4th ANNUAL EARTH RESOURCES PROGRAM REVIEW

VOLUME I
NATIONAL AERONAUTICS AND SPACE ADMINISTRATION PROGRAMS

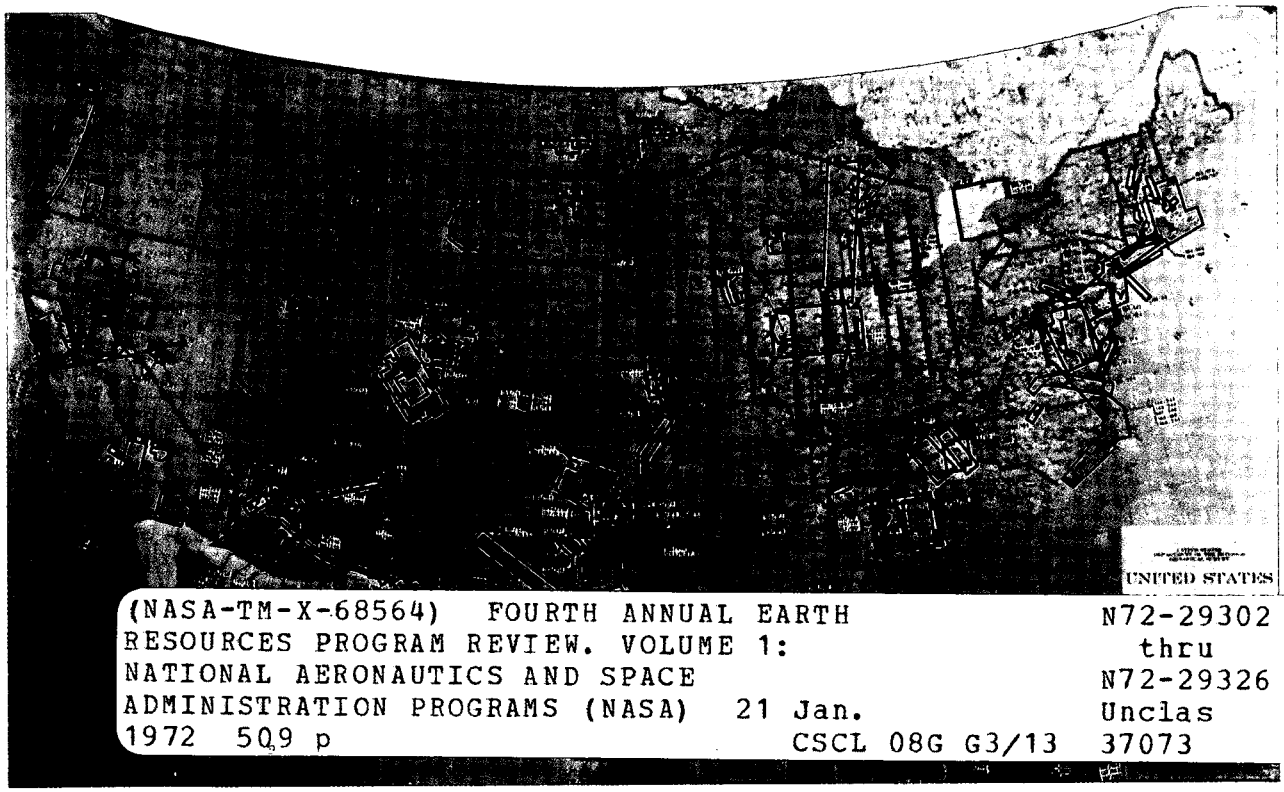

(NASA-TM-X-68564) FOURTH ANNUAL EARTH RESOURCES PROGRAM REVIEW. VOLUME 1: NATIONAL AERONAUTICS AND SPACE ADMINISTRATION PROGRAMS (NASA) 21 Jan. 1972 509 p CSCL 08G G3/13

N72-29302 thru N72-29326 Unclas 37073

Presented at the
Manned Spacecraft Center
Houston, Texas

January 17 to 21, 1972

FOREWORD

A review of various aspects of the Earth Resources Program was held at the Manned Spacecraft Center, Houston, Texas, January 17 to 21, 1972. Particular emphasis was placed on the results of analysis of data obtained with the Manned Spacecraft Center and other aircraft which have contributed data to the program.

The review was divided into the disciplinary areas of Geology, Geography, Hydrology, Agriculture, Forestry, and Oceanography. Program investigators presented the results of their work in each of these areas. The material presented is published in five volumes:

VOLUME I - NATIONAL AERONAUTICS AND SPACE ADMINISTRATION PROGRAMS

VOLUME II - UNIVERSITY PROGRAMS N72-29327

VOLUME III - U.S. GEOLOGICAL SURVEY PROGRAMS N72-29355

VOLUME IV - NATIONAL OCEANIC AND ATMOSPHERIC ADMINISTRATION PROGRAMS AND U.S. NAVAL RESEARCH LABORATORY PROGRAMS N72-29378

VOLUME V - AGRICULTURE AND FORESTRY PROGRAMS N72-29409

The review provided a current assessment of the program for both management and technical personnel. Note that the material presented represents the current status of ongoing programs and complete technical analyses will be available at a later date.

Where papers were not submitted for publication or were not received in time for printing, abstracts are used.

FRONT COVER

The map on the front cover depicts the NASA Earth Resources aircraft coverage of the United States through June 1971.

CONTENTS OF VOLUME I

CONTENTS OF VOLUME II

CONTENTS OF VOLUME III

CONTENTS OF VOLUME IV

CONTENTS OF VOLUME V

SECTION 1

N72-29303

AMES RESEARCH CENTER

SR&T PROGRAM AND EARTH OBSERVATIONS

by

I. G. Poppoff
Earth Science Applications Office
Ames Research Center
Moffett Field, California

INTRODUCTION

In this paper we present an overview of the research activities in earth observations at Ames Research Center and highlight some of the results of our FY '72 program.

Almost all of the tasks that will be described involve the use of our research aircraft platforms. The aircraft are used in three ways: (1) As intermediate platforms in the development of future satellite instrumentation, (2) as platforms for the development of techniques that are uniquely suitable for aircraft, and (3) as vehicles for the obtaining of data directly from the atmosphere through which the aircraft fly.

Our program is also directed toward the use of the Illiac IV which will be installed at Ames Research Center within the next few months. We have several environmental modeling programs underway and within six months they should be developed to the point requiring the capabilities of the Illiac IV to extend them to three dimensions.

Most of our SR&T tasks are heavily weighted toward Pacific coast and Pacific basin problems. In particular, we have developed a very close and formal relationship with the State of California resource agencies in which we will be lending them whatever talents and facilities we have in earth observations in an effort to help solve some of their very difficult resource management problems.

The SR&T effort at Ames presently involves some thirty researchers. Most of the work is being done in-house or through collaborative arrangements with Universities and government agencies. The tasks can be grouped for convenience into water applications, air applications, animal migration studies, and geophysics.

WATER APPLICATIONS

In water applications the principal activity revolves around the airborne differential radiometer system that was discussed in a preceding paper. In brief, the differential radiometer operates by tuning one channel to the wavelength of the material that is to be sensed and tuning the other channel to a reference wavelength. For example, one channel can be tuned to the chlorophyll A absorption band and the other channel can be tuned to an unaffected reference wavelength. With this device several lakes in the state of California have been over-flown, considerable ground truth has been obtained, and it is found that the output of the differential radiometer is proportional to the logarithm of the chlorophyll concentration. Figure 1 shows the use of this instrument in determining the characteristics of the outflow plume of the Sacramento and San Joaquin rivers through the Golden Gate of San Francisco Bay. Figure 2 shows the use of this instrument in plotting the distribution of chlorophyll in Clear Lake. Figure 2 also illustrates the result that can be obtained by the use of a dual channel television system utilizing false color intensity-slicing for real-time viewing of the chlorophyll distribution in bodies of water. This dual channel instrumentation has also been applied to the problem of detecting and measuring the extent of oil slicks. The problem is to determine what conditions can provide the greatest contrast between the oil and the water. The spectral characteristic of the reflected sunlight was examined as was the effect of polarization, the effect of sun angle and the effect of sky brightness. It was found that the reflected sunlight has highest contrast in the ultraviolet and that by using the polarization characteristics of the reflected beam one could further increase the contrast. Figure 3 shows a flight over two oil slicks with a differential radiometer which has one channel tuned to the UV and the other channel tuned to a reference wavelength in the visible.

We have also had a more concentrated activity at one specific lake in California, Lake Tahoe. This is a very clear lake with relatively sterile water; it is now experiencing a great deal of pressure from urban development at both the north and south ends. There is some concern that the lake is starting to become more eutrophic; and, in fact, algal blooms have been observed. One theory is that the algae are growing because of the nutrients that are carried by tributaries discharging into the lake. Therefore, this study, which was done in collaboration with the University of California, was directed toward an analysis of this particular hypothesis. Ames Research Center conducted the photographic over-flights and interpretation of photographs, the University of California team provided the ground truth, analyzing

the water samples for nutrients and bacterial and algal productivity. Figure 4 shows that the major discharge period is in the spring and early summer during the thaw of the Sierra snow pack. Figure 5 is one of the aerial photographs clearly showing the sediment plumes discharged into the south end of Lake Tahoe by the upper Truckee River. Figure 6 shows contours of the density of sediment in the plumes, together with some of the analyses of productivity. You will notice that there is a fair correlation between the density of sediment and the productivity of bacteria.

Recognizing that the primary source of water in California is the Sierra snow pack, we are developing techniques to measure the thickness of the pack and the water content. Because of the economic importance of the snow pack, forecasts of the year's water supply are important to many people; therefore, a fairly accurate accounting of the water content of the snow pack would be a very valuable contribution. A plane radio wave impinged on the surface of the snow is partially reflected and partially transmitted. The amount transmitted depends upon the thickness of the snow, the frequency of the radio wave, and the density of the snow. The technique that we are using was originally developed to study subsurface layers on the moon; we have done extensive computer modeling to see how this technique could be applied to measuring a snow pack. Figure 7 shows the geometry of the model. Figure 8 shows one of the traces determined by our theoretical modeling program. You should note that as the frequency is varied, a dip occurs at a frequency that is characteristic of the thickness and the dielectric constant of the snow. The depth of that dip is characteristic of the dielectric constant; therefore, the dielectric constant can be determined and, subsequently, the depth of the snow pack. The dielectric constant itself is a function of the snow density and therefore provides us information on the water content. Notice also that at regular quarter-wave intervals, additional dips are seen, and eventually a dip is seen (labeled ν_{ice} in the diagram) which is characteristic of the thickness of the ice under the snow pack. Therefore, ice thickness can also be measured with this technique, even under a snow pack. We are testing this technique using towers in the snow region. Instead of scanning the frequency, however, we're using a fixed frequency and fixed transmitter power and monitoring the reflected amplitude of the signal as the depth of the snow pack increases. You can see in figure 9 the results of one preliminary run where we do get the frequency dips that the model predicts; there is a marked difference between moist snow and very wet snow. These are very preliminary results, of course, and we will continue this investigation throughout the winter.

AIR APPLICATIONS

We have several tasks in the general category of atmospheric applications. The first of these tasks is an effort to determine the environmental impact of such operations as the SST and the Space Shuttle on the stratosphere. At the same time we wish to learn about the impact of lower atmosphere sources such as volcanoes, thunderstorms, and smog. In this effort, we are constructing theoretical models and developing instrumentation (to be flown on the U-2) to make analyses of specific gases in the stratosphere. The modeling program, as you can see in figure 10, will account for a number of constituents. In addition to those listed, we currently include many carbon compounds. The series of continuity equations that make up this model take into account time dependence, photochemistry, and mass transport. To date, we have developed a one-dimensional version of this model; it is on the computer and appears to be operating correctly. Figure 11 shows the results of using this model to determine the equilibrium stratosphere. Notice that the ozone concentration, which is one of the products of this model, agrees fairly well with measurements and with other steady-state models. Figure 12 shows the effect of introducing excessive amounts of nitric oxide and water vapor at 20 kilometers, which is the hypothesized altitude. A considerable amount of nitric oxide was introduced in this model and yet, as can be seen, there is very little impact on the ozone profile. These are, of course, very preliminary results and illustrate more the capabilities of the model than the actual evaluation of the impact of an SST on the stratosphere.

Figure 13 illustrates the sampling equipment that is being developed for the U-2. We will be able to analyze the atmosphere for CO, CO_2, ozone, water vapor, and nitric oxide. This package is being flown on the Ames 990 in order to debug it. Results to date have possibly established an upper limit for the nitric oxide concentration at 10 parts per billion at 39,000 feet (tropopause was at 33,000 feet). This information will serve at least to bound some models. We have also obtained some aerosol collections at this altitude. The particles in figure 14 are all one micron or less in size, the largest particles that you can see appear to be droplets; when they are touched by the electron beam for analysis, they deform and move around on the slide as droplets should. Approximately 1/3 of the particles are clearly droplets, perhaps another 1/3 are solid with liquid surface and perhaps another 1/3 are solid. The preliminary analysis that we have made accounts only for elements over atomic weight 11; we find silicon, aluminum, calcium, iron and sulphur. The large droplets contain only sulphur (probably sulphuric acid), the smaller particles contain the metals as well as sulphur, and the smallest particles apparently do not contain

sulphur. This would seem to indicate a fairly strong influx of volcanic material into the stratosphere. This again, however, is only preliminary information and cannot be viewed as definitive.

A second task in the area of air quality is an airborne survey of the vertical structure and areal extent of photochemical smog in the Los Angeles and San Francisco basins. These data are intended for use as input into revised air pollution models for these areas. In brief, we have instrumented an aircraft for the collection of carbon monoxide, nitric oxides, ozone, temperature, dew point, hydrocarbons and aerosols. Figure 15 shows the layout of these instruments in a Cessna 401A which was used for the surveys. Figure 16 shows a typical ozone stratification observed at Riverside. Notice that the concentrations of ozone at the inversion layer at approximately 2,000 feet are much greater than those at ground level. Figure 17 shows a survey flown 200 nautical miles west of the coast of California; here we see that ozone occurs at several levels and that a particularly high concentration exists at an altitude of almost 20,000 feet. It was also found that smog is dispersed several hundred miles away from each of the basins that were investigated. This work is being done in cooperation with the University of California at Riverside and with the San Francisco Air Pollution Control District and with the Livermore Laboratory of the University of California.

Another task in this area, a rather unique one, is the study of atmospheric microorganisms. The work done this summer revolved around the larger NASA study of the Midwestern corn blight. Two aircraft were instrumented to make collections of microorganisms. Figure 18 shows the area flown by an Aerocommander instrumented with an aerosol collector and figure 19 shows the area flown by a DC-3, instrumented with a different kind of collector. The result indicated that there were microorganisms over all the three states that were surveyed, that these organisms occurred in strata, that they were found at altitudes as high as 6,000 feet, and that they were frequently concentrated at the base of clouds. One of the difficulties that was encountered early in the survey is that the researchers were looking for the spore shown in figure 20 and could not find any in the collected slides; figure 21 shows a typical collection. Now, if one will notice the body in the middle of that collection and compare it with figure 22, you will see that it actually was a dehydrated form of the corn blight spore. When this was recognized, it was realized that all the collections had been successful; now there is a large body of data being analyzed to show the distribution, vertically and horizontally, over the corn-growing states.

Another task in this area that is just starting is a study of the atmospheric mercury budget for the San Francisco Bay area. This mercury study is now in the planning stage.

ANIMAL MIGRATION

Work in animal migration studies is just starting. The objective of the three tasks that are now getting underway is to study the migration of marine animals, utilizing the unique advantages of the satellite for long distance relaying of information about the global distribution and migration paths of the particular species under study.

The goal of the first task (figure 23) is to study the behaviour of whales. Since whales migrate over most of the globe, the use of a satellite is uniquely necessary for such studies. The second task (figure 24) is an attempt to use dolphins as platforms to carry instrumentation down to the biomass and to study its characteristics and extent. Inasmuch as dolphins must eat, they will find the biomass; and inasmuch as they surface often, the information could be picked up through telemetry. The third application (figure 25) is for the tracking of salmon in the northwestern United States. The management of the salmon harvest is a very difficult one and requires data on the number of salmon moving into the salmon fishing grounds. These particular data must then be analyzed in terms of parameters that are needed for management decisions; and this often must be done in just a matter of hours. This task involves the development of sonic bouys to be anchored along the Aleutian chain which can detect the number of salmon moving into the area (and perhaps their species and size) and relay this information via satellite to a large computer where the management program is stored; the results then would be relayed back to the fisheries managers.

We are also planning programs that involve the application of miniaturized physical function sensors to the studies of the behaviour of mammals during their migration and feeding.

GEOPHYSICS

The first task is the use of vector magnetometry to analyze various geological characteristics under the surface of the oceans or below the surface of the land areas. We have used this vector magnetometer in a flight over the Pacific Ocean; the data will be used in analysis of sea floor spreading, and thus provide some information to corroborate theories of plate tectonics. We have also overflown the United States and this data is being requested by NOAA as input to their world geomagnetic maps. In collaboration with the USGS, we made a very thorough magnetic survey of the northwestern corner of the state of Washington in the vicinity of Neah Bay.

The second task is a study of the application of thermal infrared instruments to the problem of detecting and mapping potential landslide areas. This appears to be feasible because landslide areas are caused by the underground damming of water drainage. The resulting differences in soil moisture cause changes in surface temperatures and these can be detected with thermal infrared sensors. Our preliminary studies have shown that this technique is very feasible and valuable; it is being continued in collaboration with the US Corps of Engineers and the State of California.

STATISTICAL CORRELATIONS

The last task is the development of techniques for the analysis of statistical data. The objective of this study is to provide computer techniques that will allow the determination of statistical relationships between variables whose relationships are unknown. Figure 26 illustrates a three-variable relationship plotted in three-dimensional space. It is very noisy data, and no apparent relationship is evident to the naked eye. However, when this data is processed with the program developed in this task, we see that this is a noisy spiral (figure 27). This sort of analysis, we believe, will be very valuable in attempts to correlate many ecological paramaters that are being measured, and for which no known relationships exist.

Figures

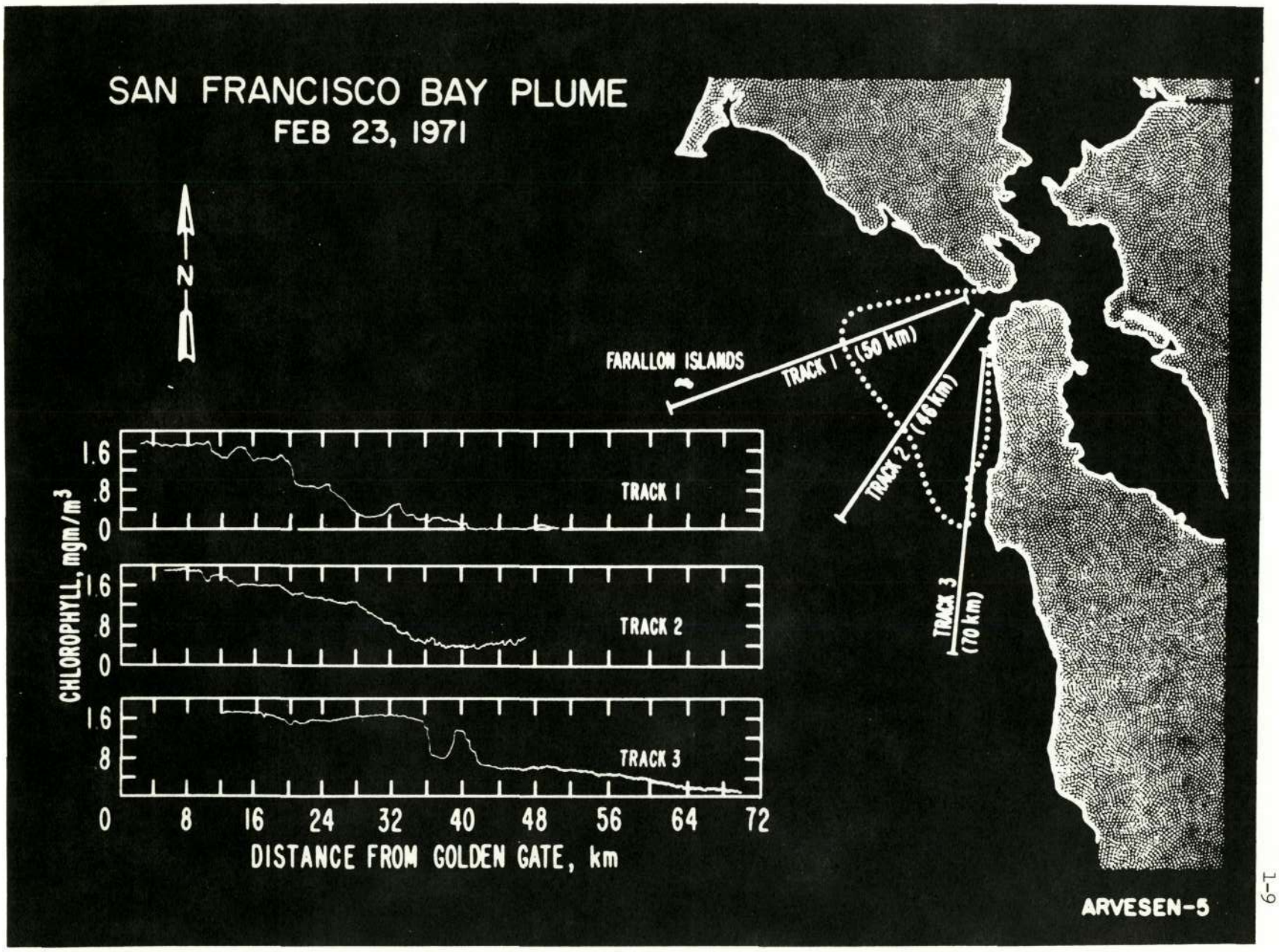
SAN FRANCISCO BAY PLUME
FEB 23, 1971
N
FARALLON ISLANDS
TRACK 1 (50 km)
TRACK 2 (46 km)
TRACK 3 (70 km)
CHLOROPHYLL, mgm/m³
1.6
.8
0
TRACK 1
TRACK 2
TRACK 3
0
8
16
24
32
40
48
56
64
72
DISTANCE FROM GOLDEN GATE, km
ARVESEN-5

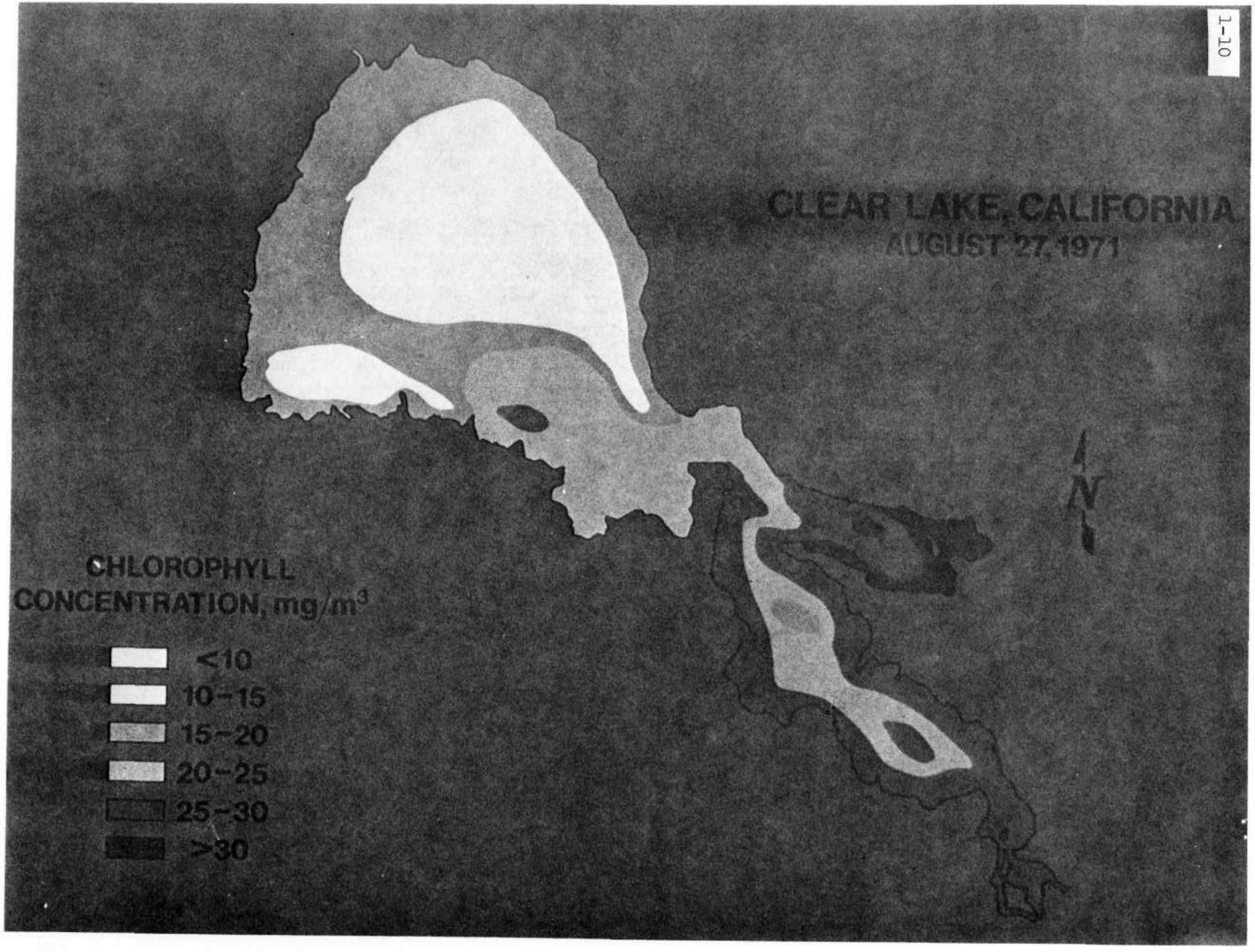
CLEAR LAKE, CALIFORNIA
AUGUST 27, 1971
N
CHLOROPHYLL
CONCENTRATION, mg/m³
<10
10–15
15–20
20–25
25–30
>30

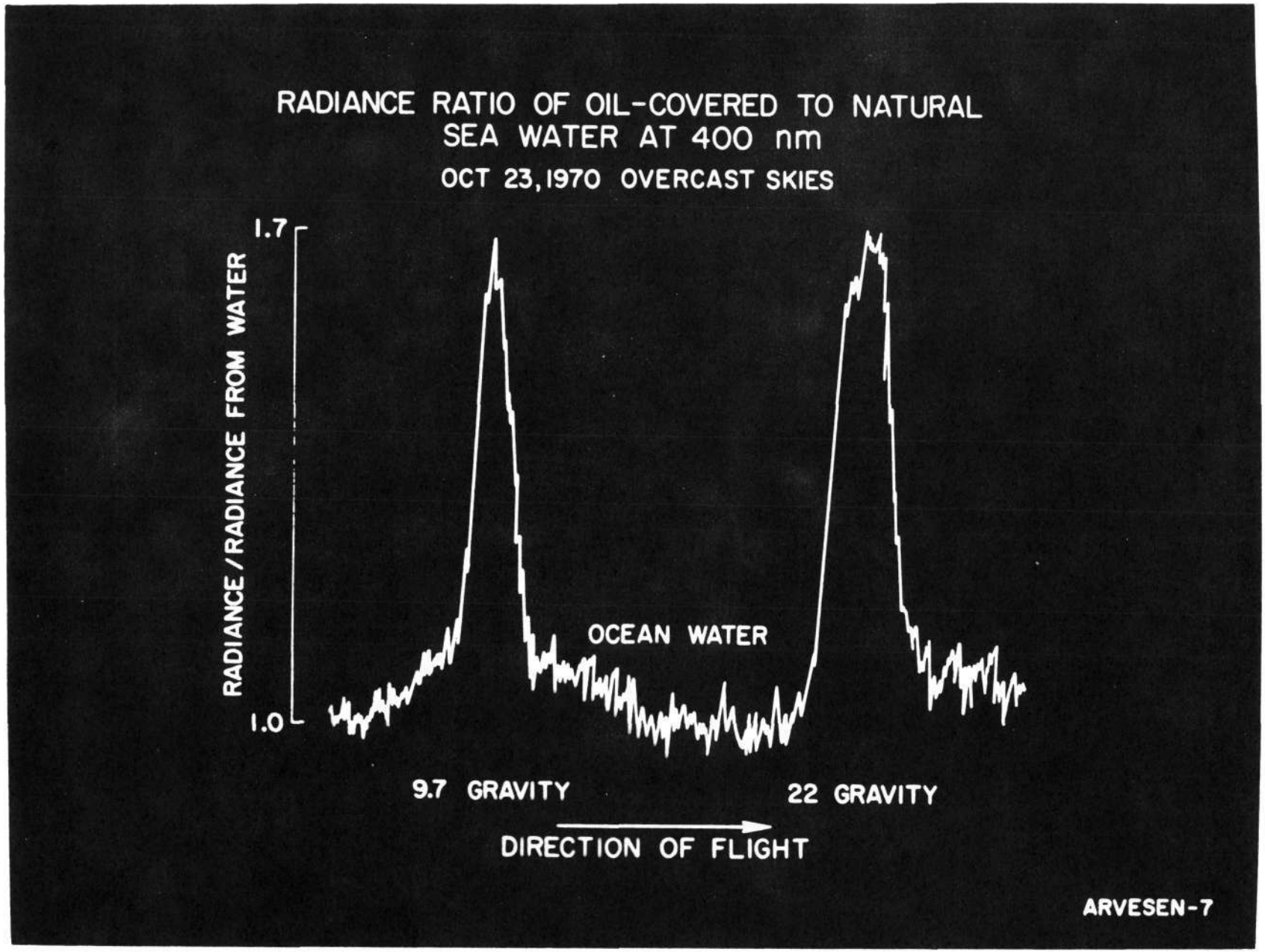
RADIANCE RATIO OF OIL-COVERED TO NATURAL SEA WATER AT 400 nm
OCT 23, 1970 OVERCAST SKIES
RADIANCE / RADIANCE FROM WATER
1.7
1.0
OCEAN WATER
9.7 GRAVITY
22 GRAVITY
DIRECTION OF FLIGHT
ARVESEN-7

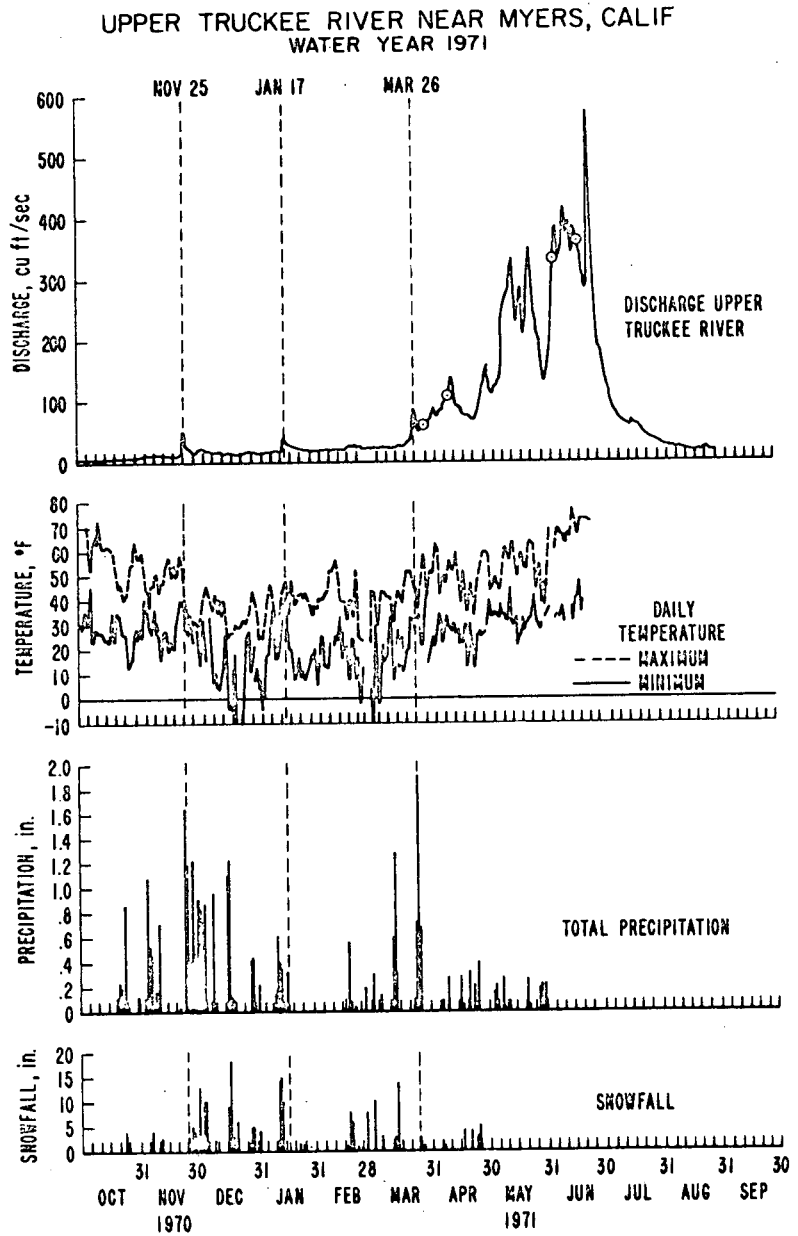
UPPER TRUCKEE RIVER NEAR MYERS, CALIF
WATER YEAR 1971
NOV 25
JAN 17
MAR 26
DISCHARGE, cu ft/sec
600
500
400
300
200
100
0
DISCHARGE UPPER TRUCKEE RIVER
TEMPERATURE, °F
80
70
60
50
40
30
20
10
0
-10
DAILY TEMPERATURE
MAXIMUM
MINIMUM
PRECIPITATION, in.
2.0
1.8
1.6
1.4
1.2
1.0
.8
.6
.4
.2
0
TOTAL PRECIPITATION
SNOWFALL, in.
20
15
10
5
0
SNOWFALL
31 30 31 31 28 31 30 31 30 31 31 30
OCT NOV DEC JAN FEB MAR APR MAY JUN JUL AUG SEP
1970
1971

HETEROTROPHIC PRODUCTION RATE--UPPER TRUCKEE RIVER SEDIMENT PLUME, 6-20-71 AM
(μg acetate/m^3-hr)

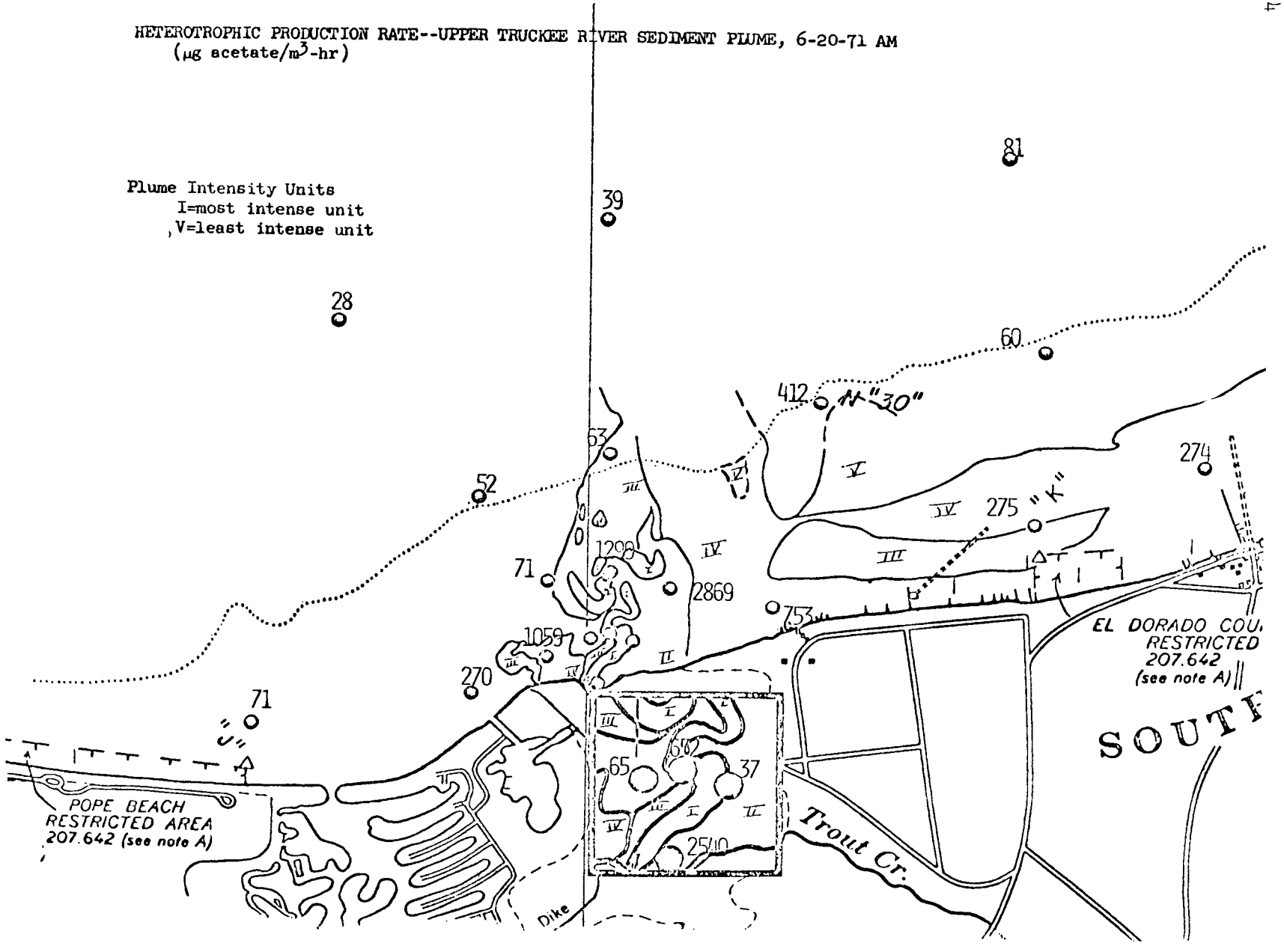

FIVE-LAYERED MODEL

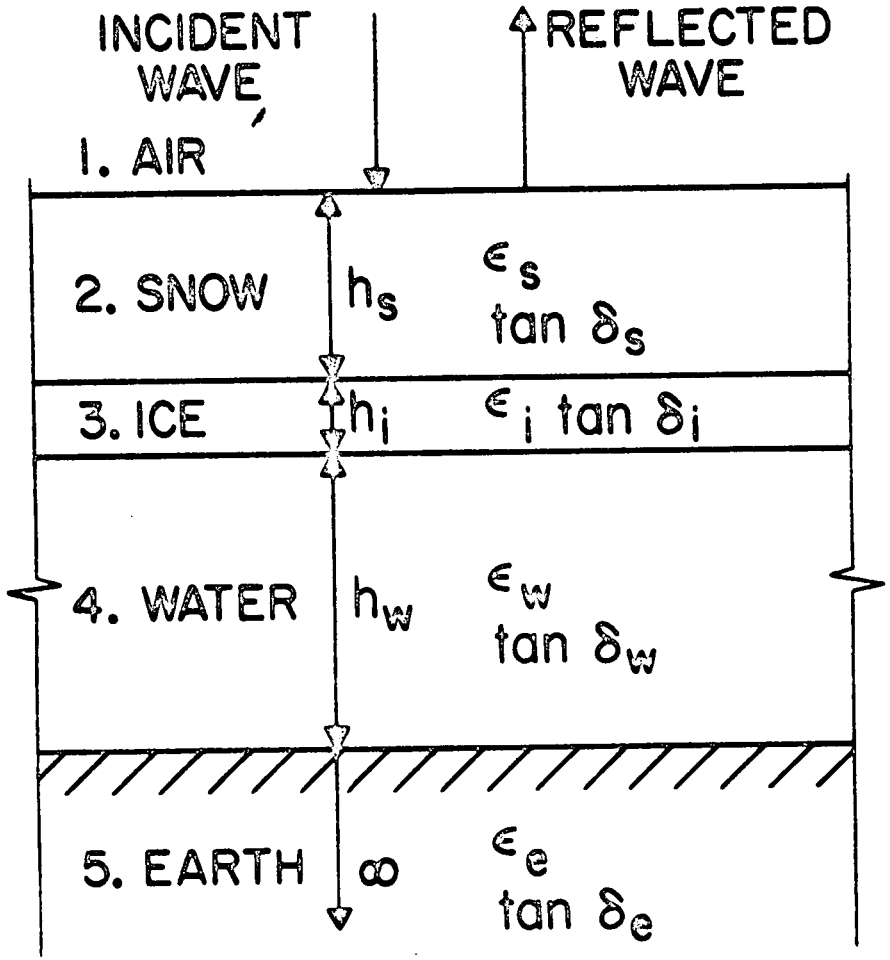

REFLECTION AMPLITUDE VS. FREQUENCY

SNOW THICKNESS: 91.4 cm (3 ft)
ICE THICKNESS: 7.56 cm (3 in.)
WATER DEPTH: LAKE

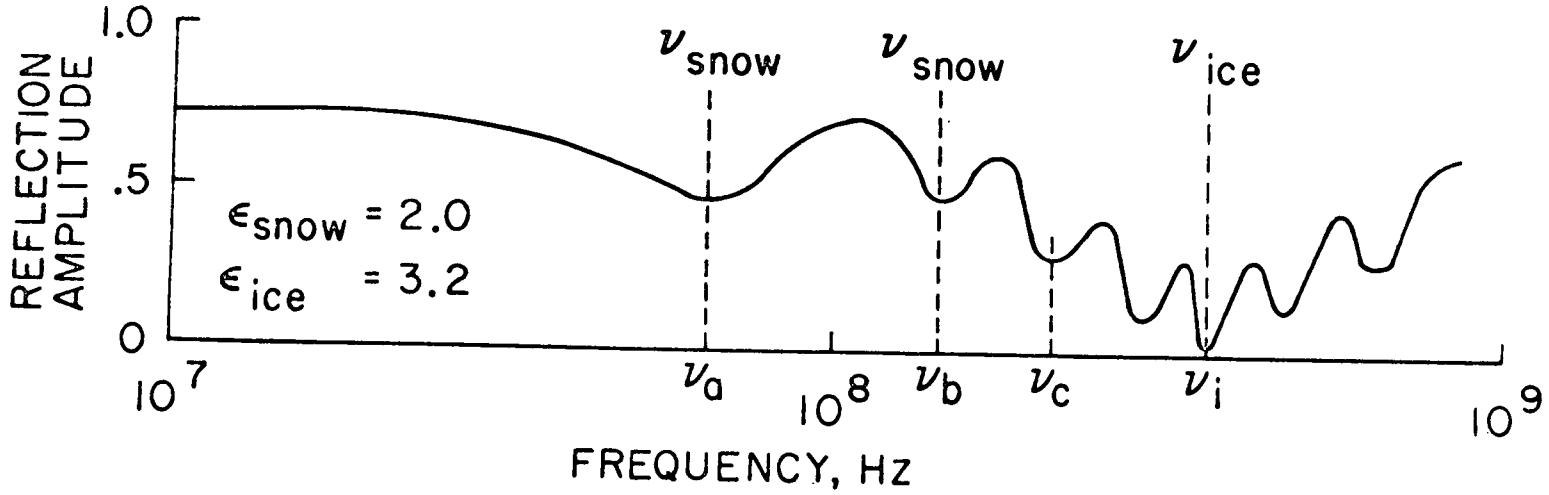

SYSTEM RESPONSE VS. SNOW DEPTH

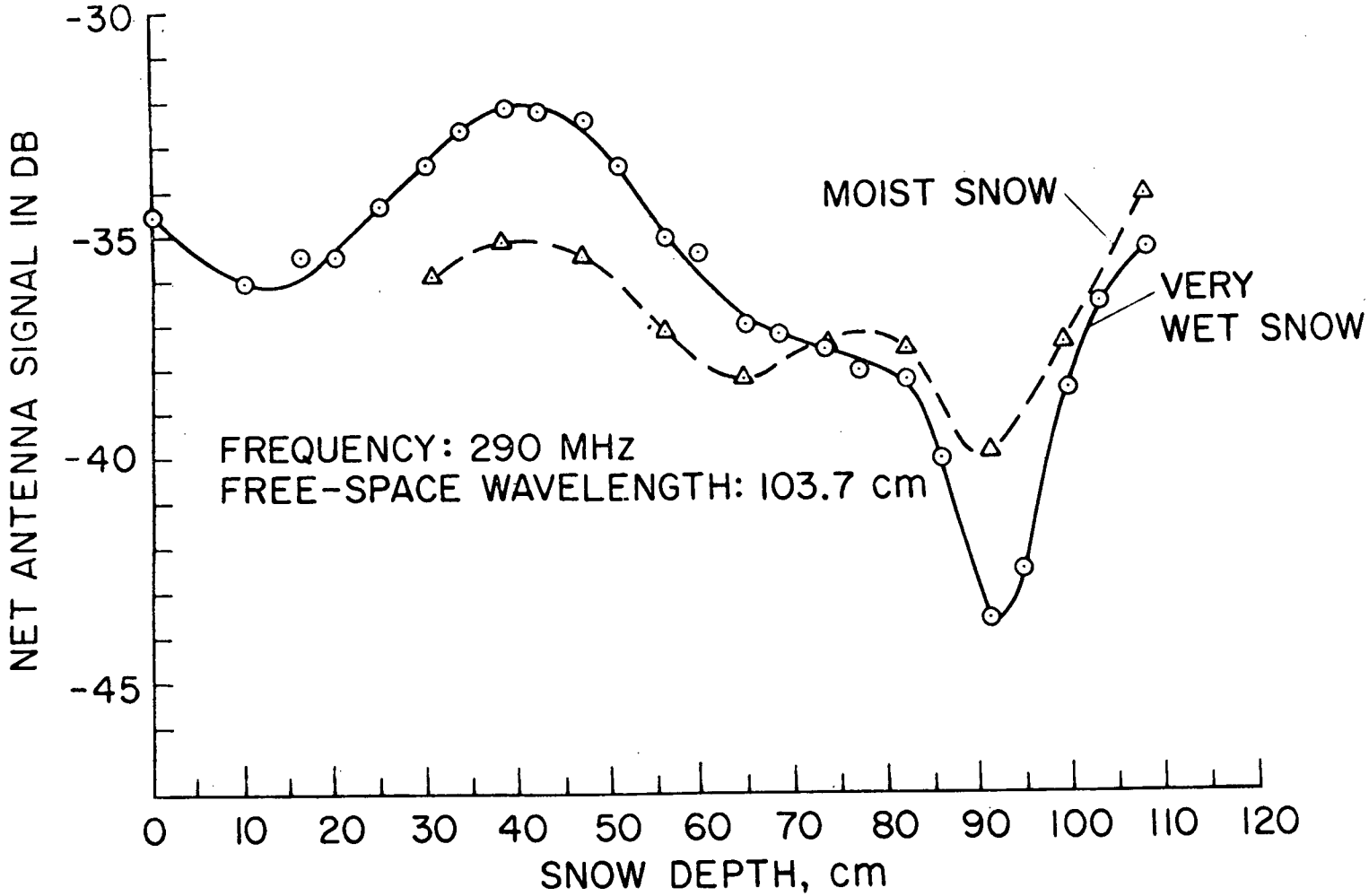

CHEMISTRY AND TRANSPORT

CONSTITUENTS:

O, O (^1D), O_3, H, OH, HO_2, H_2O_2, H_2O, NO, NO_2, NO_3, N_2O_5, HNO_3

CONTINUITY EQUATIONS:

$$\frac{\partial M_i}{\partial t} + \frac{\partial \Phi_i}{\partial z} = P_i - L_i$$

$$\Phi_i = -K\left[\frac{\partial M_i}{\partial z} + \left(\frac{d(\ln T)}{dz} + \frac{1}{H_i}\right) M_i\right] + VM_i$$

STRATOSPHERIC MODEL EQUILIBRIUM, DAYTIME

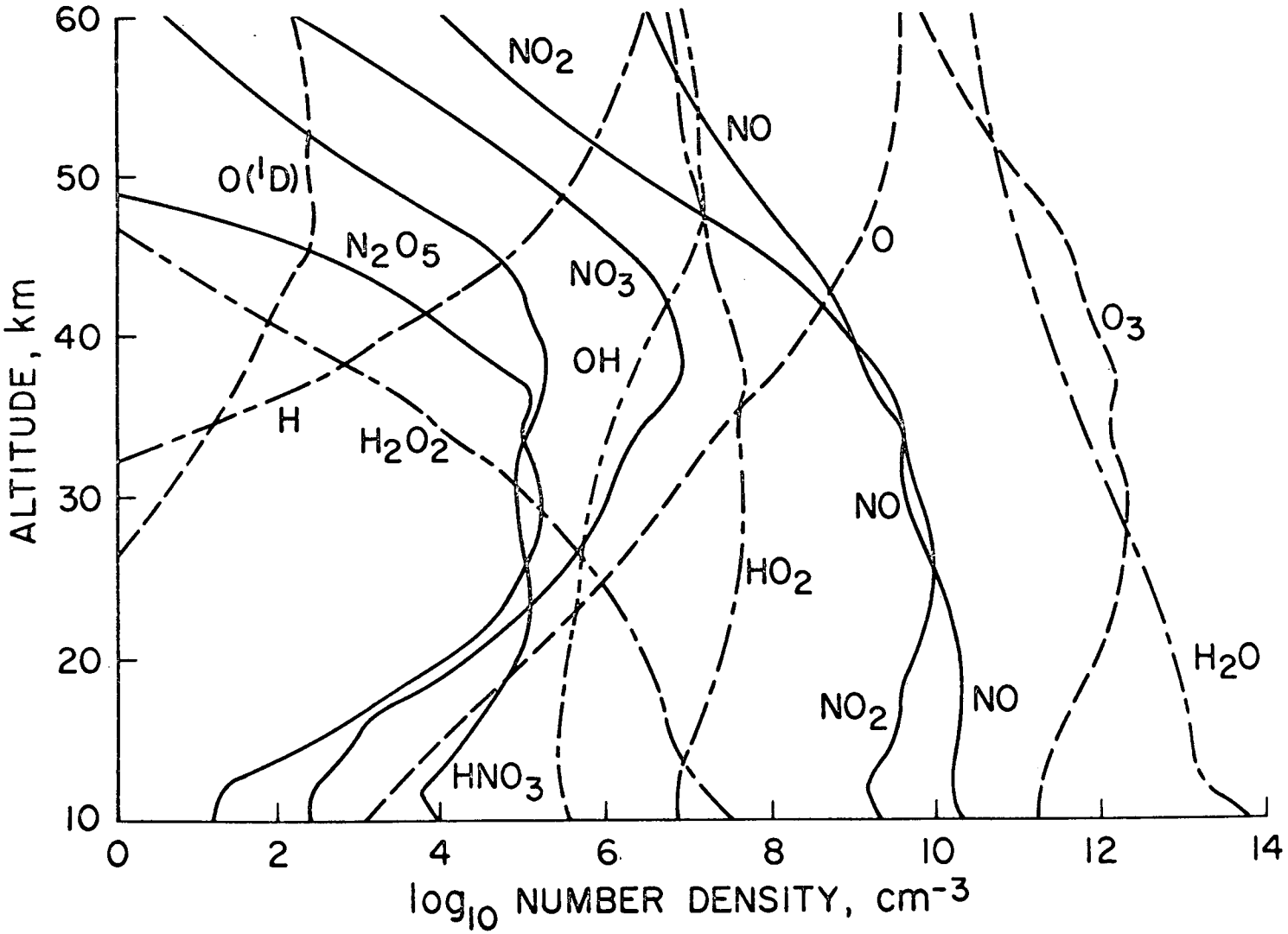

PERTURBED STRATOSPHERE AFTER 3×10^7 sec

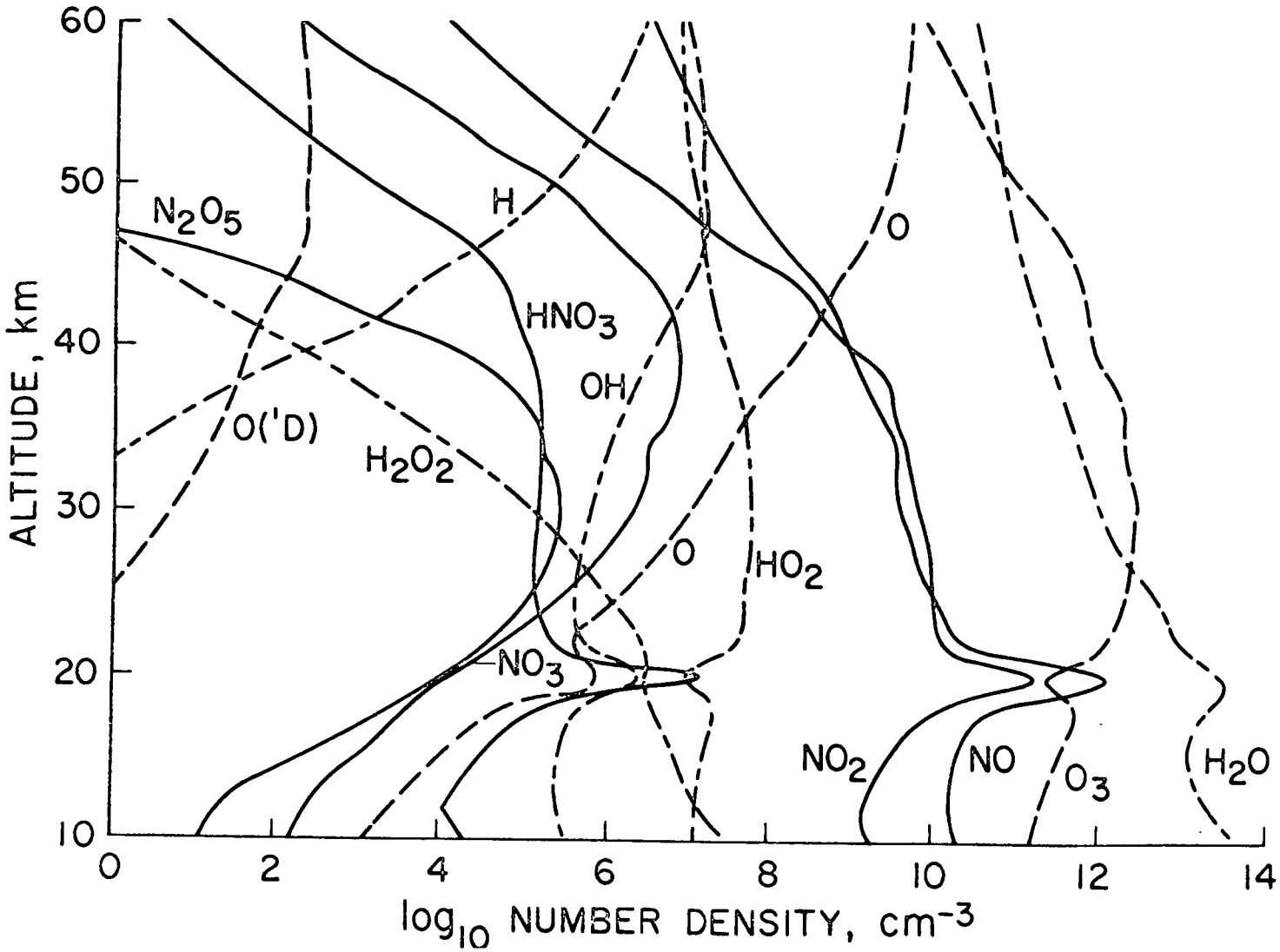

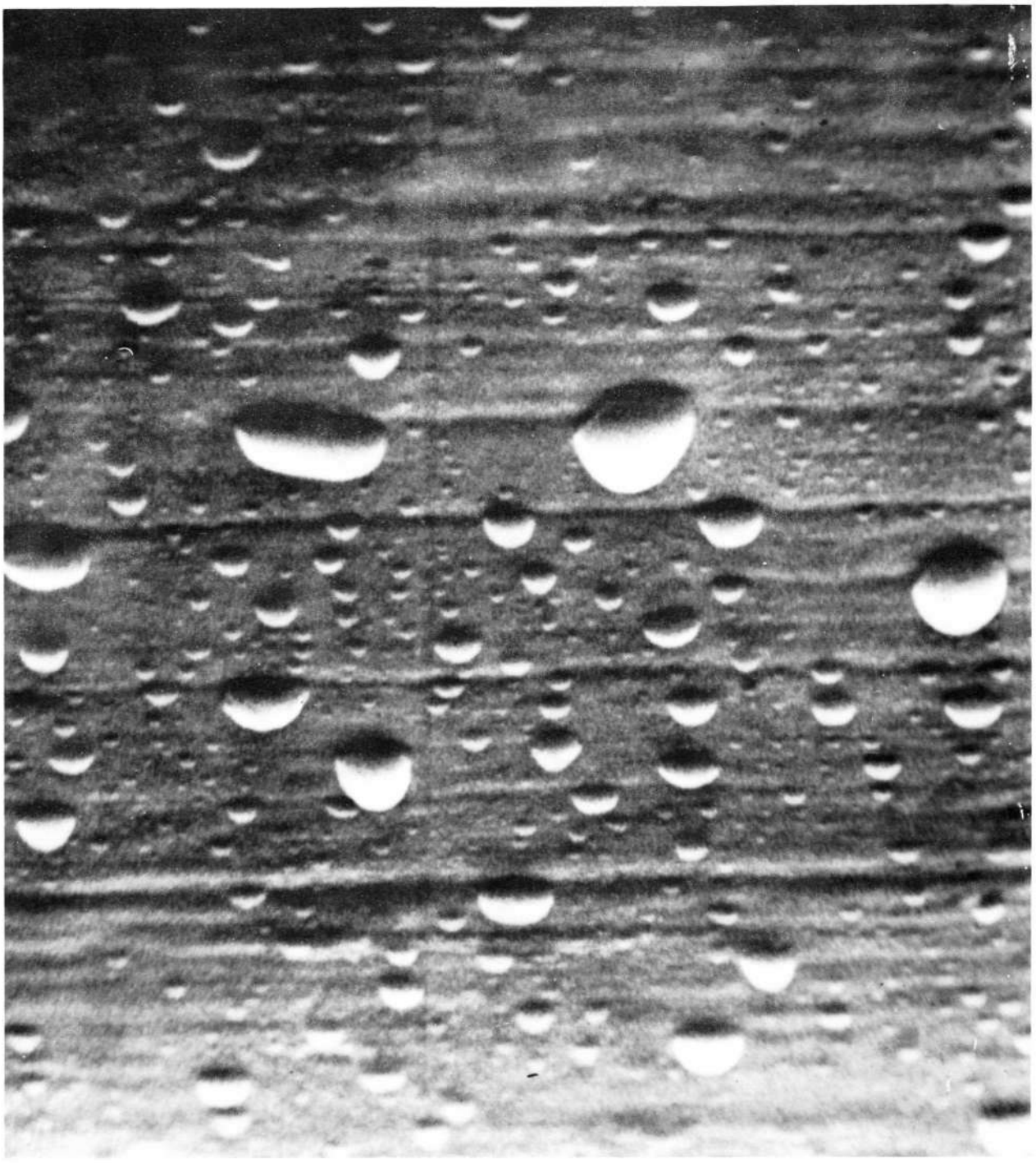

CESSNA 401-A CONFIGURATION

FALL 1971 FLIGHTS

EQUIPMENT WEIGHT - 440 lbs
GROSS WEIGHT - 6400 lbs

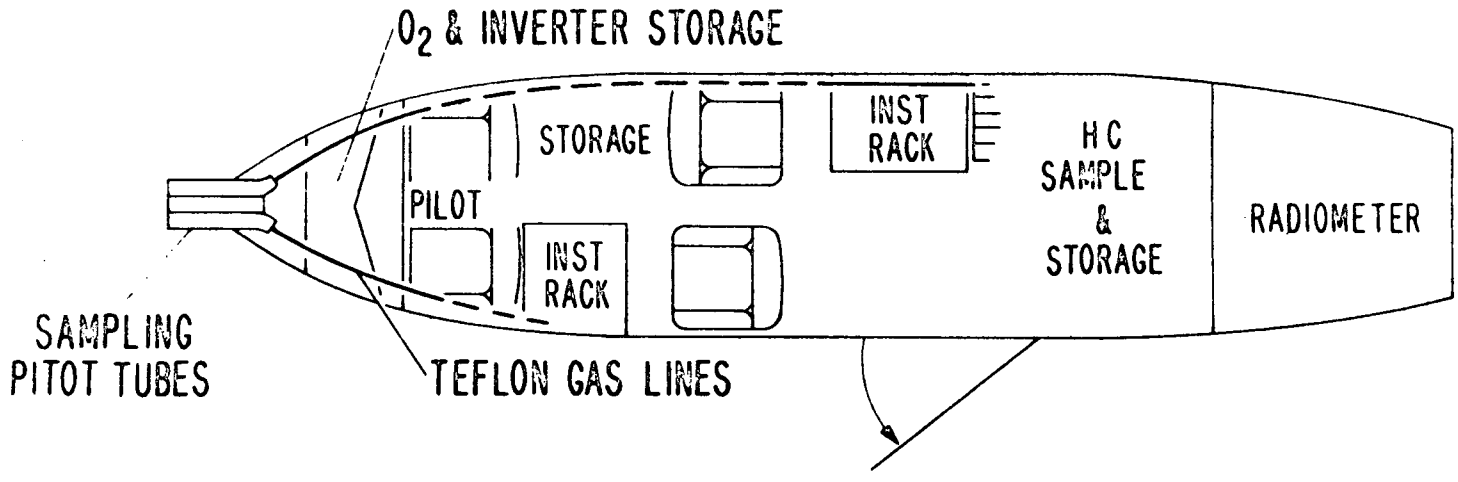

INSTRUMENTATION:	CO	TEMPERATURE	HYDROCARBON SAMPLES
	NO_X	DEW POINT	NEPHELOMETER
	O_3	RADIOMETER	RECORDERS

H. GLORIA

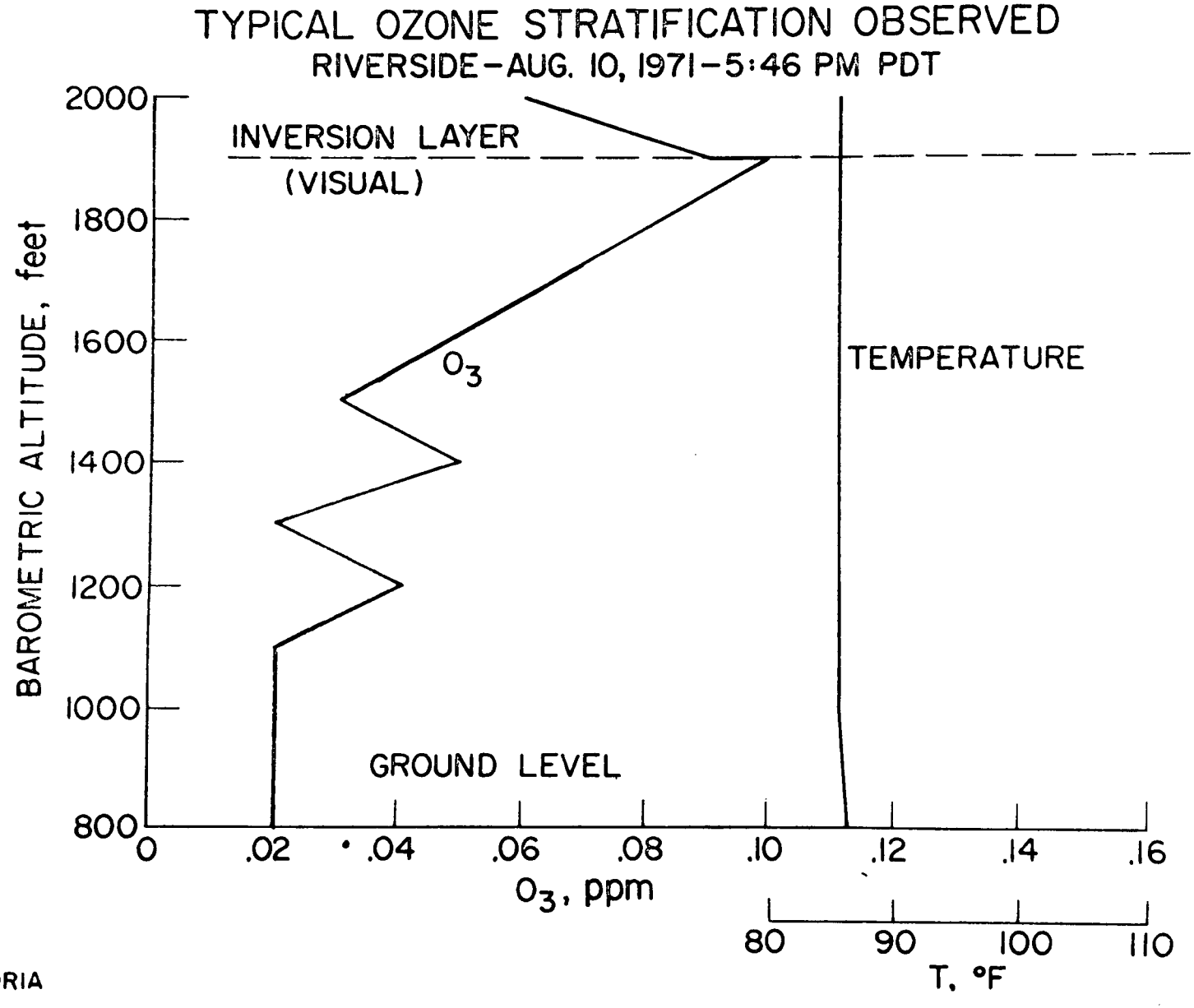
TYPICAL OZONE STRATIFICATION OBSERVED
RIVERSIDE – AUG. 10, 1971 – 5:46 PM PDT
INVERSION LAYER
(VISUAL)
O_3
TEMPERATURE
GROUND LEVEL
BAROMETRIC ALTITUDE, feet
2000
1800
1600
1400
1200
1000
800
0
.02
.04
.06
.08
.10
.12
.14
.16
O_3, ppm
80
90
100
110
T, °F

H. GLORIA

OCEAN BACKGROUND OXIDANT SURVEY
200 NM WEST OF COAST – FLIGHT 9A
SEPT. 11, 1971 – MIDAFTERNOON DATA

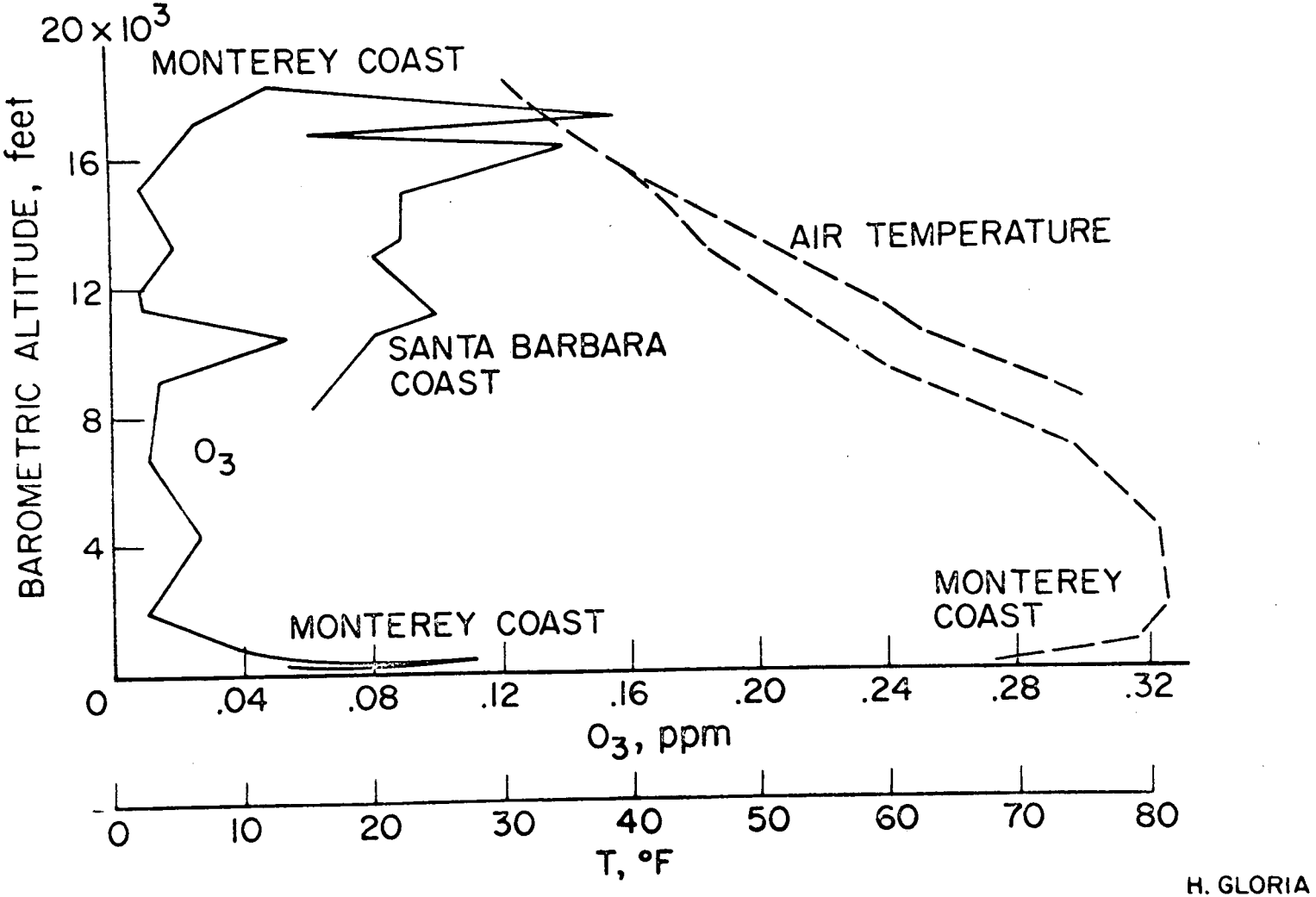

H. GLORIA

SAMPLING AREAS COVERED BY AEROCOMMANDER

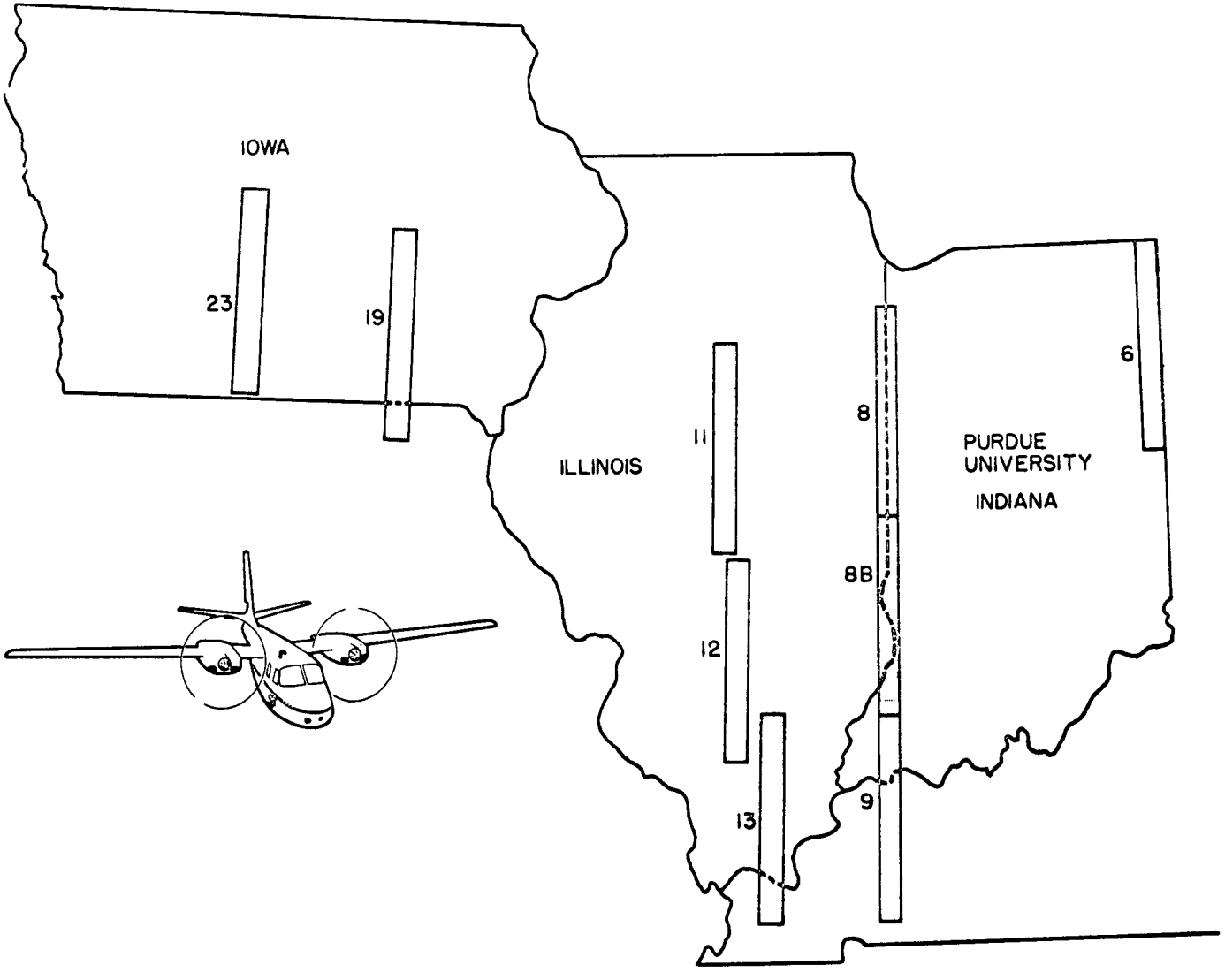

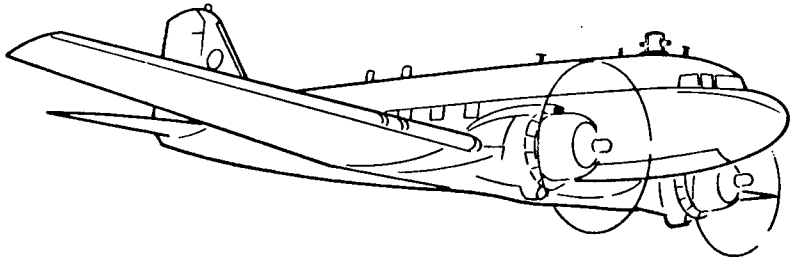

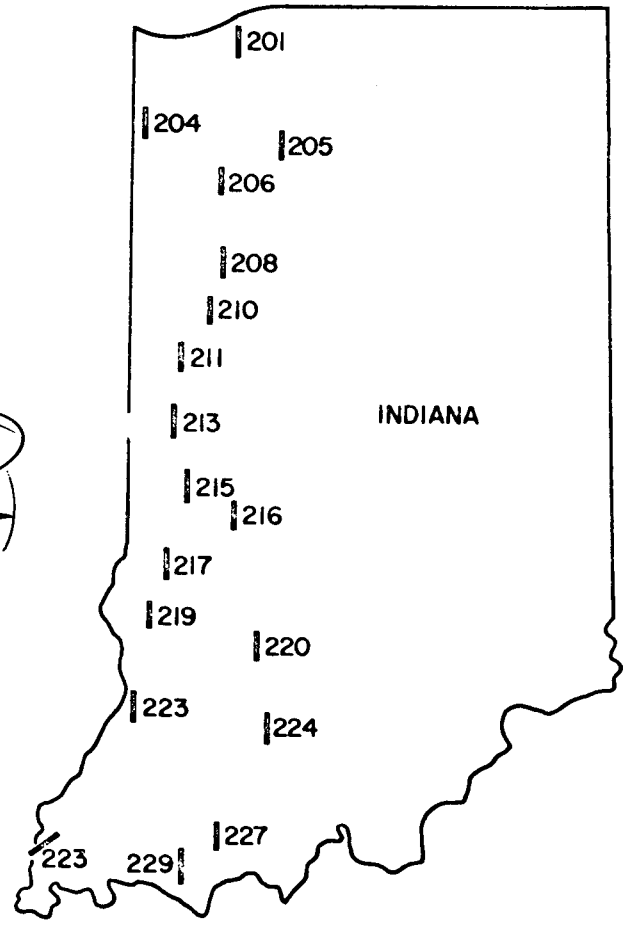
201
204
205
206
208
210
211
213
INDIANA
215
216
217
219
220
223
224
227
223
229

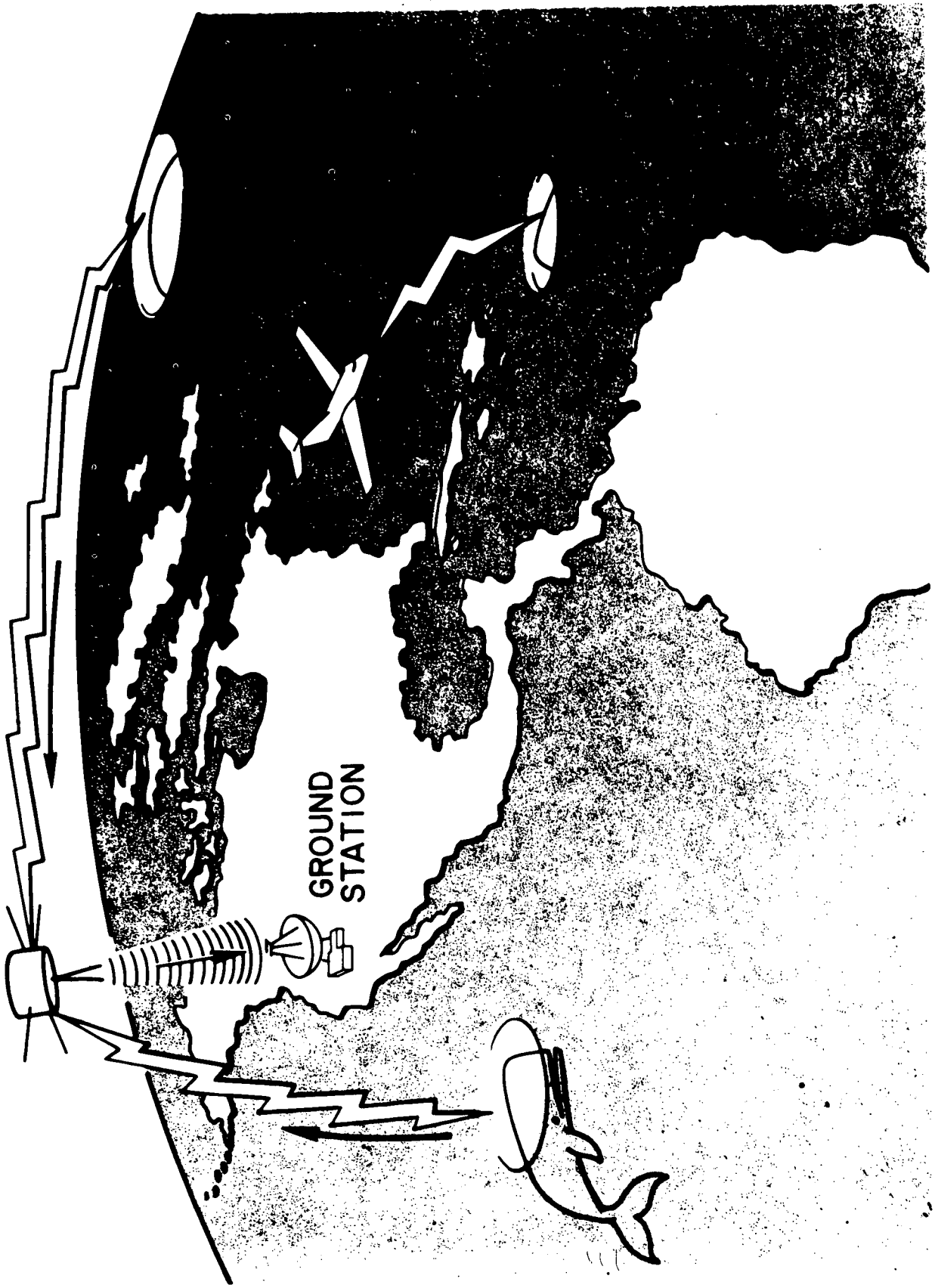
GROUND
STATION

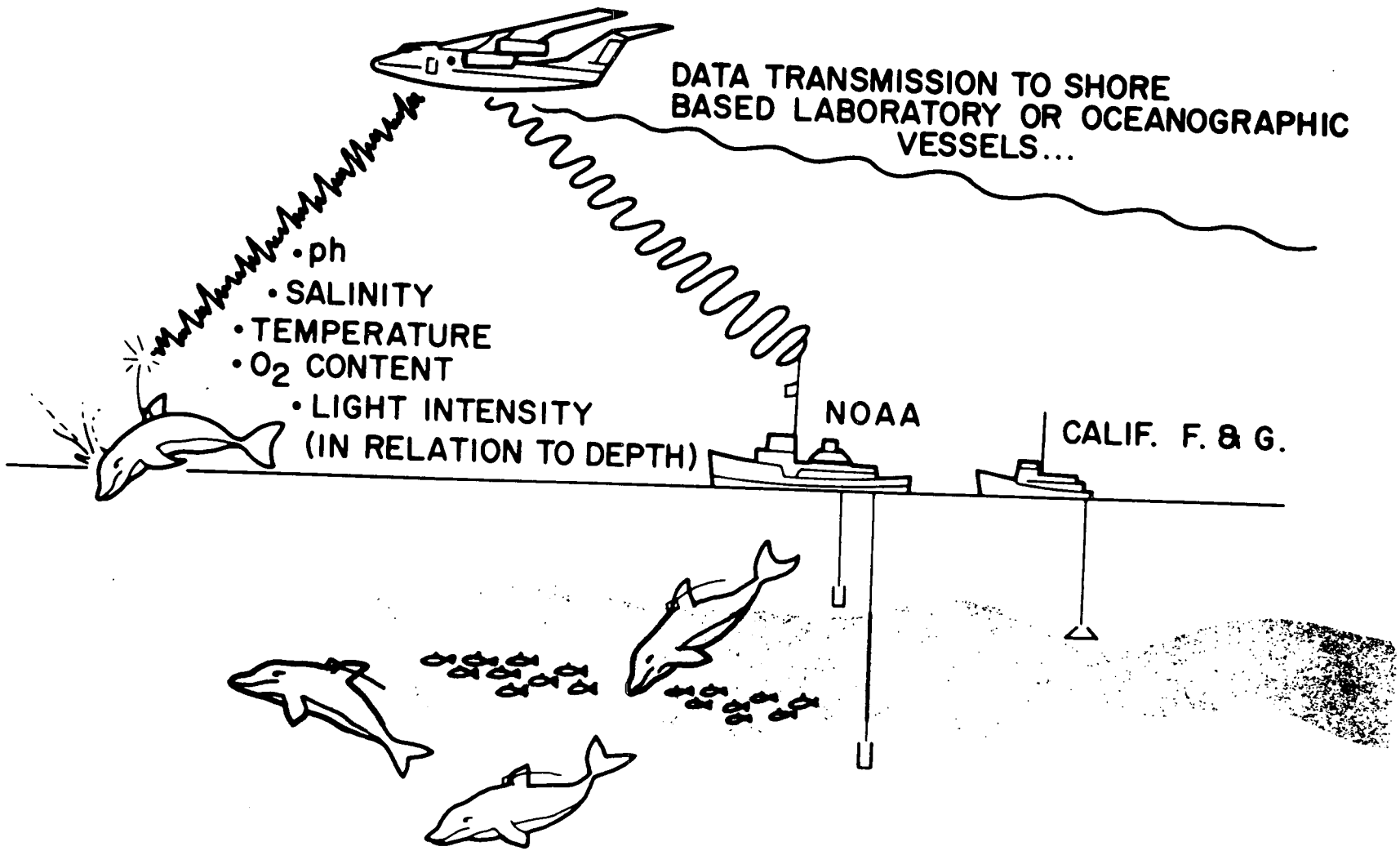
DATA TRANSMISSION TO SHORE
BASED LABORATORY OR OCEANOGRAPHIC
VESSELS...
• ph
• SALINITY
• TEMPERATURE
• O_2 CONTENT
• LIGHT INTENSITY
(IN RELATION TO DEPTH)
NOAA
CALIF. F. & G.

MANAGEMENT OF OCEAN PROTEIN RESOURCES

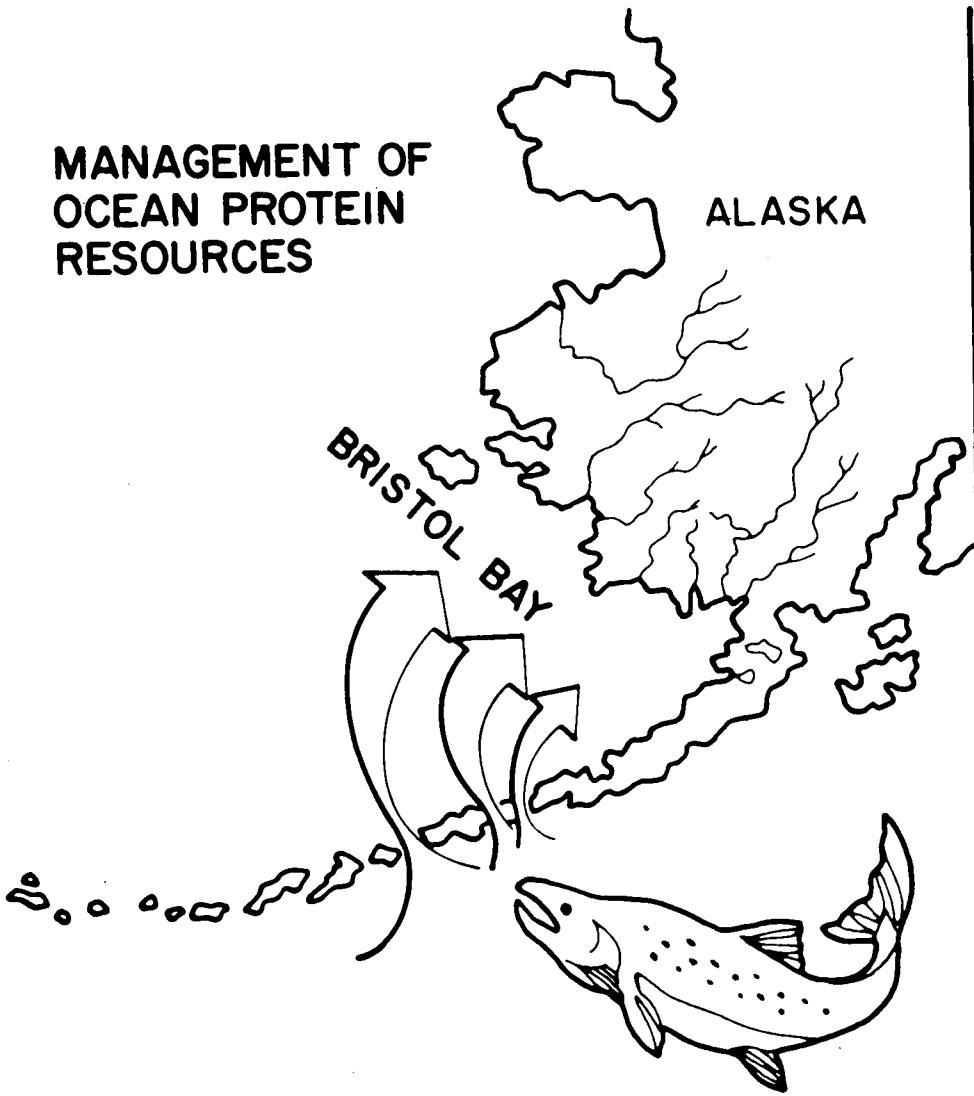

PACIFIC OCEAN

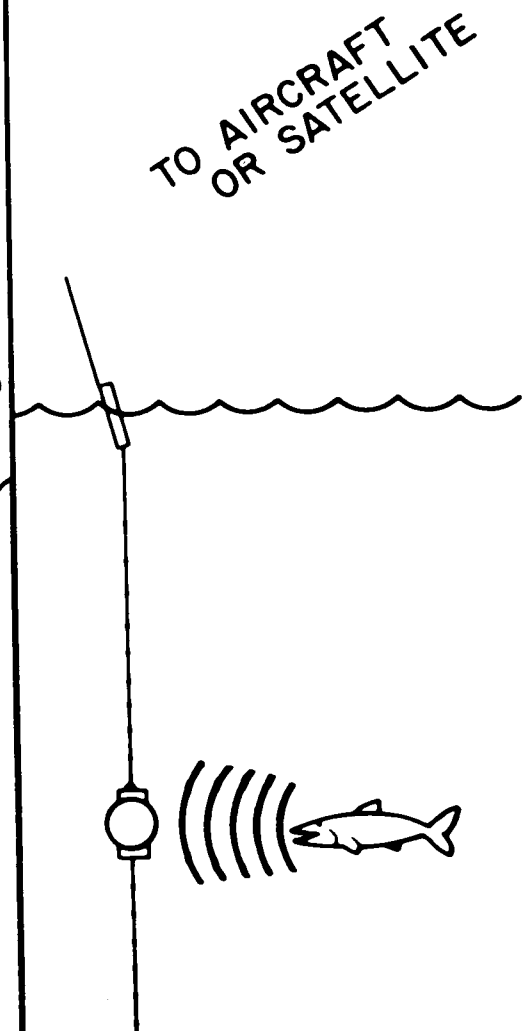

SONAR FISH SCHOOL DETECTION

TWO DIMENSIONAL PLOTS OF THREE DIMENSIONAL DATA

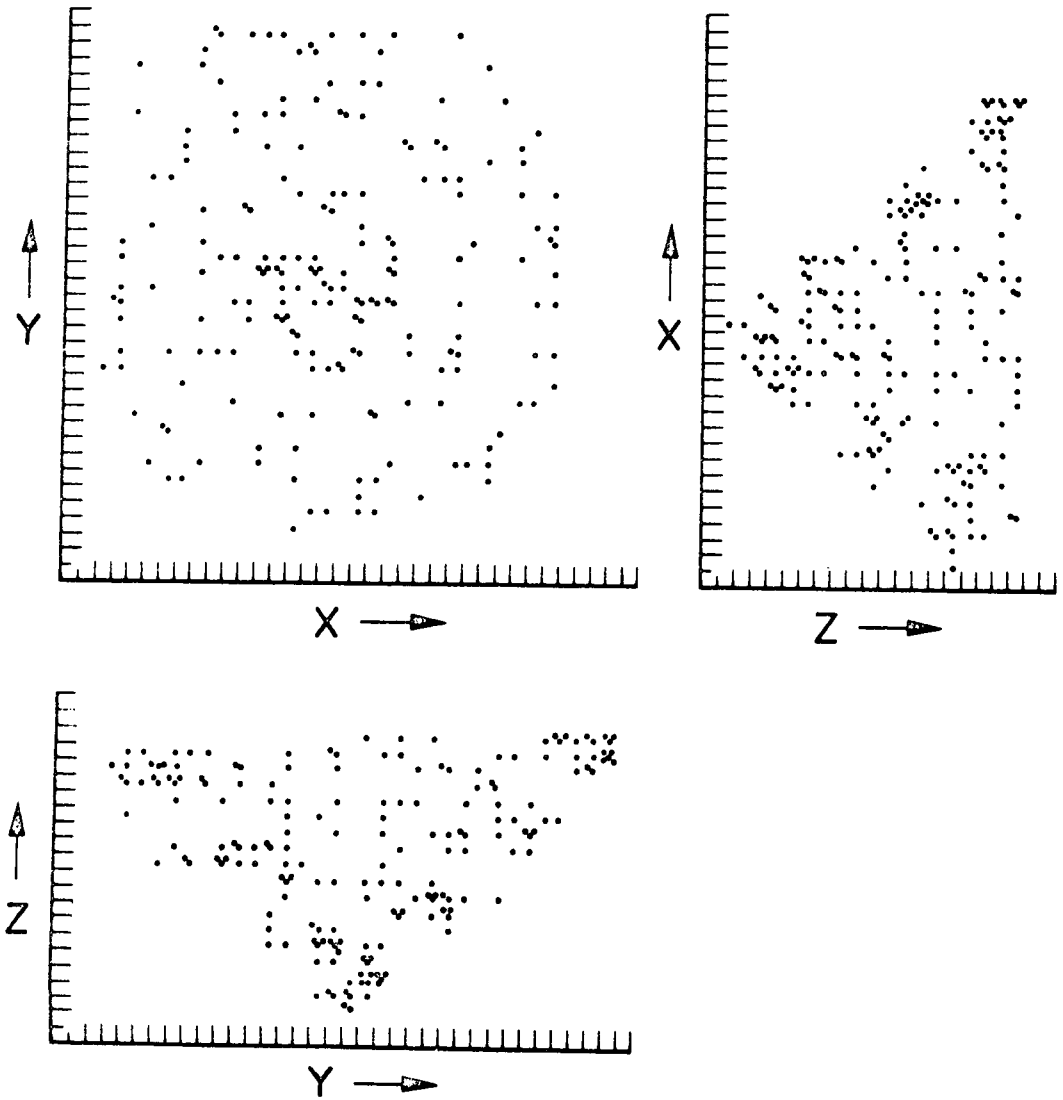

"THREE DIMENSIONAL" PLOT OF DATA FROM A NOISY SPIRAL

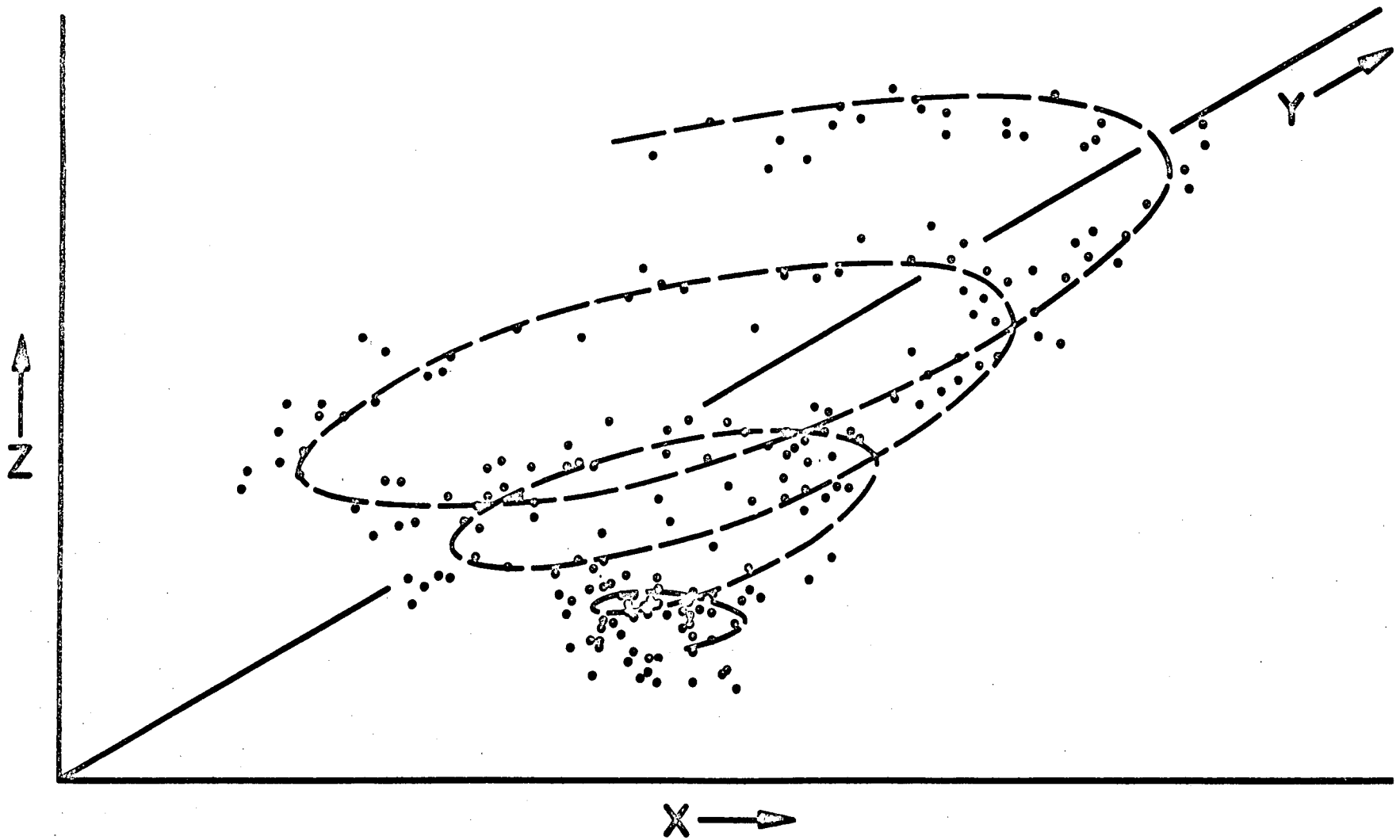

(PAPER NOT SUBMITTED FOR PUBLICATION)

SECTION 2

DEVELOPMENT OF CHESAPEAKE BAY TEST SITE FOR REMOTE SENSING APPLICATIONS

by James Bettle

ABSTRACT

(Not available)

SECTION 3

N72-29304

DEVELOPMENT OF EARTH RESOURCES SURVEY TECHNIQUES AT GSFC—OVERVIEW

by

W. Nordberg
Laboratory for Meteorology
and Earth Sciences
Goddard Space Flight Center
Greenbelt, Maryland 20771

I should like to give a necessarily brief overview over the Earth resources survey activities at the Goddard Space Flight Center.

First, I should try to put these activities into the context of an overall Program rationale for Earth resources surveys from space (Figure 1). I believe, that such a basic programmatic framework applies to all Earth observations from space, regardless of their ultimate application, be it for weather forecasting or crop inventory. Within this programmatic framework, I will show you that activities at GSFC are primarily focussed on the following:

(1) Definition and demonstration of remote sensing techniques which lead to the measurements of physical quantities from which Earth resources related parameters can be determined. The presentations by Hovis, Curran, Shenk, and Gloersen which will follow are examples of this activity.

(2) Development of sensors, spacecraft, and on-board as well as ground based data management systems. These developments are geared to the flight of automated space observation systems such as NIMBUS and ERTS. These systems are operated by GSFC when they are flown. There will be no presentations of this part of the GSFC program since, I believe that our activities in this area are quite well known. I will, however, present a table which shows how the various remote sensing concepts relate to the sensors flown on ERTS and NIMBUS or to those which are yet to be developed for later missions (Figure 2). I will also show a chart to demonstrate the clear parallelism between the various characteristics of meteorological satellite missions, with which we have had more then 10 years of experience, and Earth resources survey missions, of which ERTS is our first (Figure 3).

(3) Determinations of Earth Resources related parameters from the remote sensing observations and measurements. Examples of these activities will be given in the presentations by Salomonson, MacLeod and Short.

(4) Applications of Earth observations to resource management, i.e., to the exploration and conservation of natural resources and to the protection from environmental hazards. This activity has just begun at GSFC in the sense that we consider the applications which will result from the ERTS observations as pilot experiments in this very important area. In this activity we expect to work very closely with User Agencies, with over 200 individual ERTS investigators and with other NASA centers, particularly as they will apply the observations in their own geographic regions to solve resource management problems.

SECTION 4

N72-29305

RADIOMETRIC IMAGES OF IR RESTSTRAHLEN EMISSION FROM ROCK SURFACES

by

Warren A. Hovis
Laboratory for Meteorology
and Earth Sciences
Goddard Space Flight Center
Greenbelt, Md. 20771

INTRODUCTION

Measurements by a number of investigators, principally Lyon (1), have shown that the reststrahlen feature of silica bearing rocks, soils and unconsolidated segments, is variable with silica concentration. The maximum intensity of the reststrahlen band is found to vary from 8.8 micrometers for acidic materials rich in silica to 10.7 micrometers for ultrabasic rocks poor in silica. For remote sensing purposes the reststrahlen bands are of interest since they reduce emissivity selectively. Figure 1 shows the effect of the reststrahlen of granite, an acidic rock, and durite, an ultrabasic rock, on the emitted energy of samples at 290°K. The effect of the reststrahlen is to reduce the emitted energy and hence reduce the equivalent blackbody temperature that would be measured by a radiometer. The effect of the 9.6 micrometer ozone band, as seen from satellite measurements, is shown to illustrate why the reststrahlen of intermediate rocks cannot be sensed from a space platform. The ozone band completely masks the wavelength interval in which intermediate reststrahlen bands occur.

INSTRUMENTATION

In order to test the feasibility of remote sensing of the reststrahlen effect, a two-channel radiometer was constructed that sensed radiance in two channels simultaneously. The channels selected were 8.3 to 9.3 and 10.2 to 11.2 micrometers. The instrument had an instantaneous geometric field of view of 2° x 2° and a rotating mirror scan mechanism designed to produce contiguous scans from a DC-3 aircraft at approximately 10,000 ft. altitude. Signals were recorded on a magnetic tape recorder and subsequently converted to equivalent blackbody temperatures for both channels.

RESULTS

Measurements were made over a number of rock types in the Maryland-Pennsylvania region and samples were acquired of surface material from all areas observed. Figure 2 shows the measured emissivity of a sample of serpentine from Rockville, Md. together with the transmission of the filters used to define the two channels. Since the detectors used were thermistor bolometers there should be little spectral associated with them and it is reasonable to expect that the response functions closely follow the filter transmissions.

It can be seen in Figure 2 that the emissivity of the sample is lower in the 10.2 to 11.2 micrometer region than in the 8.3 to 9.3 micrometer region. A lower equivalent blackbody temperature would then be expected in the long wavelength channel than in the short. Figure 3 shows the measured equivalent blackbody temperatures along the aircraft nadir across the serpentine. The equivalent blackbody temperatures are in good agreement over the fields and trees bordering the exposed serpentine but differ by up to 2.5°C over the serpentine. It should be noted that reduction of particle size reduces the intensity of reststrahlen but does not shift the wavelength unless particle size is extremely small. In this case quarry dust was present on the samples and was included in the laboratory measurements shown in Figure 2.

Another area of exposed serpentine was overflown near Cedar Hill, Pennsylvania. Figure 4 shows the measured emissivity of two samples from the area overflown and Figure 5, the equivalent blackbody temperature observed in the nadir direction. Again the long wavelength channel shows a lower equivalent blackbody temperature than the short wavelength channel as would be expected for a low silica content rock.

A region of exposed slate was overflown near Peach Bottom, Md. to cover an intermediate case. Figure 6 shows the laboratory measured emissivity of the slate with its reststrahlen approximately midway between the two channels. Figure 7 shows the equivalent blackbody temperatures measured along the nadir. Small temperature variations are seen; never as much as 1°C.

Beach sand is rich in silica and was used to examine the effect of acidic materials. Assategue Island, on the Eastern Shore of Maryland and Virginia, was overflown and surface samples collected. Figure 8 shows the laboratory measured emissivity of the beach sand with a very pronounced reststrahlen feature corresponding quite closely to the short wavelength channel. Figure 9 shows the equivalent blackbody temperatures, measured at nadir, during a flight from over the Atlantic, across the island, and then over Chincoteague Bay. Over water the two

channels agree very well and show the bay water slightly warmer than the ocean. Over the island differences up to 5 and 6°C are seen with the short wavelength channel now indicating the cooler temperature. The inland or bay side of the island is marshy and more heavily vegetated than the ocean side, so the temperature differences are reduced as the sand within the instrument field of view is partially covered by water or vegetation.

The mapping ability of the instrument is shown in Figure 10. A flight was conducted parallel to the shore line of the island with the Atlantic on the left and the island on the right. Various methods of presenting a map where both a difference and the polarity of the difference could be shown were examined. The best results were obtained with a color plot where green represents little or no difference in equivalent blackbody temperature, colors tending toward red represent the case where the short wavelength channel appears cooler and colors tending toward blue represent the reverse case. Over the beach sand the color map shows the material to be rich in silica while over the ocean the green color indicates a material that is reasonably black in both channels, water. This format has been adopted for presentation of the data from the Nimbus E HRSCMR.

REFERENCE

1. Lyon, R. J. P. , Econ. Geol. 60, 715 (1965).

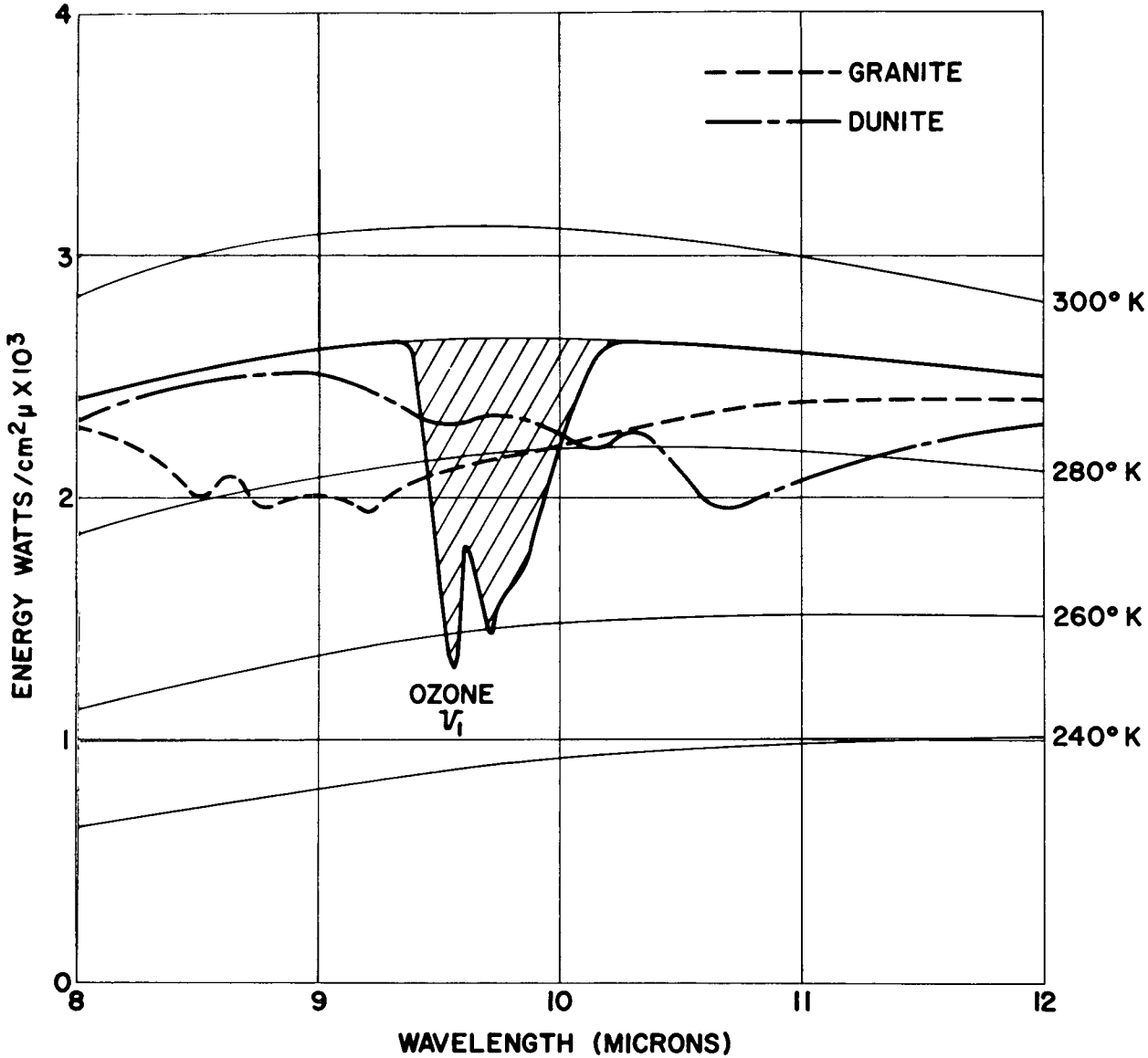
GRANITE
DUNITE
300° K
280° K
260° K
240° K
OZONE
ν_1
ENERGY WATTS/cm$^2\mu$ X10^3
WAVELENGTH (MICRONS)
0
1
2
3
4
8
9
10
11
12

Fig. 1

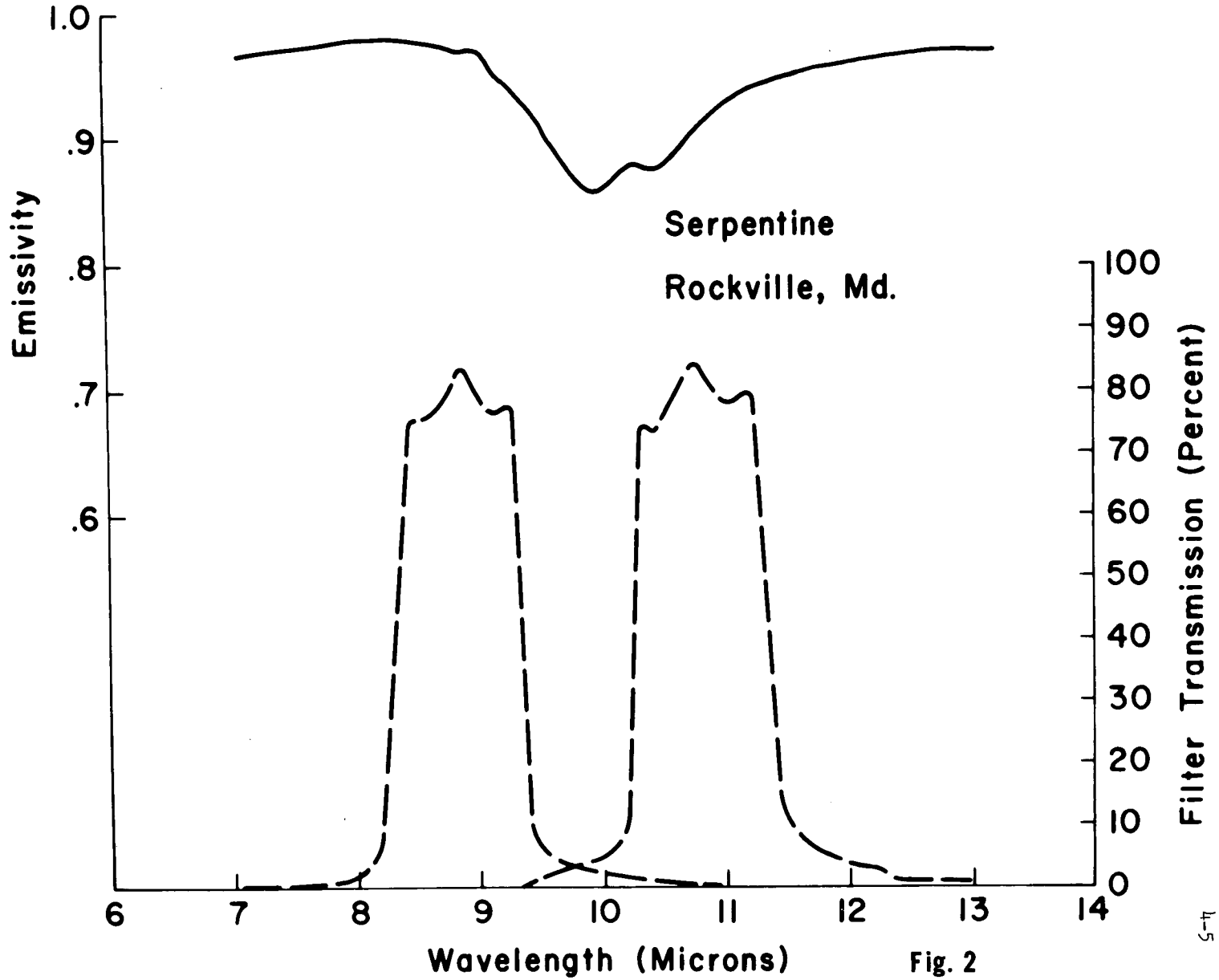
1.0
.9
.8
.7
.6
Emissivity
Serpentine
Rockville, Md.
100
90
80
70
60
50
40
30
20
10
0
Filter Transmission (Percent)
6
7
8
9
10
11
12
13
14
Wavelength (Microns)

Fig. 2

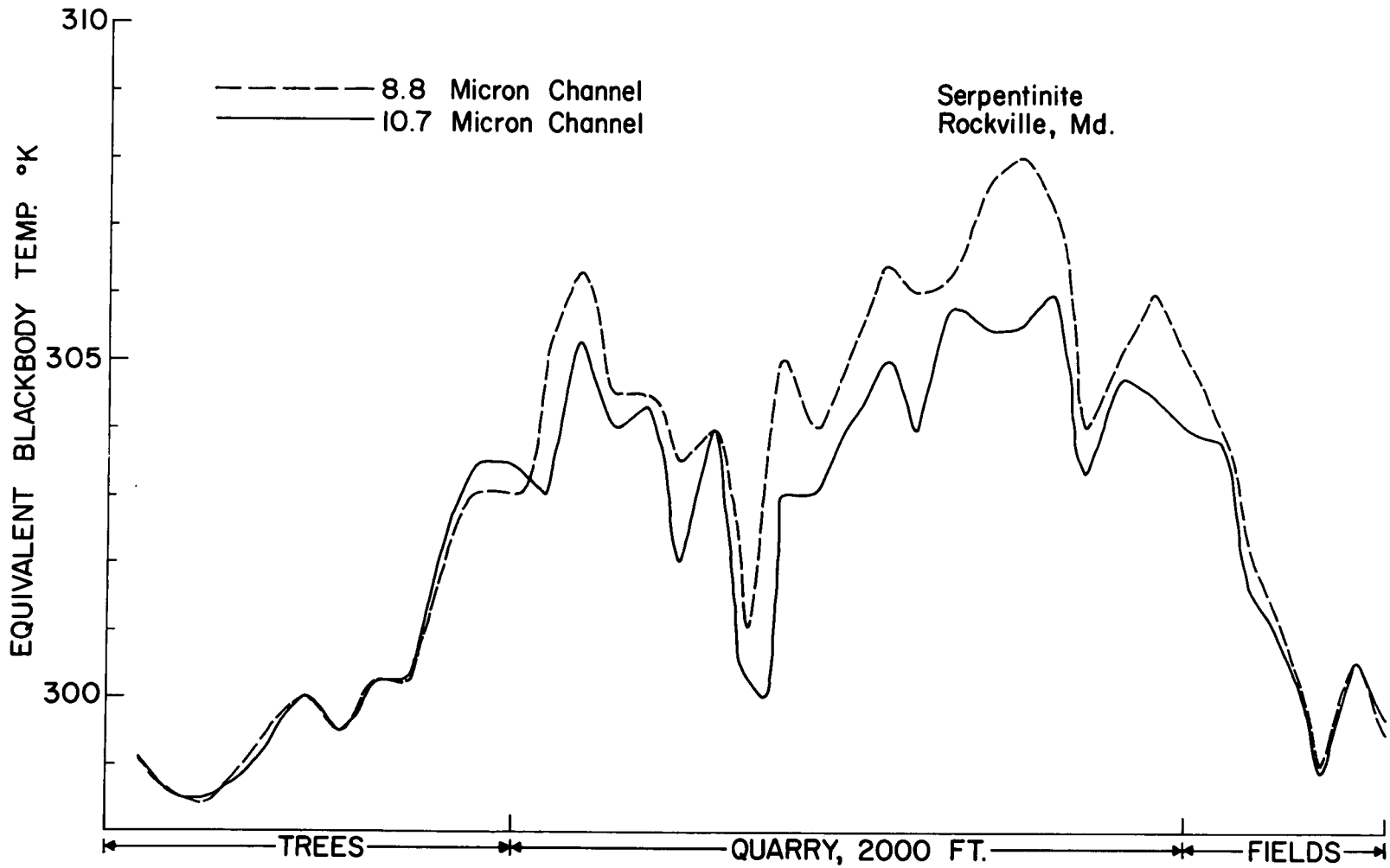
310
305
300
EQUIVALENT BLACKBODY TEMP. °K
8.8 Micron Channel
10.7 Micron Channel
Serpentinite
Rockville, Md.
TREES
QUARRY, 2000 FT.
FIELDS

Fig. 3

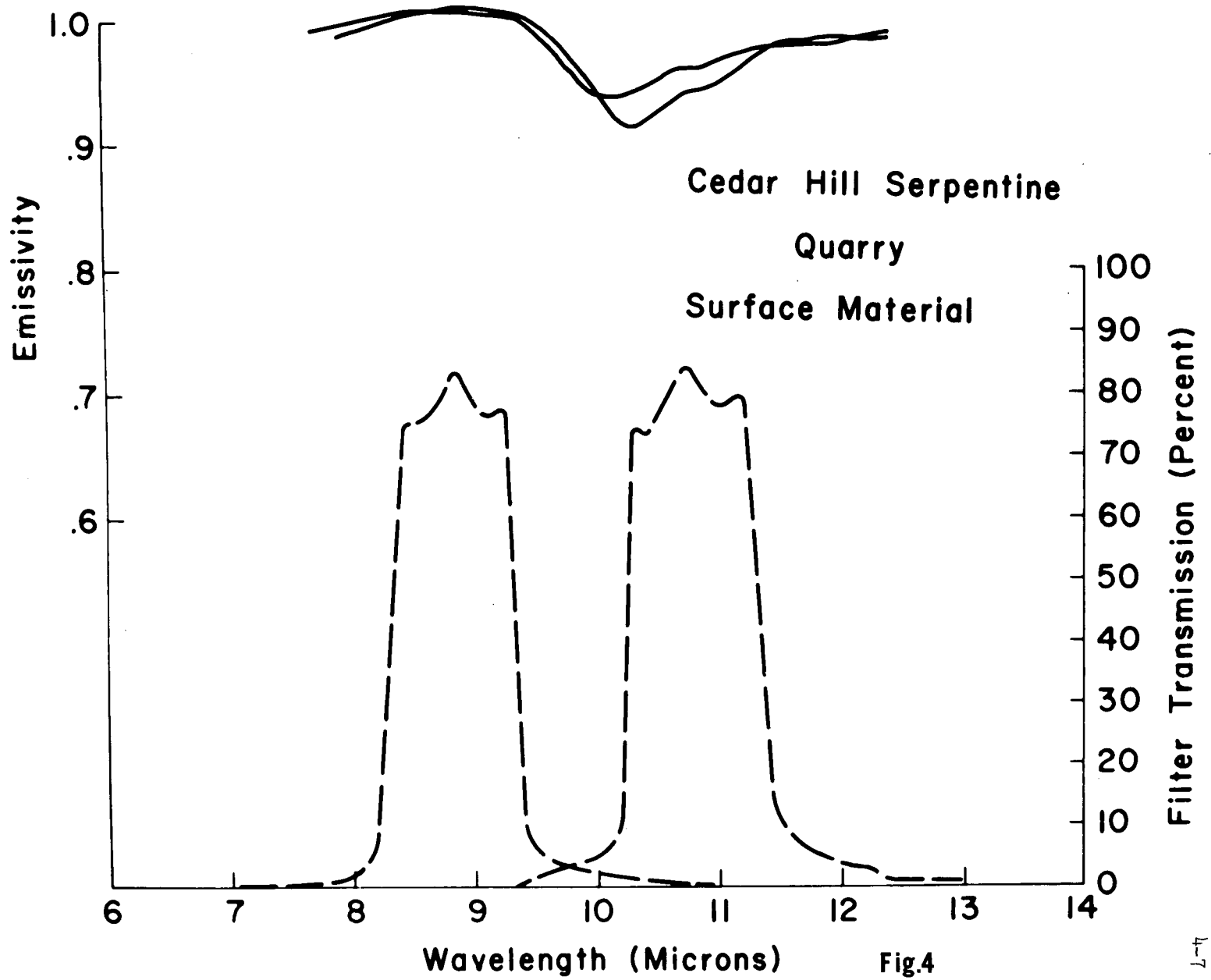
Cedar Hill Serpentine
Quarry
Surface Material
Emissivity
1.0
.9
.8
.7
.6
Filter Transmission (Percent)
100
90
80
70
60
50
40
30
20
10
0
6
7
8
9
10
11
12
13
14
Wavelength (Microns)

Fig.4

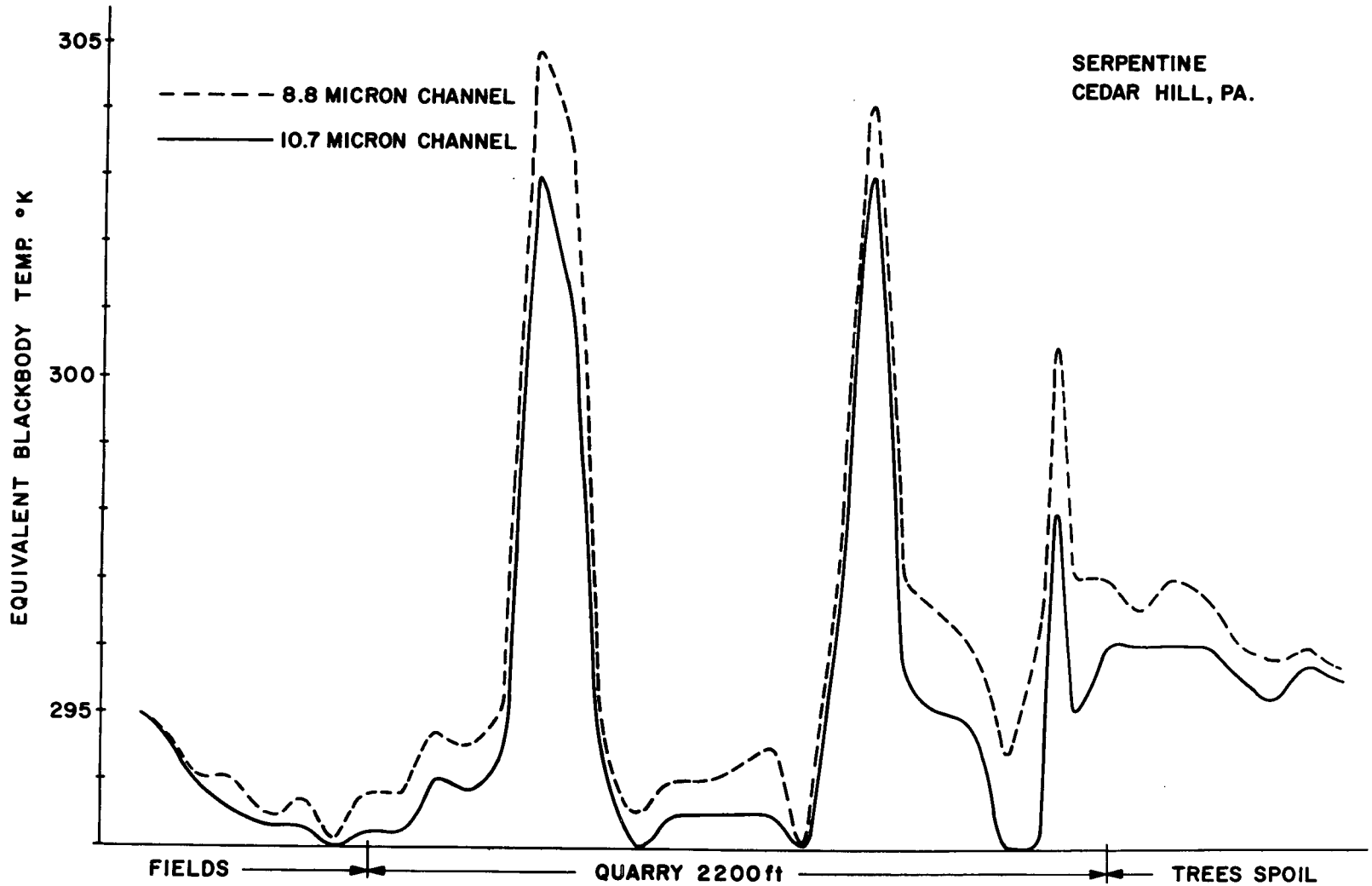
305
300
295
EQUIVALENT BLACKBODY TEMP. °K
8.8 MICRON CHANNEL
10.7 MICRON CHANNEL
SERPENTINE
CEDAR HILL, PA.
FIELDS
QUARRY 2200ft
TREES SPOIL

Fig.5

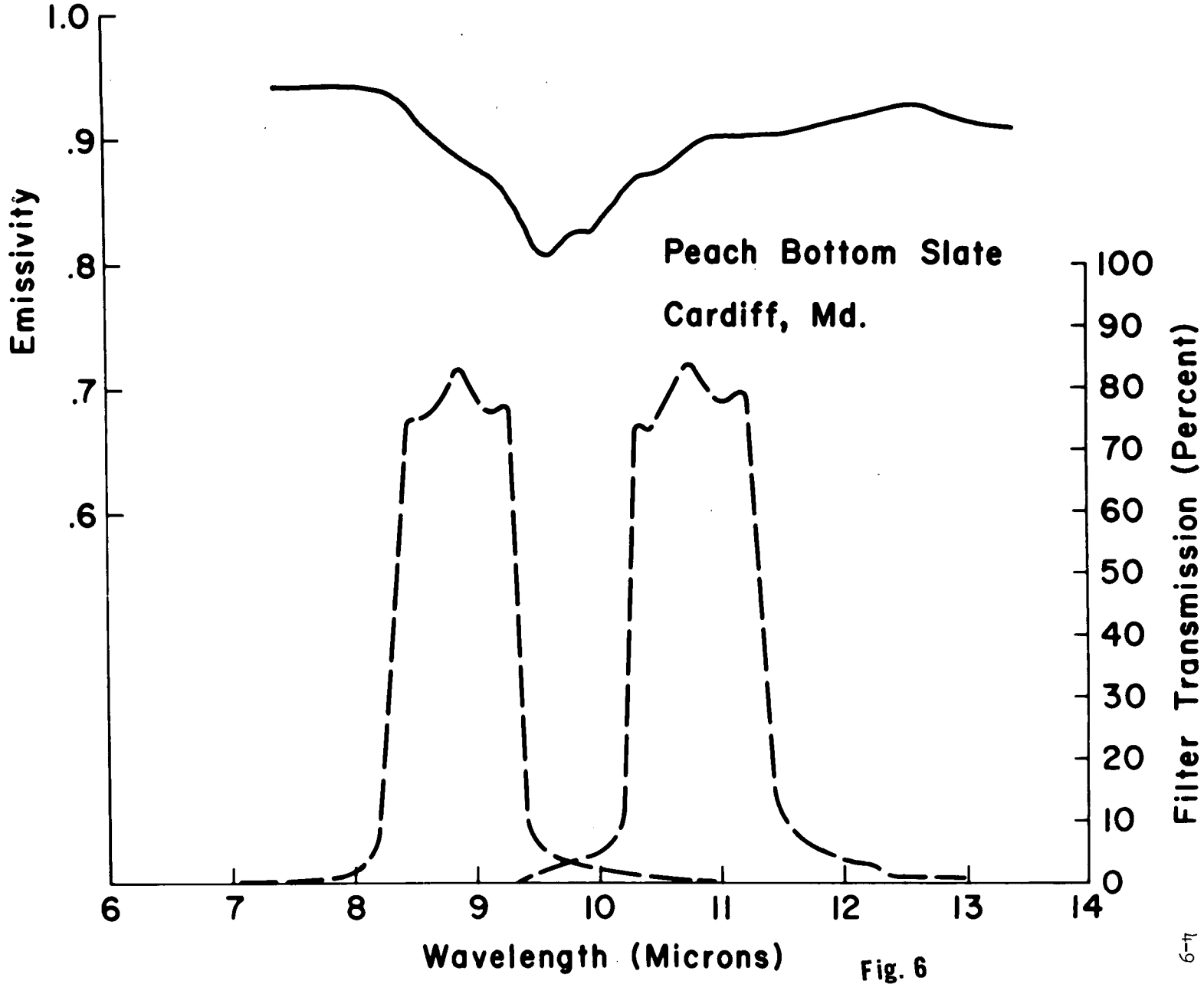
1.0
.9
.8
.7
.6
Emissivity
Peach Bottom Slate
Cardiff, Md.
100
90
80
70
60
50
40
30
20
10
0
Filter Transmission (Percent)
6
7
8
9
10
11
12
13
14
Wavelength (Microns)

Fig. 6

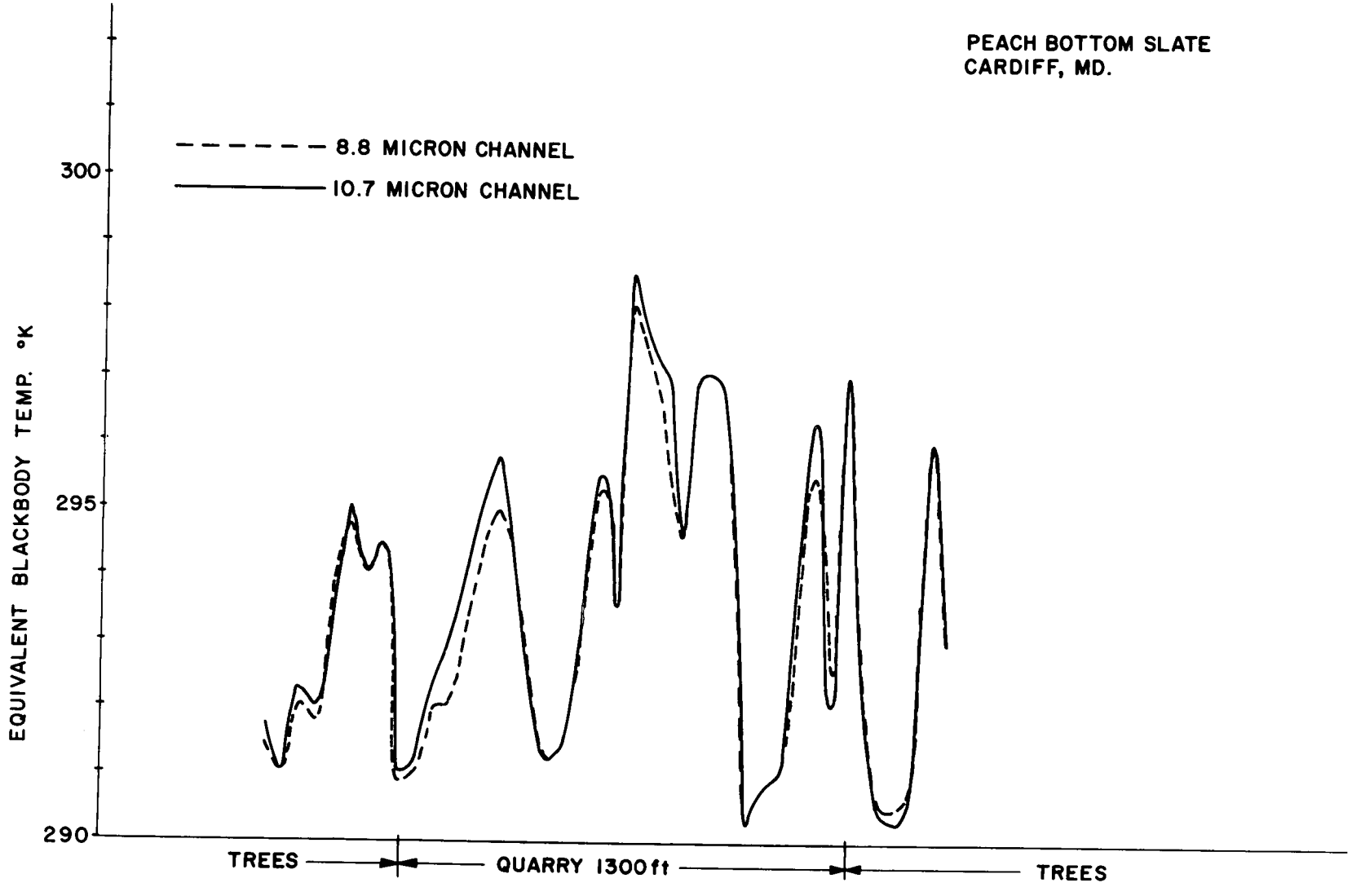
PEACH BOTTOM SLATE
CARDIFF, MD.
8.8 MICRON CHANNEL
10.7 MICRON CHANNEL
300
295
290
EQUIVALENT BLACKBODY TEMP. °K
TREES
QUARRY 1300ft
TREES

Fig. 7

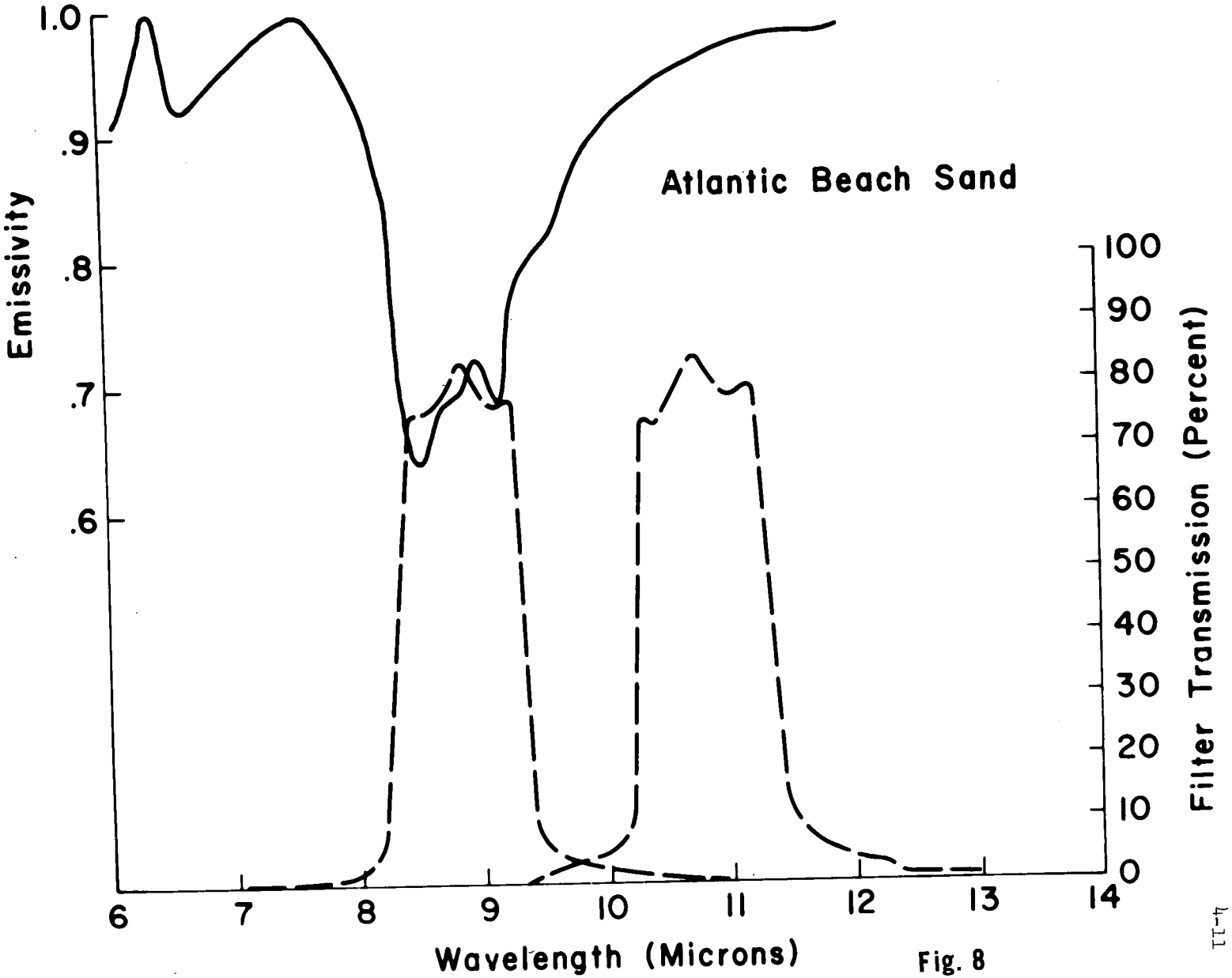
Atlantic Beach Sand
Emissivity
1.0
.9
.8
.7
.6
Filter Transmission (Percent)
100
90
80
70
60
50
40
30
20
10
0
6
7
8
9
10
11
12
13
14
Wavelength (Microns)

Fig. 8

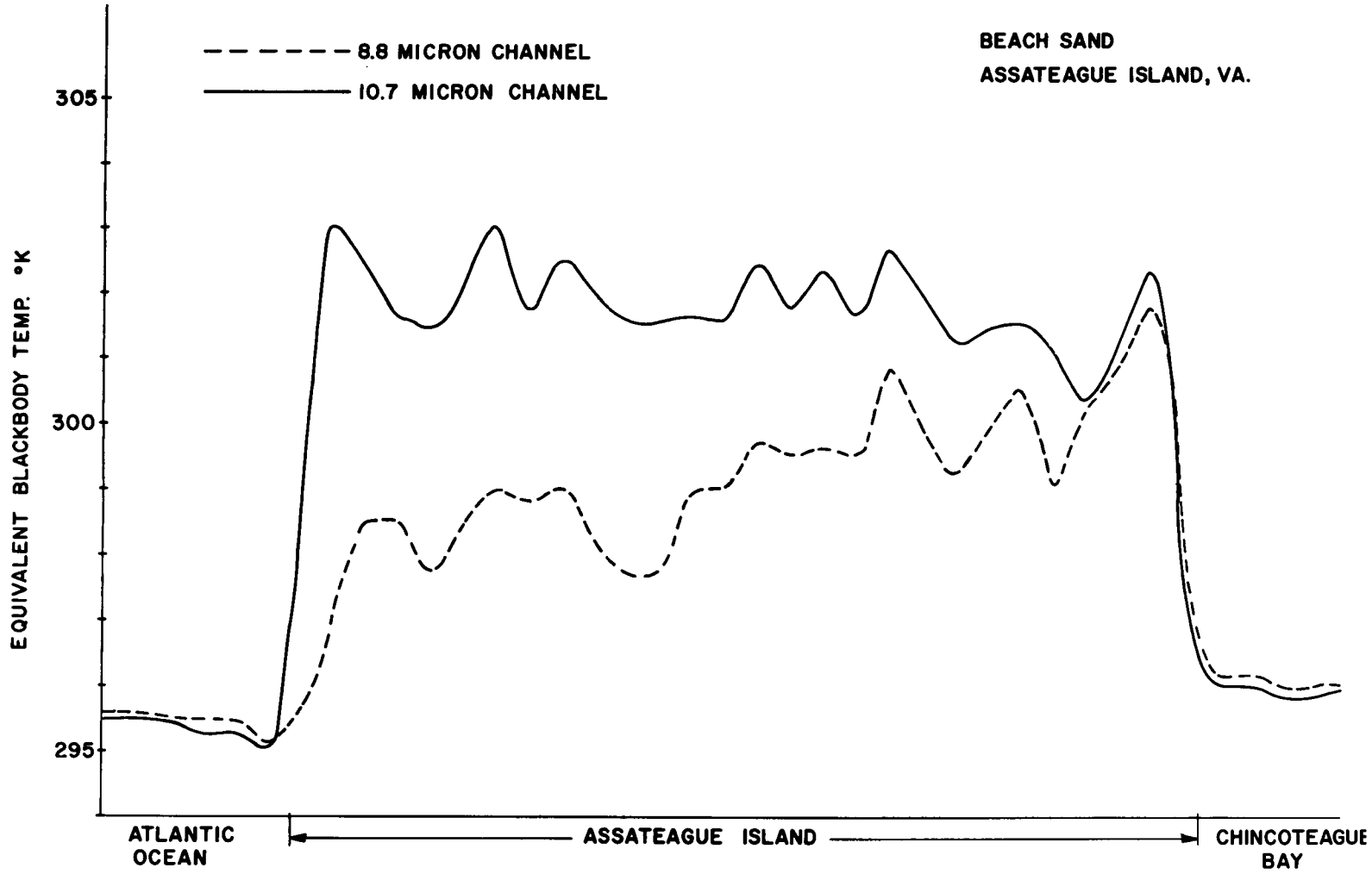
8.8 MICRON CHANNEL
10.7 MICRON CHANNEL
BEACH SAND
ASSATEAGUE ISLAND, VA.
305
300
295
EQUIVALENT BLACKBODY TEMP. °K
ATLANTIC OCEAN
ASSATEAGUE ISLAND
CHINCOTEAGUE BAY

Fig. 9

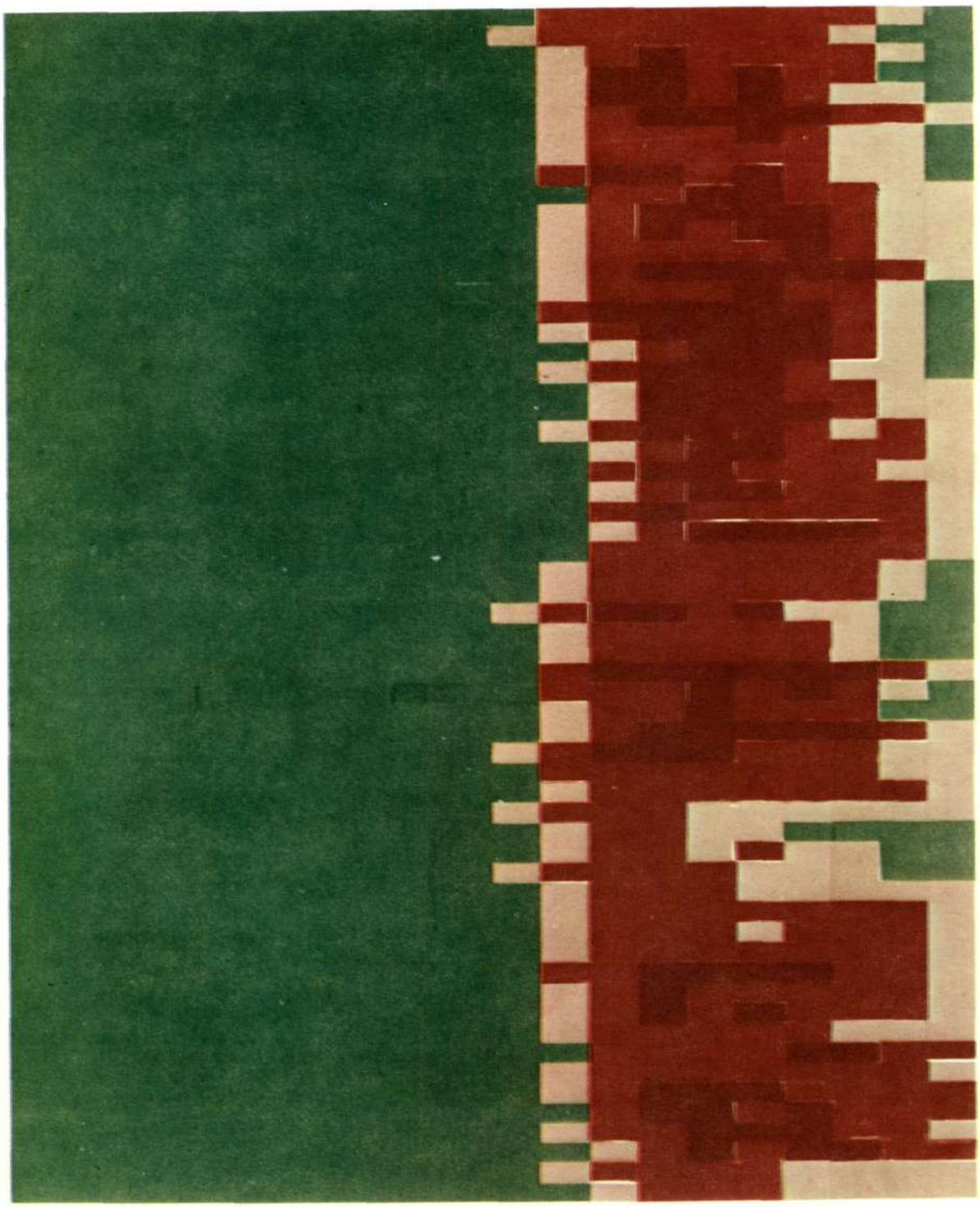

Fig. 10

ASSATEAGUE ISLAND, VA.

SECTION 5

NIMBUS HYDROLOGICAL OBSERVATIONS OVER THE WATERSHEDS OF THE NIGER AND INDUS RIVERS

by

Vincent V. Salomonson
and
Norman H. MacLeod

Laboratory for Meteorology
and
Earth Sciences

Goddard Space Flight Center
Greenbelt, Md. 20771

INTRODUCTION

The sensors on the Nimbus Meteorological satellites have permitted daily and synoptic observations that cover large regions. Although these sensors have a relatively low spatial resolution capability they nevertheless give one a unique perspective for studying the hydrological features over large watersheds and for observing their inter-relationship in the total watershed system. This capability has been utilized to increase our understanding of the Niger and Indus River watershed systems. The size of the two watersheds and the major rivers are given in Table 1 along with comparative statistics showing the size of the Missouri River and its drainage area. As one can easily ascertain, these systems are all considerably larger than the areal extent of the entire state of Texas. Besides the general objective of better understanding the major physical processes occurring in these watersheds, the study of these watersheds has also been conducted so that one might better identify the location of those hydrological phenomena requiring the use of higher spatial resolution systems on future earth resources satellites.

NIGER RIVER RESULTS

For the mapping of surface water, one of the most useful spectral regions is the near infrared where the solar reflectance contrast between water and vegetated or bare soil surfaces is relatively large. Observations in a portion of this spectral region, namely 0.7-1.3μm, are available from the Nimbus 3 High Resolution Infrared Radiometer (HRIR) which was launched in April of 1969. The HRIR is a horizon to horizon

scanning radiometer with a spatial resolution at the subsatellite point of 8 kilometers.

The imagery and digital data from the HRIR was utilized to study regional features and large scale changes in Western Africa and the Niger River watershed. A particular feature and process that was examined was the flooding in and around the Niger Inland Delta that occurred between May and November of 1969. Fig. 1 shows seven HRIR views of West Africa taken in each of these seven months. As can be seen from the map in the center, the Niger River originates in Gambia, flows northeastward through the Republic of Mali, and then goes south-southeastward through Nigeria toward the Atlantic. The arrows radiating from the map locate the position of the Niger Inland Delta in each of the imagery frames proceeding counter-clockwise from May 1969 in the upper right-hand corner. Another point for comparision is Lake Fagubine just above the northeastern portion of the Delta. This lake remains filled with water throughout the period shown in this slide and its reflectance changes very little.

There are at least five major features and/or events that can be located in these imagery frames. One can most easily note the general decrease in the reflectance of the total Niger Delta as one proceeds in time from May through November. This results from the inundation of the delta as flooding progresses. Closer examination of the imagery reveals that the progression in flooding from the southwestern portion of the Delta toward the northeast can be seen, particularly from August through November. It is also possible to see the high flow in the river west of the Delta in July, August, and September. In October and November this high flow to the west disappears and appears to the east of the Delta, thereby indicating how the presence of the Delta acts like a detention basin and slows the progression of the flood down the river.

The response of the Savannah vegetation to monsoonal rainfall can also be observed as manifested by decreased reflectance which is associated with greater plant growth and vigor. This progression of the vegetation response is most visible in the August through November imagery.

One may note, furthermore, that we are possibly seeing the ancient cource of the Niger River as it proceeded north from Segou toward a joining with the Senegal River. The interesting tonal feature suggesting this interpretation can be seen in the June through November images. The greatest contrast in the images along the ancient path travelled by this river appears in August and September suggesting plant and soil moisture response to subsurface flow coming from the Niger and moving along the route of the old channel.

Corroboration of the interpretations obtained from these images is best achieved by examining digitized HRIR data. This has been done for the images obtained in May, July, and November and the results as obtained after careful registration, interpolation, and contouring of the data on a 1:400,000 scale are presented in color processed form are shown in Fig. 2. The range in normalized reflectance represented in these results goes from 0.5 percent to 17.0 percent. Low reflectances are blue and green, higher ones are tan and red. One can see that the reflectance in the Delta goes from an average reflectance near 12 percent to 5 percent between May and November as a result of the flooding during this period. The higher reflectances in the northeastern portion of the Delta are also visible in all three sets of results. Furthermore, one can see the northward progression between May and July of the vigorous vegetation and dense canopy boundary as represented by the green shades in Fig. 2. Some retreat southward between July and November in the vigorous vegetation area is indicated which would be associated with the decrease in the monsoonal rainfall.

INDUS RIVER RESULTS

The Niger River results showed the progression of runoff down the course of the river as observed in 0.7-1.3μm spectral region by the Nimbus 3 HRIR. Another aspect of watershed hydrology is the deposition of the precipitation on the watershed and its relationship to surface runoff. In this regard, the Indus River watershed situation encourages the application of satellite technology because of its generally larger size, its inaccessibility for monitoring by conventional techniques, and the fact that most of its flow results from the melting of snow deposited in the Western Himalayas. The location of the portion of the Indus River watershed that was most closely examined is shown in Fig. 3. The volume of flow in this river is roughly equal to that of the Columbia River System in the U.S. and affects the lives of millions of people who depend on it for irrigation and development of agriculture in this semi-arid region of the world. The Tarbella Dam which is being built a few miles above Attock will contain 5 million acre-feet of water and provide irrigation water for 300,000 acres of land.

The most appropriate satellite sensor on Nimbus 3 and 4 for observing snow cover was the Image Dissector Camera System because it had the best spatial resolution (4km) and monitored reflected solar radiation in the visible portion of the spectrum where the contrast between snow and bare soil or rock surfaces is greater then in the near or far infrared. Fig. 3 shows six IDCS frames taken over the Indus River watershed above Attock, Pakistan during the major snowmelt months of May, June and July for two years, 1969 and 1970. These IDCS frames were obtained in 70mm black and white positive transparency form and used to

construct Fig. 4. The outline of that portion of the watershed above Attock was sketched and superimposed on the original 70mm black and white transparencies; therefore, this outline can be seen in the views presented in Fig. 4.

The bright shades seen over the Indus watershed generally correspond to the snow-covered portions of the watershed. Some ambiguity can be introduced where clouds are present, but only in the June 1969 frame do some clouds exist over the watershed and obscure a small portion of the snow-covered area. It is readily apparent that in both 1969 and 1970 the areal extent of the snow cover and its change with time can be observed. Closer study of the photographs reveals that the snow cover decreases in a spatially systematic way as time progresses from May to July. Generally the snow cover disappears first from the northwestern and southern portions of the watershed and by July only persists in the highest and northeastern parts of the watershed that contribute to flow of tributaries like the Shyok and Nubra Rivers lying in the Baltistan and Ladakh regions of Kashmir.

In order to quantify the changes in snow cover observable in Fig. 4, the original black and white 70mm transparencies were enlarged and the percent of the watershed covered by snow measured by planimetering. In an operational way one is very much interested in the relationships between observations such as presented here and surface runoff. Therefore, the results obtained from planimetering the areal extent of the snow cover in that portion of the watershed above Attock, Pakistan have been graphically related in Fig. 5 to the runoff observed at Attock. The areal extent of the snow cover has been plotted in such a way as to relate a decrease in the snow cover to an increase in the mean monthly runoff with the areal extent results for 1969 and 1970 being plotted as dashed lines and the runoff as solid lines.

The first result to notice in Fig. 5 is that the areal extent of the snow cover is consistently less in 1970 as compared to 1969. Secondly, the change with time in the snow cover is very similar in both years. The decrease in the overall snow cover in 1970 is reflected in the lower overall runoff observed in 1970. In addition, it is encouraging to see that there is some correlation between the change in the snow cover from month to month and the mean monthly runoff, particularly in 1969.

The results so far suggest that some success might be achieved in predicting the total runoff volume or the level of peak discharge if one were to use the satellite to monitor the areal extent and location of the snow cover in late winter and early spring. It is intended that a few more years data be analyzed to see if this hypothesis can be established. At the very least, these results indicate that the satellite data can be used as an additional source of information and understanding in the management of the water resources in this region.

CONCLUSIONS

As a result of studying the Nimbus imagery over these two large watersheds, it is felt that a perspective and understanding of the large scale hydrological processes and their interrelationship has been obtained which could be obtained by no other means in so short a time. In the case of the Niger River a much better appreciation of the flooding process has been obtained along with the role of the Inland Delta in this process. Obviously a knowledge of the spatial and temporal distribution of the snow-melt process in the Indus River watershed is now available that was obtained with minimal effort as compared to the effort and time that would be required using conventional methods. It seems clear that even the low resolution data easily available from meteorological satellites can be a valuable source of information in the better management of the water resources in these regions. In addition, it has also been substantiated and concluded that the daily and synoptic views over large regions provided by these types of sensors will be in future studies a valuable and even necessary set of information to be combined with the relatively high resolution sensor data forthcoming from systems like the Earth Resources Technology Satellite (ERTS).

TABLE I. A COMPARISON OF THE DRAINAGE AREA AND RIVER LENGTH ASSOCIATED WITH THE NIGER AND INDUS RIVERS, THE MORE FAMILIAR MISSOURI RIVER, AND THE AREA OF THE STATE OF TEXAS

NIGER RIVER

TOTAL DRAINAGE AREA = 580,000 sq. mi. (1,502,000 sq. Km.)

LENGTH OF MAIN RIVER = 2,600 mi. (4,184 Km.)

INDUS RIVER

TOTAL DRAINAGE AREA = 372,000 sq. mi. (970,000 sq. Km.)

LENGTH OF MAIN RIVER = 1,900 mi. (2,900 Km.)

MISSOURI RIVER

TOTAL DRAINAGE AREA = 529,400 sq. mi.

LENGTH OF MAIN RIVER = 2,466 mi.

AREA OF TEXAS = 267,338 sq. mi.

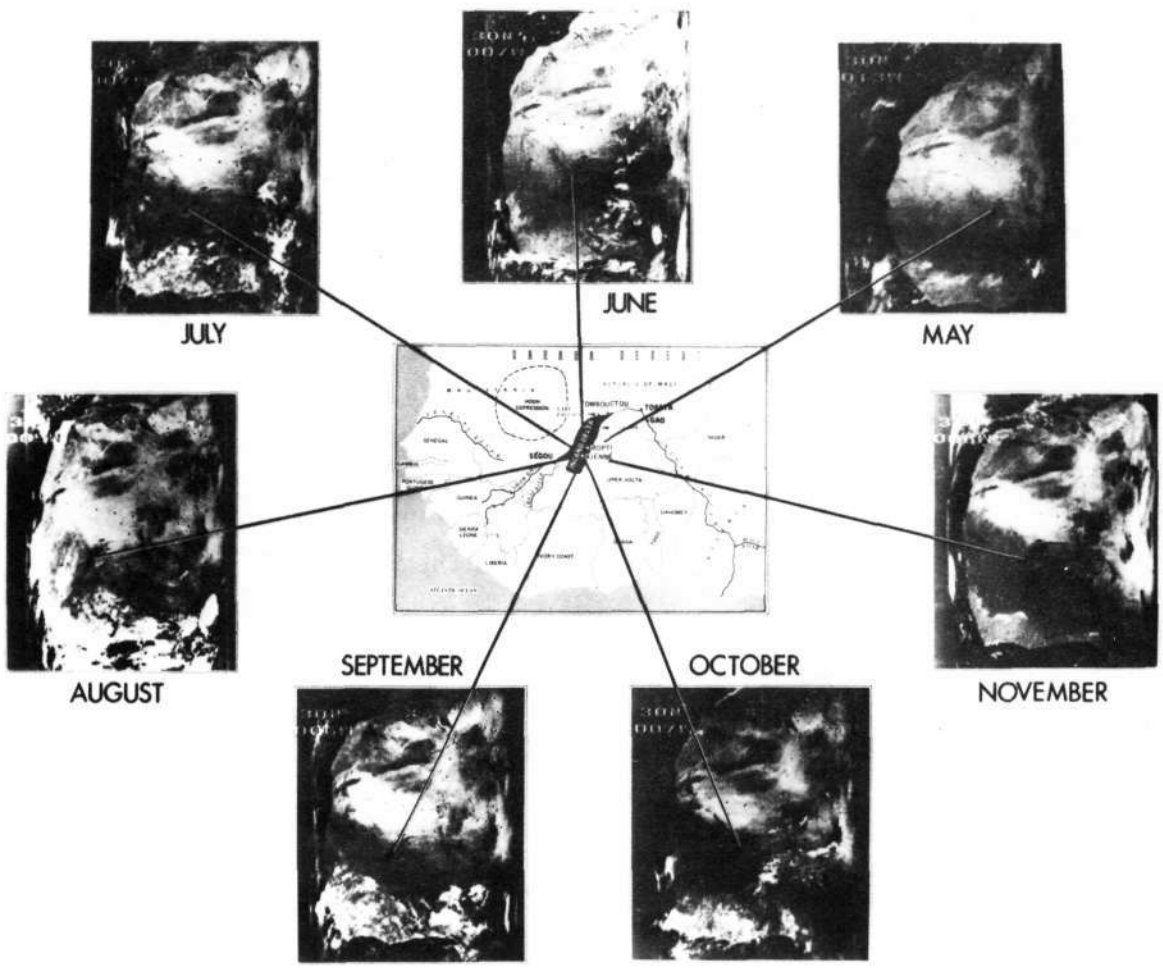

Figure 1.-Nimbus 3 HRIR images over Western Africa showing the progression in the flooding of the Niger Inland Delta

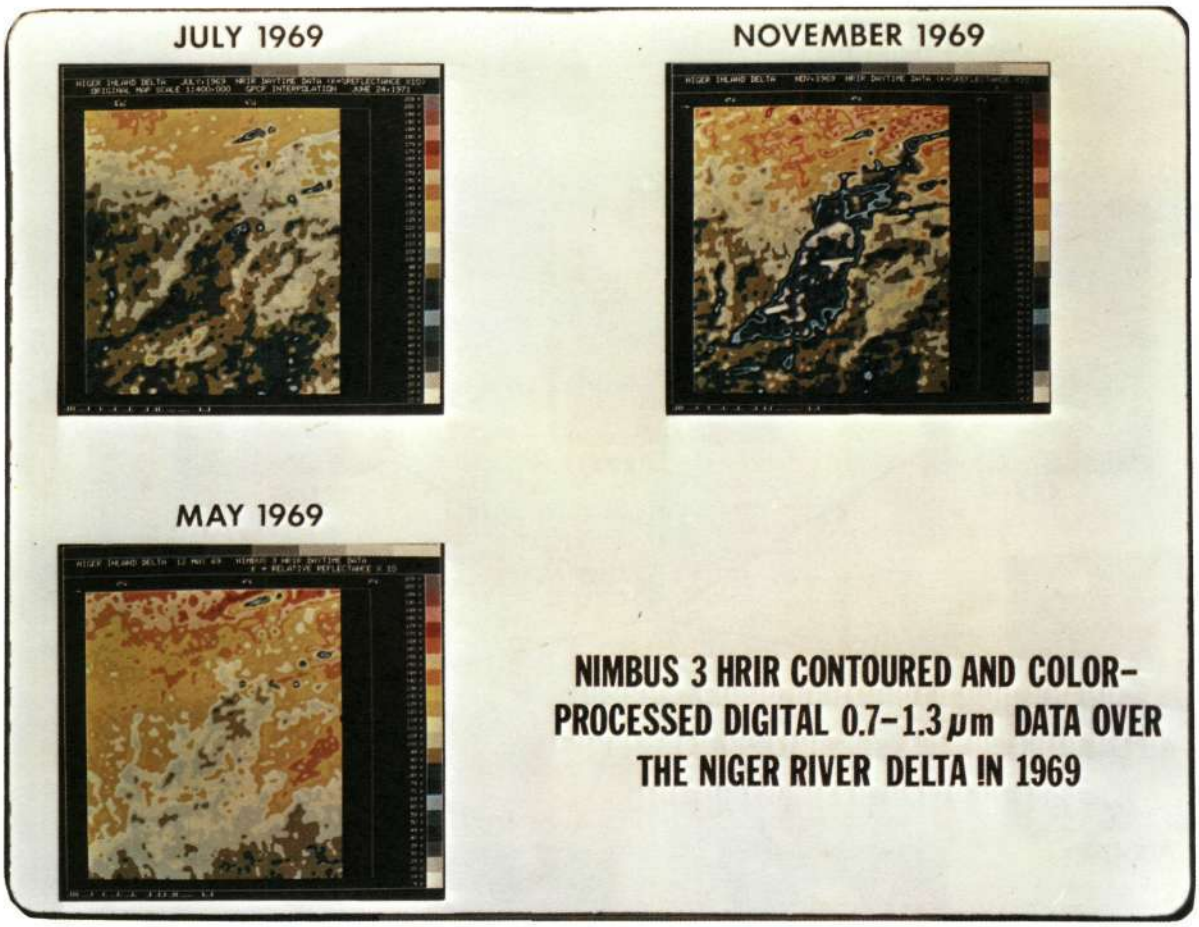

Figure 2.-Nimbus 3 HRIR data that has been processed to show quantitative changes in reflectance over the Niger Inland Delta

Figure 3.-A map of the area in the Western Himalayas where observations of snow cover were made using the Nimbus 3 and 4 Image Dissector Camera System (IDCS). The dark boundary delineates that portion of the Indus River watershed above Attock, Pakistan.

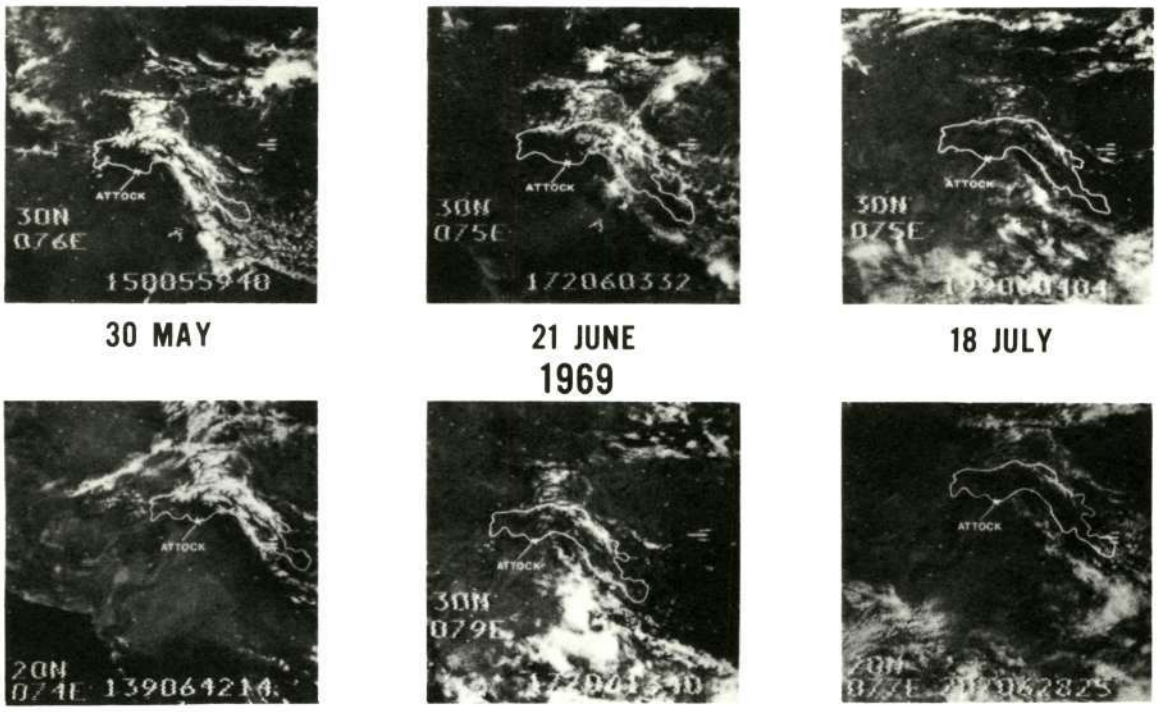

NIMBUS 3 AND 4 IDCS OBSERVATIONS OF SNOW COVER OVER THE INDUS RIVER WATERSHED DURING MAJOR SNOWMELT PERIOD

Figure 4.-Six views of the Indus River Watershed above Attock, Pakistan showing satellite-observed changes in snow cover

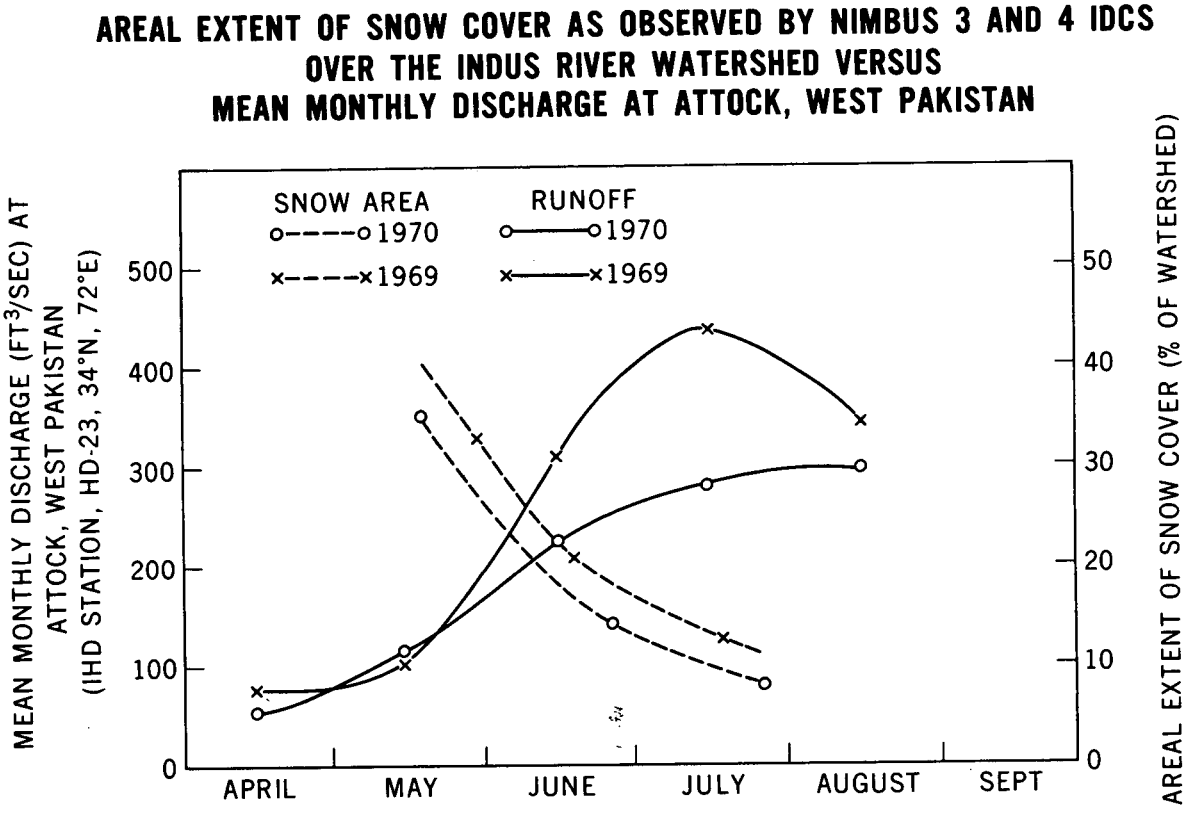

Figure 5.-A graph showing the observed relationship between mean monthly discharge measured at Attock, Pakistan and the snow cover over the Indus River watershed.

SECTION 6

N72-29307

SPECTRAL REFLECTANCE MEASUREMENTS OF PLANT-SOIL COMBINATIONS

by

N. H. MacLeod

Laboratory for Meteorology
and Earth Sciences

Goddard Space Flight Center
Greenbelt, Maryland 20771

As part of the Goddard Space Flight Center, Earth Observations Program, we have made field and laboratory observations of plant and soil reflectance spectra to develop an understanding of the reflectance of solar energy by plants and soils. A related objective is the isolation of factors we feel contribute to the image formed by multi-spectral scanners and return beam vidicons carried by ERTS or film-filter combinations used in the field or on aircraft.

In this work we want to develop a set of objective criteria for identifying plant and soil types and their changing condition through the seasons for application of space imagery to resource management. This is because the global scale of Earth Observations Satellites requires objective rather than subjective techniques, a particularly where ground truth is either not available or too costly to acquire.

Before we started we knew that people can visually discriminate between plant species, between sick and healthy plants and, with training, between soil types. People correlate in their minds clues from a scene such as the shape and arrangement of leaves on a plant, the color of leaves and soils - the motion and even the sound of crops and forests. But these clues are not available for use with space imagery because of spatial and spectral limitations.

As the acquiring of ground truth for training sets may be impractical in many cases, we have attempted to identify objectively standard responses which could be used for image interpretation. These are the responses or factors we are especially interested in to form a base for detecting changes in a scene or series of images.

In the laboratory we started with the question of whether or not plant leaves have specific reflectance spectra or whether the reflectance of leaves is the same for all species. Using single, normal, mature leaves, we measured the reflectance spectra of many species in a Cary 14 Reflectance Spectrometer.

Figure 1 shows the spectra for four of these species. The now familiar leaf reflectance curve is very similar for all of the species used. This observation was supported by a statistical analysis in which no significant differences between the species were found at any wavelength. The 1.6 micrometer wavelength values were most nearly significant and with more replication may show significance in future tests. Replication is not easy to achieve with space imagery, however.

We investigated the source of the leaf spectra similarities by taking the leaves apart. Figure 2 shows the reflectance spectra of chlorophyll extracted with methanol from fescue leaves. Chlorophyll extracts from other species appear to be the same. In the top curve we see the reflectance spectrum of chlorophyll over a bright background. It is essentially a chlorophyll absorption spectrum. The fiberglass background is very bright across these wavelengths. Therefore where chlorophyll does not absorb, the percent reflectance is high. The regions where chlorophyll does absorb are those of the typical features of leaf reflectance at 0.45 and 0.68 micrometers.

The lower curve is the percent reflectance obtained when chlorophyll was placed over a black matte background. Any reflectance is due to chlorophyll with perhaps some influence from the glass disc upon which the chlorophyll was placed. We find virtually no reflectance occurring in this case. Thus the reflectance features noted at 0.45 and 0.68 micrometers cannot be due to light back scattered from chlorophyll. Instead, the features are produced by chlorophyll absorption of light scattered by some other substance or structure in the leaf.

Figure 3 demonstrates that this is indeed the case. Here normal fescue leaves are compared to fescue leaf matter from which chlorophyll has been extracted, and to intact leaves where water was removed by simple drying at low heat. Removal of the chlorophyll results in increased reflectance in the visible, chlorophyll absorption regions. Removal of water results in increased reflectance in the IR regions where water absorbs at 0.9, 1.1, 1.45 and 1.9 micrometers. The reflectance of leaf material with minimal amounts of either chlorophyll or water is typically very high in the IR and decreases smoothly in the visible.

Normal mature leaves have much the same constituents and arrangements of cellular material - pigments, such as chlorophyll; cellulose cell walls, water; thus it is not surprising that, most plants have similar reflectance spectra, if these constituents are the absorbers and reflectors of light energy in these regions. The data indicate that we do have an adequate baseline from which to detect changes from normal leaf conditions.

In **Figure** 4 we see the reflectance spectra from two soils in the wet and dry condition. The Goddard soil is a sandy loam typical of the mid atlantic states coastal plain. The Houston soil is a highly organic, well aggregated soil from the Houston area. The Houston soil is black in color, while the Goddard soil is light tan. The spectra are smooth, except in the water absorption bands. It is expected that a large difference would be found in their spectra. The effect of wetting the soils is, of course, to deepen the water absorption features, less in the case of the light textured Goddard soil than in the Houston soil. In most soils the percent reflectance is reduced by about 50% across the spectrum shown here. Using a collection from around the world we find this to be quite constant. In the Houston soil the reflection of the dry soil is already quite low. It may even be increased slightly in the visible by wetting, though the water absorption features deepened as expected.

Unlike plant leaves, soils do differ in brightness, and red soils, white sands and black loams can be differentiated. Knowledge of the reflectance of a soil when dry can be used as a baseline to develop information on soil moisture content.

Figure 5 shows that these differences in soils appear in the reflectance spectra of leaves and soils combined. The differences appear in the wavelengths where neither water nor chlorophyll are strong absorbers. The two leaf cases presented are one and, then, nine leaves of normal mature soybean. The soils are a bright Salt Lake City soil, the Goddard soil and a red laterite of Kenya. The effect of a difference in soil brightness (these are air dry soils) is seen in both leaf cases. The difference between soils is, of course, much obscured by the presence of leaves. The major effect in this experiment is the increase in reflectance due to increase in leaf numbers. The location and intensity of the absorption features is not shifted, but the difference of intensity of reflectance in the non-absorbing regions is statistically significant. This latter effect is being well studies at Weslaco by USDA. In essence, increasing the number of leaves results in a smooth increase in reflectance except at the chlorophyll and water absorption peaks. The effect in a series of images can be interpreted in terms of plant growth, where the number of leaves over a particular unit area of soil increases with growth.

So far we have dealt with normal leaves. Diseased leaves differ from normal leaves in a rather limited number of ways. They lose chlorophyll and become yellow; they die and become brown as a result of oxidation of cell contents. Leaves may develop transparent spots due to virus attack, they may wilt. Nutritional diffeciencies produce specific patterns of color change. Southern corn leaf blight produces dead leaves and yellow leaves in additon to the typical lesions. In Figure 4 we compare normal corn leaves to blighted leaves and to leaves infected with ring virus. In all the leaf cases, three backgrounds are used. Black, in which only the reflectance of the leaf itself is observed; white background where the full effect of leaf transmission is added to leaf reflectance and a background of Miami silt loam, the soil in which the corn was grown. The measurements were made at Goddard but the materials came from Lewis Research Center through their cooperative program in SCLB study with the Ohio State Agricultural Experiment Station.

In the normal leaf the background effect is pronounced only in the infrared. In the dead SCLB leaf (100% necrotic), the chlorophyll has been lost and its absorption features are not seen. But the oxidation products are apparently absorbing energy reflected from the background as the soil and white backgrounds are not really different in effect. Before corn leaf tissue not directly infested with the fungus dies, it becomes yellow or chlorotic. We see that some absorption still occurs in the blue by some of the accessory leaf pigments, but the chlorophyll features in the red band have disappeared. In this leaf condition the background effect is very pronounced both in the IR and the visible. This leaf is not a very bright reflector by itself as seen in the black background curve. It has become more transparent in wavelengths longer than 0.5 micrometers. Thus, over a bright soil, the chlorotic condition should be distinquishable from the dead condition both in terms of spectral differences and in terms of brightness. Over a darker soil, the two conditions would be perhaps more difficult to separate.

The virus disease has produced a third spectral response. Over a bright soil it would appear as a brighter green and orange than a normal leaf. However, over a black background it is not distinquishable from a normal leaf. Thus we have found that reflectance of single normal leaves provides us with information upon which to base separation of normal and abnormal conditions, to follow leaf area with growth and to distinquish some disease or pathological conditions. In dealing with such conditions we can explain much of the change in reflectance in terms of loss of pigment, oxidation products and changes in water content. As these are very common changes, and the spectral effects of all diseases in all plants have not yet been studies, we should use great caution in interpretation of remote sensing imagery in regard to disease.

The effect of soil background is two fold. First, the specific brightness of various soils will have a direct effect on the observed brightening of diseased leaves. Second, the effect of soil moisture will be to darken the radiance of a scene across the spectrum studied here.

This discussion has led us to recognize some predictable changes in observed reflectance from leaf-soil combinations in the laboratory. Most of these are explainable in terms of pigment and water absorption in leaves and as variations in soil spectral brightness and variations in soil moisture.

The laboratory observations of factors affecting tone and spectral content of the scene are useful as a start. But it is quite obvious that, if normal leaves have virtually indistinquishable reflectance features, there must be other factors in the scene which permit us to tell one plant from another or one plant community from another. Thus leaf spectra do not yield complete information on differences seen in the MSS and Nimbus imagery of seasonal change or geographic differences in complex plant communities discussed by Drs. Short and Salomonson at this session.

Therefore, to predict quantitatively the content of an image requires isolation of additional objective factors associated with the plant-soil combinations and the reflected energy. Some such factors might be leaf arrangement, effective leaf area normal to the sensor viewing angle, extent and depth of canopy cover, proportion of open soil in the scene and so on. Crop and soil management practices also may be effective in changing radiance of a scene, but our understanding of these factors is still incomplete.

In going from the laboratory to the field to study plants and soils as they exist in nature, we will be able to use some of the baseline response information presented here, but even more emphasis must be placed on identification of new additional objective factors which relate the physical objects in a scene to a remotely sensed image.

Again, for Global Applications of Space acquired imagery to problems or resource management, understanding of the factors which change the plant and soil reflection of solar energy - the principal source of remote sensing information is essential. We have just scratched the surface.

Figure 1

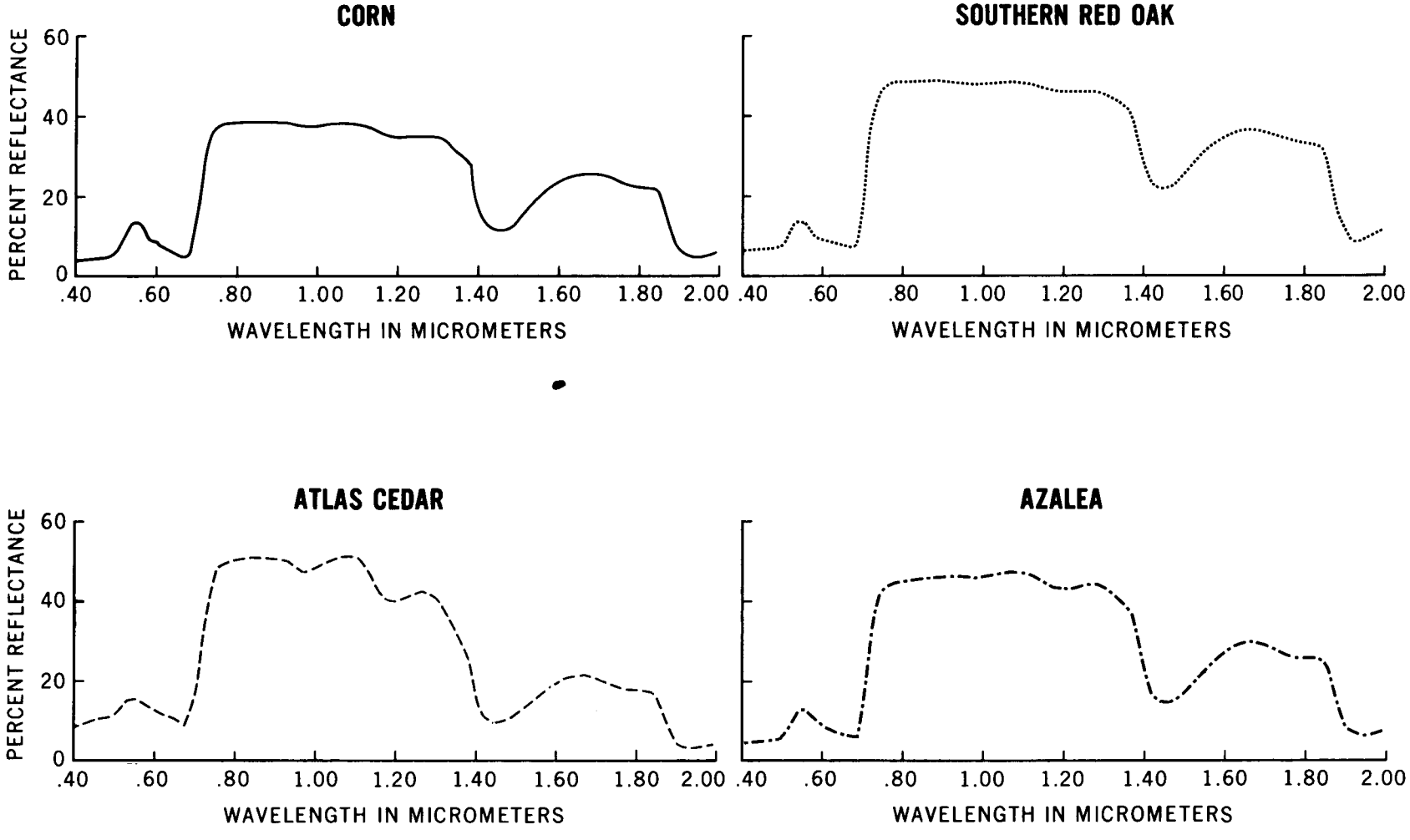
CORN
SOUTHERN RED OAK
ATLAS CEDAR
AZALEA
PERCENT REFLECTANCE
0
20
40
60
.40
.60
.80
1.00
1.20
1.40
1.60
1.80
2.00
WAVELENGTH IN MICROMETERS

Figure 2

CHLOROPHYLL EXTRACT

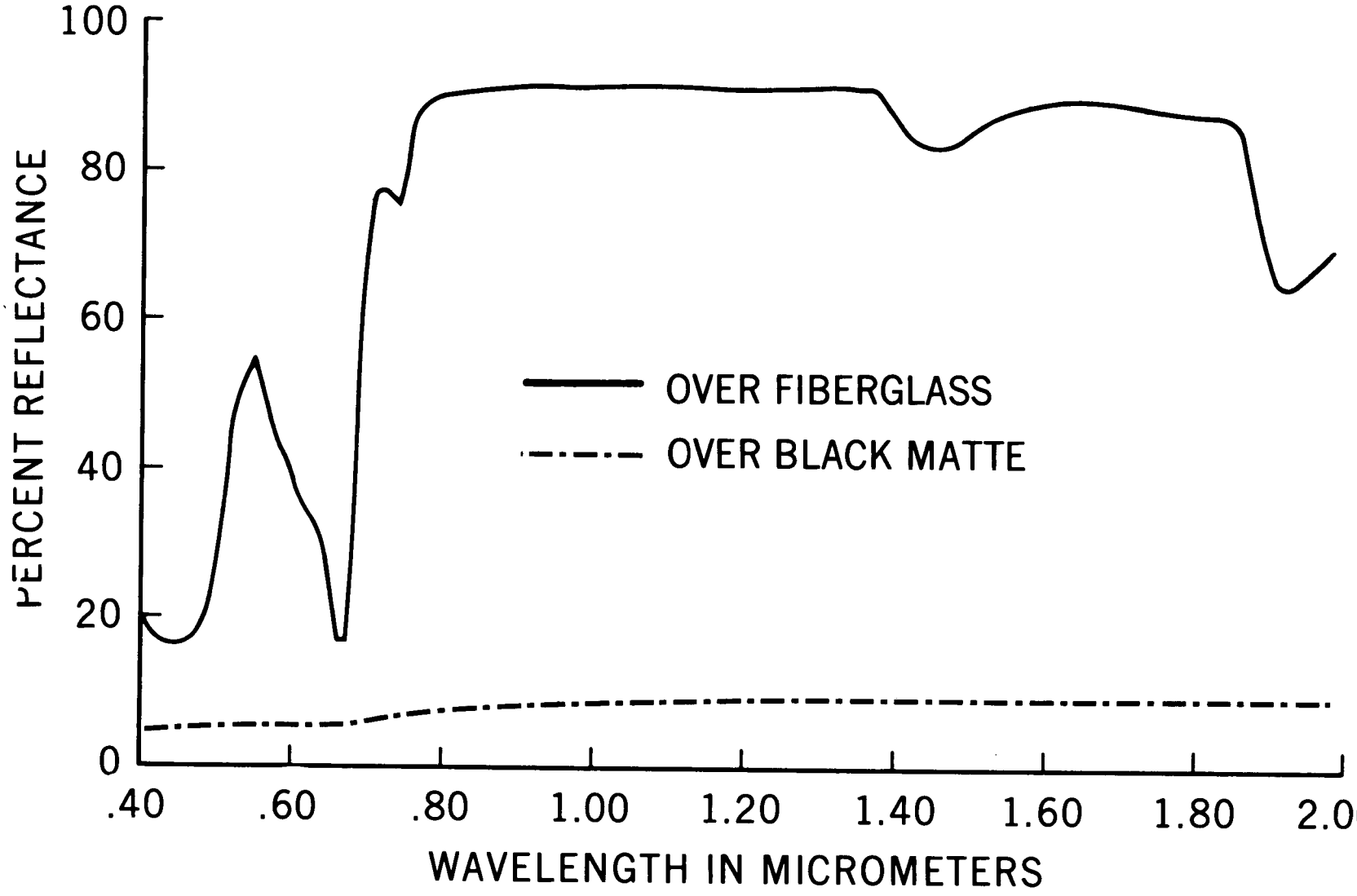

Figure 3

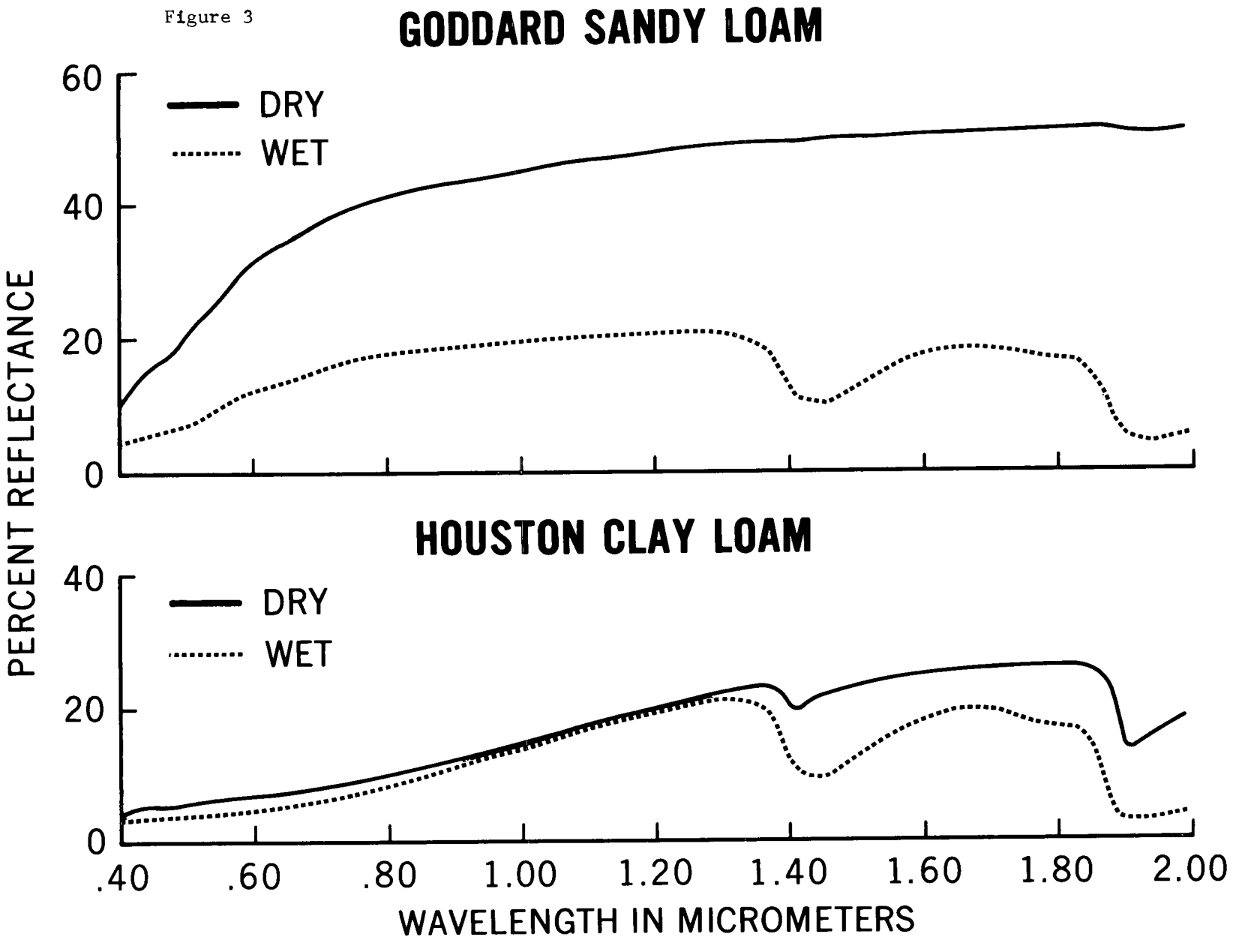
GODDARD SANDY LOAM
DRY
WET
60
40
20
0
HOUSTON CLAY LOAM
DRY
WET
40
20
0
PERCENT REFLECTANCE
.40
.60
.80
1.00
1.20
1.40
1.60
1.80
2.00
WAVELENGTH IN MICROMETERS

Figure 4

PERCENT REFLECTION OF SINGLE SOYBEAN LEAF

PERCENT REFLECTION OF NINE SOYBEAN LEAVES

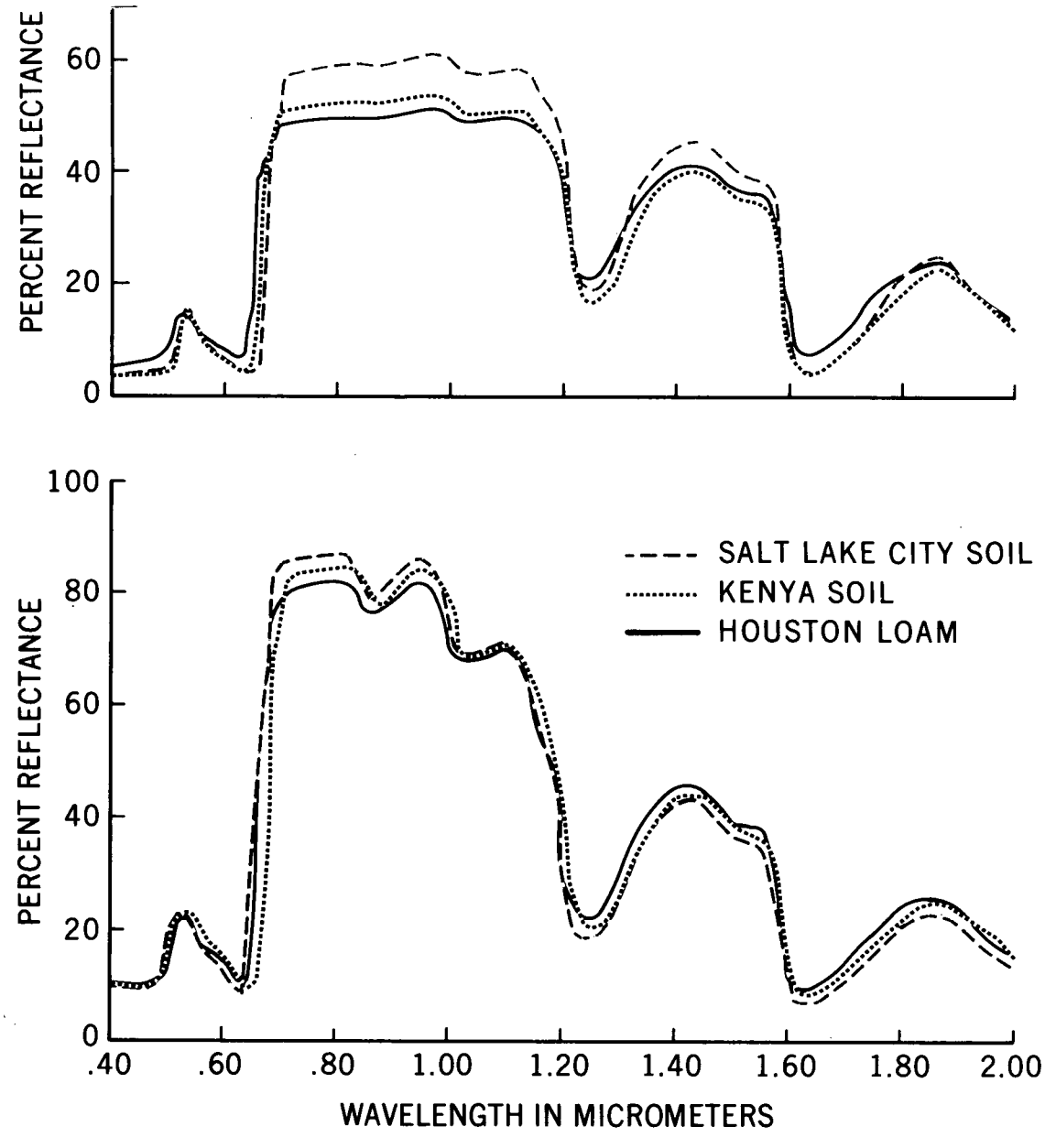

Figure 5

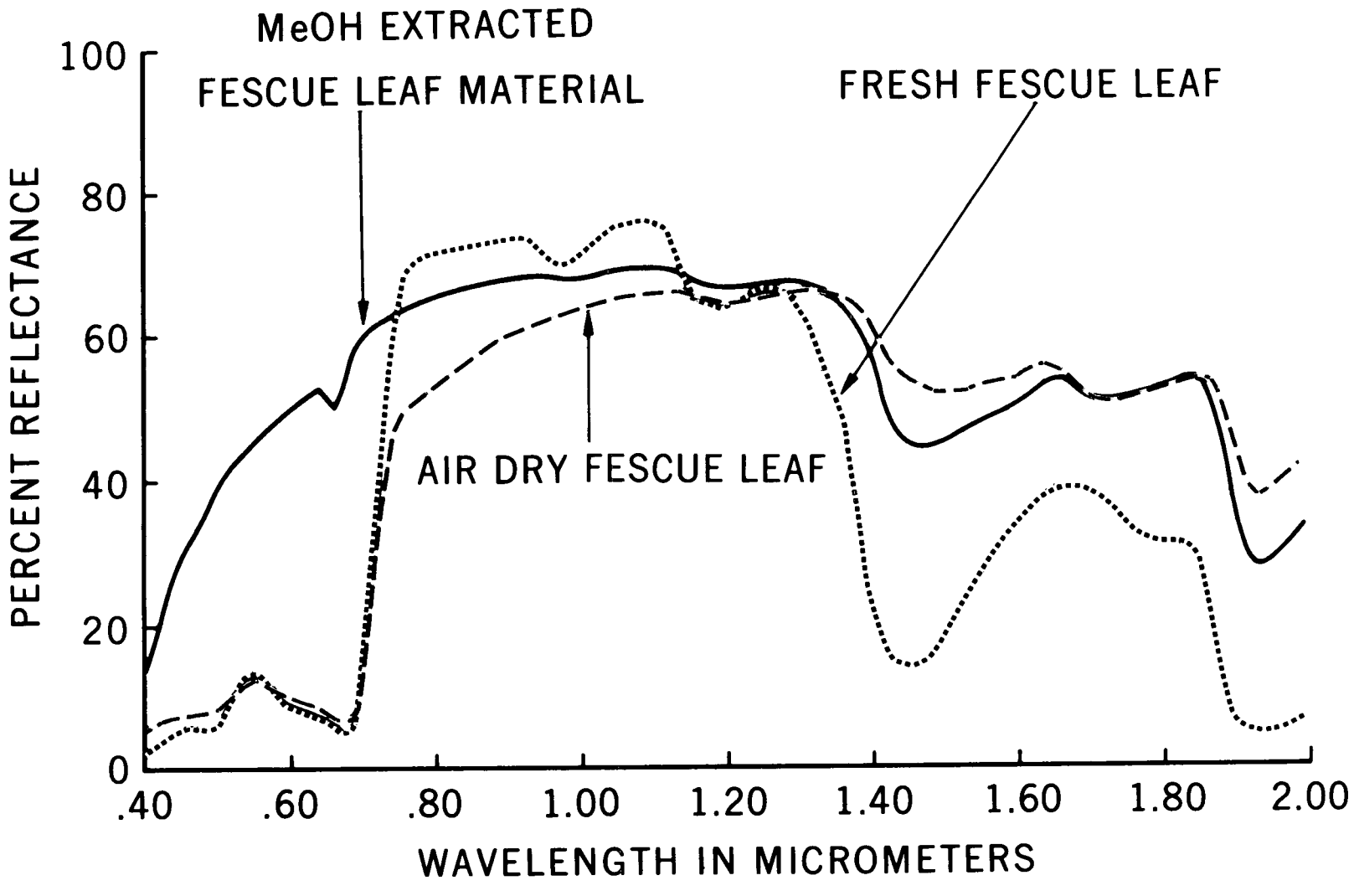
MeOH EXTRACTED
FESCUE LEAF MATERIAL
FRESH FESCUE LEAF
AIR DRY FESCUE LEAF
PERCENT REFLECTANCE
100
80
60
40
20
0
.40
.60
.80
1.00
1.20
1.40
1.60
1.80
2.00
WAVELENGTH IN MICROMETERS

Figure 6

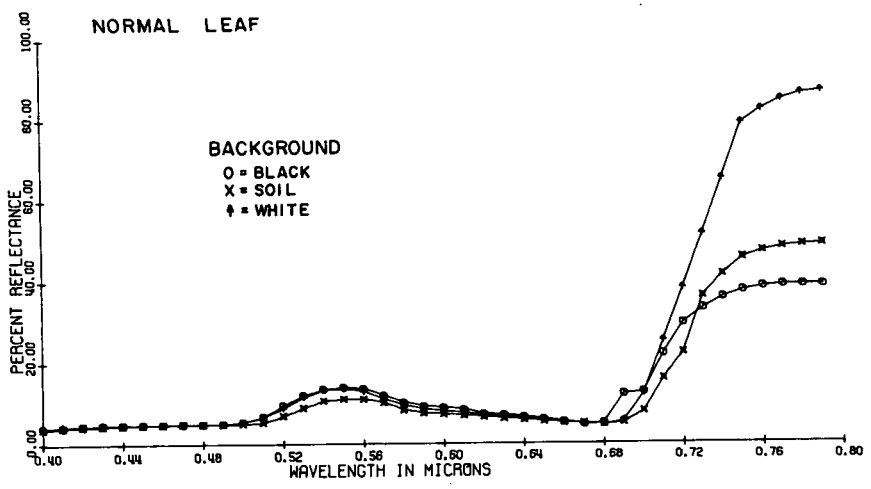
NORMAL LEAF
BACKGROUND
O = BLACK
X = SOIL
♦ = WHITE
PERCENT REFLECTANCE
WAVELENGTH IN MICRONS

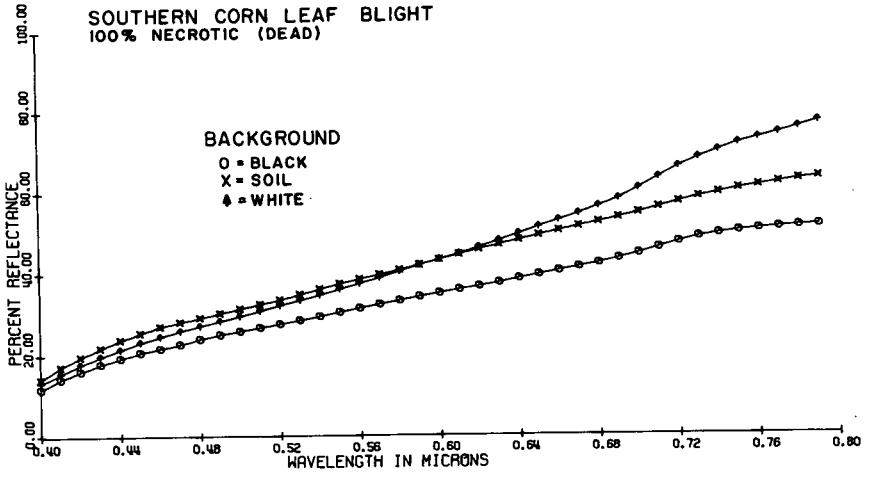
SOUTHERN CORN LEAF BLIGHT
100% NECROTIC (DEAD)
BACKGROUND
O = BLACK
X = SOIL
♦ = WHITE
PERCENT REFLECTANCE
WAVELENGTH IN MICRONS

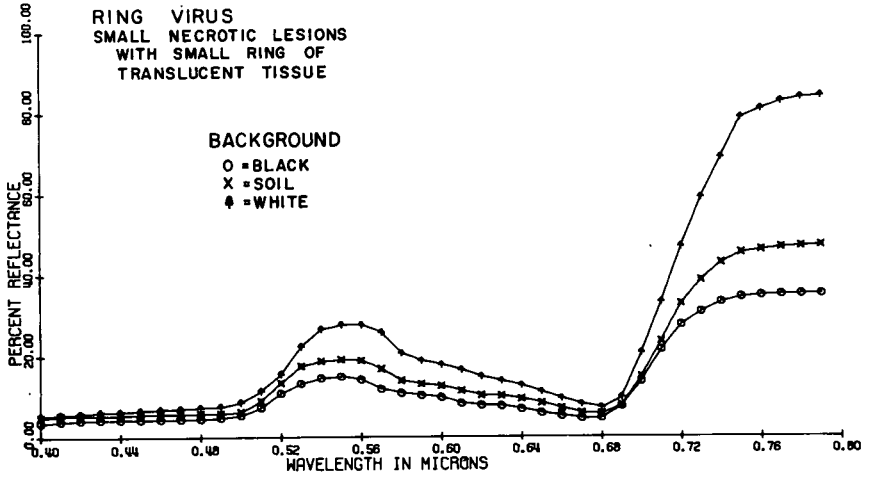
RING VIRUS
SMALL NECROTIC LESIONS
WITH SMALL RING OF
TRANSLUCENT TISSUE
BACKGROUND
O = BLACK
X = SOIL
♦ = WHITE
PERCENT REFLECTANCE
WAVELENGTH IN MICRONS

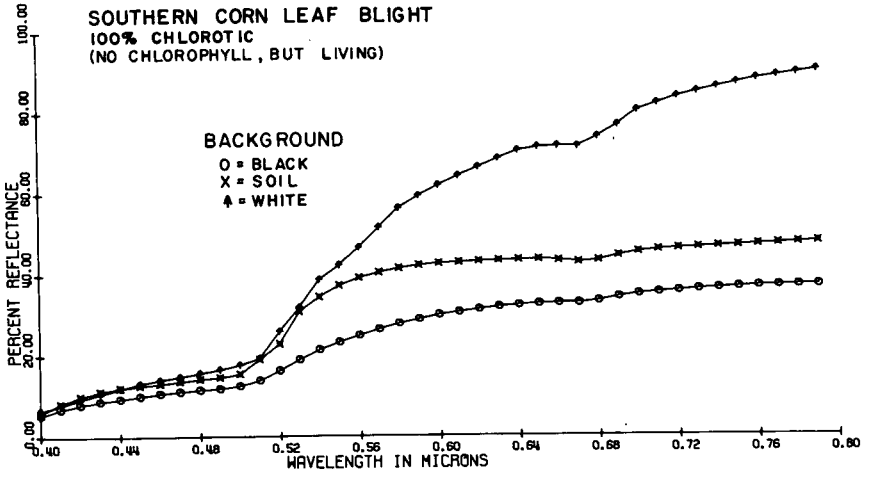
SOUTHERN CORN LEAF BLIGHT
100% CHLOROTIC
(NO CHLOROPHYLL, BUT LIVING)
BACKGROUND
O = BLACK
X = SOIL
♦ = WHITE
PERCENT REFLECTANCE
WAVELENGTH IN MICRONS

SECTION 7

ANALYSIS OF MULTISPECTRAL IMAGES SIMULATING ERTS OBSERVATIONS

by

Nicholas M. Short & Norman H. MacLeod
Earth Observations Branch
Goddard Space Flight Center
Greenbelt, Maryland

INTRODUCTION

In response both to the anticipated desires of the User Community for simulated imagery prior to launch of the first Earth Resources Technology Satellite (ERTS-A) and to the need for such products suited to scientific and technological evaluation at Goddard, a simulation study of selected aircraft- and spacecraft-acquired images was initiated in 1971 within the Earth Observations Branch at Goddard Space Flight Center. The principal modes of simulation include: first, areas of coverage comparable to ERTS, that is, approximately 183 km (100 nm) on a side; second, spatial resolutions within these images similar to ERTS (namely, about 100 meters for the two ERTS sensor systems at optimum signal to noise ratios); third, spectral responses analogous to that expected from each channel on both the Return Beam Vidicon (RBV) and Multispectral Scanner (MSS), leading to production of photographic images that should appear similar to those representing each band in the two sensors (spectral response curves for each band are shown in Figure 1); and, fourth, runthroughs of several analytical techniques, such as color density slicing, color additive viewing, and computer-generated reflectance and surface temperature maps, by which ERTS data can be analyzed, interpreted, and applied.

The two regions involved in the simulation study are Wyoming - selected as typicalof a semi-arid surface dominated by geological features and considerable topographic variation, and the Chesapeake Bay region around Washington, D.C. and eastward - chosen as characteristic of a humid climatic environment, dominated by vegetation, flat, and bounded by a marine coastline.

NIMBUS STUDIES

The first step in these simulation studies began with examination and analysis of certain Nimbus meteorological satellite images. Nimbus I, a short-lived satellite with an eccentric orbit, produced many intriguing pictures of the Earth's surface at resolutions of a kilometer or better near perigee. The scene depicted in Figure 2 represents one of the finest

examples of high altitude synoptic imagery obtained from unmanned satellites to date. Comparison of the image - covering parts of southwest Wyoming, northwest Colorado, northeast Utah, and eastern Idaho - with the geological map of the same area shows that nearly all major structural and topographic units can be readily recognized. The light, highly reflective basins stand out in sharp contrast to the uplifted mountains which appear dark in the image because of the much more extensive vegetation cover - mainly thick grasses and conifers. These contrasts can be further enhanced by converting the photographic grey levels into colors by use of a TV color density slicing system. (Figure 3). In general, the lack of high resolution in Nimbus photos is offset by these distinct differences in contrast that allow ready recognition of major vegetation groups and moisture variations on a regional, synoptic scale.

Dr. V. Salomonson of the Meteorology Branch at Goddard has produced a surface temperature distribution map of the entire state of Wyoming from emitted thermal radiation at 11.5 micrometers as dectected by the THIR or Temperature-Humidity Infrared Radiometer on Nimbus IV. This channel is similar to the thermal channel peaked between 10.4 and 12.6 micrometers planned for ERTS-B, although the THIR resolution of 8 kilometers is much less than that of about 300 meters being designed for ERTS-B. A schematic relief map of Wyoming appears in Figure 4c. This should be compared first with a computer-generated map of THIR-sensed data for the entire state obtained during a daytime pass on July 4, 1970 (Figure 4b). Color codes show the surface temperature range after appropriate corrections are made. It is immediately evident that, again, most of the principal topographic features within the state are well defined by the temperature variations. These variations are accentuated primarily by the pronounced relief or differences in elevation between the relatively cool uplands and the hotter intermontane basins. Broad patterns coincident with structural uplifts within the basins or with major drainage systems can even be discerned. However, when THIR looks at this same surface at night (Figure 4a), on the same July 4th, the temperature distribution pattern becomes far less recognizable when attempts to correlate with topography are made - although the general positions of basins and mountains are crudely defined.

WYOMING AIRCRAFT SIMULATIONS

Let us turn now to efforts to simulate ground scenes of the same general size or areal extent and spatial resolution as expected from ERTS. Invaluable experience pertinent to this was already available through the studies of Gemini and Apollo orbital photography made by Lowman, Abdel-Gawad, and others. The chief conclusions reached by these workers and by many other specialists in remote sensing are that such small scale (that is, large areas of coverage) images have a tremendous inherent capability for providing synoptic overviews of extensive sections of the Earth's surface and that many individual ground features at or near the limits of resolution could be successfully identified by classification techniques based on diagnostic spectral and spatial characteristics or signatures.

Rather than retread the path laid out by these orbital photography experts, we have followed a somewhat different approach. Largely through the ingenuity of R. Sabatini and others of the Allied Research Corporation supporting Nimbus, a simple technique for progressively degrading images with initially high resolutions has been developed. In its essence, this technique involves reprinting a photograph at various sizes smaller than the original, photographing these again as is, and then enlarging the variously reduced negatives to a single constant size before final printing. Control in the process is maintained through use of a grey level scale and a three-bar resolving-power target that aids in calculating new resolutions.

As a first test of the method, a remarkable photomosaic of the Los Angeles area made at an initial scale of 1: 400,000 by Aero Service Corp. of Philadelphia, Pa from over 10,000 individual aerial photos was systematically degraded from an initial ground resolution of about 15 meters (Figure 5a; reduced through steps of 30 and 55 meters) through steps of 25, 50, 100, and 200 meters (using an 8 x 10 print) (Figure 5b). Two conclusions are strikingly obvious. First, regardless of resolution, all the first- and second-order land features are visible and generally identifiable at all these resolutions. The various mountain units, some major geological structures expressed topographically (including the San Andreas fault zone), most larger drainage systems, and the bigger agricultural fields remain evident in the lower resolution renditions. Second, however, useful and sometimes essential details relevant to mapping or to feature identification are lost in the low resolution (e.g., 200 meter) image. This is best demonstrated by examining the cultural features present in the Los Angeles basin, preferably with the aid of a magnifying glass.

We have now tried essentially the same type of progressive degradation on an area within central Wyoming (Figure 6) whose dimensions approximate that of a single ERTS field of view or frame reproduced photographically. The region covered centers on the Wind River basin surrounded by uplifted mountain blocks some 1500 to 3000 meters higher in elevation. In the Nimbus TV imagery, these uplifts appear significantly darker in a processed photofacsimile. In an Aero Service-produced composite photomosaic at a 1:250,000 scale (put together from more than 12,000 aerial photos in a 1952 flight sequence), shown in Figure 7a, it is very hard to spot the uplifts or the deformed structures within the basin. This is one of the weaknesses associated with this type of photomosaic - in which the aerial surveying plane usually flew around high noon to minimize shadows and some contrasts are later removed by dodging during preparation of the mosaic. This tends to obscure some of the structural and topographic relationships that make a synoptic view so attractive for interpreting large units of the Earth's crust. Still, careful examination of the photograph shown in Figure 7b, degraded to about 130 meters resolution, reveals that many critical details have remained detectable. When degraded to 285 meters resolution (Figure 7c), most major elements of interest in the scene are still recognizable and can be adequately mapped. What is sacrificed in this scene are specific details of secondary drainage, individual rock units, cultural layouts in towns, and the like; however, changes in tonal

patterns as seen under magnification can sometimes be interpreted to correctly identify these features.

On October 21, 1971, a U-2 flight over essentially the same area of central Wyoming was conducted for the first co-author by NASA Ames Research Center. The aircraft carried four Vinten cameras, three of which contained film-filter combinations designed to simulate the ERTS RBV sensor system. Each camera produced individual pictures about 26 km (14 nm) on a side, with slight overlap and sidelap among photos in the flight lines. The effective ground resolution is between 15 and 20 meters. We have prepared an uncontrolled photomosaic from some 54 individual frames using the red band images (Figure 8). Because the red band optimizes contrasts in a scene dominated by geologic features, some of the structural, topographic, and geomorphic features scarcely discernible in the Aero Service mosaic are more readily picked out in the U-2 composite mosaic.

Instead of decreasing the resolution of the entire scene, a sequence of degradations was carried out on a single 26 km frame. The area selected is in the vicinity of Ocean Lake near the northwest corner of the Wind River basin. An Aero Service photomosaic that covers this area appears in Figure 9a and an undegraded (resolution about 18 meters) U-2 frame extending over much the same area is shown in Figure 9b. Figure 10a illustrates the scene at a resolution of about 45 meters. As before, most of the essential information remains intact. When degraded to 100 meters, the principal loss of information again is in the fine structure of drainage systems, rock and soil distribution, etc. But the overall synoptic aspects of the scene continue to stand out in their proper context.

This same scene can also be examined through different regions of the photographic spectrum. The simulated green band view (Figure 11a), when compared to the red band view (Figure 11b), discloses one evident difference. The photographic contrasts between various areas of rock and soil and between agricultural fields (most of which were harvested and barren by October 21) are distinctly less in the green than in the red. On the other hand, sediment in the lake is evident only in the green band photo. Next, compare the IR band (Figure 11c) with the red band. Contrasts within the cultivated areas are reduced - mainly because most of the crops are gone. During growing season the IR band could show stronger contrasts than in the red band. Moisture variations in the desert wastes south of the lake show up well in the IR and also in the red bands but less so in the green. Another example appears in Figures 12a, b, and c. Once more, maximum contrast, and hence scene definition, occurs in the red band. Some contrasts are evident in the IR but the green band photo looks more or less washed out and rather dark.

These observations agree with Lowman's conclusions for desert areas seen in the SO-65 Apollo 9 experiment. The explanation is straighforward: In Wyoming, most of the surface in the basins is dominated by rocks and soils whose colors range from reds to browns to grays to buff. As viewed within the visible red wavelength region, color variations on such sur-

faces should lead to large photo density contrasts. Sparsity of vegetation causes minimal changes in the green and IR band photos.

STUDIES IN THE CHESAPEAKE BAY (CARETS) REGION

Lets switch our attention now to simulation studies in the eastern United States. Figure 13 presents a synoptic photomosaic of the Chesapeake Bay region, enclosing an area about 220 km (120 nm) across the view and 275 km (150 nm) from top to bottom. This picture was constructed from over 110 individual red band frames obtained during a U-2 flight on September 15, 1971. The U.S. Department of Agriculture has completed a similar photomosaic with the green band photos from this flight. Comparison of the two products, at nearly equivalent scales, reveals a sharper contrast among the major land features - mostly farm and forest plots - within the green band. This is observed repeatedly in individual frames covering rural areas in the Delmarva peninsula.

Figure 14a, b, and c consists of the green, red, and IR band photos of an area which includes Goddard Space Flight Center, the Beltway northeast of Washington, D.C., and the Washington-Baltimore Parkway. Again, the heavily vegetated areas, such as those within the Beltsville Agricultural Experiment Farms, show up best in the green band. But because of the extensive cultural - or suburban - development in this area and the presence of many sand and gravel pits, the contrast seems even greater in the red band panorama. In the IR band photo, the overall tone of the picture is bright, with subdued contrast except for the water backed up behind a dam on the Pawtuxent River north of Laurel, Maryland. Towns and other cultural features are hard to distinguish from surrounding vegetation at first glance. This particular scene indicates the effects in the IR of a suburban environment in which everyone is still trying to keep his lawn and shrubery in growth as late as September 15. The uniform brightness, then, gives a different impression than that of the IR band views of the farmlands in eastern Maryland, where considerable harvesting had already altered the growth pattern by then.

A red band U-2 frame that covers an area in Maryland's eastern shore where Highway 50 crosses the Choptank River is reproduced in Figure 15a. Ground truth data for many of the features clustered along the highway in this section were obtained by N. H. MacLeod. Figure 15b shows a reconstructed false color IR image, produced on an I^2S color additive viewer, which should approximate the type of color photo that will be produced routinely from the three RBV images on ERTS. In this image, the green band is projected through a blue filter, the red through a green, and the IR band through a red filter. As expected, the forest areas reappear as dark red, the growing field crops as lighter red, and fallow fields, excavations, and town areas mainly as shades of blue or green.

In mid-October, 1971 the multispectral scanner developed by Warren Hovis of the Earth Observations Branch at Goddard for ERTS simulation was

flown on an aircraft at an altitude of 2500 meters over this same Choptank River area and other parts of the Delmarva peninsula. The photo imagery was produced by converting the analog voltage data recorded on magnetic tape into video signals processed through an electron beam recorder into a picture. The four channel MSS image obtained over a strip along Highway 50 appears in Figure 16. The numbers refer to individual identified features, labelled in Figure 17, within which photo densities of corresponding areas in each band image were measured. It should be stressed that these measurements, plotted graphically in Figure 17, cannot be considered as quantitative owing to non-calibration of either the raw MSS data or photographic reproduction and to the relative simplicity of the densitometer used. Note too that noise has not been removed, as is evident in channel 4. The signature data are thus only approximations of the kinds of results expected from the ERTS MSS system.

The following generalizations can be summarized from interpretations made on Figures 16 and 17:

1) The images produced from the first two channels - the visible green and red bands - are, in general, similar to one another in terms of the densities associated with specific feature categories.

2) The two IR channels are, to a lesser extent, also similar to one another.

3) The two pairs of channels - visible and IR - produce images that are distinctly different from one another.

4) The signatures of the same feature classes appear to be reproducible throughout the scene, as suggested by the very similar density values obtained for the two separate mixed hardwood stands and the two fields containing old hay.

5) Ambiguities about whether bright (light grey tones) areas in the visible channels represent fallow fields or growing crops are clearly resolved by the IR channels.

6) At the resolution of the MSS images - about 10 meters - the identification of dark-toned areas in the first two channels as forests of taller trees is confirmed by the third channel, in which tree canopy patterns give rise to a distinctive texture.

Now, to counter the impression that two of the four MSS channels may seem redundant, look at the last illustrations. The U-2 RBV-simulated photographs for part of the Atlantic coastline along Assateague Island (Maryland-Delaware) appear in Figure 18. The MSS counterpart for the offshore bar area is shown in Figure 19. Close inspection of patterns representing beach sand and dune sand distributions and vegetation along drainage paths or in tidal marshes, etc. will reveal that channels two

and four add significant new information in relation to channels one and three. Visual differences in tone or grey level, not too apparent to the eye at first glance, prove larger than suspected when areas are densitometered and channel density levels are ratioed.

SUMMARY

In conclusion, these main points are reiterated:

First, even at resolutions around 100 meters, the synoptic character of diverse ground scenes extending over wide areas remains strongly expressed and, in some respects, is emphasized by loss or reduction of details.

Second, each band on the RBV or MSS sensors appears to have a useful function for certain specific tasks. Thus, on one type of land surface, one visible band may be superior to another but with the converse true in another region with different land surface types.

Lastly, interesting and exciting though these simulation images may be, they'll pale and be forgotten the day we begin to get the real products from ERTS itself.

ACKNOWLEDGEMENTS

We are particularly grateful to Mr. Ronald Sabatini and Mr. Walter Ahlin of the Allied Research Corporation for their generous assistance in preparing many of the illustrations appearing in this paper.

SPECTRAL RESPONSE FOR ERTS-A

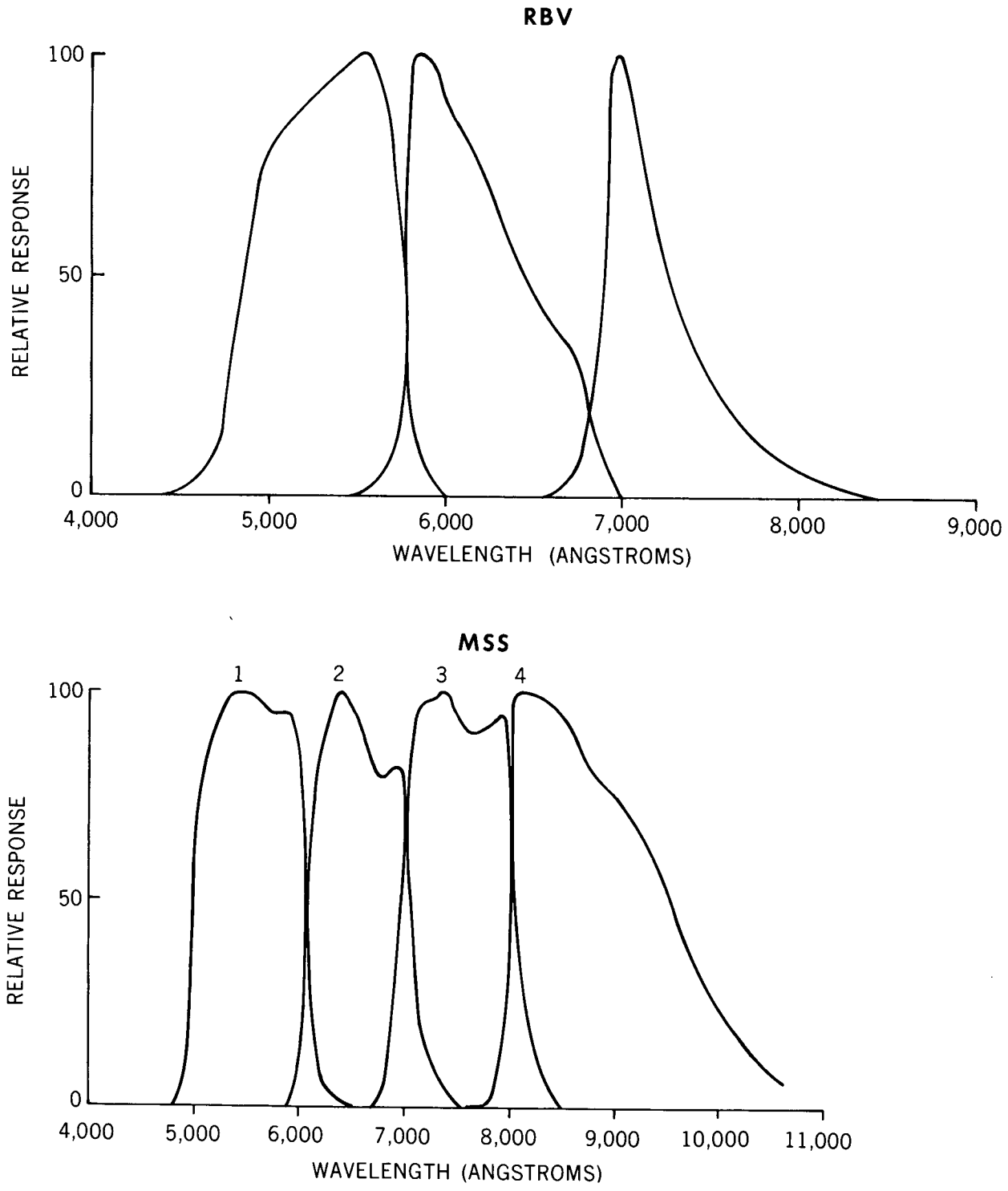

Figure 1. - Spectral response curves for the Return Beam Vidicon (RBV) (calculated) and Multispectral Scanner (MSS) (measured) sensors on ERTS-A

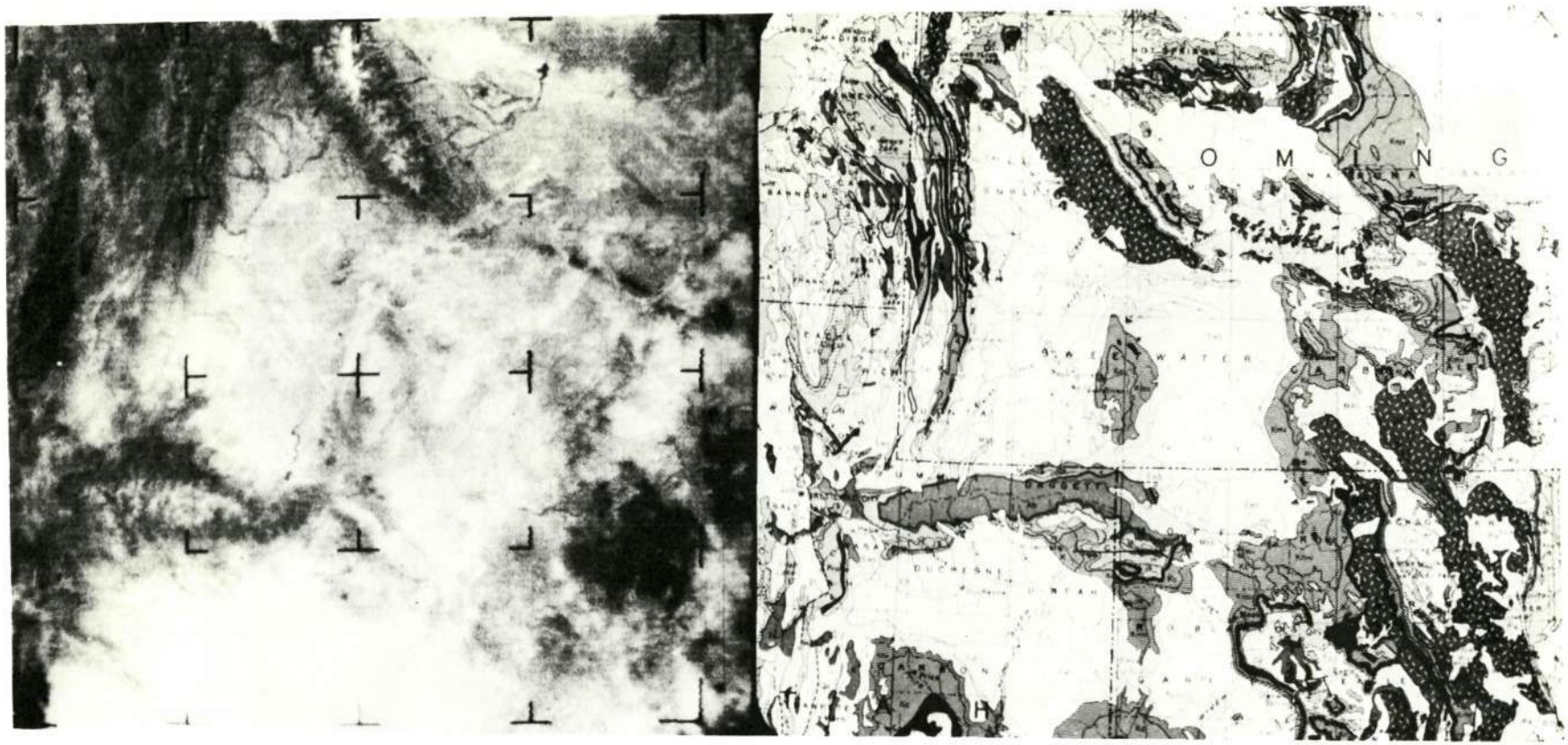

Figure 2. - Left: Nimbus I AVCS (television) photofacsimile of southwestern Wyoming, northwestern Colorado, and northeast Utah taken on September 4, 1964 (orbit 109) from an altitude of approximately 890 km. The large, light area in the center is the Green River basin; a similar area to the south is the Uinta basin. The Wind River mountains appear in the top center, the Wyoming-Hoback Ranges to the left of these, and the east-west Uinta Range on the lower left below center. Right: A geological map (from U.S. Geological Survey map of the U.S.) showing the region covered by the Nimbus I image.

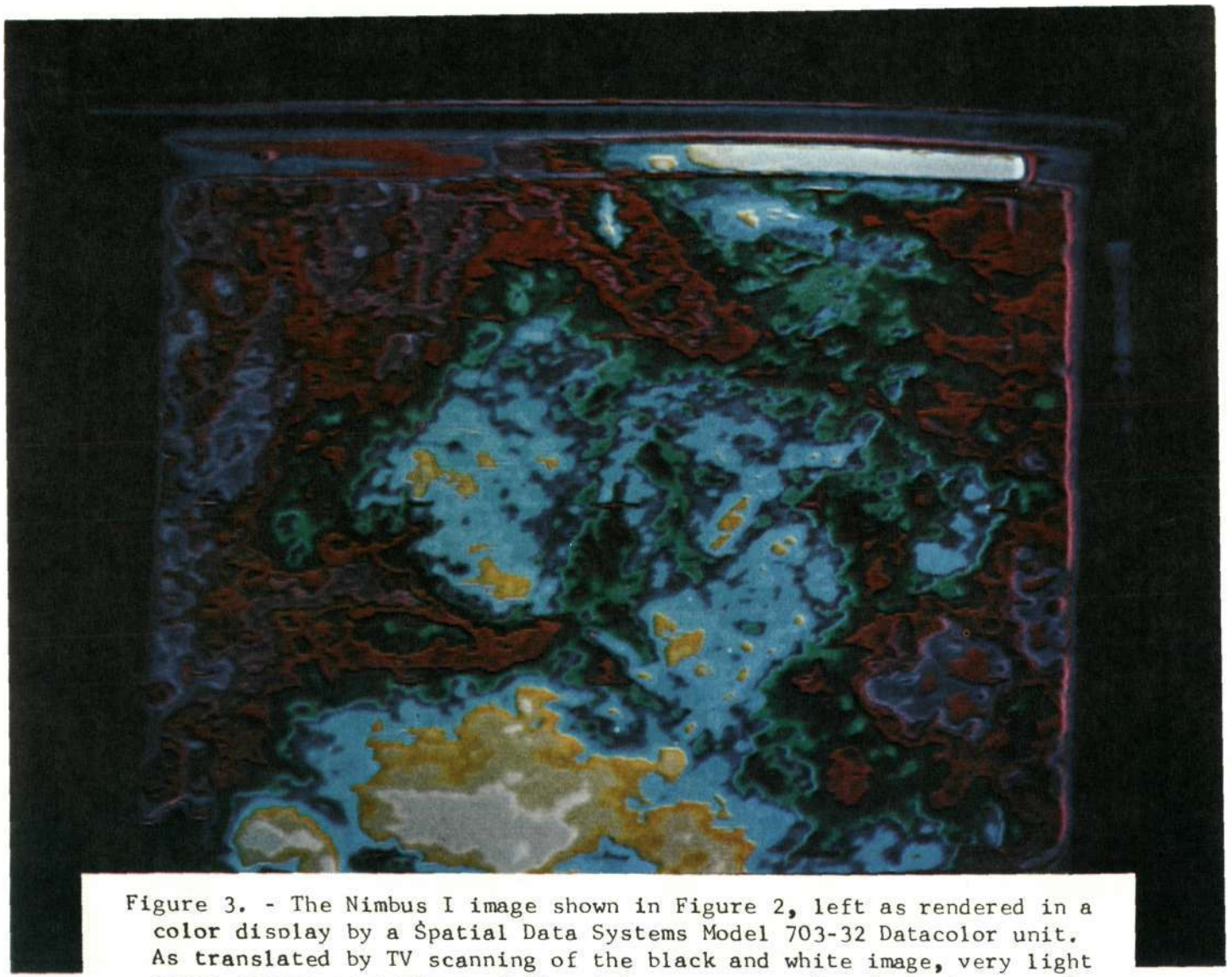

Figure 3. - The Nimbus I image shown in Figure 2, left as rendered in a color display by a Spatial Data Systems Model 703-32 Datacolor unit. As translated by TV scanning of the black and white image, very light greys appear as yellows, followed by a sequence for darkening grey levels through blues, greens, dark olive, red, mauve, and bluish-purple.

NIMBUS 4 THIR 10.5–12.5 μm OBSERVATIONS OVER WYOMING

JULY 4, 1970

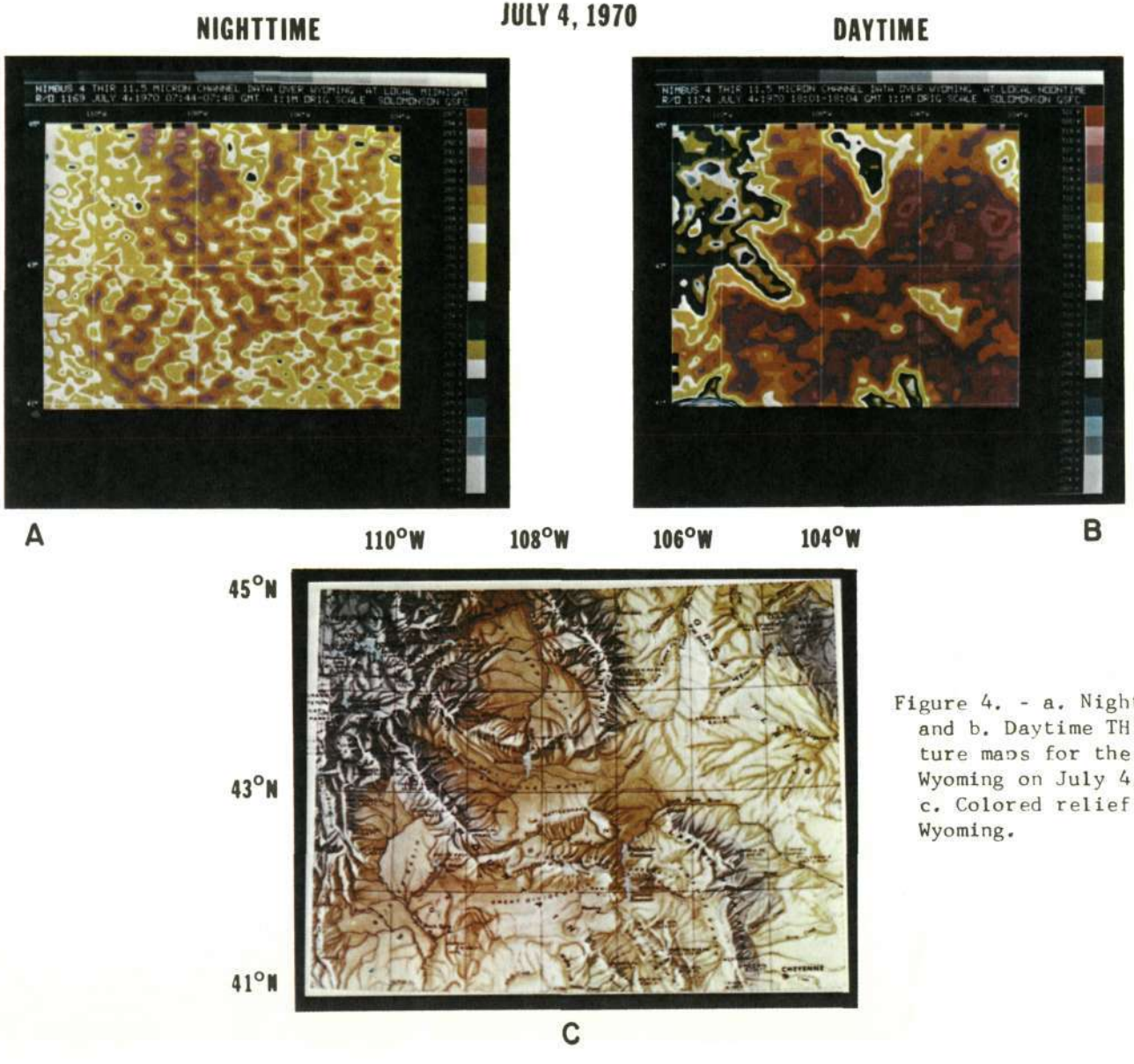

Figure 4. - a. Nighttime THIR and b. Daytime THIR temperature maps for the surface of Wyoming on July 4, 1970. c. Colored relief map of Wyoming.

(A)
Aerial Photomosaic of Los Angeles and Mojave Desert Areas

(B)
Degraded Image of (A)
Resolution is approx. 200 meters.

PRODUCED BY ALLIED RESEARCH ASSOCIATES, CONCORD, MASS.

Figure 5. - a. Composite aerial photomosaic of the Los Angeles basin - Mojave desert areas of California; San Gabriel Mountains in the center. The resolution of the original 8 x 10 inch photo before reduction to illustration size is about 30 meters; as reproduced here it is about 55 meters. b. Same scene reduced in resolution to approximately 200 meters; or about 350 meters as printed.

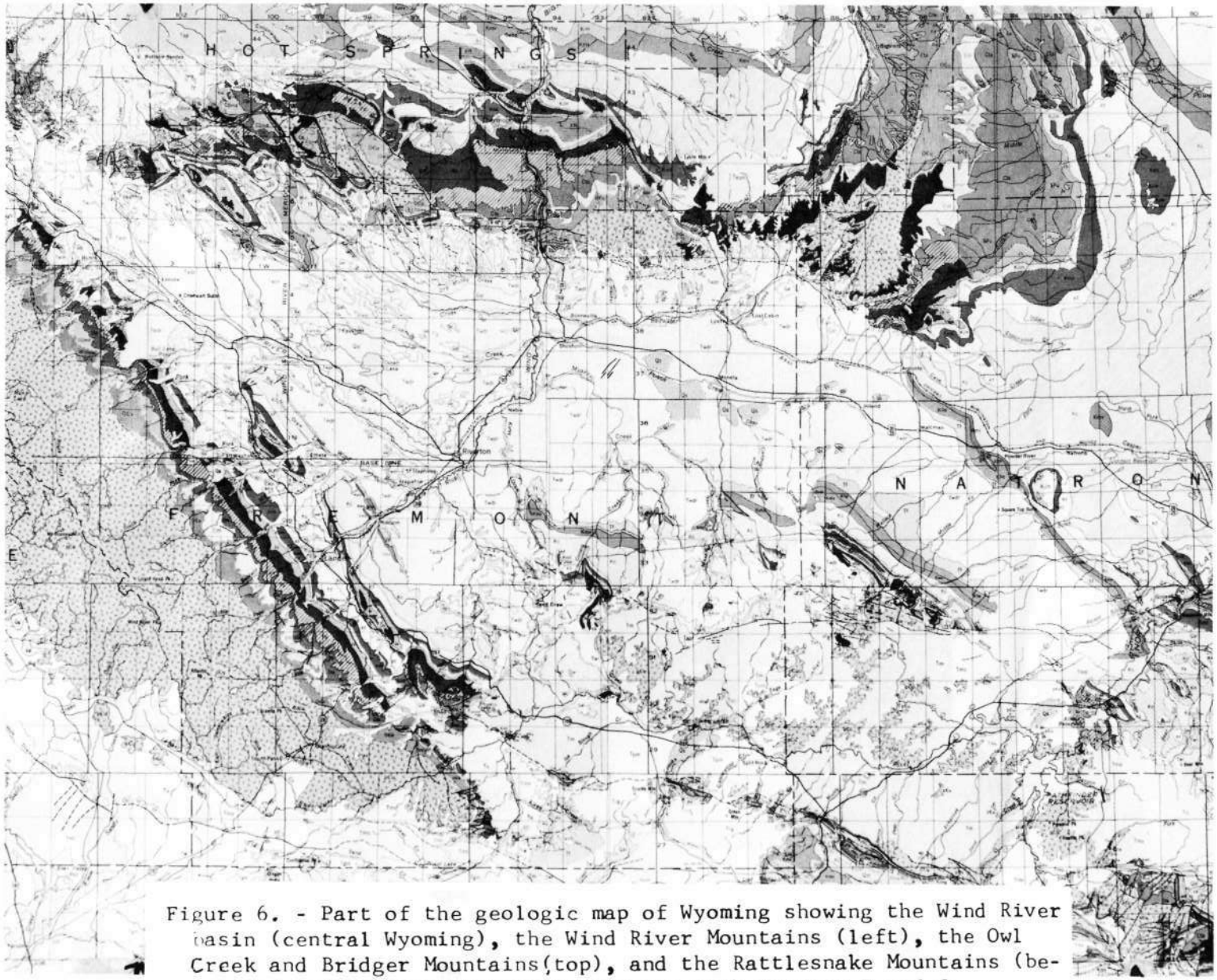

Figure 6. - Part of the geologic map of Wyoming showing the Wind River basin (central Wyoming), the Wind River Mountains (left), the Owl Creek and Bridger Mountains (top), and the Rattlesnake Mountains (below and left of word Natrona); compare with Figures 7 and 8.

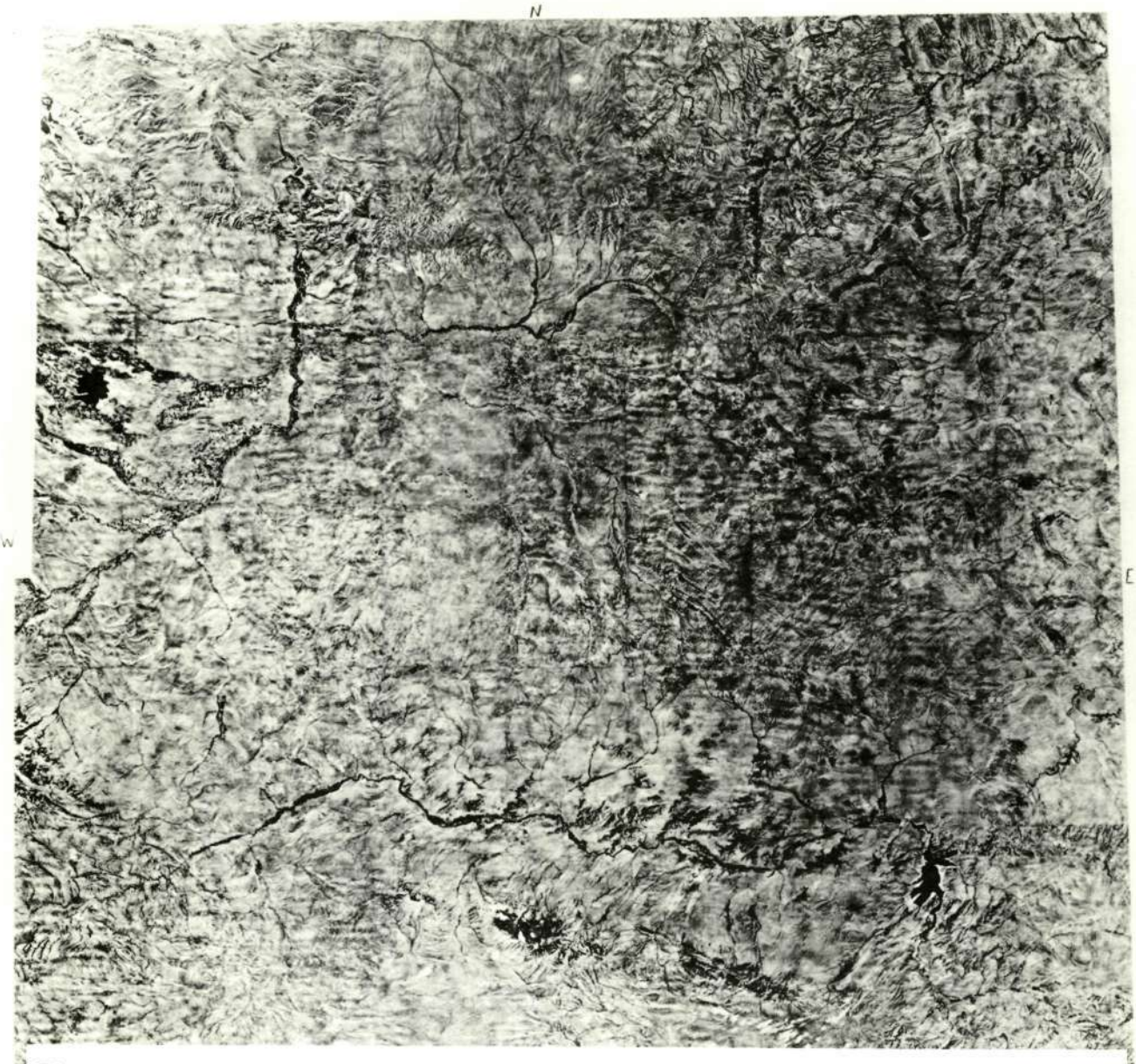

Figure 7a. - A composite photomosaic of the Wind River basin region; produced by Aero Service, Inc. at an initial scale of approximately 1:425,000 and a resolution of about 15 meters. As reduced in this illustration, resolution is estimated to be near 60 meters.

a.

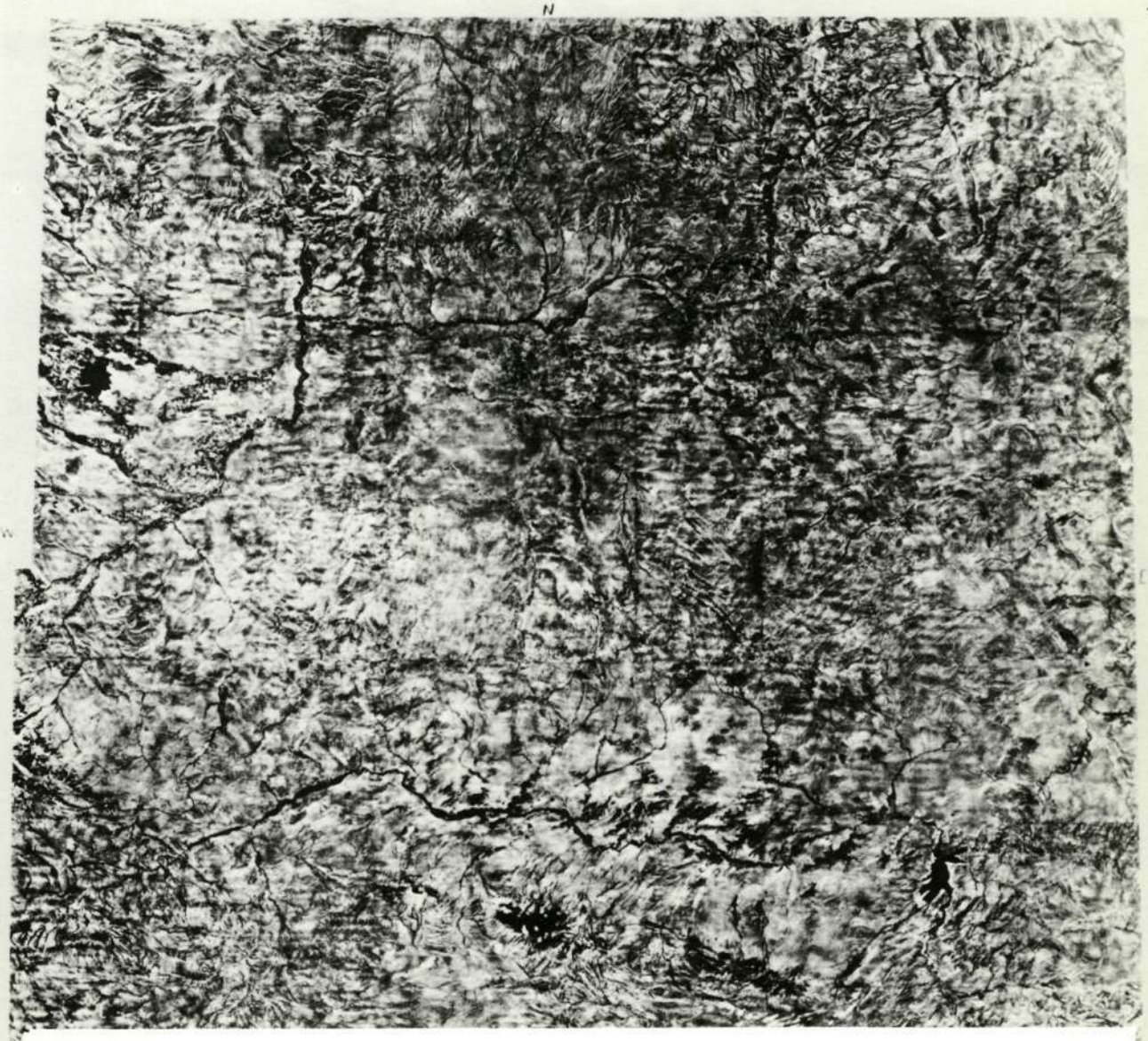

Figure 7b. - Reduction of the Wind River photomosaic to a resolution near 130 meters (estimated with aid of target). Note light and dark horizontal banding in this and other pictures of the scene; this is a form of "noise" apparently introduced during either initial photography or photomosaicing.

b.

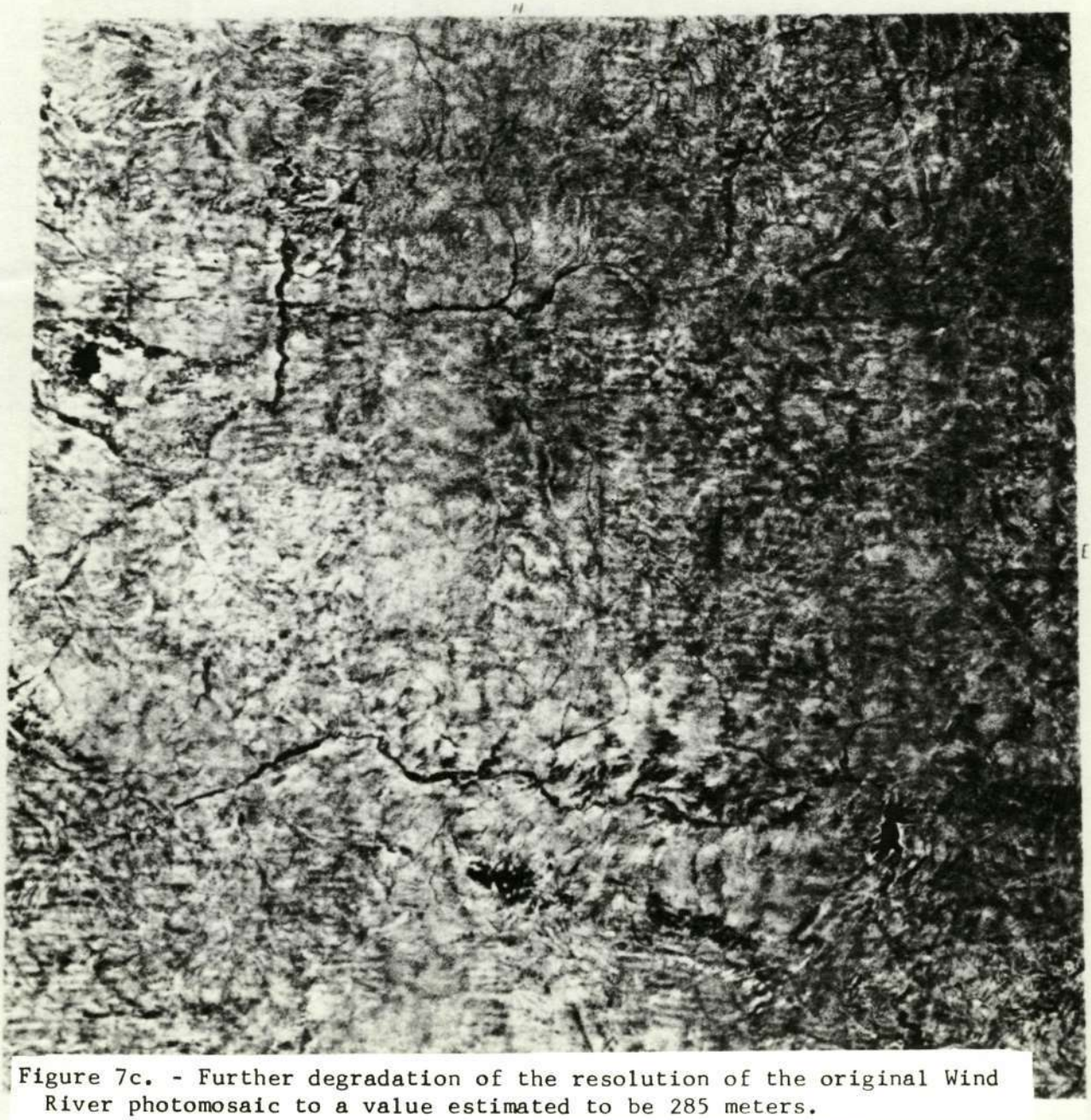

Figure 7c. - Further degradation of the resolution of the original Wind River photomosaic to a value estimated to be 285 meters.

c.

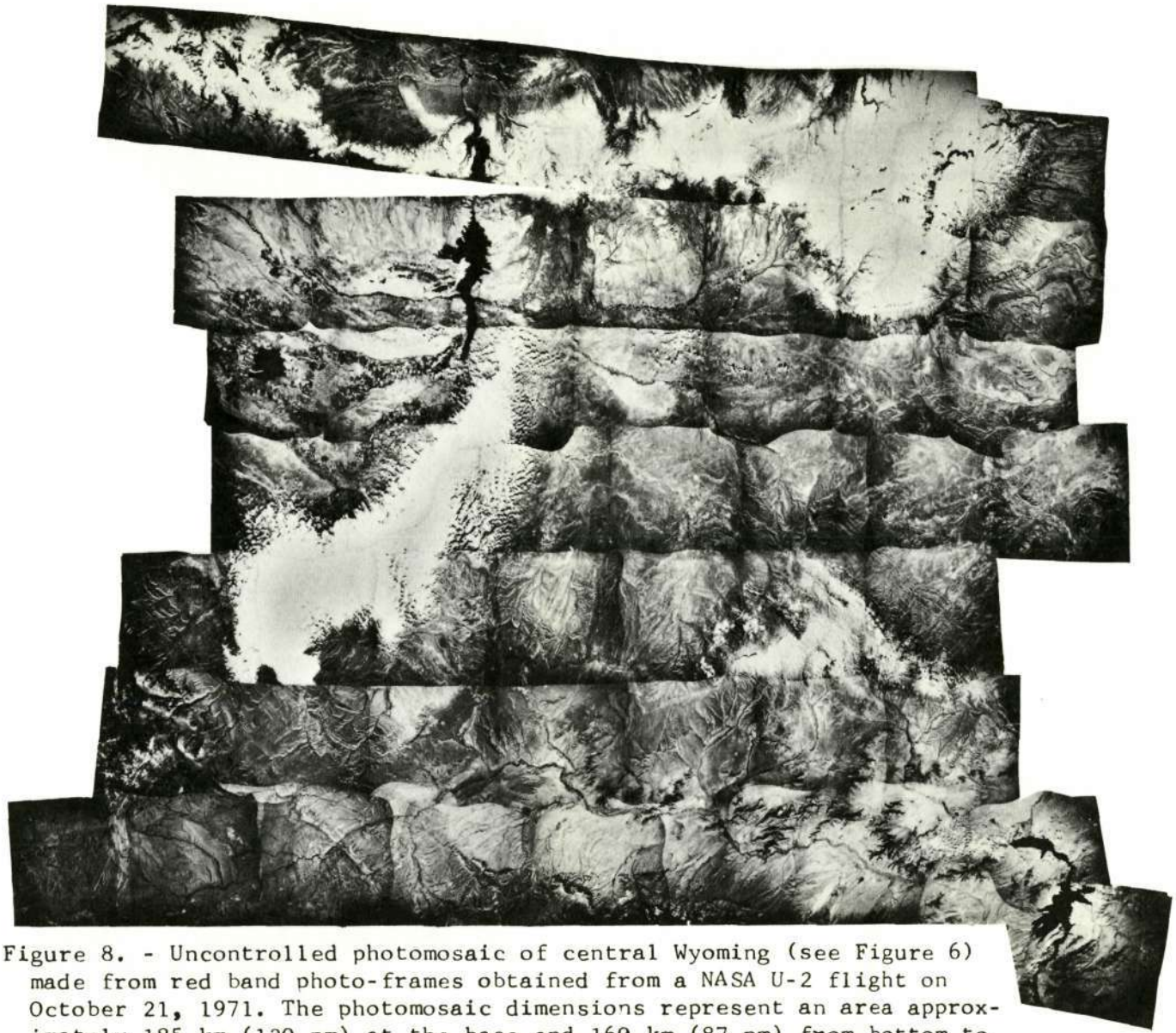

Figure 8. - Uncontrolled photomosaic of central Wyoming (see Figure 6) made from red band photo-frames obtained from a NASA U-2 flight on October 21, 1971. The photomosaic dimensions represent an area approximately 185 km (120 nm) at the base and 160 km (87 nm) from bottom to top. Resolution of original photomosaic is about 18 meters; as printed in this illustration, the resolution is near 75 meters.

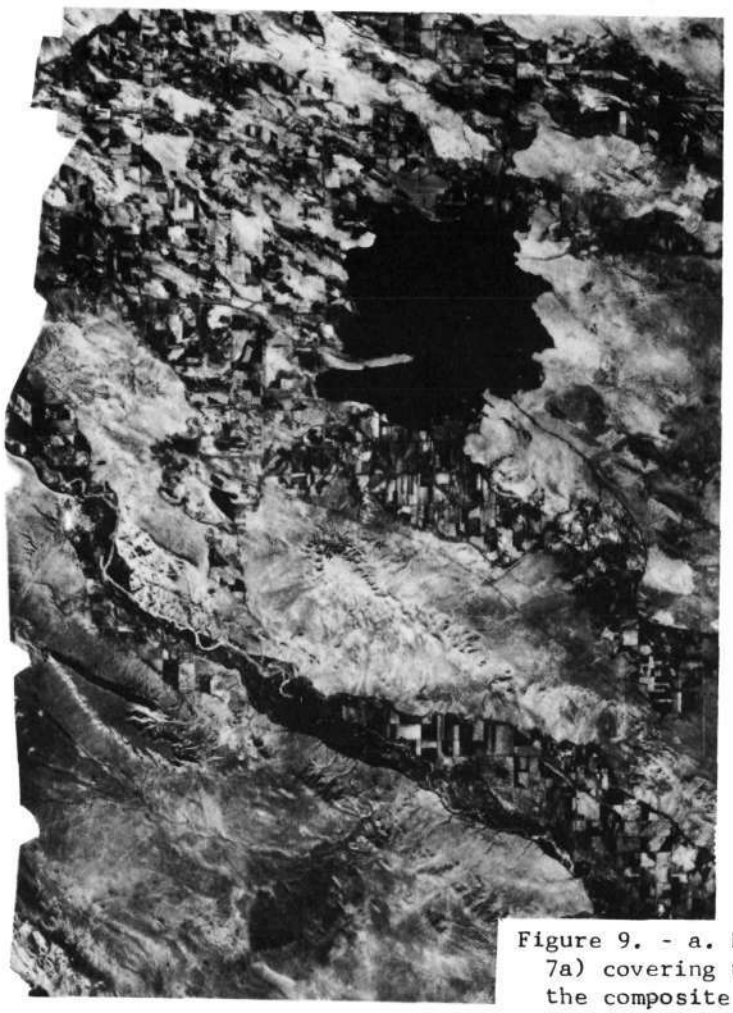

a.~50m

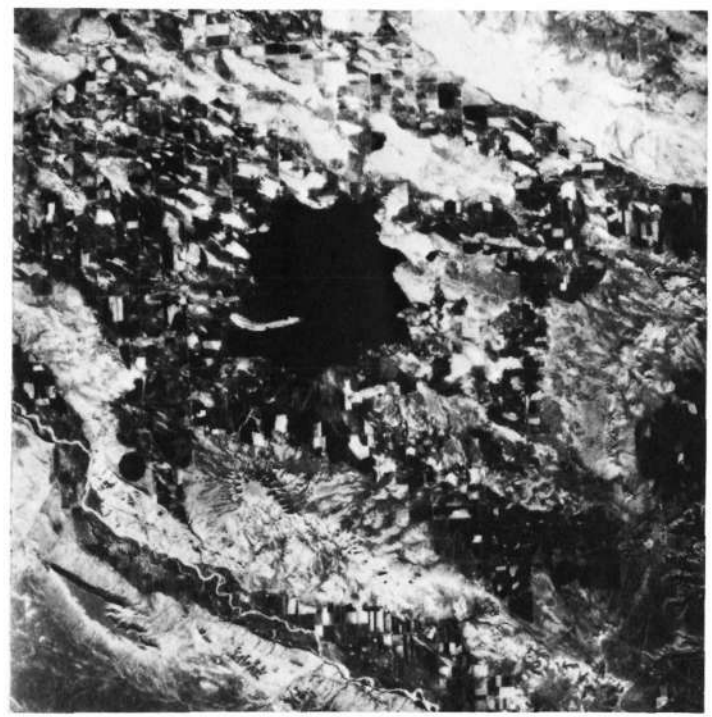

b.~64m

Figure 9. - a. Reproduction of the Aero Service photomosaic (see Figure 7a) covering the region around Ocean Lake, Wyoming (upper left edge of the composite photomosaic). Vertical dimension of photo is equivalent to 25 km on the ground; b. A red band U-2 photo that includes Ocean Lake and its surroundings. This and succeeding photos of Ocean Lake have been degraded by the technique described in the text. Stated resolutions refer to images as printed.

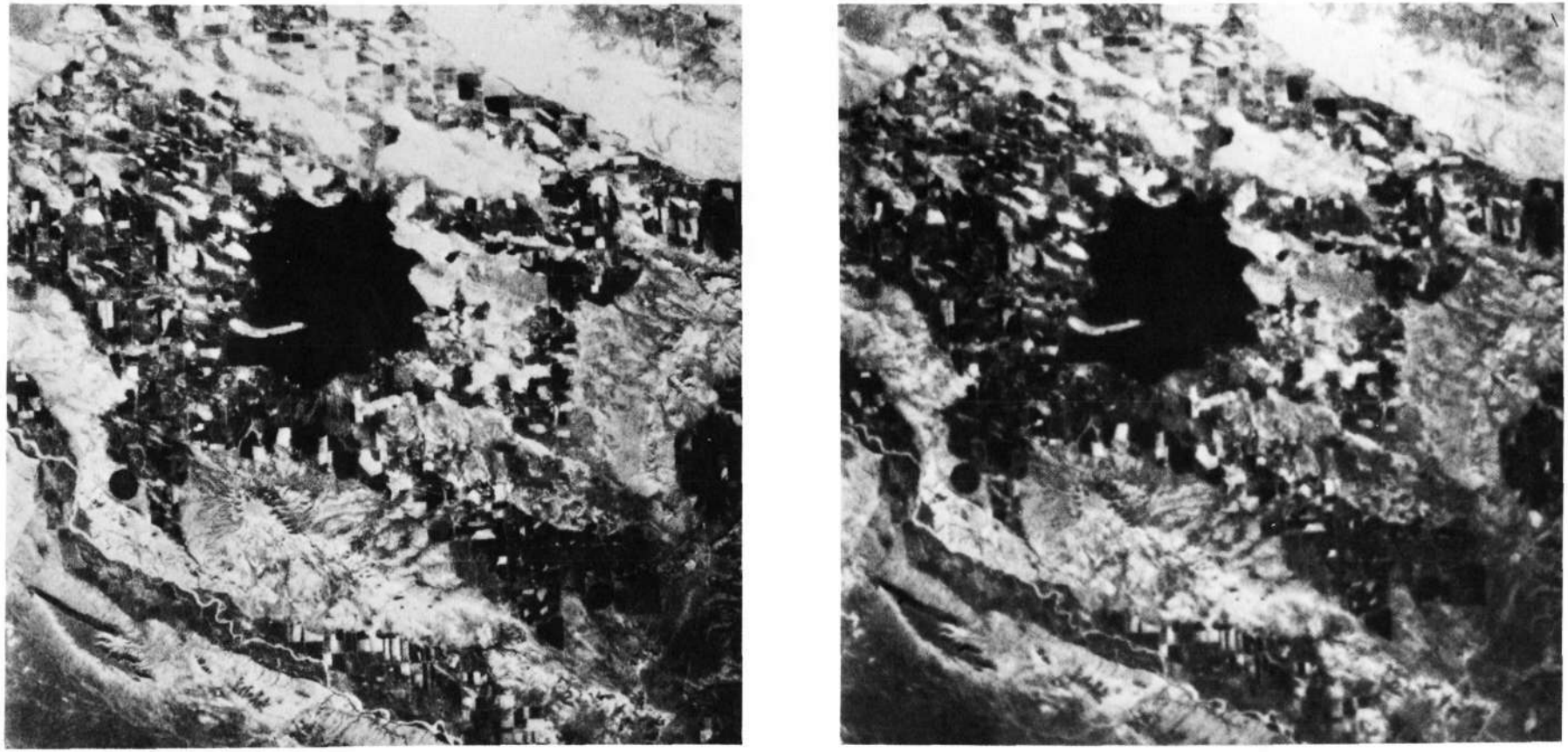

a.~120m

b.~260m

Figure 10. - a. U-2 photo of Ocean Lake region with resolution degraded to 120 meters; b. Same scene with resolution now at 260 meters.

a. Green

b. Red

c. IR

Figure 11. - U-2 photographs of the Ocean Lake, Wyoming region as imaged on the October 21, 1971 flight. a. Green band; b. Red band; c. IR band. See text for discussion of principal features in each multispectral image.

a. Green

b. Red

c. IR

Figure 12. - U-2 photographs of area east of Split Rock and north of Lamont in south-central Wyoming (see third photo from right along base of Figure 8) a. Green band; b. Red band; c. IR band. Edge of Ferris Mountains visible at lower left corner. The Sweetwater River crosses from left to right and part of the Granite Mountains (note joints) appear above the river.

Figure 13. - Composite photomosaic (made by Allied Research Corp.) of the Chesapeake Bay region, using individual frames (red band) obtained from the September 15, 1971 U-2 flight from NASA Wallops Island. Note Washington, D.C. near center left edge; Cape May appears at the upper right corner. See text for equivalent ground dimensions. Resolution in this reduced version estimated to be approximately 60 meters.

a. Green

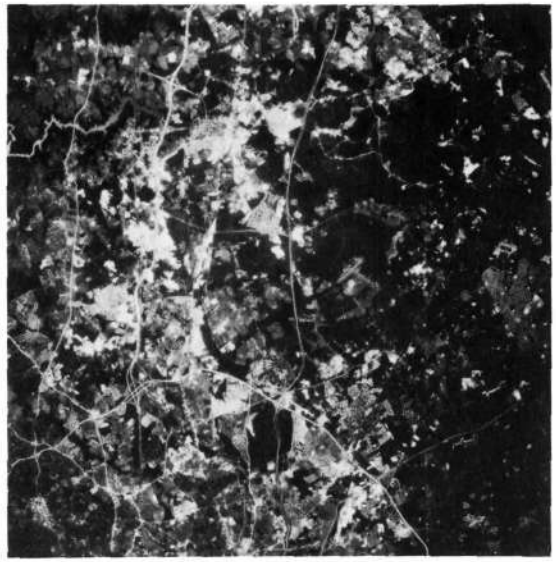

b. Red

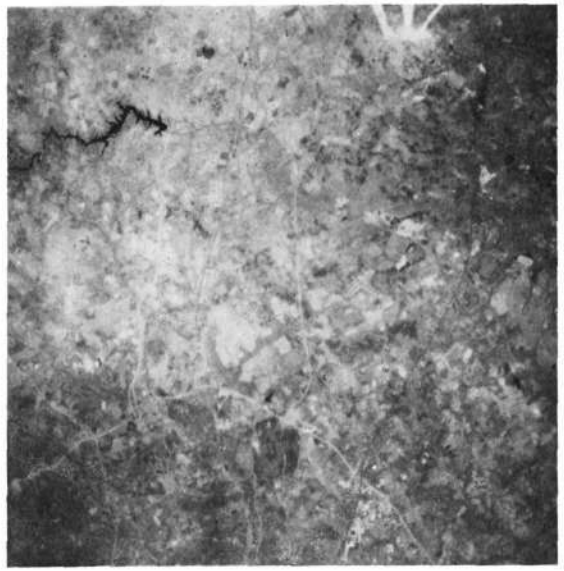

c. IR

Figure 14. - Three multiband frames (a. Green; b. Red; c. IR) obtained during the U-2 flight of September 15, 1971, showing an area northeast of Washington D.C. (near center left edge of Figure 13). The Washigton Beltway (appearing as part of a loop) is seen in the lower left and center; the Washington-Baltimore Parkway runs through the center, bottom to top. The community of Belair (Bowie) is shown at the right center edge. See text for discussion of differences indicated in the band images.

a.

b.

Figure 15. - a. A portion of the red band frame (September 15, 1971 U-2 flight) showing a part of the Choptank River estuary near its mouth at Chesapeake Bay, the town of Cambridge, and the farmland along Highway 50 running north (photo appears just above and left of the center of Figure 13); b. The same scene rendered in false color IR by combining the Green, Red, and IR images on a color additive viewer (see text).

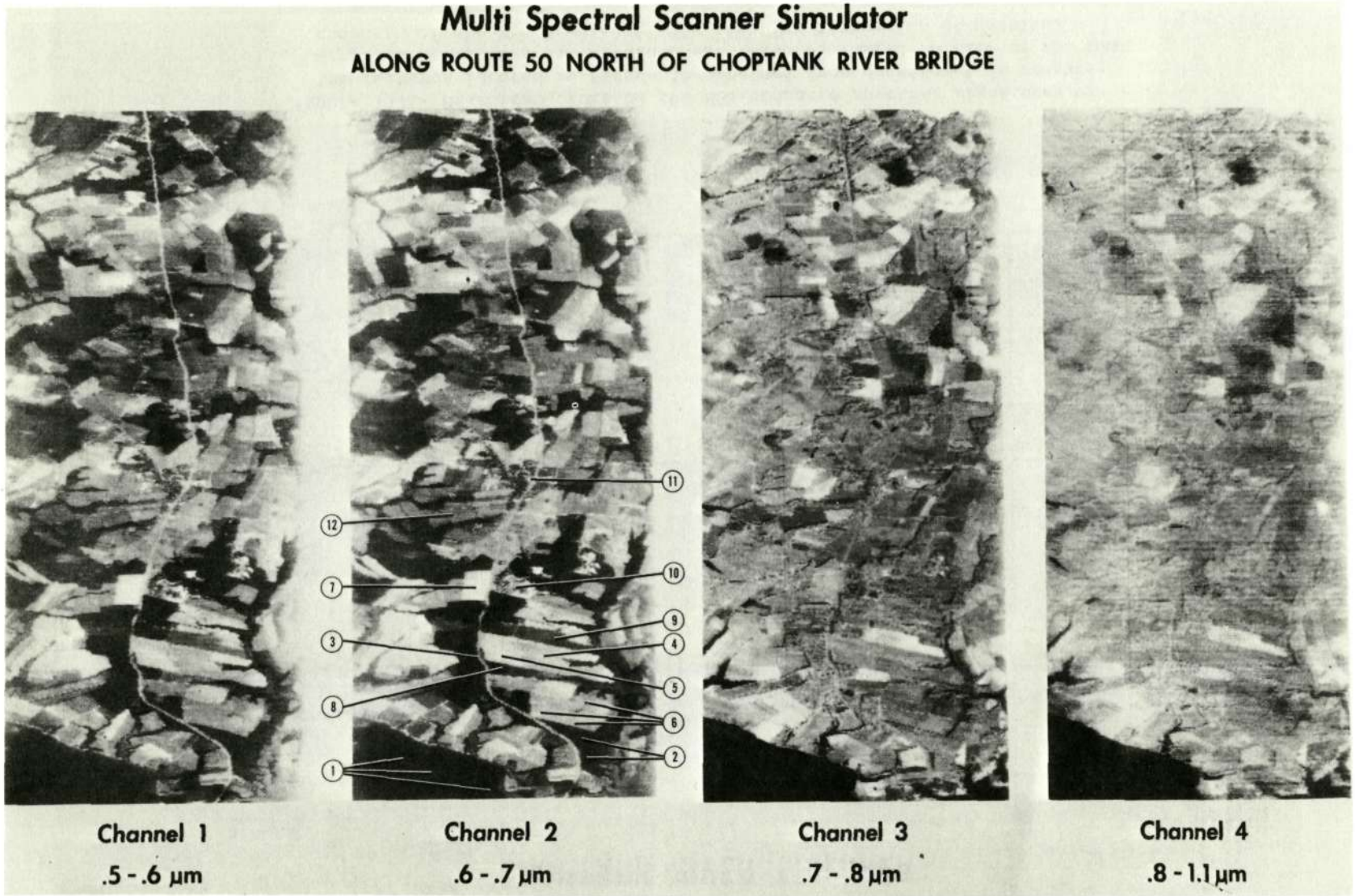

Figure 16.-A segment of the farmland along Highway 50 north of the Choptank River bridge (see Figure 15) as imaged in each of four channels by a prototype ERTS multispectral scanner (MSS) flown on a DC-3 in the fall of 1971. The numbers associated with the channel 2 image refer to various agricultural fields and other features identified in Figure 17.

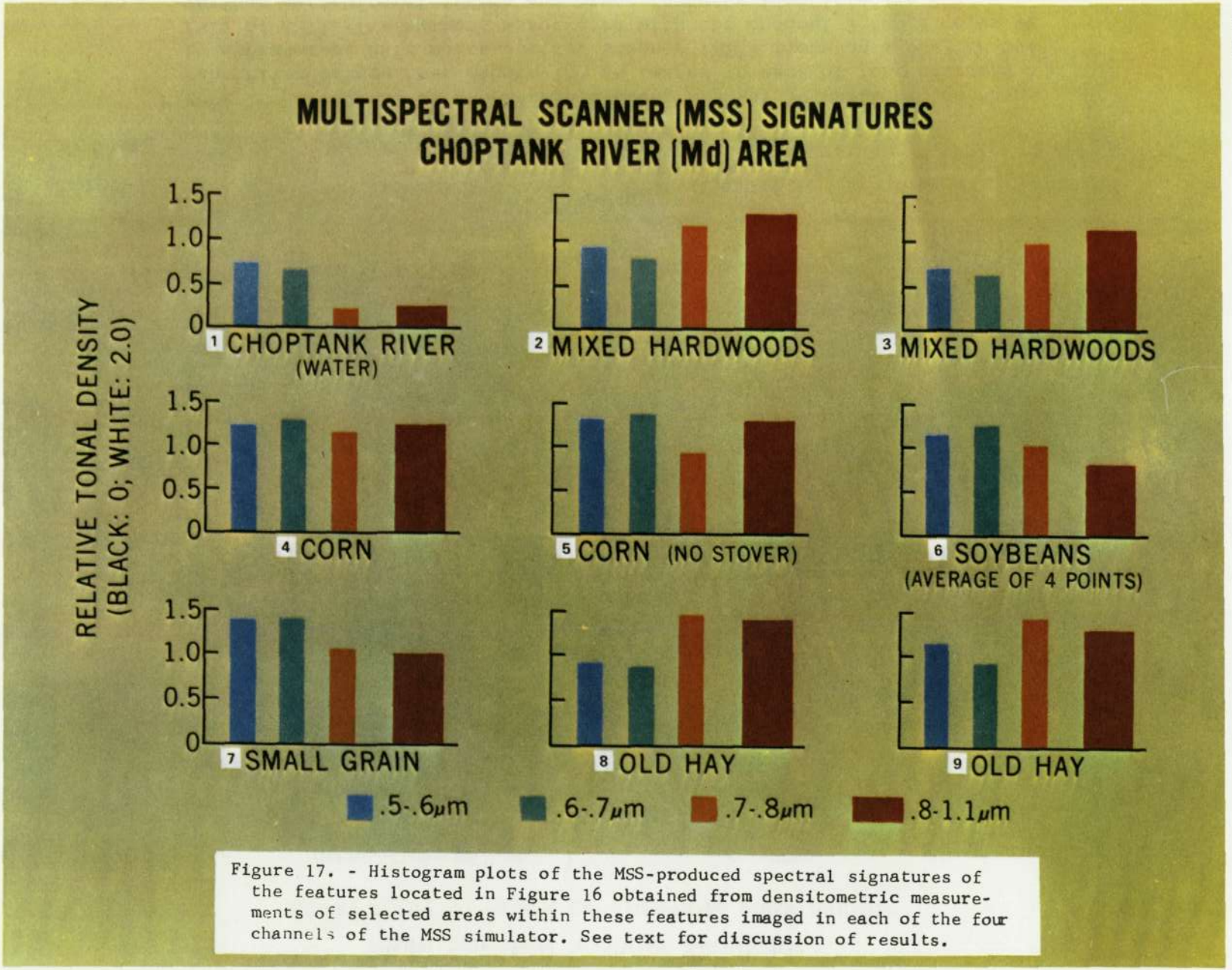

Figure 17. - Histogram plots of the MSS-produced spectral signatures of the features located in Figure 16 obtained from densitometric measurements of selected areas within these features imaged in each of the four channels of the MSS simulator. See text for discussion of results.

a. Green

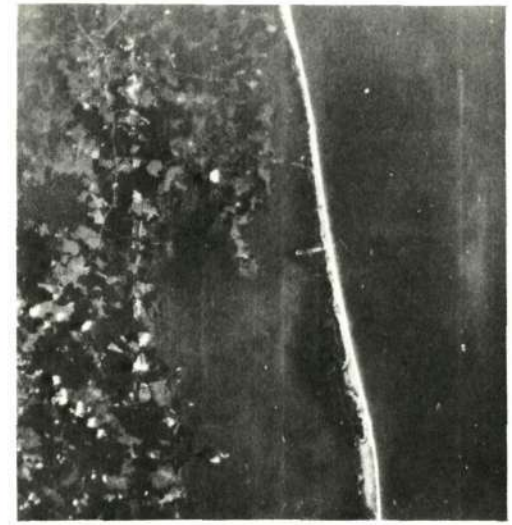

b. Red

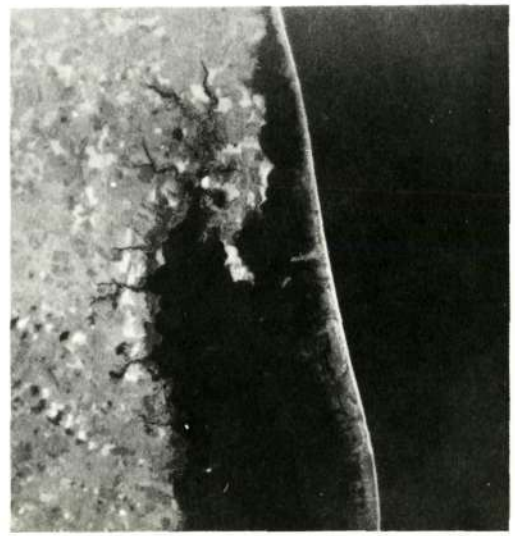

c. IR

Figure 18. - A section along the Atlantic Ocean coastline of Maryland, south of Ocean City, showing the northern end of Assateague Island and Chincoteague Bay. This set of U-2 multiband photos (a. Green; b. Red; c. IR) from the September 15, 1971 flight appears just above the center right edge of Figure 13.

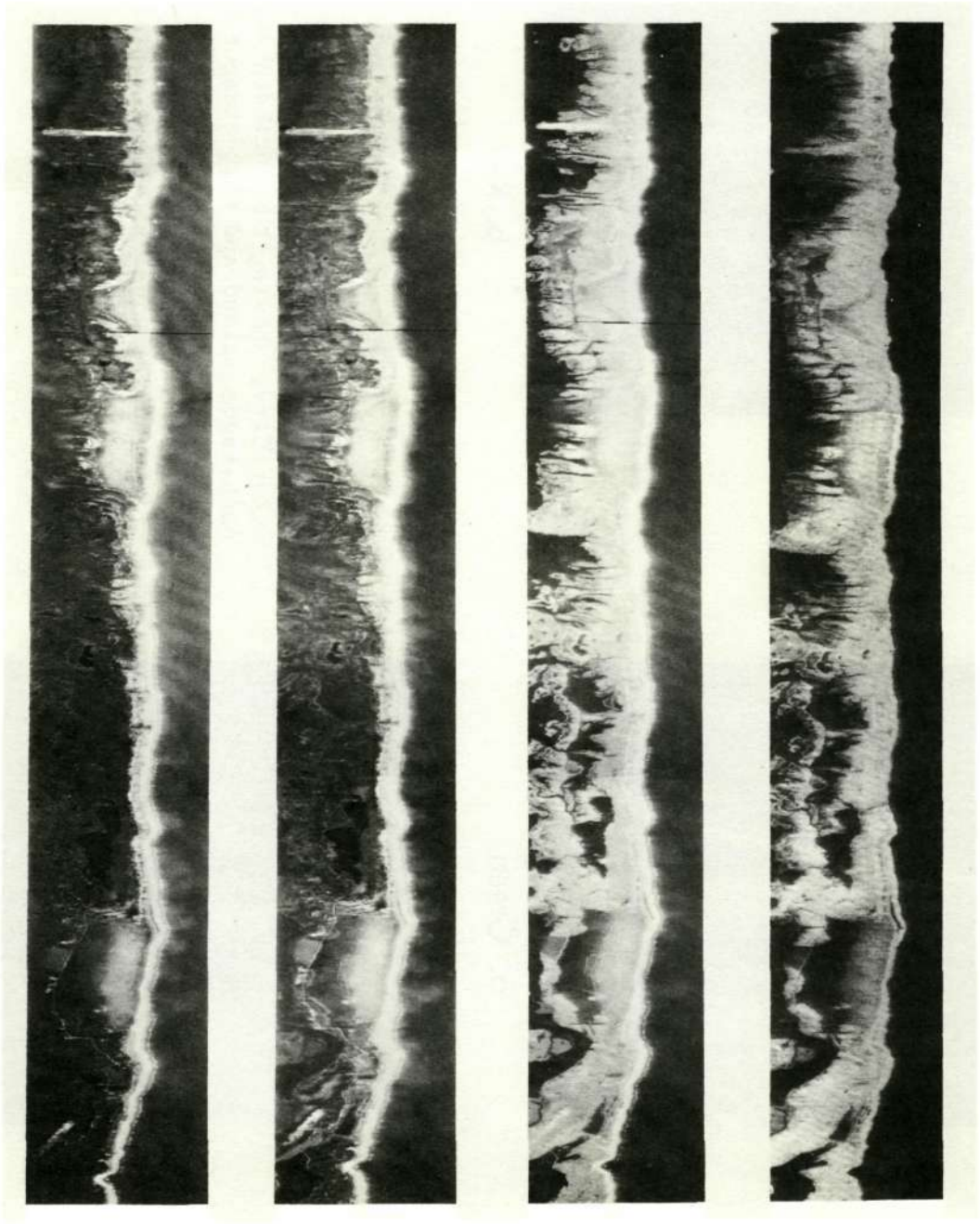

Figure 19. - Images made from the four channel data obtained by the multispectral channel simulator during a flight over the Assateague Island offshore bar. The top half of each image corresponds to the lower portion of the island shown in Figure 18.

SECTION 8

MICROWAVE EMISSION MEASUREMENTS OF SEA SURFACE ROUGHNESS, SOIL MOISTURE, AND SEA ICE STRUCTURE

by

P. Gloersen, T. Wilheit, and T. Schmugge
Laboratory for Meteorology
and Earth Sciences
Goddard Space Flight Center
Greenbelt, Maryland 20771

In order to demonstrate the feasibility of the microwave radiometers to be carried aboard the Nimbus V and VI satellites and proposed for one of the Earth Observatory Satellites, remote measurements of microwave radiation at wavelengths ranging from 0.8 to 21 cm have been made of a variety of the Earth's surfaces from the NASA CV-990 A/C. The instrument complement has been described elsewhere[1]. Brightness temperatures of sea water surfaces of varying roughness, of terrain with varying soil moisture, and of sea ice of varying structure were observed. In each case, surface truth information was available for correlation with the microwave brightness temperature. Radiation at 1.55 cm was mapped with an image-forming radiometer over these areas, while radiation at the other wavelengths was measured at fixed viewing angles with respect to the aircraft, primarily to determine the wavelength dependence of the phenomena mapped at 1.55 cm.

The physical basis for the interpretation of such measurements is given by the equation shown in Figure 1. In this wavelength region, the Rayleigh-Jeans approximation holds for all cases of interest, therefore the signal received by the radiometer is proportional to the brightness temperature of the source. The surface contribution is shown in the brackets; it is reduced before arriving at the radiometer by the atmospheric transmissivity, τ. It consists of an emission term given by the product of the emissivity and thermometric temperature of the surface, and a reflection term given by the product of the surface reflectivity, or one minus the emissivity, times the sky temperature as viewed from the surface, averaged over the hemisphere. The last term is the contribution from the atmosphere, as viewed from the spacecraft or aircraft; it is negligible for the low altitude data to be discussed in this paper. We shall concentrate on only one of the factors shown in this equation, the emissivity ε, which is a function of the wavelength λ, the look angle β, and various surface characteristics i.

The general nature of such surface characteristics variation is illustrated in Figure 2 for the measurements to be discussed here. In each case we have plotted the emissivity normal to the surface as a function of frequency in gHz : a few select wavelengths are indicated on the abscissa for reference. For the ocean surface, the effect of surface winds disturbing the sea is to increase the emissivity of the surface. In the case of terrain, the effect of wetting unvegetated soil is to lower the emissivity of the surface; heavily vegetated terrain is uniformly high in emissivity over a wide range of moisture conditions in the soil. For sea ice, first year thick sea ice is a glossy medium which has high emissivity as long as the thickness exceeds one wavelength, that is, as long as it is optically thick. Multi-year ice, on the other hand, is a good dielectric, and would be quite transparent to the microwaves except for the presence of many scattering centers such as unfilled brine cells; thus, it becomes a good diffuse reflector and, therefore, a poor emitter at least at the shorter wavelengths. First year thin ice, that is, less than a wavelength thick, represents a third type for which the emissivity lies somewhere in between and the thick first year ice curve, depending on the thickness of the ice. The calm sea curve is repeated on this graph. Intermediate emissitivies are, of course, obtained also when open water is observed in the ice pack in non-beam-filling situations, but of course, in all channels at once, as opposed to the wavelength dependences seen when viewing various ice types. In the remainder of the paper, we shall be a bit more quantitative in discussing these various pheonmena.

Let us discuss sea ice in more detail. Figure 3 is a view of the Point Barrow, Alaska, test area, showing sea ice as blue or yellow, snow-covered terrain as white or pink, and open water as black, in the order of decreasing brightness temperature. Further north, on the Arctic ice canopy, two different types of sea ice were observed, as shown in Figure 4. This is the same area Bill Campbell discussed in an earlier paper at this meeting, describing the activities at AIDJEX Camp 200, located near the center of this image. This view is a computer-produced mosaic of five separate parallel tracks flown by the aircraft over the test area at an altitude of 10 km: the area shown is about 70 x 80 km in extent. The two ice types shown here are first year thick, as indicated by the yellow and orange colors, and multi-year, as indicated by the blues; we have a high degree of confidence in this interpretation in view of the surface observations available to us thru the AIDJEX activities. The large multi-year ice floe on which Camp 200 was located can be seen to be segmented into three large pieces, separated by first year ice in the refrozen leads. Evidently, this large flow had begun to break up late in the last summer season, but had been frozen into this position by the formation of new ice. A refrozen polynya can be seen at the apex of the inverted v-shaped pattern of the refrozen leads.

Very close scrutiny of the high altitude photography revealed the presence of these features also, thereby supporting this interpretation. With the total cloud cover common to this area, it would, of course, be impossible to see the surface visually, with photography, or, for that matter, infrared or visible imagery in general. On the following day, the area was completely covered by clouds. However, on that next day, the microwave view of the area was substantially unchanged, as shown in Figure 5. If you look closely you can also see about an 8° shift in temperature between these two scenes; as we found out on our low-level passes, this was mostly due to a corresponding change in surface temperature. Some multi-spectral data were obtained for these two ice types as the aircraft took a low altitude pass starting in the northeast quadrant of the scene, passing over the AIDJEX and crossing the ice floe in a southwesterly direction. The results are shown in Figure 6. The edges of the ice floe are clearly shown; the spikes appearing on the ice floe data result from a leg of the v-shaped refrozen lead (actually several refrozen leads when viewed at the higher resolution shown here). As indicated earlier, the contrasts of this particular feature diminish with frequency. Our on-board infrared radiometer indicated surface temperatures to be constant within $\pm$ 5°K over a good portion of this track, independent of ice type and in agreement with thermometric measurements of Camp 200. Figure 7 shows evidence of a third type of ice, first year thin. The ice represented by the largest dip at 1.42 gHz is the order of a wavelength thick, or less, so that the ocean water can be partly seen through the sea ice; in this particular example, the ice was evidently the order of 10 cm thick, since the shorter wavelengths show no corresponding decreases in brightness temperature. As you can see, this effect diminishes as frequency increases; for the 1.42 gHz or 21 cm case, the largest dip shown goes about half way to the calm sea limit; at a wavelength of 11 cm, the same feature dips only about 1/4 of the way. The rough estimate of ice thickness quoted is based on the assumption that the e-folding length of the absorption in the ice is about a wavelength. Careful inspection reveals that the dips shown at longest wavelengths correspond to small peaks at the shortest wavelengths; these were identified from the 1.55 cm image of the area as first year ice between patches of small multi-year floes.

Next we will discuss the changes in emissivity resulting from variations of soil moisture. The image formed from the data obtained during a low altitude pass over an agricultural area near Phoenix, Arizona is shown in Figure 8. In spite of the image distortion resulting from the low altitude of the pass and the low scan rate, the pattern of the individual cultivated fields can be recognized in the rectangular patterns displayed here. Dry fields are indicated as red rectangles,

very wet fields as black rectangles, and intermediate cases as yellow, green, and blue. A more quantitative presentation of such data is given in Figure 9, obtained from one of the other radiometers at a fixed viewing angle. Here the brightness temperature is plotted against the percent soil moisture by weight. According to the on-board infrared radiometer, the surface temperature corresponding to these data was 291°K, with a maximum deviation of + or -4K, hence the maximum emissivity, at the inqercept, is about 0.96. The summary of this and some data taken at other wavelengths is shown in Table I. Noteworthy here is the gradual decrease in slope with the decrease in wavelength and an uncertainty in the brightness temperature at a given moisture content of 5 - 6K. The variation in the intercept is more due to errors in the absolute temperature calibrations of each instrument than anything else.

We now change the topic to some sea surface observations, taken entirely at the 1.55 cm wavelength. These results have been published but they are included here for the sake of completeness. The observations are summarized on the graph shown in Figure 10, where we have plotted brightness temperature changes vs. sea surface winds. As can be seen, the brightness temperature, and hence the emissivity, was observed to increase linearly with wind speed at the surface above a threshold of about 7 m/sec. This increase has been interpreted to be due largely to the presence of foam to varying extent at wind speeds above this threshold, as indicated by the data in the Figure 11. The segments of data shown here are for increasing wind speed, going from left to right. The large spikes that appear with increasing frequency as the wind speed, or average brightness temperature, increases are <u>not</u> noise spikes, but are due to small patches of foam, observed also on the photographs of the sea surface taken at the same time. In Figure 12 the correlation betwee the % foam cover measured from photographic data and the radiometric data is shown. Again, the relationship is linear, within the available measuring accuracy. For comparison, we show also a straight line from the origin to a data point obtained from a foam patch that was 100% beam-filling, along the lower part of which the results of some computations from Cardone's whitecap model also fall.

In summary, we have demonstrated the utility of passive microwave radiometry in determining ocean surface wind speeds, at least for values higher than 7 meters per second. In addition, we have shown that such radiometric signatures have been used to determine soil moisture in unvegetated terrain to within five percentage points by weight. Finally, it has been shown that we can distinguish between first year thick, multi-year, and first year thin sea ice by observing their differing microwave emissivities at various wavelengths. We can also determine the extent of sea ice coverage in the polar ice canopies; the amount of open water present in the Arctic polar ice canopy apparently

has profound effects on the long-term weather in our part of the Northern Hemisphere[1,3,4].

Our future plans include continuation of these aircraft missions to improve our data base, and initiating satellite-borne instrumentation to extend our studies to a global scale. In 1973, we are scheduled to fly a 1.55 cm imager on Nimbus V; a year later, a 0.8 cm imager with dual polarization and constant incidence angle is scheduled to be carried on Nimbus VI. Beyond that, we are working on a multichannel microwave radiometer covering the wavelength range from 0.8 to 6 cm to be flown on the follow-ons to the Nimbus and ERTS satellite series, and on tehcniques for improving the present surface resolutions with a multi-beam approach.

REFERENCES

1. T. Wilheit, J. Blinn, W. Campbell, A. Edgerton, and W. Nordberg, "Aircraft Measurements of Microwave Emission from Arctic Sea Ice", to be published in Remote Sensing of Environment (1972).

2. W. Nordberg, J. Conaway, D. B. Ross, and T. Wilheit, "Measurements of Microwave Emission from a Foam-Covered, Wind-Driven Sea", J. Atmos. Sci., 28, 429-435 (1971).

3. F. I. Badgley, "Heat Budget at the Surface of the Arctic Ocean", Proc. of the Symp. on the Arctic Heat Budget and Atmospheric Circulation, edited by J. O. Fletcher, The Rand Corporation (RM-5233-NSF) (1966).

4. W. Wittmann and J. Schule, "Comments on the Mass Budget of Arctic Pack Ice", Proc. of the Symp. on the Arctic Heat Budget and Atmospheric Circulation, edited by J. O. Fletcher, The Rand Corporation (RM-5233-NSF) (1966).

Table I

LINEAR REGRESSION RESULTS
MICROWAVE BRIGHTNESS TEMPERATURE
VS
SOIL MOISTURE CONTENT

WAVELENGTH	INTERCEPT	SLOPE	STANDARD ERROR OF ESTIMATE
21 CM	280	-2.22	6.22
6 CM	307	-1.65	5.46
1.55 CM	281	-1.44	4.34.
0.8 CM	292	-1.16	5.50

$$T_{B_{H,V}} = \tau_o \left\{ \epsilon_{H,V}(\lambda, \beta, \gamma_i) T_T + \left[1 - \epsilon_{H,V}(\lambda, \beta, \gamma_i) \right] \overline{T}_{B_{SKY}} \right\} + T_{B_{ATM}}$$

- $T_{B_{H,V}}$: OBSERVED RADIOMETRIC TEMPERATURE
- τ_o: ATMOSPHERIC TRANSMISSIVITY
- $\epsilon_{H,V}(\lambda, \beta, \gamma_i) T_T$: THERMAL CONTRIBUTION FROM SURFACE
- $\left[1 - \epsilon_{H,V}(\lambda, \beta, \gamma_i) \right] \overline{T}_{B_{SKY}}$: REFLECTED CONTRIBUTION FROM SURFACE (SKY SOURCE)
- $T_{B_{ATM}}$: DIRECT ATMOSPHERIC CONTRIBUTION

$$\left(T_{B_{ATM}} = \int_0^{h_\infty} T_{T_{ATM}}(h) \frac{\partial \tau}{\partial h} \, dh \right)$$

Figure 1 **Microwave brightness temperature as a function of several variables**

SPECTRAL CHARACTERISTICS OF VARIOUS SURFACES

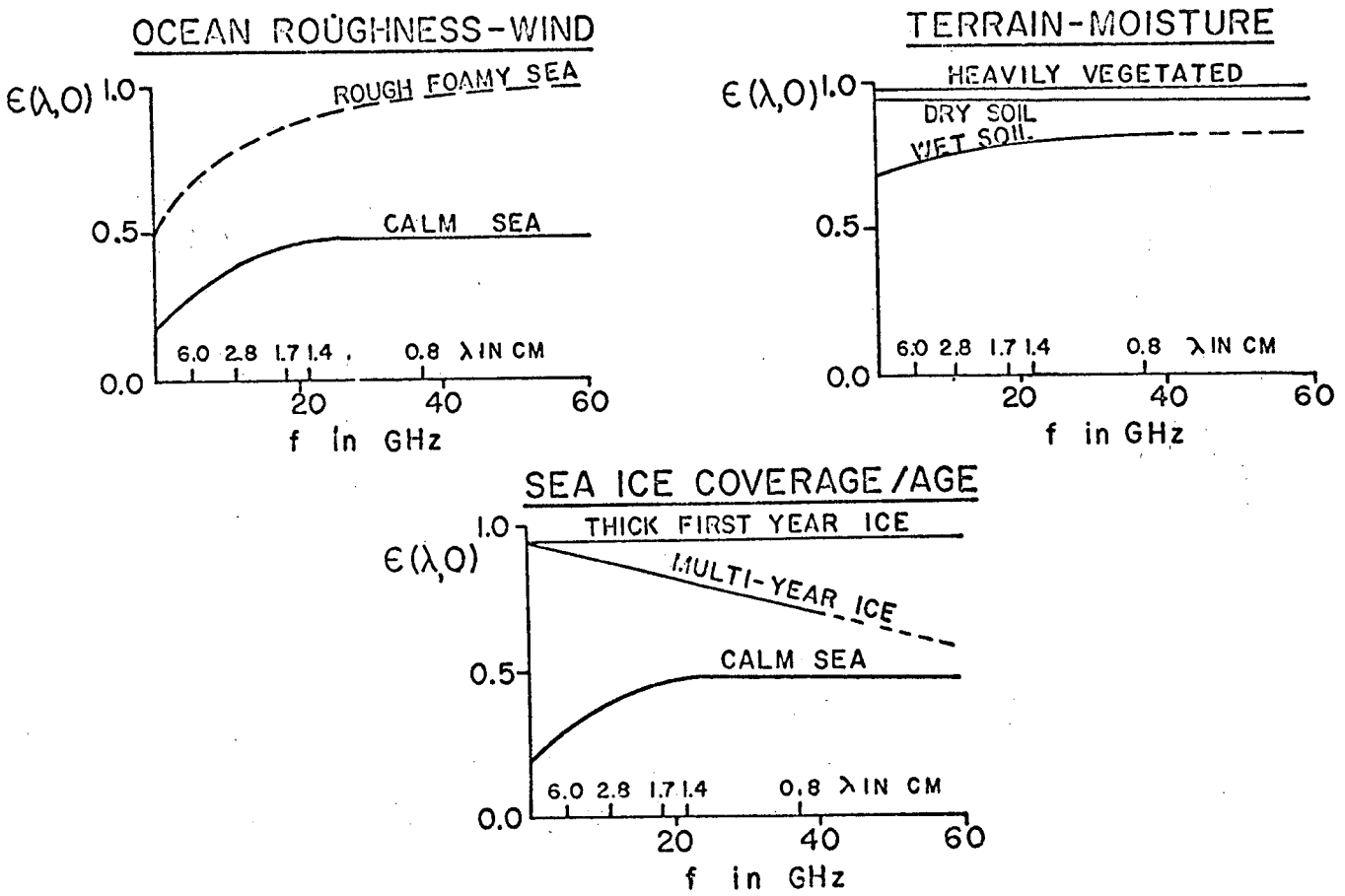

Figure 2 **Spectral variations of the emissivity of various surfaces**

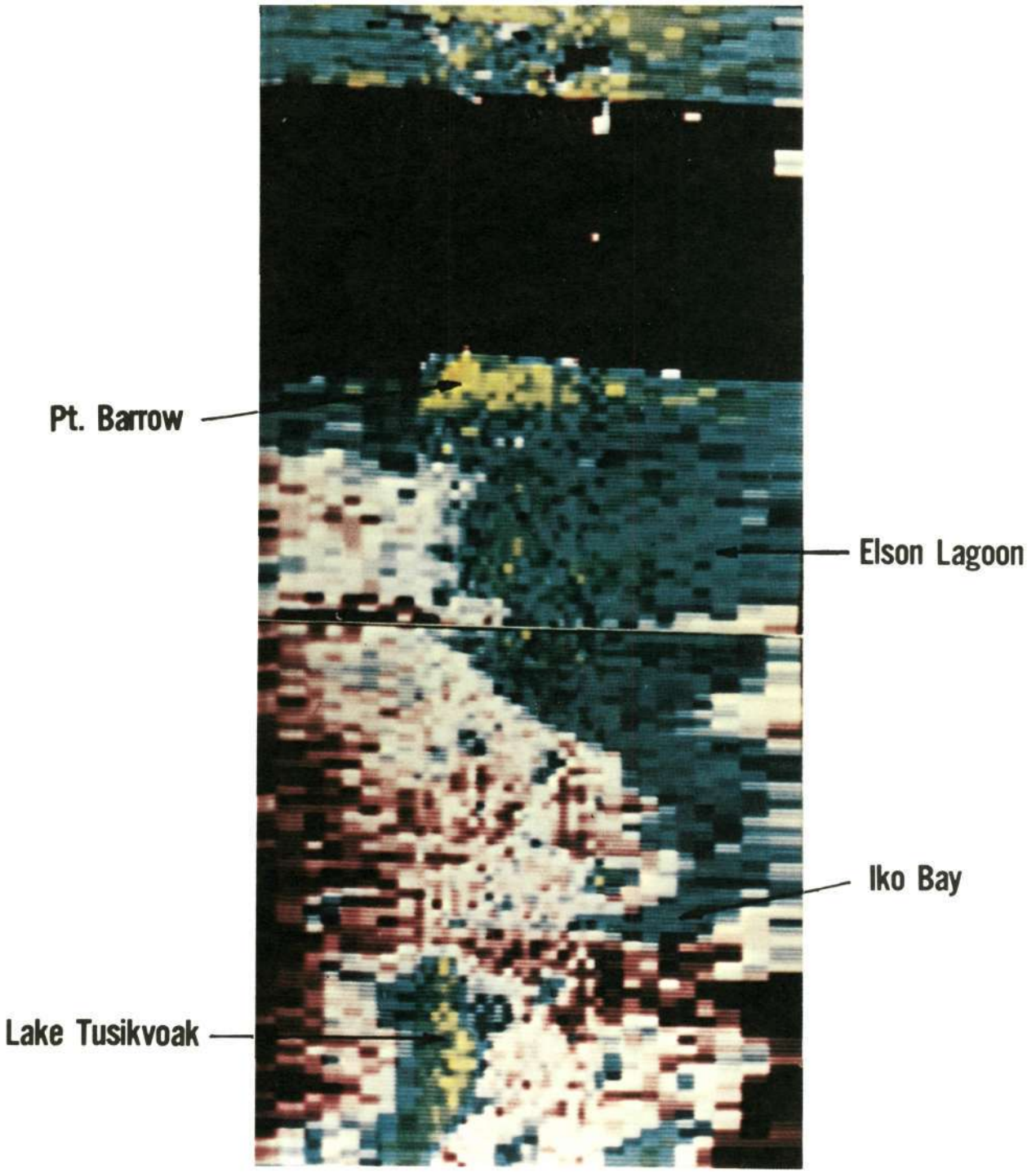

Figure 3 19.35 GHz image of the Point Barrow Test Area

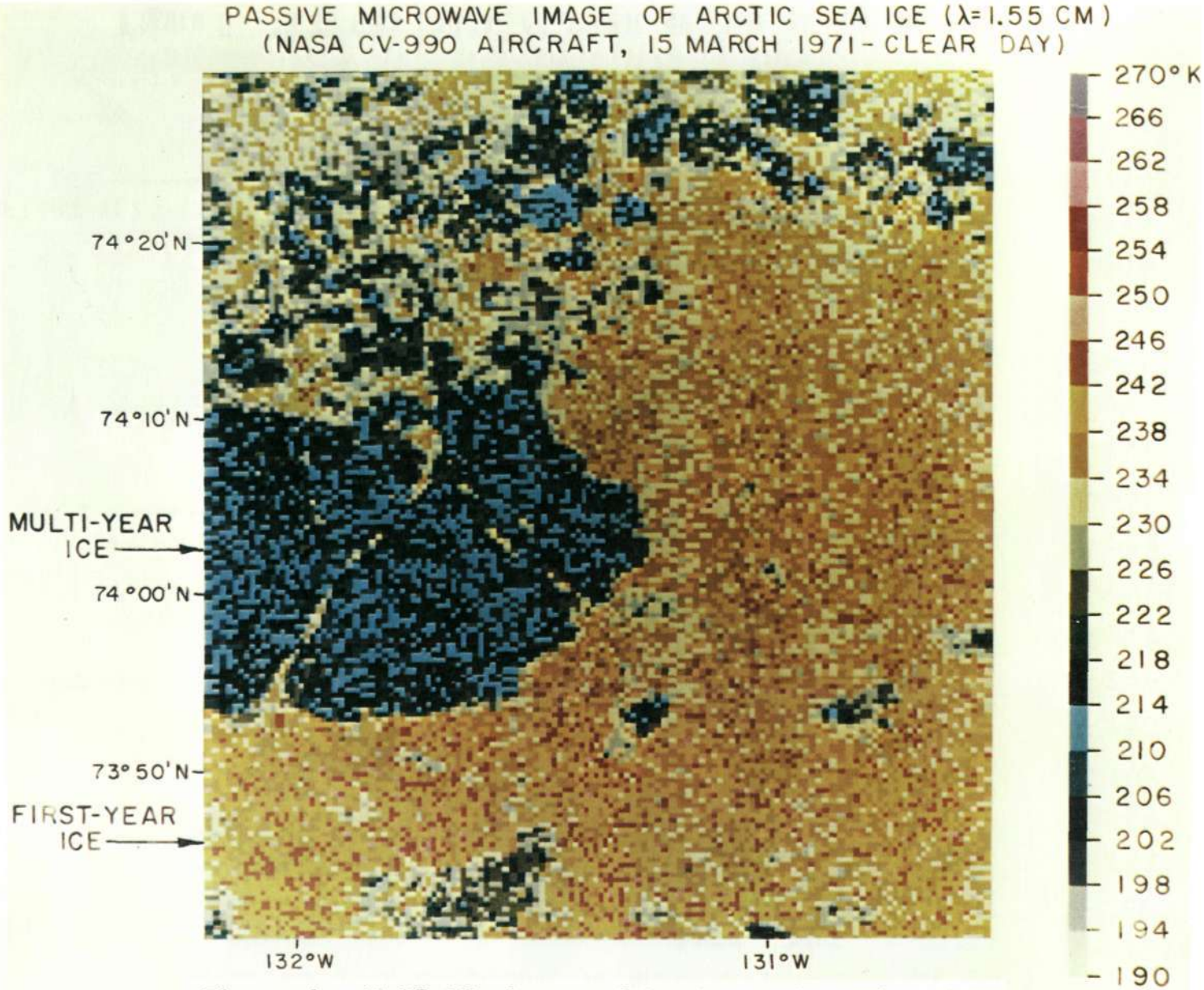

Figure 4 19.35 GHz image of Arctic sea ice, clear day

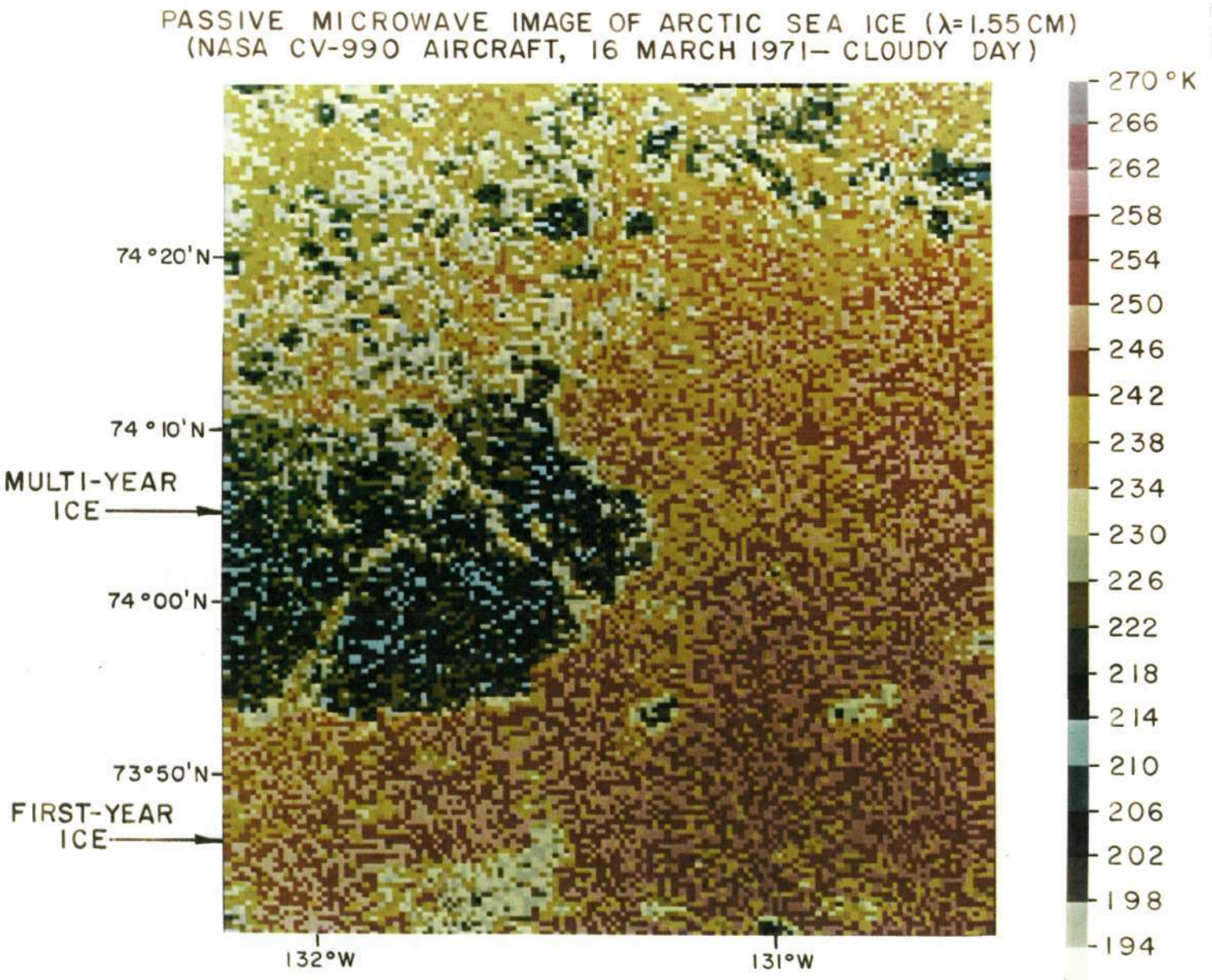

Figure 5 19.35 GHz image of Arctic sea ice, cloudy day

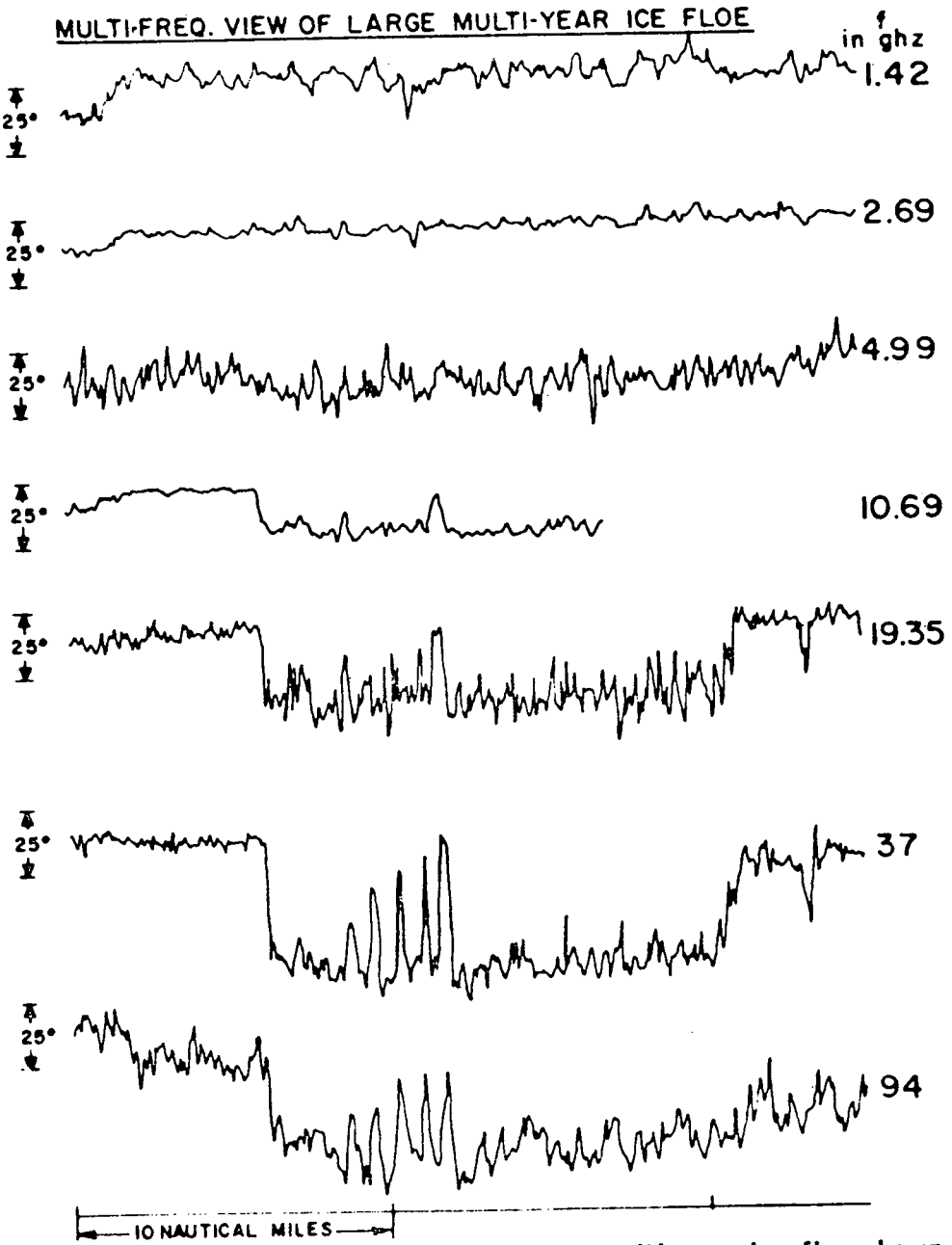

Figure 6 Multispectral view of the large multiyear ice floe shown in Figures 4 & 5; low-altitude pass in a southwesterly direction

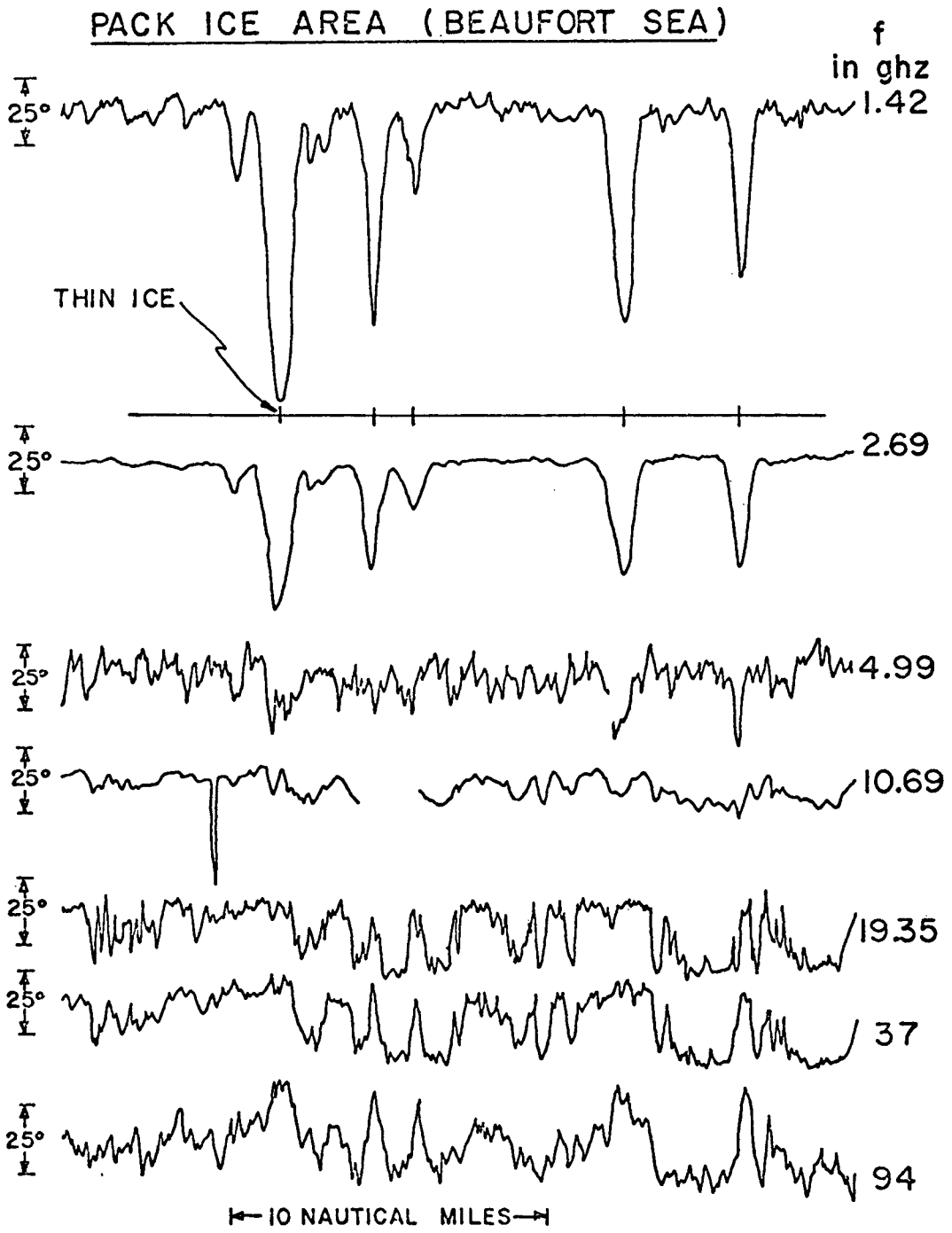

Figure 7 Multispectral view of sea-ice in the Beaufort Sea

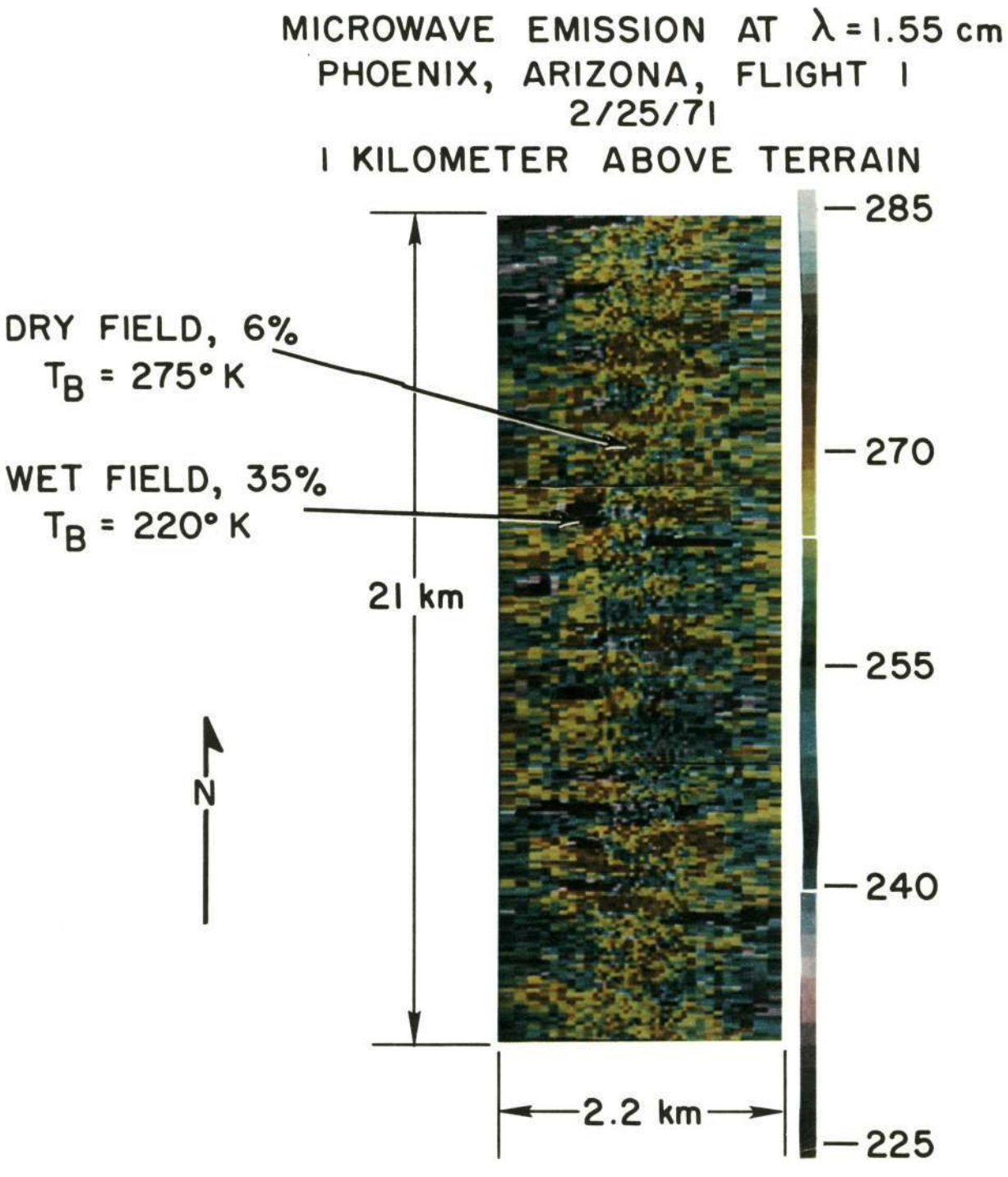

Figure 8 19.35 GHz image of an agricultural area near Phoenix, Arizona

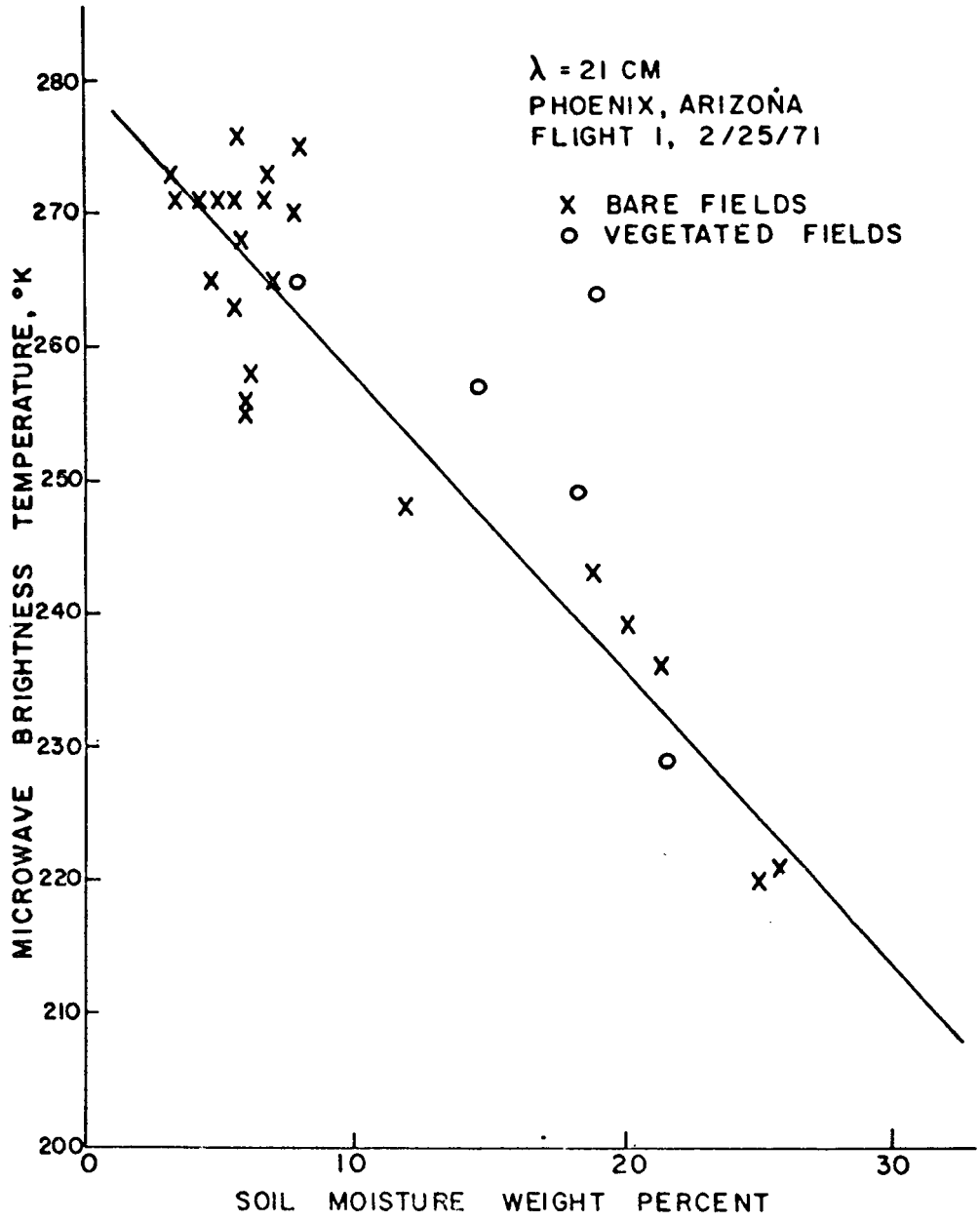

Figure 9 Radiometric temperature vs % soil moisture, by weight at 1.42 GHz

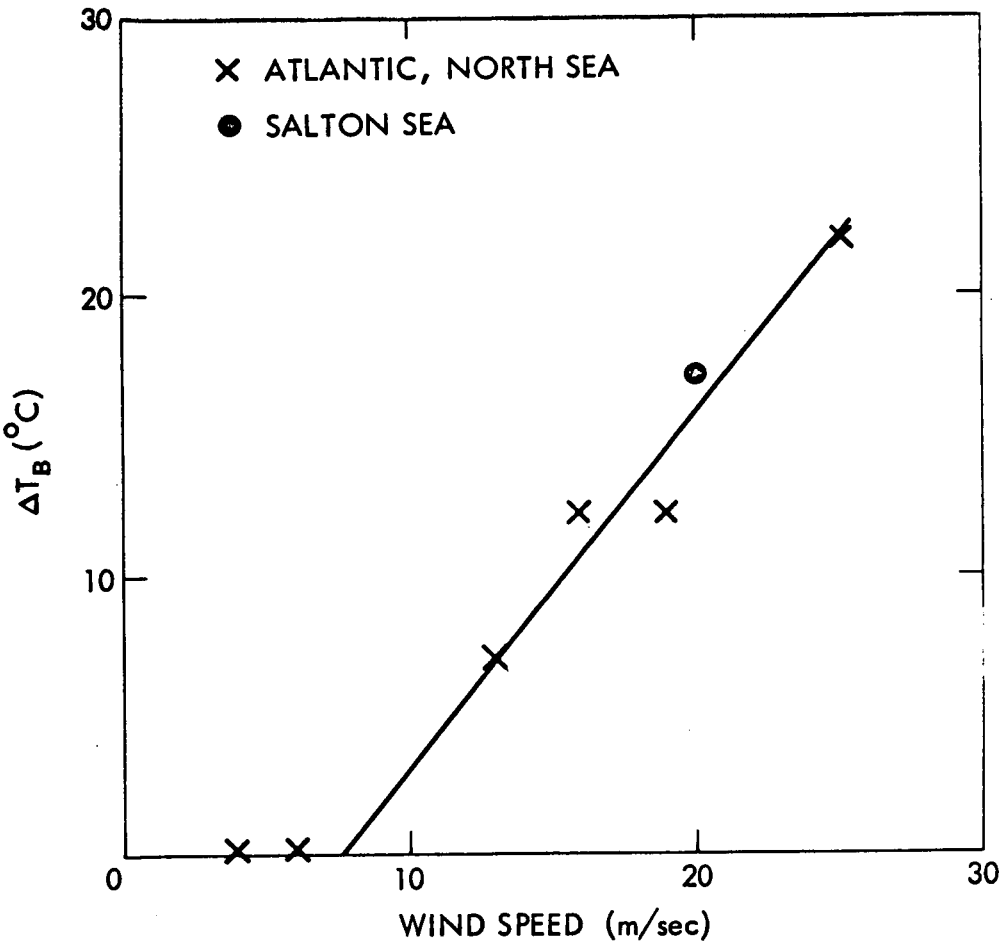

Figure 10

Change in brightness temperature vs wind speed at the sea surface at 19.35 GHz

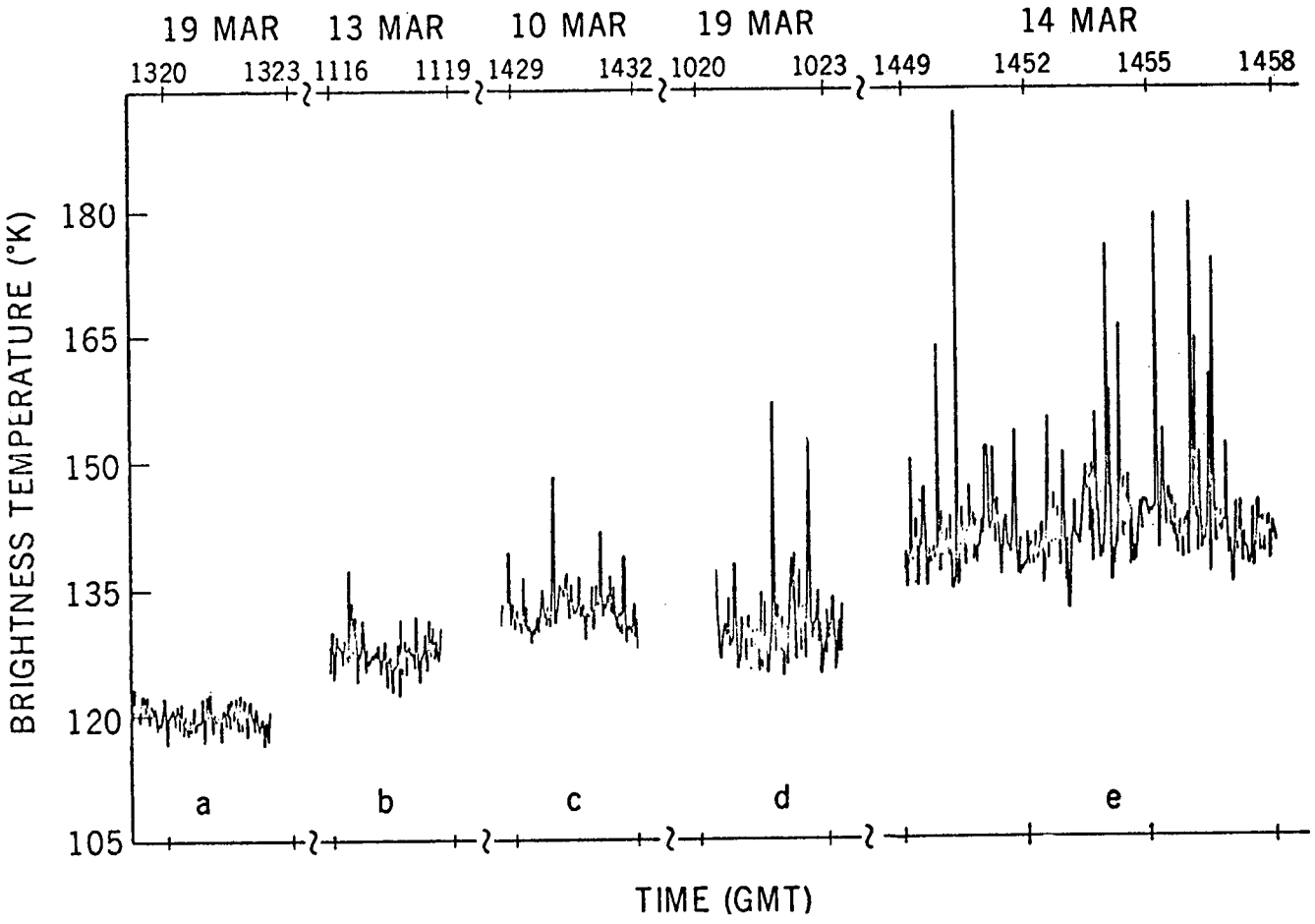

Figure 11 Radiometric temperature records of the sea at 19.35 GHz for various surface wind speeds, increasing from left to right

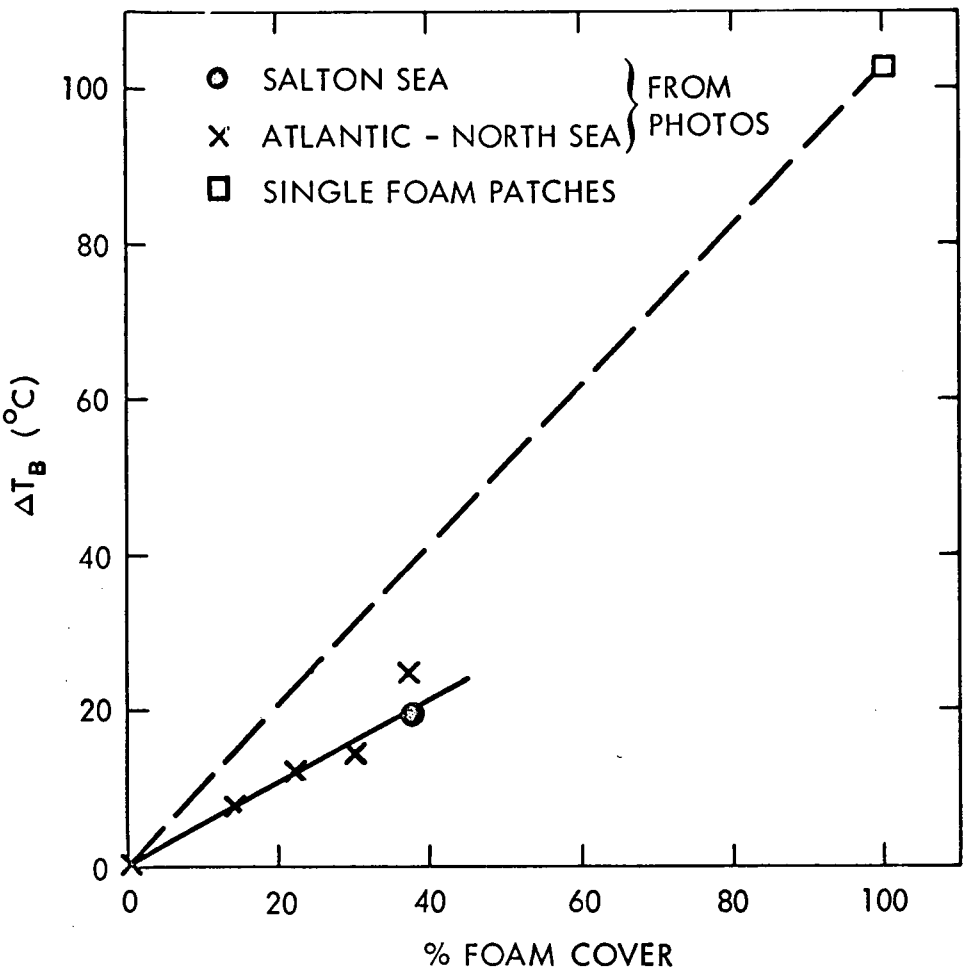

Figure 12

Radiometric temperature of the sea as a function of percent foam cover, as determined by photogrametry

N72-29310

SECTION 9

RADIOMETRIC OCEAN COLOR SURVEYS THROUGH A SCATTERING ATMOSPHERE

by

Robert J. Curran
and
Warren A. Hovis

Laboratory for Meteorology
and Earth Sciences

Goddard Space Flight Center
Greenbelt, Maryland

INTRODUCTION

The color of the ocean surface is strongly dependent upon the amount and type of material suspended in its top layers. Low altitude aircraft spectral reflectance measurements have shown that the color signature of water can be related to the concentration of chlorophyll in the top few meters of water. White in 1969 and Clarke, Ewing and Lorenzen in 1970 presented measurements of the spectral reflectance of the ocean surface for several different chlorophyll concentrations. Some of these spectral reflectance measurements together with a determination due to Ramsey (1968) for water with extremely low chlorophyll concentrations are presented in Figure 1. The measured data plotted here is surface level reflectance versus wavelength in nanometers. For each curve the chlorophyll concentration, in units of milligrams per cubic meter of water, is noted on the left hand portion of the diagram. It may be noted in this figure that as the chlorophyll concentrations increase the reflectance in the blue decreases and the reflectance in the green stays roughly constant. As a result of this change in reflectance with change in chlorophyll concentration, Clarke, Ewing and Lorenzen have suggested that two wavelengths will be an efficient measure of the chlorophyll concentration. The wavelengths suggested by these authors are 460 nanometers and 540 nanometers.

Dr. Hovis of our Laboratory has initiated a series of aircraft flights to measure the spectral reflectance of ocean waters containing various concentrations of chlorophyll. The first of these flights occurred during August 1971 and was made off Santa Catalina Island

near southern California. During this set of measurements two distinct values of chlorophyll concentration were encountered. The color ratios and chlorophyll concentrations measured are shown in Figure 2. This figure shows the relationship between the color ratio and the chlorophyll concentration in millgrams per cubic meter. The low level aircraft measurements made off southern California are indicated by the circled-crosses. Previously existing data values are indicated by symbols corresponding to the previously mentioned reference. The general relationship between the two variables is indicated by the diagonal line. For low values of the chlorophyll concentration the correlation between color ratio and chlorophyll concentration is not satisfactory. However, it should be noted that some of this problem is related to the difficulty of measuring the low chlorophyll concentrations and also some of the difficulty can be attributed to the presence of other particulates suspended in the water. The increased turbidity of the water obscures the lower values of color ratio more easily. More measured data is required to define the relationship satisfactorily.

The data shown in this slide pertain to low altitude aircraft measurements and presumably should be free of the effects of atmospheric transmission losses. Because of the interest in observing the global distribution of the chlorophyll containing phytoplankton it is anticipated that scanning satellite borne radiometers will be used to collect data. To simulate the problems one may encounter in measuring ocean color from satellite altitudes further aircraft measurements have been made at higher altitudes.

Figure 3 gives a comparison between the nadir spectral radiance measured at very low and high altitudes. These measurements were made for a solar zenith angle of approximately 60 degrees. The high altitude measurement made at 14.9 kilometers has more than two thirds of the atmosphere below it. In general the radiance is much larger at the high altitude because very little of the incident solar irradiance has been attenuated before reaching this level. In comparing the measurements made at two different altitudes, the enhanced atmospheric reflectance at the shorter wavelengths is very much in evidence. This wavelength dependent distortion of the surface level reflectance poses the problem of "how to correct for the light scattered in the atmosphere when observing the surface from satellite altitude?"

METHOD OF ANALYSIS

We have approached this problem by modelling the radiative transfer properties of the atmosphere. Figure 4 gives a schematic representation of the various transfer processes which occur. The

incident solar irradiance may either be scattered in the atmosphere and returned to space or be transmitted to the air-water interface and then be reflected, or finally be transmitted through the interface and then be scattered back by the phytoplankton and particulates which are suspended in the water. It is the radiation which suffers this latter process which contains the spectral information as to the presence of chlorophyll. Because of the high probability of light being scattered or reflected before reaching the turbid water, and also because of the probability of being reflected or scattered before the satellite radiometer; a very small fraction of the incident solar radiation accomplishes this latter process.

We have used a numerical model for the transfer of radiation through a mixed molecular-aerosol atmosphere. The molecular and particulate scatterers in this model are distributed with altitude according to a climatological mean model. The scattering properties of these particulates are further made to correspond to nature. The results of a large number of calculations were parameterized in order to be easily usable for predicting the effects of viewing ocean color through the earth's atmosphere. It was found that the most useful parameter to use in defining the optical state of the atmosphere for a given wavelength and given solar zenith angle, was the aerosol optical depth of the atmosphere. This quantity is directly related to the total number of aerosol particles in a verticle column of atmosphere.

Figure 5 demonstrates the dependence of the reflectance of the atmosphere only on the aerosol optical depth. The two wavelengths chosen further demonstrate the contribution due to the molecular constituents. For aerosol optical depth equal to zero the reflectance is due only to the molecular atmosphere and since the molecular optical depth of the atmosphere is greater for shorter wavelengths shown. As the aerosol optical depth increases in both cases the reflectance is seen to increase.

RESULTS AND CONCLUSIONS

Naturally occurring aerosol optical depths most frequently equal 0.1 or 0.2. For the reflectances given in this graph it is seen that the color ratio for the atmosphere only, is in the interval 0.4 to 0.6 for naturally occurring aerosol optical depths. The radiation returning from the ocean surface level is attenuated before reaching a satellite borne detector. As a result of this attenuation and further because the reflectance of the ocean surface level is a fraction of the atmospheric reflection, the color ratio calculated for the ocean-atmosphere system are only slightly modified by the surface reflectance. Putting this simply the surface level color ratio is obscured

by the atmosphere and forced to be closer to the value of the atmosphere alone when observed at satellite altitudes.

This effect is graphically displayed in Figure 6 where the color ratio at the top of the atmosphere is related to the color ratio at the surface by a family of intersecting lines. Each line corresponds to a different aerosol optical depth extending from a pure molecular atmosphere to an optically dense atmosphere as noted by the values for the aerosol optical depth written along the left-hand margin of the graph. If one knows the optical depth of the atmosphere at the time of a satellite measurement then using a family of curves such as these, one could relate the color ratio at the top of the atmosphere to that at the surface level. Thus, a measurement of the color ratio at the top of the atmosphere can be related to the chlorophyll concentration of the ocean water.

A comparison of the theoretical calculations and the measured data from Santa Catalina Island is given in the table of Figure 7. After correcting for ozone absorption it is seen that the measured and predicted intensities are in close agreement. To improve the quality of the models and to gather more data to support the correlation between surface level color ratio and chlorophyll concentration, several further flights are anticipated for measuring ocean color.

The results of both the experimental and theoretical investigations made to date indicate that satellite borne radiometers can sense ocean color. However, the accuracy to which the chlorophyll concentration can be measured appears to be 0.1 to 0.4 mg/m^3 depending upon solar zenith angles. These accuracies are less than desired by many of the oceanographers and presently an effort is being made to improve the quality of the chlorophyll concentration determination.

To alleviate the lack of data further ocean color measurements are planned in June 1972. These measurements will include locations with higher chlorophyll concentration in order to better understand the relationship between chlorophyll concentration and ocean color. Also the effects of high water turbidity will be investigated.

REFERENCES

Clarke, G. L., Ewing, G. C., Lorenzen, C. J., 1970: Spectra of Backscattered Light From the Sea Obtained From Aircraft as a Measure of Chlorophyll Concentration. Science, 167, 1119 - 1121.

Ramsey, R. C., 1968: Study of the Remote Measurement of Ocean Color. Final Report. TRW, NASW-1658, 89 pp.

White, P. G., 1969: Experimental Results of the Remote Measurement of Ocean Color. Second Annual Earth Resources Aircraft Program Status Review, Sept. 16-18, 1969. NASA Manned Spacecraft Center, 3, Sec. 50, 1 - 9.

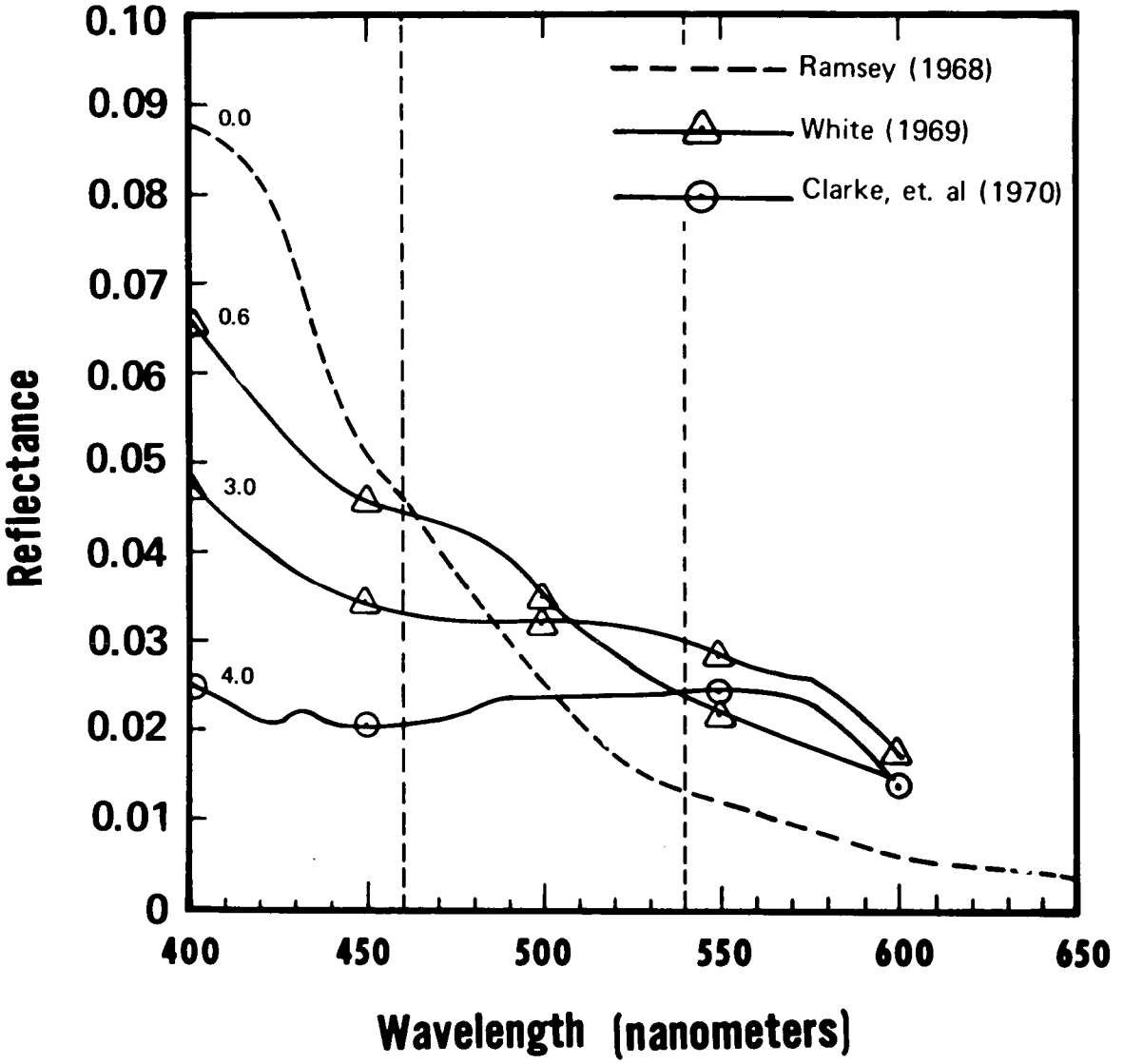

Figure 1 - Ocean reflectance as a function of wavelength. The measured chlorophyll concentrations in units of milligrams per cubic meter are noted in the left hand column of the figure.

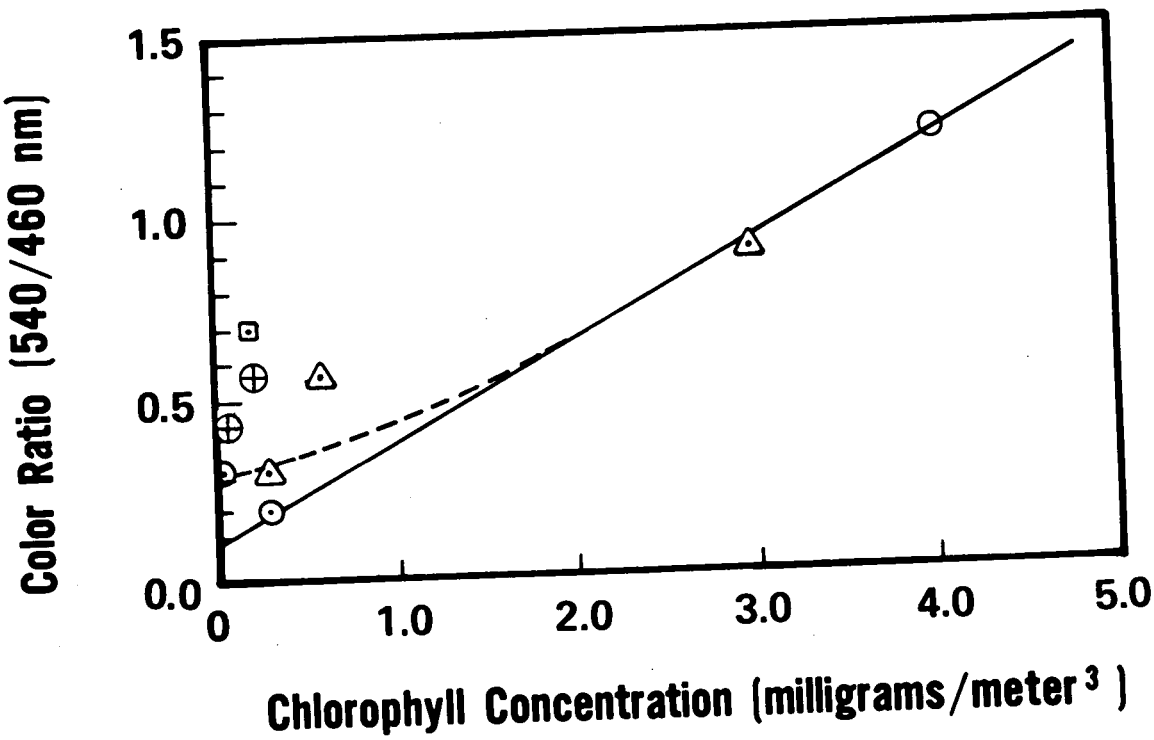

Figure 2 - Measured values of ocean color ratio for several values of chlorophyll concentration. The diagonal line represents a linear approximation to the data and the dashed line has the intercept value as given by Ramsey (1968).

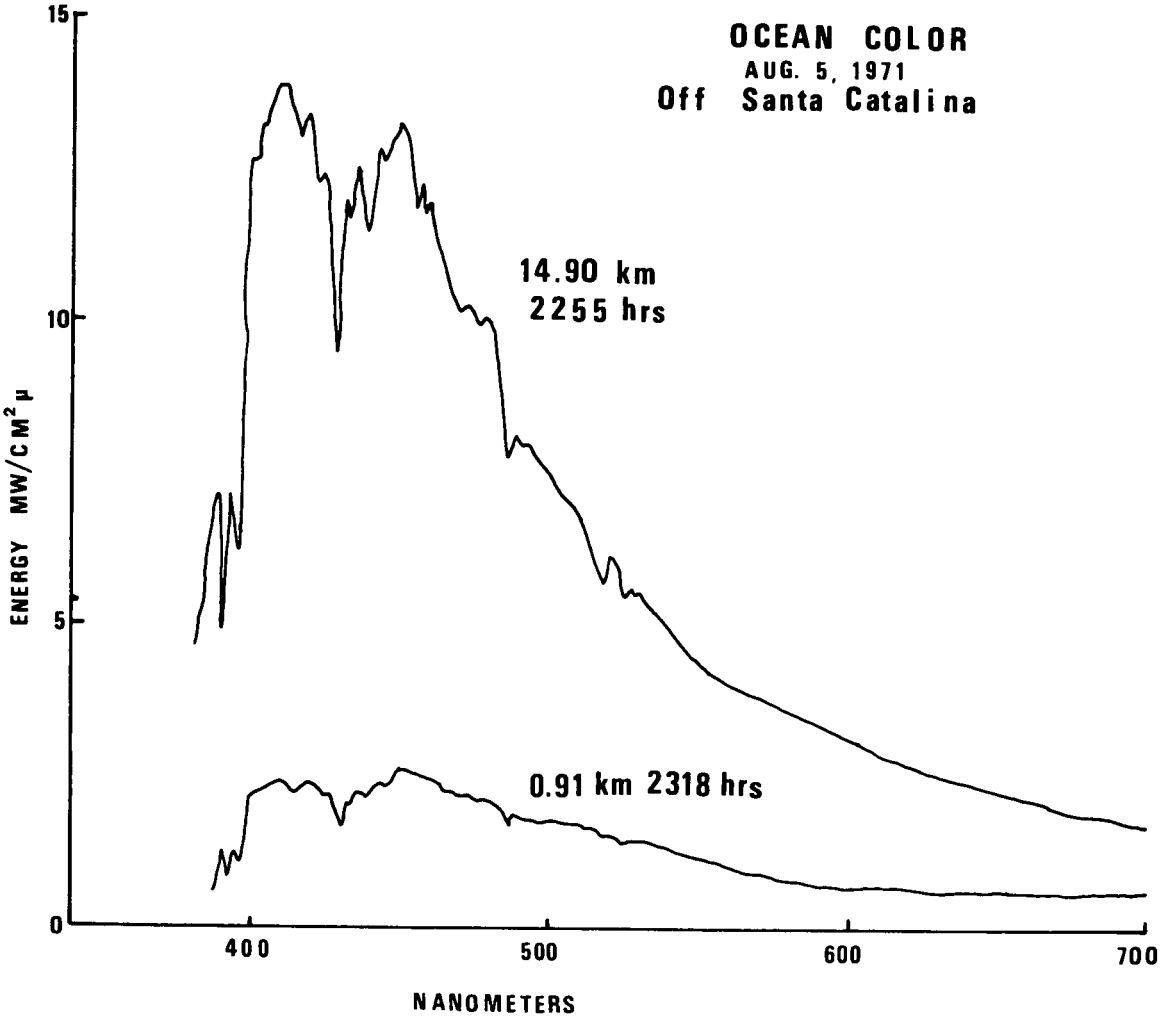

Figure 3 - Comparison between nadir spectral radiance measured at very low and high altitudes.

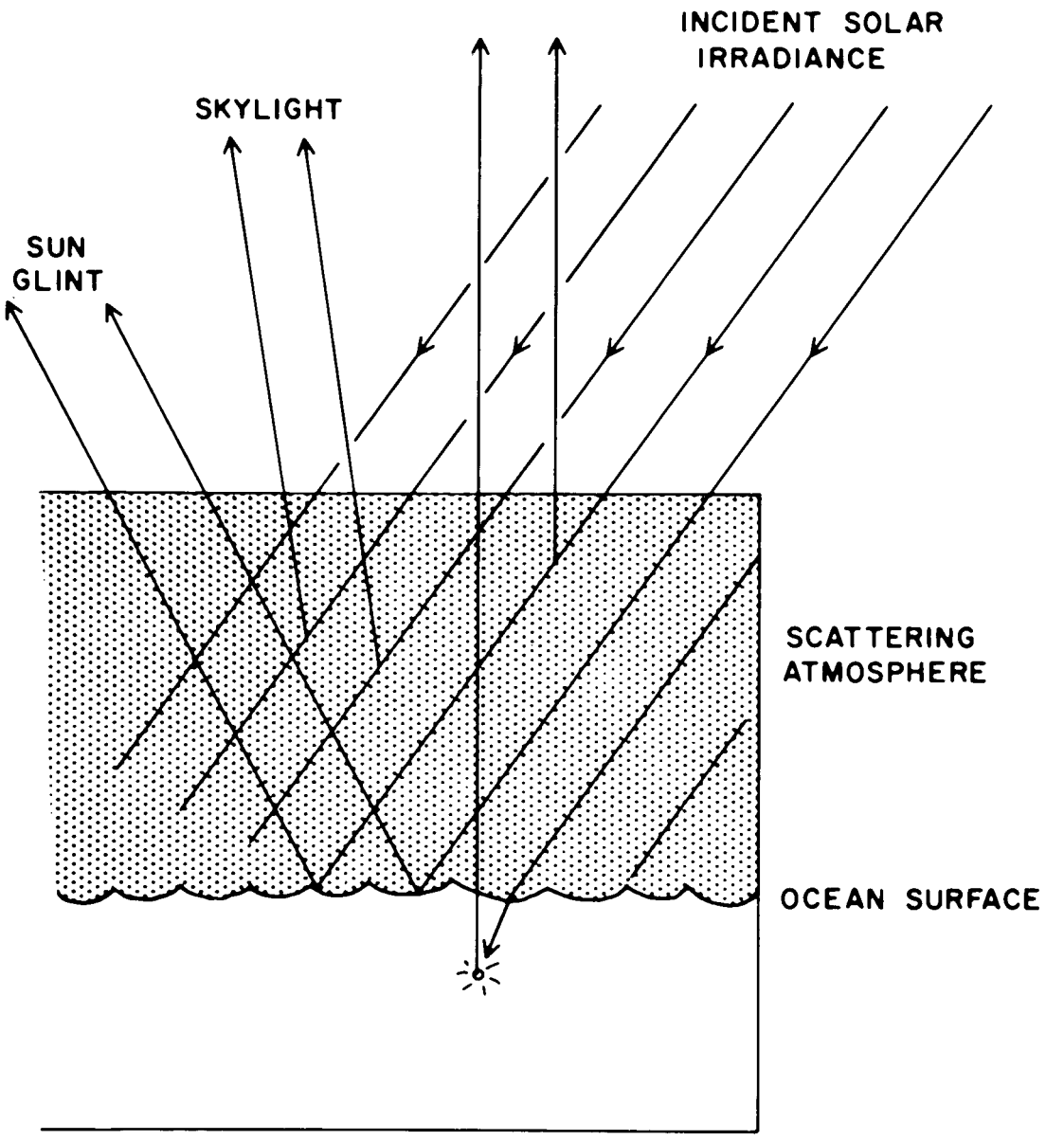

Figure 4 - Schematic representation of the various transfer processes which occur in the atmosphere-ocean system.

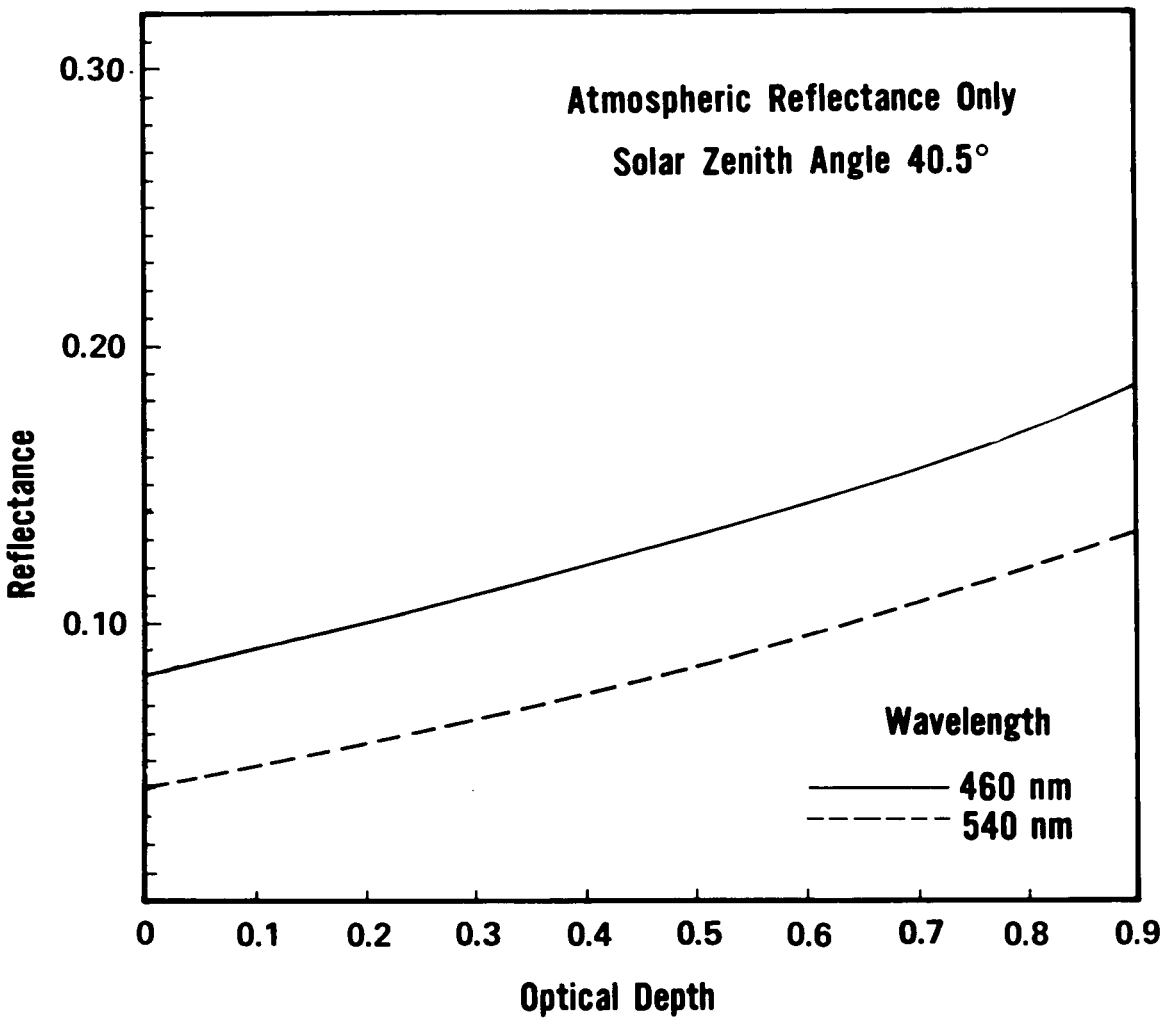

Figure 5 - Reflectance of the atmosphere as a function of optical depth.

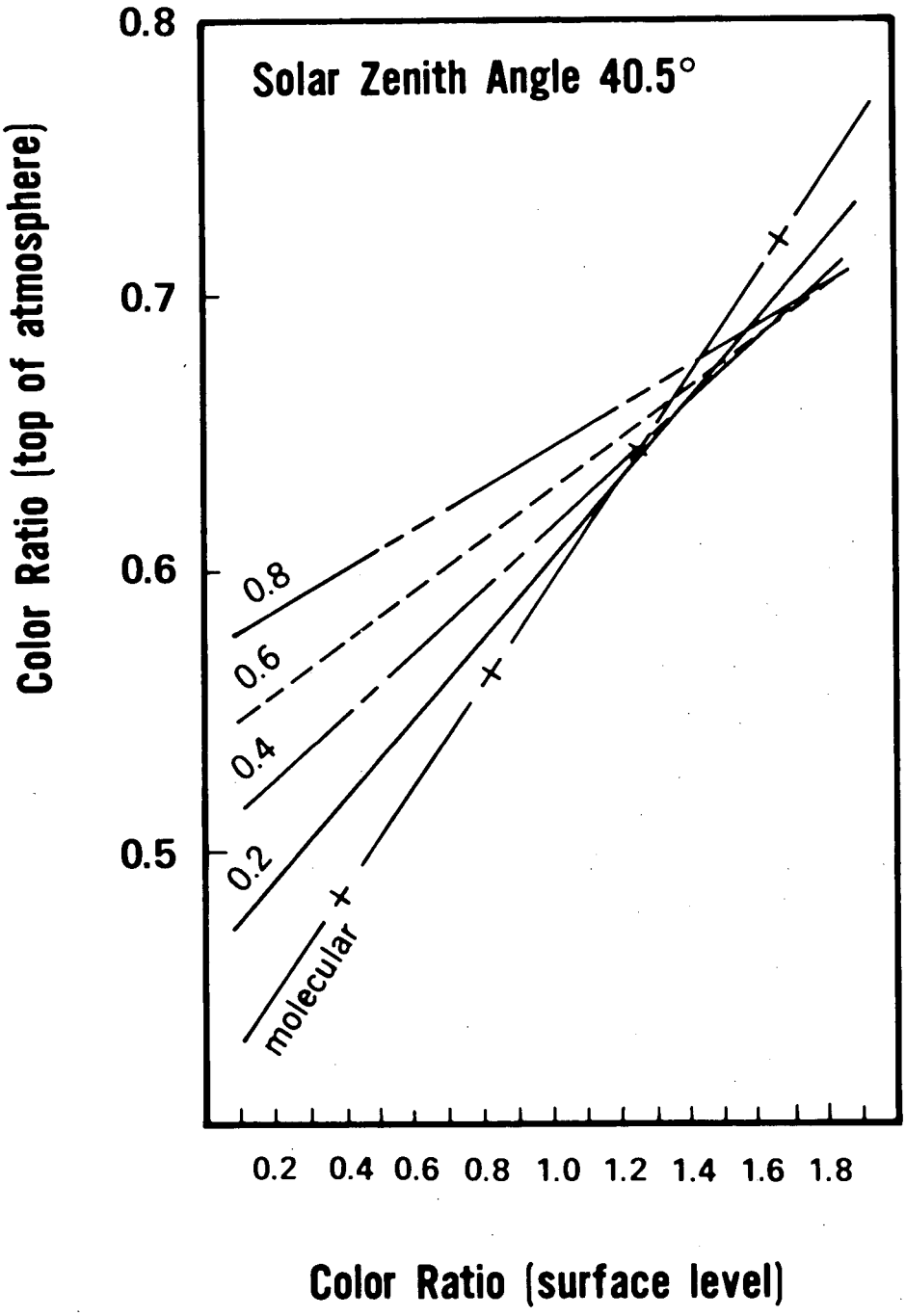

Figure 6 - Relationship between the color ratio as predicted for the top of the atmosphere and the color ratio at the surface level. The optical depth of the atmosphere is noted in the left hand column of the figure.

COMPARISON OF THEORETICAL AND EXPERIMENTAL VALUES OF OCEAN COLOR

	(CHLOROPHYLL) < 0.01mg/m^3		(CHLOROPHYLL) = 0.23 mg/m^3	
WAVELENGTH	460nm	540nm	460nm	540 nm
REFLECTANCE (SURFACE)	0.0218	0.00914	0.0180	0.0101
I (THEOR.) ★	3.90	1.68	3.83	1.69
I (MEAS.) ★	3.88	1.56	3.77	1.52
% DIFFERENCE	0.513	7.50	1.58	11.22
COLOR RATIO(SURFACE)	0.419		0.562	
COLOR RATIO TOP (MEAS.)	0.439		0.440	
COLOR RATIO TOP (THEOR.)	0.453		0.466	

★ Units of radiance are given in mw/cm2, ster., μm and are evaluated for 14.9 meters altitude.

Figure 7 - Comparison of measured and calculated values.

SECTION 10

N72-29311

A MULTISPECTRAL METHOD OF MEASURING SEA SURFACE TEMPERATURES FROM SATELLITES

by

William E. Shenk
and
Vincent V. Salomonson
Laboratory for Meteorology
and Earth Sciences
Goddard Space Flight Center
Greenbelt, Md. 20771

INTRODUCTION

High chlorophyll concentrations are associated with areas of the oceans where nutrients are plentiful. Nutrients are supplied from the ocean bottom in regions of upwelling characterized by relatively low temperatures. Algae growth is aided in coastal waters where relatively high temperatures are found. Therefore, measurements of sea surface temperatures are important in the detection of the areas of upwelling and warm coastal waters. As a result of satellite measurements it has been possible to study the temporal sea surface temperature fluctuations in areas where, before the satellite observations, changes were virtually unknown. A good example is the study of the strong upwelling off the Somali Coast. Upwelling along the northeast African coast begins in connection with the development of the southwest monsoon in May. From May to July the temperature gradient increases and the relatively cold temperatures, which first appear near the coast, move offshore to form an anticyclonic gyre that has a characteristic diameter of about 600 km. Figure 1 shows a view of the gyre on July 3, 1966 where the equivalent blackbody temperature pattern (uncorrected for atmospheric effects) was obtained from the 3.5-4.1 μm measurements of the Nimbus 2 High Resolution Infrared Radiometer (HRIR). The gyre is fully developed with a temperature gradient of 5°K and the width of the cold temperature tongue is about 100 km. The lower portion of Figure 1 depicts chlorophyll concentrations measured during a similar event by an Indian Ocean expedition vessel. Highest concentrations are seen in the meridional cross section near the coast and in the offshore area of the gyre whereas the minimum concentrations were found in the relatively warm waters in between.

There are two problems associated with remotely sensing the sea

surface temperature with infrared measurements that dominate the total error budget. There are the effects of the atmosphere on the emission in an atmospheric window and clouds. The greatest potential error is obscuration of the sea surface by clouds since the emission from the clouds can come from a wide temperature range that is associated with the cloud top levels. Thus, it is imperative that a remote sensing technique for ocean temperature measurement contain a means for determining that the emitted energy is coming from a cloud free source. A multispectral technique has been developed (Shenk and Salomonson, 1972) using the measurements from the Nimbus 2 Medium Resolution Infrared Radiometer (MRIR) that tests for the presence of clouds before accepting the concurrent window infrared emission from what was assumed to be sea surface and the intervening cloud free atmosphere.

METHOD

The Nimbus 2 MRIR was a scanning radiometer operating in 5 spectral regions. All observations in these five channels were geographically registered at the same point and had an instantaneous field-of-view at the subsatellite point of 55 km. Three of these spectral regions were used in this study; namely, the 0.2-4.0 μm region where the observed reflectivity of clouds is generally quite high relative to the ocean surface, the 6.4-6.9 μm region that responds to upper tropospheric water vapor and clouds thereby offering a descriminator for the presence of cirrus, and the 10-11 μm window region permitting the observation of sea surface temperature in cloud free areas. This approach consists of establishing thresholds for the 0.2-4.0 μm reflectance channel and the 6.4-6.9 μm water vapor channel which indicate when a particular concurrent observation in the 10-11 μm channel is cloud free. In this study several threshold combinations in the reflectance and water vapor channels were selected based on observed frequency distributions of the MRIR observations taken from four relatively cloud free days during a one-month period from mid-June to mid-July, 1966 over an area encompassed by the latitudes from 30-50°N and longitudes stretching from 30°W to a line that was parallel to and no closer than 50 nautical miles (more than 1 MRIR resolution element diameter) from the United States coastline. The four relatively cloud free days were selected over this region by looking at the pictures taken by the Advanced Vidicon Camera System (AVCS) on the Nimbus 2 satellite which had a nominal spatial resolution of 0.9 km.

Figure 2 shows the frequency distribution of the observations taken for the four days in the reflectance region. Normalization of the 0.2-4.0 μm reflected energy for solar zenith angle was accomplished with the expression:

$$\bar{r} = \frac{\pi \bar{N}}{H^* \cos \delta}$$

where $\bar{r}$ is the normalized reflectance, $\bar{N}$ is the effective radiance, H^* is the effective solar constant and δ is the solar zenith angle. The strong peak at low reflectances corresponds to the normalized reflectances occurring over the ocean surface. Larger reflectances are associated with clouds and cloud/clear sky combinations. The cloud-no cloud threshold was positioned at a point displaced a distance Δr on the high reflectance side of the frequency peak resulting from observations from what was most likely the cloud-free ocean surface. The magnitude of Δr was set equal to the difference between the lowest observed reflectance and the reflectance corresponding to the above-mentioned frequency peak. In Figure 1 there were no $\bar{r}$ values less than 3. Thus, with the frequency peak at $\bar{r} = 6$, $\Delta r = 3$ and the reflectance cutoff was placed at $\bar{r} = 9$. The Δr on the low reflectance side of the peak was assumed to be produced by random instrument noise and other minor factors such as sea surface glitter.

The layer emitting most of the radiation from which the sensed radiance emanated in the 6.4-6.9 μm spectral band is from 7-11 km for a U.S. Standard Atmosphere with 2.0 cm of precipitable water. This is within or slightly below the level where cirrus clouds are generally located. When this layer was relatively dry the radiation was emitted from a slightly lower layer and thus, in general, from a region of warmer temperatures. With a dry upper troposphere the likelihood of the presence of cirrus clouds was considered to be small.

A frequency distribution approach was also followed in setting the thresholds for the water vapor channel equivalent blackbody temperature observations. Two separate criteria were used to establish these thresholds. One criterion consisted of setting the threshold at the 1σ location on the warm side of the mean of the water vapor channel observations that were taken over specified latitude zones (Figure 3). The second criterion was less restrictive and the threshold was established at the 70% point of the cumulative frequency distribution of equivalent blackbody temperatures (where the cumulative frequency curve started at the lowest temperatures).

RESULTS AND DISCUSSION

Using the threshold selection techniques described above, Nimbus 2 window channel observations, which were objectively selected as being cloud free, were collected over the month period for the area in the

Atlantic already described. Using different threshold combinations and ranges in radiometer observation nadir angle (η), 4 different sets of these measurements were assembled and composited on 1:5 million Mercator grid print maps (Nimbus Project, 1966[2]) with a grid point spacing of 0.625° of longitude.

For comparison purposes with the window radiation measurements all available ship observations of sea surface temperature were obtained for the time period already specified and from 31-43°N and 58°W westward to the U.S. coast. These ship observations (about 4500) were composited on the same map projection and scale as that employed for the radiometric observations. The differences between the ship observed temperatures and the window channel temperatures at a grid point were computed wherever 4 or more radiometric and ship observations occurred. The results were tabulated in histograms for each of four equally-spaced latitude bands from 31-43°N. Figure 4 shows the results for the set with the most relaxed thresholds where the 70% cumulative frequency threshold for the water vapor channel was used and the nadir angle limits were 0-50°. The differences between the ship observations and the observed window equivalent blackbody temperatures (ΔT) are caused by atmospheric effects. These effects were greatest in the 31-34°N region where the frequency peak occurs at ΔT = 8K whereas ΔT = 4-5K for the frequency peak at 40°N-43°N. The dispersion in the results within a latitude band occur because of variability in atmospheric attenuation effects, η, some nonconcurrence in time of the ship and radiometric observations, possible clouds, and random errors in the ship reports. The best comparisons were achieved between 31-34°N where a total dispersion of 2.0K about the mean difference between the ship and radiometer equivalent blackbody temperatures (ΔT) occurred. Larger dispersions further north were believed to be mostly attributable to greater ocean temperature fluctuations occurring during the month period. Despite the relaxed water vapor channel threshold and the wide nadir angle limits the results were similar to those for the other sets with the more stringent thresholds.

Another important result was an experiment to examine the possibility of using just one of the two cloud filtering channels. The conclusion was that the two channel cloud filter was substantially superior to the use of either of the channels alone.

The magnitude of the atmospheric correction to the sensed window radiance depends on the spectral interval, the vertical temperature profile, particulate matter, η, and the vertical distribution of the absorbing constituents. For the Nimbus 2 MRIR window channel the principal absorbing constituents are ozone and water vapor. Therefore, the smaller differences between observed ship temperatures and the window equivalent blackbody temperatures at the higher latitudes was

probably caused by smaller atmospheric water vapor content and colder vertical temperature profiles. Any difference in the particulate concentration as a function of latitude was uncertain.

In order to correct the radiometric observations for the atmospheric effects, a stepwise multiple regression approach was employed. This permitted the evaluation of a simple linear correlation which fitted each grid print window channel radiometric observation average to each grid print ship observation average. In addition, the multiple correlation approach was used to assess the utility of including not only the two parameters just mentioned, but also the observations in the reflectance and water vapor channels, and the nadir angle at which the measurements were made. The multiple regression approach permitted the specification of the ship sea surface temperatures to an r.m.s. error of approximately 1.5K for all latitudes. When the results were stratified into two equal latitude bands, the temperatures in the lower latitudes could be determined to approximately 1K.

The two regression equations were then used to process the radiometric information and arrive at a map of sea surface temperature. This map is shown in Figure 5. The corrected sea surface temperature map shows the basic ocean features that would be expected in the June-July period over the western North Atlantic. A short distance east of the United States coast is the warm axis of the Gulf Stream with sea surface temperatures of about 300K. The strong thermal gradient of about 10K occurs in connection with the north wall of the Gulf Stream just north of 40°N. This gradient is not as steep as it normally is on a given day due to the one month data collection period and the spatial resolution of the MRIR.

Other investigations have successfully employed this technique over different oceanic regions. Figure 6 shows the temperature gradients for a consecutive 3-week period in June-July, 1966 over the southern Indian Ocean, from 10° to 45°S (Shenk and Szekielda[3]). The 10-11 um equivalent blackbody temperatures have not been corrected for atmospheric effects. The radiation measurements detected the Agulhas Current flowing southwestward along the African Coast to 38°S. An area of upwelling was located just off the south coast of Africa and north of the warm axis of the Agulhas Current.

The oceanic polar front is pronounced between 40-45°S which is associated with a convergence of the surface currents. Thus, the front separates the cold polar surface water from the warmer water masses of the lower latitudes. The center of this front lies in the Indian Ocean in the region where the water temperatures are, according to the uncorrected satellite data, in the range of 281-283°K. This cold water is found in the tropics at a depth of 300-400 m and in the

subtropics between 500-1000 m which originates at the surface at about 40°S.

The analysis of remotely sensed radiation data from the satellite gave a temperature gradient at 52°E and 43°S of 0.055C km^{-1}. This is a sharper horizontal gradient than that associated with the upwelling region along the Somali Coast and more pronounced than in the nautical charts for this area. Considering the ground resolution of the radiometer and the time period of approximately three weeks during which the radiation data were sampled, it is concluded that the temperature gradient should be still greater if synoptic measurements over shorter periods are made and that the polar front had a very stable position. This gradient is comparable with similar temperature gradients in the Gulf Stream. The Gulf Stream temperature boundary oscillates so much that a temperature analysis over a few weeks substantially smoothes the original sharp temperature gradients.

Szekielda[4] has discussed in more detail upwelling along the south African west and south coasts. Figure 7 shows his analysis from mid-May to mid-June, 1966. The prominent warm axis of the Agulhas Current is seen to extend south of 40°S with a small area of upwelling (285°K uncorrected isotherm) appears just off the south African Coast. A stronger region of upwelling produced by southerly winds is found associated with the Benguela Current along the west coast between 30°S and the Cape of Good Hope.

CONCLUSIONS

A multispectral technique has been developed which independently tests for the presence of clouds before a registered window radiance measurement is accepted as coming from the sea surface and the intervening atmosphere. The spatial resolution of ocean temperature mapping can be the same as that of the radiometer. With the 55 km subsatellite track resolution of the Nimbus 2 MRIR, current boundaries and upwelling areas have been successfully identified. Knowledge of the position of these regions and temperatures within them are important to the detection of areas of high chlorophyll concentrations.

These three registered channels will hopefully be flown on radiometers that are proposed for space flight on the TIROS N, ATS-G, and EOS missions. The spatial resolutions will vary from 0.9 km (TIROS-N) to 11 km (ATS-G) for the 11 μm channel. In the interim it may be possible to implement this technique where the appropriate channels are flown on the same satellite but are not part of the same instrument (Nimbus E).

REFERENCES

1. Shenk, W. E. and V. V. Salomonson, 1972: "A Multispectral Technique to Determine Sea Surface Temperature Using Nimbus 2 Data", J. of Phys. Ocean. (to be published in April, 1972).

2. Nimbus Project, 1966: "Nimbus 2 Users' Guide", Goddard Space Flight Center, Greenbelt, Maryland, 229p.

3. Shenk, W. E. and K-H. Szekielda, 1971: "Satellite Ocean Temperature Analysis of the Indian Ocean", Paper presented at the Symposium on Indian Ocean and Adjacent Seas, Cochin, India, Jan. 12 - 18, 1971.

4. Szekielda, K-H., 1971: "Upwelling Studies with Satellites", NASA X-651-71-298, 17p.

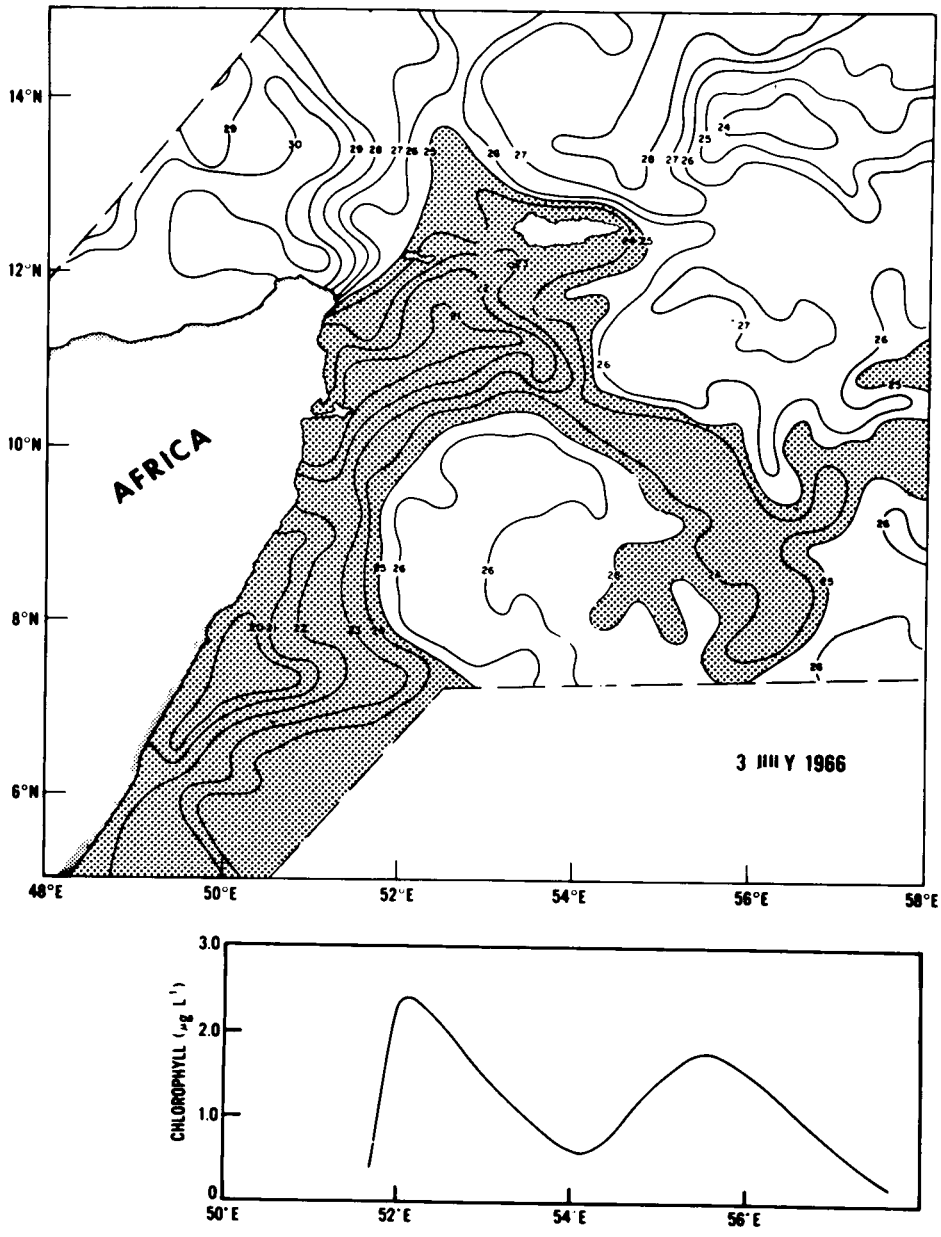

Figure 1 - Top - Nimbus 2 High Resolution Infrared Radiometer Equivalent Blackbody Temperatures (uncorrected for atmospheric effects) of the fully developed upwelling gyre off the Somali Coast on July 3, 1966 (after Szekielda). Isotherms are in °C and equivalent blackbody temperatures $\leq$25°C within the gyre are shaded.

Bottom - An east-west cross-section of chlorophyll concentrations recorded by an Indian Ocean Expedition vessel during a similar event.

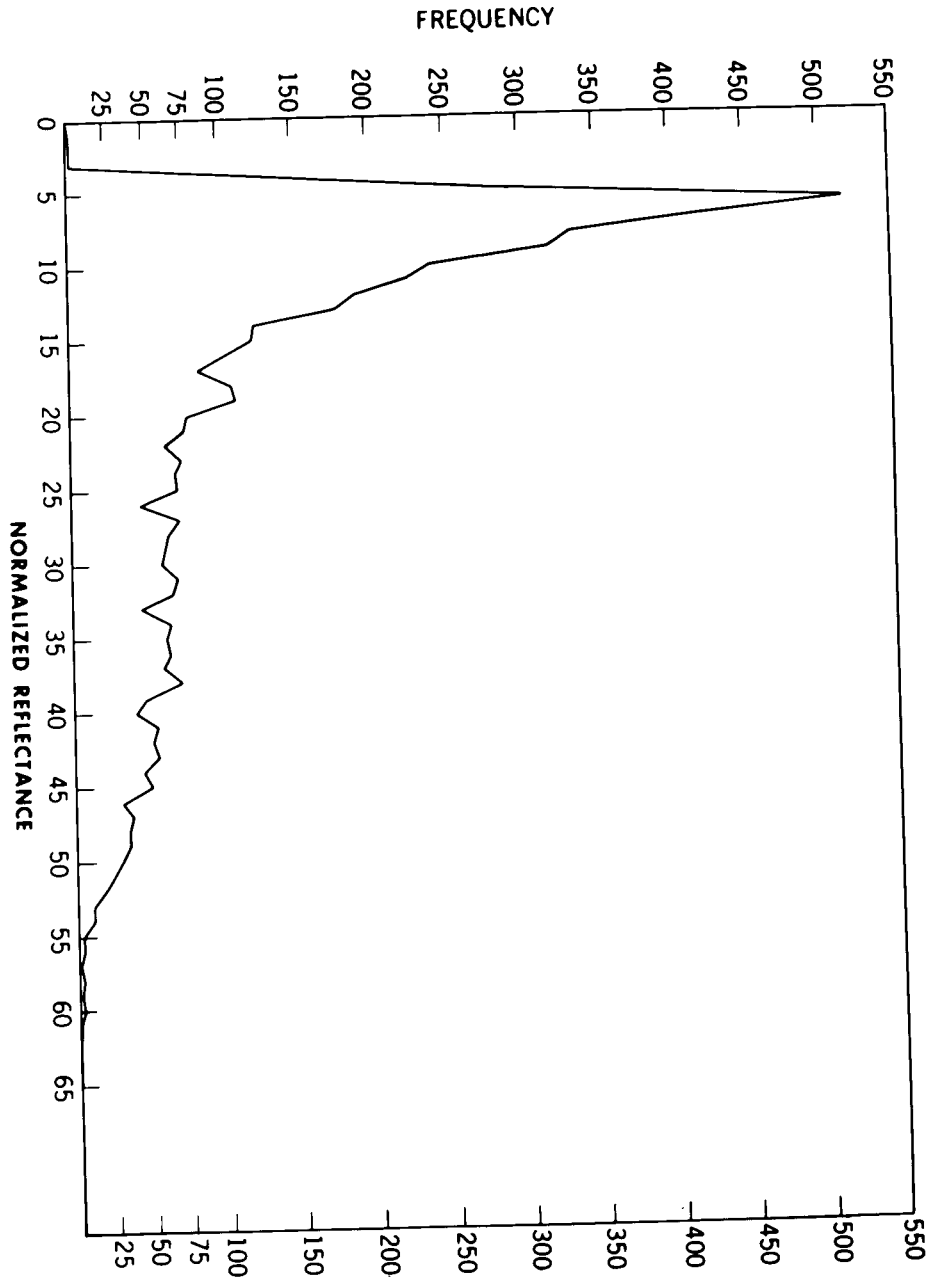

Figure 2 - Frequency distribution of normalized reflectance measurements from the 0.2-4.0 μm channel of the Nimbus 2 Medium Resolution Infrared Radiometer for 4 relatively clear days over the western North Atlantic between mid-June and mid-July, 1966.

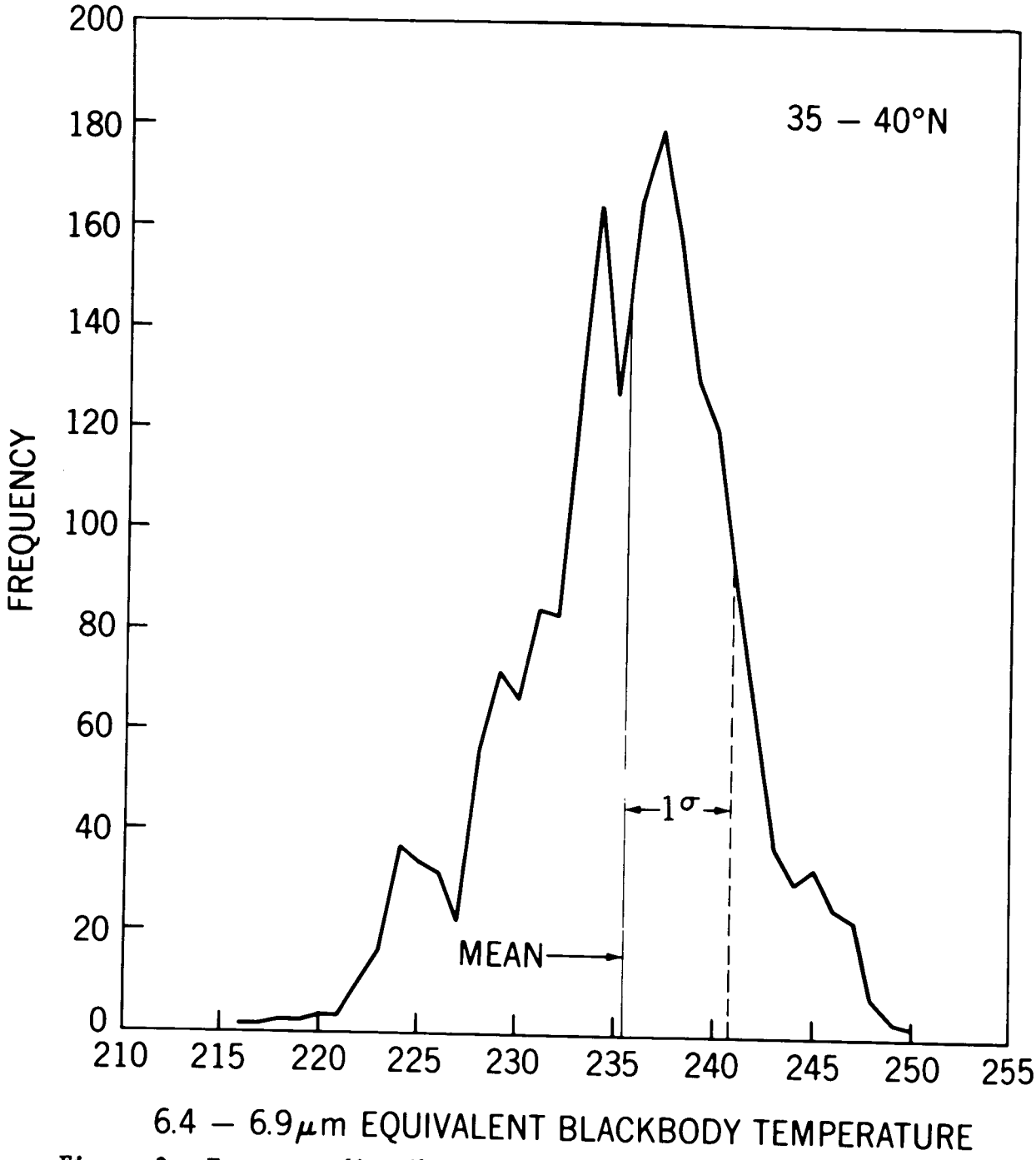

Figure 3 - Frequency distribution of 6.7 μm equivalent blackbody temperatures ($T_{BB's}$) for the same 4 days as in Figure 2. The mean and 1 σ to the warm side of the mean are indicated where the $T_{BB's}$ on the warm side of the 1 σ point were assumed to be associated with a cloud free upper troposphere.

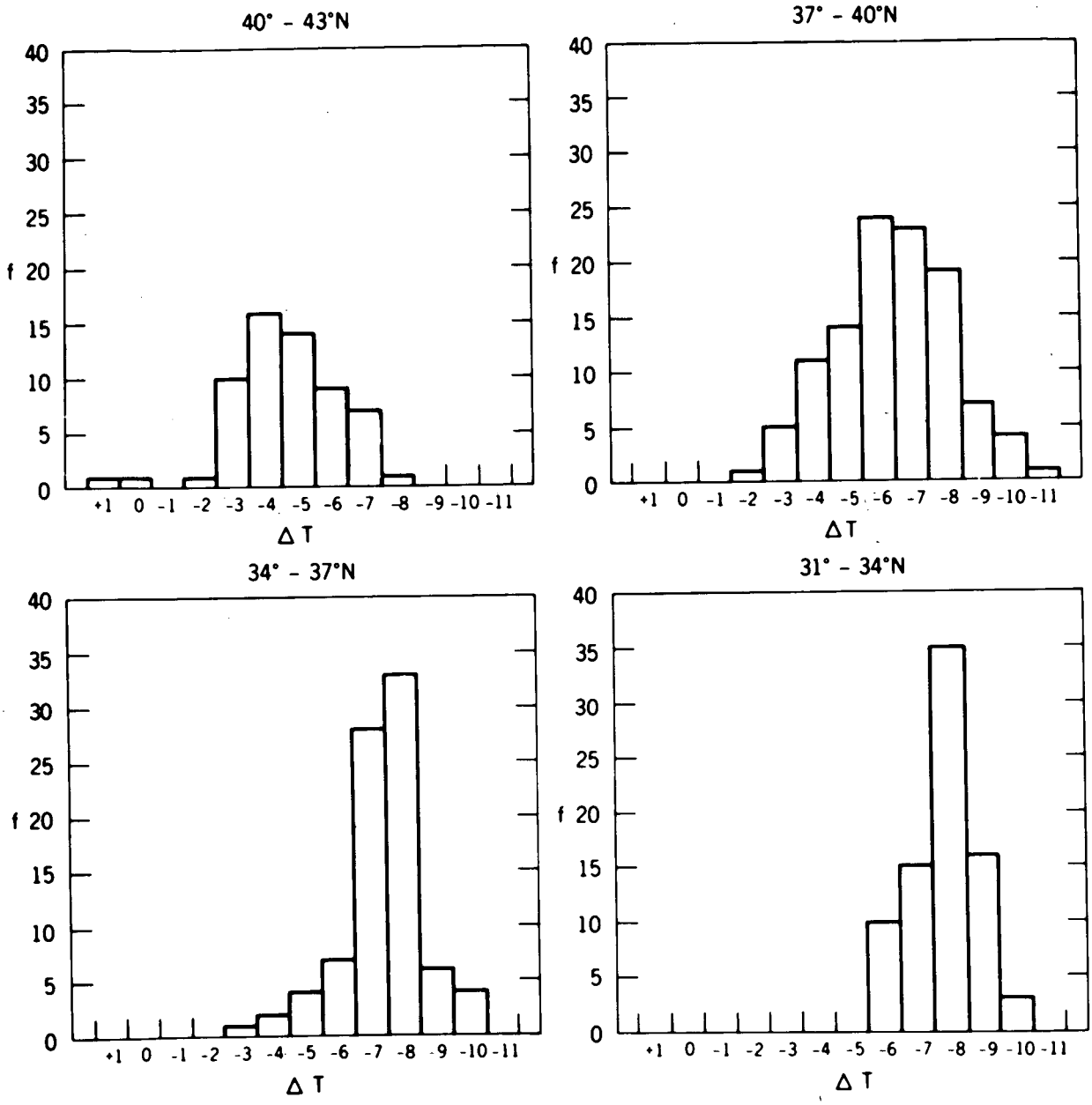

Figure 4 - Frequency distributions for 4 equally spaced latitude bands over the western North Atlantic of the difference between ship sea surface temperatures and 10-11 μm window equivalent blackbody temperatures associated with assumed cloud free conditions.

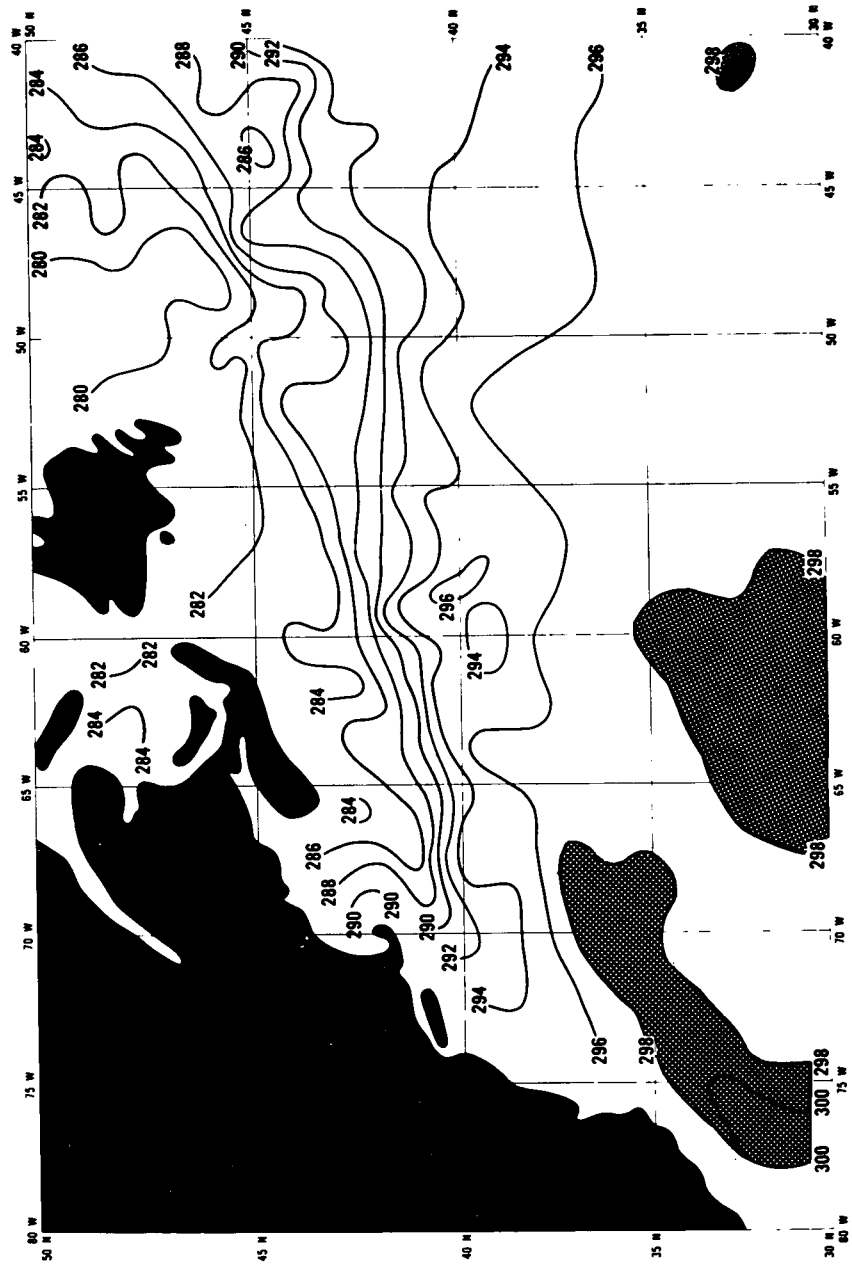

Figure 5 - Satellite generated map of sea surface temperature (mid-June to mid-July, 1966) over the western North Atlantic where the assumed cloud free 10-11 μm equivalent blackbody temperatures have been corrected for the effects of the atmosphere. Isotherms are in °K with the warmest areas (≥298°K) stippled.

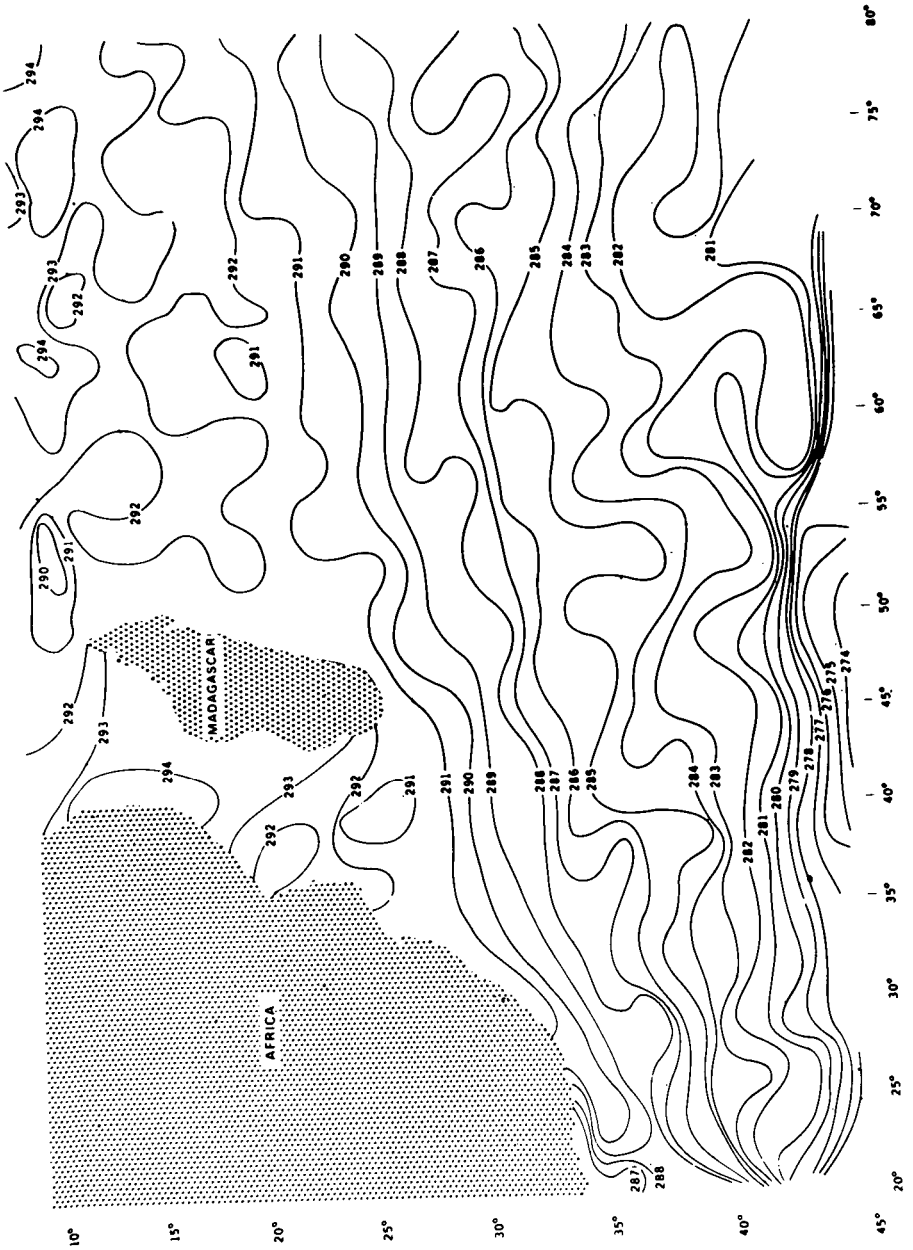

Figure 6 - June, 1966, southern Indian Ocean map of assumed cloud free 10-11 μm equivalent blackbody temperatures (°K) that are uncorrected for atmospheric effects.

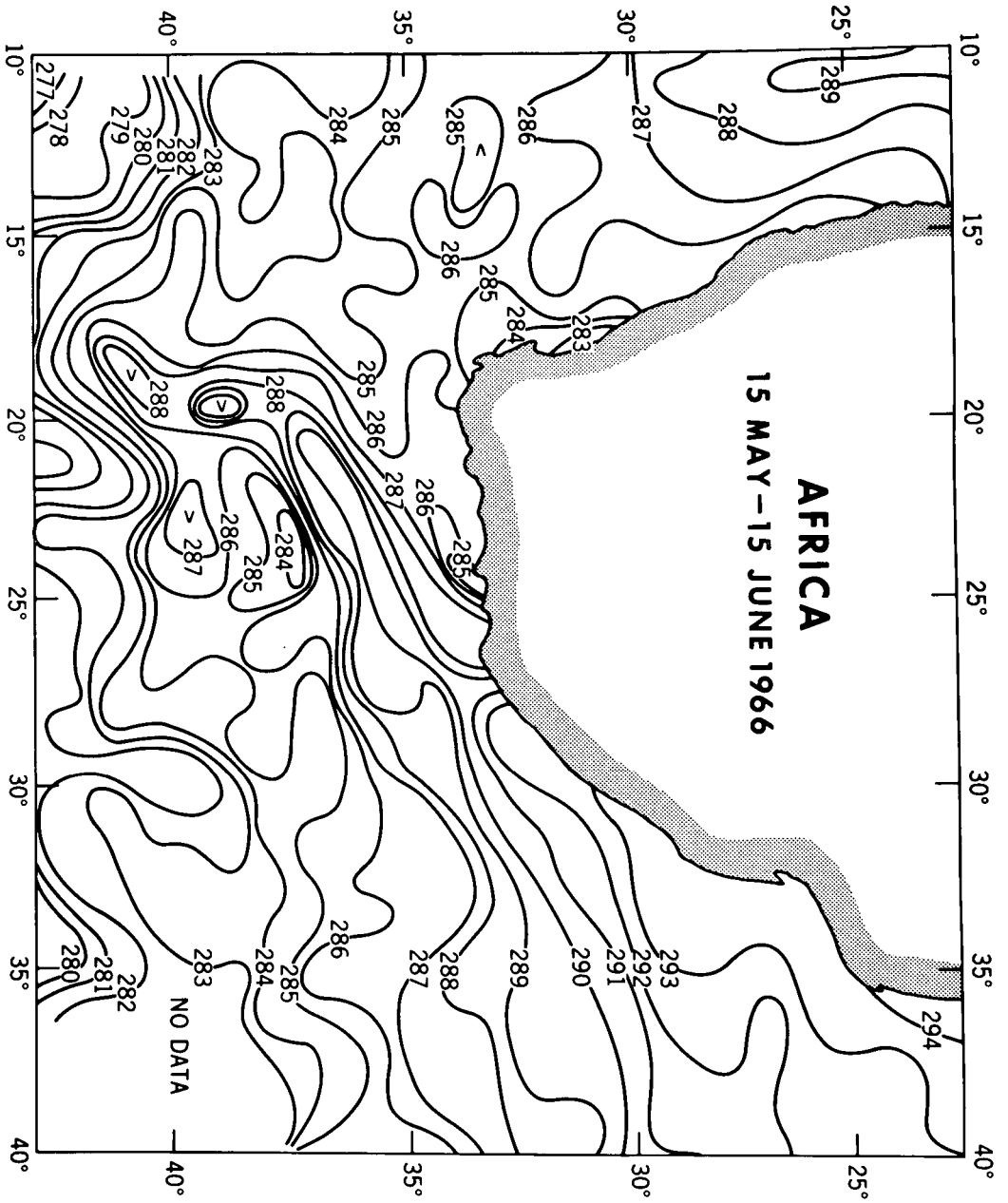

Figure 7 - Mid-May to mid-June, 1966 chart of assumed cloud free 10-11 μm equivalent blackbody temperatures (°K), uncorrected for the atmosphere, over portions of the southwestern Indian Ocean and southeastern Atlantic Ocean.

A SUMMARY OF ACTIVITIES OF THE EARTH RESOURCES LABORATORY AT THE MISSISSIPPI TEST FACILITY DURING 1971

by

Robert O. Piland
Earth Resources Laboratory
@
Mississippi Test Facility

INTRODUCTION

The NASA Earth Resources Laboratory at the Mississippi Test Facility was approved for implementation in the latter part of 1970, consequently 1971 represents the first full year of operation. A short paper was presented at the Third Annual Earth Resources Aircraft Program Review approximately a year ago which described initial concepts and plans for the Laboratory. The five papers which follow describe activities at the Laboratory during 1971. They are presented in the context of status reports. Technical reports covering various aspects of the program are published separately and in addition to the present papers.

The initial concepts for the Laboratory may be summarized as follows:

(1) Conduct research investigations in the Mississippi/Louisiana/Gulf area in the application of remote sensing.

(2) Stress the interests and/or needs of agencies in the area in the selection of activities.

(3) Utilize existing aircraft and satellite programs as a source of data.

(4) Collect and analyze surface data for correlation with flight data.

(5) Conduct systems studies to consider all aspects of potential applications to guide selection of research investigations.

The first item was intended to delineate the geographical area within which investigations were to be undertaken. It was not intended to encompass this total area. The second item is self-explanatory. The third item emphasizes the fact that the new activity will not be directly involved in the development of satellite systems

or sophisticated aircraft operations such as at MSC-Houston or Goddard. Conversely, the fourth item indicates the requirement for significant data acquisition at or near the surface for correlation activities. The last item indicates a need for an overall look at the potential application so that undue emphasis will not be placed on one technical aspect of an area, but that balanced R&D support will be directed towards the definition of a total future operational application system.

The initial plan for the Laboratory also outlined a general implementation plan. Elements of the plan were as follows:

First Year

Recruit Personnel

Bring Support Contractor Onboard

Procure Specialized Equipment

Second Year

Continue Personnel Buildup

Initiate Technical Investigations with Aircraft and Surface Measurements

Implement Data Processing Techniques

Third Year

Extend Projects to Include Data from ERTS and Skylab Projects

This plan recognizes the fact that the Laboratory was being started from essentially a zero capability. No existing groups or organizational elements nor equipments were being transferred from existing Earth Resources activities.

In addition to the items listed, there was the inherent requirement to develop a technical program which is by far the most difficult task for a new organization. Such a program must complement rather than duplicate existing efforts, it must be paced to the development of capability to conduct the activity, and it must properly direct itself towards technique development or demonstration type experiments in lieu of operational activities.

The remainder of the paper will be directed towards summarizing our activities in carrying out the implementation plan and developing and initiating a technical program. Specifically, the following

elements are treated:

Personnel

Organization

Technical Equipments

University Program

Agency Relationships

Minor Projects

Technical Program

Reports/Products

Milestone Summary

PERSONNEL

Personnel buildup is presented in figure 1. Authorization to hire 25 civil service personnel was received in October 1970. These personnel were onboard in September 1971. A procurement plan for a technical support contract was approved in November, 1970. After a competitive selection, the Lockheed Electronic Corporation was selected and initiated work on February 1, 1971. A buildup to approximately 70 personnel was reached in the early fall of 1971. Consequently, the staff of the Laboratory has remained essentially constant for the last four months at approximately 95.

ORGANIZATION

The organization of the Laboratory is presented in figure 2 for the NASA and contractor groups. The Laboratory reports to the Director of the Manned Spacecraft Center, Houston. The Land and Sea Remote Sensing Applications Groups are concerned with land and water projects respectively. These groups consist of specialists including a hydrologist, forester, agronomist, ecologist, cartographer, regional planner and an oceanographer, meteorologist, and a microwave engineer, mathematician and computer specialists, photographic scientist, instrumentation and data systems engineers. The numbers next to the organizational blocks on figure 2 indicate the number of personnel in the group.

The Lockheed Electronics Technical Support Contractor is organized as shown on the lower half of figure 2. A modest complement of disciplinary specialists support the data analysis activity with larger groups involved in data preparation, instrumentation, and data systems. The latter two being heavily involved in the operations related to surface data acquisition.

TECHNICAL CAPABILITY
(Equipments)

The Mississippi Test Facility and nearby Slidell Computer Complex have been primarily involved in the testing of large scale rockets over the past several years. While these pursuits lead to a firm basic technical laboratory capability, items uniquely related to the remote sensing activities were not available. Consequently, in this first year of operation, a significant effort has had to be directed towards the planning and purchasing of necessary equipments. The following paragraphs describe the major items involved.

In the area of remote sensors for surface measurements to be used from boat, truck or light aircraft the plan was to obtain relatively inexpensive, commercially available devices requiring no development. These sensors would cover the same general spectral bands or ranges as those on ERTS, Skylab EREP, or used in the Earth Resources Aircraft Program. With these criteria we have acquired the following:

A set of general purpose cameras (Yashicas, Hasselblads, Nikons)

An I^2S Multiband Camera System

Barnes Precision Radiation Thermometers (PRT-5 and 6)

A Texas Instruments Single Channel Scanner

An Exotech Field Spectrometer

These equipments have all been delivered with the exception of the field spectrometer which will be delivered within the next month.

In addition to the remote sensors a family of relatively simple in-situ sensors and associated equipments have been obtained. These range from simple thermometers to Secchi disks to a pyronometer.

We have employed a number of platforms or carriers in conjunction with obtaining measurements on or near the surface. A 27 foot power boat (J-Boat) was available at MTF. Evaluation of this craft indicated it to be suitable for work in the calm waters of the nearby river but its slow speed and limited stability made it unusable in the coastal

waters such as the Mississippi Sound. For major coastal experiments we have depended on agencies, universities and individuals located in the area.

A truck has been purchased suitable to accommodate an extensible boom, instrumentation and data recording systems. This will be available in May. Its primary use will be in the local area relative to correlation measurements in agricultural and natural target areas to obtain information on variables for which it is impractical to maintain long term or very frequent aircraft coverage.

As stated earlier our investigations have been built around the data gathering capability of the Earth Resources Aircraft Program including the P3A, C130 and RB57. Locally a smaller aircraft supports our near surface measurements on a rental basis. This allows for the gathering of preliminary data prior to large aircraft coverage, limited but frequent data acquisition between large scale missions and low altitude measurements during the course of the mission. We have obtained out-the-window photography and PRT-5 and camera data employing a simple mount on the door. In the near future we will be able to obtain vertical data through floor areas where removable hatches have been installed.

In addition to measurements in natural areas of interest we have found it necessary to have a limited laboratory capability for spectral tests and calibration and several outdoor calibration areas. Two spectrometers, a Cary 17 with a spectral range of .18μ to 2.65μ and a Perkin-Elmer instrument with a range of 1.0μ to 15.5μ have been obtained. The former has been used for a variety of tasks including the analysis of sea water content for chlorophyll as will be discussed by a subsequent speaker.

An optical bench and associated equipment has been obtained for limited camera and lens calibration and black body sources have been obtained for calibrating the thermal IR equipment.

For use outside the Laboratory (figure 3 a) we have obtained and are using a set of Data Corporation photographic targets (figure 3 b) and have instrumented a 13 acre reservoir (figure 3 c) on the site with thermocouples to support calibration of the thermal sensor operation. In the summer we will have access to a series of agricultural fields on a nearby farm (figure 3 d) where arrangements with the owner will provide a series of forty-acre fields containing cotton, soy beans, rice, wheat and milo. The first three, plus sugar cane, represent the major crops of the Mississippi-Louisiana area. Their nearby location and size will allow a convenient site for ERTS and Skylab investigations and a variety of near surface investigations of second order variables.

The discussion to this point has emphasized equipment relating to the acquisition of data. Our activity in the past year has been equally concerned with acquiring data preparation equipment and

arranging for data processing. Processing of data for the Laboratory is accomplished primarily at the Slidell Computer Complex and the MTF Photographic Laboratory. The former is equipped with a series of Univac 1108 computers and the latter has been equipped in the last year to provide up to 9 inch format, automatic color processing as well as a variety of related capabilities. The MTF photo processing capability is augmented by a small, manually operated, processing capability in ERL which is used for special purposes. While the Univac 1108's represent a significant capability, their usefulness is directly geared to available and suitable programs. A considerable effort has been directed towards the transfer of a series of pattern recognition programs into these computers. Mr. Whitley will describe this activity in more detail in a later paper.

The data processing capability must be augmented with the necessary equipments for data preparation and analysis. A variety of light tables ranging from field units to photo interpretation stations have been acquired. The previously mentioned I^2S Mini-Addcol Color Additive Viewer for registration, combining, and display of the several bands for analysis. A second I^2S device, consisting of a Digicol Image Color Transformer was obtained to provide a capability for enhancing discrimination between features in an image. The most significant capability which will be located at the Laboratory will be a Data Analysis Station to be delivered in May. This equipment is similar to that located at MSC-Houston and will allow for the screening, editing and tape reformatting of multispectral data from the C130, 24-channel scanner, the Skylab EREP and ERTS scanners. This equipment will be described in more detail in a subsequent discussion.

UNIVERSITY PROGRAMS

The initial plan for the implementation of this Laboratory envisioned the development of relations with a number of universities in the area. It was felt that the universities, with their specialized personnel, afforded a knowledge of the area and represented one of the bridges to operating groups who hopefully will desire to use remote sensing techniques as they develop.

Contracts were let with the following universities:

Louisiana State University

Tulane

Mississippi State University

University of Southern Mississippi

Gulf Coast Research Laboratory

The purpose of this initial activity was not to conduct specific remote sensing investigations but to gather a set of information regarding the area, to evaluate it in the context of helping to guide the development of projects at the Laboratory, and to afford the universities an opportunity to increase their familiarity with the remote sensing program.

These studies have been completed and are now being evaluated. Two of the universities, Mississippi State and Tulane, have submitted ERTS and/or Skylab proposals which have been favorably received. All have proposed continuing activities with the Laboratory and we hope funding will allow continued support of these universities.

AGENCY RELATIONSHIPS

Contacts with federal and state agencies have been many and diverse. As you know, a number of government agencies, including USGS, NOAA, and EPA, have laboratories and activities located at MTF. We have had minor cooperative activities with a number of these groups and would expect these efforts to grow. Particular elements of those groups with which we see expanding activity include the EROS office, National Marine Fisheries, and the Data Buoy Project of NOAA.

There is also located at MTF a State Liaison Officer who reports to the Governor. He provides convenient access to state agencies and officials and, conversely, a channel into our operation for these interested groups.

During the first several months at MTF we conducted a series of visits to a variety of state and federal agencies located in the area. These are too numerous to list in this paper but they provided us with an excellent assessment of current interests in the area and the status of current use of remote sensing techniques. Subsequent papers will detail areas where we have entered into more definitive collaborative areas with local groups such as the Mississippi Sound and the Atchafalaya Basin Projects.

MINOR PROJECTS

During the first year as we were striving to develop a capability and define a longer range program, we undertook a number of minor projects, some by choice and some by plan. These projects hopefully served a technical purpose, but also were valuable in orienting our staff and developing procedures.

The projects included the following:

- Tornado Survey
- Pine Blight
- Corn Blight
- Land Use Update
- Soil Moisture

All of these activities have been reported with the exception of the Pine Blight Project. In addition, the appendix of Mr. Mooneyhan's paper will describe these activities in more detail.

TECHNICAL PROGRAM

Earlier in the paper it was noted that one of the most difficult but important tasks of the first year's activity was to develop a technical program. Such a program has been developed based on studies, discussions with university and agency personnel, and knowledge of the ongoing program. Three technical areas of activity have been selected for study, as follows:

- Automated techniques for the annual updating of land use.
- Circulation and associated characteristics of a semi-enclosed water body and a deep water current.
- Definition and monitoring of the characteristics of a wetland area.

These areas are recognized as being quite broad in scope, however we have selected detail technical objectives within these broad areas and these will be described by Messrs Tilton and Mooneyhan respectively.

The program is structured to proceed from an initial base of technique development to one of demonstration experiments. The latter is being done in conjunction with operating agencies and the former may or may not depending on the status of the technique.

Figure 4 presents a summary of test areas within which work is going on or is planned for the future. The automated techniques for land use classification is concentrated in the Mississippi Gulf Coast counties with a planned extension to the rich "delta" farming region in the coming year. Mississippi State University will work in both

these areas with satellite data. Techniques related to the preparation of high altitude photography for land use and other application is being studied in the Jackson area. Additionally, the University of Southern Mississippi will attempt to exploit multiband photography in relation to sedimentation in the neighborhood of a reservoir and associated land use in the Jackson area.

Water studies were initiated in the Mississippi Sound and Mobile Bay. The Sound is defined by the coast and a string of barrier islands extending from Lake Pontchartrain to Mobile Bay. The Gulf Coast Research Laboratory will participate with ERL in a more concentrated study of an estuary emptying into the Sound, namely Biloxi Bay. Tulane's ERTS proposal relates to a preliminary study of Lake Pontchartrain and we hope to support a more concentrated study of the eastern area of the Lake employing light aircraft.

We have received a specific request to study Barataria Bay in Louisiana using an approach similar to that used in the Sound. This would be an example of a demonstration experiment after previously exercising the techniques. We have delayed answering this request until we could evaluate initial results of the Sound Study.

We have also initiated a study extending into the deep Gulf built around the Gulf East Loop Current. Initial tests cover the area in the figures but since the current varies in its location through the year, subsequent tests will move with the current.

Our wetlands study is being conducted in the Atchafalaya Basin in Louisiana which is defined by the Atchafalaya River, a distributary of the Mississippi and a series of levees. Louisiana State University proposes to conduct a more concentrated study of the Bayou La Fourche and the land area contained within its levee system. Details of this water system offer controlled conditions which make the site of interest.

As stated earlier, the ERL projects mentioned here will be discussed in more detail by subsequent speakers. The university projects have not developed sufficiently at this time to warrant further detail at this review.

1971 REPORTS/PRODUCTS

Table I presents a list of reports prepared by ERL in 1971. These include primarily the results of the minor projects previously mentioned and the documentation of surface measurements or ground truths for a number of the projects.

SUMMARY

In summary, figure 5 presents a milestone chart which presents typical highlights of our year's activity. We received authorization to hire personnel in October of 1970 and initial funding in January of 1971. During February the Technical Support Contractor initiated work, the university contracts were let, and our first project activity was initiated with the Tornado Survey. The I^2S Multiband System was received in June and the first Mississippi Sound measurements were obtained in July. The Gulf Coast Counties Land Use tests were initiated in September and the Atchafalaya tests in October. The first Deep Gulf tests were in November and the infrared scanner was delivered in December.

We feel we have developed a reasonable foundation for the Laboratory in this first year. The second and third years will be more critical as the results of our efforts reach a position which will allow us to evaluate their usefulness in terms of the overall Earth Observation Program.

EARTH RESOURCES LABORATORY 1971 REPORTS/PRODUCTS

Earth Resources Activity at Mississippi Test Facility - A Proposal and Implementation Plan August 12, 1970

Photographic Survey in Post Tornado Relief Activities February 21, 1971

Observations of the Southern Corn Leaf Blight November 1971

Soil Moisture Remote Sensing Study, Part 1, Surface Measurements July 20, 1971

Hancock County Land Use Study, Experiment 1, Part 1, Surface Measurements September 9, 1971 (draft)

Mississippi Test Sites Land Use Study Photographic Experiment, Mississippi Land Use Study Preliminary Report September 30, 1971 (draft)

Mississippi Sound Remote Sensing Study, Experiment 1, Part 1, Surface Measurements July 22, 1971

Mississippi Sound Remote Sensing Study, Experiment 2, Part 1, Surface Measurements November 10, 1971

Eastern Gulf of Mexico Remote Sensing Study, Experiment 1, Part 1, Surface Measurements November 21, 1971

Atchafalaya River Basin Study, Experiment 1, Part 1, Surface Measurements October 29, 1971 (draft)

Atchafalaya Basin Mosaic with Surface Classification Overlay from October 1970 data December 1971

Table I. - Reports/Status Chart

ERL & SUPPORT CONTRACTOR PERSONNEL

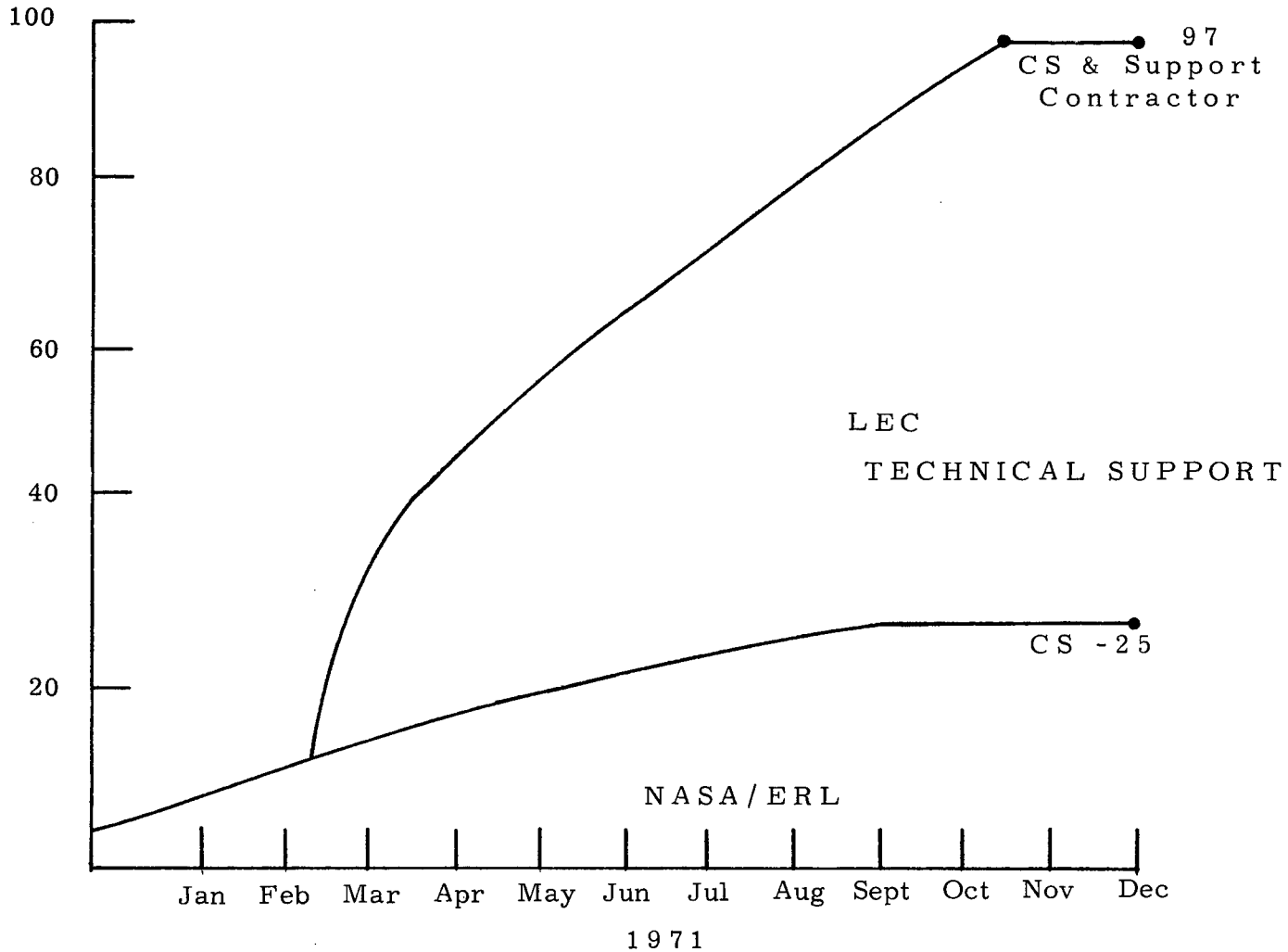

Figure 1. - Personnel Curve

As of January 1, 1972

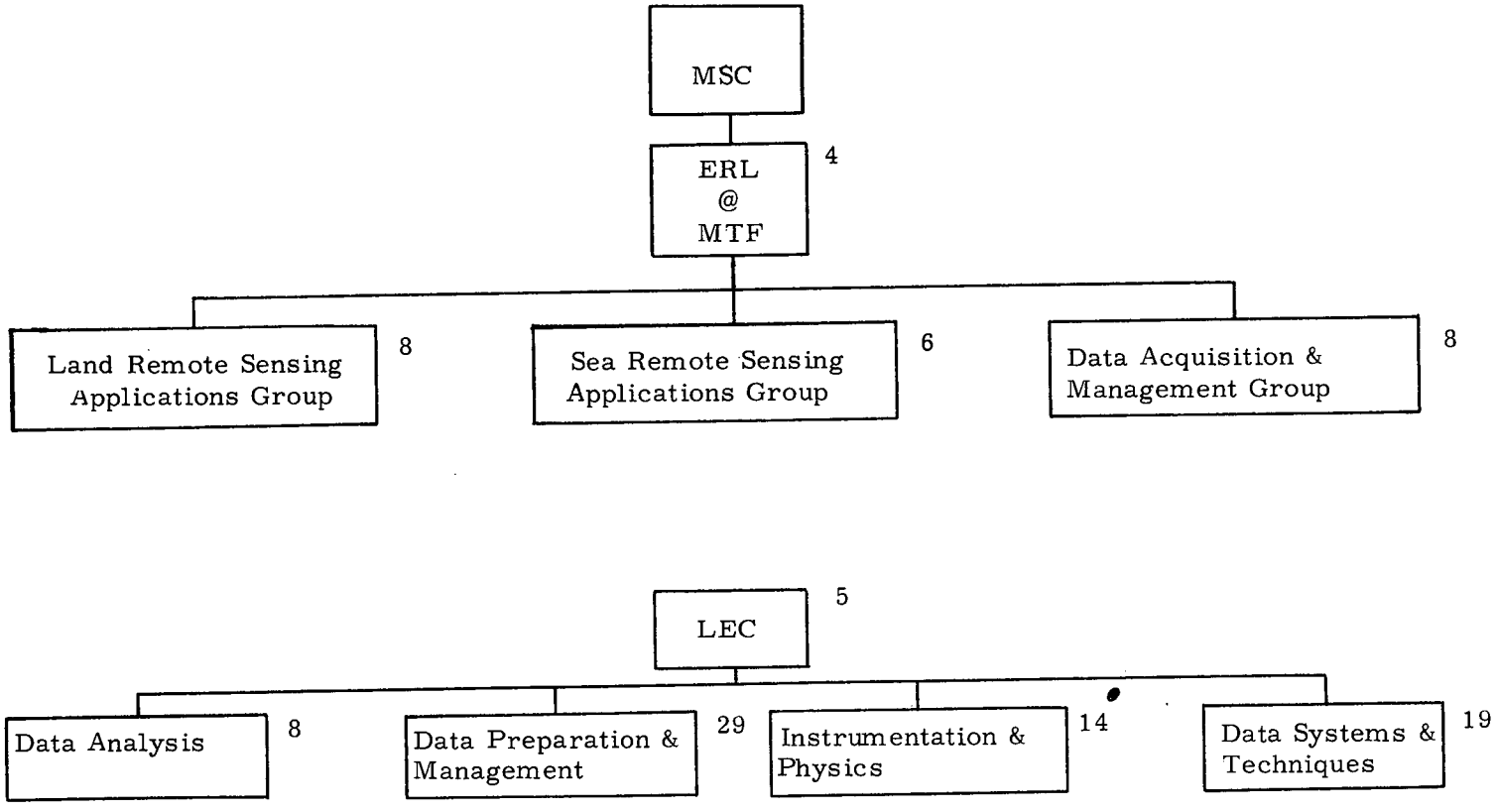

Figure 2. - Organization Chart

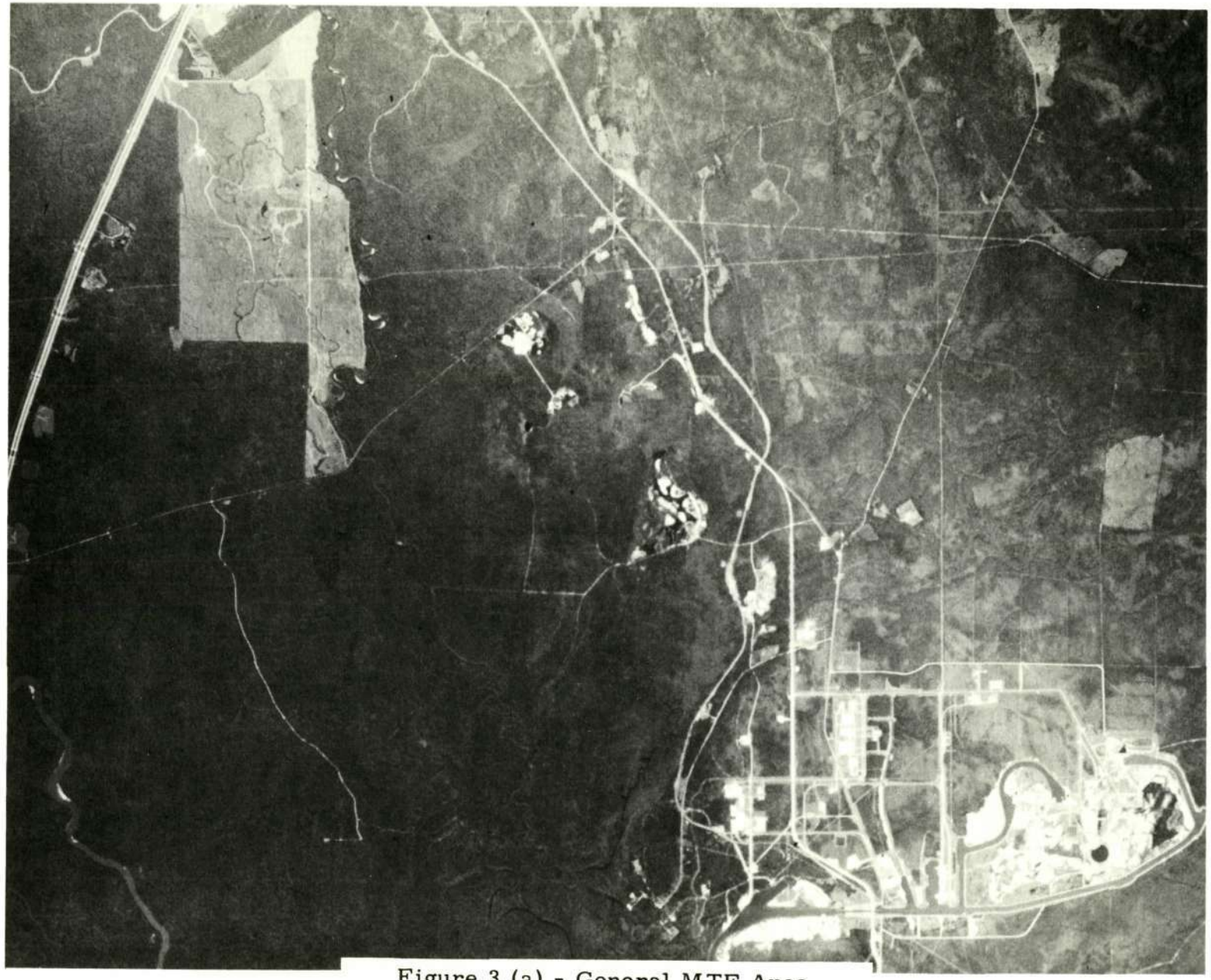

Figure 3 (a) - General MTF Area

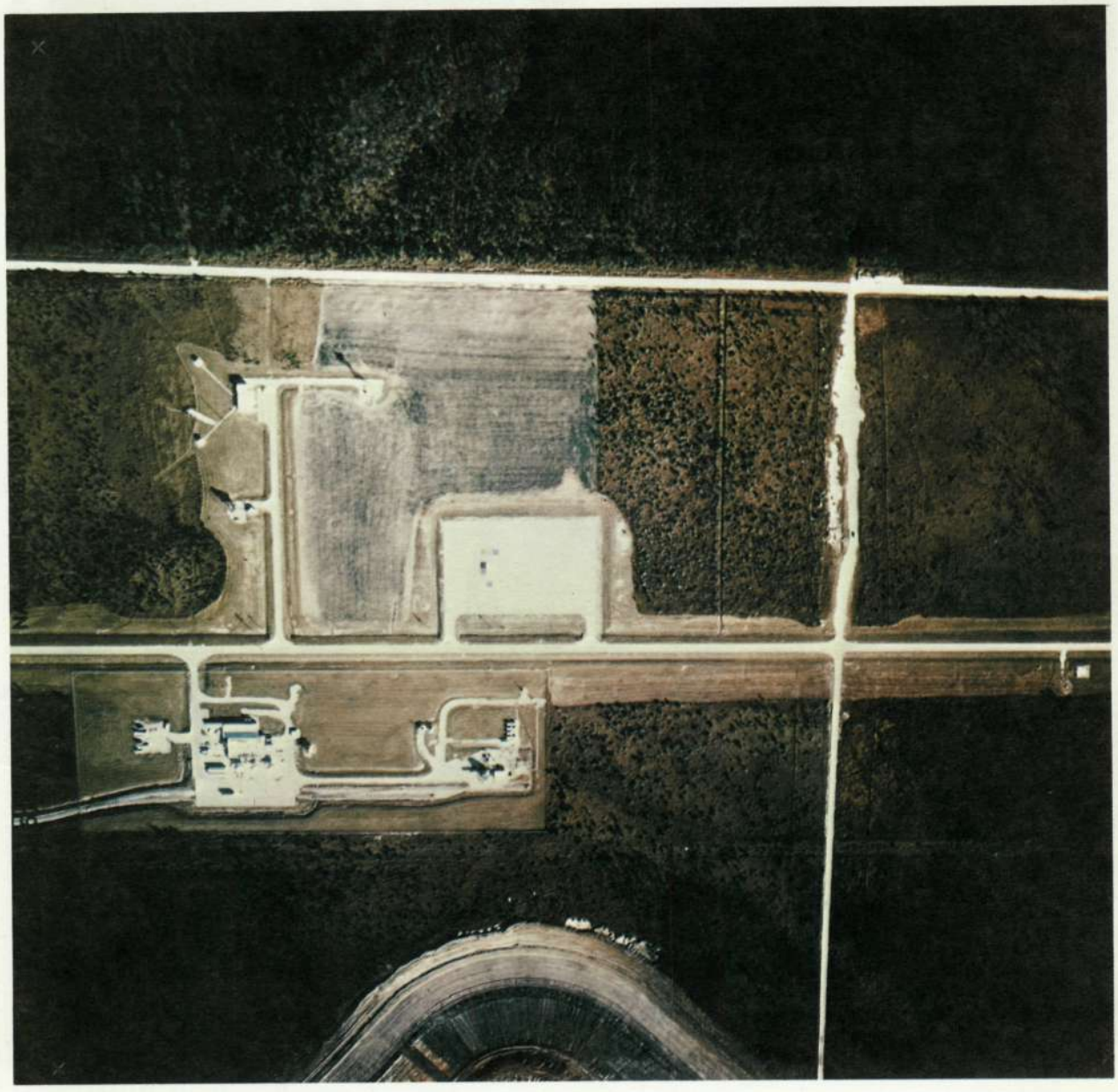

Figure 3 (b) - Target Array

Figure 3 (c) - Instrumentated Thermal Calibration Reservoir

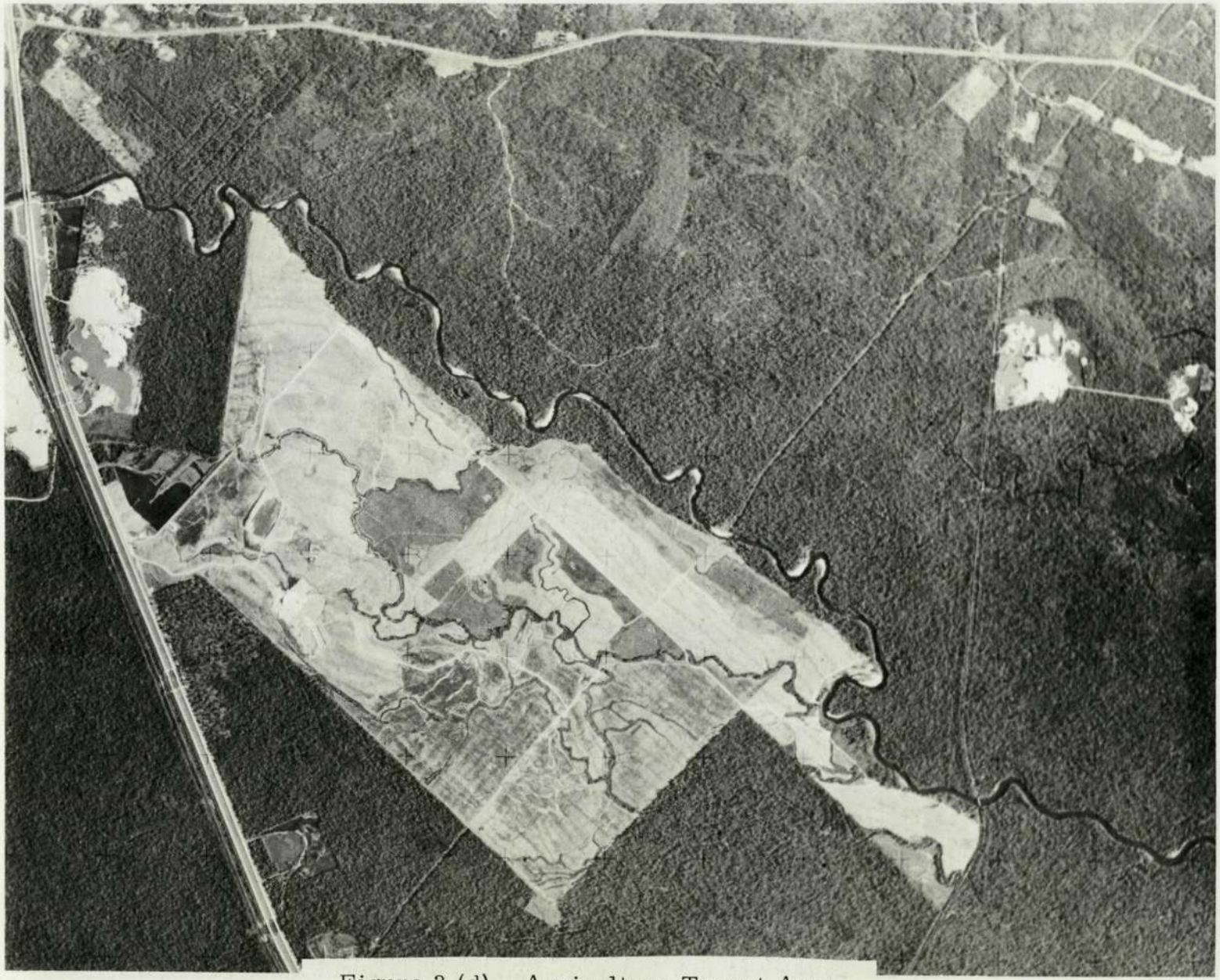

Figure 3 (d) - Agriculture Target Area

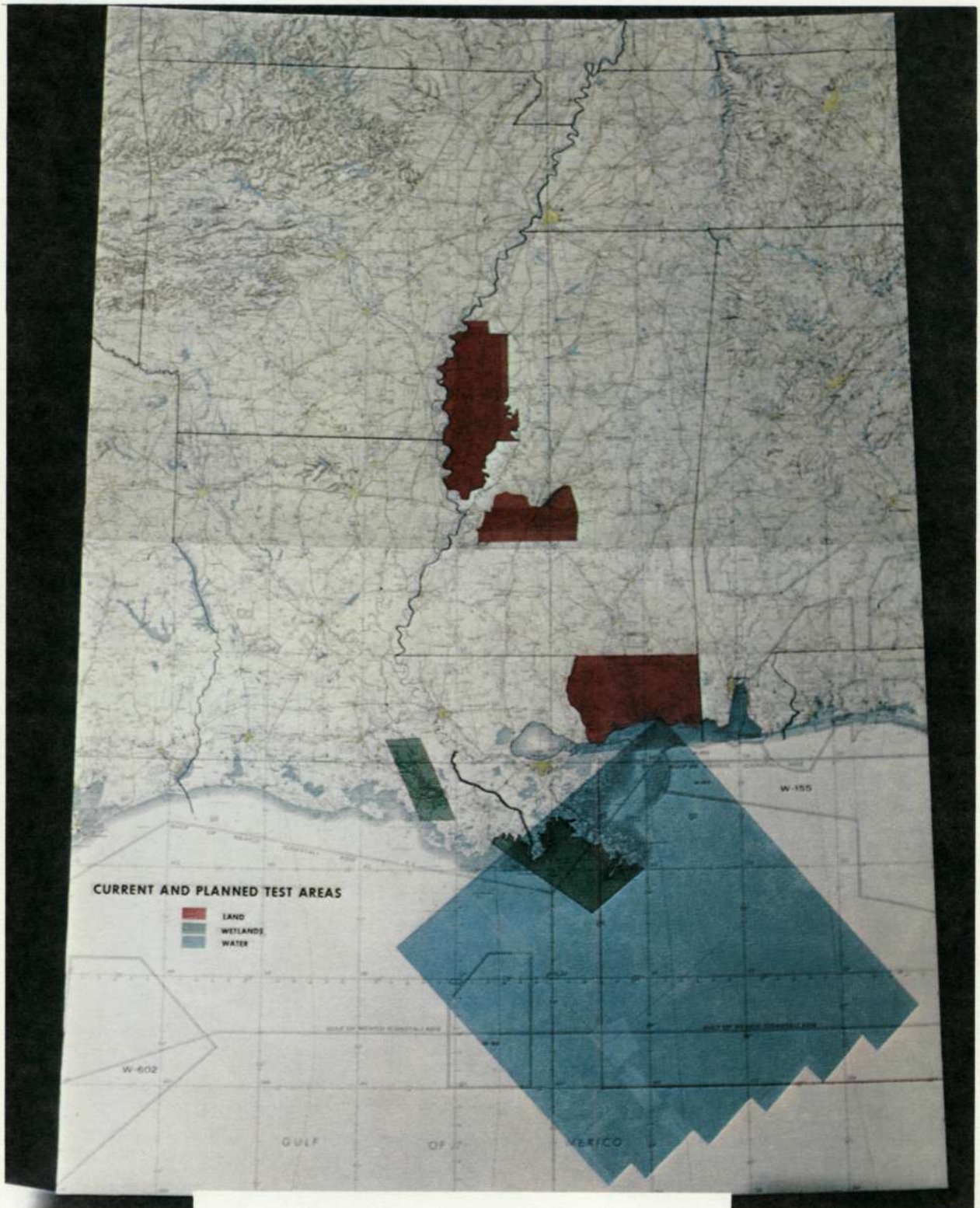

Figure 4. - State Target Areas

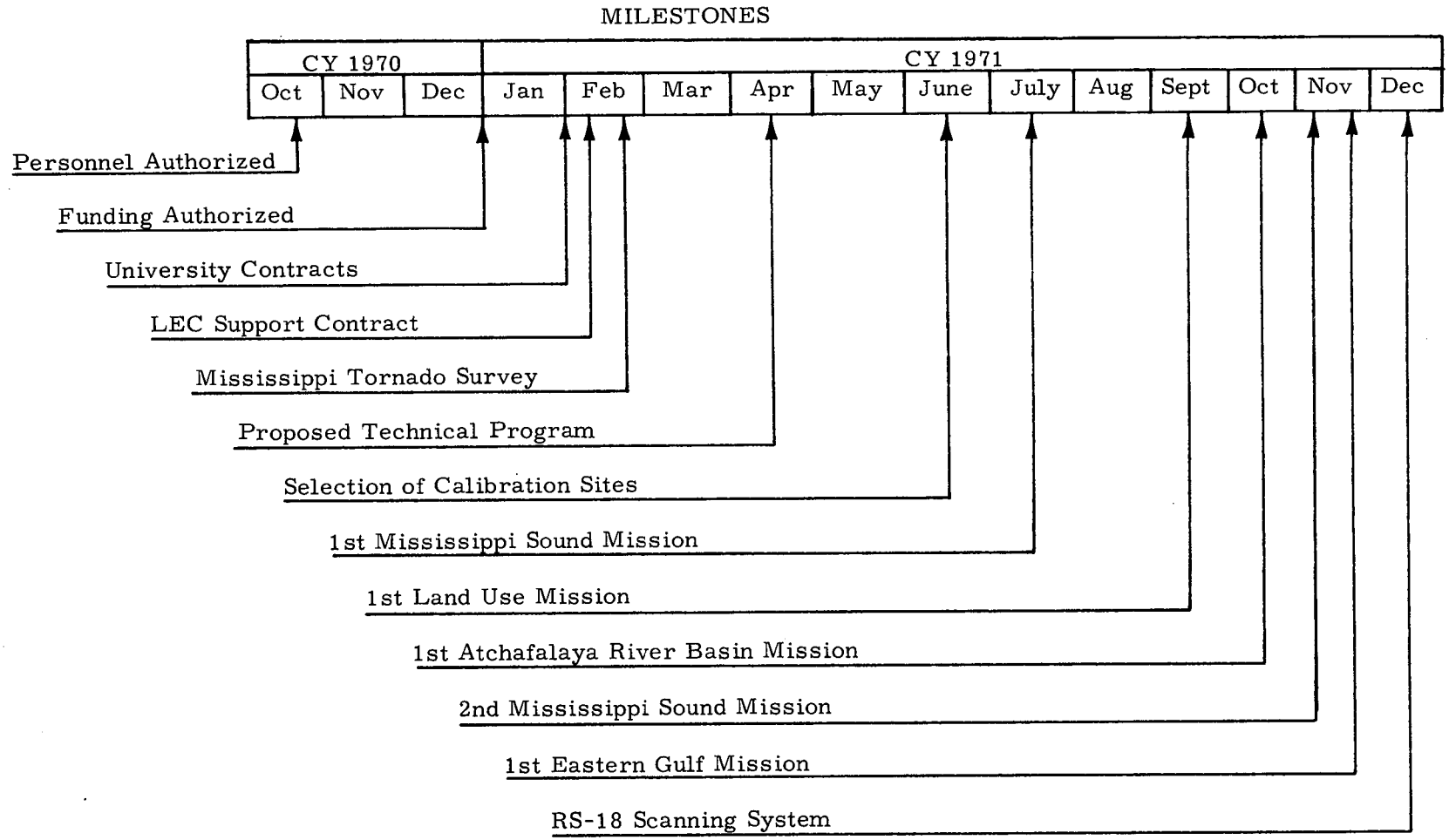

Figure 5. - Milestone Chart

SECTION 12

N72-29313

SUMMARY OF 1971 WATER REMOTE SENSING INVESTIGATIONS

by

Edward Lee Tilton, III
National Aeronautics and Space Administration
Earth Resources Laboratory
Mississippi Test Facility

INTRODUCTION

The Earth Resources Laboratory (ERL) has undertaken a Sea Remote Sensing Program designed to use multispectral instruments and techniques to characterize near shore and deep bodies of water. It is recognized that other investigations on remote sensing techniques and the evaluation of remote sensing instruments have preceded the ERL program and are ongoing. It is the intention of the ERL program to build on these other elements of the Earth Resources Program throughout the investigations described herein.

The fundamental ERL concept is to define and use the appropriate combination of available remote sensing instruments which measure radiant energy in different parts of the electromagnetic spectrum to determine the physical and biological parameters that characterize a given water system. Furthermore, it is intended to formulate interrelationships of these parameters to define techniques that are of general applicability to water system problems and to demonstrate their application to channel management (dredging), pollution definition and tracking, probable fish location, and marine resource assessment and management.

A major parameter of any water system is its circulation. Unfortunately, this is a difficult one to measure directly using remote sensing techniques. However, it is one which, when defined, forms the basis for the physical characterization of the body of water. The transport of suspended matter and bottom materials, the mixing of chemical constituents and the distribution of nutrients and pollutants are all elements of the water system which may be more easily studied once the circulation is known. Therefore, circulation has been chosen as a focal point around which the characterization of a water system may be built.

Because circulation is a difficult parameter to measure directly by remote sensing, an approach must be devised to infer this parameter from measurements of other water system parameters. Techniques are available or under development for measuring parameters such as surface

temperature, surface salinity, and chlorophyll. Photographic data allows an assessment of turbidity patterns, water color and some bottom features. Also, photographic dye marker techniques are being developed for obtaining circulation information that may be correlated with that inferred from the interrelationship of other parameters mentioned above. The intent, therefore, is to devise a method of interrelating these parameters such that circulation may be inferred.

In designing the initial laboratory programs, primary consideration was given to a program structure that would result in future technique application guidelines for the proper choice of (1) the type and combination of instruments to be used, (2) the quantity and location of surface measurements required, and (3) light, medium or high altitude aircraft or satellite sensor platforms depending on the physical nature of the water body such as its geographic size and shape or its depth. Three categories were selected around which to build the program. A large, deep body of water was to be selected for study using high altitude aircraft and satellite data. A coastal, medium sized body of water, relatively shallow and having typical estuarine characteristics, was to be selected for study using light and medium aircraft. And finally, a small body of water, a subsystem to the near shore water body, was to be selected for development of light aircraft techniques.

STATUS OF ACTIVITIES IN CY71

Two major investigations were initiated early in 1971 to develop remote sensing techniques for water systems and to evaluate presently available remote sensing instruments.

Deep Water Bodies

First an investigation was planned to develop remote sensing techniques to be applied to deep water bodies. The initial data on this project is being gathered by high altitude aircraft. However, it is intended that the techniques developed be extended to satellite altitudes and that optimum systems and procedures be defined for general applicability to the ocean current systems. It is not felt that the data from ERTS A will be directly applicable to this work. However, ERTS B and the Skylab EREP data will be used as an integral part of the project to develop ocean current remote sensing techniques. Dr. Robert D. Boudreau is the Principal Investigator on this investigation. The following is a brief discussion of the project.

The Eastern Loop Current in the Eastern Gulf of Mexico was chosen for this investigation because it represents a deep water current system with seasonal variations and because of its proximity to the Laboratory. The Eastern Loop Current enters the Gulf through the Yucatan Straits and exits through the Straits of Florida. The current is a seasonal phenomena in that its northern most extent proceeds northward during the spring and summer. The Loop becomes detached during the fall and the gyre drifts into the Northern Part of the Gulf. Figure 1 shows thermal contours in the Gulf indicating the boundaries of the Loop. This data was taken on the EGMEX program in April 1970.

This deep water current phenomena affords the opportunity of developing remote sensing techniques for defining surface thermal characteristics of a large body of water using high altitude, broad coverage instruments. Initial efforts have been directed at using the RB57F aircraft at 60,000 foot altitude and an instrument complement of a thermal scanner (RS-7), a thermal radiometer (Block and PRT-5), a filterwheel spectrometer and cameras to determine surface thermal patterns, and deep water chlorophyll concentration. It is planned to incorporate the Scanning Imaging Spectroradiometer (SIS) into the chlorophyll investigation when the instrument becomes available although it is recognized that recent information from Goddard indicated that the SIS capability may be limited for chlorophyll work.

The placement of aircraft flight lines has been and will be arranged in future flights to give total imagery coverage over a large area of the Gulf in an attempt to delineate the fine as well as the gross thermal features of the current system. The thermal radiometers are being used to measure radiation temperature along the flight lines while the thermal scanner imagery allows an assessment of thermal patterns. The filterwheel spectrometer is being used to develop techniques for the correction of data errors due to atmospheric effects. The photographic imagery provides data for the measurement of chlorophyll concentration and also provides knowledge of the percent and type of cloud cover as well as an indication of sea state.

The first mission in a series of four seasonal missions was flown on November 21, 1971. The area surveyed on that date is shown in Figure 2. The RB57F as well as the NP3A, a light aircraft and five surface vessels were involved. The NP3A, light aircraft and one surface vessel, as well as the RB57F, each carried a radiation thermometer (PRT-5) for the purpose of establishing radiation temperature and atmospheric effects on these measurements from several different altitudes. The five surface vessels took thermometer readings and water samples for chlorophyll analysis to establish surface calibration data for the remote instruments. A 200 mile surface temperature transect taken along Flight Line 3 by one of the surface vessels on an aborted

attempt to perform this mission on November 12, 1971, indicated a surface temperature distribution very similar to that shown in Figure 1. This data along with oral reports received from the Oregon II research vessel which was running transects in the Gulf for the EGMEX V program during the first three weeks in November gave confidence that the area to be surveyed covered at least a portion of the Eastern Loop Current. It was not possible at that time to extend the RB57F flight lines further into the Loop Current region because of aircraft navigation limitations. In addition to the surface water measurements, radiosonde data and surface weather observations were gathered during the mission to establish atmospheric parameters for use in an atmospheric data correction model being developed as a part of the project.

At the time of this writing approximately sixty percent of the NP3A and RB57F data from the November mission has been received from Houston and is being prepared for analysis. All surface data has been analyzed and reported in "Eastern Gulf of Mexico Remote Sensing Study, Experiment #1, Part 1, Surface Measurements," dated November 21, 1971.

Coastal Water Bodies

An investigation was planned to characterize the physical parameters of a coastal body of water leading to the development of techniques for prediction of circulation from remotely sensed data. While the project described above is aimed at techniques to be used from satellites, it is appropriate to develop techniques for near shore bodies of water from medium altitude aircraft because of geographic size and instrument resolution required. This project is described in more detail in a companion paper, "Mississippi Sound Remote Sensing Study," by Dr. B. Houston Atwell, the Principal Investigator, and Dr. G.C. Thomann who is investigating the microwave aspect of the project. The following is a brief discussion of this phase of the program.

The Mississippi Sound was selected for the near shore study because of its nearness to the Earth Resources Laboratory, thus minimizing operational problems, and because of the interest of many local, state and federal agencies in its marine resources and protected water for shipping (Figure 3). Mobile Bay was included in this study because of the direct interaction of the Bay waters with the Sound waters. Also, the Sound interacts directly with the Eastern Gulf of Mexico.

The first two of four seasonal missions have been carried out in the Sound on July 22, 1971 and November 10, 1971. The missions have been scheduled to obtain seasonal and tidal variations in the data. Instrument complement, flight line placement, and altitudes flown have

been arranged to achieve definition of an optimum set of procedures for the determination of circulation and the associated parameters.

An integral part of this approach to studying coastal water systems through the use of remote sensing is the establishment of proper surface measurement techniques. During the development stage detailed surface parameter coverage is required so that the physical phenomena being measured may be understood and so that correct interpretation techniques may be established for the remotely sensed data. This detailed surface measurement coverage is being obtained in the Mississippi Sound Study through the cooperation of university, state and federal agencies in the Louisiana, Mississippi and Alabama coastal areas.

The participants in the study are shown in Figure 4. Their interest and cooperation in the study has made it possible to develop a very complete description of the water parameters from surface measurements during an overflight. Furthermore, these participants are considered among the eventual users of the remote techniques being developed and this cooperative effort has enhanced the pursuit of potential remote sensing applications in each of their respective areas of interest and responsibility.

At this time all of the NP3A data from the first mission and seventy percent of the NP3A data from the second mission have been received from Houston. Two reports on the surface measurements have been issued thus far entitled, "Mississippi Sound Remote Sensing Study, Part I, Surface Measurements from Experiment #1," dated July 22, 1971, and "Mississippi Sound Remote Sensing Study, Part I, Surface Measurements from Experiment #2," dated November 10, 1971. An interim report on the remotely sensed data from the July 22, 1971 mission is in preparation. It is planned to prepare and issue in the summer of 1972 a final report covering the four Mississippi Sound Missions.

SUPPORTING ACTIVITIES

A supporting activity receiving close attention and requiring considerable effort during ERL's first year was the establishment and implementation of efficient data preparation techniques for both the surface measurements and remotely sensed data. A major goal is to have all contour charts, plots, imagery mosaics and laboratory analyses of surface samples for the major water parameters completed in a timely fashion. Goals of one month for the preparation of a surface measurement report and three months for preparation of the remotely sensed data collected by Houston aircraft have been established. The one

month goal has been met on the last two missions carried out in mid November and it is expected the three month goal will also be met on those two missions.

The method used to achieve these goals was to identify a standard product to be prepared for each type of data. For example, upon receipt of the photographic imagery the first step is to prepare actual flight line maps noting the time of the imagery on the map and the orientation of the frame. Throughout the rest of the analysis all data are keyed to this map. All surface data and radiometer data are contoured on 1/250,000 charts for ease of comparison in establishing interrelationships between the parameters. These standard products are illustrated in the paper "Mississippi Sound Remote Sensing Study," by Dr. B. Houston Atwell and Dr. Gary C. Thomann.

Another area of supporting activity during the first year of the program was the establishment of standardized procedures for taking surface measurements such as temperature, salinity and chlorophyll, the establishment of coordination methods for taking surface measurements over large areas during aircraft overflights and the proper distribution of sampling points to allow correct interpretation of the remotely sensed data. Methods have been devised and successfully demonstrated that allow fifty surface crews from several different universities, state and government agencies to sample more than 100 different surface locations over a 1000 square mile body of water during a three to five hour aircraft mission. As the techniques are developed it is intended to reduce the number of sampling points to the minimum required for general usage of the procedure.

Similar coordination procedures were also required and developed for the several aircraft usually participating in these missions as well as for the retrieval of surface samples and the gathering of weather information. Requirements documents, flight plans, instruction packages and sampling kits for surface crews, and premission briefings have all become part of the standard operating procedure prior to a mission.

PLANNED ACTIVITIES FOR CY72

Plans for CY72 include the completion of the remaining flights on the Mississippi Sound and Eastern Gulf of Mexico investigations and the publication of reports on the results of these technique development activities. These reports will include a description of the instrument complement, appropriate sensor platforms and altitudes, and the procedures necessary to characterize bodies of water and an

assessment of the products to be derived from the techniques. Figure 5 shows a schedule perspective for the Sea Remote Sensing Program.

In addition, several other investigations will be initiated in 1972. A more intense study on a relatively small body of water will be conducted to develop low altitude, light aircraft remote sensing techniques. Biloxi Bay on the coast of Mississippi has been chosen for this study because of its relationship as a subsystem in the Mississippi Sound water system and because it is a biologically productive area with significant historical data available from previous studies. This will be a cooperative effort with the Gulf Coast Research Laboratory playing a significant role in the gathering and analysis of surface measurements and in the correlation and interpretation of the data. It is planned to make monthly remote and surface measurements of the physical and biological parameters in the Bay over a one year period. Again the objective is to develop the technique for defining the physical and appropriate biological parameters using remote sensors. The use of a light aircraft at low altitudes over small bodies of water can be a useful, economical tool for developing techniques that may later be extended to higher altitudes as procedures and atmospheric correction techniques are developed.

It is also planned to conduct an investigation in the Barataria Bay region on the Louisiana coast for the purpose of further development of microwave/salinity techniques and to demonstrate the water system characterization techniques developed during the Mississippi Sound investigation. This effort will be planned and implemented in cooperation with the Corps of Engineers (New Orleans District) and with several universities already doing research in the area. The Gulf Universities Research Corporation has chosen the Bay as a primary test area thus making available a capability for collection of detailed surface measurement data for correlation with the remotely sensed data.

SUMMARY

The first year of the ERL Sea Remote Sensing Program was concentrated on project planning, data acquisition procedures and data preparation techniques to establish a firm procedural basis for the program. Most of these procedural elements were established and proven during the three missions conducted in CY1971. It is anticipated that the program in CY1972 will see the analysis completed on the Mississippi Sound series and the first series of Eastern Gulf experiments allowing increased emphasis to be given to more intensive technique development studies, the interrelationship of parameters for the measurement and prediction of water circulation, and the demonstration of the application of these techniques.


GULF OF MEXICO
ATLANTIC
OCEAN
23
23.5
24
24.5
25
25.5
26
26.5
EGMEX - 1970
NOAA ART
OVERFLIGHT
APRIL 23 - 27 1970
TEMP °C
PENINSULA
DE YUCATAN

FIGURE 1

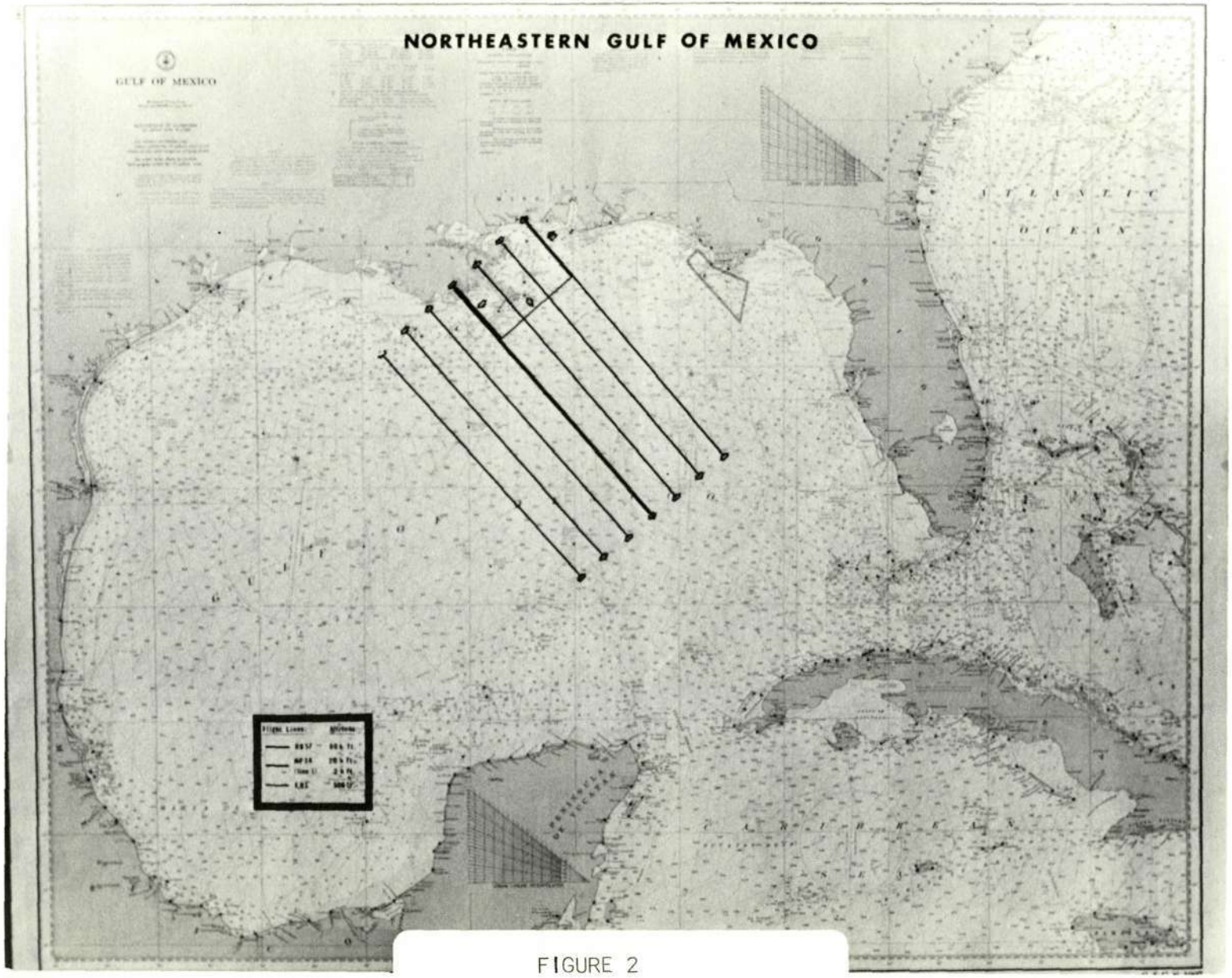

FIGURE 2

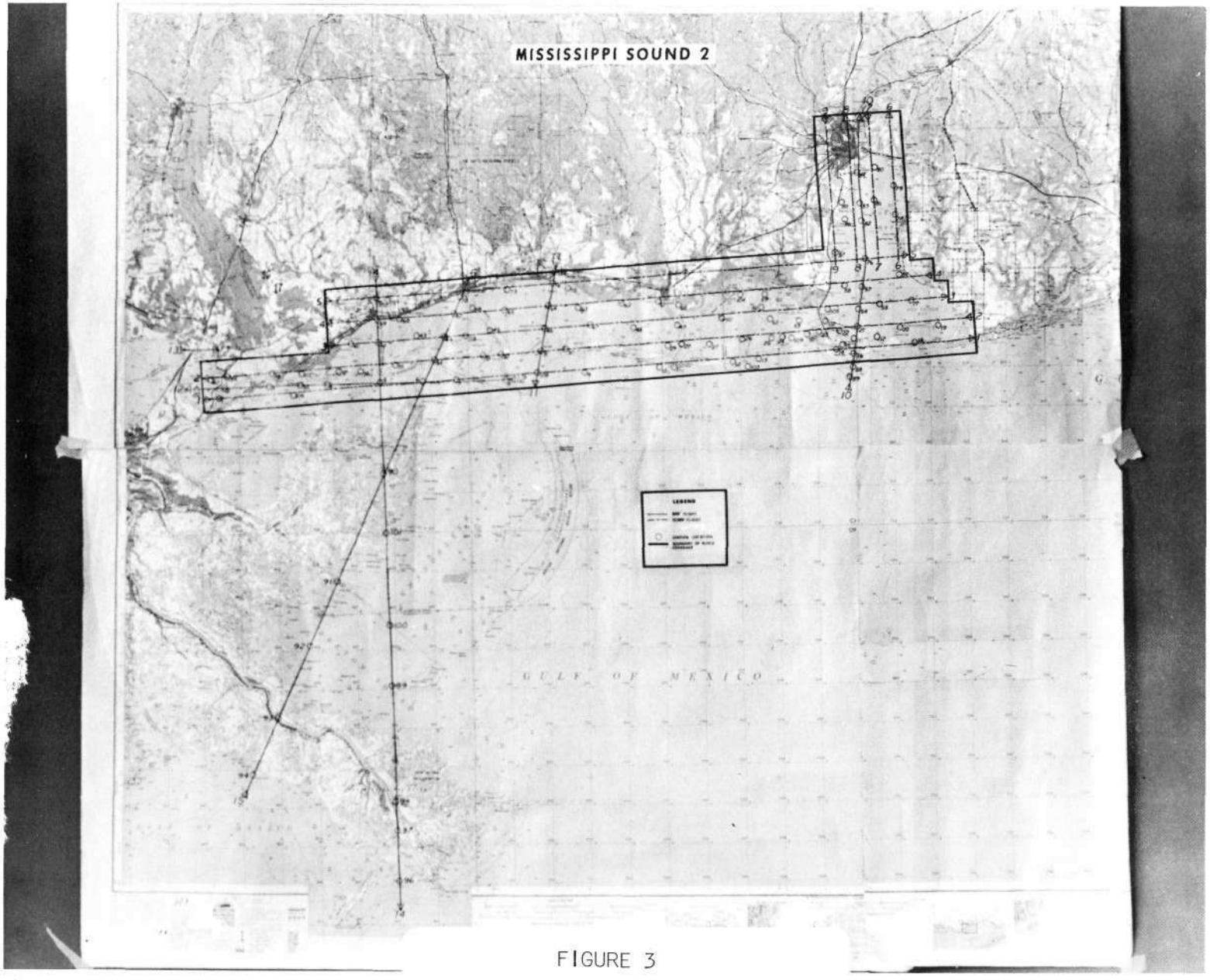

FIGURE 3

MISSISSIPPI SOUND STUDY PARTICIPANTS

ALABAMA DEPARTMENT OF CONSERVATION
GULF COAST RESEARCH LABORATORY
LOUISIANA STATE UNIVERSITY
LOUISIANA WILDLIFE AND FISHERIES
MISSISSIPPI MARINE CONSERVATION COMMISSION
MISSISSIPPI STATE UNIVERSITY
NATIONAL MARINE FISHERIES SERVICE
NOVA UNIVERSITY
TULANE UNIVERSITY
UNIVERSITY OF ALABAMA, MARINE SCIENCE INSTITUTE
U.S. FOOD AND DRUG ADMINISTRATION
U.S. CORPS OF ENGINEERS - MOBILE, ALABAMA
U.S. CORPS OF ENGINEERS - NEW ORLEANS, LOUISIANA

FIGURE 4

SEA REMOTE SENSING PROJECTS
SCHEDULE PERSPECTIVE

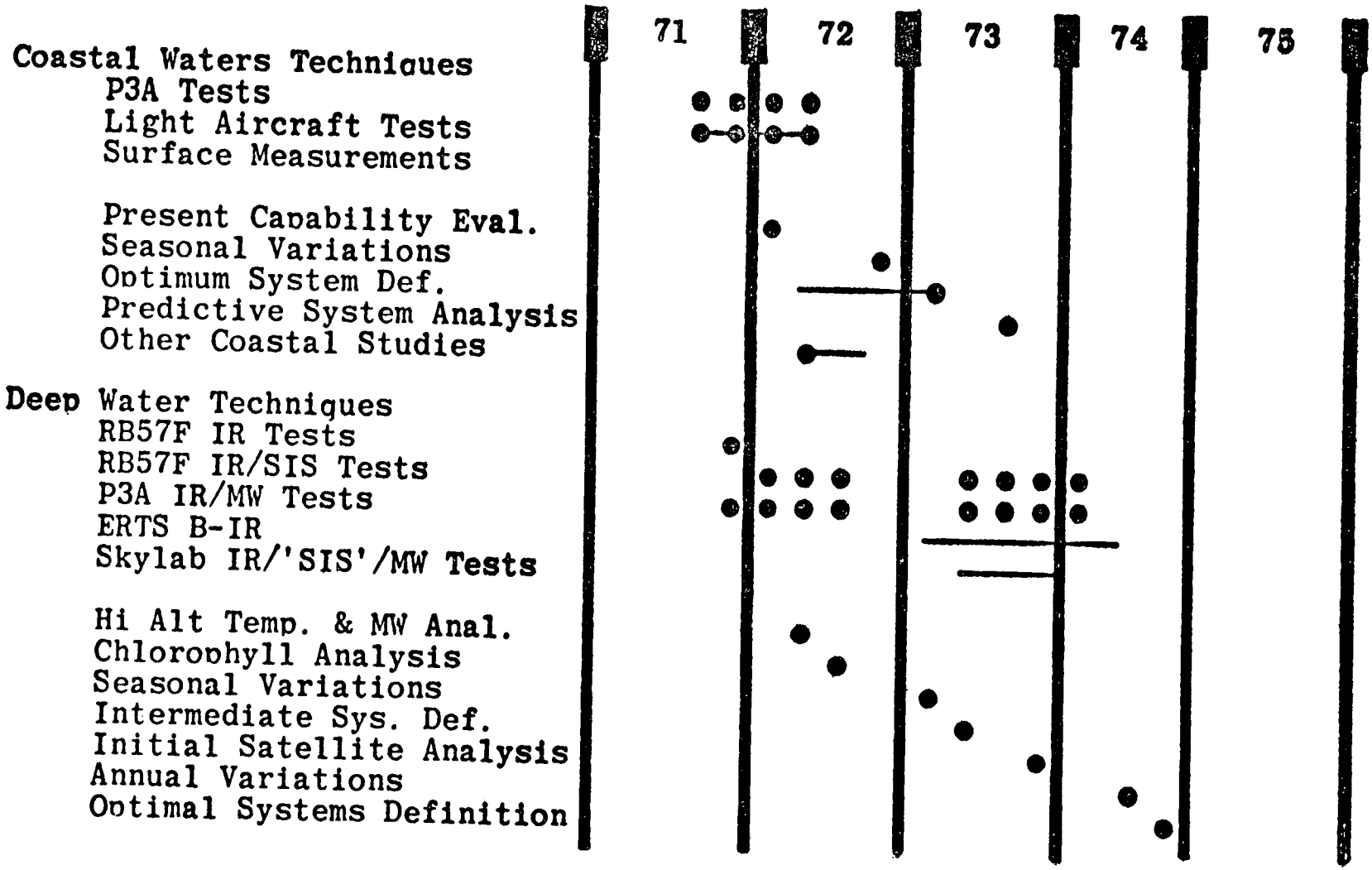

FIGURE 5

SECTION 13

N72-29314

MISSISSIPPI SOUND REMOTE SENSING STUDY

by

Dr. B. Houston Atwell & Dr. G.C. Thomann
National Aeronautics and Space Administration
Earth Resources Laboratory
Mississippi Test Facility

As a part of the research program of the NASA Earth Resources Laboratory, a remote sensing study of the Mississippi Sound was initiated in April, 1971. The objective of the study is the development of remote sensing techniques to study near shore marine waters. In directing our efforts toward this general goal, the following specific elements have been included in our study plan: (1) evaluate existing techniques and instrument capabilities for remote measurement of parameters which characterize near shore water, (2) integrate these parameters into a system which will make possible the definition of circulation characteristics, (3) conduct applications experiments and (4) define hardware development requirements and/or system specifications.

A list of parameters which characterize coastal water bodies is shown in Table I. Determination of these parameters is prerequisite to evaluating the condition of near shore waters. Also shown in Table I are remote sensing techniques which have been developed to varying degrees to evaluate these parameters. It is our goal to continue this development, and furthermore, to integrate these techniques with conventional measurements into a system which will allow assessment of conditions to determine what effects natural and man-made stresses will have on a coastal water body.

DATA ACQUISITION

Aircraft Measurements

The data acquisition phase of this study was planned to be framed about a series of overflights by NASA aircraft equipped with remote sensing data systems.

The first overflight, Mississippi Sound I, took place July 22, 1971. Two aircraft were used: the NASA NP3A equipped with camera systems, PRT-5 radiation thermometer, RS-14 infrared scanner, and the multi-frequency microwave radiometer; and a light aircraft equipped with a second PRT-5.

Figure 1 shows a map of the test area including flight lines flown by the NP3A and the light aircraft. The aircraft and flight line altitudes are shown in the legend.

The flight lines were planned with the following objectives: (1) adequate PRT-5 coverage to develop a temperature contour map from aerial measurements, (2) RS-14 scanner imagery along one flight line at an altitude of 20,000 feet to assess temperature anomalies associated with waters being exchanged through passes connecting the Mississippi Sound to the Gulf of Mexico, (3) low altitude flight lines (800 ft) in areas where strong salinity gradients exist to evaluate effects of salinity on microwave emission from the water surface and (4) multiband photography coverage for sea color studies related to chlorophyll concentration.

Surface Measurements

Surface measurements were made by a total of 43 boats which occupied eighty-five (85) stations (Figure 1) throughout the Mississippi Sound. The measurements made by each of the boats are shown in Table II.

Meteorological data, including radiosondes, were taken at several stations adjacent to the Mississippi Sound as an aid in reduction of the remotely sensed data.

Surface water temperatures were obtained by taking "bucket" samples of water as near to the surface as possible and measuring the temperature of this water immediately with a thermometer.

Tide measurements were obtained from the U.S. Corps of Engineers for stations at Mobile, Alabama; Dauphin Island, Alabama; Gulfport, Mississippi and Pascagoula, Mississippi.

Laboratory Analysis

Water samples collected were subjected to laboratory analysis for parameters listed in Table III.

Salinities were run with a Bissett-Berman Laboratory Salinometer. Standard (35 $^{o}/oo$) sea water was used as a reference, and salinities were determined from the conductivity ratio of the sample to that of the standard. Temperature and instrument drift corrections were made according to the Bissett-Berman Instruction Manual.

Water samples at each station were analyzed for chlorophyll content, which gives a measure of the phytoplankton present. The

technique used was essentially that proposed by SCOR-UNESCO Working Group 17 in Determination of Photosynthetic Pigments in Sea-Water, UNESCO, Paris, 1969. Each water sample for chlorophyll analysis was filtered through a millipore 0.45 micron acetate filter. The filters and their residue were stored at -5°C over activitated silica gel. Each filter and its residue was ground in a teflon tissue grinder. Ninety percent acetone was used as the extracting agent. The acetone homogenates were stored in the dark for ten minutes, then centrifuged at 2000 g for forty minutes instead of the recommended ten minutes because the extract was too turbid. The volume of each extract was recorded and the absorption spectrum of the chlorophyll extract measured against a blank acetate filter dissolved in 90% acetone. The measurements were made on a Cary 17 Spectrophotometer.

Scientists from Mississippi State University performed water chemistry analysis described below. Although these analyses may not be directly related to the remote measurements, there may be indirect relations and they were also of general interest to participants in the surface measurement study.

Light transmission measurements were made using a Bausch and Lomb Spectronic 20 at a wavelength of 625 nm.

Primary productivity and metabolic activity measurements were made by filling two 300 ml B.O.D. bottles with samples and the dissolved oxygen (in one of the bottles) determined using a YSI portable oxygen meter. The bottles were immediately stoppered and one of the pair covered with aluminum foil. Both bottles were placed in a circulating water bath (20 gal. aquarium) at 26 $\pm$ 1°C; incubated for eight hours, and the dissolved oxygen determined on both bottles.

Turbidity measurements were conducted on a Coleman Nephocolorimeter. Total coliform, chloride ion, salinity, phosphate, and nitrate procedures used were those listed in Standard Methods for the Examination of Water and Wastewater, 12th ED. P. 234.

pH determinations were made using a Coleman Model 12 pH meter.

All measurements made by the "ground truth" boats, results of the laboratory analysis of water samples, and meteorological and tidal data have been published by the NASA Earth Resources Laboratory.[1] Copies of this report have been distributed to all participants of the study. Contour maps of surface temperature, surface salinity and surface chlorophyll content over Mississippi Sound were developed from the surface measurements and laboratory analysis. These maps are shown in Figures 2, 3, and 4 respectively.

Each of these contour maps has many interesting features. The contours of chlorophyll concentration show a variation from 2 to 20 mg/m^3 throughout Mississippi Sound. In general, there is a monotonic decrease in chlorophyll content with increasing distance from the coast; however, in areas where influxes of Gulf of Mexico water enter the Sound, variations to this pattern exist. The Gulf of Mexico waters have a much lower chlorophyll content, differing by an order of magnitude to the richest Mississippi Sound water.

Surface temperature, as measured by the "ground truth" boats, showed a variation of about $2^{o}C$ throughout the Mississippi Sound. The patterns shown by the contour map indicate that most of the surface temperature variations are associated with waters being introduced into Mississippi Sound from the Gulf of Mexico on an incoming tide. The water in the Gulf of Mexico during this season of the year (late summer) is characteristically cooler than the Mississippi Sound water.

The surface salinities were lower in the western part of the Mississippi Sound near Lake Borgne. Salinities of 10 $^{o}/oo$ were measured here. The highest salinities were in the area of the passes and offshore islands; here the values approach normal open ocean salinities of 35 $^{o}/oo$. The fresh water influx from the Pearl River in the western part of the Mississippi Sound is shown very clearly. Also the effect of high salinity water entering through the passes is distinctly displayed by the contour maps.

These contour maps, and the data from which they were constructed provide an excellent set of "ground truth" data for evaluation of the remotely sensed data.

REMOTELY SENSED DATA

Radiometric Water Temperature

The NASA NP3A was equipped with a Barnes PRT-5 radiation thermometer and an RS-14 infrared scanner for the Mississippi Sound I experiment. The PRT-5 was operated on all NP3A flight lines shown in Figure 1; whereas the scanner was used only on flight lines at altitudes of 3,000 and 20,000 feet. The PRT-5 data at 20,000 ft. altitude contained noise (thought to be due to air frame vibration) that made the data unsuitable for further analysis. Thus the usable thermal data obtained from the NP3A was PRT-5 data on all flight lines at 800 and 3,000 feet and RS-14 Scanner imagery on the 3,000 and 20,000 foot altitude flight lines.

A light aircraft, equipped with a second PRT-5, flew flight lines in the eastern portion of the Mississippi Sound (Figure 1). The combined radiometric temperature data from both aircraft along with qualitative information from the RS-14 scanner imagery were used to develop a radiometric surface temperature contour map (Figure 5). Radiometric temperature data used to construct the contour map shown in Figure 5 were obtained from altitude of 800 and 3,000 feet. In order to combine these all temperatures were reduced to a surface datum. The corrections due to the atmosphere were +3.2°C and +2.0°C for the flight lines at 3,000 feet and 800 feet respectively. These corrections were determined emperically by an analysis of points where surface temperatures and radiometric temperatures from both altitudes were obtained within a 1/2 hour time interval.

The flight lines for the experiment were planned so that the high altitude line (20,000 feet) would provide infrared scanner imagery of the passes connecting Mississippi Sound to the Gulf of Mexico. It was assumed that surface temperature anomalies associated with waters being exchanged through these passes would provide information pertaining to the water circulation in the Mississippi Sound. Scanner imagery of Petit Bois Pass between Dauphin and Petit Bois Islands (Figure 6) provides an interesting illustration in this respect.

On July 22, 1971, the day of the experiment, the water in the Gulf of Mexico was generally cooler than that in the Mississippi Sound. On the day of the experiment, there had been an incoming tide all morning with high tide at approximately 12:00 Noon. The infrared scanner imagery shown in Figure 6 was collected between 11:51 a.m. and 11:52 a.m. The cool water from the Gulf of Mexico that entered the Mississippi Sound through Petit Bois Pass on the incoming tide and its course after entering the Sound is shown very clearly by this imagery.

From an analysis of both the scanner imagery and video signal from the scanner recorded on magnetic tape, the temperature difference between the incoming Gulf of Mexico water and the resident Mississippi Sound water was determined to be between 0.4°C and 0.6°C.[2] This difference compares very well with the temperature contour maps drawn from shipboard measurements (Figure 2) and remote radiometric measurements (Figure 5).

Chlorophyll Studies

The development of techniques to remotely determine the phytoplankton concentration of near shore waters has been an integral part of the Mississippi Sound Remote Sensind Study. A parameter related to the concentration of phytoplankton in marine water is the amount of phytoplankton pigments in the water, and, in particular, the various

types of chlorophylls present.[3] In pure open ocean waters the wavelength of maximum reflectance is about 462 nm. As phytoplanktons are added there is a shift toward longer wavelengths. This phenomena has been the basis for much of the research done in remote sensing of marine phytoplankton concentrations. A similar approach has been followed in our study.

In open ocean waters the ratio of the Blue to Green reflectance as measured by photographic densitometry has been used with reasonable success as a measure of algal concentration.[4] In the case of nearshore waters such as Mississippi Sound, however, complications exist which make modifications to this technique necessary. These factors are: (1) turbid waters with large sediment content, (2) high concentrations of phytoplankton which make scattering of light as well as absorbtance important,[4] and (3) in shallow water, bottom reflectance may introduce errors. In order to take some of these factors into account, we have used a ratio of Blue to Green•Red and have related this ratio to chlorophyll concentration.

Examination of the KA-62 multiband photography taken during the mission showed that photographs of 11 of the "ground truth" vessels had been obtained. The chlorophyll concentration determined from water samples collected by these surface vessels (method described in previous section) was plotted against the ratio of film densities Blue/Green•Red (Figure 7). The correlation between this ratio and chlorophyll concentration is generally encouraging although a few points show a wide divergence.

Salinity Measurement

Emissivity of Sea Water: Ionic solutes alter the real and imaginary part of the dielectric constant of pure water in the microwave region. A conductivity term is also introduced, as an addition to the imaginary term. The Debye type equation,[6,7] with the conductivity term added, can be used to express the dielectric constant as a function of frequency.

$$\varepsilon_c = \frac{\varepsilon_s - \varepsilon_\infty}{1 + \frac{j\lambda_s^{1-\alpha}}{\lambda}} + \varepsilon_\infty + \frac{\alpha}{jw\varepsilon_o}$$

ε_c - complex dielectric constant

ε_s - low frequency dielectric constant of the solution

ε_∞ - high frequency dielectric constant of the solution

λ_s - relaxation wavelength

λ - wavelength

σ - conductivity

ω - frequency

ε_o - permittivity of a vacuum

α - spread parameter

The four parameters, ε_s, λ_s, σ, and α are functions of the normality and temperature of the solution. ε_s and λ_s decrease with increasing normality due to hydration;[8] the conductivity increases almost directly with concentration, at least for dilute solutions, due to the increasing number of ions available. The importance of the spread parameter, α, is relatively minor and will be ignored for the present. At low microwave frequencies the dependence upon conductivity is strong enough to cause a measurable decrease in the radiation emissivity of the solution as normality increases. As an illustration of this effect, the emissivity of a NaCl solution at a temperature of 30°C is shown in Figure 8. The Fresnel reflection coefficient equations for a flat surface were used to relate the emissivity to ε_s. The incidence angle is 0°.

Sea water is a complex solution, containing every element presently known, although many only as trace elements.[9] The complex dielectric constant of sea water as a function of salinity and temperature has not presently been measured. Since NaCl accounts for 78% of the salts in sea water, a NaCl solution is usually used as a sea water substitute. The substitution can be made in a manner to produce sea water and NaCl solutions of either equal normality, or equal salinity. The latter appears to be most often used.[10,11] The gram equivalent weight of sea water is 57.85, that of NaCl is 58.45, so the substitutions are nearly equivalent. Since the effects on ε_s λ_s, and α of some of the salts other than NaCl in sea water are not precisely known, both probably introduce error. Diregarding these difficulties, a sea water salinity scale is added to Figure 8 positioned according to a equal normality substitution.

Radiometric and Salinity Measurements: Radiation upwelling from the Mississippi Sound was measured at the frequencies of 1.420, 10.625, and 31.4 GHz along flight lines 1, 2, 3, and 4 of the Mississippi Sound I mission. The flight lines are drawn in Figure 1. The aircraft altitude was 800 feet. The instrument used was the Multifrequency Microwave Radiometer, a conventional Dicke type radiometer, part of the instrument complement of the NP3A.

Surface values of salinity were obtained from water samples taken at the time of the aircraft overflight. The sampling positions are represented by large dots on the flight lines in Figure 1. The salinity of the samples was determined with a salinometer, as explained above. Standard sea water was used for calibration.

The apparent temperature at 1.42GHz and the measured salinity values along flight lines 1, 2, 3,and 4 are shown in Figures 9, 10, 11 and 12. The emissivity for sea water was calculated by substituting a NaCl solution of equal normality, except the conductivity of sea water rather than the salt solution was used. Hopefully, this improved the calculation accuracy. Each of the radiometric temperature data points is an average of the radiometer output voltage after calibration corrections were inserted. The averaging period is 16.6 sec., which corresponds to a ground distance of about 3,600 ft. Averaging over this distance would conceal any fine salinity structure which exists at the water surface. The averaging was necessitated by the high standard deviation (about 6°K) when the direct radiometer output with an averaging period of .20 sec. was used. Part of this large variance is believed due to interference from other equipment. It is not believed that sufficient fine salinity structure was present to appreciably affect the comparison of the average radiometric temperature with measured salinity. The radiometric temperature confidence interval shown in the graph is a 2σ interval for the averaged output variable, where σ is the standard deviation of the averaged output.

Actual surface temperatures along each flight line varied only slightly (about 1.5°K), hence water temperature was assumed to be a constant for each line. No corrections for either sea state or atmospheric effects have presently been made. Sea states were mild when the first four lines were flown. Wind velocities and wave heights for the four flight lines are shown in Table IV. Neither whitecaps nor sea foam, which has considerable effect upon apparent temperature,[12] were present. The four graphs demonstrate the correlation between salinity and apparent temperature obtained for this experiment. The fixed bias of about 30°K is probably due to a combination of system errors, uncertainties in the salinity/emissivity relationship, and to the reflected sky temperature, which has not been removed. It should be possible to eliminate this bias with the ground truth information and, in fact, if 30°K is subtracted from the measured apparent temperature, the salinity and apparent temperature curves align closely in many parts of the four graphs. However, discrepancies still exist, in particular in parts of Figures 9 and 12. Because of the large offset in the measured apparent temperature, and because of the larger than expected variance of the radiometer output, the authors hesitate to compare the data in an absolute sense. However, it is believed that the apparent temperature data maintains its relative integrity over the

short term, and the similarity of the curve shapes in the figures, especially the long flight line in Figure 9, demonstrate the sensitivity of apparent temperature to salinity and the possibility of measuring salinity values in this range remotely.

CONCLUDING REMARKS

The information presented thus far was primarily from the experiment which took place on July 22, 1971. Since that time there has been a second experiment on November 10, 1971. Aside from being at a different season of the year, there were other variations from the first experiment - the flight lines were revised (Figure 13) to provide complete infrared scanner coverage of Mississippi Sound. A different tide stage was chosen - an outgoing tide instead of the incoming tide occurring during the first experiment. It is hoped that viewing the Sound under these varying conditions will better aid us to understand the processes taking place.

At present, the status of the Mississippi Sound study is as follows: (1) we have developed a satisfactory system to gather "ground truth" over the entire area of Mississippi Sound to aid us in evaluating the remotely sensed data, (2) we have conducted two data acquisition experiments, (3) we are proceeding in analysis of individual sensor data from flights completed, and (4) we are pursuing methods which will allow interrelations between data from individual sensors in order to add another dimension to our study.

ACKNOWLEDGMENTS

Chlorophyll analysis from photographic densitometry was performed by Dr. S.R. Baig of NOVA University, Florida, under NASA Contract NAS9-12025.

REFERENCES

1. Mississippi Sound Remote Sensing Study, July 22, 1971, Part I, Surface Measurements, NASA Earth Resources Laboratory, NASA Mississippi Test Facility, Bay St. Louis, Mississippi.

2. Eppler, W.G., et al., "RS-14 Data Handling Technique Development," LEC Interdepartmental Communication, J.O. 151, January, 1972.

3. Yentsch, C.S., "The Influence of Phytoplankton Pigments on the Color of Sea Water." Deep-Sea Research, Vol. 7, pp. 1-9, 1960.

4. Baig, S.R., Final Report, NASA Contract NAS9-12025, December, 1971.

5. Baig, S.R., Personnal Communication, January, 1972.

6. Lane, J.A., and J.A. Saxon, "Dielectric Dispersion in Pure Polar Liquids at Very High Radio Frequencies, III. The Effect of Electrolytes in Solution." Royal Soc. Proc., Vol. A214, pp. 531-545, 1952.

7. Grant, E.H., et al.,"Dielectric Behavior of Water at Microwave Frequencies." J. of Chem. Phy., Vol. 26, No. 1, pp. 156-161, January, 1955.

8. Haggis, G.H., et al., "The Dielectric Properties of Water in Solutions." J. of Chem. Phy., Vol. 20, No. 9, pp. 1452-1465, September, 1952

9. Neumann, G. and Pierson, W.J., Jr., Principles of Physical Oceanography. Prentice-Hall, Inc., Englewood Cliffs, N.J., p. 40, 1966.

10. Saxton, J.A. and J.A. Lane, "Electrical Properties of Sea Water." Wireless Engineer, pp. 269-275, October, 1952

11. Paris, J.F., "Transfer of Thermal Microwaves in the Atmosphere." Vol. 1, Department of Meteorology, Texas A&M University, College Station, Texas, May, 1971.

12. Droppleman, J.D., "Apparent Microwave Emissivity of Sea Foam." J. of Geophy. Res., Vol. 75, No. 3, January, 1970.

Parameters	Applicable Remote Sensing Technique
Circulation	
Sediment Plumes	Visible Imagery and Radiometry
Thermal Patterns	Infrared
Salinity	Microwave Radiometry
Tides	
Winds	
Fresh Water Inflow	
Water Chemistry	
Biological Productivity	
Chlorophyll	Visible Imagery and Radiometry
Bathymetry	

Table I

Parameters Characterizing Coastal Waters
and Related Remote Sensing Technique

Surface Water Temperature
Air Temperature
Humidity
Wind-Direction and Speed
Secchi Transparency
Sea State Observation
Water Sample Collection

Table II

Measurements From Boats at Each Station

Parameters	Performed By
Salinity	ERL/LEC
Chlorophyll	ERL/NOVA Univeristy
Primary Productivity	Mississippi State University
Metabolic Activity	"
Turbidity	"
Coliform	"
pH	"
Chloride Ion	"
Sodium	"
Potassium	"
Calcium	"
Magnesium	"
Iron	"
Phosphate	"
Nitrate	"
Total Solid	"
Suspended Solids	"

Table III

Laboratory Analysis of Water Samples

		Wind Speed	Wind Direction	Wave Height
Line	1	0-5 knots	Variable	6 in
	2	5-10	NE	6
	3	3-5	NE	6-12
	4	3-5	NE	6

TABLE IV
Wind velocities and wave heights for flight lines 1, 2, 3, and 4 of Mississippi Sound I Mission

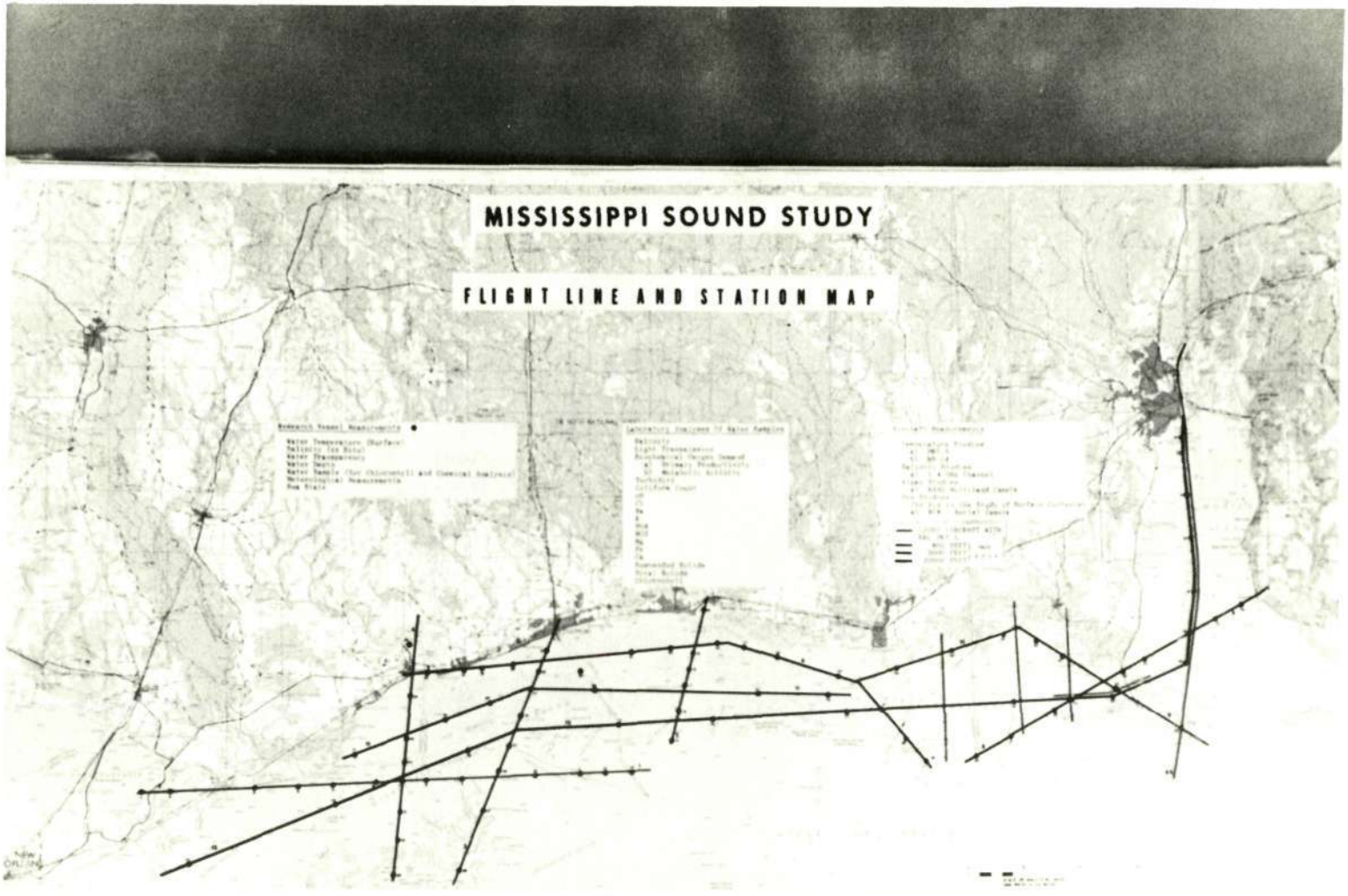

FIGURE 1
Mississippi Sound I, Flightline and Station Map,
July 22, 1971

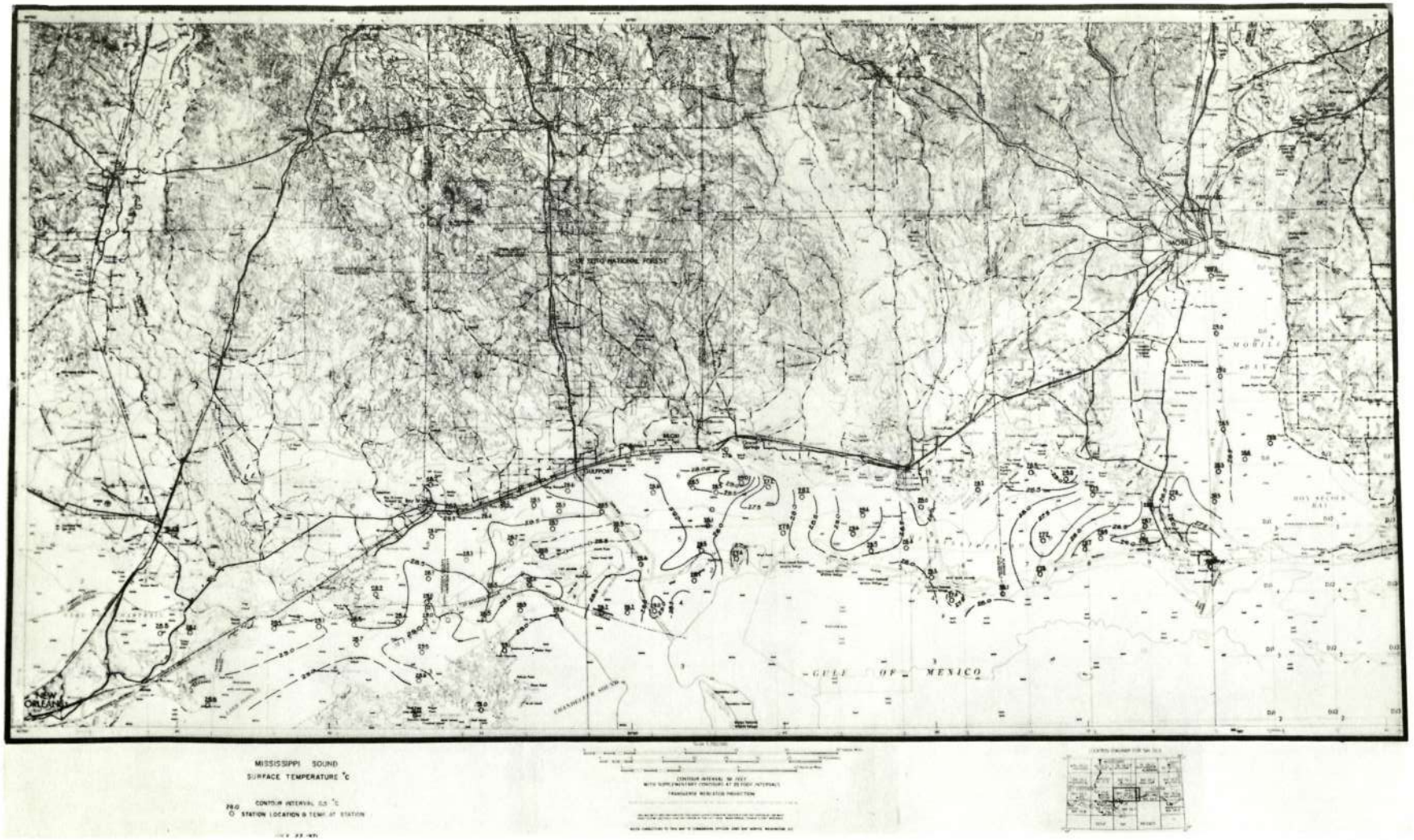

FIGURE 2
Mississippi Sound Surface Temperature ^{o}C,
July 22, 1971 - Shipboard Measurement

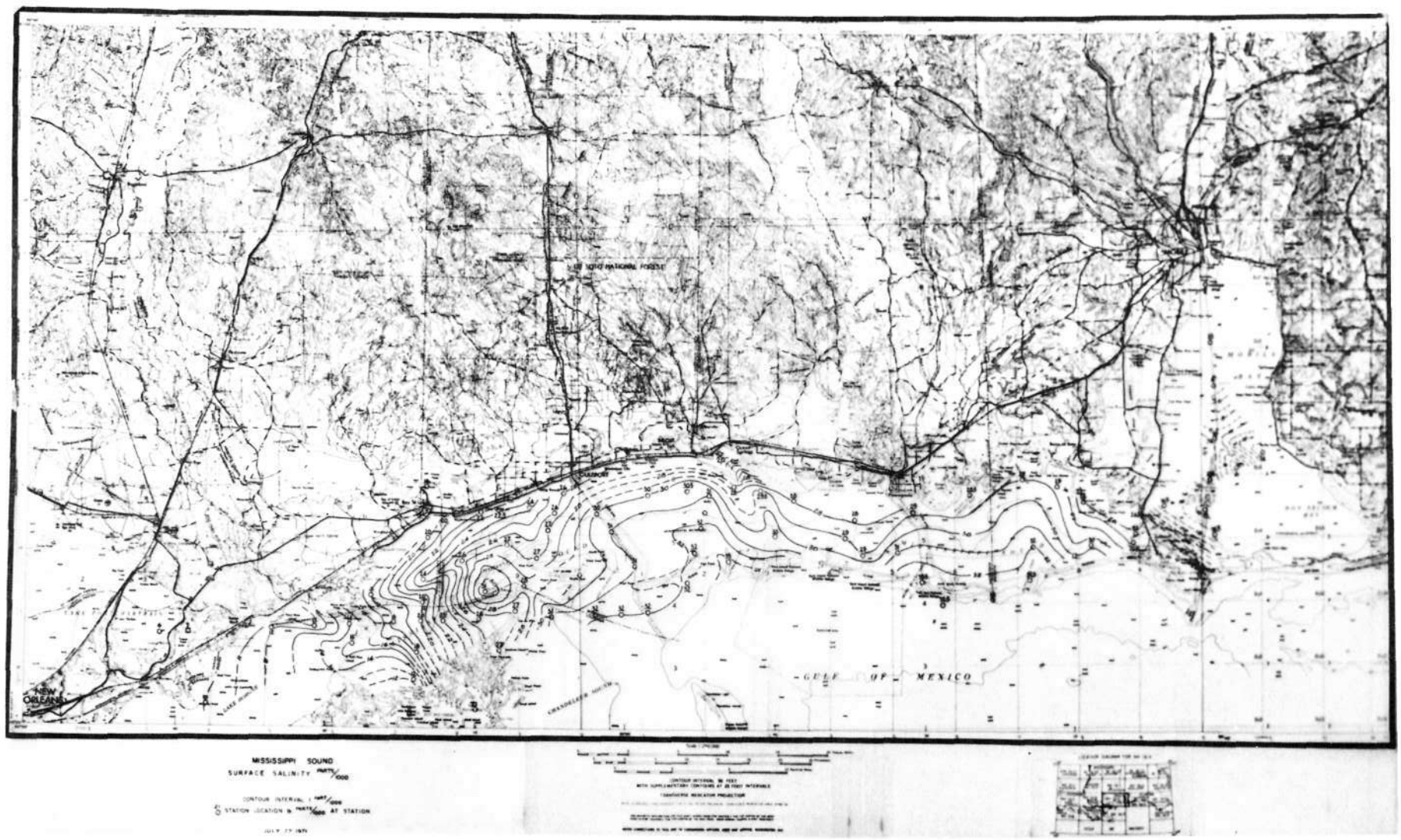

FIGURE 3
Mississippi Sound Surface Salinity o/oo,
July 22, 1971 - Laboratory Analysis

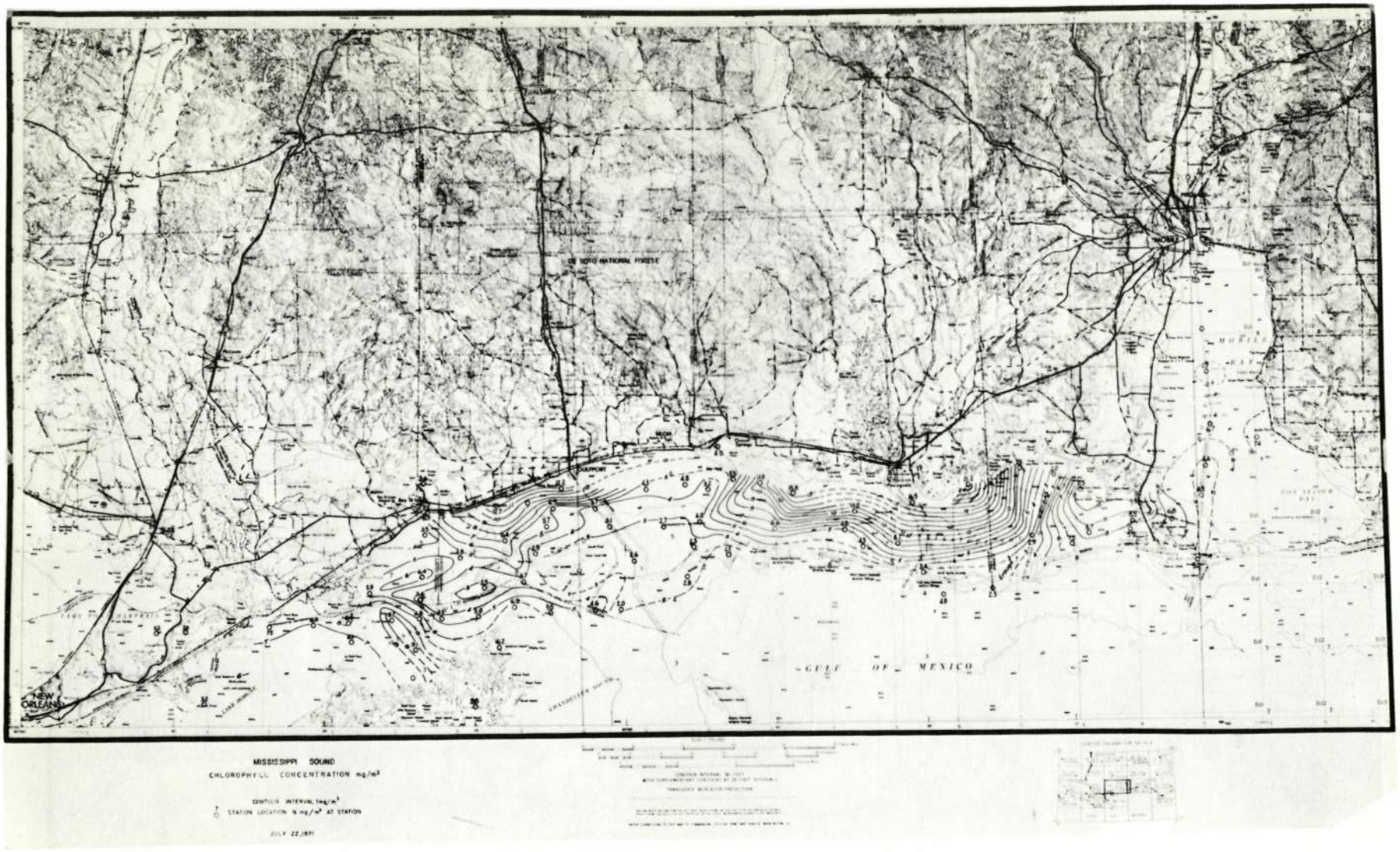

FIGURE 4
Mississippi Sound Surface Chlorophyll Concentration mg/m^3,
July 22, 1971 - Laboratory Analysis

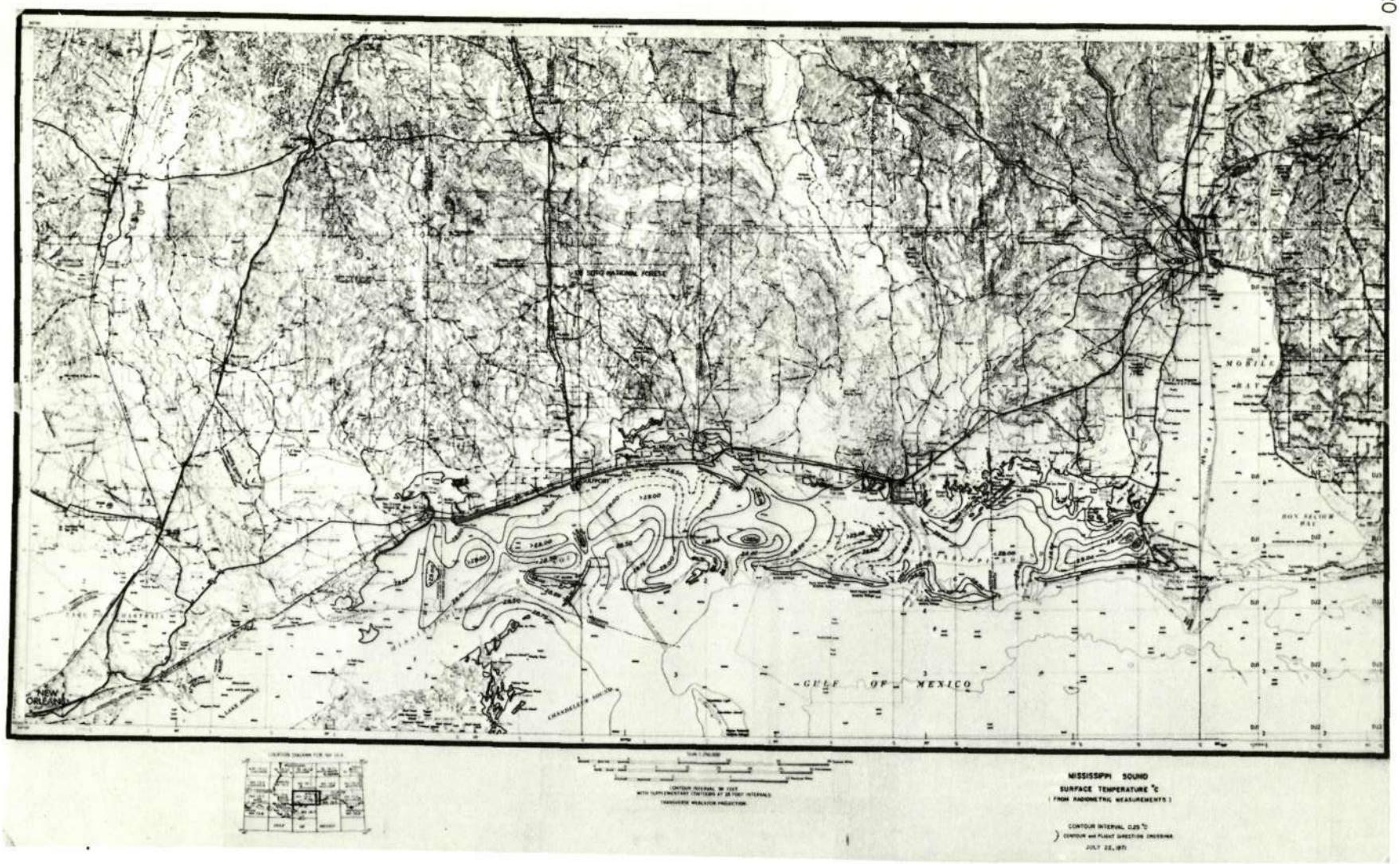

FIGURE 5
Mississippi Sound Surface Temperature ^{o}C,
July 22, 1971 - From Radiometric Measurements

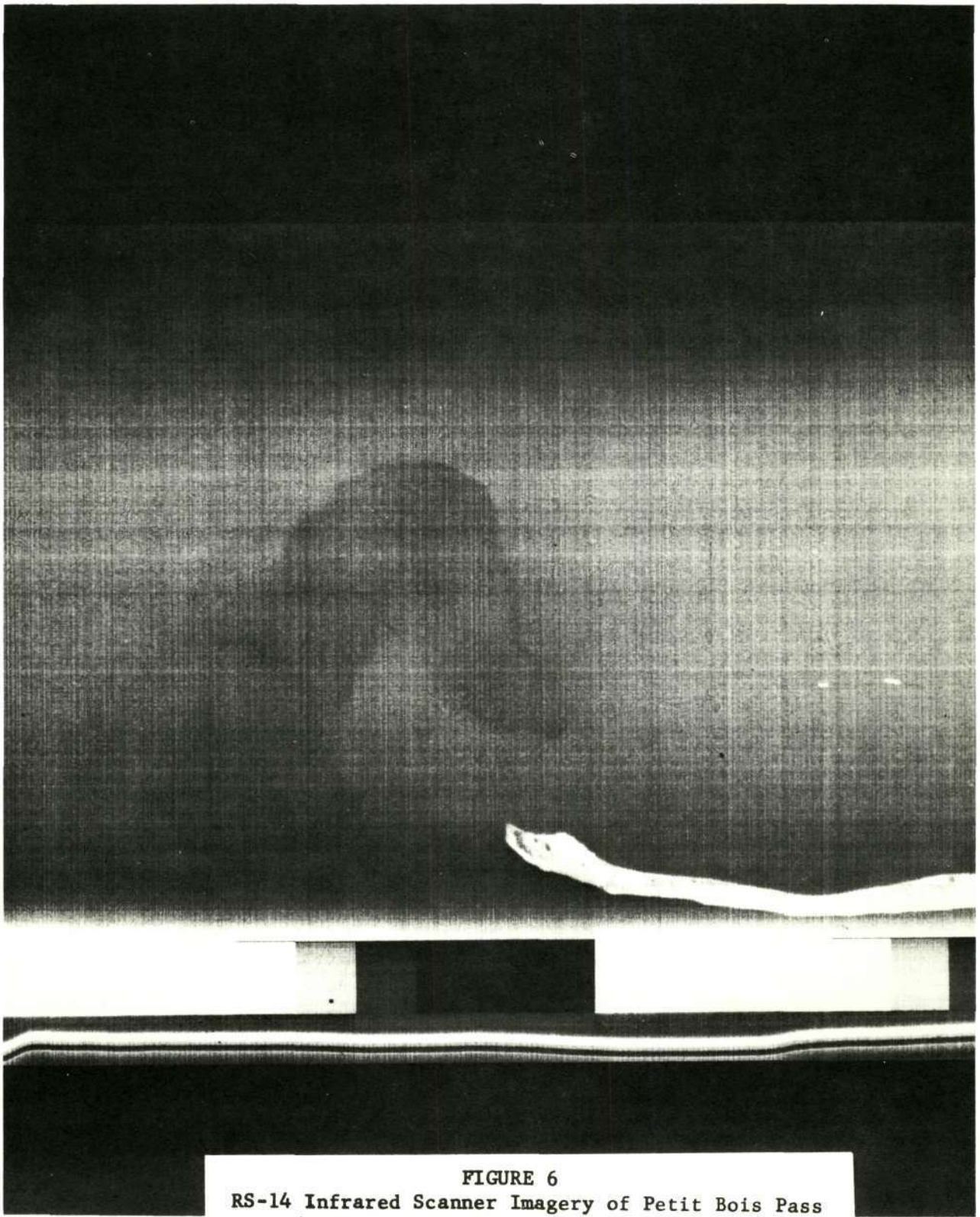

FIGURE 6
RS-14 Infrared Scanner Imagery of Petit Bois Pass
(Between Petit Bois and Dauphin Island)

MISSISSIPPI SOUND I
JULY 22, 1971
FILM DENSITY CHLOROPHYLL CURVE

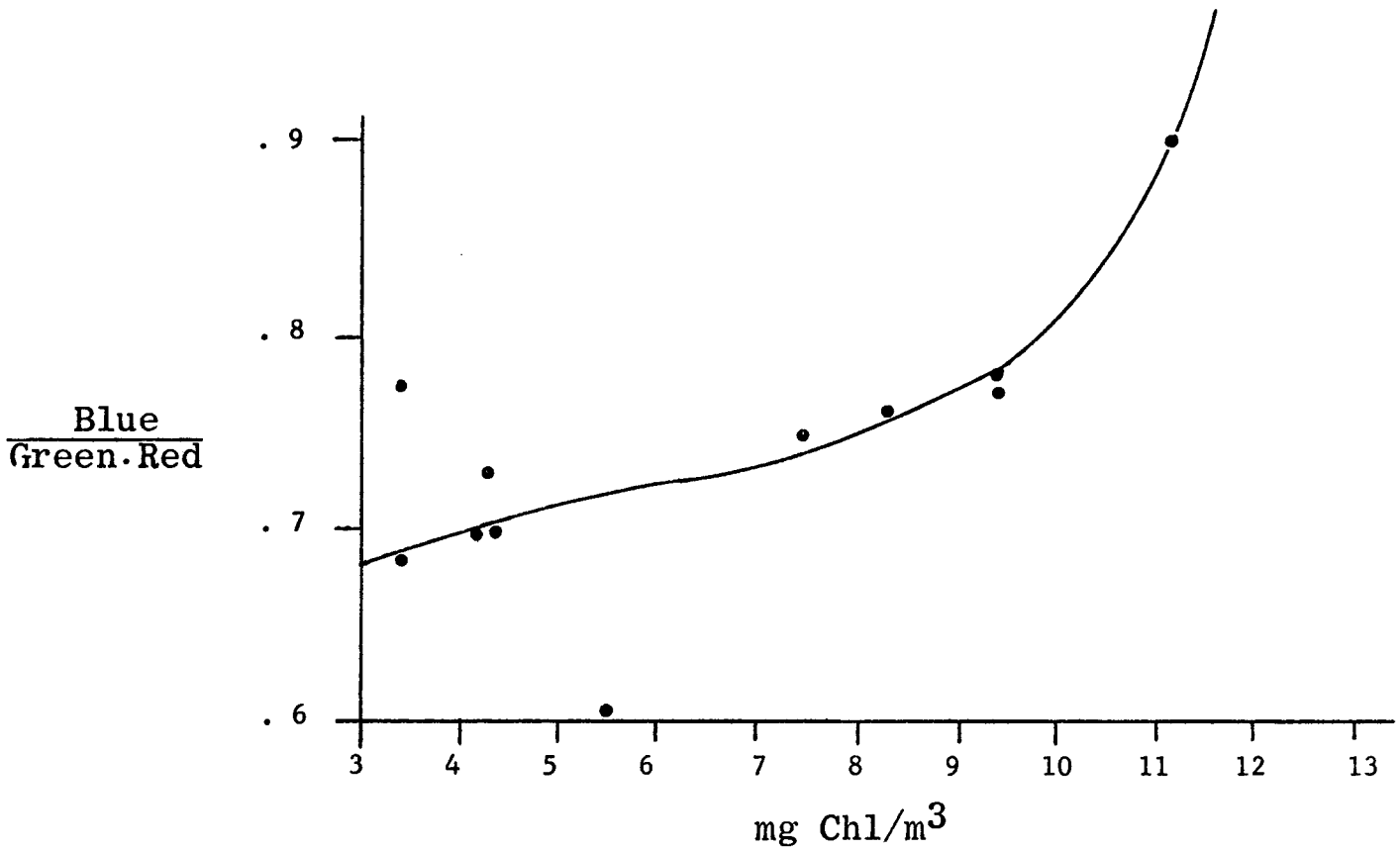

Figure 7

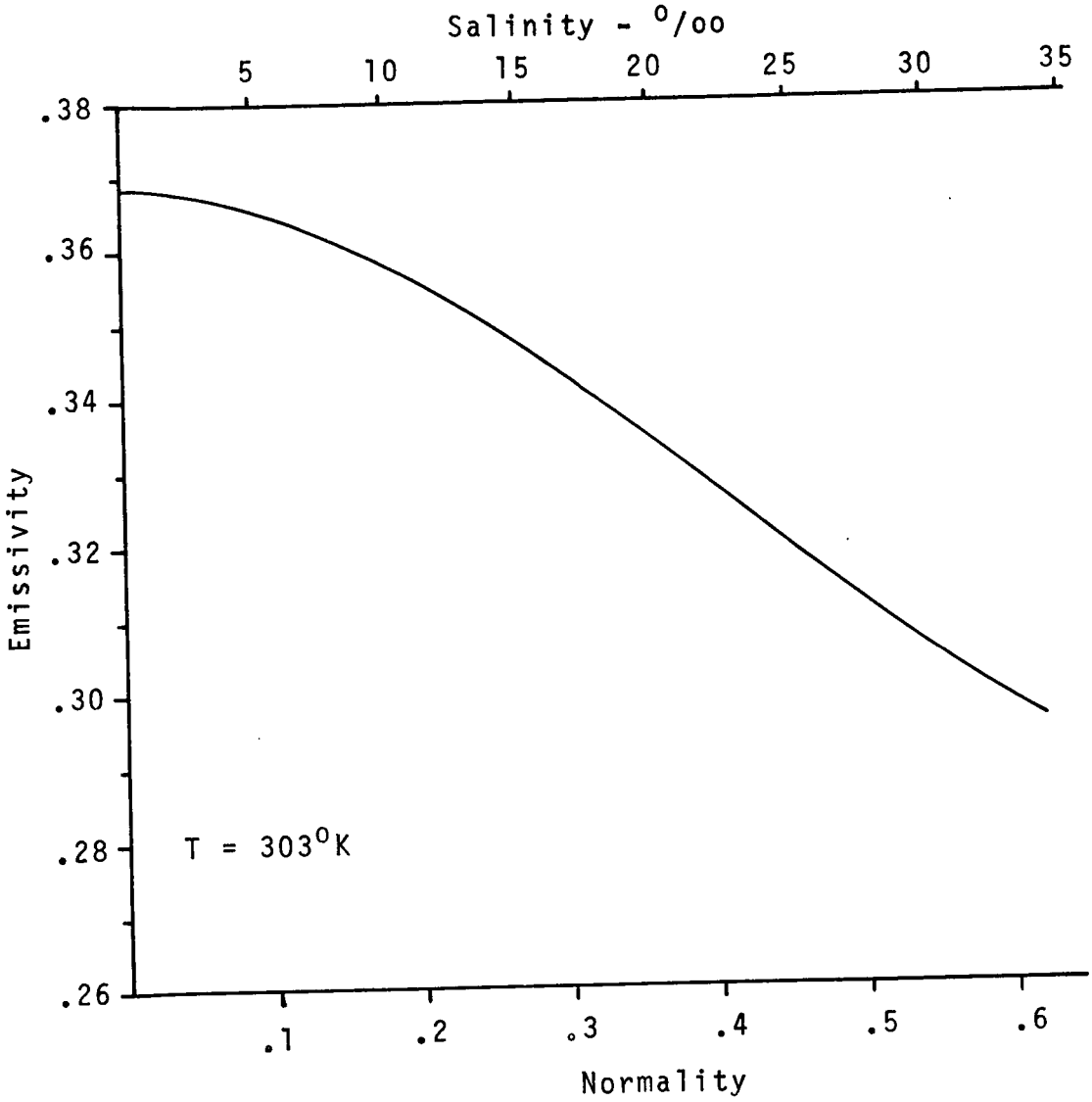

FIGURE 8
Emissivity of a 30°C NaCl Solution as a function of normality

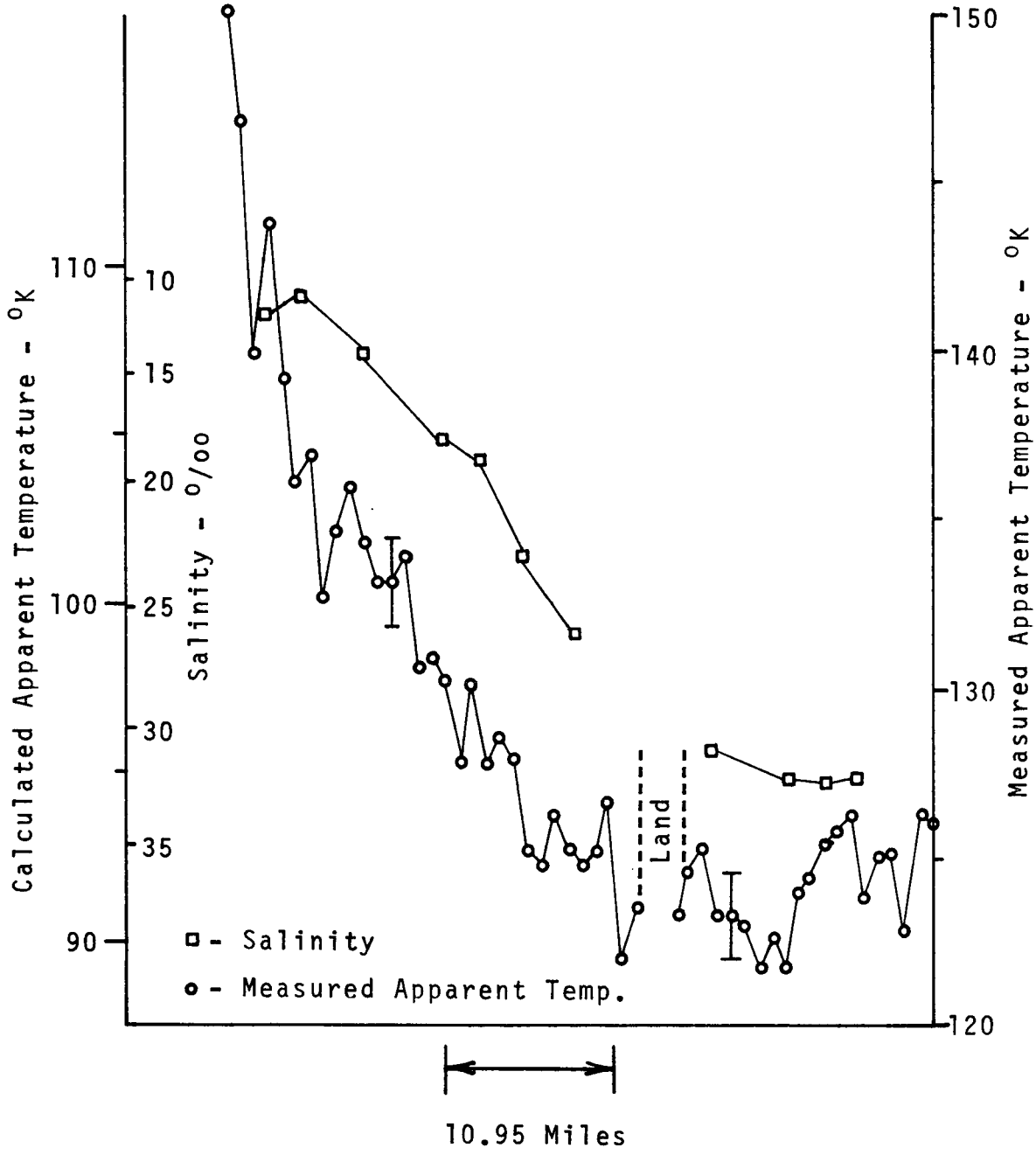

FIGURE 9
Measured apparent temperature and salinity for line 1 of Mississippi Sound I Mission. Water temperature = 28.8°C, incidence angle = 9.33°, vertical polarization

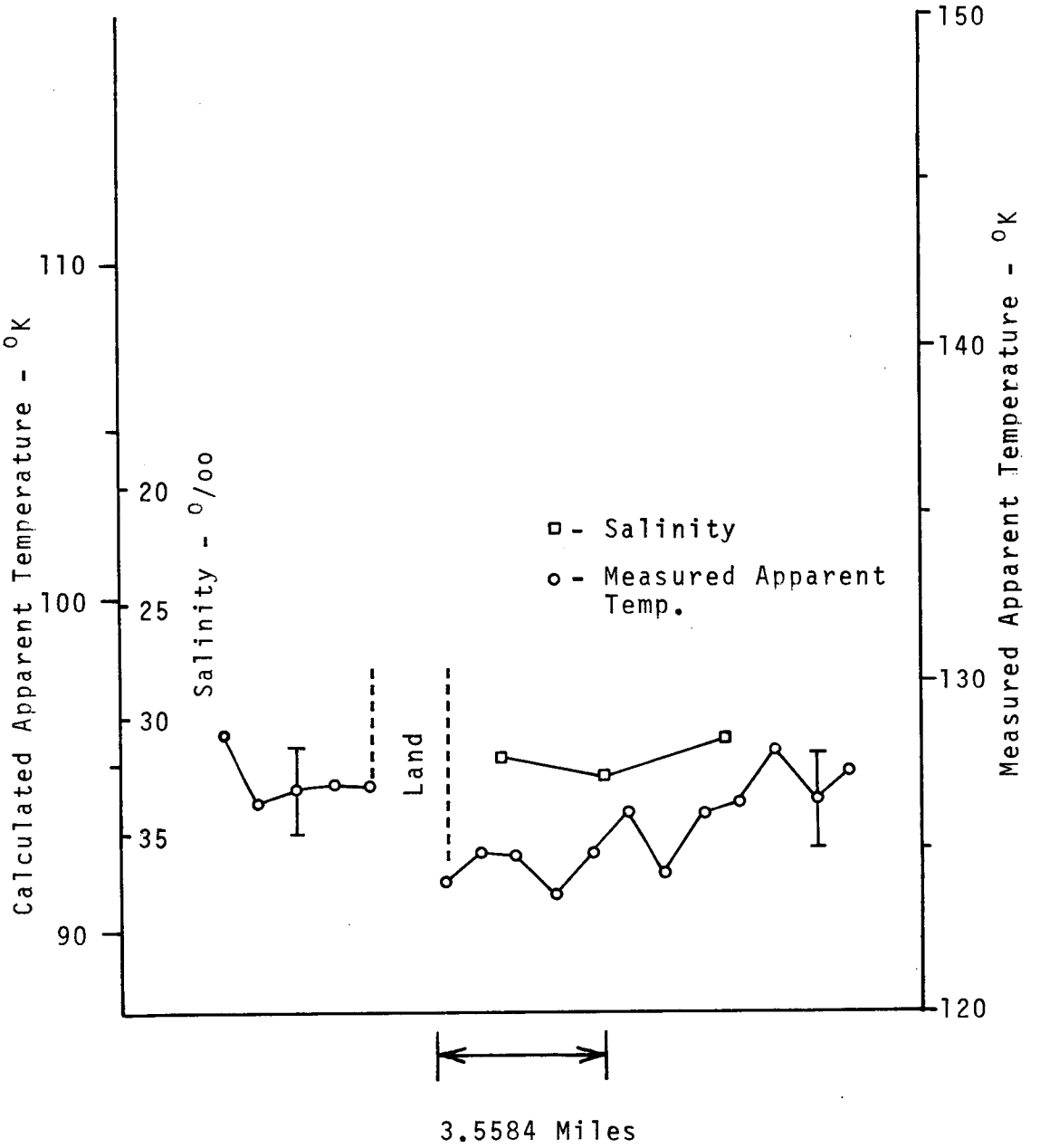

FIGURE 10
Measured apparent temperature and salinity for line 2 of Mississippi Sound I Mission. Water temperature = 28°C, incidence angle = 9.33°, vertical polarization

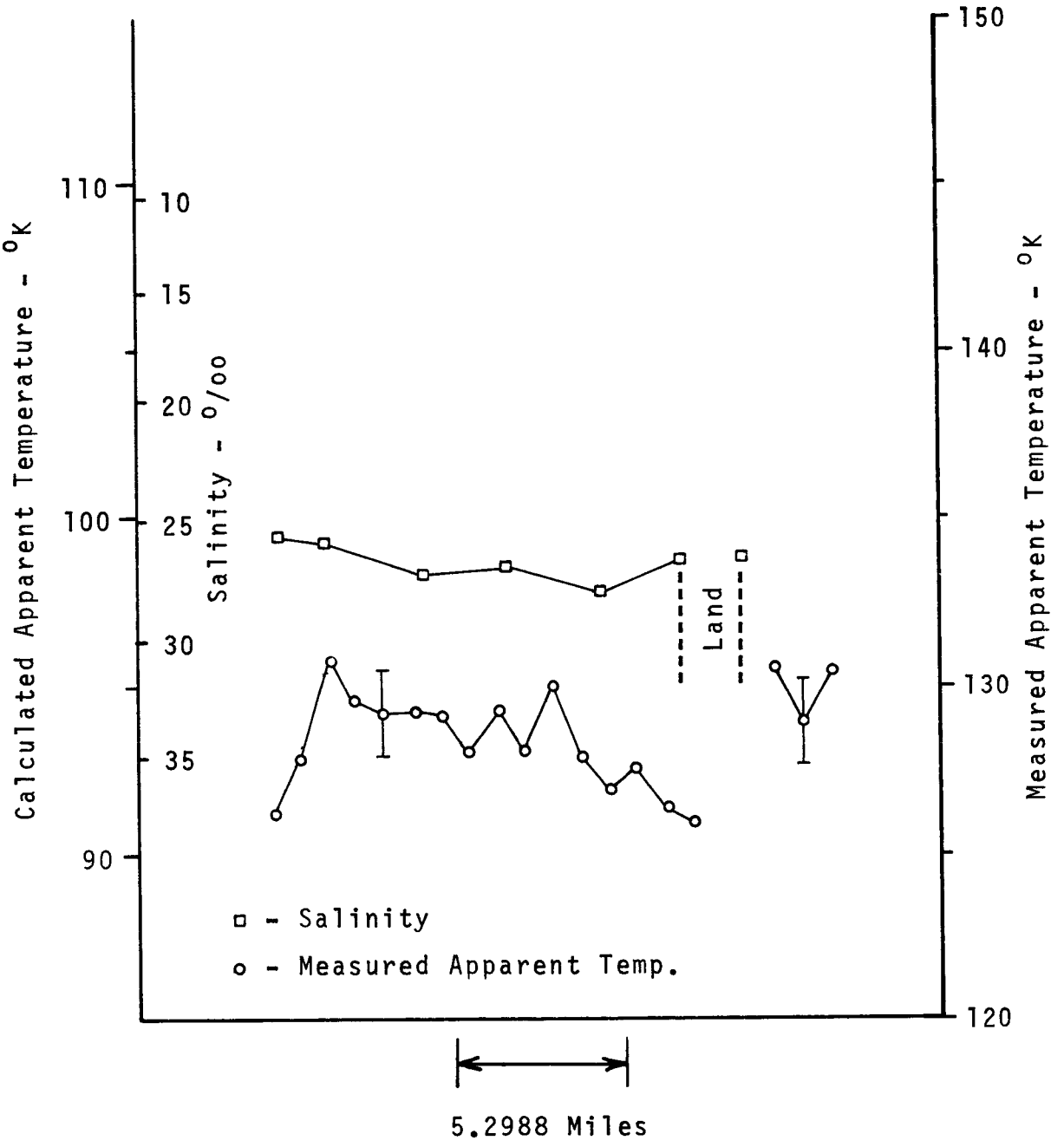

FIGURE 11
Measured apparent temperature and salinity for line 3 of Mississippi Sound I Mission. Water temperature = 28.5°C, incidence angle = 9.33°, vertical polarization

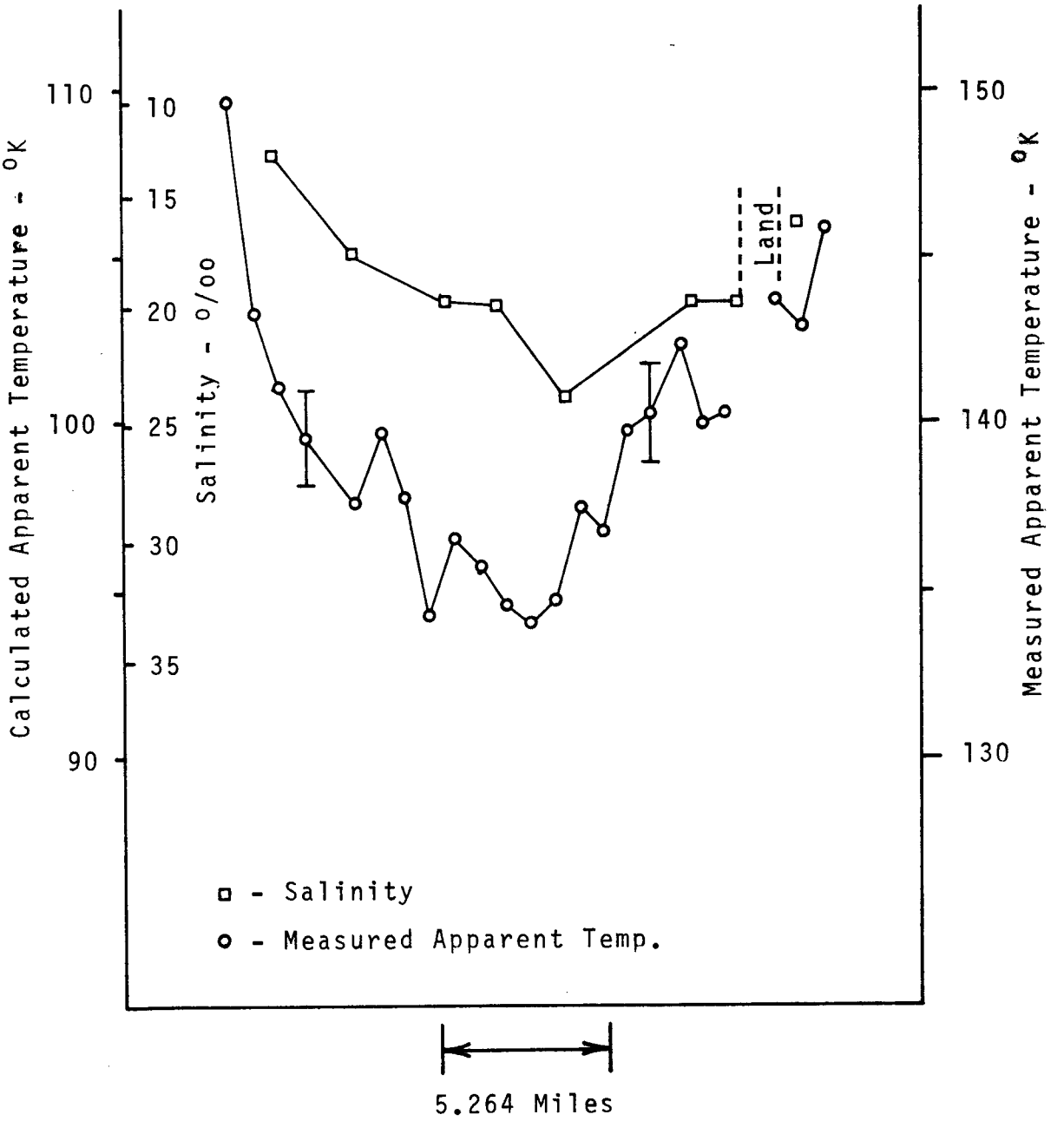

FIGURE 12
Measured apparent temperature and salinity for line 3 of Mississippi Sound I Mission. Water temperature = 28.5°C, incidence angle = 9.33°, vertical polarization

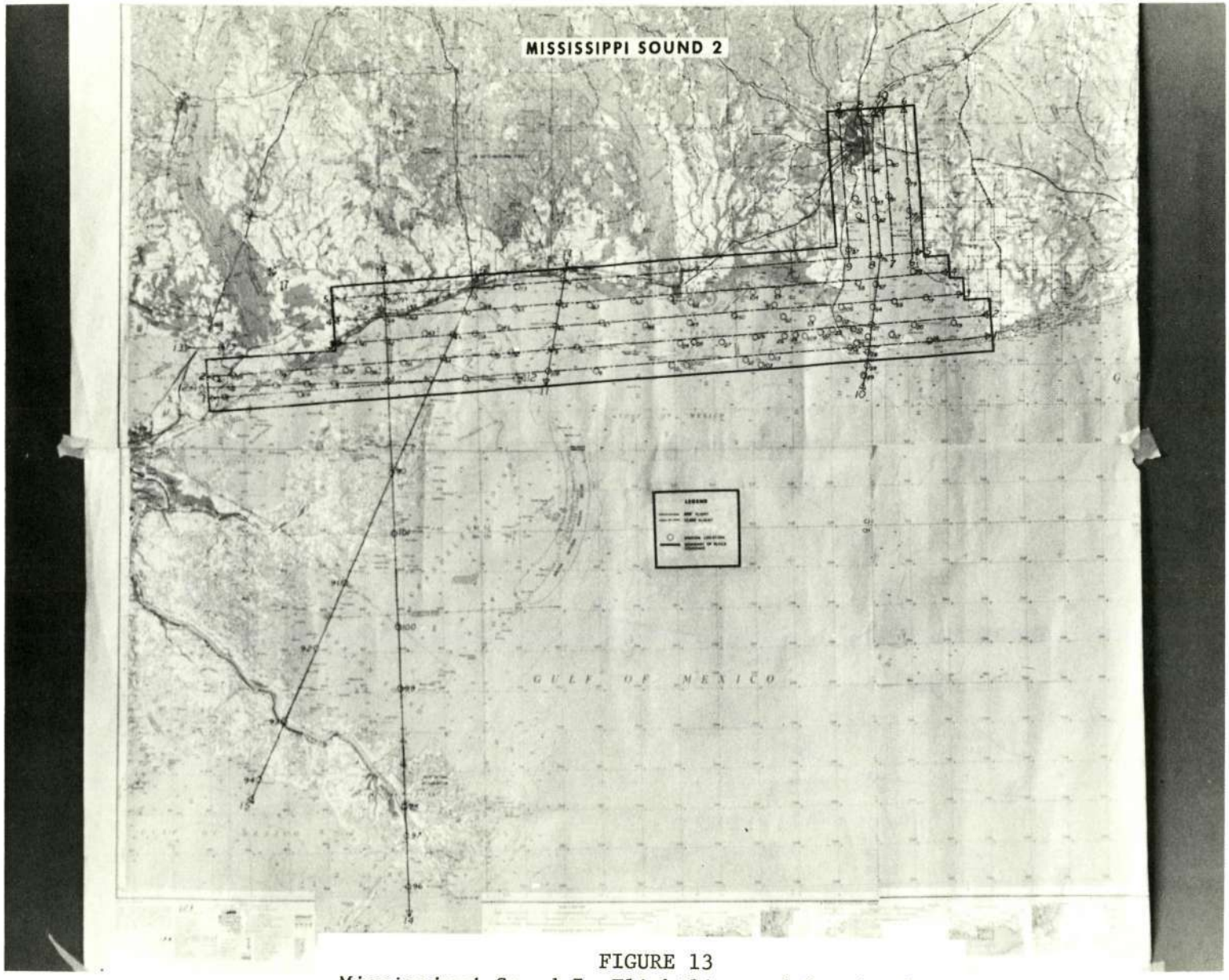

FIGURE 13
Mississippi Sound I, Flightline and Station Map,
November 10, 1971

SECTION 14

SUMMARY OF 1971 LAND REMOTE SENSING INVESTIGATIONS

by

Darden Wayne Mooneyhan
National Aeronautics and Space Administration
Earth Resources Laboratory
Mississippi Test Facility

INTRODUCTION

The Land Remote Sensing Application Group of the Earth Resources Laboratory has as its primary objective to develop techniques to provide land use up-date information using remotely sensed data and automatic data processing technology.

The approach to this objective is to utilize the multispectral scanners, the associated Data Analysis Station, and the Pattern Recognition Programs to identify and classify land surface characteristics, including Wetlands, and to convert these data to demonstration type experiments in the various disciplines.

Within the framework of developing these techniques, application studies are being conducted which utilize remote sensing and its products and which are more immediately useful. A summary of some of these application studies is presented in the Appendix.

The detailed objectives of these land studies are:

1. The evaluation of the 24-channel multispectral scanner as a tool for identifying and classifying surface characteristics to altitudes of 20,000 feet.

2. The evaluation of the 10-channel Bendix multispectral scanner as a tool for identifying and classifying surface characteristics to altitudes of 60,000 feet.

3. The evaluation of existing and modified Pattern Recognition techniques and scanner resolutions for mixed target areas; for example, urban, forest, agriculture, and marshland.

4. The demonstration of techniques to applications; for example, surface classification for land use planning and plant community delineation for mosquito control.

5. The evaluation of extension capabilities of techniques to larger areas of varying geography.

6. The definition of elements of a system for area land use up-date; for example, satellite measurements and accuracies and computer output formatting for the user community.

It is recognized that at this time the 24-channel MSS and the associated DAS have not passed performance specification checks and are not fully operational. However, it is felt that system requirements for technique development can be met by the system in its present operating condition. It is also felt that the data system refinement and technique development can progress together and produce a useful product at the earliest possible date.

LAND USE STUDY

The initial step toward the primary land use objectives was the selection of a study area along the Gulf Coast region of Mississippi. The area is a typical flat land coastal area which is representative of a considerable amount of land in Mississippi and Louisiana. The site was selected because in addition to being convenient to the location of the Earth Resources Laboratory, it is a rapidly developing urban complex along the Coast with agriculture and forest in the hinterland and this provides a study area with mixed land use practices. There is an active planning commission (Gulf Regional Planning Commission) in the area which provides a point of application for land use information for the purpose of regional planning. In addition, there are other active user applications of land use information such as mosquito control and forest management. For the initial experiment specific areas in Hancock County, Mississippi, plus three Agricultural Experiment Stations in Louisiana, were chosen for targets.

The team of investigators on this experiment are Dr. R. H. Griffin, Soil Scientist and Agriculturist; Dr. Armond T. Joyce, Forester; Dr. Robert H. Cartmill, Hydrologist/Meteorologist; and Mr. Paul L. Vegas, Regional Planner.

With the area selected a ground truth gathering exercise was started in the target area in June 1971. It was decided that the most effective way to gather ground truth information for this type mission would be to conduct a 100% field check of a one-mile wide strip along the flight lines (Figure 1) and to select primary training sample and test sample areas from within the areas of 100% ground truth coverage. Approximately one hundred square miles of detailed ground truth information was gathered. The procedure followed to gather this ground truth information was:

1. To obtain from the files existing vertical photographic data.

2. To enlarge the vertical photographs to a workable scale and mosaic them into strips covering the selected ground truth areas.

3. Using these strip mosaics and mylar overlays, the field inspection teams transcribed the ground truth information directly onto the overlays.

4. A legend and scale were added and through a photographic process the information on the mosaic and the overlay were transferred to a black and white presentation with land use classifications identified.

An example of the final product of the factor map is shown in Figure 2.

With the aid of the factor maps and photographs taken by the field teams, the team of investigators selected several training sample areas for each of the land use classifications. Figures 3 through 6 are photographs of typical test sample areas. These selected sites were studied by the investigators to confirm that they were good homogeneous samples and large enough to be utilized as training samples. These confirmed areas were then identified as the final training samples for the individual flight lines.

The procedures followed in ground truth acquisition on mission day were:

1. A photographer visited each training sample site and photographed the area in prescribed detail.

2. A photographer in a light aircraft obtained oblique photographs for all selected training sample areas as well as any noticeable changes in other areas.

These mission day photographs were then packaged with the appropriate factor maps and identified so that the investigators could make ready use of them.

At this time it appears that one of the most important operations in this type of experiment is the adequate gathering of ground truth information. It has been the experience that the proper selection of training samples can be assured only with good ground truth coverage.

Also in June 1971 copies of the Pattern Recognition Program software were obtained from the Manned Spacecraft Center and the modifications to adapt them for use with the Univac 1108 computers at

the Slidell Computer Center were started. In addition, each step in the processing of MSS data with these programs was studied in detail by each of the team members.

With a background of ground studies and data processing technique development, a MSS data acquisition flight was requested. The mission was flown on September 7, 1971 in very poor weather conditions. The flight plan called for four flight lines to be flown at 20,000 feet, and seven flight lines to be flown at 4,000 feet. Three of the 4,000 foot flight lines were underflights of portions of the 20,000 foot flight lines and were flown to provide data for evaluating the effects of scale differences. A layer of scattered clouds at approximately 4,000 feet, varying from 10% to 80% cloud cover, was present most of the day. The 20,000 foot flight lines were flown and it appears at this time that the data from areas with 20% or less cloud cover is useable. Only two of the 4,000 foot flight lines were flown on September 7 because of the cloud layer.

On September 7 the scanner was operating with 20 of the 24 detectors on line with the roll compensation system inoperable and with some noise in Array 3 (2.1 to 4.75 microns). While this noise presented some problems, the primary loss of data on September 7 was due to cloud cover with only about 40% being useable. The mission day ground truth activities were conducted with no anomalies or loss of data.

A second attempt to complete the mission was conducted on September 9, again with inclement weather. On this second mission the scanner was operating with 22 of the detectors on line, with the roll compensation system inoperable, and with Array 3 cleared of the noise that was present on September 7. Although the 4,000 foot lines were flown with scattered clouds, most all of the data was generally useable. Again, on the second day, the ground truth was gathered without anomalies.

The photographic data from the MSS mission was processed in approximately ten days. The investigators used this data in three ways:

1. Cross-checking against the earlier ground truth data,

2. Locating cloud cover and evaluating its effects,

3. Correlation of time of flight and training sample locations as an aid to the DAS operator in locating training samples on MSS tape.

Approximately two weeks after the mission, the MSS data was screened and reviewed on the DAS. During this review the samples were identified by scan line and a tape containing all training coordinates was produced.

It was decided at this point that a small amount of data should be processed end to end through the system to confirm that the Pattern Recognition Programs as adapted to the local computer system were operational before starting the bulk data processing efforts.

The next step in the processing of the MSS data is built around the Purdue Pattern Recognition Programs. The "Pictout" program was run on the pilot data using a single channel (1.18 to 1.3 microns) for the purpose of confirming location of training samples. Figure 7 is a presentation of the product of "Pictout" for that one channel. The "Stat" program was run against training sample data for the various classifications and the "Select" program was used to determine from those statistics the best six data channels for the classifications. These six channels were then processed using the "Classify" and "Display" programs and the first product of this experiment is a color display showing six categories of land use from the pilot project. Figure 8 is a color presentation of that product.

The results of the pilot project, which was a very small amount of data, are encouraging and it appears that there is considerable improvement to be gained by better selection of training sample and threshold values and by improved versions of the Pattern Recognition Program.

It should be noted that the Pattern Recognition Programs are for the most part not capable of handling a 24-channel multispectral scanner with 700 resolution elements per scan; instead the programs are written to accommodate 12-channel data with 222 resolution elements per scan. Because of these limitations, the Earth Resources Laboratory is expending considerable effort in modifying these programs to accept the 24-channel data and also in incorporating a much faster "Classify" program which will allow the same amount of data to be processed using much less computer operating time. The details of these program modifications will be covered in the next presentation made by Mr. Sid Whitley of this Laboratory.

To date the data from one other flight line from the September missions has been reduced to computer tapes and those tapes are presently being processed through the Pattern Recognition Programs at the Slidell Computer Center. The schedule for the Land Use Study is shown in Figure 9.

In summary, the 1971 activities have centered around planning the study projects and cooperative efforts supporting the studies, conducting data acquisition, and completing a pilot data processing project. During 1972 data acquisition phase will continue but the big objective is to move data processing to large scale processing and demonstration of application of the techniques.

ATCHAFALAYA WETLANDS STUDY

Early in October 1971 the Chairman of the Joint Legislative Committee on Environmental Quality for the State of Louisiana requested that NASA, along with other agencies, participate in a wetlands study project involving the lower Atchafalaya Basin.

The Atchafalaya River became a distributary of the Mississippi River in 1500 A.D. and the uninhabited basin serves as a floodway for the Mississippi River with flood gates at Old River and Morganza. The average flow in non-flood stage is one-third of the Mississippi River flow or about 150,000 CFS. The designed maximum flood stage flow is 1,500,000 CFS. The basin is indeed a great wetland swamp that has created much interest in ecological circles. The river dumps 100,000 tons of sediment each day in the lower basin such that 60 square miles of new land was formed by accretion between 1930 and 1950. Based on a two to eight year flood cycle there is sufficient sediment to fill the Atchafalaya Lakes by the year 2000. Also in the basin are large reserves of oil and gas as well as much valuable timber resources and rich farm lands. The lower Atchafalaya Basin, in addition to being of significant economic and ecological interest to the State, has features which make it a suitable candidate for the study and demonstration of remote sensing techniques. Specifically, it is a relatively large area, it is for a large part inaccessible by surface means, and it is very dynamic in its land/water make up. Figure 10 shows the location of the study area.

There are both Federal and State agencies participating in the study; a partial list follows:

Louisiana Legislature, Joint Committee on Environmental Quality
Louisiana Forestry Commission
Louisiana Highway Department
Louisiana Department of Wildlife and Fisheries
Louisiana Stream Control Commission
Louisiana State Geologist
Louisiana State Land Office
Louisiana Department of Public Works
Corps of Engineers, New Orleans District
Corps of Engineers, Waterways Experiment Station, Vicksburg, MS
Corps of Engineers, Topographic Research Station, Ft. Belvoir, VA
U. S. Forestry Service, Southern Regional Office, New Orleans
U. S. Geological Survey, Department of Interior
U. S. Environmental Protection Agency, Water Quality Office
Bureau of Outdoor Recreation, Department of Interior
National Oceanographic Atmospheric Administration

The ERL participation plan developed detail objectives and experiments that held some promise of being accomplished by remote sensors in support of the broad objective of the program proposed by the Joint

Legislative Committee. These detail objectives are:

1. Evaluate techniques for monitoring accretion/decretion.

2. Demonstrate technique for determining salt water intrusion by classification of pertinent plant communities. Correlate with adjacent remotely sensed salinity measurements.

3. Demonstrate technique for location and classification of aquatic plants.

4. Evaluate techniques for determination of water characteristics, e.g. turbidity, source, inlet-outlet conditions.

5. Evaluate techniques for locating water/land areas through forest species identification and vice versa.

The study was initiated with a search for existing data in the files, where a considerable amount of valuable data was found. The New Orleans District of the Corps of Engineers has been gathering data in the basin since 1917, the U. S. Forestry Commission has on record some inventory data in the basin and many other agencies have records of environmental and water quality data. After studying some of this data, including film from a 1970 RB57 mission, the ground truth effort was started during mid October 1970 with ground truth teams in boats and a light aircraft.

The initial MSS mission was scheduled for the week of October 25 and the ground truth teams worked in the basin during the entire week. A map of the area showing the flight lines is shown in Figure 11. The team of investigators for this study are Dr. Robert H. Cartmill, Hydrologist/Meteorologist; Dr. Armond T. Joyce, Forester; and Mr. William G. Cibula, Marshland Ecologist. Four ground crews worked in the lower Atchafalaya Basin taking various water samples and hundreds of ground level photographs of the various vegetation covers, from the heavily forested areas, to the mixed swamp lands, to the marsh areas near the Atchafalaya Bay. Participating in the ground truth teams were members of the Louisiana Wildlife and Fisheries Commission, the Louisiana Department of Public Works, and the Corps of Engineers, New Orleans District, along with numerous ERL personnel. In addition to the ground level teams, oblique photographs were taken from a low-flying aircraft in the areas that were inaccessible to the ground teams. The acquisition of ground truth in the basin is difficult because of inaccessibility of many areas. 100% ground coverage of the area is impossible. Therefore, the investigators relied very heavily upon data taken along the waterways and low altitude oblique photographs for their training sample selection. Examples of ground truth photography are shown in Figures 12 through 17.

On October 27 the scheduled MSS mission was flown in very good weather; however, initial screening of the data on the night of October 27 revealed that the scanner recorder had malfunctioned and essentially all data had been lost. The flight and the ground truth activities were rescheduled for October 29. The mission was flown again in very good weather on October 29 with 14 of the 24 channels operating and with two of those noisy. However, it was decided that the twelve good channels would be processed and an attempt to carry out the first part of the study will be made using this data.

The photographic data from both missions was processed; however, the sensitivity of the IR layer was down more than 50% on both rolls of film and the IR qualities were lost. An attempt to enhance the IR qualities by filtering in the duplicating process was only partially successful. This data is being used by the investigators in their interpretation and an uncontrolled mosaic is under construction for the purpose of identifying gross land use classifications.

The investigators using the mission photography as a base located training samples for the MSS data with regard to time, and mylar overlays were constructed showing the location of each sample. The use of the overlays helped insure that training sample boundaries were maintained while locating the samples on the DAS screen for transfer to tape. During the week of December 6 the investigators reviewed the MSS data using the Data Analysis Station and identified the training samples. The coordinates and data from the training samples were transferred to nine-track computer compatible tapes. The training sample data as well as the coordinates was transferred to a nine-track tape in order that the "Stat" program can be run against the training sample tape instead of the bulk data tapes. The twelve good channels of data were identified and nine-track computer compatible tapes have been requested. It is anticipated that the computer tapes will be available to start data reduction with the Pattern Recognition Programs about February 1, 1972. The target date for land use overlays constructed from Pattern Recognition Program output is April 1, 1972.

The October 1971 data provides coverage of the basin while it was at its most dormant state with regard to vegetation cover and at the driest season with regard to rainfall. A second MSS mission has been requested for May 1972 to obtain data of the region in the more lush green and wet time of the year.

In addition to these MSS data, ERL will participate in late February in a major study effort being coordinated by the Louisiana Joint Legislative Committee. All of the participating agencies are involved in this effort and ERL will gather multiband photographs and thermal data for selected areas using a light aircraft. In addition, several ERL ground truth teams will participate in that effort. A schedule for the wetlands study is shown on Figure 18.

A list of the ERL products from this experiment to support ERL studies as well as the other participants are as follows:

1. Color uncontrolled mosaic, 1970 data.

2. Color infrared uncontrolled mosaic, 1971 data.

3. Land use overlay of seven major categories derived by photo interpretation techniques.

4. Land-water characteristics overlay of 20-25 categories transposed from scanner data/pattern recognition computer printouts.

5. Thermal pattern and temperature transect overlays.

6. Partial area controlled mosaic for accretion experiment.

7. Accretion maps as derived from a variety of scales, spectral bands, time variations for experimental area.

Although none of the MSS data has been processed to completion, the combination of ground truth studies, photo-interpretation studies and the review of the MSS data on the DAS indicates that the proposed objectives of this study should be obtainable by this approach.

Figure 1
Flight lines for September 7 and 9 MSS Mission, Hancock County, Mississippi.

NASA–ERL/MTF

PHOTOMAP

FLIGHT LINE 1-1 SHEET No. 3

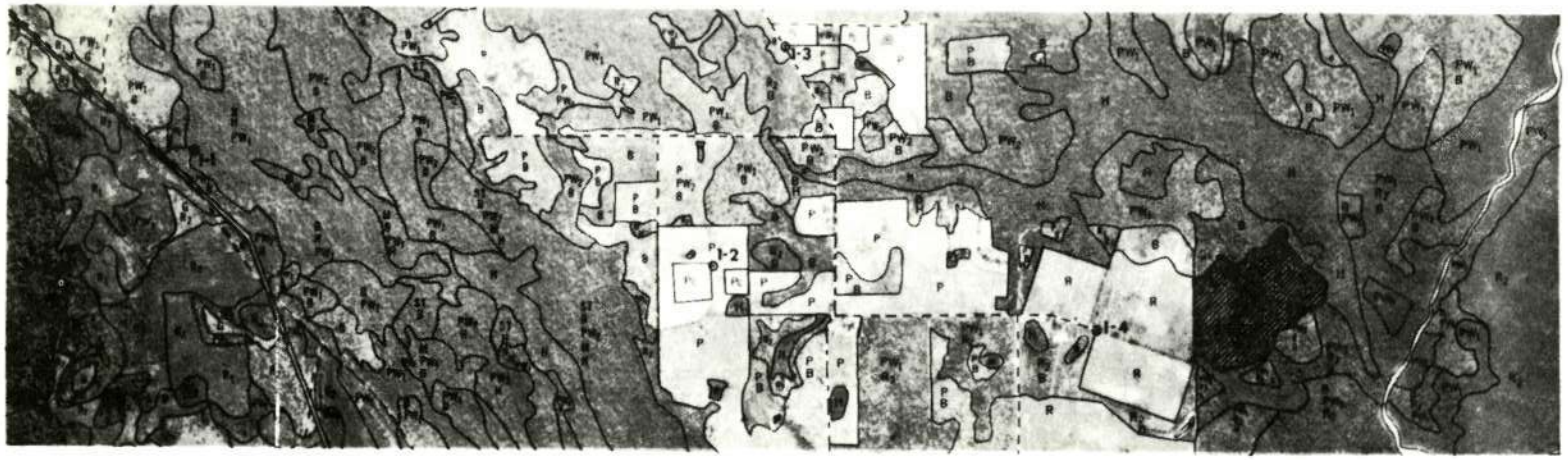

Compiled by Lockheed Electronics Company
Aerial photography 31 October 1970
Ground survey 0 July to 6 August 1971
Uncontrolled mosaic photo base

FLIGHT LINE LOCATION MAP

SCALE 1:12,000

SHEET INDEX

1 2 3 4 5 6

LEGEND

	PRIMARY ROAD	M	MARSH (WETLAND)
	SECONDARY ROAD	W	WATER
	RAILROAD	ROW	RIGHT OF WAY
	STREAM	B	BRUSH
	INTERMITTENT STREAM	G	GRASS
U	URBAN	H	HARDWOOD
R	ROW CROP	ST	SAWTIMBER
S	EXPOSED SOIL	PW_1	9"– 11" DBH
P	PASTURE	PW_2	5"– 9" DBH
P_C	CULTIVATED PASTURE	R_2	2"– 5" DBH
O	ORCHARD	R_1	UP TO 2" DBH

● PICTURE POINT

FOREST STAND TEST PLOT

Figure 2
Example of ground truth factor map showing land use classification.

C-5

Figure 3
Typical training sample for soybeans; ladder used for photographs and PRT-5 reading.

Figure 4
Typical training sample for cotton.

Figure 5
Typical pastureland training samples. Interface shows differences in management practices.

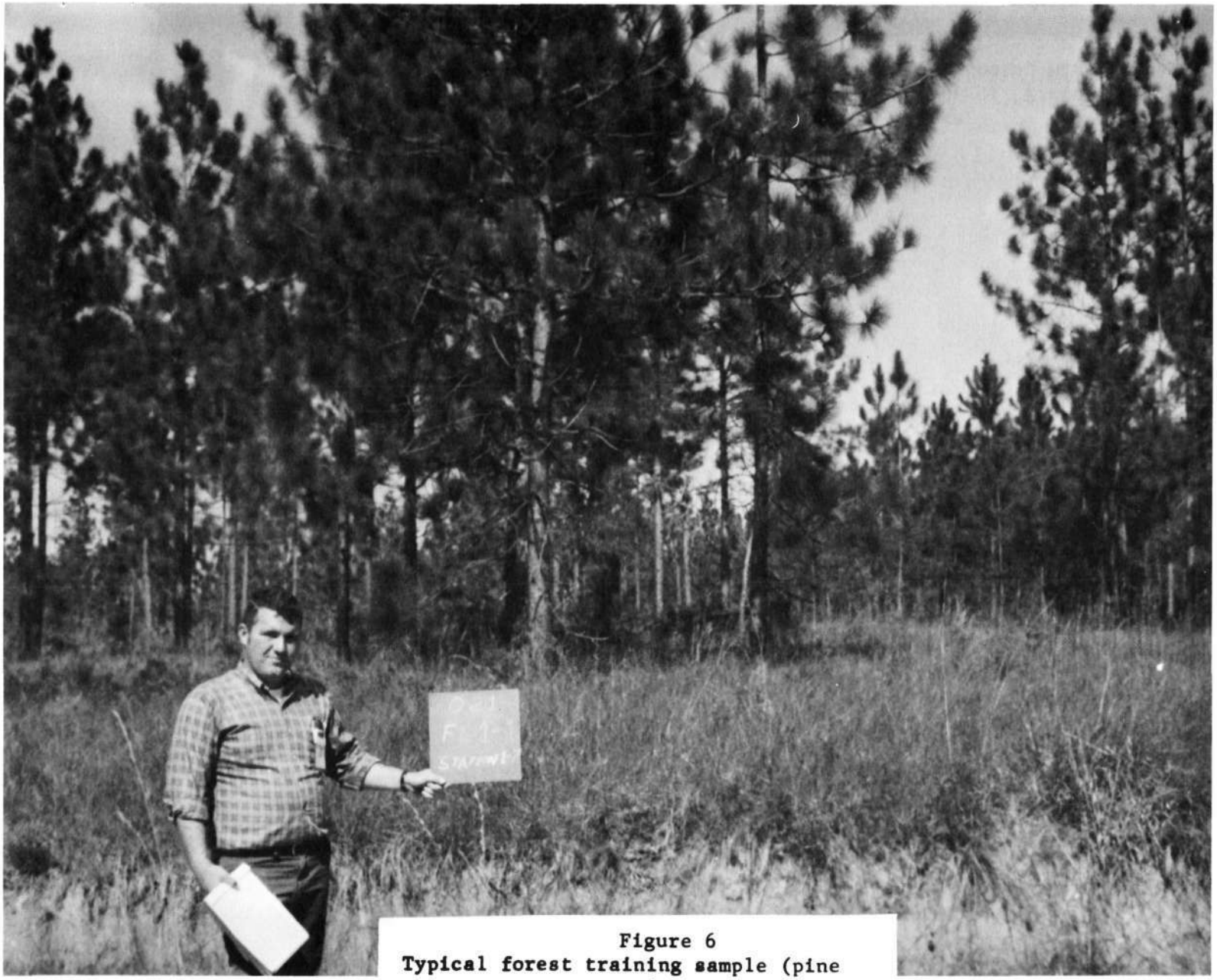

Figure 6
Typical forest training sample (pine reproduction).

MISSION MSS FLIGHT 10 LINE 4 RUN 1

SEPT. 9, 1971
BAY ST LOUIS, MISS.

OUTPUT FROM CHANNEL 11 1.18 to 1.30 MICRONS

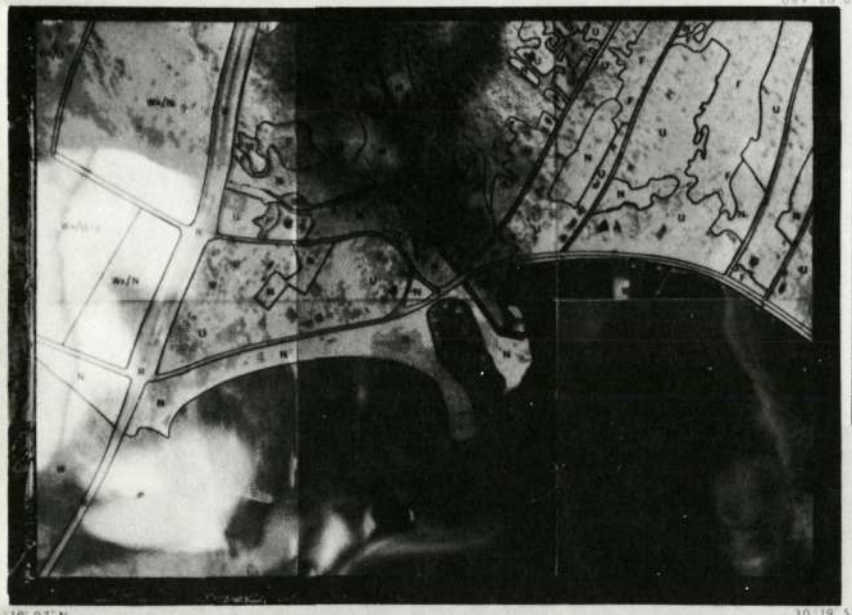

SCALE 1:4000

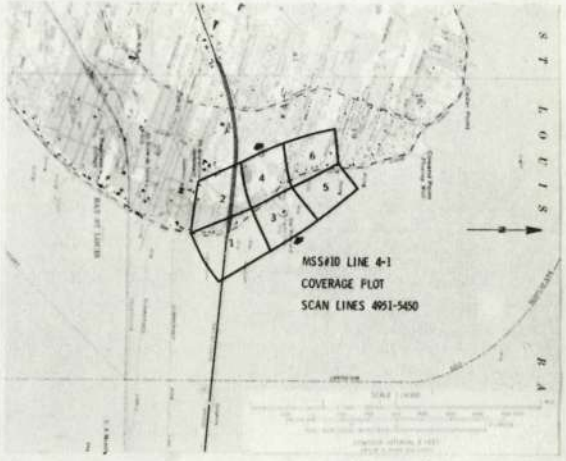

Figure 7
Photographic presentation of "Pictout" Program Channel 11, Bay St. Louis, Mississippi.

MISSION MSS FLIGHT 10 LINE 4 RUN 1

SEPT. 9, 1971
BAY ST LOUIS, MISS.

COMPUTER DERIVED LAND USE CATEGORIES

SCALE 1:4000

W WATER 105 ACRES
U URBAN 74 ACRES
N UNDEVELOPED 41 ACRES
F FOREST 31 ACRES
R RIGHT OF WAY 17 ACRES
M MARSH 7 ACRES
UNCLASSIFIED 120 ACRES

Figure 8
Color presentation of computer generated output of "Classify" Program.

SCHEDULE

LAND USE STUDY

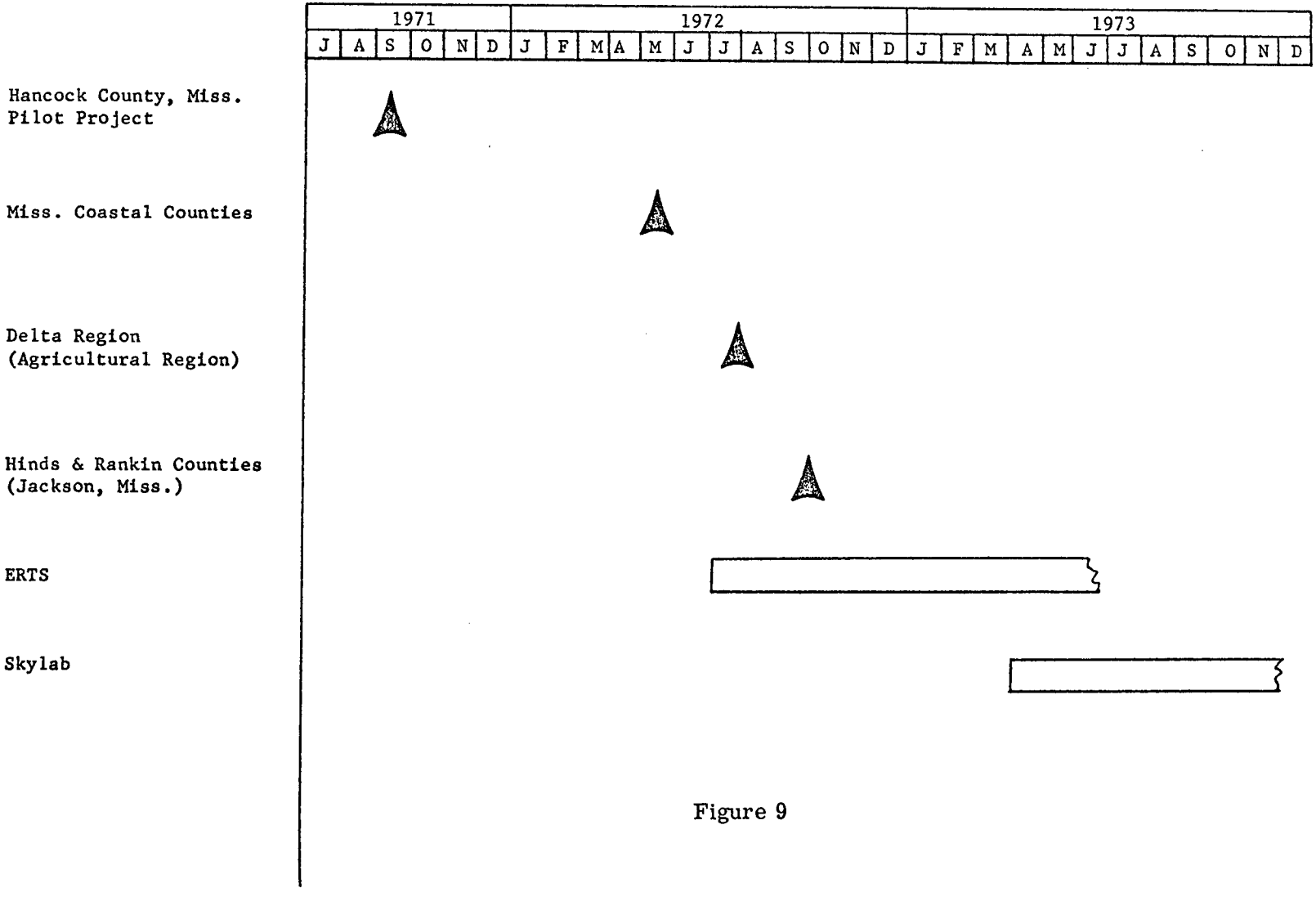

Figure 9

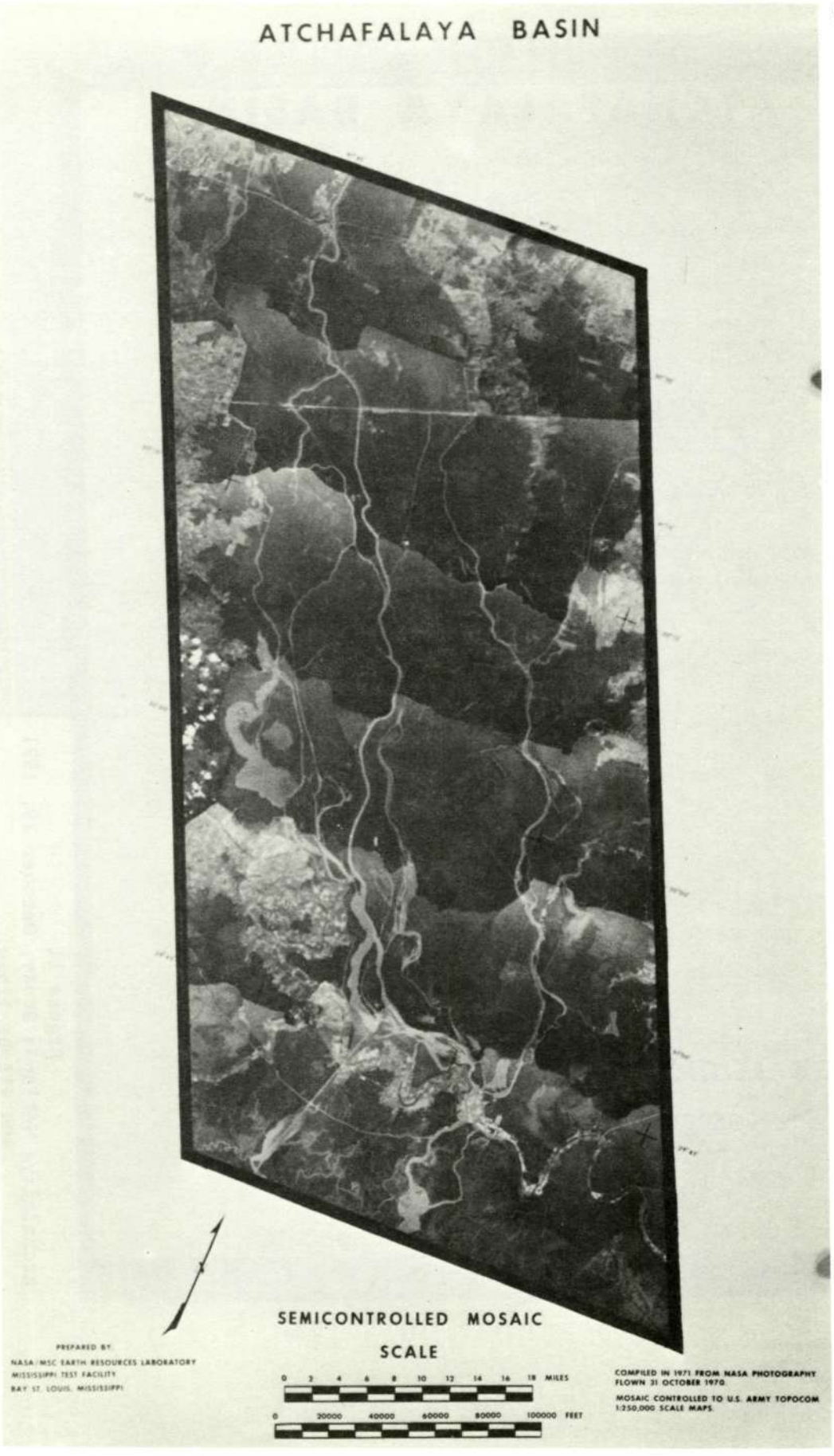

Figure 10
Atchafalaya Wetlands Study area.

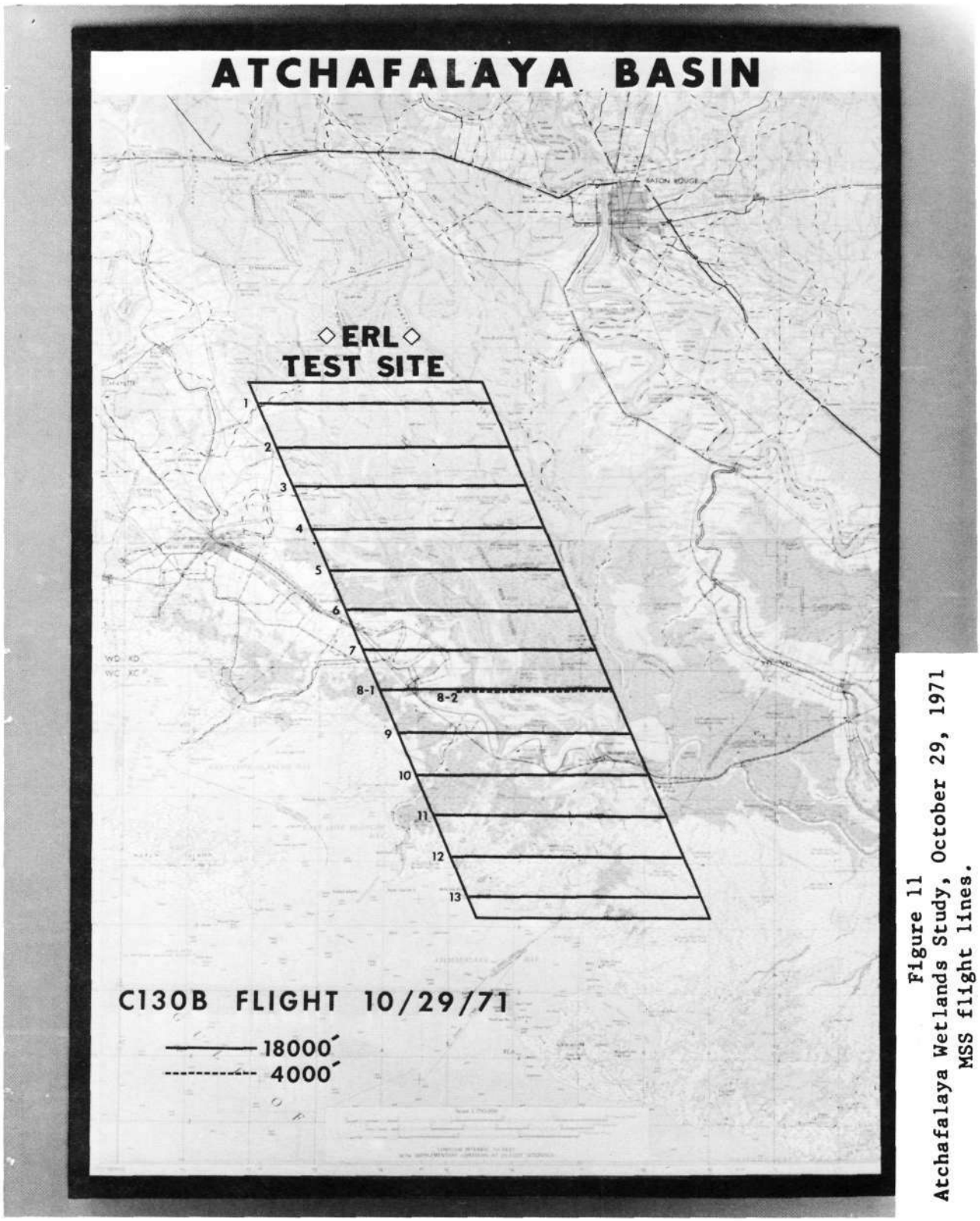

Figure 11
Atchafalaya Wetlands Study, October 29, 1971
MSS flight lines.

Figure 12
Typical forest training sample, Atchafalaya Basin, Water Tupelo trees.

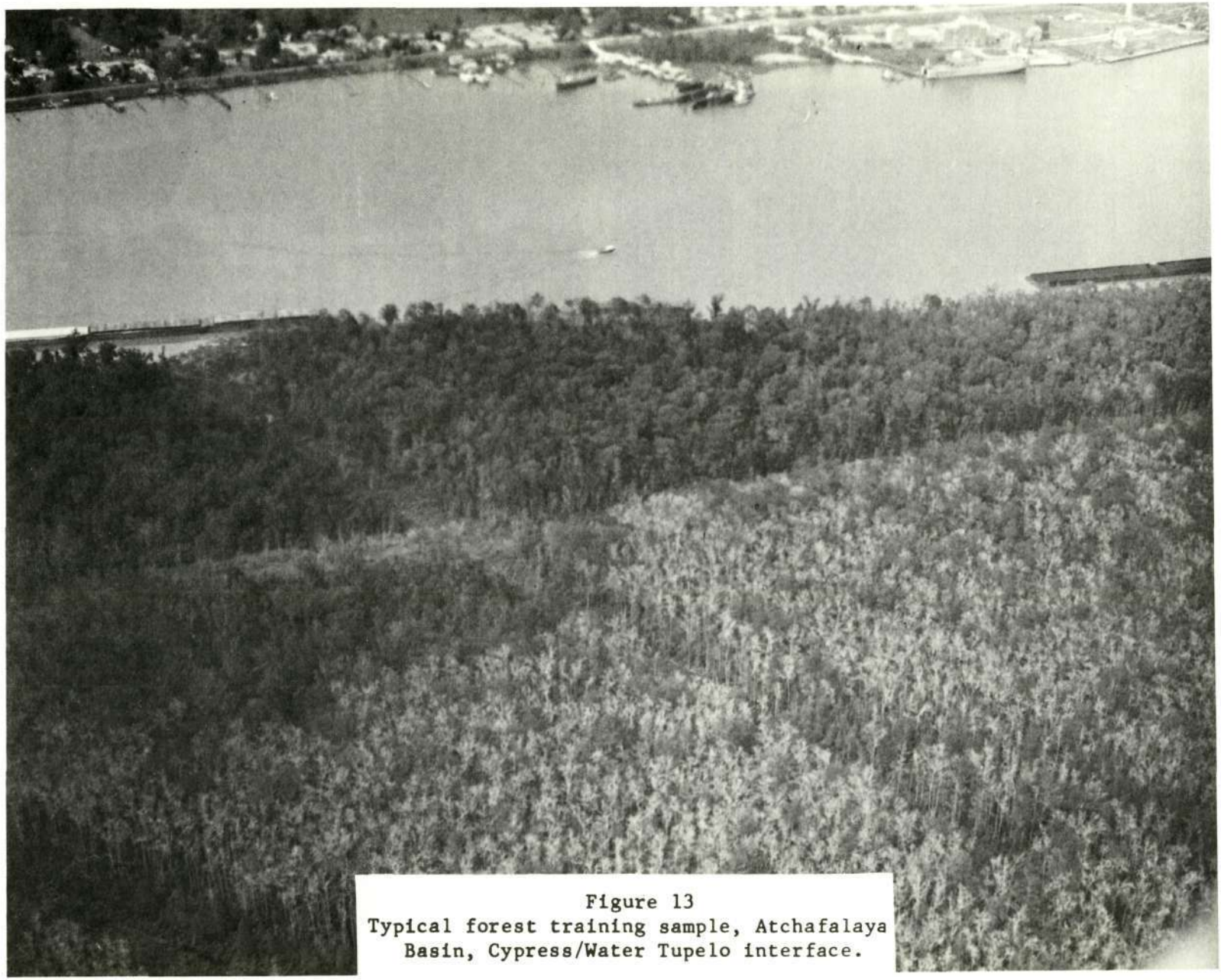

Figure 13
Typical forest training sample, Atchafalaya Basin, Cypress/Water Tupelo interface.

Figure 14
Lower Atchafalaya wet marsh, fresh water standing 100% of time, water hyacinth and Bull Tongue.

Figure 15
Lower Atchafalaya marsh with some filling from sedimentation, dry part time, Smart-

Figure 16
Lower Atchafalaya marsh, goldenrod including first plant primary succession from wet to dry land.

Figure 17
Lower Atchafalaya marsh, goldenrod and Cotton Seed tree, first succession of forest on dry sediment formed land.

SCHEDULE

ATCHAFALAYA WETLANDS STUDY

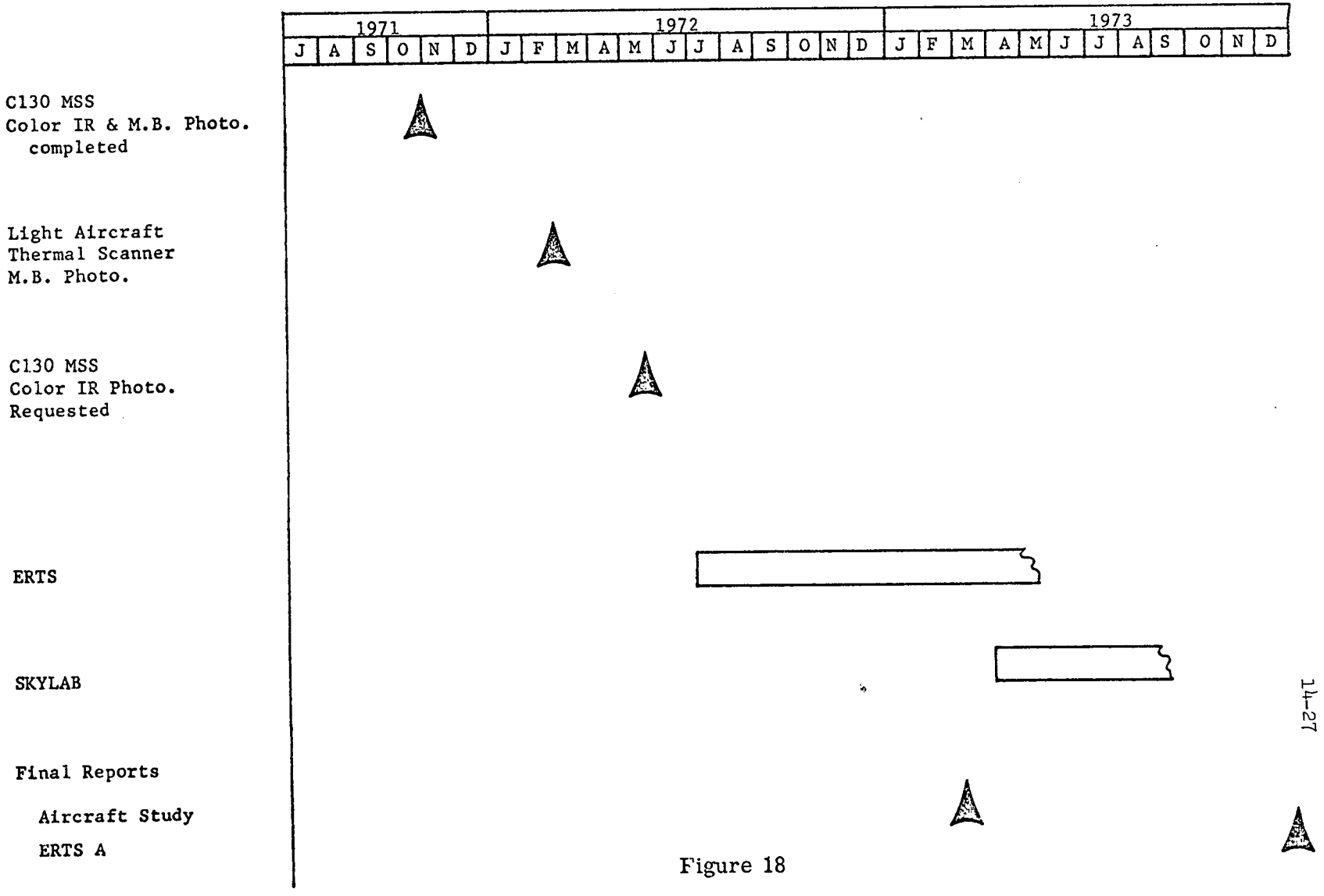

Figure 18

APPENDIX

APPLICATION STUDIES

Mississippi Tornadoes - Disaster Operations Plan

On February 1, 1971 a series of tornadoes occurred in the Mississippi Delta region causing severe damage in numerous small communities and rural areas over a 200-mile path. On February 22, at the request of the Office of the Governor, personnel from the Earth Resources Laboratory acquired low-altitude oblique photographs and ground photographs in the stricken area for the purpose of assessing the need for more extensive vertical photography and to determine the best flight path for obtaining vertical coverage. On February 23 the Manned Spacecraft Center (MSC) C-130 aircraft obtained vertical photography of the tornado paths from altitudes of 2,500 and 8,000 feet. The data was processed on the night of February 23 at the MSC Photographic Laboratory. At 8:00 the following morning, February 24, the data was presented to the Mississippi Office of Civil Defense, Office of Emergency Preparedness, and the Office of the Governor. Accompanying the data were appropriate disciplinary personnel to provide interpretation of the data and assist the disaster recovery teams in their application and use of the data. The results were a very efficient utilization of the imagery by seven agencies engaged in the disaster recovery effort. The utilization ranged from a damage estimate by the Corps of Engineers, to the routing of emergency supplies by the Red Cross, to the location of suitable trailer camp sites by HUD, and many others. An example of the data is shown as Figure A-1. As a result of this experience which proved to be of considerable assistance to the disaster recovery agencies, the Earth Resources Laboratory has been requested to provide similar coverage of disasters occurring in the Office of Emergency Preparedness Southeastern District and has formulated a disaster operations plan which follows the plan used in the tornado recovery and which is shown in Figure A-2.

The total involvement of the Earth Resources Laboratory in the disaster recovery is documented in an ERL report entitled "The Use of an Aerial Photographic Survey in Post Tornado Relief Activities (Mississippi Tornado - February 21, 1971)" dated March 17, 1971.

Participation in the Southern Corn Leaf Blight Study

In the spring of 1971 the corn blight study group at Purdue University requested that the Earth Resources Laboratory monitor several test plots of Texas Male Steril Corn (T cytoplasm) that had been planted in the southern counties of Mississippi for the purpose of determining the severity of the blight in that region. The major part of the corn crop

in the State of Mississippi was planted using N cytoplasm corn, a variety not susceptible to southern corn leaf blight. The leaf blight was detected on the T cytoplasm corn located in a test plot in Jackson County, Mississippi when the corn was only 8-10 inches in height. During the unusually dry spring, the infestation appeared to occur at a slower rate than it did later during the wet summer months. Once the drought had ended, the blight progressed at a very rapid rate and the test plots were severely damaged to the point of premature death and yield losses estimated at 50%-100%.

The sites were monitored on a weekly basis from ground level and several observations were made from low-flying aircraft. The results were transmitted to the study group at Purdue each week during the growing season.

A series of photographs of one of the blighted areas from the first notice of the presence of the blight through the end of the study is shown in Figure A-3. The total results of the ERL participation is documented in a report entitled "An Observation of Southern Corn Leaf Blight on Corn Containing Texas Male Sterile Cytoplasm" dated November 1971, by Dr. Gary C. Thomann.

Soil Moisture Study

An experiment was conducted in an effort to determine if the moisture content of the soil could be determined by remote sensors. The equipment used was a multiple frequency microwave radiometer (MFMR) and thermal infrared measuring devices. The scope of the experiment also included the practical problems of obtaining the necessary ground truth, appropriate processing of sensor data, preparation and control of suitable test plots, and conducting the overflight of the prescribed flight line.

The approach of the investigation was to examine the feasibility of measuring soil moisture by two different concepts. The first concept was measurement of the relative thermal response of vegetation under different degrees of moisture stress to the affects of solar radiation. The equipment used for this method was the RS-14 scanner and the PRT-5 radiometer. The second concept was the measurement of radiation intensity in the microwave region of the spectrum. The equipment used for this method was the MFMR operating on frequencies of 1.42, 10.625, and 31.4 GHz.

Several different soil types of different moisture contents were measured. In addition, the cover and surface conditions of the plots were varied in order to determine the effect of these conditions upon the measurement by the sensors. The primary objective was to define in a general manner the most promising techniques for measuring soil moisture using remote sensors.

The investigation is still in progress, the microwave data has been received and is being evaluated, and results of the study should soon be available. A report on the compilation of the ground truth measurements has been published and is entitled "Soil Moisture Remote Sensing Study, Part 1, Surface Measurements" dated July 20, 1971.

Utilization of Photographic Data

Three experiments have been conducted using small scale photography (scale 1:120,000) to determine the optimum cost-effective format and packaging to make widespread use of high-altitude photographic data practical. There are in the NASA files and in the files of other agencies, many rolls of very high quality small scale photographic data. At the same time small regional planning groups are spending a considerable part of their funds to acquire large scale photographic data and ground level data to support their planning efforts.

The first of the experiments was conducted using one frame of small scale photography, enlarging it to the exact scale of the local regional planning commission's base maps, and conducting a cost study of transferring that data by tracing it directly onto the base maps as opposed to the cost of transferring from large scale photography by normal practices of photo-interpretation. At this level, it appears that savings of approximately 40% in cost could be realized and even a larger bonus realized in the time to produce the product.

The second experiment involved an entire county, approximately eleven photographs from an old mission were used and was conducted primarily to determine the practicality of handling and packaging the data at the county level.

The third experiment, presently underway, involves various planning agencies and approximately eight counties covered by these agencies. The area covered is shown on Figure A-4. This phase is a total experiment from packaging to cost effectiveness to accuracy determination. An example of the product of this experiment is shown in Figure A-5. The results of this experiment will be evaluated by follow-up contacts with the involved planning groups. The final product of this experiment should be a proposal to market, through some appropriate arrangements, the existing data in the MSC files, packaged and formatted in some optimum way as determined by the on-going experiments.

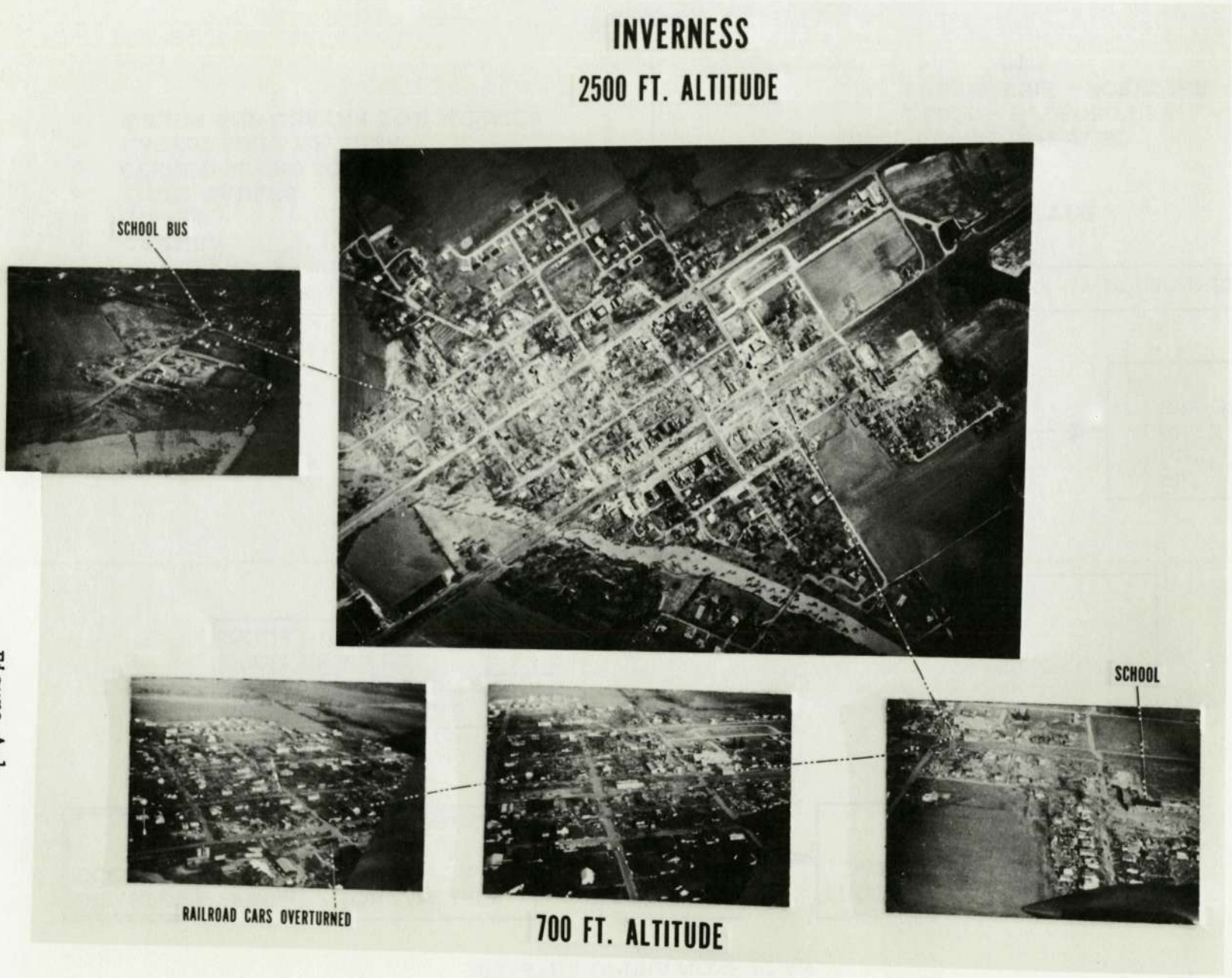

Figure A-1
Example of tornado data.

DISASTER OPERATIONS PLAN

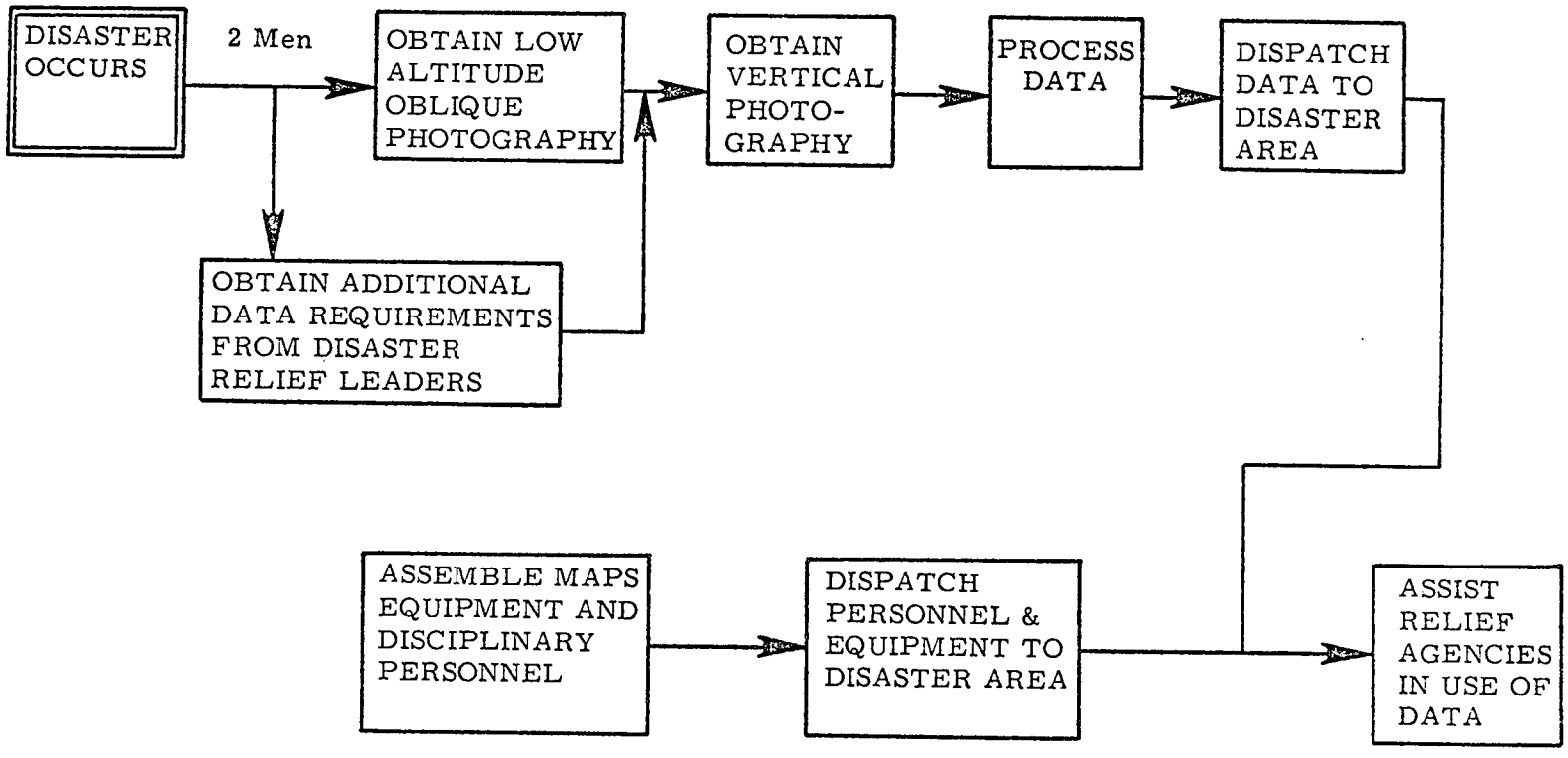

TYPICAL EQUIPMENT	TYPICAL TEAM OF PERSONNEL
o CAMERA o COPIER o LIGHT TABLES o STEREO-MICRO SCOPES o LATEST MAPS OF AREA o WAXER AND COATER FOR MOSAICS	o PHOTOGRAPHER o PHOTO INTERPRETER o CARTOGRAPHER o PLANNER o DISCIPLINARY SCIENTIST FLOOD - HYDROLOGIST FOREST FIRE - FORESTER ETC.

Figure A-2

Figure A-3
Example of corn blight data.

Figure A-4
Test area for small scale photography experiment.

Figure A-5
Example of a product of small scale photography study.

SECTION 15 N72-29316

SUMMARY OF 1971 PATTERN RECOGNITION PROGRAM DEVELOPMENT

by

Sidney Lanier Whitley
National Aeronautics and Space Administration
Earth Resources Laboratory
Mississippi Test Facility

INTRODUCTION

This paper is a summary of activities in the area of digital Pattern Recognition Analysis Programs at the Earth Resources Laboratory at the Mississippi Test Facility during 1971. This paper addresses eight areas related to Pattern Recognition Analysis at the Earth Resources Laboratory as follows: (1) Background; (2) Earth Resources Laboratory Goals; (3) Software Problems/Limitations; (4) Operational Problems/Limitations; (5) Immediate Future Capabilities; (6) Earth Resources Laboratory Data Analysis System; (7) General Program Needs and Recommendations; (8) Schedule and milestones.

BACKGROUND

In the mid-sixties when the Earth Resources Survey Program was much smaller, the University of Michigan, Purdue University, and the University of Kansas developed basically similar techniques for the analysis of multispectral data. The techniques developed by Michigan and Purdue were oriented toward multispectral scanner data analysis while the Kansas technique was oriented toward all kinds of imagery analysis; i.e., photographic, radar imagery, infrared scanner imagery, etc. The Pattern Recognition Analysis Technique implemented by the University of Michigan was, in the early days, an analog computer solution. Its chief limitations were long setup time, and dependence upon operator judgement. Its desirable feature was that, after long setup time, the classification run was very rapid.

The Pattern Recognition Analysis Technique developed at Purdue University was a series of algorithms which were implemented on an IBM 360/44 Computer. Figure 1 is a flow diagram describing the general flow of multispectral scanner data through the Purdue University Laboratory for Applications of Remote Sensing (LARS) Pattern Recognition Analysis System.

The analog tape-recorded multispectral scanner data were digitized and fed through a series of programs whose functions are as follows:

PICTOUT - To display an image on a conventional line printer to simulate gray shades with selected symbols. This was used to identify training samples, test fields, and areas to be analyzed in detail.

STAT - To compute and print on a line printer the following parameters for training classes and fields only:

- o Means
- o Covariance matrices
- o Histograms
- o Spectral plots
- o Coincident spectral plots

SELECT - To determine the best n bands where $2 < n < 12$ by a divergence calculation.

CLASSIFY - To classify unknown materials by computing the probability that the unknown material is the same as one of the training samples for which a means and covariance has been stored as a signature.

DISPLAY - To print the results from classify as a coded computer generated map, and to generate a score card to tell the investigator how well his run worked in designated test fields.

The Purdue Pattern Reocgnition Programs were comparatively easy to set up, were very repeatable when identical inputs were used and equipment operator judgement was at a minimum.

In late 1969, MSC/Houston acquired the Purdue Pattern Recognition Programs, implemented them on an IBM 360/44 Computer at the Manned Spacecraft Center, Houston, and developed a set of documentation for the series of programs. To demonstrate the complexity of the programs, it took approximately 9 months to get the system operational on a very similar computer. Some of the problems were:

a. Systems routines delivered by the computer manufacturer contained errors. These particular systems routines had never been used by MSC programmers before, and the bugs had not been discovered.

b. A small number of coding errors were found in the programs.

c. Test case results did not match the results presented in Purdue's reports. It was finally determined that the report results were slightly in error.

Dr. David Landgrebe, Director, Laboratory for Applications of Remote Sensing at Purdue University, once stated that it was not sufficient to just have a correctly operating Digital Pattern Recognition Program, but that a lot of knowledge was required to run it effectively. That is a very true statement. To effectively operate the system, a team of engineers, computer programmers, statisticians and discipline scientists are required. An expertise in operating the programs comes with experience and careful study.

EARTH RESOURCES LABORATORY GOALS

Figure 2 is a list of the objectives of the Earth Resources Laboratory. As discussed in a previous paper, a major interest of the Earth Resources Laboratory is to apply current data analysis techniques to experimentally demonstrate their applicability in the test area around the Mississippi Test Facility. Our interest was not to develop new programs and analysis techniques, but to use and evaluate previously established techniques, and to modify them as necessary to meet our needs.

To meet these objectives of the Earth Resources Laboratory we acquired copies of the latest versions of the Manned Spacecraft Center's Pattern Recognition Programs in May and June of 1971. By that time, MSC had begun the process of converting the Pattern Recognition Programs to run on UNIVAC 1108 Computers. At the time ERL acquired the UNIVAC 1108 programs, they still contained a number of errors caused by incompatibility between the IBM 360/44 and the UNIVAC 1108.

As ERL personnel started to convert the Digital Pattern Recognition Programs to run on the UNIVAC 1108 Computer at the Slidell Computing Center, we felt that we needed to familiarize our analysis personnel with the operational procedures, capabilities, and limitation of the programs. To accomplish this, we established a Pilot Automated Land Use Experiment following the step-by-step procedure shown in Figure 3. The area selected for a test case is shown in Figure 4, and is located in Harrison County, Mississippi. We used a frame of Color IR film for our source of data. We digitized our data with a scanning microdensitometer making tri-color separations to give us our multispectral data. We exercised all of our pattern recognition subprograms with this pilot set of data. Figure 5 shows the flow of the data through the initial programs. Figure 6 gives an example of the PICTOUT display of one of the channels. Figures 7, 8, and 9 are examples of part of the output from Program STAT. Figure 10 is an example of the output from Program CLASSIFY, and Figure 11 is an example of output from program DISPLAY. Figure 12 is a score card showing the results of the classification.

Our first version of the program worked well with three channels of data. We moved on at the completion of the pilot study and software conversion to complete preparation for handling our first set of data from the 24-band Multispectral Scanner. Mr. Mooneyhan has shown a sample result of the first run of Multispectral Scanner data through ERL's pattern recognition programs.

SOFTWARE PROBLEMS/LIMITATIONS

In our preparation for handling 24 channel (MSDS) Multispectral Scanner Data, we found that there were many problems in the programs. The programs we received from MSC had a capability of reading MSDS data with 24 channels, and 700 elements per scan line, but a subset of 12 channels and 222 picture elements were all that the programs could process. At this point ERL assessed the tasks of modification of the programs to handle MSDS data before a C-130 MSDS checkout mission was flown. A decision was made to use an interim procedure for processing MSDS checkout mission data where the 700 element scan lines were divided into three parts; left third, middle third, and right third. After completion of the data processing, these segments are mosaiced together to reconstruct the entire swath width. Appendix A describes the interim data flow, assumptions, investigator participation requirements, computer processes and computer time estimate for using the interim procedure for processing 30,000 scan lines of data.

A major limitation of the digital pattern recognition programs is long computer run time due to its many calculations. Although there are a number of equations used in the series of programs, the following listed equation seems to be the greatest user of computer time. The following equation is used to compute the probability that material i gave rise to the measurement vector X for a particular ground cell or picture element in the multispectral imagery:

$$P_i(X) = \frac{1}{(2\pi)^{N/2} |K_i|^{\frac{1}{2}}} \exp\left[-\tfrac{1}{2} (X-M_i)^T K_i^{-1} (X-M_i)\right]$$

Where: P_i = Probability density function from training fields for the i^{th} material
X = Measurement vector for a particular ground cell
N = Number of channels used
M_i = Mean vector for the i^{th} material
K_i = Covariance matrix for the i^{th} material

K_i is an N X N matrix where N is the number of channels used in the solution. $P_i(X)$ is evaluated for each material for which a training sample is designated. This evaluation causes the matrix K_i to be

manipulated for every picture element in the scene for every material to be classified.

OPERATIONAL PROBLEMS/LIMITATIONS

In addition to the software problems/limitations described above, we have found some operational problems and limitations which are listed below:

a. All Multispectral Scanner Data from the 24-band Scanner, and the S-192 EREP Scanner must be funneled through a Data Analysis System prior to computer analysis.

b. Data Analysis Systems produce only 9-track computer tapes, causing users with only 7-track tape drives to have to procure 9-track tape drives or have the tapes converted.

c. Software, Hardware, and procedural bugs still exist in the 24-channel Scanner and its Data Analysis System. This is not intended as a criticism, as the system is still in checkout. We have been able to work around all problems encountered to date.

d. Interim display capabilities being used by ERL in the MTF area for computer generated color coded maps are cumbersome to use.

IMMEDIATE FUTURE CAPABILITIES

In view of the software problems/limitations discussed above, we have begun to modify and extend our series of pattern recognition programs, as necessary, to handle data from the newer multispectral scanners. Program STAT has been modified to accept Multispectral Scanner training sample data which is formatted by a Data Analysis System. STAT can now handle up to 24 bands of data and up to 700 picture elements per scan line. Program SELECT is being modified to accept up to 24 bands of Multispectral Scanner Data. We intend to always use fewer than 12 bands of data in our CLASSIFY program due to the long run time. We are still evaluating whether we should modify program CLASSIFY to accept 700 element per scan line data or if we should use our much faster Digital Table Look-Up classification, which gives equivalent results.

In addition to these software problems, digital pattern recognition programs have a basic problem of running slowly. A little over

a year ago an effort was initiated at MSC to develop a classification technique which would perform a pattern recognition analysis at a much faster rate and with results comparable to the Purdue Programs. Dr. Walter G. Eppler, while an LEC Direct Support Contractor at MSC, conceived a new Digital Table Look-Up pattern recognition technique which was many times faster than the LARS Pattern Recognition Analysis Programs. The Digital Table Look-Up (DTL) avoided computations by looking up the identity of materials from stored decision tables. These stored decision tables were based upon the Maximum Likelihood decision rule used in the Purdue Pattern Recognition programs. Dr. Eppler reported on the Table Look-Up Approach to Pattern Recognition at the Seventh International Symposium on Remote Sensing of Environment in May 1971. The DTL was implemented on an IBM 360/44 Computer at MSC as a machine language program.

A Digital Table Look-Up Pattern Recognition Analysis Program is being developed by the Earth Resources Laboratory at MTF for use on a UNIVAC 1108 Computer. Figure 13 shows the flow of data through the Digital Table Look-Up Program. It is estimated that this series of programs will be checked out and ready for operational verification by July 1972.

EARTH RESOURCES LABORATORY DATA ANALYSIS SYSTEM

The important role played by the Data Analysis Systems in preparing Multispectral Scanner Data for computer processing by users has been pointed out already. The format of flight tapes are not compatible with conventional data processing facilities. The Earth Resources Laboratory is acquiring a Data Analysis System to be installed at MTF because we are planning to emphasize the use and applications of Multispectral Scanner data acquired from aircraft and space. The scheduled delivery date for our DAS is in May 1972, with an operational date of about one month later. Figure 14 is an artists conception of the Data Analysis System. The ERL-DAS is similar to the two existing DAS's at MSC. It is completely compatible with the two MSC DAS's and has a number of features that do not exist in the MSC versions. These features, for the greatest part, were added at little or no cost, and were based upon experience gained in the design, manufacture, and checkout of the MSC-DAS's which were earlier models. The ERL DAS has one major capability that does not exist in the MSC DAS's. The ERL DAS can read, register, and display on the DAS up to four bands of Multiband Photography and process the data as though it were Multispectral Scanner Data. The same optical input subsystem can separate the three dye layers on color or color IR film and input them into the DAS as three-band multispectral data.

During the development and checkout of the two MSC-DAS's it was determined that the cursor system which was designed to designate training samples, test fields, and areas to be analyzed was more cumbersome to operate than necessary. To make the cursor system more convenient to use, the ERL DAS employs a light pen cursor.

Figure 15 is a functional block diagram of the ERL-DAS showing inputs, data processor, control and display, and output subsystems. Figure 16 gives the ERL-DAS Characteristics.

The ERL-DAS will be delivered with the necessary software to screen, evaluate, and reformat data from the 24-band Multispectral Scanner, the S-192 Skylab EREP Scanner, S-190 Multiband Photography (or any multiband photography), and Microwave Imager Data. The necessary software will be included to convert the S-192 curved scan lines to straight scan lines.

GENERAL PROGRAM NEEDS AND RECOMMENDATIONS

The Digital Pattern Recognition Programs are, as pointed out earlier, designed for processing 222 picture elements per scan line and twelve or fewer data bands. It should be recalled that the following numbers of scan lines must be processed in the near future:

SCANNER	ELEMENTS/SCAN	DATA BANDS	SCAN RATE
MSDS	700	24	10 to 100 scans/sec.
ERTS Scanner	2400	4	
SKYLAB EREP S-192	1200	12	100 scans/sec.

Prior to the time of the ERTS flight we have a need to modify our Pattern Recognition Programs to give them the capability to handle as many as 2400 picture elements per scan line.

Due to the large amount of resources required to analyze multispectral data it is highly desirable to make some preliminary checks to determine the quality of the data before proceeding with the full analysis. Since we have so much data these checks must be made automatically. For instance, tests can be run on each training sample to determine if it is sufficiently like other training samples of the same material, and if it is significantly different, the training sample can be rejected on the basis of investigator's criteria. If the data distribution is significantly different from a normal distribution, which is assumed by the maximum lilelihood ratio classifier, the investigator can be given an opportunity to determine if processing should continue. At this point preprocessing algorithms such as

the ones previously used by the University of Michigan could be applied so that the analysis results will be more correct.

Regardless of how well we do in the development of either a pure digital pattern recognition analysis system or a pure analog pattern recognition analysis technique, each will have inherent disadvantages that are not solvable in pure analog or pure digital. By clever programming, the processing speed can be improved in the digital programs with larger and faster computers, but for all digital techniques processing speed will remain prohibitive. The setup time can be improved in the analog system with state-of-the-art systems, but it too will remain prohibitive. A hybrid computer implementation of the analog and digital solutions developed at the University of Michigan and Purdue can avoid both the long analog setup time and the long computation time by accomplishing the setup tasks with the digital portion of the hybrid computer, and by accomplishing the classification tasks with the analog portion of the hybrid computer. Both the University of Michigan and MSC are doing some development work using hybrid computers. I believe that we can expect some great improvements in analysis time and in reduced cost of analysis. I would like to urge that this area of development be continued.

SCHEDULE AND MILESTONES

Figure 17 is a schedule and some milestones for pattern recognition analysis development, the acquisition of equipments that will be used to prepare data for pattern recognition analysis, and some of the missions which will have pattern recognition analysis requirements.

Figure 1

Flow of Data Through LARS Pattern Recognition System

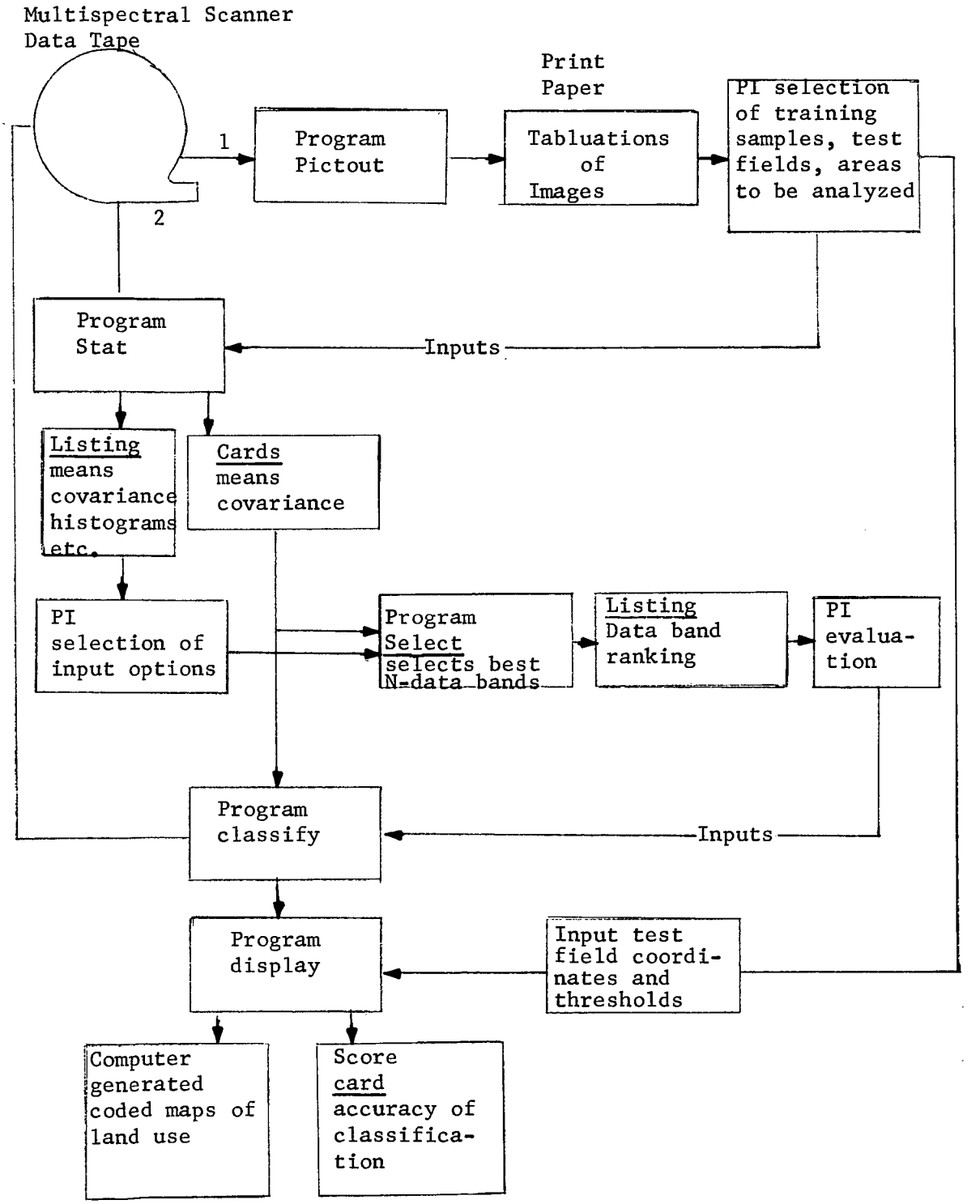

DETAIL OBJECTIVES

LAND

- EVALUATION OF 24 CHANNEL MULTISPECTRAL SCANNER TO 20K ALTITUDE
- EVALUATION OF 10 CHANNEL BENDIX SCANNER TO 60K ALTITUDE
- EVALUATION OF EXISTING AND MODIFIED PATTERN RECOGNITION TECHNIQUES AND SCANNER RESOLUTIONS FOR MIXED TARGET AREAS, e. g. URBAN, FOREST, AGRICULTURE, MARSH
- DEMONSTRATION OF TECHNIQUE TO APPLICATIONS, e. g. SURFACE CLASSIFICATION FOR LAND USE PLANNING; PLANT COMMUNITY DELINEATION FOR MOSQUITO CONTROL
- EVALUATION OF "EXTENSION" CAPABILITIES OF TECHNIQUES TO LARGER AREAS OF VARYING GEOGRAPHY
- DEFINITION OF ELEMENTS OF SYSTEM FOR AREA LAND USE UPDATE SYSTEM, e.g. SATELLITE MEASUREMENTS AND ACCURACIES, COMPUTER OUTPUT FORMATTING

Figure 2

Figure 3 COLLECTION AND PROCESSING OF REMOTE SENSING DATA FOR LAND USE INVENTORY

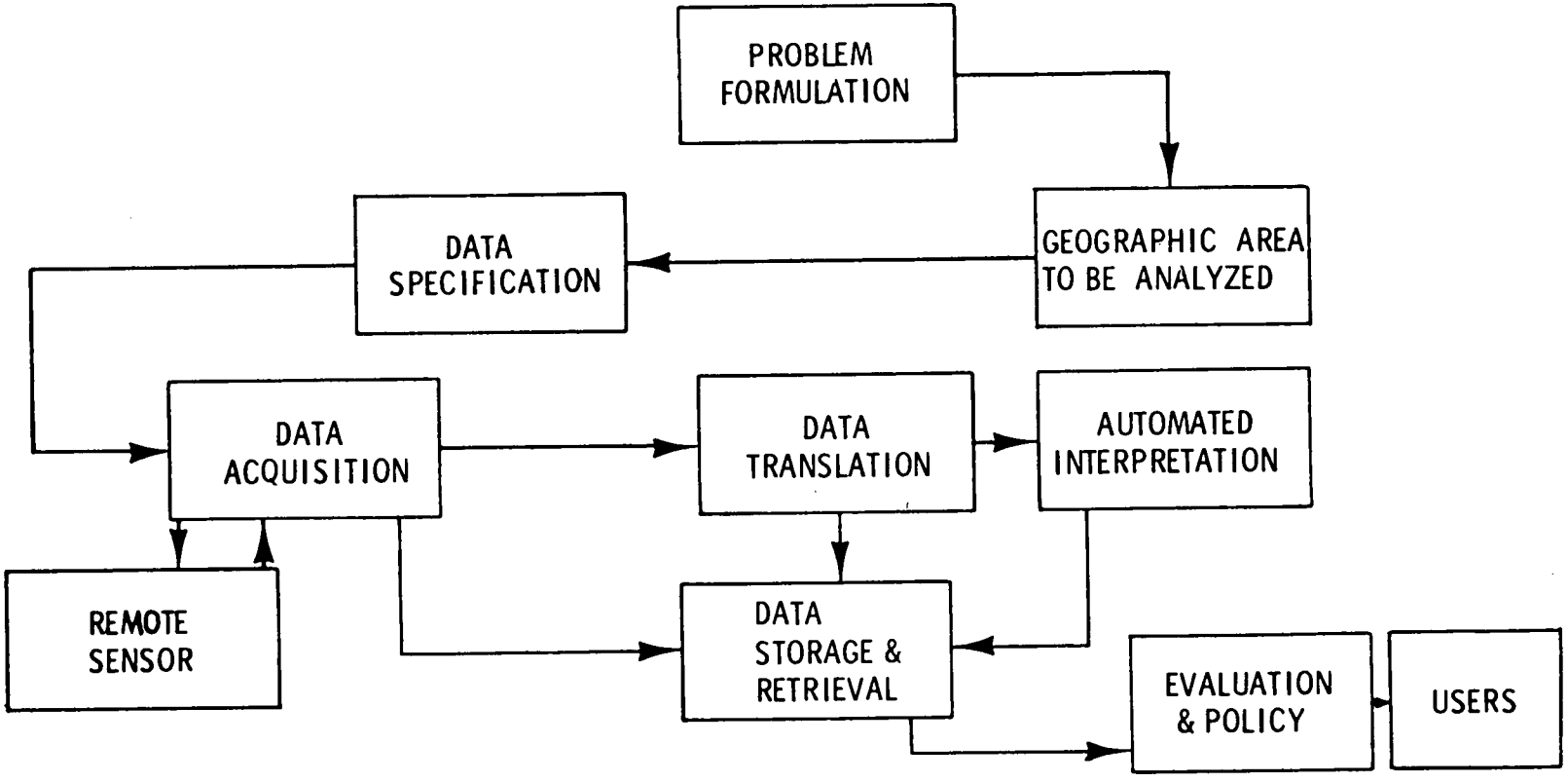

PILOT AUTOMATED LAND USE UPDATE

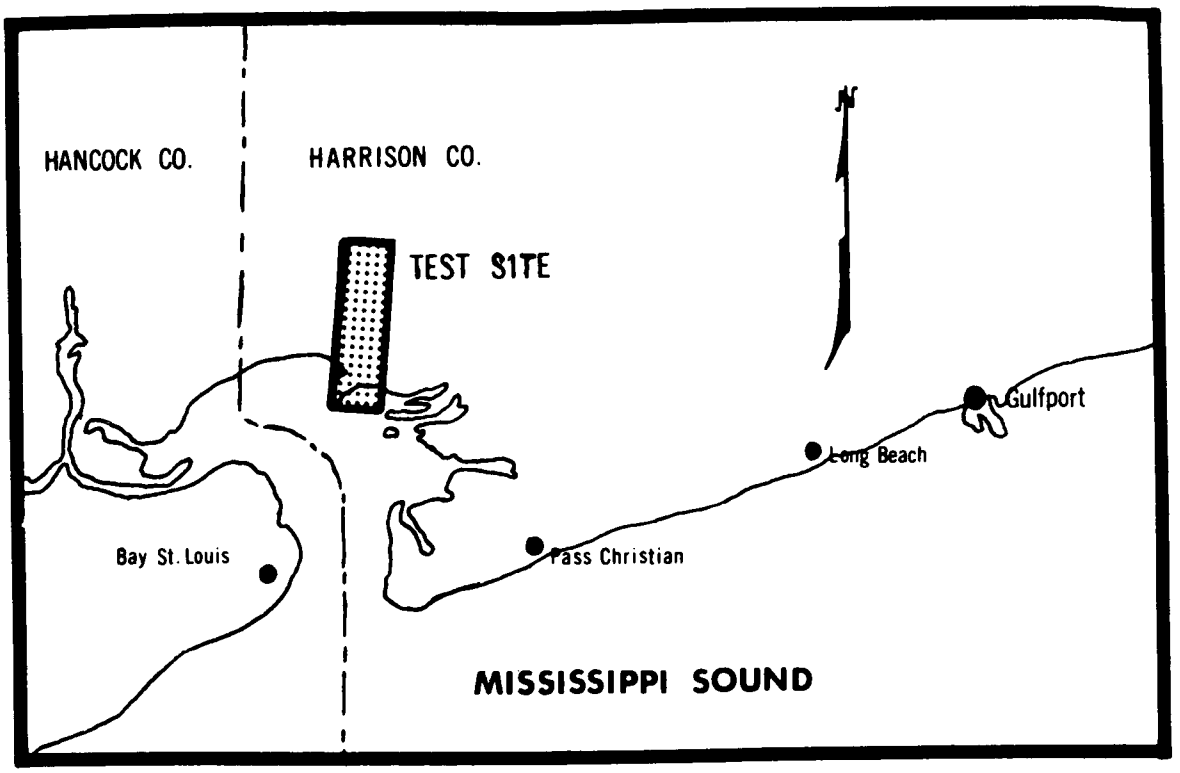

Scale 1:250,000

5 0 5 Statute Miles

Fig.4. Existing photography covering the 1 x 3½ mile strip of land indicated above was chosen as the test area on which to introduce and exercise automated pattern recognition capabilities at MTF/ERL.

Figure 5 DATA TRANSLATION AND AUTOMATED INTERPRETATION SYSTEM EMPLOYED IN PILOT LAND USE DETECTION STUDY

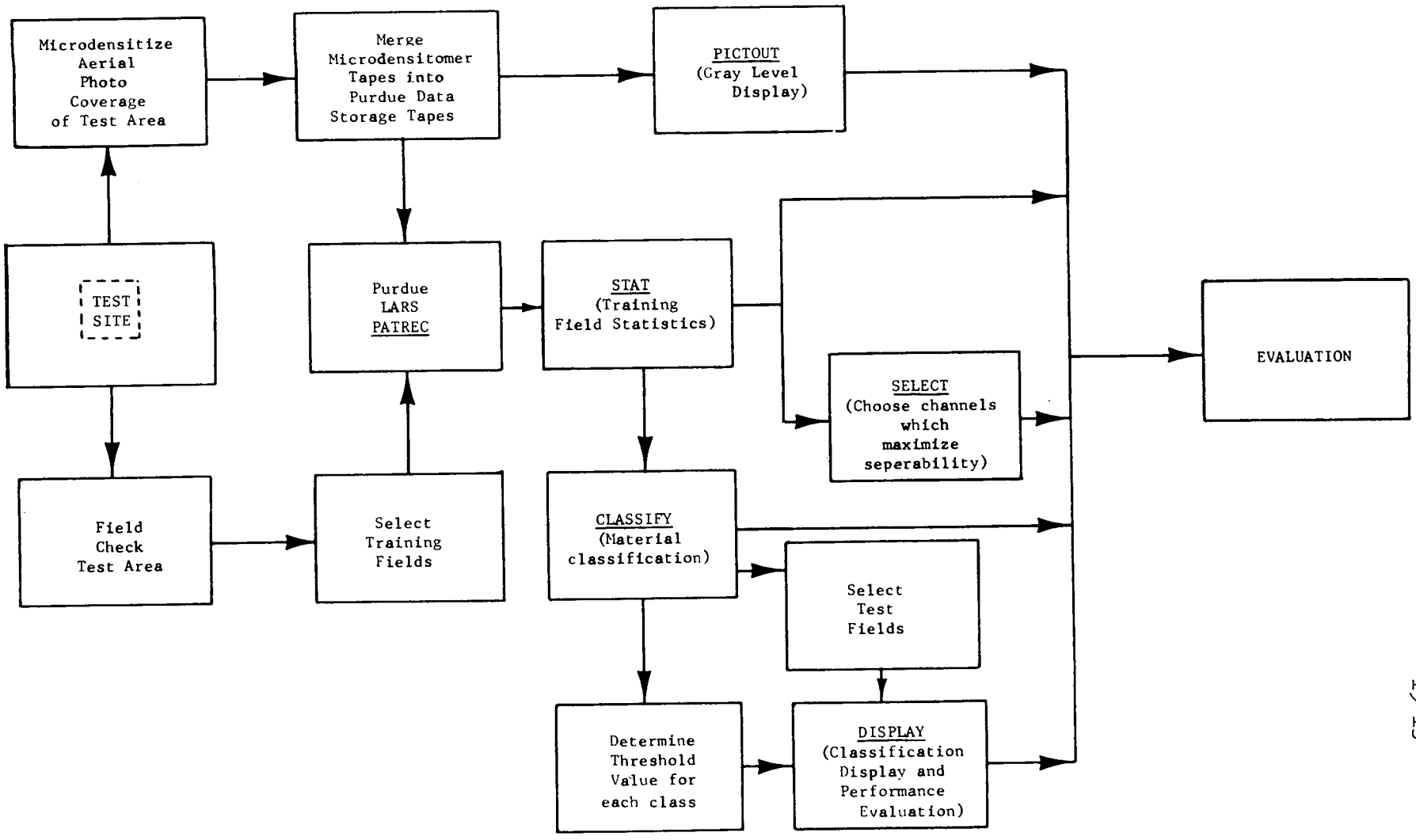

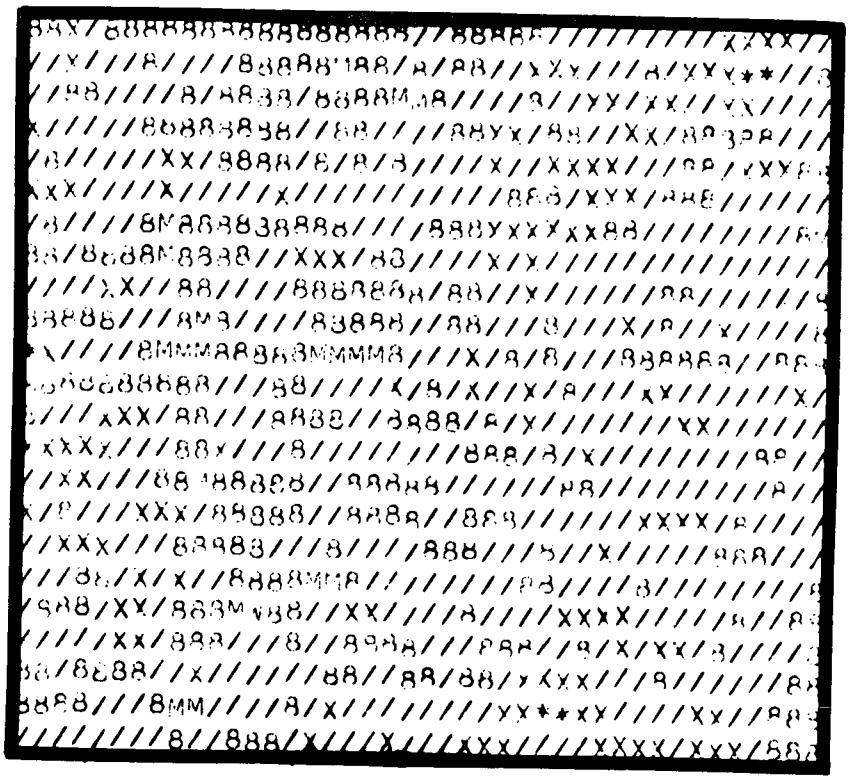

Figure 6. PICTOUT display, channel 2 (.52 - 58 microns).

Symbol	Film Density Interval (relative)
*	89 - 93
X	94 - 96
/	97 - 98
8	99 - 100
M	101 - 103

Pw

RUN NO. 26600061, FIELD 60-1
NO OF SAMPLES = 861, FROM LINES 180 TO 200
(EVERY 1 LINE(S)), SAMPLES 3 TO 43 (EVERY 1 SAMPLE(S))

THE COVARIANCE AND MEAN FOR TRAINING FIELD 60-1

	.43- .49	.52- .58	.62- .66
MEAN	100.70	77.79	51.35
ST DEV	1.97	2.14	3.56

COVARIANCE MATRIX

	.43 - .49	.52 - .58	.62 - .66
	3.90		
	2.00	4.56	
	.45	.59	12.70

CORRELATION MATRIX

	.43 - .49	.52 - .58	.62 - .66
	1.00		
	.66	1.00	
	.06	.08	1.00

Figure 7. Example of STAT printout for training field 60-1.

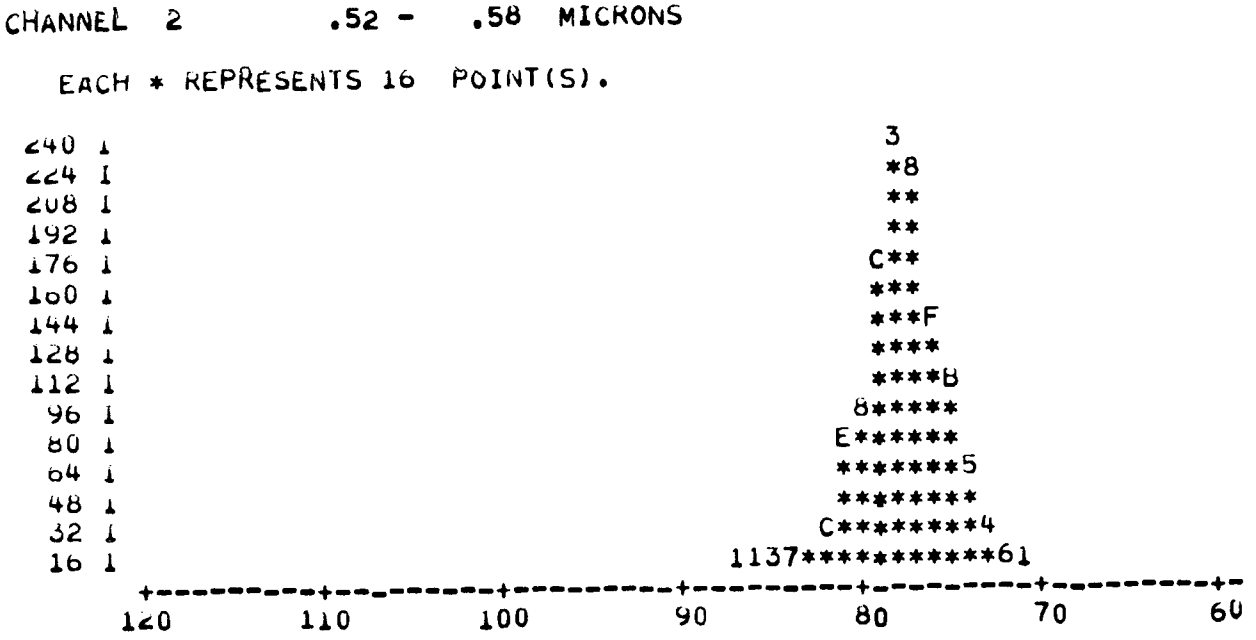

Figure 8 Reflectance histogram for pine (pulpwood), channel 2 (.52 - .58 microns).

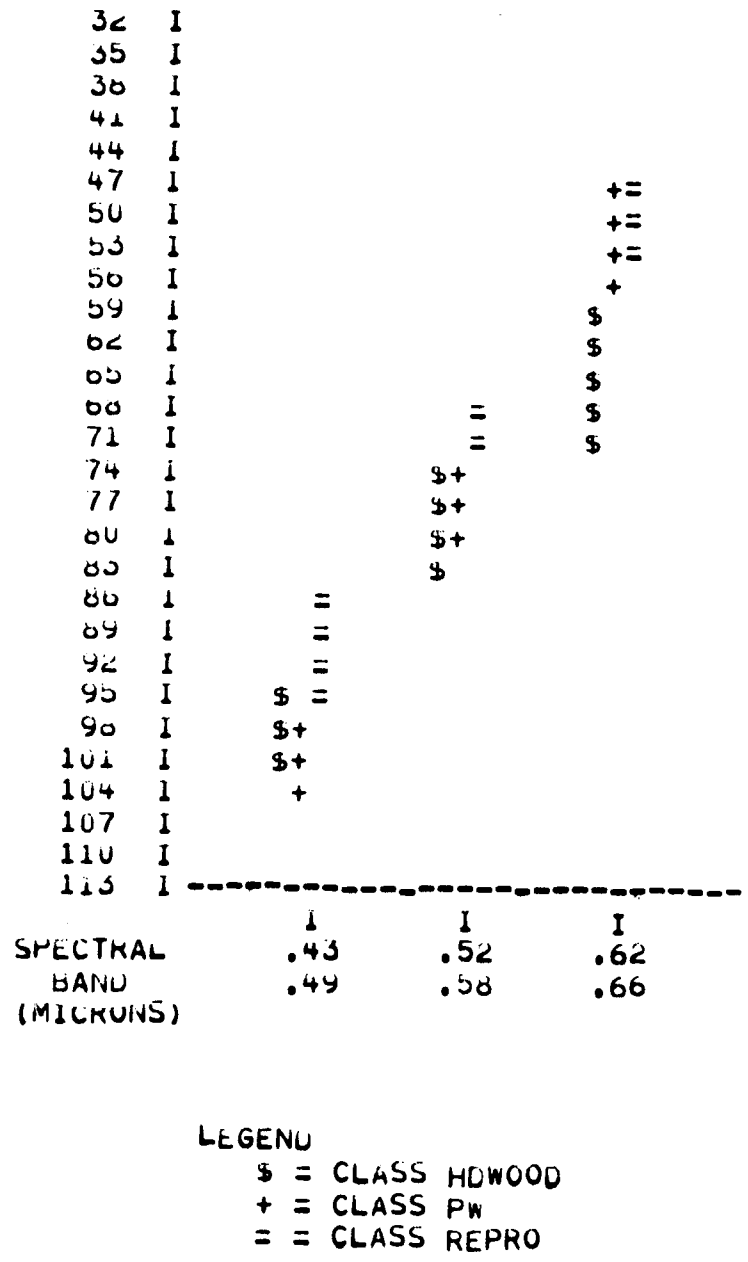

Figure 9. Comparison of spectral reflectance of training areas of three classes of material. Reflectance or radiance, increasing upward, is shown for each of three channels used in the pilot study. A vertical line two standard deviations long, centered about the mean radiance, is drawn using alphanumeric symbols.

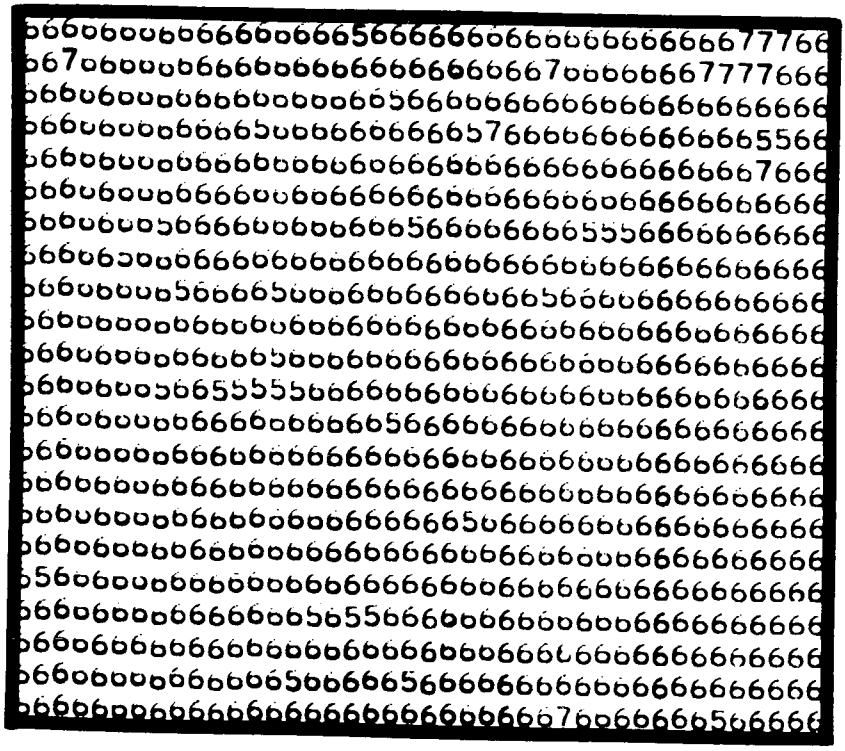

Figure 10 Example of CLASSIFY printout for training field 60-I. Using maximum-likelihood scheme actual classification is made for each ground resolution cell.

Symbol	Class
5	Hardwood
6	Pine (pulpwood)
7	Pine (reproduction)

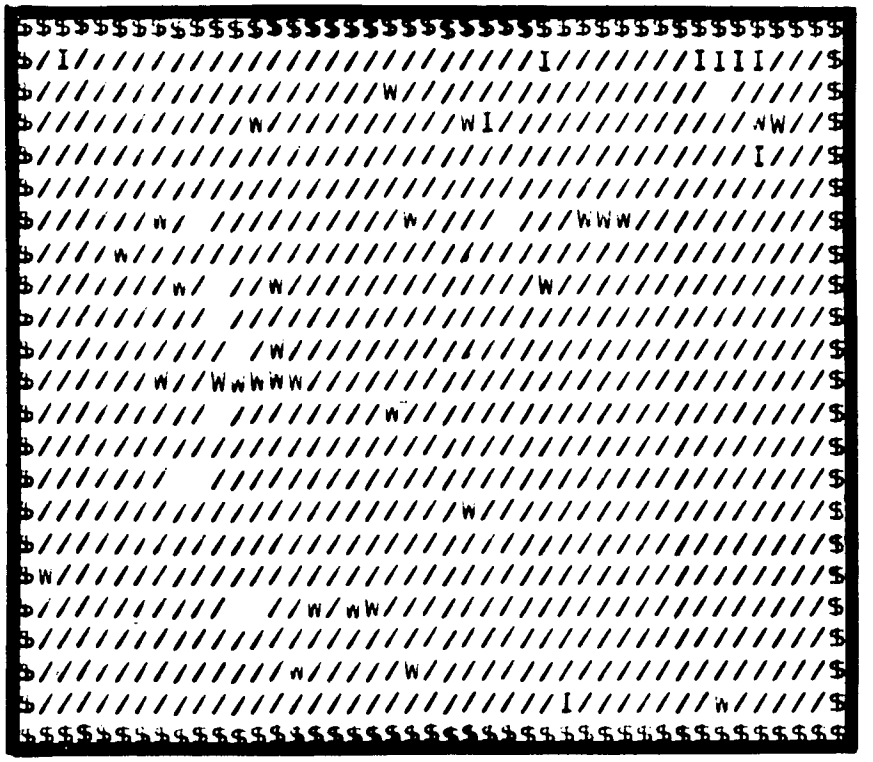

Figure 11 Example of DISPLAY printout of training field 60-I, utilizing the threshold option, the classification made for each ground resolution cell is displayed, and left blank where value at that cell did not exceed threshold value.

Symbol	Classification
W	Hardwood
/	Pine (pulpwood)
I	Pine (reproduction)
Blank	Not classified

CLASSIFICATION SUMMARY BY TEST CLASSES

	CLASS	NO OF SAMPS	PCT. CORCT	NO OF SAMPLES CLASSIFIED INTO SWAT	MARS	ROW	PAST	HDWO	PW	REPR	THRS
1	SWAT	12113	95.8	11599	0	0	0	0	0	0	514
2	MARS	9968	84.5	0	8424	0	0	756	4	1	783
3	ROW	2141	87.9	0	0	1882	63	0	2	23	171
4	PAST	3050	86.9	0	5	22	2651	6	0	118	248
5	HDWO	1587	89.3	0	90	0	0	1417	71	5	4
6	PW	3566	78.8	0	1	0	0	262	2810	424	69
7	REPR	1656	77.7	0	1	0	90	117	32	1287	129
	TOTAL	34081		11599	8521	1904	2804	2558	2919	1858	1918

OVERALL PERFORMANCE = 88.2

PERFORMANCE BY CLASS = 85.8

Figure 12 Example of a Summarization of Classification Results, Using Training Samples. All fields of a particular material are grouped together and correct recognition percentage is shown. Also given is the number of ground resolution elements being classified into each category.

DIGITAL TABLE LOOK-UP
DATA PROCESSING FLOW

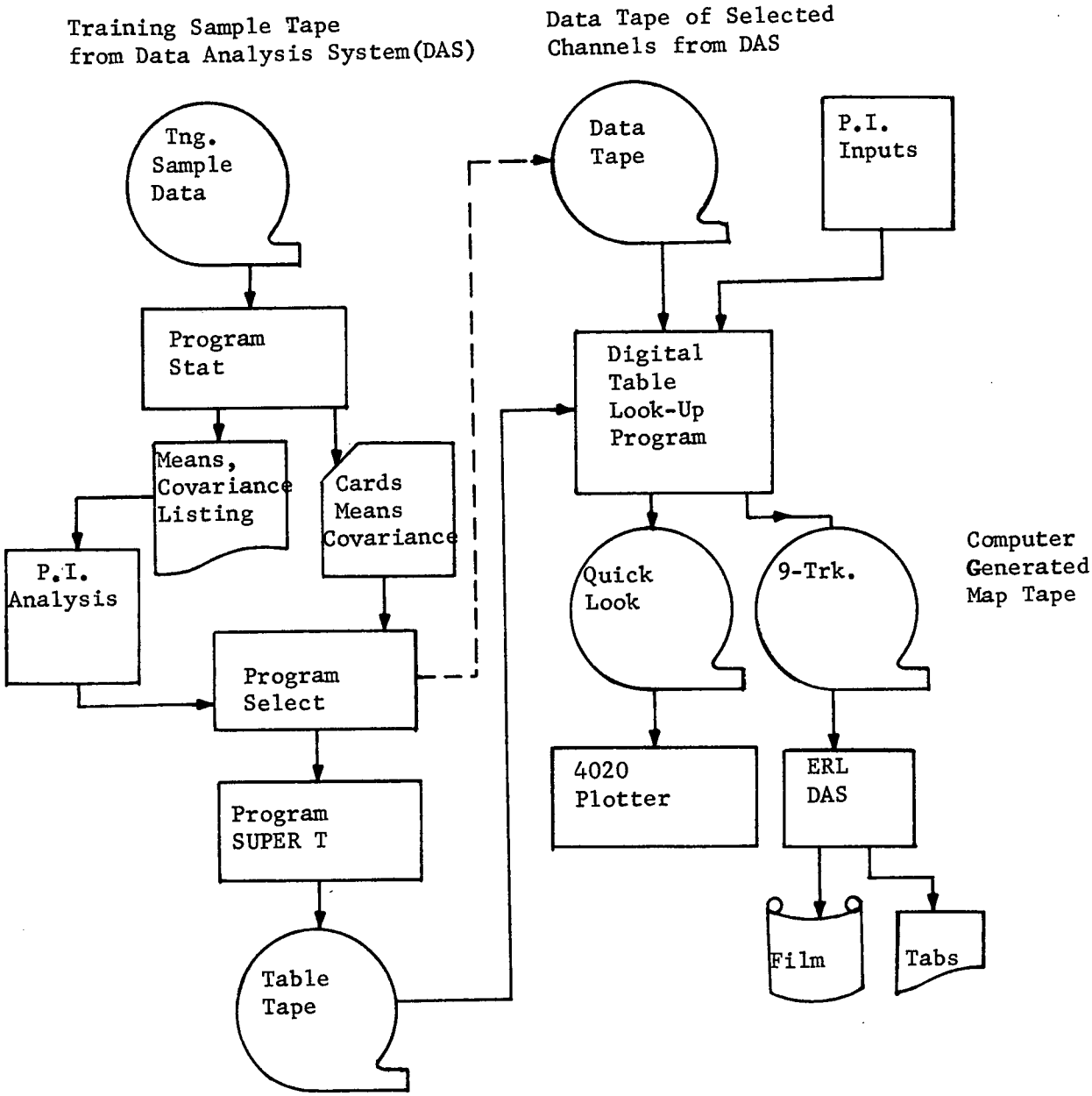

Figure 13

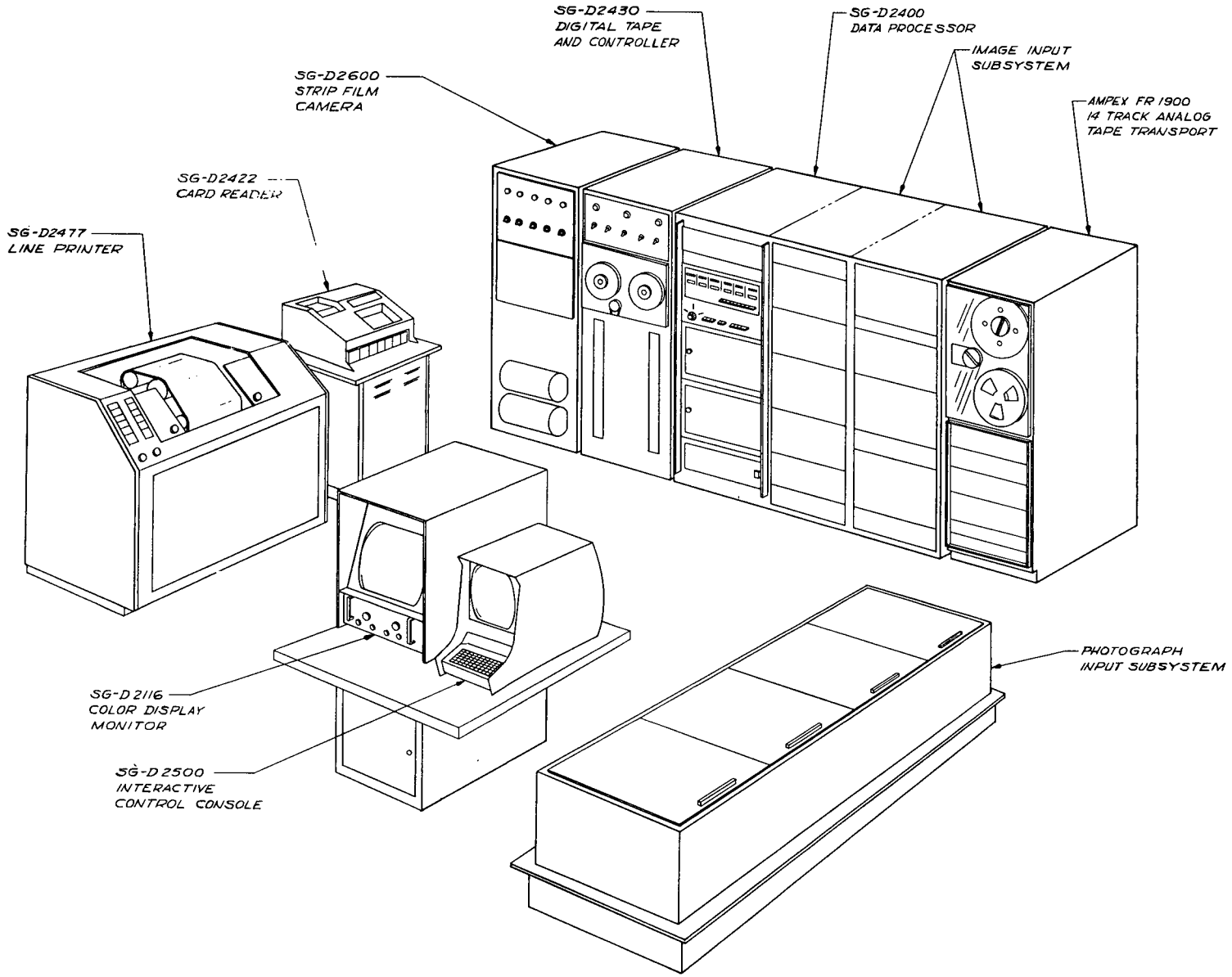

Figure 14 Perspective View of Earth Resources Data Analysis System

ERL - DATA ANALYSIS SYSTEM

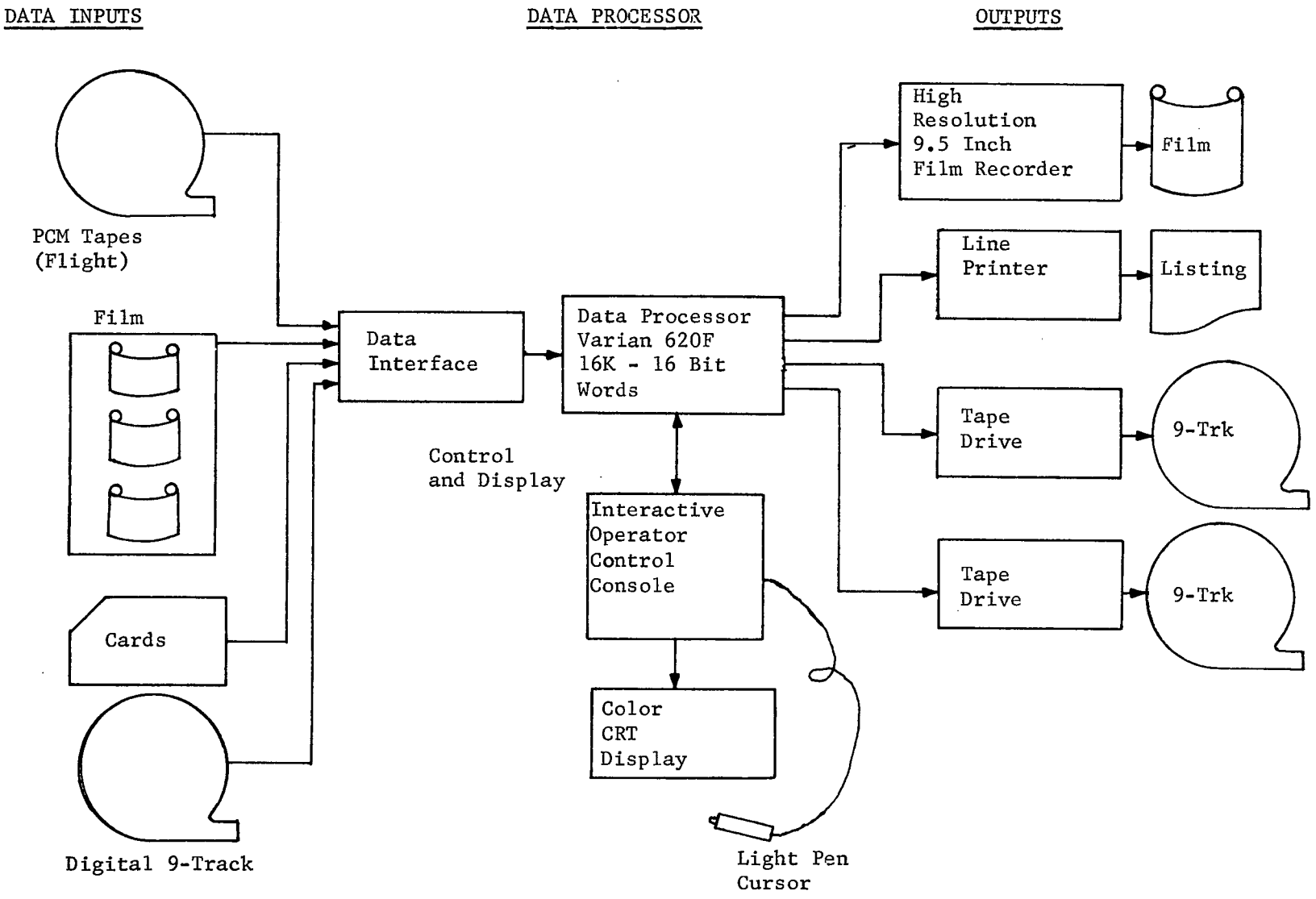

Figure 15

Figure 16 ERL DAS CHARACTERISTICS

PURPOSE: TO SCREEN, EVALUATE, REFORMAT AND RECORD DATA FROM MULTISPECTRAL SCANNERS, MICROWAVE IMAGERS, MULTIBAND FILMS, AND SCANNING IMAGING SPECTRORADIOMETERS FOR FURTHER ANALYSIS ON LARGE COMPUTERS.

INPUTS:
- A) FROM TELEMETRY 1-INCH TAPES RECORDED IN BI-PHASE L PULSE CODE MODULATED (PCM) FORMAT
- B) UP TO 4 BANDS OF MULTIBAND CAMERA FILM.
- C) COLOR OR COLOR IR PHOTOGRAPHY FOR TRI-COLOR SEPARATIONS INTO THREE DATA BANDS
- D) IBM CARDS
- E) DIGITAL 9-TRACK TAPES OF IMAGERY

DISPLAY:
- A) COLOR CRT (525 TV LINE RESOLUTION)
- B) FALLING RASTER MOVEMENT
- C) REFRESHED AT STANDARD TV RATES

CONTROL: INTERACTIVE OPERATORS CONSOLE
- A) SELECTION OF DATA BANDS
- B) LINEAR COMBINATION OF DATA BANDS
- C) REAL TIME COLOR DISPLAY MODIFICATION

DATA PROCESSOR:
- A) VARIAN 620F COMPUTER
  - 1) 16K, 16 BIT WORDS
  - 2) 750 NANO-SECOND CYCLE TIME

OUTPUTS:
- A) FILM RECORDER
  - 1) COLOR OR B&W
  - 2) 9.5 INCH FILM
  - 3) CONTINUOUS STRIP RECORDING
- B) LINE PRINTER
- C) TAPE DRIVES
  - 1. 9-TRACK 800 BPI
  - 2. SPEED 150 IPS

Figure 17

SCHEDULE AND MILESTONES

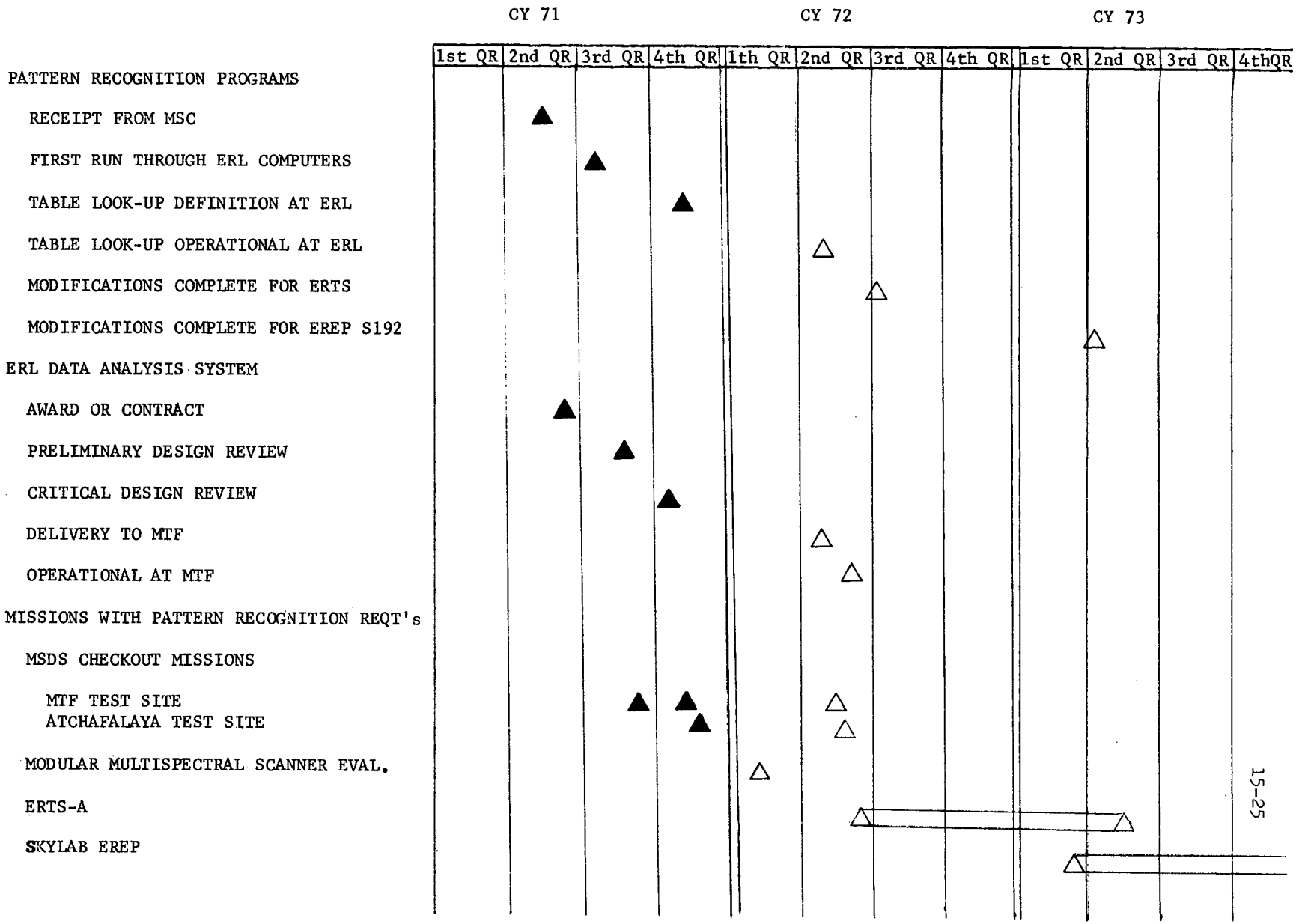

APPENDIX A

TRAINING FIELD PROCESSING

Assumptions:

- One 7 track tape contains all training field data.
- All tapes are error free and properly formatted.
- Overnight turnaround provided by SCC.

Investigator Participation:

- Provides histogram and spectral plot scales.
- Determine best 12 channels.

Computer Processes:

Computer Time	25 min.
Manhours	60 hrs.
Calender Time	1 wk.

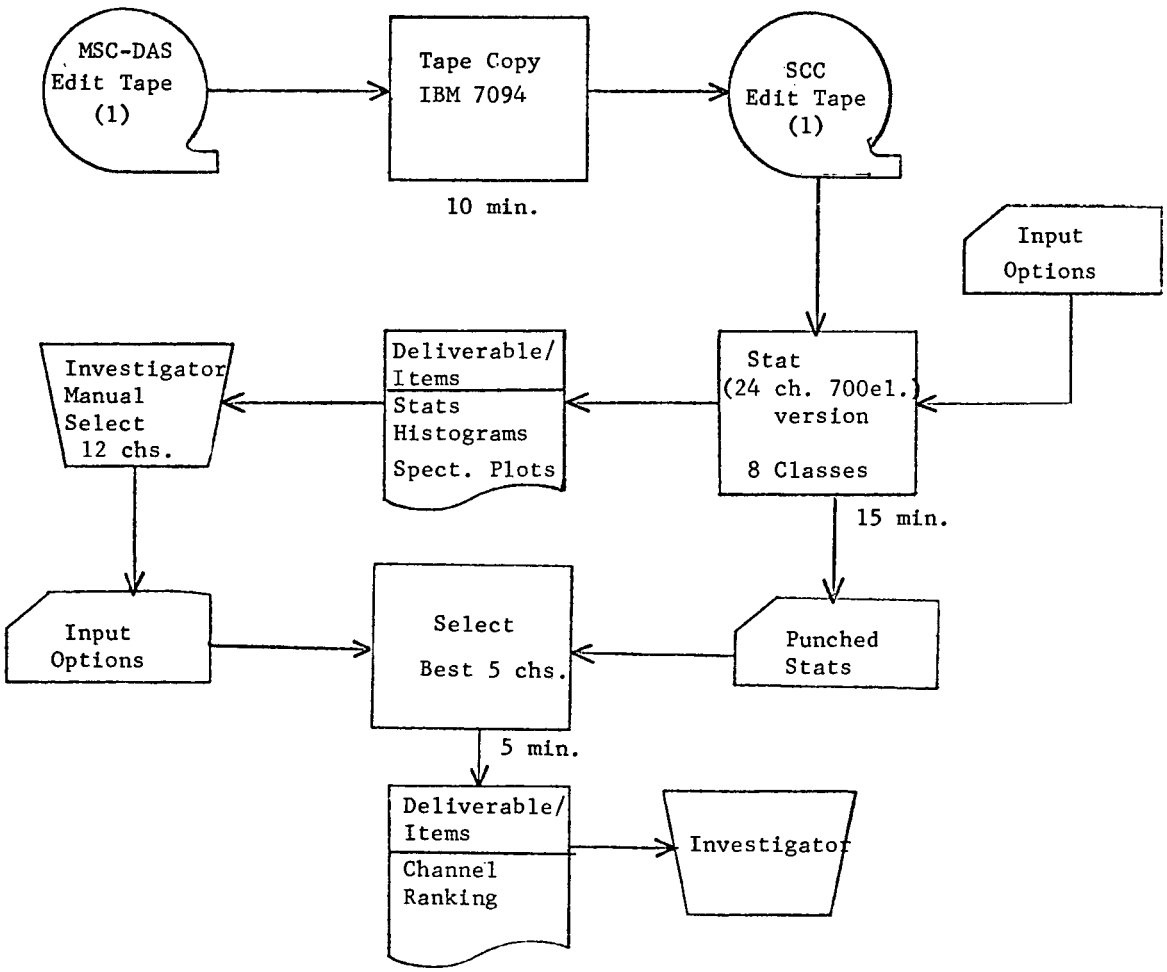

CLASSIFICATION

Assumptions:

- 7 track tapes of 5 desired channels.
- All tapes are error free and properly formatted.
- All scans and elements will be classified.
- Overnight turnaround provided by SCC.

Investigator Participation:

- The channels to be used (subset of STAT)
- The classes to be used (subset of STAT)

Computer time	2530 min.
Manhours	200 hrs.
Calender Time	4 wks.

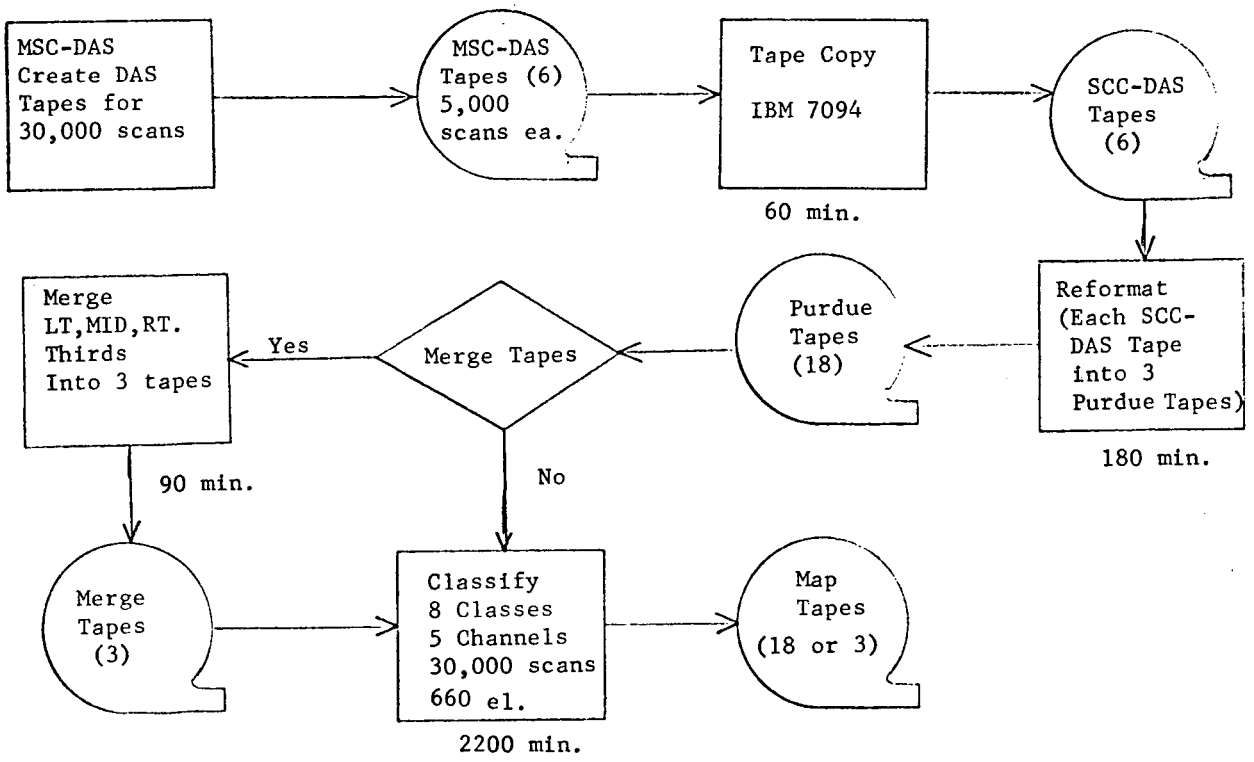

DISPLAY

Assumptions:

None

Investigator Participation:

- Provide the threshold values for each class.
- Provide test field coordinates.

* Computer time	440 min.
Manhours	370 hrs.
Calender time	6 wks.

* Character plot from printer available in one week; 60 min. computer time and 30 manhours.

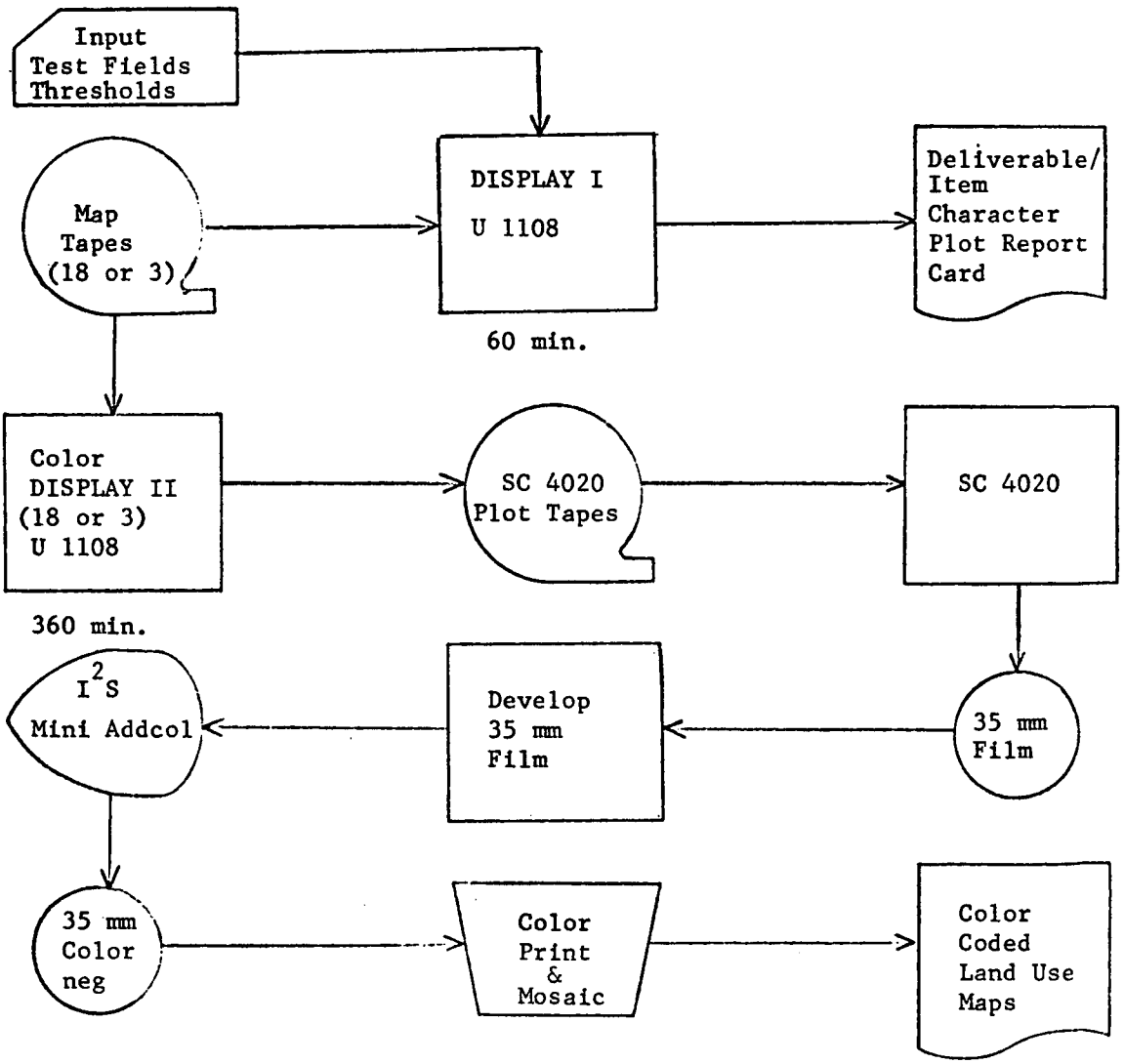

The time required to complete all processing steps would be :

Step	Comp Time Min.	Man Hrs.	Cal. Time Wks.
Training Field Processing	25	60	1
Classification	2530	200	4
Display I	60	30	1
Display II	360	340	6
Total	2975	630	12
	49 hrs.35min.	16 wks.	12 wks.

A more detailed description of the steps required to process this data are:

1. Receipt of MSC-DAS edit tapes.
2. STAT (24 ch., 700 ele. version).
3. PI manual select of best 12 chs.
4. SELECT (best 5 of 12 chs).
5. MSC-DAS data tapes for best 5 chs.
6. REFORMAT
7. MERGE
8. CLASSIFY
9. DISPLAY I (character plot)
10. DISPLAY II (color coded land use map)

The flow chart estimates are for a typical mission consisting of 30,000 scan lines of MSS data. It is assumed that eight materials or classes and the best five data channels are to be used.

Basic assumptions are:

1. MSC-DAS Tapes
   a. Only 7-track tapes are received.
   b. All tapes are error-free..
   c. All required data are properly formatted.
2. STAT
   a. The operational 24 ch., 700 ele. version will be utilized.
   b. Training field data will be on a single MSC-DAS edit tape.
   c. STAT will be run for only the training fields contained on the MSC-DAS edit tape.

d. The PI will provide the following input options:

- o Histogram high end
- o Histogram low end
- o Histogram height
- o Histogram number of bins
- o Spectral plot low end

e. Deliverable items, training classes and fields (for all good chs.) will include:

- o Means
- o Covariance matrices
- o Histograms
- o Spectral plots
- o Coincident spectral plots (classes only)
- o Punched means and covariance matrices on cards (classes only)

3. PI Manual Select

The PI will either perform a manual select to determine the best 5 channels or determine which channels (max. of 12) should be utilized by SELECT to determine the best 5 channels.

4. SELECT

a. The production 12 channel LARS Purdue version of SELECT will be utilized.

b. The PI will provide:

- o Which training classes and STATS will be utilized.
- o The number of channel combinations to consider.
- o Which channels (max. of 12) will be considered.

- o Any weights to be assigned a class.
- o The number of combinations desired to print the results for.

c. If statistics are not available for the selected classes and channels (max. 12) in the STAT module training deck, STAT will be required to be re-run for only those selections.

d. Deliverable item is a listing of the required number of the best channel combinations.

5. MSC-DAS Data Tapes

a. The PI after analyzing SELECTS output will notify the MSC-DAS to generate data tapes for the desired best channels.

b. No multi-reel tapes.

c. Only 7-track tapes to be delivered to ERL.

d. All tapes are error free.

e. Data is properly formatted on tapes.

6. REFORMAT

a. In order to use the 12 channel, 222 element production version of CLASSIFY, the MSC-DAS data tapes must be reformatted to the Purdue Bulk Data Tape Storage format (i.e., maximum of 12 channels and 222 elements).

b. Since the production version of CLASSIFY can handle only 110 elements at a time, the REFORMAT tapes will contain data for only 220 elements.

c. Each MSC-DAS data tape will be reformatted into 3 REFORMAT tapes. Each tape will contain data for 220 elements (approximately 1/3 scan consisting of 700 elements) and be designated LEFT, MIDDLE, and RIGHT thirds).

7. MERGE

The running of MERGE is optional and beneficial in that it merges the REFORMAT tapes into 3 tapes (one each for the left, middle, and right thirds).

8. CLASSIFY

a. The current operational 12 channel, 222 element LARS version of CLASSIFY will be utilized.

b. The PI will provide:

- o The channels to be used which are a subset of the STAT data.
- o The classes to be used (subset of STAT data).

c. All scans and elements will be classified.

d. Deliverable items

- o Listing (character plot) of classified data.

9. DISPLAY I

a. The current operational LARS version of DISPLAY will be utilized.

b. The PI will provide:

- o The threshold values for each class.
- o The desired test fields.

c. Deliverable items include:

- o A "report card" giving performance results on a per field and per class basis.
- o A line printer character plot.

10. DISPLAY II

a. This is optional and results in a color coded land use map.

b. The STAT histograms will be utilized to determine bins to be utilized for each color (class).

c. Combining of colors will be done on the Mini Addcol viewer.

d. A 30,000 scan line mission will produce 360 frames of color photography. Prints and a mosaic of these photos will be required to produce a color coded land use map.

SECTION 16

N72-29317

LEWIS RESEARCH CENTER EARTH RESOURCES PROGRAM

by

Herman Mark
National Aeronautics and Space Administration
Lewis Research Center
Cleveland, Ohio

INTRODUCTION

In our Earth Resources program at Lewis Research Center we are attempting to bring NASA technical capabilities to bear on regional problems that would benefit from such attention. We have, quite frankly, made it a point to select problems existing in our region from among those which we believe are possible to do, and we've added the requirement that solution of the problem will directly make many people in the area happy that the NASA had the technological capability to provide the solution, while at the same time making very few of our local citizens mad at us. Our goals thus include visibly demonstrating NASA technical capability to the general community along with conducting the scientific effort itself. The areas of effort (fig. 1) because of our location, seemed most appropriately to be the following: Monitoring and rapid evaluation of water quality, determination of ice-type and ice coverage distribution to aid operations in a possible extension of the Great Lakes Ice Naviation and Shipping Season and preliminary efforts to monitor the spread of crop viruses and the extent of damage to strip-mined areas as well as the success of efforts to rehabilitate such areas for agriculture. These problem areas are listed in figure 1.

DESCRIPTION OF THE STUDIES

Water Quality

The first of these, the study of water quality, is being done in two parts. The first is in cooperation with the Environmental Protection Agency and their Headquarters Office of Research and Monitoring. Under the Office of Research and Monitoring, as you might guess, there is an Office of Research and an Office of Monitoring. At present they are not sure under whose management this effort should come in their Headquarters Office, but they agree that the work should be done. The local EPA people that we deal with in the Lake Erie Basin Office in Cleveland, and the Measurements Laboratory people in Cincinnati are very enthusiastic, as are the EPA people in the 5th District Office in Chicago. What we

have done is to obtain several IRLS-Nimbus IV data collection packages and we have deployed one on the Great Miami River near Cincinnati, Ohio (fig. 2).

The IRLS, or Interrogation, Recording and Location System data collection package is inside this trailer near the Miami River. This package can be interrogated by Nimbus IV several times a day. It is provided with the capability of transmitting seven analog channels of data of which two are housekeeping voltages and five are input data. The parameters we are reading in the Miami River are dissolved oxygen, conductivity, temperature, pH, and a standard voltage. These are simultaneously being sent by telephone to EPA offices in Cincinnati. The data that Nimbus receives is recorded, then subsequently dumped to a ground station, sent by hard-line to Goddard, and Goddard sends it to Lewis by mail. The EPA is delighted with this installation and we're presently discussing with them the deployment of another IRLS package at the outflow from the Eastlake Power Plant in Lake Erie, as well as the possible use of 20 ERTS DCS packages to aid them in their essential monitoring duties since they are extremely short of people to monitor the areas in this district for which they have responsibility. With the present antenna, we're getting two to six responses for every twelve interrogations, so we designed an 11dB gain antenna for these fixed location applications (fig. 3), and now we get >nine responses for every twelve interrogations.

We plan to continue using the conical helix shown in figure 2 for moving applications, however, to maintain axi-symmetry. In a cooperative effort with the Canada Centre for Inland Waters in the IFYGL studies on Lake Ontario, we are planning to use the locating feature of the IRLS to determine surface currents on the lake by placing a package on a high water drag buoy which CCIW is designing and building. At the same time, we are designing circuitry to integrate surface winds in time and store the integrated values for interrogation. CCIW will have two ships on the lake 24 hours a day to care for the buoy and package.

In another cooperative program with the Canada Centre we have overflown their research vessel, the C.S.S. Limnos (fig. 4), with a scanning spectrometer while the Limnos has made chemical and organic particle density measurements at five depths, at each of six stations in Lake Erie.

At each station shown in figure 5, the Limnos makes a measurement 1 meter below the surface, 6 meters below the surface, one just above the thermocline, one just below, in the hypolimnion, and one on the bottom. As soon as CCIW can reduce the data, we will attempt to see if the measurements of organic material at depth can be correlated with the surface density values, thereby to obtain a correlation for the entire column

of water with the overflight spectral readings. We have similarly overflown their M.S. Martin Karlsen (fig. 6), which makes measurements at 50 points in Lake Erie shown in figure 7. The Canadians have formally agreed to work together with these data as well. On one of our flights over the Cleveland Sewage Treatment Plant, we caught a color IR of a serious accidental spill of millions of gallons of raw sewage (fig. 8). When we looked more closely, there was a man in a boat sailing right through it (fig. 9). We have some really tough sailors in Cleveland.

Ice Type Distribution Monitoring

Our second area of interest is that of ice type evaluation and monitoring (fig. 10). This program grew out of discussions we had early in the year with Captain E. F. Walsh, Chief of Operations, 9th Coast Guard District. He agreed that if his Ice Information Center could get really good information on the kind and distribution of ice coverage on the Lakes, it would make operating into the ice season much easier. At the present time, shipping on the lakes moves for about 8 months. From the latter part of December to the middle or latter part of April, most shipping ceases due to ice covering the lakes, channels, and harbors. Since a total of 250×10^6 tons of cargo are shipped on the lakes (20 percent of total U.S.), the value of lengthening the shipping season has become apparent to others and some months ago, Congress passed a bill authorizing a group of Federal Agencies led by the U. S. Army Corps of Engineers and the Coast Guard to perform a 3-year demonstration to determine the feasibility of extension of the shipping season. Last year, with Captain Walsh's cooperation, we had already made flights to look at the ice coverage and the variation in ice types. Figure 11 is a photograph of ice in a channel. In figure 12 is shown the pattern seen when ice sheets begin to come together. In figure 13 can be seen a photograph of ice with a large opening and the results of automatic processing programs put together to determine the area of such openings in the ice. In figure 14 we see broken-up ice, starting to refreeze. Notice how definite the patterns are. It occurred to us that the information determining lake ice type might often be there, but that much of it would be in patterns. Questions such as: How big are the pieces? Are they getting bigger or smaller? How many holes? How big are the holes? appeared to be the type that would require answering. So we developed some programs to permit us to count objects. We felt that the counting of objects would be valuable in other applications as well as in the ice program and this will be discussed later where it does apply.

In figure 15 the left figure is a pictorial representation of an object; the right figure shows how a computer would view the object after it had been "seen" by some sensor and suitably digitized.

In the computer study of the object, the array is scanned one line at a time (top to bottom) and one element at a time (left to right). An algorithm has been developed in which scale-independent geometric features (heads = H, tails = T, splits = S, and joins = J) are recognized as the scanning proceeds and the sums are recorded. Actually at any one time only two lines need to be known by the computer: the line being scanned and the previously scanned line. Thus the entire two-dimensional array need not be stored at one time -- a space-saving feature.

Note that the first relation ($\Sigma H + \Sigma S - \Sigma T - \Sigma J = 0$) provides a way of telling when an object has been completely scanned -- the expression equals 0 when the object is complete. As each object is completed, the object counter is incremented. Although only a single object is shown in the figure, the computer can keep track of multiplicity of complicated objects as they unfold during the scanning (even spirals, objects within objects, etc.)

Notice that once the H T S J sums have been obtained for an object, the second relation can be used to tell how many holes each object has. This, along with the object count, gives two scale-independent pieces of information about an image.

Since the algorithm for recognizing H T S and J's considers in turn each element making up an object, we can concurrently keep track of <u>any</u> property of the object which can be calculated one element at a time. For example:

area = A
perimeter = P
center of mass
inertia tensor

From these, useful scale-independent parameters such as $P/\sqrt{A}$ ('jaggedness' parameter) can also be constructed.

Figure 15 shows an object consisting of either x or no-x elements ("black and white"). If objects are recorded in different shades of grey or in different colors, or if there are several kinds of objects (as is the case for most real images), the problem is handled by simultaneously performing the above analysis for each shade, color, or type of object. Each additional kind of object requires additional storage for keeping track of the sums.

Algorithms have been developed for other interesting tricks, such as "counting" composite objects (objects consisting of the union of two or more types of distinguishable objects) and detecting which objects

border selected sets of other objects.

As work progresses we hope to branch from the "counting" stage of analysis just described to more sophisticated techniques of pattern recognition.

In figure 16 is shown the organization of the Federal Ice Board mentioned earlier. At the formal request of Major General Ernest R. Graves, the Division Engineer of the U. S. Army Corps to the NASA Administrator's Office, I was named to fill the NASA slot on the board in December 1971. We are hoping that Lewis' effort to fly over and make remote images together with ground truth measurements made for us by the Coast Guard, as well as additional ground truth provided by the Lake Survey Center, will result in operational frequency ice type and coverage maps. These will be used by the Coast Guard operations to deploy optimumly their small fleet of ice-breakers which have been added for the season extension program. To provide for the problem of cloud cover periods when visible and thermal wavelength band images may be useless, we are planning for Houston P3 16.5 gigahertz SLAR flights in February 1972, as well as an Ames Convair 990 flight in March 1972, using the Goddard 19.1 gigahertz microwave passive scanner. The final goal will be to provide upgraded ice-information to the Coast Guard which can be used, not only in the demonstration, but beyond, during extended shipping seasons. Additional information from satellites will be provided to determine the value of such synoptic views, especially those from ERTS next winter.

Additional Regional Efforts

The third area of effort I'd like to discuss today is shown in figure 17 and is made up of two cooperative efforts with the Ohio Agricultural Research and Development Center. The first is one in which we have attempted to aid USDA entomologists stationed at OARDC in tracking the spread in corn of Maize Dwarf Mosaic Virus of a number of varieties while they keep track of the population distribution of the insects spreading the disease. Toler of Texas A & M has done a similar optical study of St. Augustine Decline Virus with that grass as the model host. In figure 18 we see the test plots of corn being subjected to the disease. In figure 19 we show a sample of a plant infected with MDMV. A lab plot (fig. 20) of optical properties of healthy corn compared with corn suffering from the virus indicates that it is transmission that is increasing in the infected leaves. A lab composite indicates that this should result in increased reflectance at 5600 Å and field spectra of diseased plants do indeed exhibit this increase (fig. 21).

The Ohio Agricultural Research and Development Center at Wooster, Ohio, is an outstanding agricultural scientific group, and they've been

working diligently on a test strip-mined area in Noble County, Ohio (fig. 22) for some years to determine what should and can be done about the devastation to the countryside caused by the strip-mining activities in Ohio. Discussions we have had with Dr. R. Davis, Assistant Director of OARDC and with Dr. Burley Schmidt, Head of the Department of Agronomy there, have resulted in a cooperative effort at their test site. Our present plan is for Dr. Paul Sutton, the agronomist in charge of the test site and his crew to provide us with soil and sample classifications which we are to try to identify remotely. If we can identify the samples of interest by remote sensing, we will have the beginnings of a system to determine rapidly the damage being done. Figure 23 is a photograph (near IR) of the test area. Figure 24 shows how clearly the stripped areas stand out against the remaining vegetation. Dr. Sutton has provided us with eight samples (fig. 25) which are of interest, and the color photo shows how distinguishable these soil types are. In figure 26 lab spectra show that the soil types are detectable, and our cooperative effort continues to see if the extent of these various soil types can be determined for the test plot. Since a major purpose of the effort is the rehabilitation of such areas for agriculture, various types of agricultural efforts have been made. For example, orchards (fig. 27) have been planted in the ruined areas. Our efforts are involved here in determining the success of such efforts at agricultural rehabilitation, hopefully in a rapid and automatic way. For evaluating the success of orchard plantings, here we have developed (fig. 28) our object counting programs to include the ability to determine the state of the orchard, tree by tree, automatically permitting rapid large area evaluations. It should be pointed out here that strip-mining in Ohio is a $500 million a year industry and everyone, including the mining industry, would like a proper and realistic cost of rehabilitation to be determined. At present, an acre brings in $25,000 from coal but less than $200 per acre in fines. Since such efforts could never be halted, it is necessary to make proper estimates of damages and costs so that increased charges be made when necessary, and even as important, made smaller -- even zero -- when appropriate, say when soil easy to rehabilitate is turned up. The goal of our cooperative effort with OARDC is to provide some of the capability to permit this eventually on an operational basis to assist everyone concerned. The mining industry, the agricultural industry, as well as the state and its people, will all benefit from the development of such a capability.

Page intentionally left blank

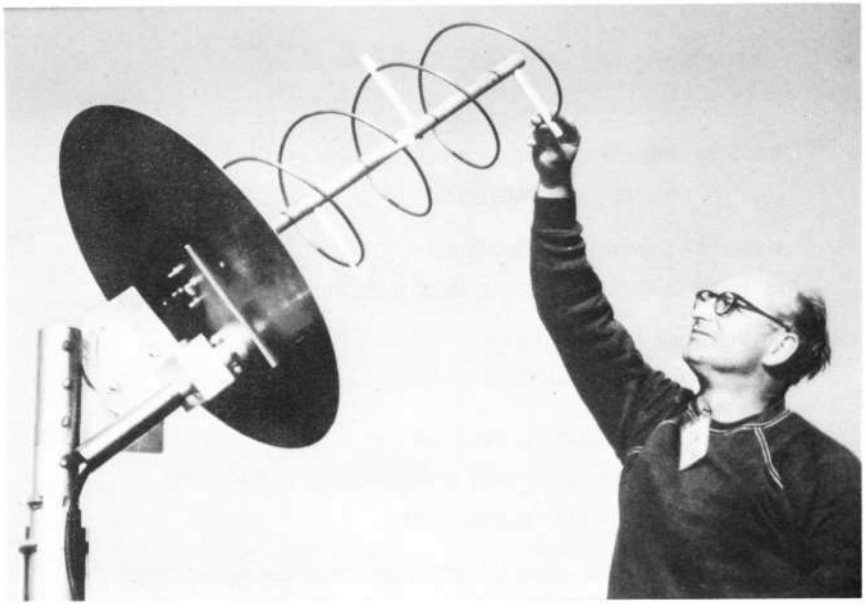

Figure 3. - High gain antenna for fixed location IRLS packages.

Figure 4. - Canadian steamship LIMNOS making in the water measurements in Lake Erie.

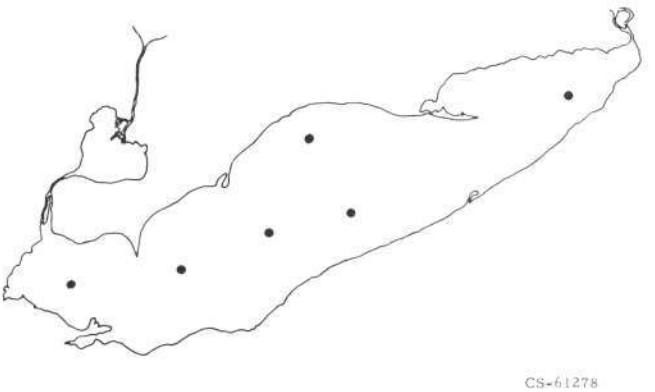

Figure 5. - Lake Erie organic particle measurement stations of the C. S. S. LIMNOS.

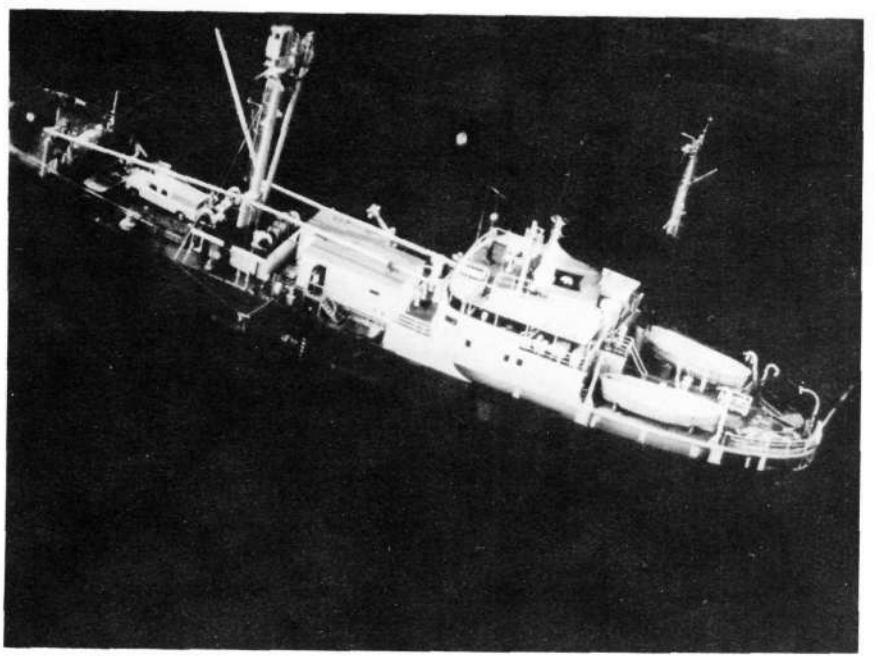

Figure 6. - Canadian motor vessel Martin Karlsen making in the water measurements in Lake Erie.

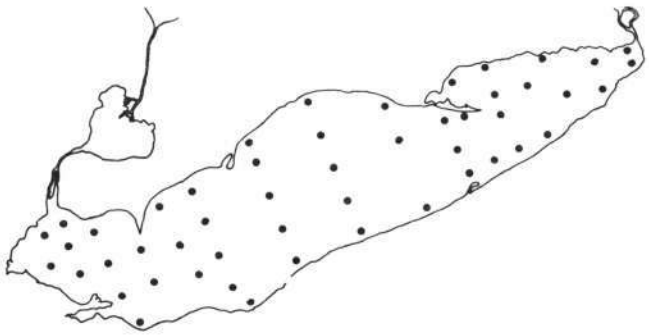

Figure 7. - Lake Erie measurement stations for the C.M.V. Martin Karlsen.

Figure 8. - Accidental sewage spill at Cleveland Sewage Treatment Plant (near IR).

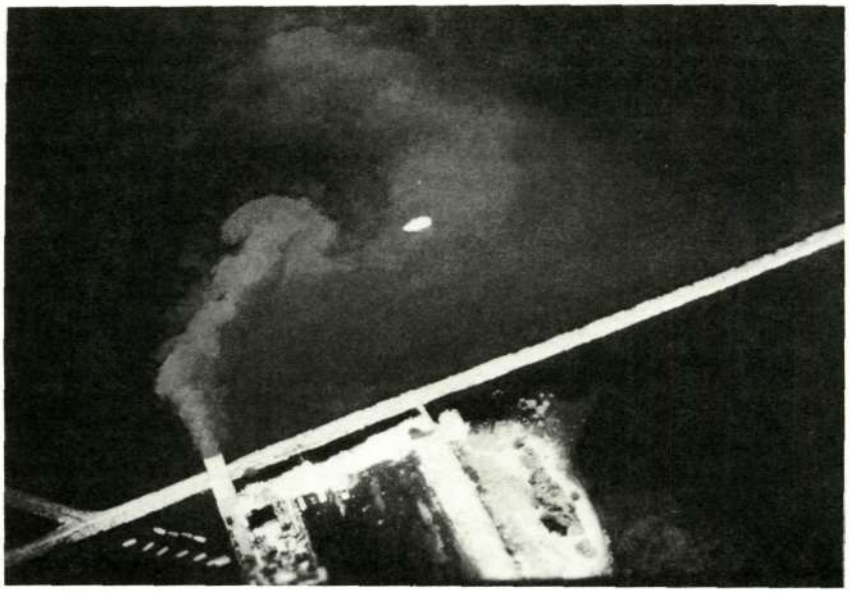

Figure 9. - Closeup view of raw sewage spill at Cleveland Sewage Treatment Plant (near IR).

160-75-60: MIDWEST/GREAT LAKES APPLICATIONS OF

EARTH OBSERVATIONS SATELLITES

2. HYDROLOGY, LIMNOLOGY - HL-1

GREAT LAKES ICE EVALUATION & MONITORING

CS-61289

Figure 10. - Lewis Research Center Ice Monitoring Program.

Figure 11. - Channel ice seen from 1000 foot altitude.

Figure 12. - Ice sheets beginning to overlap as seen from 1000 foot altitude.

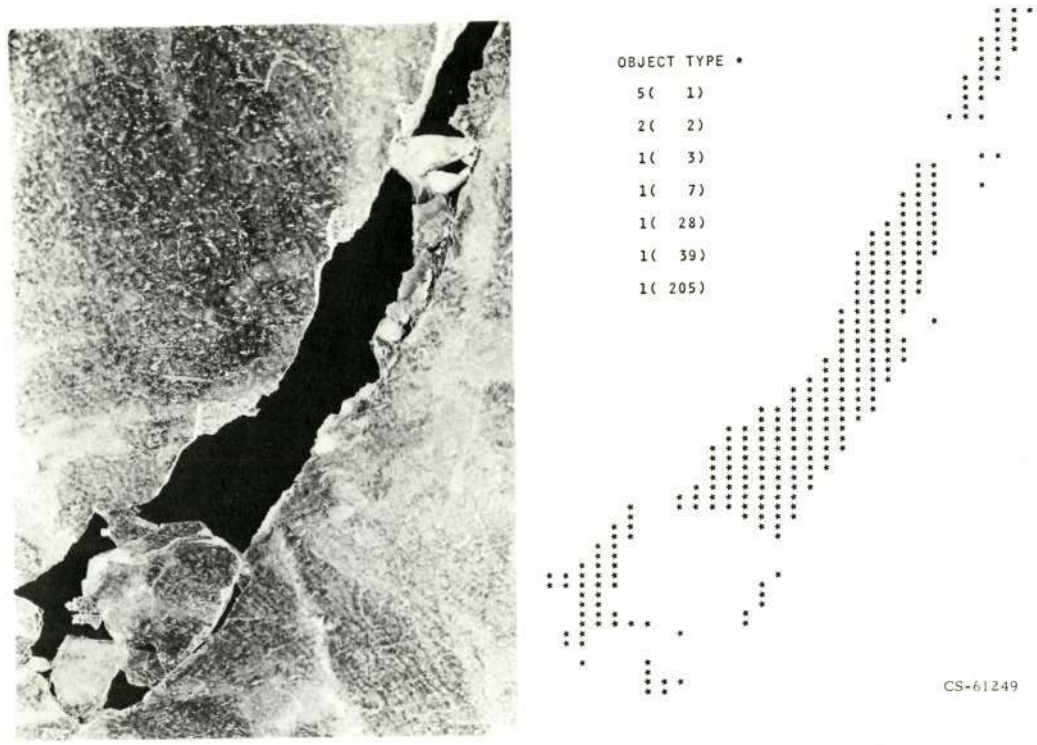

Figure 13. - Photo showing large opening in ice and results of automatic processing of the photo.

Figure 14. - Patterns of broken ice starting to refreeze seen from about 1000 foot altitude.

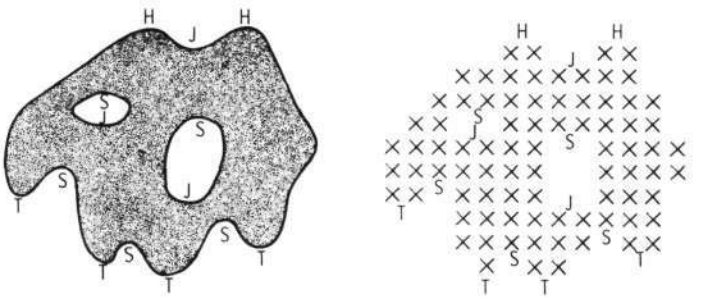

FOR ANY OBJECT:

$$\Sigma H + \Sigma S - \Sigma T - \Sigma J = 0$$

$$\text{NUMBER OF HOLES} = \frac{(\Sigma S + \Sigma J - \Sigma H - \Sigma T + 2)}{2}$$

CS-61790

Figure 15. - Example of computer object counting.

ORGANIZATION FOR GREAT LAKES - ST. LAWRENCE SEAWAY
NAVIGATION SEASON EXTENSION DEMONSTRATION PROGRAM

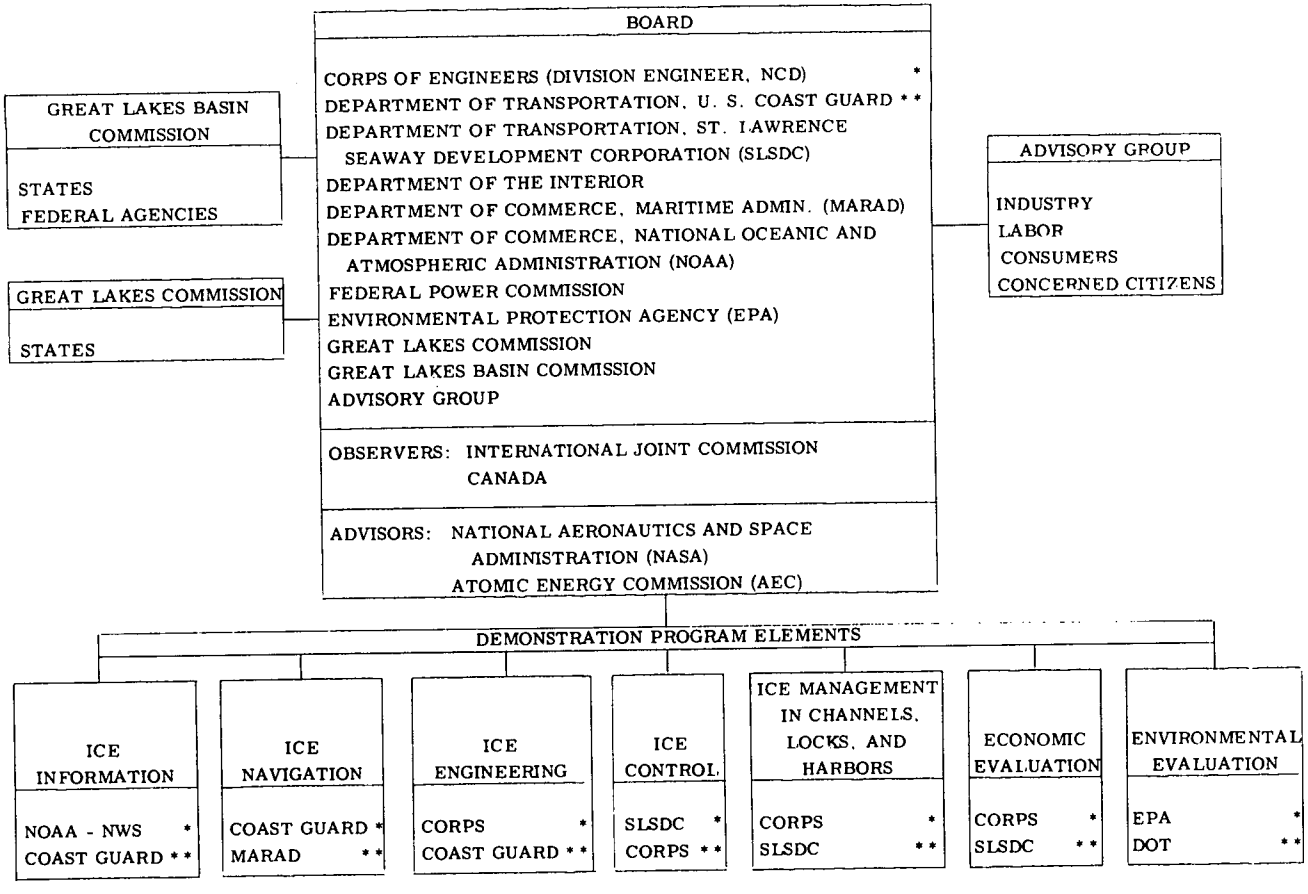

CS-61279

* Lead Agency (Chairman of Work Group)
** Vice-Chairman of Work Group

Figure 16. - Organization of the Federal Ice Board.

160-75-60: MIDWEST/GREAT LAKES APPLICATIONS OF
EARTH OBSERVATIONS SATELLITES

3. AGRICULTURE, FORESTRY, & RANGE - AF-2, 4
PRELIMINARY STUDIES OF CROP DISEASE SPREAD
& STRIP-MINED AREA REHABILITATION FOR
AGRICULTURE

CS-61288

Figure 17. - Additional regional studies in Lewis Program.

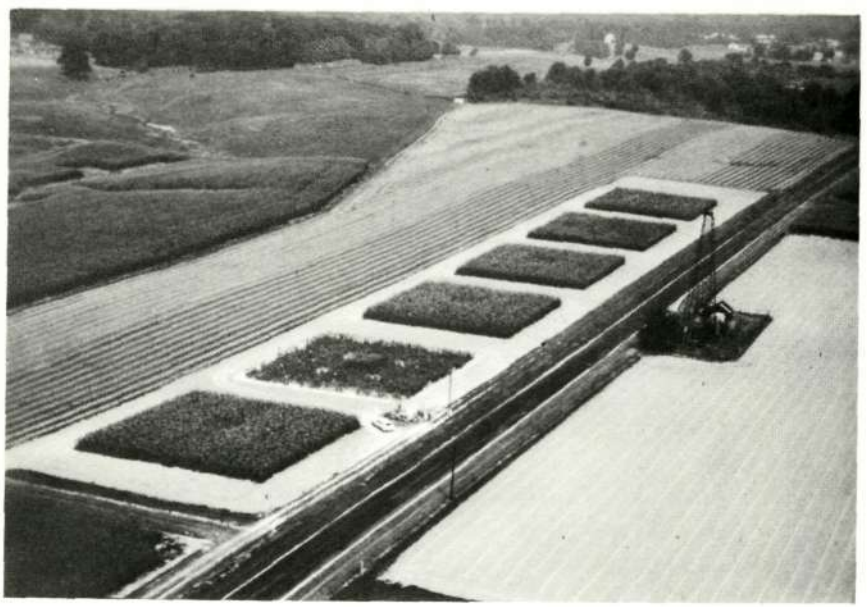

Figure 18. - Aerial photo of test plots of corn at Wooster, Ohio.

Figure 19. - Sample of corn plant infected with Maize Dwarf Mosaic Virus.

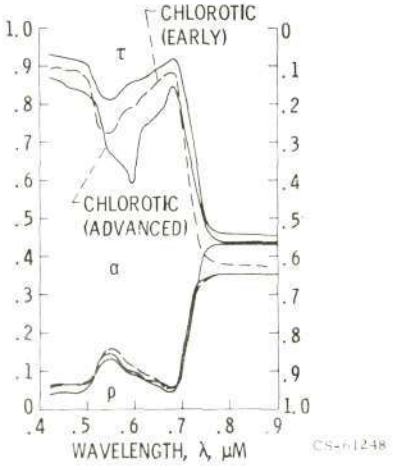

Figure 20. - Optical properties of healthy corn and corn infected with MDMV.

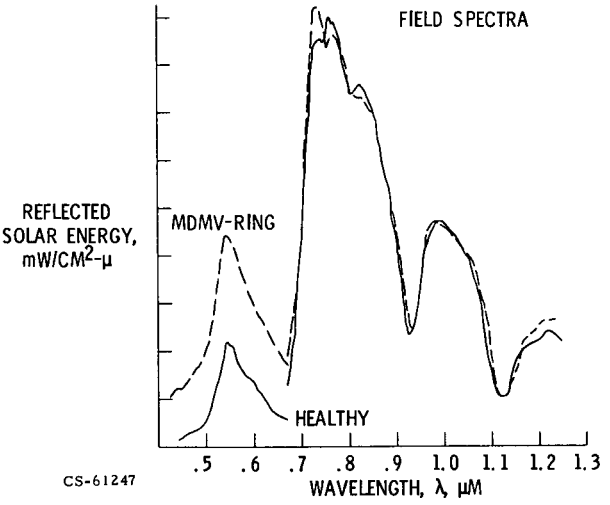

Figure 21. - Field spectra of healthy corn and corn infected with MDMV.

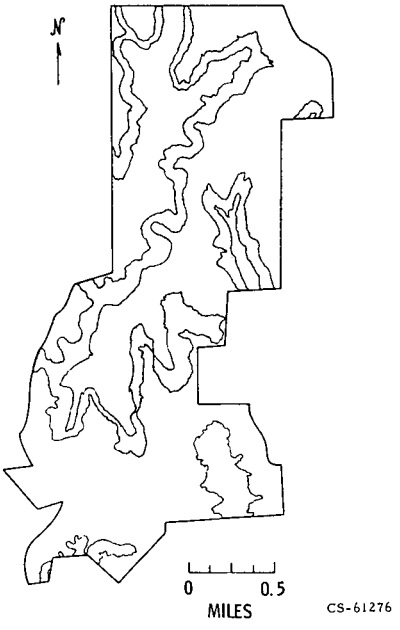

Figure 22. - OARDC test strip mined area in Noble County, Ohio.

Figure 23. - Photograph from 1000 foot altitude of OARDC test strip-mined area in S.E. Ohio.

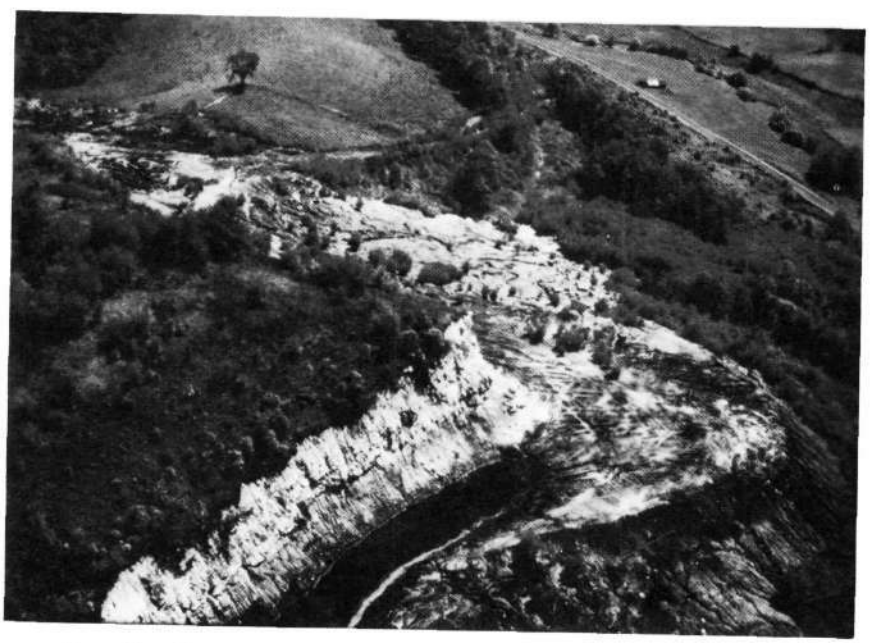

Figure 24. - Close-up aerial photo (500 foot altitude) of strip mined area in S.E. Ohio.

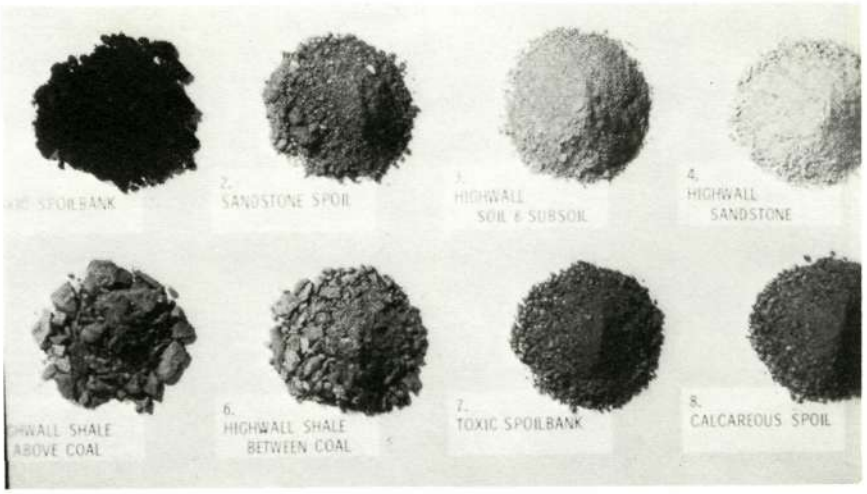

Figure 25. - Soil samples from test-strip-mined area in S.E. Ohio.

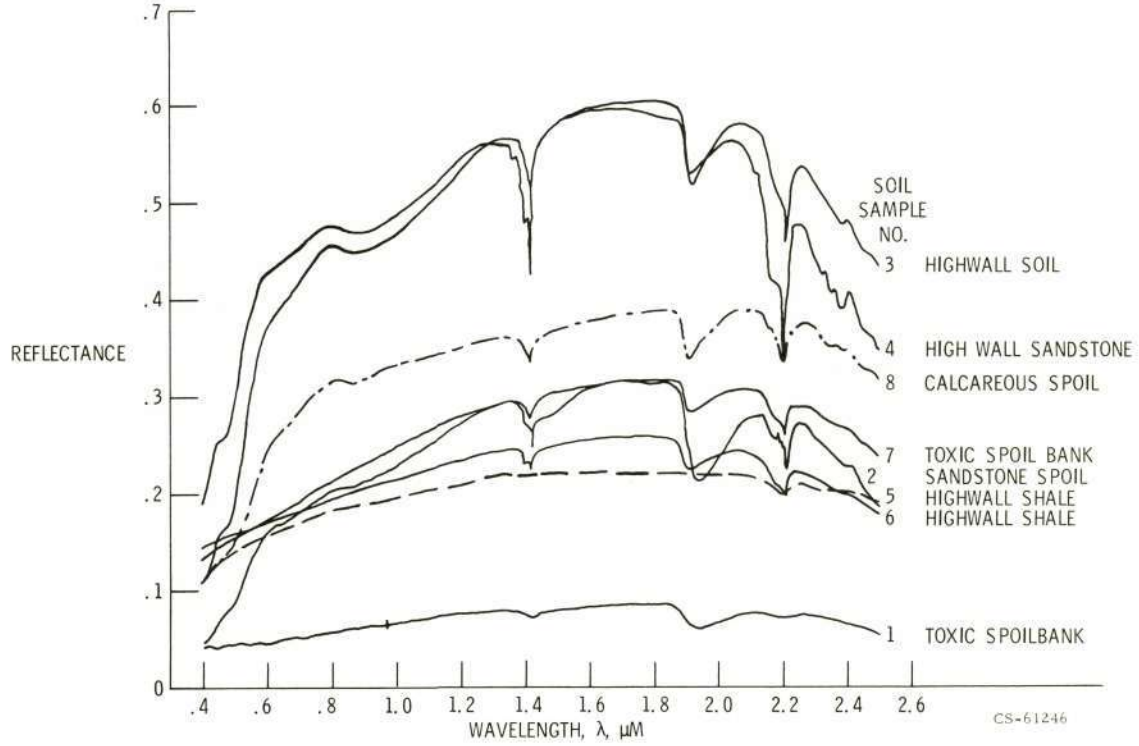

Figure 26. - Laboratory spectra of soil types from test strip mined area in S.E. Ohio.

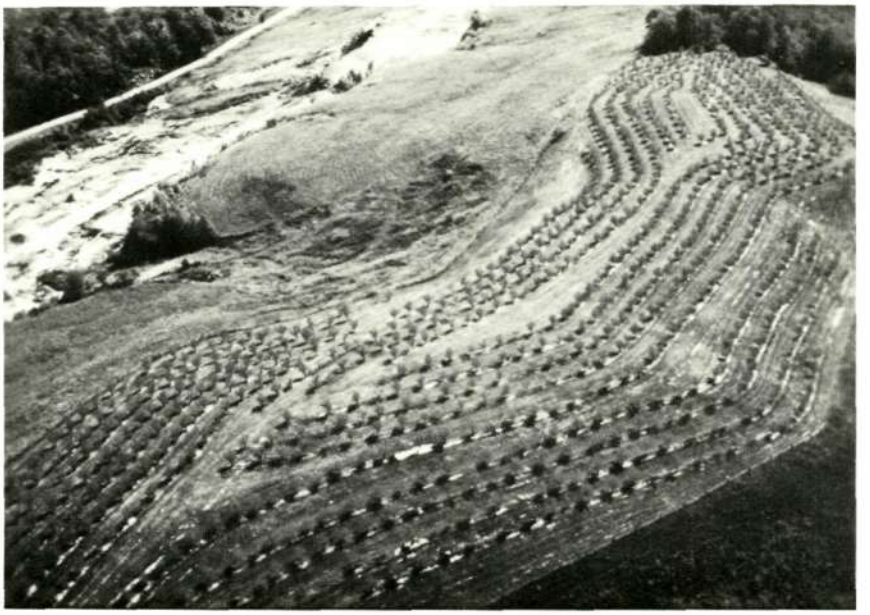

Figure 27. - Efforts at agricultural rehabilitation of test strip mined area in S.E. Ohio.

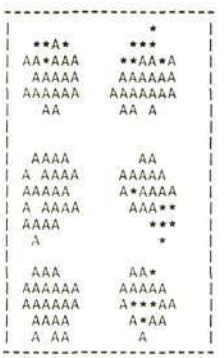

NO.	SIZE	HOLES	PERIM	* TOT	AREA	%	A TOT	AREA	%
1	23	0	24	2	4	17.4	1	19	82.6
2	26	0	28	2	7	26.9	1	19	73.1
3	24	1	34	0	0	0.0	1	24	100.0
4	22	0	24	2	7	31.8	1	15	68.2
5	22	0	24	0	0	0.0	1	22	100.0
6	19	0	22	2	5	26.3	3	14	73.7
	136			8	23	16.9	8	113	83.1

CS-61245

Figure 28. - Computer object counting technique applied to trees in test orchard.

SECTION 17

ENVIRONMENTAL APPLICATIONS ACTIVITY AT MARSHALL SPACE FLIGHT CENTER

by

Charles T. N. Paludan
Environmental Applications Office
Science and Engineering

MSFC has a history of activities in remote sensing. Many of the techniques used in the Saturn vehicles and earlier rockets involved remote detecting instruments, film cameras, television, communication equipment, and aids to data analysis. A number of these activities led to funded SR&T studies and designs. The letter from Dr. Low in November, 1970; the activity at MSFC's Mississippi Test Facility; and the 3rd Annual Earth Resources Program Review - led to a new emphasis. A new office, the Environmental Applications Office, has been established at MSFC to aid the emphasized program.

Our approach might best be summarized by mention of four points: (1) we wish to apply already-developed aerospace techniques to community problems, (2) we have not invented the problems; we have sought out potential users in the community and asked them to define problems, (3) we are applying the extensive in-house capability of our employees, and, (4) since it is a limiting factor, we have sought to apply our broad background in data management to the program.

In the short time I have, I will try to give an overall view of our activities, and to mention a few examples.

An example of SR&T oriented toward payloads for the shuttle, is the shuttle launched manned earth observatory. In this study we will define example experiments and support equipment, evaluate man's role, and develop mission requirements.

MSFC's long time role in meterology had its beginnings in problems of launch vehicles during launch and early phases of flight. This has led to a study of world-wide cloud cover as it affects ERTS and Skylab missions.

Our meterology activity also led to correlation spectroscopy as a technique for determination of atmospheric properties. This in turn led to use of similar techniques for determination of other parameters, such as correlation signatures of wet soils and snow. These parameters become inputs to hydrological models, and new data analysis methods

have resulted. Figure 1 shows a region where we are engaged in remote sensing from an airplane owned by Colorado State University. This is in the Wolf Creek Basin of Colorado -- an area already extensively instrumented for ground truth. This has also led to development of an un-supervised classification method, as reported by Smedes, et al,[1] and shown in Figure 2.

Growing out of earlier Technology Utilization work, MSFC has been engaged in a number of Environmental Applications Demonstration Projects for over a year. Emphasis has been on application of aerospace technology to community needs of Southeastern U. S. (Some of these applications fall in disciplines other than Earth Observations.) This is an incomplete list of some of these projects which are under way at the present time.

EARTH OBSERVATIONS
TYPICAL DEMONSTRATIONS PROJECTS

Hydrological Parameter Determination

Land Use Survey

Agricultural Stress Detection

New Community Site Survey

Pollution Monitoring

Urban Transportation Studies

Urban Environmental Quality

I will attempt to illustrate each of these examples.

One of the best instrumented river basins on earth is the Tennessee Valley, in which MSFC is centrally located. This has made natural several cooperative studies with TVA, University of Alabama in Huntsville, IBM, and others to apply remote sensing techniques to

---

1 Smedes, H. W., Linnerud, J. J. Woolaver, L. B., Su, M. Y., and Jayros, R. R., "Mapping of Terrain by Computer Clustering Techniques Using Multispectral Scanner Data and Using Color Aerial Film." Houston, Fourth Annual Earth Resources Program Review, January 1972.

Figure 1.-Remote Sensing from Aircraft.
(Wolf Creek Basin of Colorado)

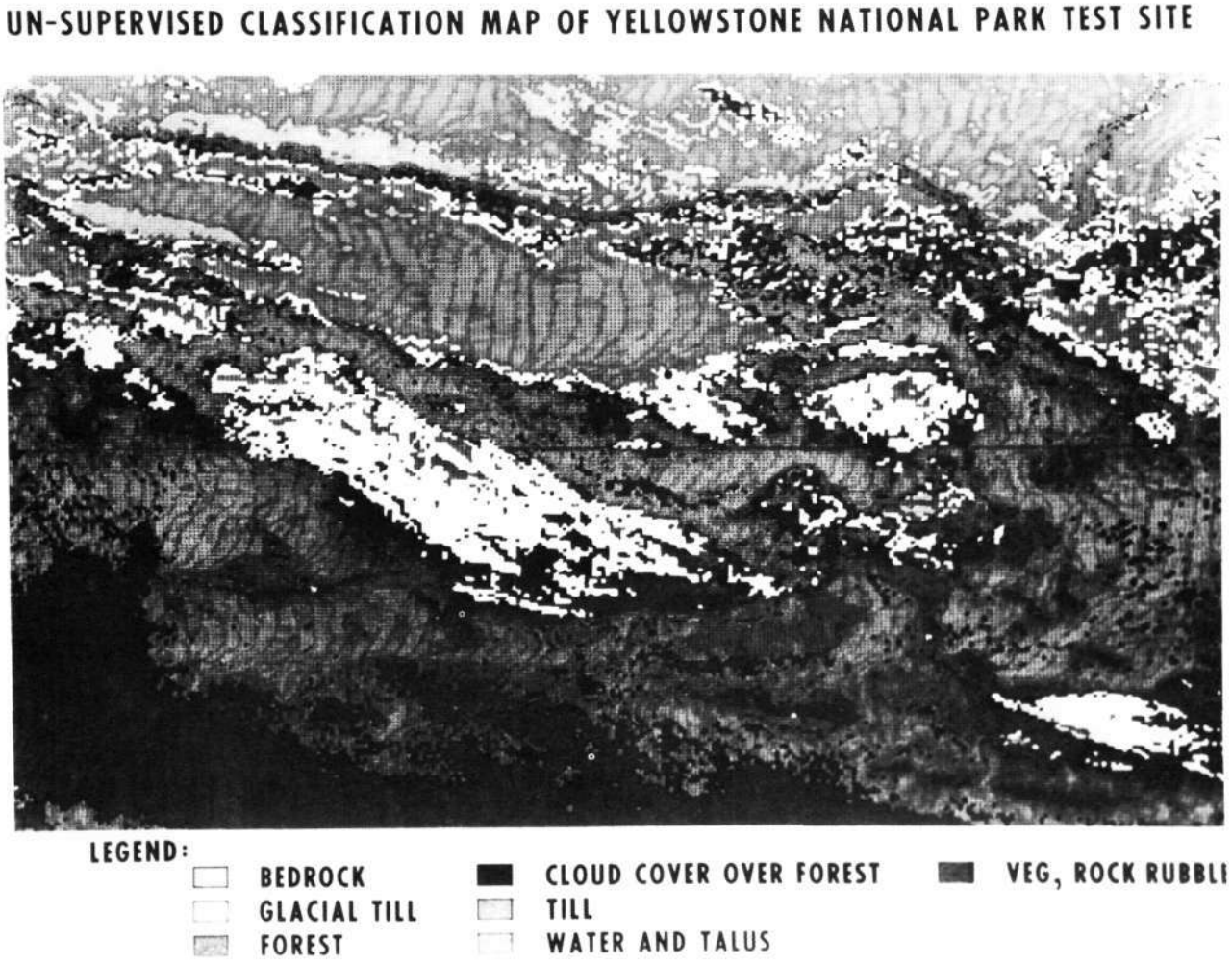

Figure 2.-Example of Un-supervised Classification Method.

determination of hydrological parameters. I have already mentioned a similar activity in Colorado.

Perhaps our most intimate local user/partner is the Top of Alabama Regional Council of Governments -- TARCOG -- five counties in Northeastern Alabama in which MSFC's main campus is located. TARCOG requested help in getting information on the most basic of planning tools - - an up-to-date study of present land-use. We had some prior experience in land-use study by means of multispectral photography, and during the past summer we collected data on the entire 10,000 km^2 area. This is now being converted into maps at the 1:24,000 scale. Ground truth support is provided by Alabama A&M University. Figure 3 shows a sample of this study. The Classification System is that growing out of the NASA/USGS June 1971 Conference.

An outgrowth of the land-use study has been study of an agricultural problem in North Alabama. Chandler Mountain, near Gadsden, has over 1,000 hectares of tomatoes, many of which are affected by nematodes. In Figure 4, the farm shown 1 lost at least $20,000 worth of tomatoes, while 7.B. , operated by a young boy using good practices, thrived.

Senator Sparkman asked us to assist HUD and the Tuskegee Alumni Housing Foundation in the study of a proposed new community site near Birmingham. Two geologists from MSFC have been conducting ground surveys, and multispectral photography has been gathered to aid in planning. Figure 5 is an index mosaic of the area. The area has scenic beauty - many rolling hills. Many of the hills turn out to be mine tailings, however, and the beautiful golden stream shown in Figure 6 is really yellow - a result of industrial pollution upstream of the site.

We are working with TVA to apply some of our Saturn instrumentation and techniques to study of air pollution.

Location of MSFC's Michoud plant in New Orleans has led to cordial relations with the planning people there. They are concerned with urban environmental quality, especially as affected by traffic. The stereo overlap on RB-57 photography results in time-lapse data of the type shown in Figure 7, which can be analysed. The amount of analysis will be large, but we have in-house research in optical processing shown in Figure 8 which is already producing results. Data taken from the Goodyear blimp before last week's Super Bowl is being analysed in this facility now.

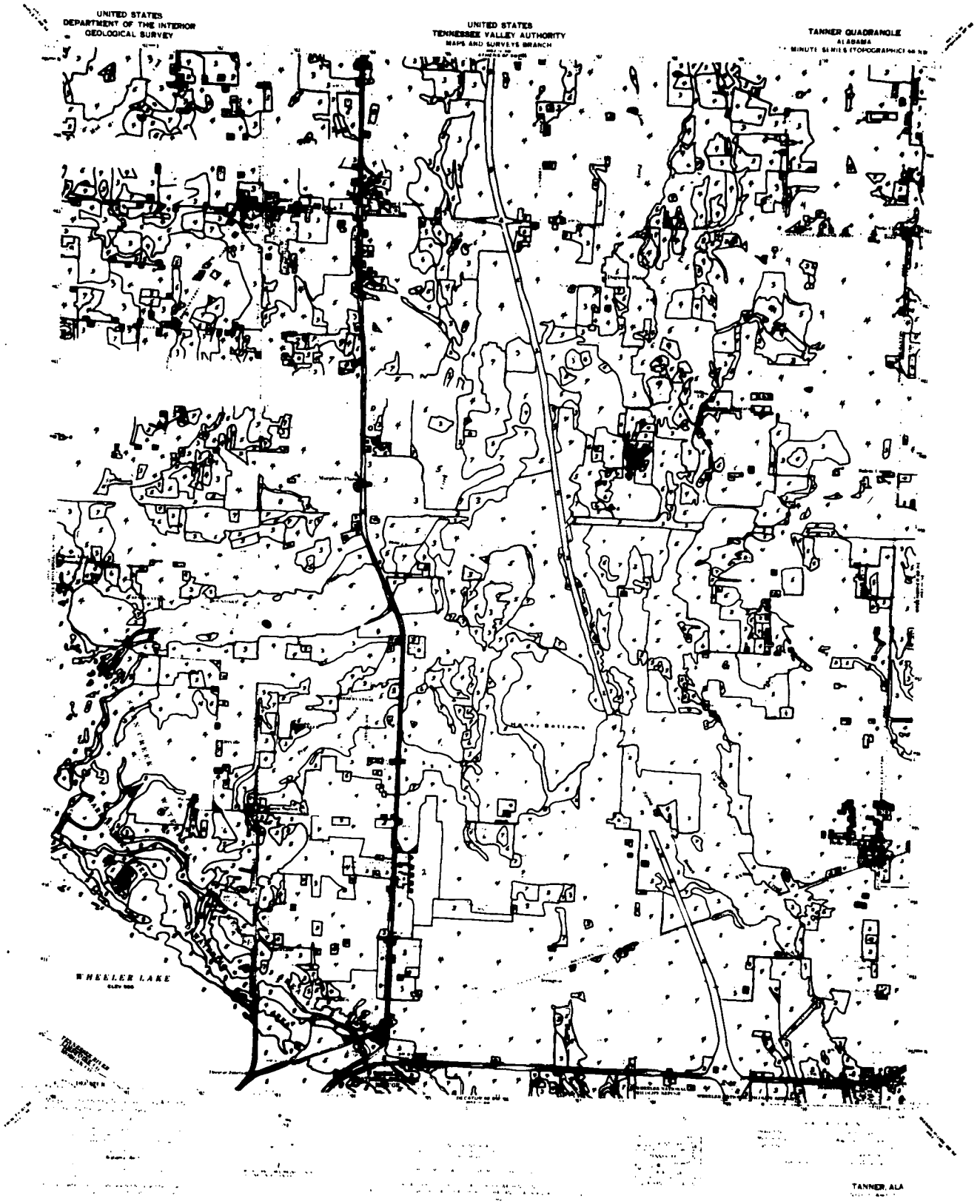

Figure 3.-Example of Land-Use Map

Figure 4.-Good and Bad Farm Practices.(Chandler Mountain)

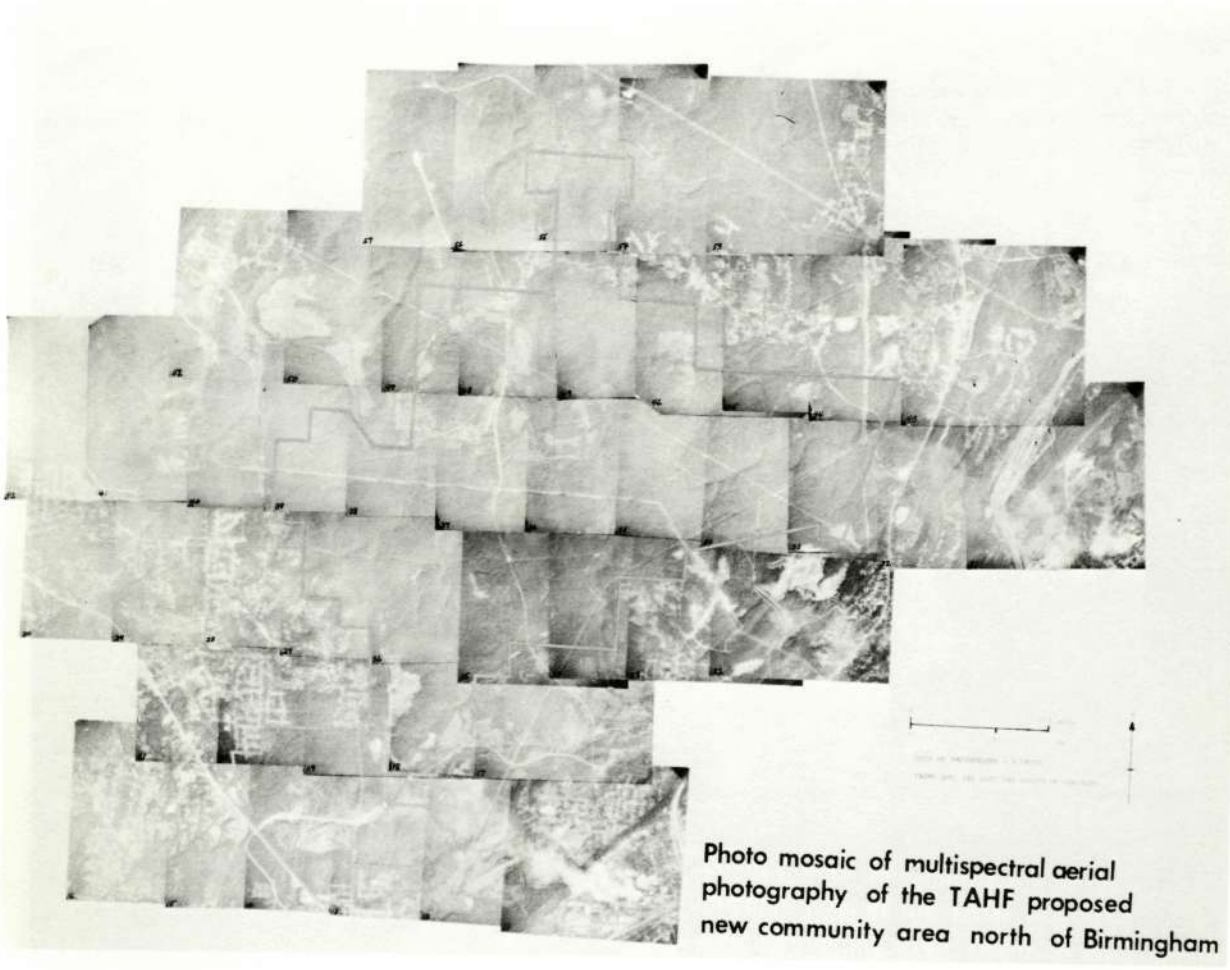

Figure 5.-Photo mosaic of North Birmingham new community site.

Figure 6.-Polluted stream in North Birmingham new community site.

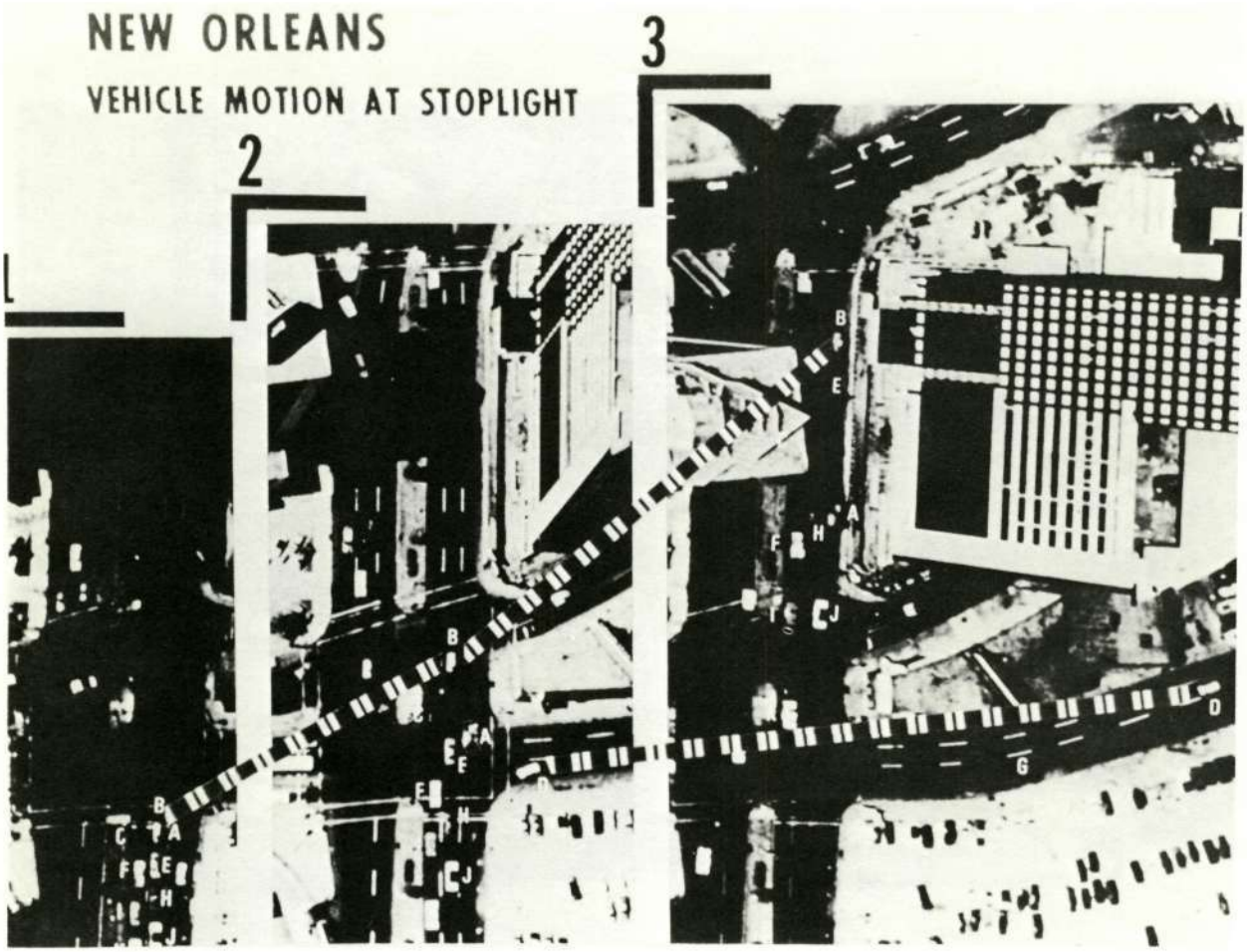

Figure 7.-Vehicle Motion at Stoplight. (New Orleans)

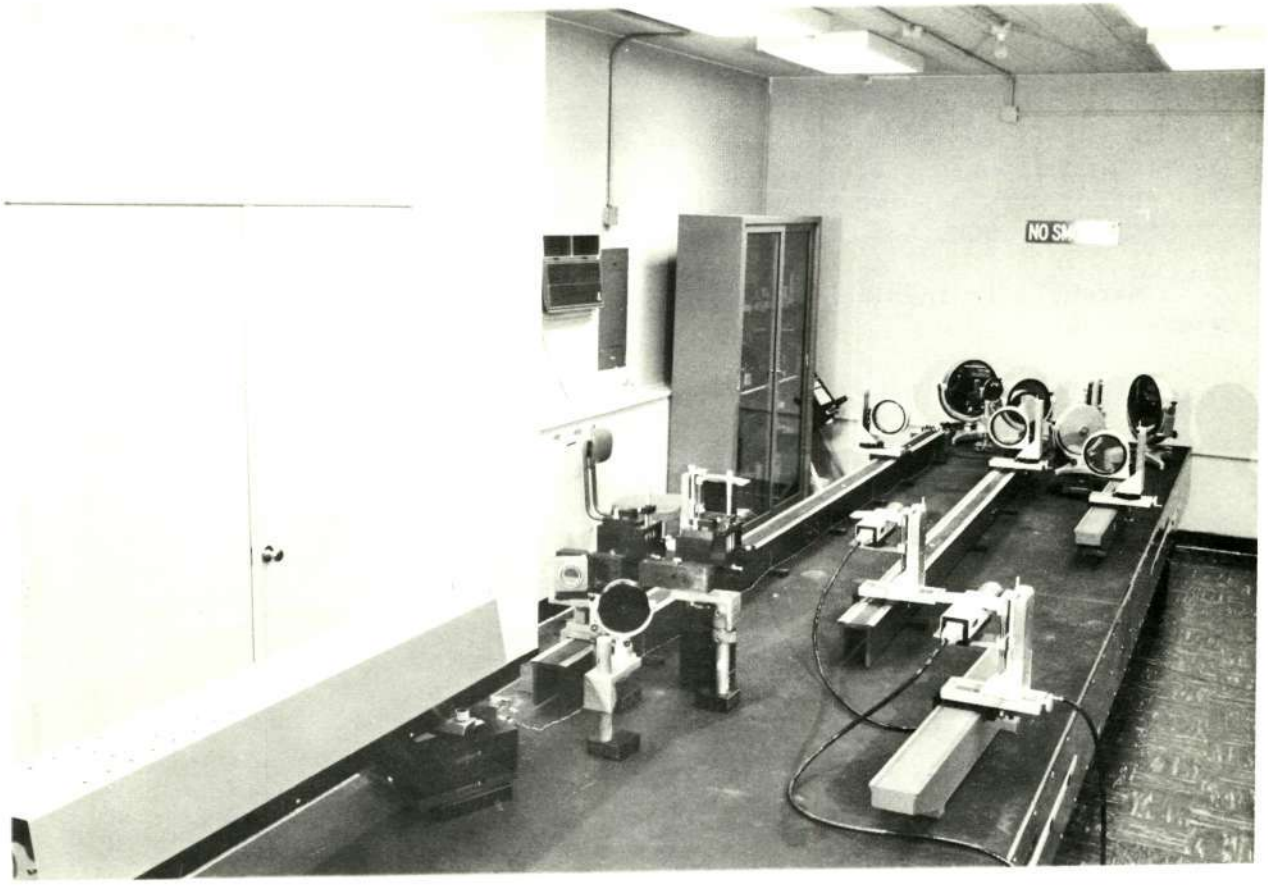

Figure 8.-Photograph of Optical Processor.

We see remote sensing from aircraft as being vital to urban problems, and expect to expand our research in this during the coming year. The City and County of Denver hopes to make remote sensing an important element in their Community Renewal Program. The entire city was imaged on Color IR film in 1969 with the help of MSC, MSFC, DOD, and others.

Marshall is involved in ERTS and Skylab EREP from a number of viewpoints:

1. Co-investigator, State of Alabama ERTS Proposal
2. Data Management Working Group
3. Scientific Monitors for ERTS
4. Data Compression Experiment for EREP
5. Proposal Evaluation Panels
6. User Identification in Southeastern States
7. Information System Studies

Marshall's Mississippi Test Facility is an important part of our involvement. It supports a number of co-located on-site activities by other agencies, and has close ties with users in the region. We consider this facility as a test bed for the long range involvement of NASA in environmental activities with other agencies of federal, state and local governments as well as an excellent model of a regional center for data analysis and dissemination. Regional modeling is a key activity at MTF and among the most interesting long range goals is the development of models of the states of Mississippi, Louisiana and Arkansas. From these models, the total impact on the region can be determined for any proposed project. Such models will be of particular utility to planning groups and to the state legislatures. The information for these models will come from the agencies located at MTF, including the NASA Earth Resources Laboratory.

SECTION 18

N72-29319

EARTH RESOURCES PROGRAMS AT THE LANGLEY RESEARCH CENTER

PART I. ADVANCED APPLICATIONS FLIGHT EXPERIMENTS (AAFE) AND MICROWAVE REMOTE SENSING PROGRAM

by

Robert N. Parker
Langley Research Center
Hampton, Virginia

INTRODUCTION

The earth resources activity at the Langley Research Center is comprised of three basic programs as follows:

1. Advanced Applications Flight Experiments (AAFE)
2. Microwave Remote Sensing Program
3. Coastal-Zone Oceanography Program

The three programs are in various stages of implementation, extending from experimental investigations within both the AAFE program and the microwave remote sensing program, to multidisciplinary studies and planning within the coastal-zone oceanography program. From a "significant results" standpoint, the reporting of the three programs is premature. The purpose of this paper is simply to identify the main thrust of the Langley Research Center activity in earth resources.

The coastal-zone oceanography program is not covered in this paper but is reported in a separate paper by W. E. Bressette. Also, the Langley Research Center air pollution program is not construed as an earth resources sub-discipline and is not reported under this meeting.

AAFE PROGRAM

The AAFE program is an Office of Applications program intended to establish strong candidate experiments for future space application missions involving both manned and automated spacecraft. The program consists of the engineering development and demonstration of promising space applications experiments, beginning with the existence of a

feasible concept from SR&T investigations, and extending to an interface with flight prototype development.

The Langley Research Center provides the implementation and project management of the AAFE program. The program involves Principal Investigators within industry, universities, other Government agencies, and the NASA Centers. Research Engineers within the Langley Research Center are assigned to each experiment during the AAFE development and experiment demonstration. Further support is also given to AAFE through related SR&T efforts within the Center.

Approximately 25 percent of the AAFE program is comprised of experiments within the earth resources discipline. The remaining experiments are distributed among the space applications disciplines of meteorology, communications, earth physics/physical oceanography, and applications technology. The AAFE/earth resources experiments are listed in Table I. The expected completion dates for the AAFE development and the possible missions which are associated with the experiments are also shown. Of the eight experiments identified, three experiments are entering an experiment demonstration phase and will be further identified with respect to the expected experiment performance and flight plans. The three experiments are the Multichannel Ocean Color Sensor (MOCS) experiment, the Composite Radiometer-Scatterometer (RADSCAT) experiment, and the Sea Surface Temperature Microwave Radiometer experiment.

The performance specifications for the Multichannel Ocean Color Sensor (MOCS) experiment are listed in Table II. The experiment consists of spectrometric measurement of ocean surface for mapping distribution, concentration, and type of organic matter. The instrument developed for this measurement is an electronic multispectral line scanner. A slit image is taken, dispersed spectrally, and read out by an image dissector tube. The instrument has two modules to allow experimental trade-offs to be made between spectral and spatial resolution. The high spectral resolution becomes important in data processing techniques such as second derivative information associated with detecting chlorophyll bands from high altitudes.

The atmospheric effects are of particular concern to the MOCS experiment, and an early phase of the development work included investigating an air-sea optical model. In this effort flight tests with a visible spectrometer, together with boat-gathered ground truth measurements, were made by the Principal Investigator during July, August, September, and October 1971. Spectral reflectance curves were obtained of various water masses overflown for altitudes from 500 to 25,000 ft. On the basis of these data, an extrapolation to the top of the atmosphere was made to indicate the expected spectral radiance obtained from ocean waters from satellite altitude. Results indicate the magnitude of the contrast to be expected from 400 to 700 nanometers and show that the

water color signatures should be measurable from satellite altitude. The results are documented in a task report, dated November 15, 1971, to contract NAS1-10908.

An engineering model of the MOCS instrument is under construction and flight tests will be performed in June 1972. Assuming a successful checkout of the instrument, the MOCS will be flown on the NASA Convair 990 in June together with a filter-wedge spectrometer from Hovis of Goddard Space Flight Center, and a differential radiometer from Arvesen of Ames Research Center. The joint flight, organized by Goddard Space Flight Center, will seek to determine the relative merits of the three instrument concepts. There is strong interest in an ocean color experiment on future missions such as the Small Applications Technology Satellite (SATS) and the Earth Observations Satellite (EOS).

The performance specifications for the RADSCAT experiment are listed in Table III. The experiment consists of inferring wind speed over the ocean surface through measurement and analysis of radar return signal and radiometer antenna brightness temperature. The RADSCAT instrument operates alternately in an active scatterometer and a passive radiometer mode. In the scatterometer mode, an electromagnetic pulse is transmitted to the ocean's surface where it is scattered by the small scale roughness element or capillary wave portion of the ocean spectrum. The amplitude of the return pulse is a function of the radar frequency, EM wave polarization, viewing angle, and the degree of surface roughness (water waves on the order of one inch length). Since the capillary water waves are in near equilibrium with the local surface wind, the amplitude of the backscattered radar pulse can therefore be used to infer wind speed. The radiometer mode is used to assess the possible contributions of clouds, rain, and surface foam to the overall measurement and analysis.

The multifrequency AAFE RADSCAT will be flown on an NOAA C-130 aircraft during April 1972, followed by flights on the NASA-MSC C-130 aircraft beginning in late June 1972. Both flights will be made over instrumented test sites off the Virginia capes. The antenna will be slewed aft in an along track mode in six steps between nadir and 60° viewing angle. Both radiometer and scatterometer signatures will be correlated with environmental conditions measured by in situ instrumentation. The earlier flights on the NOAA C-130 aircraft are intended to explore the higher wind fields which occur in the spring, prior to the schedule availability of the NASA-MSC C-130 aircraft. Calibration of the RADSCAT will be done at the Wallops Station during March 1972. The instrument will be mounted on a ground pedestal and the scatterometer will be calibrated against test spheres suspended aloft. The radiometer will be calibrated against Hohlraum temperatures and other techniques such as moon tracking, well defined stellar radio sources, and zenith measurement variations with time.

The AAFE RADSCAT instrument will be placed in the inventory of instruments available on the NASA-MSC C-130 aircraft. Future uses of the instrument would include underflight support to the Skylab-S193 experiment.

The performance specifications for the Sea Surface Temperature Microwave Radiometer experiment are listed in Table IV. The experiment consists of a single frequency (S-band) radiometric measurement of brightness temperature for deriving sea surface temperature maps on a global basis.

The relationships between brightness temperature and the effects of environmental parameters such as surface roughness and foaming, sea water salinity, and atmospheric conditions were of particular concern in this AAFE development and were explored by the Principal Investigator in a detailed investigation prior to the design and construction of the radiometer. A summary of the corrections required to the apparent temperature and the uncertainty in deriving the sea surface molecular temperature, as influenced by salinity, roughness, foaming, atmospheric absorption, clouds, and extraterrestrial background is shown in Table V. This information is published in an NASA Contractor Report, NASA CR 1960, dated February 1972.

The microwave radiometer will be test flown off the Virginia capes on an NASA C-54 aircraft operated by Wallops Station beginning in April 1972. Sea truth support will be co-shared with the RADSCAT experiment.

A survey concerning the experimental use of the microwave radiometer is now being conducted among the potential users. First consideration will be given to the continued use of the instrument installed on the NASA-Wallops C-54 aircraft.

MICROWAVE REMOTE SENSING PROGRAM

The microwave remote sensing program is a Supporting Research and Technology effort within the Langley Research Center. A specific goal of the program is to develop precision microwave sensors for day/night, all weather earth observations from satellite and/or aircraft of ocean temperature, ocean roughness, and salinity. The program also provides additional in-house support to the AAFE program.

The microwave remote sensing program involves a range of investigations extending from laboratory and theoretical analysis to systems level testing and evaluation. Descriptions of the investigations follow.

A wave tank has been constructed and will be used to isolate and independently study parameters such as wave spectrum, salinity,

temperature, and surface composition, all of which influence RF scattering and emission from water. The wave tank will also be used as a test bed to develop and calibrate sea truth instrumentation such as measurement of capillary waves.

Rigid surfaces, having a characteristic roughness which can be mathematically modeled, have been constructed for in-house experimental studies of RF scattering from rough surfaces. This technique will allow correlations between analytical and experimental results concerning RF scattering theory.

Advanced radiometer components, such as image line waveguides and associated computer design programs, are being developed to reduce internal losses and waveguide size for application in high precision radiometers. Low noise radiometer antennas, which exhibit maximum beam efficiency and minimum insertion loss, are also being developed. One such design, a corrugated horn, is also being investigated as an unfurlable concept for satellite application at S-band frequencies.

At the systems level, measurements of radiometric signatures are currently being made with a four frequency group of microwave radiometers located on a railway bridge at Buzzard's Bay in Massachusetts. Measurements are being made at .75 GHz, 1.4 GHz, 4.0 GHz, and 7.5 GHz, in conjunction with supporting sea truth and meteorological data. The measurements are taken at both vertical and horizontal polarizations and at a variable view angle from -30° through 160°. A photograph of the antennas mounted on the Buzzard's Bay bridge is shown in Figure 1. The antennas are shown in the upward-looking, stowed position.

The Buzzard's Bay radiometer investigations are intended to establish the relationship between observed radiometric signatures and ocean surface condition parameters. Information will be gathered through June 1972, a data bank established, and the data statistically analyzed. A recent computer plot of uncalibrated data taken with the Buzzard's Bay 1.4 GHz radiometer is shown in Figure 2. The increase in brightness temperature near nadir is due to reflections from the bridge.

CONCLUDING REMARKS

The earth resources program at the Langley Research Center continues as a modest effort, strongly oceanographic oriented, and characterized as entering a measurement and data analysis phase. Contributions from these SR&T and AAFE efforts, in terms of systems design, interpretive information, and confidence in specific remote sensing techniques and associated experiments, are anticipated during the current year.

TABLE I.- AAFE/EARTH RESOURCES EXPERIMENTS

Experiment Title and Investigator	Expected Completion	Possible Mission
. Fast Response, Hybrid Multispectral Processor (Kreigler; Univ. of Michigan)	Feb 74	Ground Equip.
. Earth Observation Scanning Spectro-Radiometer (Goldberg; NASA-GSFC)	Dec 74	EOS-B
. Earth Surface Mapping, Microwave Hologram Radar (Zelenka; Univ. of Michigan)	Nov 73	EOS-C
. Luminescense Detection, Fraunhofer Line Discriminator (Hemphill; USGS)	July 73	SATS
. Multichannel Ocean Color Sensor (MOCS) (White; TRW)	Dec 72	SATS
. Composite Radiometer-Scatterometer (RADSCAT) (Pierson; NYU)(Moore; U. of Kansas)(Tomiyasu; GE)	Oct 72	Skylab Support
. Sea Surface Temperature, Microwave Radiometer (Hidy; North American Rockwell)	May 72	EOS-C
. Sea-Ice Mapping Radiometer (Gloersen; NASA-GSFC)	Dec 72	EOS-A

TABLE II.- PERFORMANCE SPECIFICATIONS

MULTICHANNEL OCEAN COLOR SENSOR (MOCS)

	SPACECRAFT	AIRCRAFT
ALTITUDE	500 NM	15,000 Ft.
CROSS-TRACK SWATH WIDTH	150 NM	4,500 Ft.
ANGULAR FIELD OF VIEW	17.1°	17.1°
SPECTRAL RANGE	400-700 Nanometers	400-700 Nanometers
SPECTRAL RESOLUTION:		
(a) Modular Package MP-5	5 Nanometers	5 Nanometers
(b) Modular Package MP-15	15 Nanometers	15 Nanometers
GROUND RESOLUTION		
(a) Modular Package MP-5	3 x 1 NM	90 x 30 Ft.
(b) Modular Package MP-15	1 x 2 NM	30 x 60 Ft.
S/N (500 NANOMETERS, SCENE IRRADIANCE 1400 W/M^2-MICRON)	110	110
WEIGHT	15 lb.	20 lb.
POWER CONSUMPTION	7.5 Watts, 28 VDC	7.5 Watts, 28 VDC

TABLE III.- PERFORMANCE SPECIFICATIONS

COMPOSITE RADIOMETER SCATTEROMETER (RADSCAT)

FREQUENCY: 9.3 GHz 13.9 GHz

POLARIZATIONS: V V; V H
H H; H V

ANTENNA: 44-1/2" Dia. (S 193 Design)
ANTENNA BEAMWIDTH: 1.5° (Half Power)
ANTENNA SCAN: 0° (Nadir) to 60°, Six Steps

SCATTEROMETER TRANS. POWER: 1 Watt Peak
SCATTEROMETER MEASUREMENT RANGE: +10 DB to -35 DB
SCATTEROMETER MEASUREMENT ACCURACY: ± 1 DB (RMS Error)
SCATTEROMETER OPERATING ALTITUDES: 2 K Ft.; 10 K Ft.; 18 K Ft.

RADIOMETER, BRIGHTNESS TEMP. RESOLUTION: ± 1° K
RADIOMETER OPERATING ALTITUDES: Any

WT. (ANTENNA, GIMBAL, RF SUBSYSTEM): 300 Lbs.

TABLE IV.- PERFORMANCE SPECIFICATIONS

SEA SURFACE TEMPERATURE MICROWAVE RADIOMETER

FREQUENCY: 2.65 GHz
BANDWIDTH: 100 MHz

POLARIZATIONS: Circular; V; H

ANTENNA: Multimode Horn, Square Aperture
(35.5 cm Side, Limited by C-54 Installation)

ANTENNA BEAMWIDTH: 20.5° (Half Power)

TEMPERATURE ACCURACY:

Molecular Absolute	$\pm$ 1° K (after corrections)
Brightness Absolute	$\pm$ .3° K
Resolution	$\pm$ .1° K

RADIOMETER TYPE: Modified Dicke With Precision Nulling Feedback

POWER: 20 Watts
WT. (WITHOUT ANTENNA): 30 Lbs.

TABLE V.- SEA SURFACE TEMPERATURE MICROWAVE RADIOMETER

Contributions to Apparent Temperature and Corrections to be Applied

Effect	Contribution		Remarks
	Correction Required	Uncertainty in Molecular Temperature	
Salinity	$\Delta T_B = +1.0°$	$\pm$ 0.3°K	Correction derived from known spatial and temporal salinity variations in sea.
Roughness, Foaming	$\Delta T_B = \sim 3°K$	$\pm$ 3°K	Corrections derived from knowledge of sea state and wind conditions can reduce T_B uncertainty to $\sim 1°K$.
Atmospheric Absorption	+2.4°K	$\pm$ 0.5°K	Contribution due mainly to oxygen absorption.
Extraterrestrial Background	+3.0°K	$\pm$ 0.3°K	Excludes strong isolated radio sources near galactic center.
Clouds	$\pm$ 0.5°K*	$\pm$ 0.1°K	Corrections derived from extent and thickness of cloud cover.

*For cloud layer 1 km thick containing 1 gm liquid water per cubic meter.

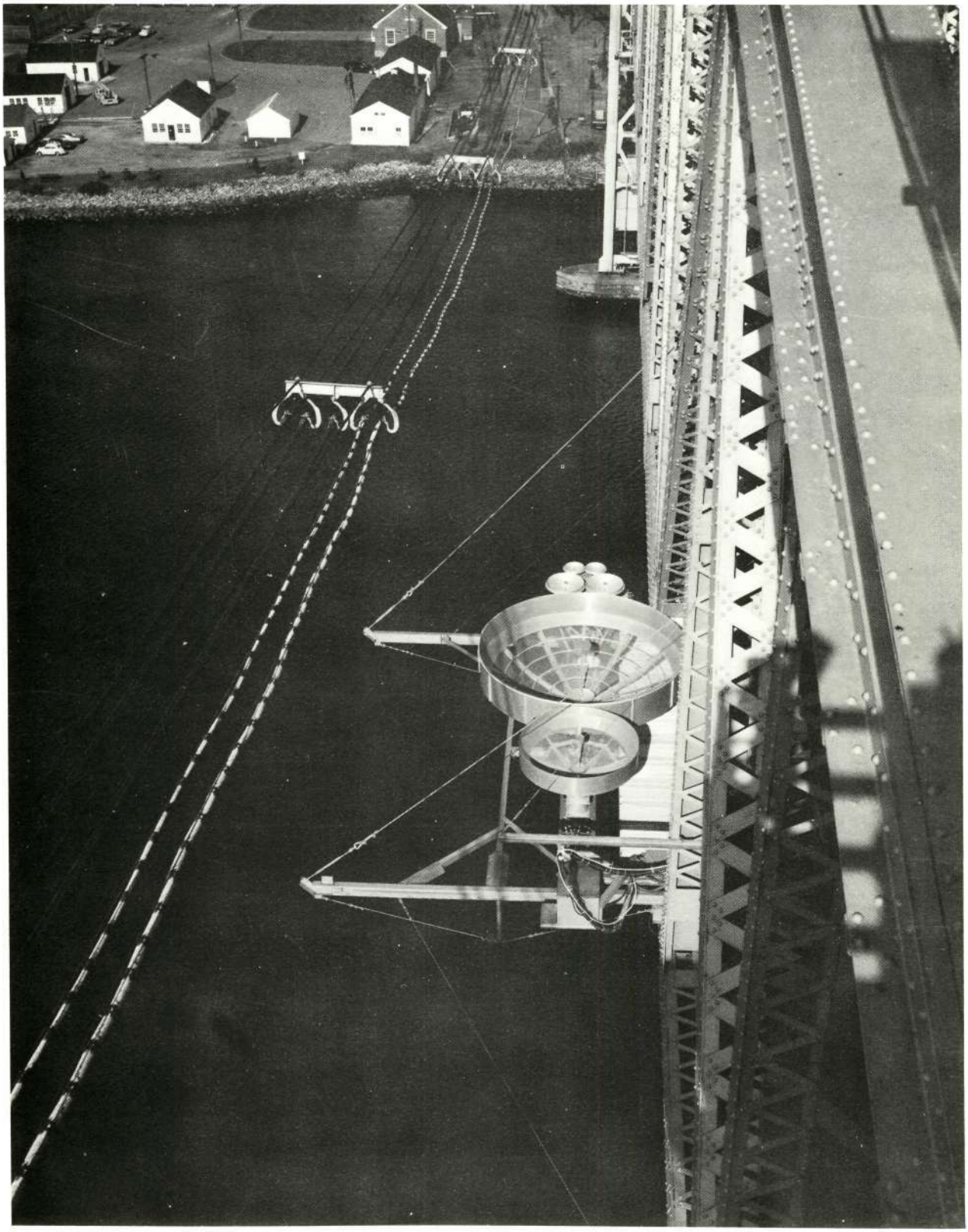

Figure 1.- Microwave radiometers located on the Buzzard's Bay Bridge in Massachusetts.

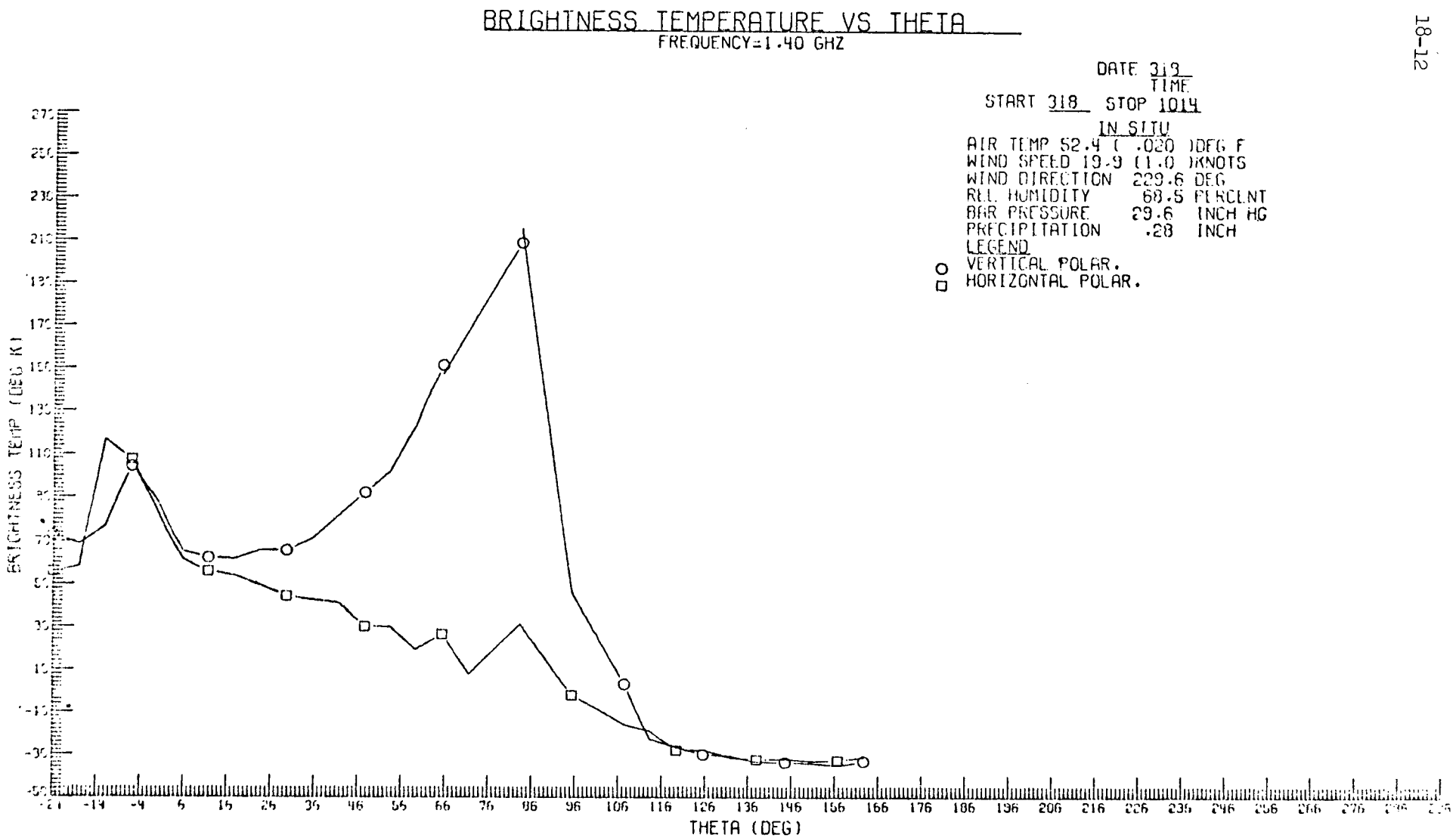

Figure 2.- Computer plot of uncalibrated data taken with the Buzzard's Bay 1.4 GHz radiometer.

EARTH RESOURCES PROGRAMS AT THE LANGLEY RESEARCH CENTER

PART II. COASTAL ZONE OCEANOGRAPHY PROGRAM

by

Walter E. Bressette
Langley Research Center
Hampton, Virginia

INTRODUCTION

One area of emphasis within the Application Program at Langley is on the coastal zone. Forty-five percent of the population of the United States lives in coastal counties, and this population is growing at twice the rate of the population of the country as a whole. As a result, there are serious pollution and other ecological problems in the coastal zones, and these problems are destined to get worse.

Most of Langley's experimental work will be carried out along the East Coast because, with both Langley and Wallops located there, the logistics will be minimized, and because most of the important coastal zone problems can be worked in this region.

Discussion

Figure 1 shows the activity in Langley's coastal zone oceanography program as a function of time separated into two groups; studies and experiments. The development of this program began with a Small Applications Technology Satellite Phase A study along with an Earth Resources Technology Satellite E&F, later to be called the Earth Observation Satellite A&B study.

The second activity was a coastal zone study to identify the environmental problems, establish the data needs, and recommend the spacecraft instrumentation to satisfy these needs.

Each summer for the past four years, we have had in cooperation with the American Society for Engineering Education, a summer study. Last summer, 23 participants, representing 13 academic disciplines, from 19 different universities, investigated problems in water quality management using the James River as a case study. The title of their report is "Clean Water: Affluence, Influence, Effluents - A Design for Water Quality Management." A similar study on the subject of Earth Resources Satellites was performed in 1969. Also, last year a NASA-sponsored conference on Remote Measurements of Pollution was held in

Norfolk, Virginia with Langley people heavily involved. The conference addressed the question of remote measurement of air, water, and land pollution. It is expected that the Remote Measurements of Pollution (RMOP) report will be published in January 1972.

The final two study items are internal NASA efforts where we had three working members on the Earth Observation Satellite Mission Review Group, and we are continuing to develop a coastal zone oceanographic experiment in the framework of the SATS concept.

In the experiments area, we did some early work with the then named Bureau of Commercial Fisheries and some balloon photography out of Wallops, but it was not until we had completed these above studies that we were able to develop and get underway some experiments in coastal zone oceanography. These experiments, which I will detail for you later, in every case were developed and are being undertaken by teams composed of both Langley personnel and people from neighboring institutions and agencies who have interest or responsibility in solving environmental problems in the coastal zone. Figure 2 lists these partners.

Wallops, who has been a long time partner of Langley in the areas of instrumentation and experimental performance, has been working in the coastal zone for some time. The Virginia Institute of Marine Science (VIMS) and Old Dominion University (ODU) are extremely important because they have people who are experts as marine scientists. VIMS is a unique institution because, besides being an educational and research institution, it has responsibilities for advising the Governor and State Legislature on marine matters. The Army Corps of Engineers with major responsibilities in marine matters is presently discussing plans for a joint program with us.

With the help of figure 3, I would like to trace our approach to the development of the program. Beginning with the following areas of concern: Pollution, Fisheries, Hazards, and Cartography, we performed contractor, in-house, and the previously described conference studies to identify the problems in various areas and established the data requirements.

For the contractor studies, we let four contracts to assure that many segments of the coastal zone would be represented. VIMS is a state institution with managerial responsibility; ODU has a research interest in the coastal zone; TRW is a large aerospace corporation; while Ocean Data System, Inc. represented the commercial interests. Although the approach was different in each study, the results were very much in agreement.

The type of problems that were identified in the area of pollution, for example, are shown in figure 4. These are as follows:
Is there pollution?
What kind is it?

What are its effects?
Will the environment accept it?
Where should industry locate?
How can pollution laws be enforced?
What can be done?

With these kinds of problems in mind, the study teams then established various data needs. In the center of figure 5 are shown the ten most relevant data needs that were established. It was from these data needs that our program in Satellite Applications, Estuaries, Continental Shelf, and Environmental Modeling evolved.

In the Satellite Applications area, we first identified the remote sensing requirements that would be needed to satisfy the data needs. Figure 6 is a chart taken from the Remote Measurements of Pollution Conference that lists the ten (10) major water pollutant types and the remote sensing requirements. For each instrumentation parameter, an optimum value and an acceptable value (in parentheses) is given. The acceptable spatial resolution value for chemical and toxic wastes, for instance, allows one to detect the pollutant and perhaps classify it. But in order to locate the source of the pollutant, 10-meter resolution will be required. With respect to temporal resolution, a 10-day viewing interval will yield gross data on thermal effluents; but to assess the dynamics of the dispersion process, a 2-hour viewing interval is desired. For oil pollution, a large field of view is desired in order to cover the entire phenomenon. However, for viewing the source of the spill and during the immediate period following the spill, a narrow (20 x 20 Km) field of view is acceptable.

A multispectral imaging concept that we believe could meet these varying requirements is shown in figure 7. The basic idea of this concept is to provide a high resolution - narrow field of view and a low resolution - wide field of view system on the same spacecraft, both of which have off-nadir pointing capability.

In our next program activity area, as shown in figure 8, that of Environmental Quality of Estuaries, a number of efforts are underway and a couple under discussion. The first of these, suspended sediment and chlorophyll activities in the lower Chesapeake Bay, is an approved ERTS-A experiment with Old Dominion University as a partner.

Figure 9 is an aerial view of one of the eight planned test sites where surface and sub-surface measurements will be made and analyzed by ODU, and correlated with aircraft and satellite imagery using Langley computers. The site will be located along the James River Bridge where the river span of nearly 5 miles will result in approximately 80 resolution elements from ERTS data.

The second activity in figure 8, volatile organics in the environment, is concerned with the exchange rates of volatile, synthetic, organic compounds, as depicted in figure 10, from the atmosphere to the water, to the organisms, the quantity of which are all unknown. Quantitatively, they are measured in fractions of a part per billion. Langley has developed a computerized, microwave spectrometer, currently being used to establish standard spectra of some of these compounds. Working together with VIMS, the most promising method of sample collection from both the atmosphere and the water will be established. Some quantitative results are expected within a year.

The effects of oil compounds on plant and animal life in the coastal estuaries, item 3, figure 8, are not understood. VIMS received a request for a proposal from the Environmental Protection Agency to determine the effects of spilled Bunker C in the marine environment, and VIMS and Langley scientists developed a joint program. Using the expertise of both institutions, major components of Bunker C will be traced through the ecosystem to measure residence times, modes of transport, concentrating mechanisms, and toxicity on plant and animal life. Mini-ecosystems, constructed in a local marsh, will be employed in this research. The proposed site for the mini-ecosystems is outlined on the map in figure 11. The populated area on the left is Williamsburg, Virginia, and the body of water at the top right is the York River.

Activity number 4, figure 8, Wetland survey for boundaries and remote sensing key for vegetation, concerns itself with the ownership and boundaries of the wetlands which in many areas of Virginia are unclear. The Governor's Council for Environmental Quality has directed VIMS to survey Virginia wetlands and to establish a legal definition of wetland boundaries for pending legislation. VIMS has been working with Langley to map wetlands from recent aerial photographs. The boundaries of the wetlands may be more adequately described by the boundaries of specific vegetation species, rather than the interface between open water and marsh, or even a prescribed mean water level. It is our belief that all four of the discrimination signatures shown in figure 12 must be employed to identify wetland vegetation remotely. To identify the shape and texture of various species will require higher resolution than usually obtained from aircraft and spacecraft photography. A goal of our investigation is to define the minimum spatial resolution required in terms of the variables listed in figure 12. Figure 13 is an aerial photo with a spatial resolution of about 1/2 meter. The texture, and some shapes, are evident. The area inside the red block is shown in figure 14. Now the resolution is down to about 1/2 centimeter and may be sufficient to determine shapes of different vegetation. Photographs like these last two will be used to relate shape and texture to various species. The relative tone and color of lower resolution pictures will then be used to relate the vegetation in this small area to other areas of like vegetation.

For the last two items in figure 8, the Coastal Engineering Research Center of the United States Army Corps of Engineers has submitted an ERTS-A proposal to study the changes in the Barrier Islands of the North Carolina coast using space imagery. Recently Goddard asked the Corps to monitor a CARETS (Central Atlantic Region Ecological Test Site - USGS) package of eight ERTS-A experiments in the vicinity of the Chesapeake Bay. The Corps has asked Langley for cooperative scientific support in both of these areas, as well as some help in instrumentation problems. Further discussions are planned.

The final activity is a cooperative effort with VIMS in the Continental shelf area. The objective of this activity is to understand the shelf waters sufficiently well so that forecasts or predictions can be made of conditions on the shelf. Let me explain with the help of figure 15 some of the reasons for such a predictive capability.

VIMS has identified the seven problems depicted in figure 15 as major ones that will require some kind of state action, including additional legislation, in the next ten years. As an example, if ocean dumping into the shelf waters is required, are there preferred locations for such activities which will minimize any unwanted effects? The area of the Continental Shelf under consideration for this program is shown in figure 16. It extends from Cape May, New Jersey, to Cape Hatteras, North Carolina, and seaward to beyond the 100-fathom line, an accepted definition of the edge of the shelf. Also shown in figure 16 is the general surface circulation that one expects in this area. The circulation pattern is complex and has both large scale and small scale features. The area is not strictly Virginia coastal waters. However, the concern is that major inputs to this system not be overlooked. For example, the concern is with the input of the Delaware Bay as well as the Chesapeake Bay, and of course, the input of the Gulf Stream. Although these boundaries are not viewed as fixed, it is emphasized that the area under consideration is roughly 20,000 square miles and, as such, requires remote sensing if synoptic inputs are to be available for inputs to predictive models. The predictive capability of the objective is approached by breaking the problem into manageable parts. These specific areas of investigation are listed in the first five items of figure 17.

The last item listed in figure 17 is really a part of each of the first five in that mathematical models are required in each. The key word is "circulation." This dynamic process is the basic phenomenon to be modeled in detail. Plans for investigations in each of these areas are now being developed.

A single surface drogue shown in figure 18 to track circulation has been designed and built at LRC. The drogue is located by an aircraft using a beacon signal and visual sighting. Tracking of the aircraft from Wallops and radio communications will provide precise position

location of the drogue. Periodic location thus allows surface current determination.

Summary

In this paper, I have presented the NASA, Langley Research Center's Coastal Zone Oceanography Program, outlined the approach used to develop the program, briefly described the activities which are in the areas of Satellite Applications, Estuaries, Continental Shelf, and Environmental Modeling, and identified the organizations who are expected to be working with us to accomplish the program mission.

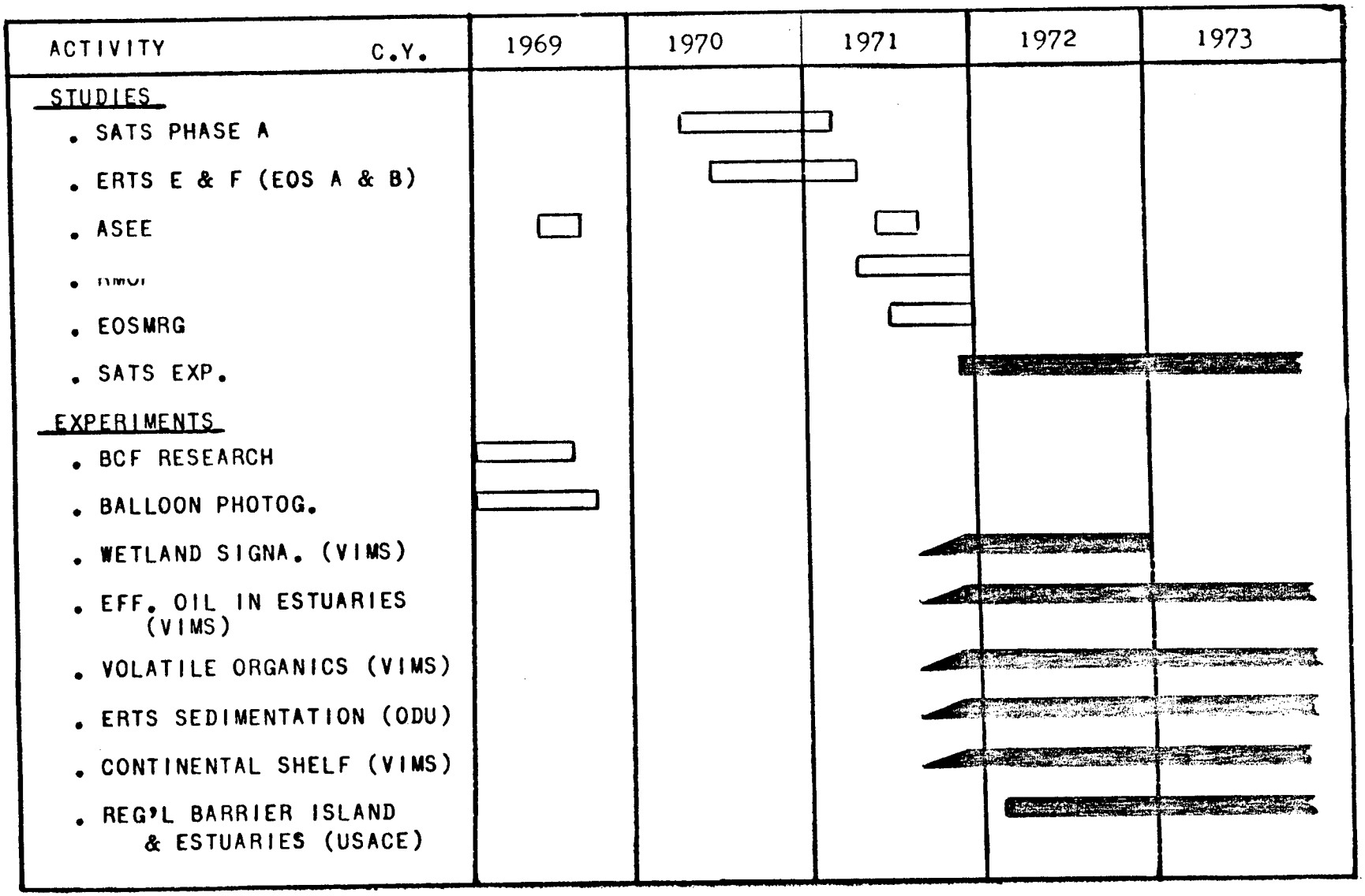

Figure 1.- The activities in the Langley Research Center's Coastal Zone Oceanography Program as a function of time.

- NASA WALLOPS
- VIRGINIA INSTITUTE OF MARINE SCIENCE (VIMS)
- U.S. ARMY CORPS OF ENGINEERS (USACE)
- OLD DOMINION UNIVERSITY (ODU)

Figure 2.- The Langley Research Center's Coastal Zone Oceanography Partners.

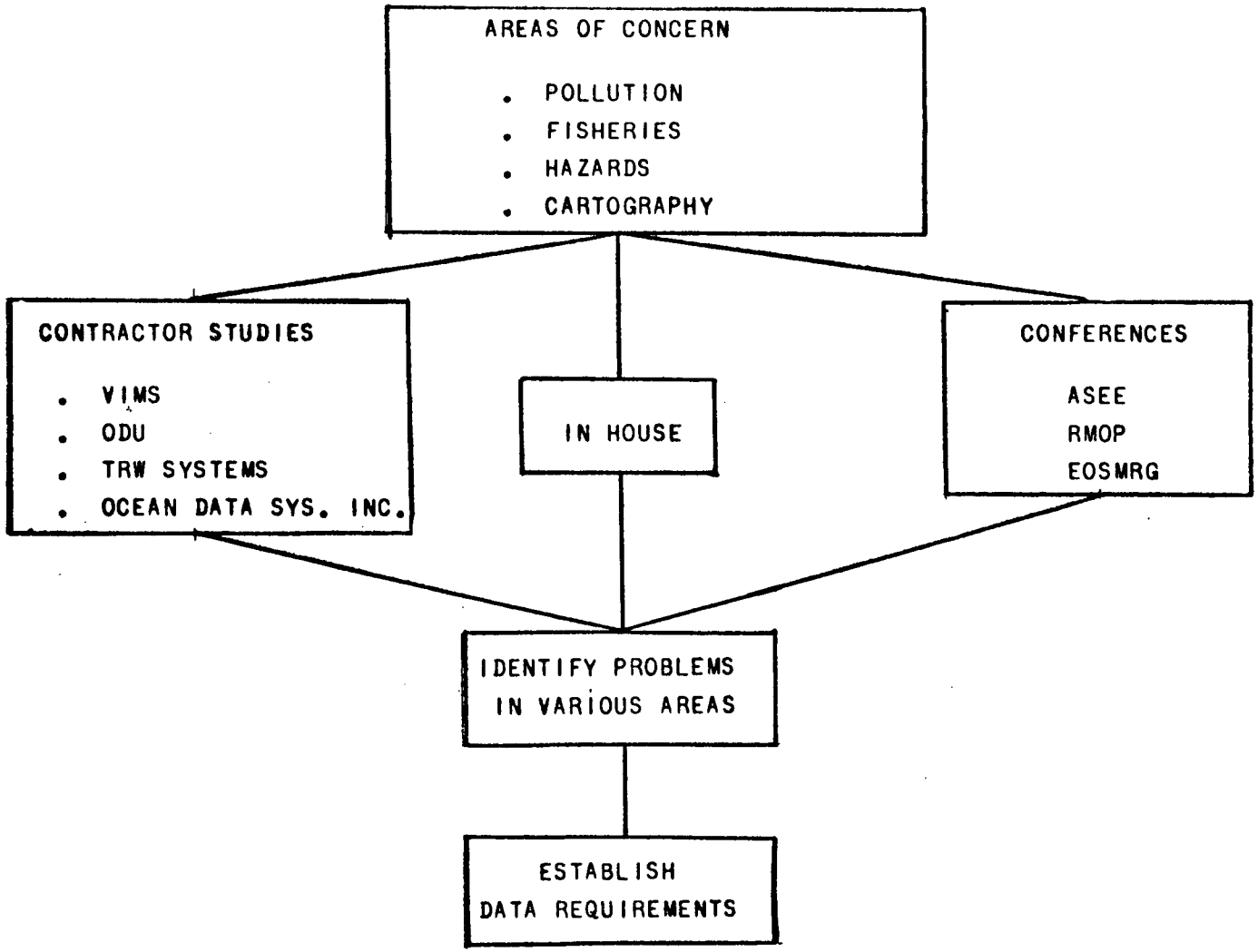

Figure 3.- The Langley Research Center's Coastal Zone Oceanography studies to identify the problems and establish the data requirements in the areas of pollution, fisheries, hazards, and cartography.

- IS THERE POLLUTION?
- DETERMINE TYPES OF DISCHARGE
- DETERMINE EXTENT OF POLLUTION EFFECTS
- DETERMINE ASSIMILATIVE CAPACITY
- OPTIMAL LOCATION FOR INDUSTRY
- EFFECT ENFORCEMENT
- ASSIST RAPID CLEAN-UP

Figure 4.- The type of problem identified in the pollution area.

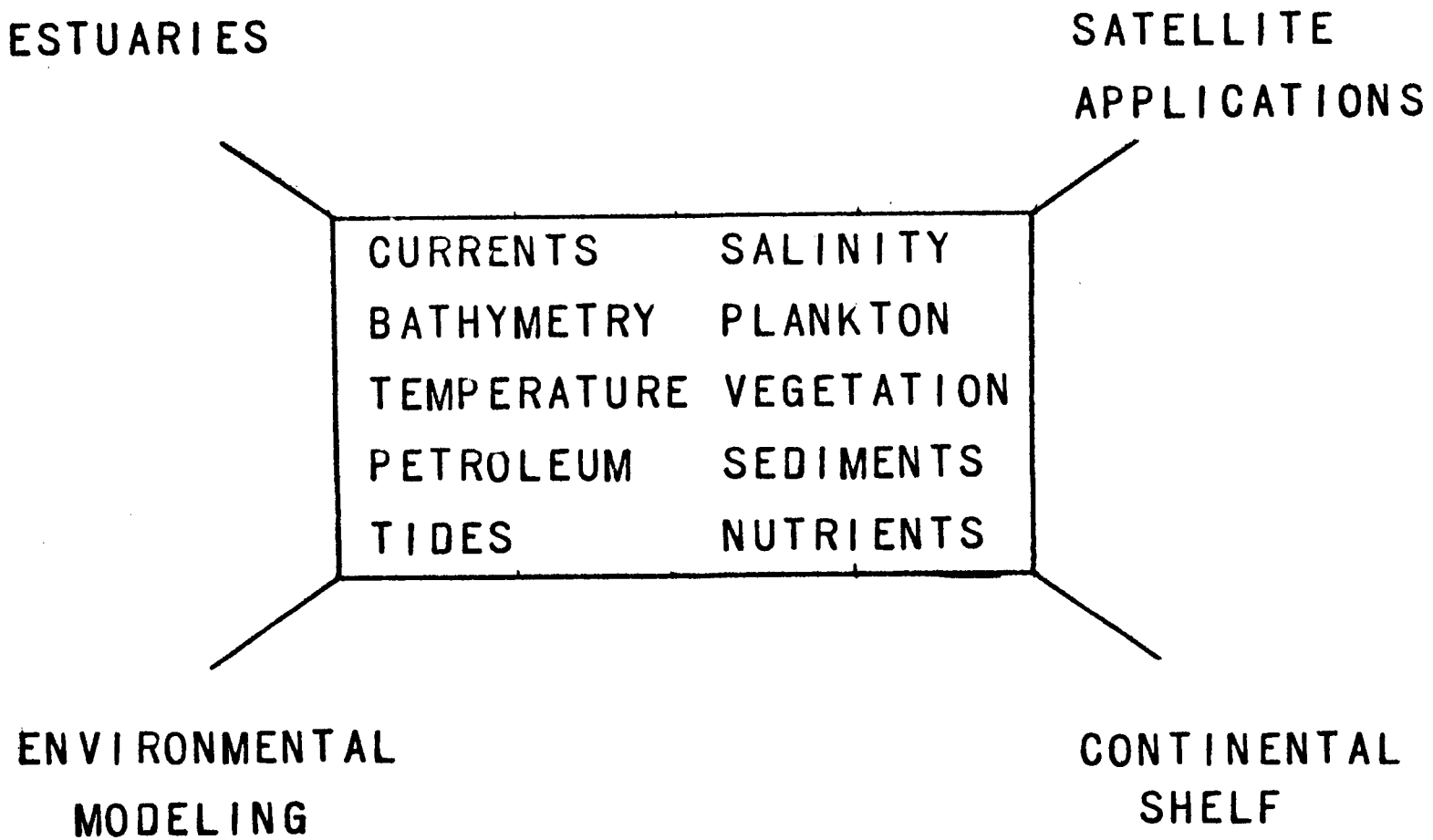

Figure 5.- The ten formost data requirements established from the coastal zone studies and the Langley Research Center's research areas for satisfying some of these data needs.

POLLUTANT TYPE	SPATIAL RESOLUTION	SPECTRAL RESOLUTION	SPECTRAL RANGE	TEMPORAL RESOLUTION	SOLAR ELEVATION	LOW ANGLE (FROM NADIR)	AREA COVERAGE
	REMOTE SENSING REQUIREMENTS						
OIL	10-30m (300m)	Broad-banc	UV,Vis. μ wave	2-4 hrs. (1 day)	only import. with glitter	only import. with glitter	200x200km (20x20km)
SUSPENDED SED.	20m (500m)	.15μm (.15μm)	350-800mm (400-700mm)	2 hrs. (1 day)	45° (30°-60°)	0 to+15° (-5°to+30°)	350x100km (10x10km)
CHEM. & TOX. WASTES	10m (200m)	.015μm (.015μm)	350-700nm (400-700nm)	5 hrs. (10 days)	45° (30°-60°)	0 to+15° (-5°to+30°)	35x35km (10x10km)
SOLID WASTES	10m (200m)	.015μm (.015μm)	350-800nm (400-700nm)	5 hrs. (10 days)	45° (30°-60°)	0 to+15° (-5°to+30°)	35x35km (10x10km)
THERMAL EFFLUENTS	30m (500m)	±0.2°C (±1°C)	10-12μm (10-14μm)	2 hrs. (10 days)	N/A	to be determined	35x35km (10x10km)
RADIOACTIVE WASTES	30m (500m)	N/A	gamma (gamma)	5 hrs. (15 days)	N/A	0° (0°)	35x35km (10x10km)
NUTRIENT WASTES	100m (2km)	.005μm (.015μm)	400-700nm (400-700nm)	2 days (14 days)	45° (30°-60°)	0to+15° (0to+30°)	350x350km (35x35km)
INTRO. OF SPECIES	to be determined	.1μm (.1μm)	Vis. (Vis.)	3 mos. (1 yr.)	N/A	N/A	350x350km (10x10km)
RED TIDE	30m (2km)	.015μm (.015μm)	400-700nm (400-700nm)	5 hrs. (2 days)	45° (30°-60°)	0to15° (-5°to+30°)	350x35km (20x100km)
HUMAN & CUL. EFFECTS	10m (100m)	Variable	UV, Vis., IR,μ wave	1 yr. (5 yrs.)	N/A	N/A	350x350km (35x35km)

Figure 6.- The ten formost water pollutant types and their remote sensing requirements identified by the remote measurements of pollution conference in Norfolk, Virginia 1972.

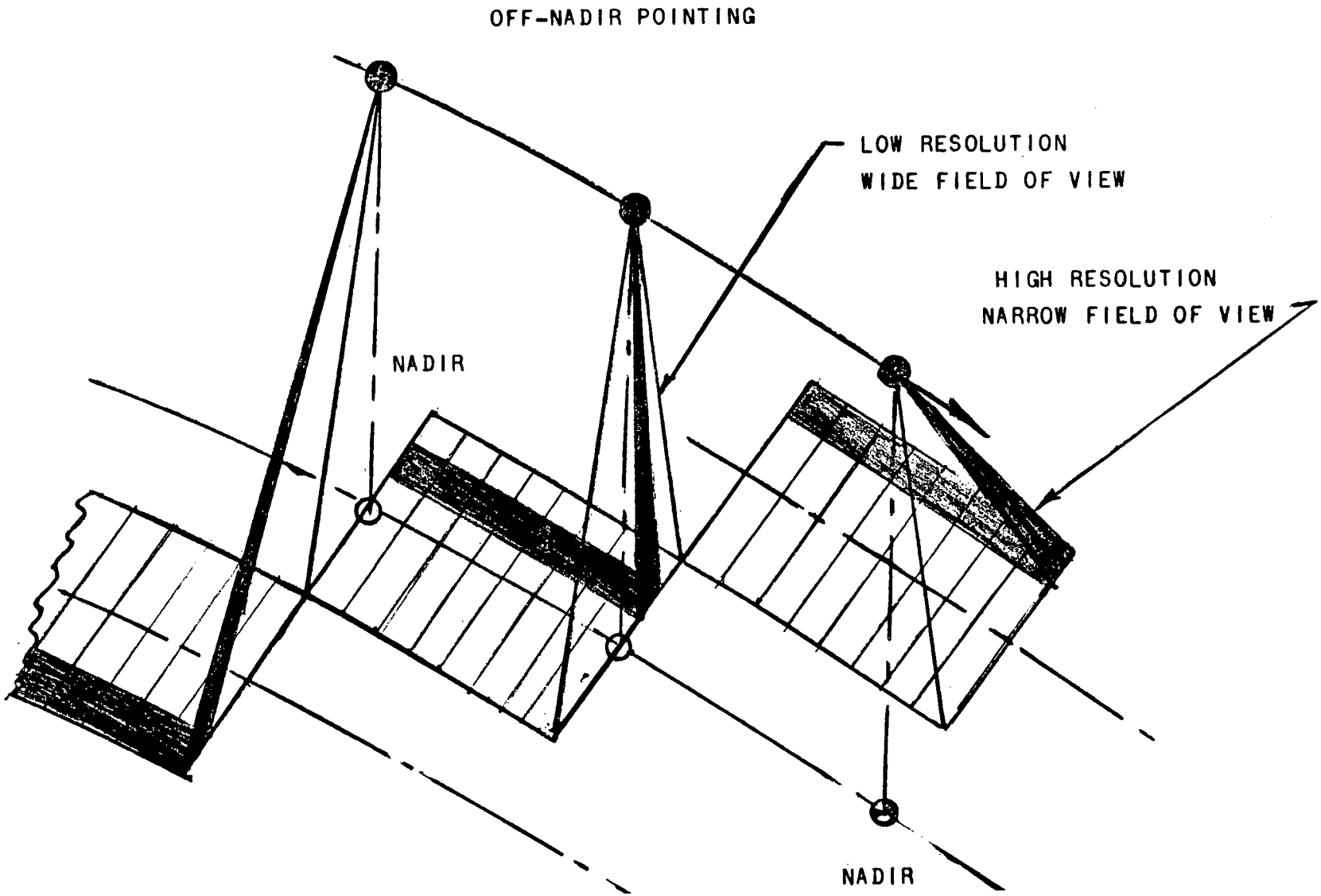

Figure 7.- A multispectral imaging system concept that could satisfy the varying data needs for the coastal zones.

- SUSPENDED SEDIMENT AND CHLOROPHYLL IN LOWER CHESAPEAKE BAY (ERTS-A & SKYLAB PROGRAMS)(ODU)
- VOLATILE ORGANICS IN THE ENVIRONMENT (VIMS)
- EFFECTS OF OIL IN COASTAL ESTUARIES (VIMS)
- WETLAND SURVEY FOR BOUNDARIES AND REMOTE SENSING KEY FOR VEGETATION (VIMS)

UNDER DISCUSSION

- NORTH CAROLINA BARRIER ISLAND & ESTUARY STUDIES WITH COASTAL ENGINEERING RESEARCH CENTER (USACE)
- SCIENTIFIC MONITORS FOR 8 ERTS-A EXPERIMENTS IN CHESAPEAKE BAY AND CENTRAL ATLANTIC REGIONS (USACE)

Figure 8.- The Langley Research Center's activities in the area of environmental quality of estuaries.

Figure 9.- An aerial photograph of the James River Bridge System. One of eight sites for the Old Dominion University-LRC, ERTS A, sediment and chlorophyll experiment.

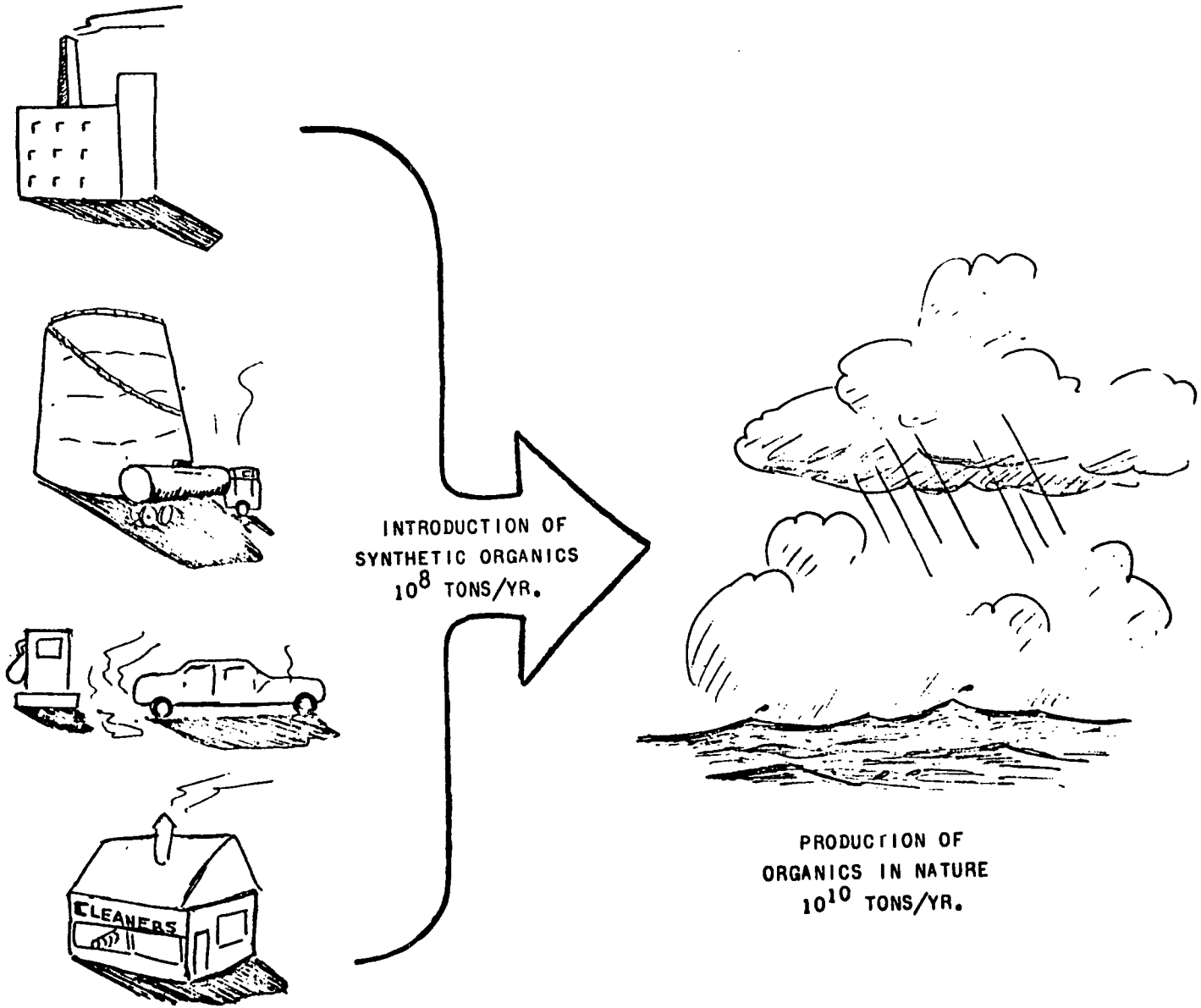

Figure 10.- Synthetic organics in the environment.

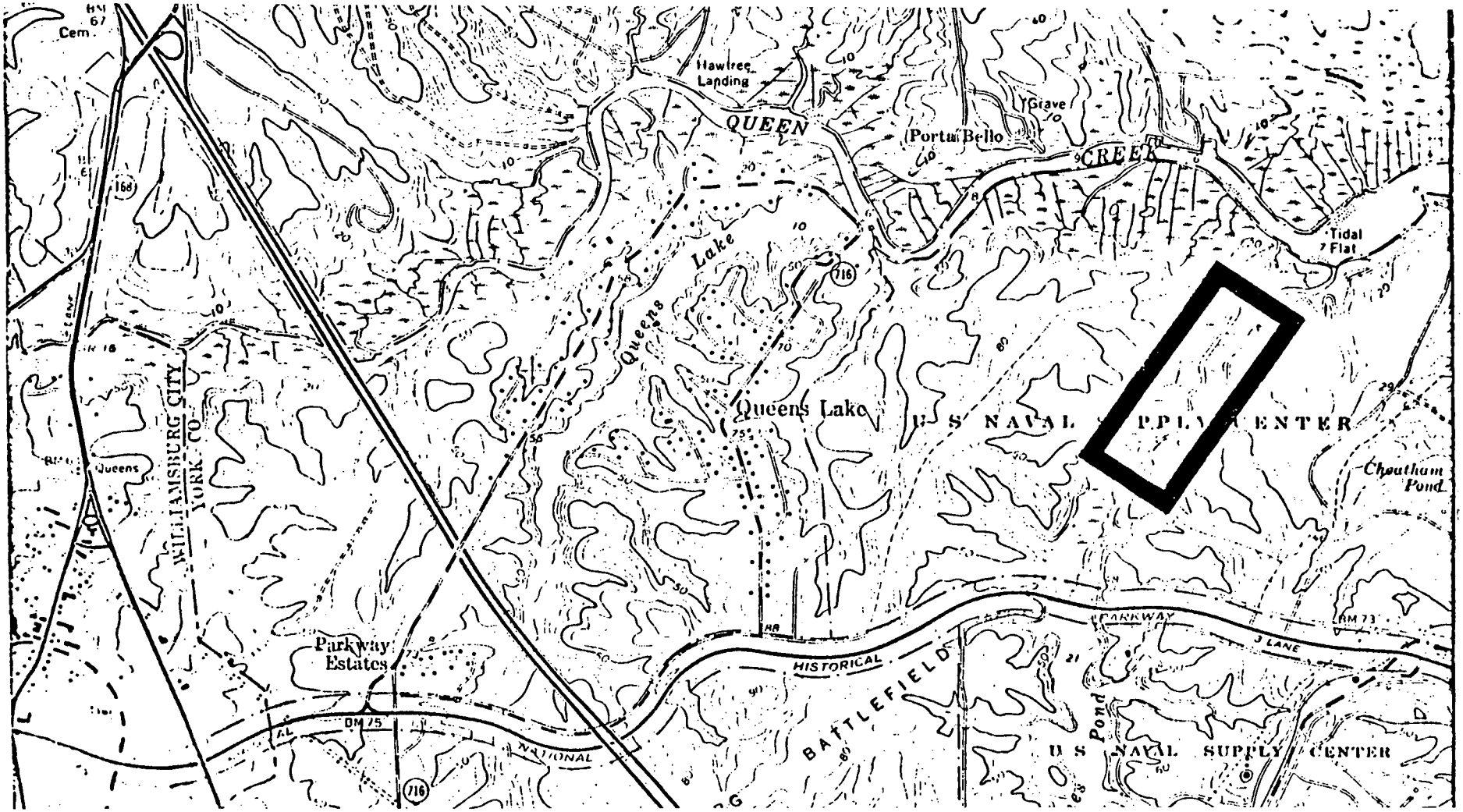

Figure 11.- The location of the Virginia Institute of Marine Sciences -LRC mini-ecosystem for the study of oil pollution on marine plant and animal life.

DISCRIMINATION SIGNATURES	VARIABLES
o SHAPE	o SPECIES
o TEXTURE	o SEASON
o COLOR	o FILM/LIGHTING
o TONE	o TIDE CYCLE
	o PLANT CONDITION

Figure 12.- Remote sensing descriminatory signatures and wetland variables.

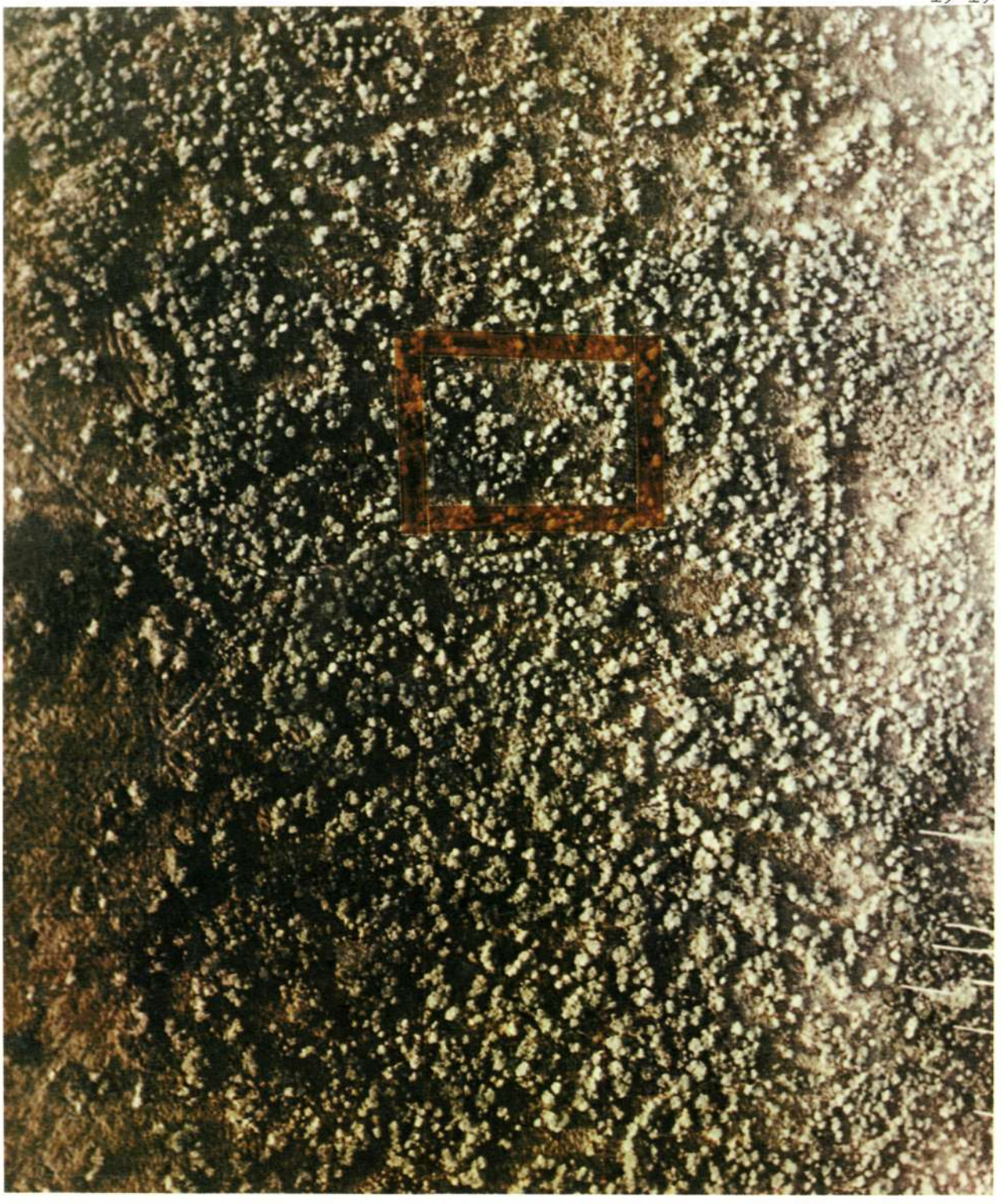

Figure 13.- Aerial photograph of wetlands with a spatial resolution of one-half meter.

Figure 14.- Aerial photograph of wetland with a spatial resolution of one-half centimeter.

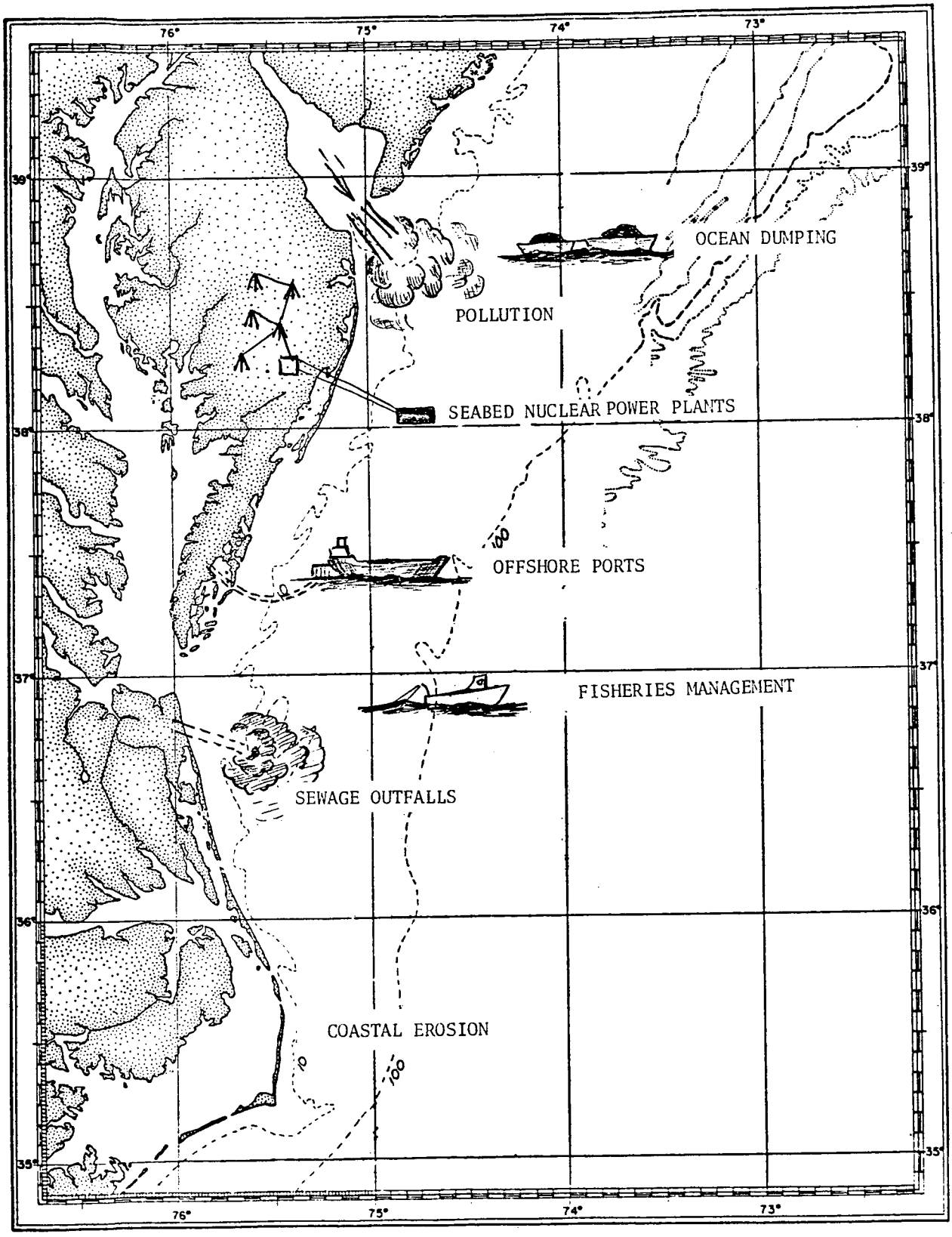

Figure 15.- Seven environmental problems on the Continental Shelf.

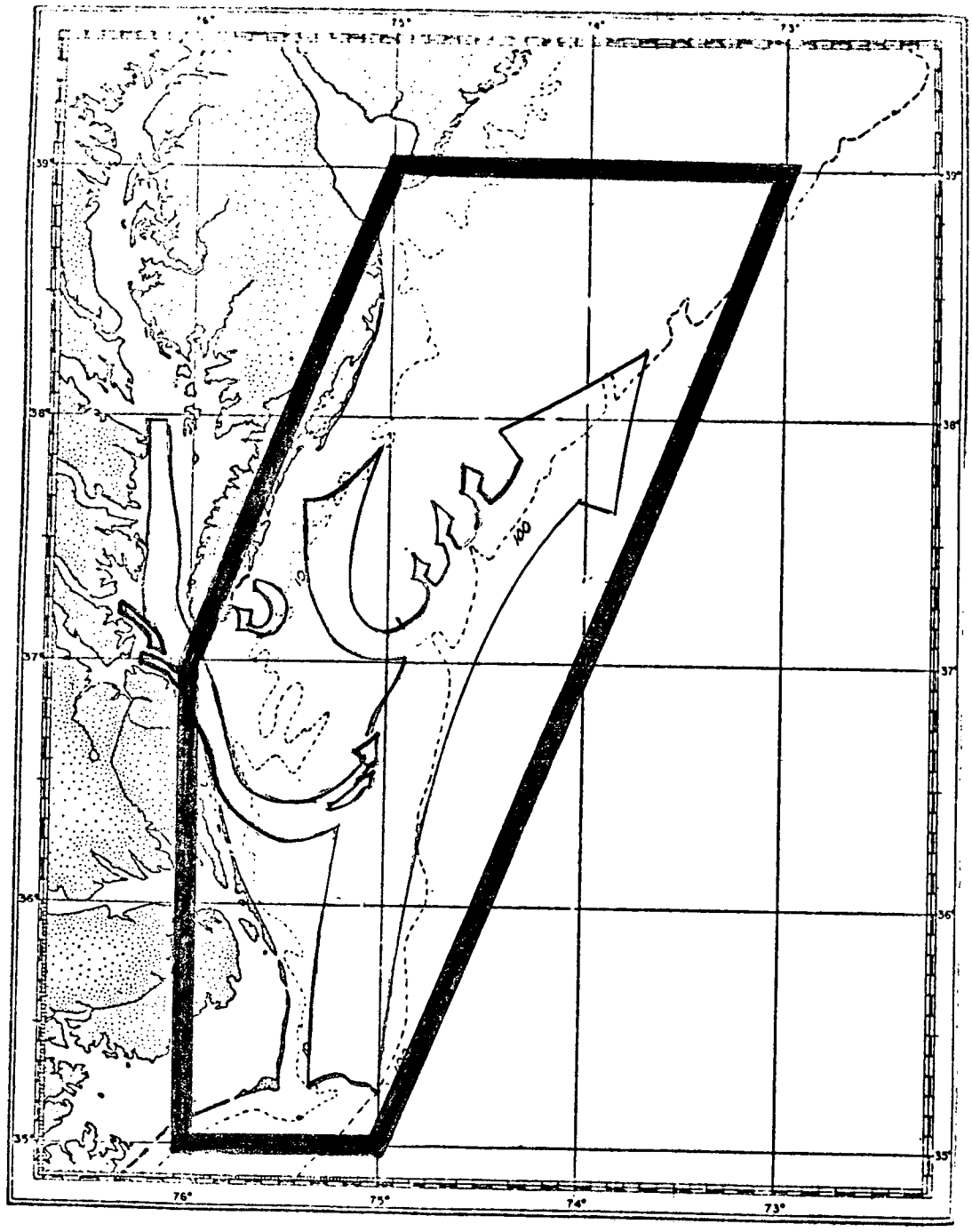

Figure 16.- The boundaries of the Virginia Institute of Marine Science-LRC Continental Shelf research area showing the normal surface flow pattern.

- CIRCULATION ON THE BROAD SHELF
- NEARSHORE CIRCULATION
- WIND DRIVEN CIRCULATION
- WAVE REFRACTION AND COASTAL EFFECTS
- SEDIMENT TRANSPORT
- MODELS

Figure 17.- The Virginia Institute of Marine Science-LRC specific areas of investigation on the Continental Shelf.

Figure 18.- A picture of the LRC drogue for detection of surface current.

SECTION 20

MSC SUPPORTING RESEARCH AND TECHNOLOGY

by Dallas Evans
Manned Spacecraft Center

ABSTRACT

(Not available)

SECTION 21

APPLICATIONS EXPERIMENTS IN THE HOUSTON REGION

by

R. Bryan Erb
Earth Observations Applications Office
NASA, Manned Spacecraft Center
Houston, Texas 77058

INTRODUCTION

Last year, Mike Holter described the Earth Observations Program here at the Manned Spacecraft Center and said that a major new thrust would be in the direction of experimental applications. The purpose, of course, was to develop a better understanding of the use of remote sensing data in pilot studies, thus aid in the definition of requirements for future remote sensing systems. I would like to give you a brief report on our first year of activity in this new direction.

OBJECTIVES AND APPROACH

The objectives of this activity are:

- To develop experimental applications of current remote-sensing technology in the Houston area.
- To develop and test a methodology for making such applications.

The approach is simple and problem-oriented in concept as follows:

- Work in concert with duly constituted operating agencies to assure implementation of the results.
- Explore a small number of specific problems, each focused on one set of operating decisions required by the agency.
- Utilize existing models of the agency information system and then augment these models with remotely sensed data.
- Develop a data acquisition, storage, and retrieval system for the test area to support the specific application studies.

We choose a specific problem of a specific resource management agency to define and bound an applications effort. A correlary of this approach is to emphasize collaboration with the operating, as well as the research arms, of the user agencies.

ORGANIZATION

The effort has been structured into major elements as shown in Figure 1. One element is the development of a simulator or facility which involves an experimental or pilot model of an Earth Resource Survey Information System with provision for acquisition and manipulation of data in conjunction with applications models. The other element is the use of the facility in a series of Applications. Each application is pursued by an interdisciplinary, interagency team. We consider it of utmost importantance to work applications as joint ventures and involve representatives of the user agency. I should also mention that the NASA effort has included many MSC groups and their support is gratefully acknowledged.

HOUSTON AREA TEST SITE

For convenience our initial efforts are being pursued in the region around Houston, NASA Test Site 175, shown in Figure 2. This area covers some 15,700 square miles of the Texas coast, an area about the size of Switzerland, but still small by Texas standards. For our purposes it offers a very reasonable selection of targets as shown in the cartoon in Figure 3.

CURRENT ACTIVITIES

I would now like to describe, very briefly, a few of our current activities.

REGIONAL INVENTORY AND MONITORING

As part of our pilot facility we have undertaken the development, for the study area, of an experimental data base for eventual use in a regional inventory and monitoring system. The purpose of such a system is to provide an up-to-date status on conditions and rates of change of

environmental features using data from sources such as ERTS and Skylab. As a starting point land-use was classified as part of an experiment to assess the utility of small scale imagery from the RB57F for developing a 20 category land-use system. An example of the final product is shown in Figure 4. This study, which was done in conjunction with the Houston-Galveston Regional Council of Governments, and the Houston Chamber of Commerce, was led by Dr. John Dornbach and Dr. Mark Chesnutwood. The base for this study was primarily color ektachrome imagery acquired on Mission 145 in November 1970. The base photo mosaic was constructed by MSC in the Mapping Science Branch. The small scale mosaic permitted interpretation and publication of the land-use at about the same scale as that of the original imagery.

This land-use information, and many other types of physical, natural, and demographic data will be stored in a computer based information retrieval system on the basis of one-kilometer square cells accessed by UTM grid designation. A trial data set has been developed to exercise the storage and retrieval system. This data base can be accessed from a remote terminal and searched for cells which satisfy one or more criteria. If, for example, we wanted all the data for a given cell we could conduct a query such as shown in Figure 5.

SAM HOUSTON NATIONAL FOREST STUDY

A joint activity has been undertaken with the U.S. Forest Service in studying the Sam Houston National Forest. Three Forest Service employees are in residence at MSC and we are providing support to a pilot study aimed at assessing the role of remote sensing in the new planning approach being pursued by the National Forest System. This planning system is shown in Figure 6. Information developed in this study will be utilized in the development of plans for the management of units of the forest, and in monitoring the implementation of the plans.

The current effort involves the use of photographic data in the inventory of forest resources such as timber stands and volume, wildlife and range resources, recreation areas, and roads. The Sam Houston National Forest includes some 160,000 acres and is located about 75 miles north of Houston. This area is typical in many ways of Southern pine forests. The area is a complex one, subject to many urban pressures from its proximity to Houston. A typical region of the Sam Houston is shown in Figure 7.

TRINITY BAY STUDY

The other major applications activity underway is the Trinity Bay Study. This effort is being carried out in cooperation with the Naval Research Laboratory, EPA, Texas Parks and Wildlife, Texas Water Quality Board, Houston Lighting and Power Company and the U.S. Army Corps of Engineers. The objectives of this effort are threefold:

1. To assess the utility of remote sensing in studying a shallow estuary, in particular, to verify mathematical and physical models of the hydraulic and thermal characteristics.

2. To make synoptic observations in the thermal infrared range of the outfall plume of a power generating station and verify the ability of a two-dimensional mathematical model to predict the location and temperature distribution of the plume, and

3. To assess the utility of remote sensing to monitor the location and distribution of a sea grass that provides important protection for juvenile shrimp.

The location of the study area is shown in Figure 8, and something of the complexity of the flow pattern in Figure 9. This activity was described in detail yesterday in the paper by Drs. Zaitzeff and Whitehead.

USE OF MULTISPECTRAL DATA

The final activity I would like to mention is our effort to utilize multispectral data. The first step has been to exercise and check out the various elements of the processing system. Three channels of spectral data were generated by digitizing each emulsion layer of a Color IR photograph. This frame of photography (Figure 10) is of the region near Katy, west of Houston. A gray map of one channel, used for the selection of training fields, is shown in Figure 11. This set of spectral data was run on the LARSYS pattern recognition program. The resulting recognition map was produced both as a grey-scale line-printer output, and as a color coded display on the Data Analysis Station (DAS) as shown in Figure 12.

FUTURE PLANS

Our activity for the next year looks in two directions: One is the use of multispectral data in applications. We have had local flights carried out by the Michigan aircraft and are currently developing the capability to process and analyze this data. We have proposed as a collective user of ERTS and EREP data and as these sources of data become available they will be applied to our applications work to augment the aircraft data. A major objective of this phase of our work will be to assess, for each application, the utility of the data from the satellite systems.

We hope also to develop additional applications and I will mention one which shows promise. This would be in conjunction with the Soil Conservation Service on Rangeland Management, and would be aimed at the identification of range sites and the monitoring of range conditions.

A study area close by has been tentatively selected. It comprises 11,000 acres of coastal prairie, near Rosenberg, southwest of Houston. A high altitude RB57F photo is shown in Figure 13. A view from space (Figure 14) shows that this region is also visible on the Apollo 9 S065 multiband experiment. A view from about 200 feet (Figure 15) shows the great variety of terrain present. I conclude from this that we will be grateful to ERTS for its role in integrating some of the local inhomogeneities.

CONCLUSION

In conclusion, we have organized, staffed, and planned an experimental applications effort at MSC. We have made many contacts in our local study area, and have started work on an experimental data base, and on several applications, which, if successful, could be replicated by the responsible agencies at other locations.

While it is too early to report much in the way of results, the heading vector of our MSC program has clearly changed.

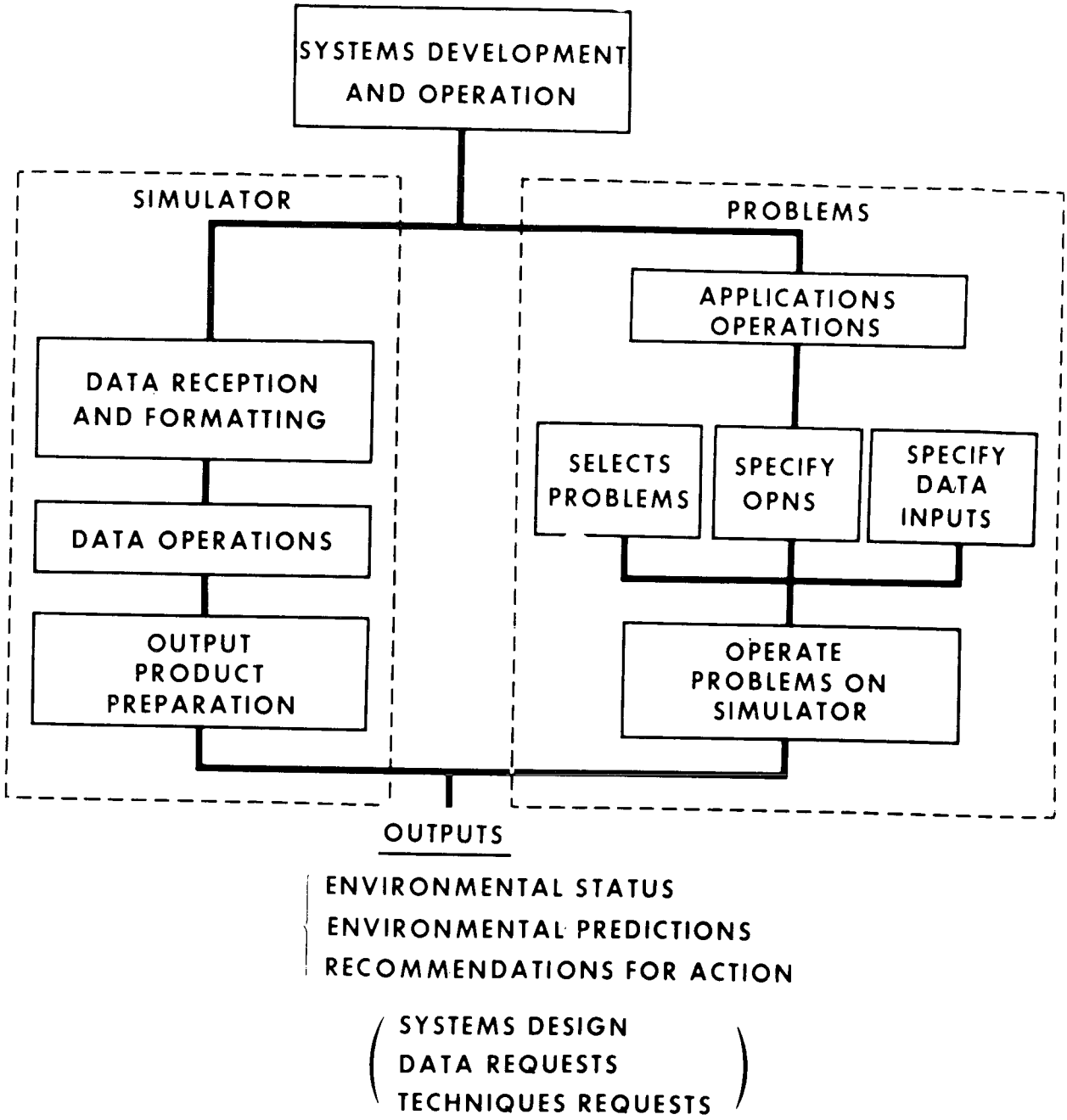

Figure 1. - Applications Organization, "The organization for undertaking applications in the Houston area comprises a simulator or facility (left) which is used in applications by carrying out the steps described (right)."

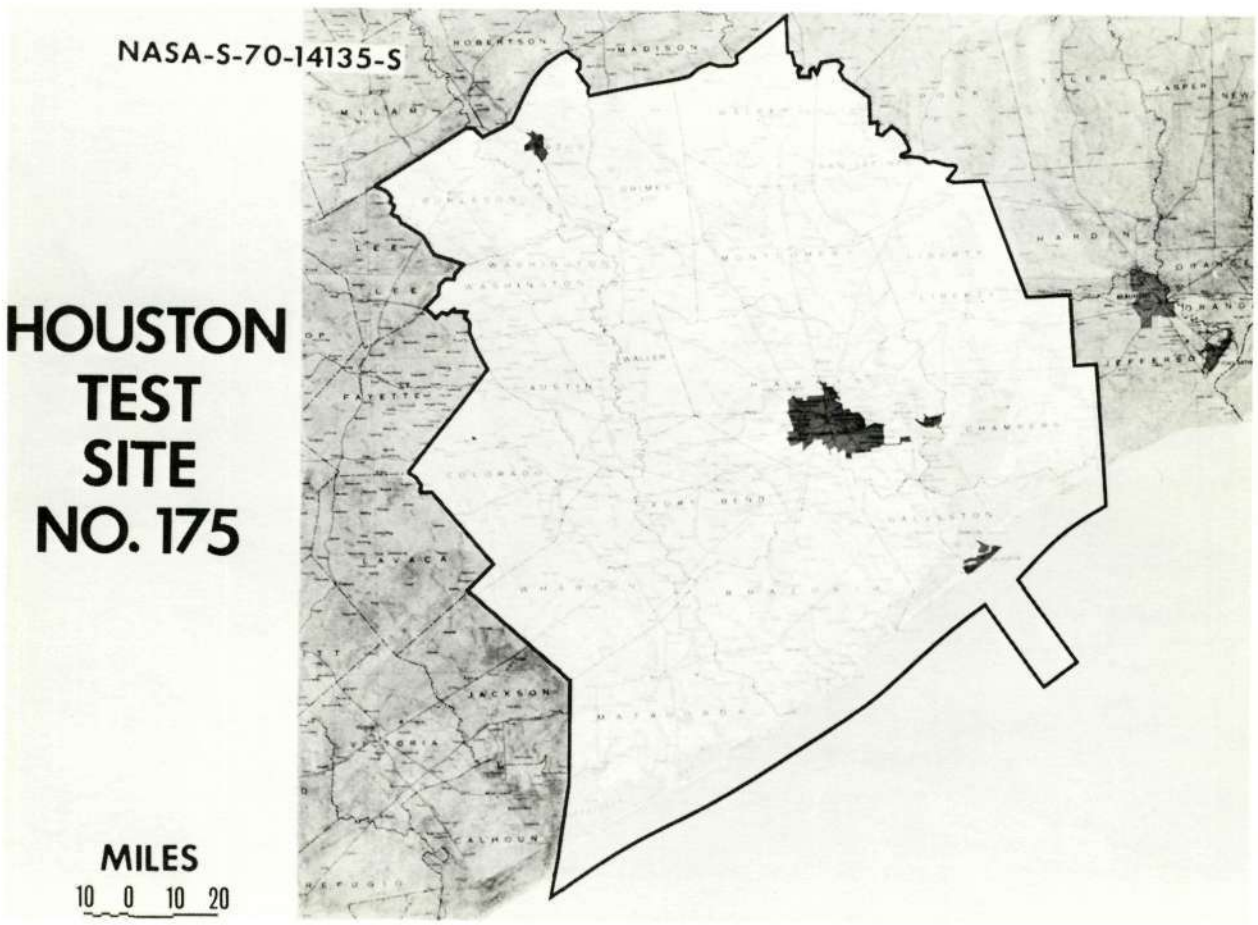

Figure 2. - Houston Area Test Site, "The Houston Area Test Site, NASA Test Site 175 comprises 15,700 square miles on the Texas Gulf Coast."

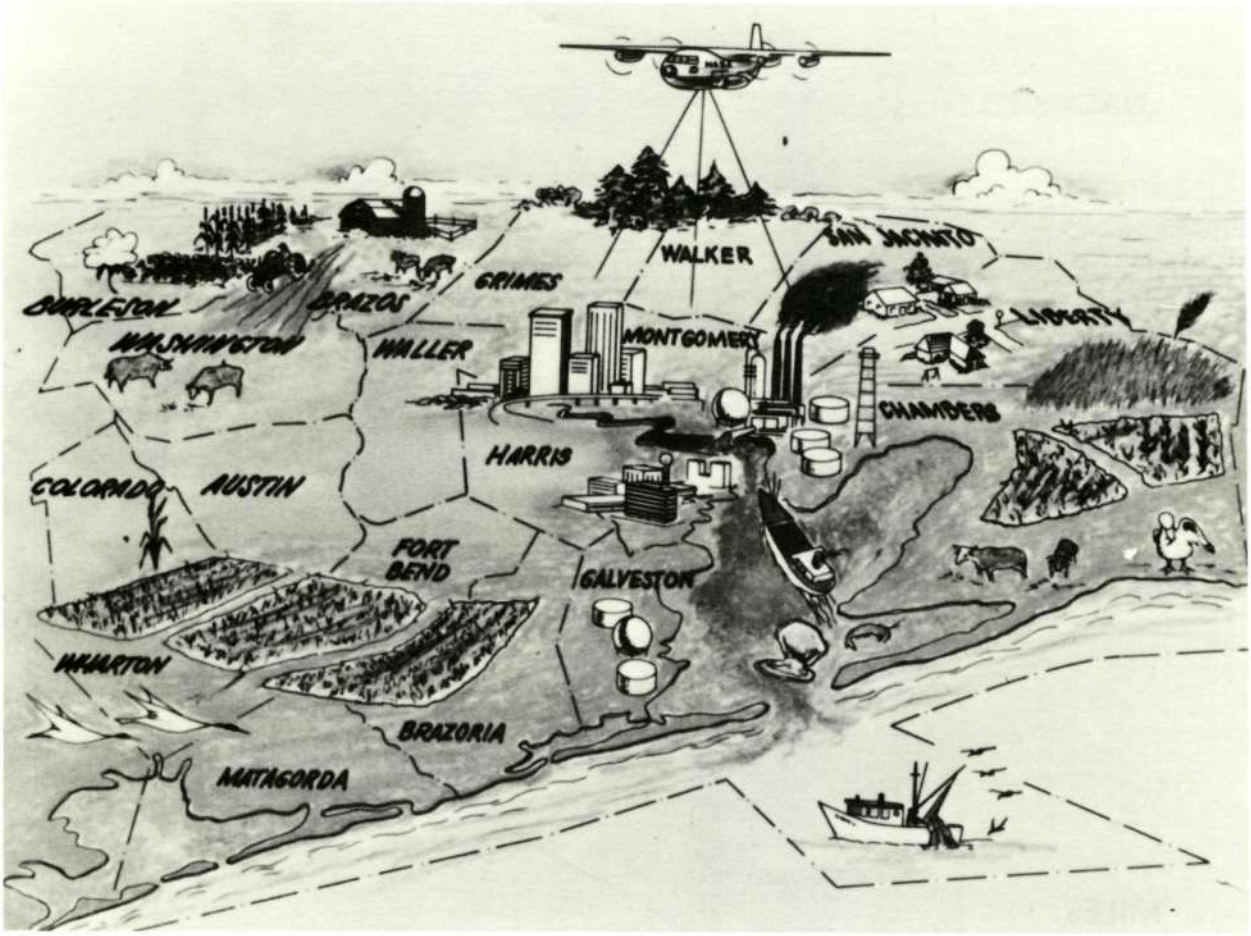

Figure 3. - Subjects Available for Study in the Houston Region, "The Houston Area Test Site offers a wide variety of subjects for remote sensing activity."

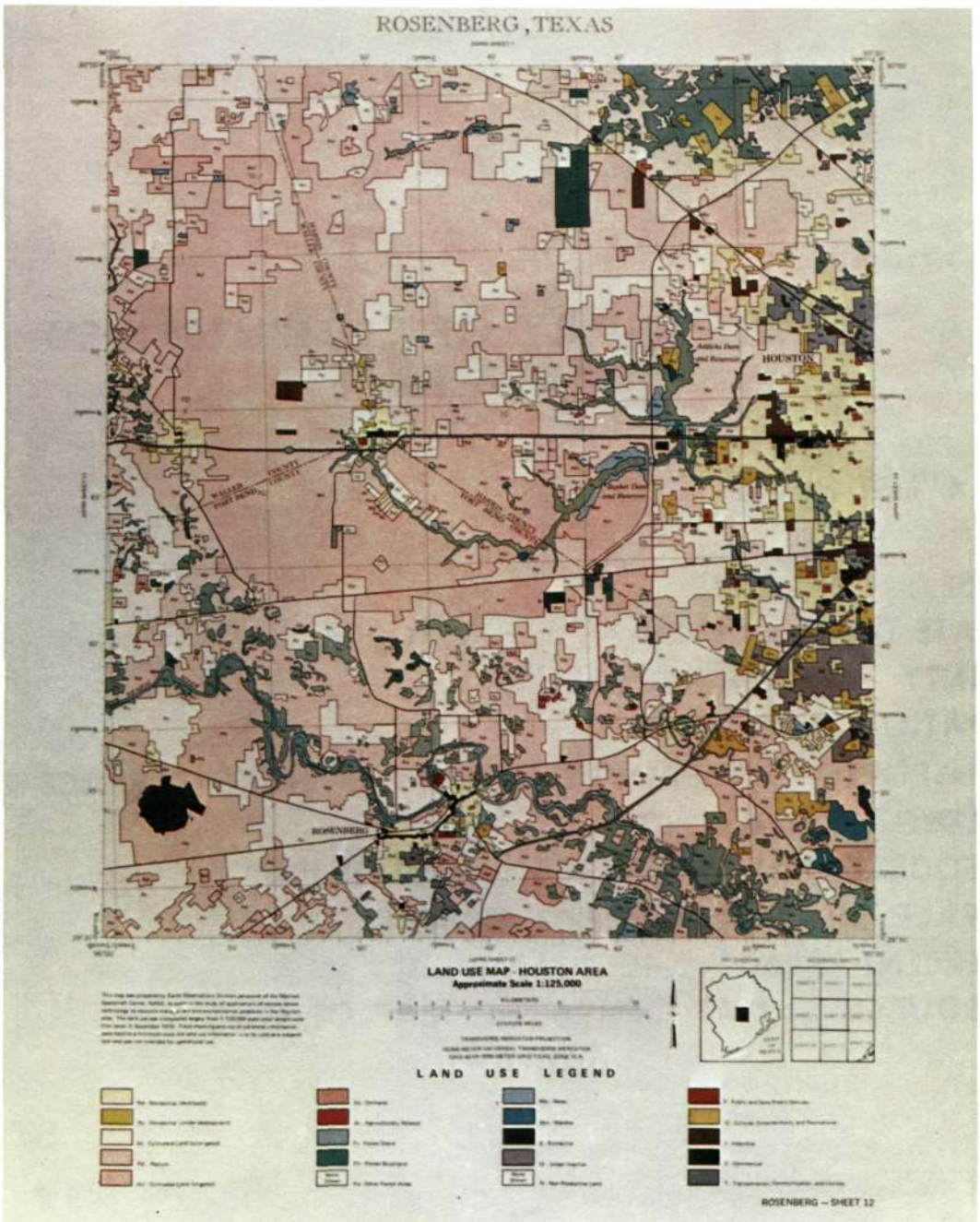

Figure 4. - Sample Sheet of Experimental Land Use Map, "This is one of 21 sheets of an experimental 20-category land use map of the Houston Area Test Site. It provides an initial data base for a regional inventory and monitoring system."

NASA-S-72-586-X

SAMPLE QUERY OF COMPUTERIZED DATA BASE

007 C"LIST HATSF '14RQJ5138'

HATSF : 14RQJ5138
UPDATE DATE : 10-20-71
COUNTY : WASHINGTON
ELEVATION : 450-350
TRANSPORTS : IMPROVED LT. DUTY : HARD SURFACE 2 LANE
TLENGTH : .6 : .7
TSOURCE : MAP OF 1963 : MAP OF 1963
SURFACE : AGRICULTURE : URBAN
PERCENT : 60 : 40
SSOURCE : MAP OF 1963 : MAP OF 1963

Figure 5. - Sample Query of HATS Data Base, "An example of the information contained in a single cell of the HATS data base. Each cell is one square kilometer, and is addressed by its UTM grid designation."

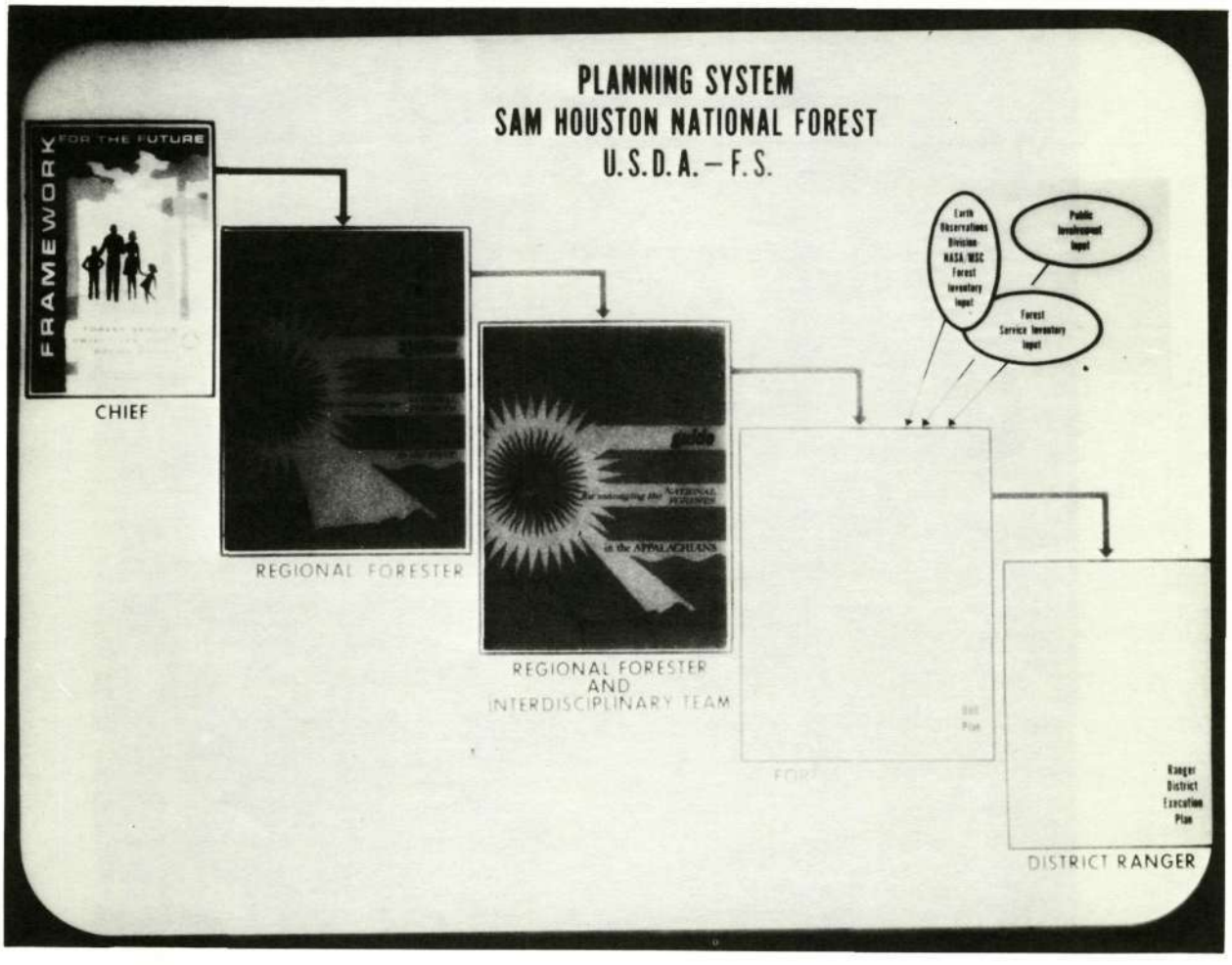

Figure 6. - Forest Planning System, "The proposed planning system for National Forests in Texas proceeds through a series of steps as shown in this figure. A unit for which actual plans are developed oped is typically a small watershed."

Figure 7. - Sam Houston National Forest, "A Typical Region of southern pine forest showing a variety of stands, adjacent private timber (lower left), and pasture lands (bottom), regeneration area (center), seed tree cut (center right) and encroaching urbanization (lower right)."

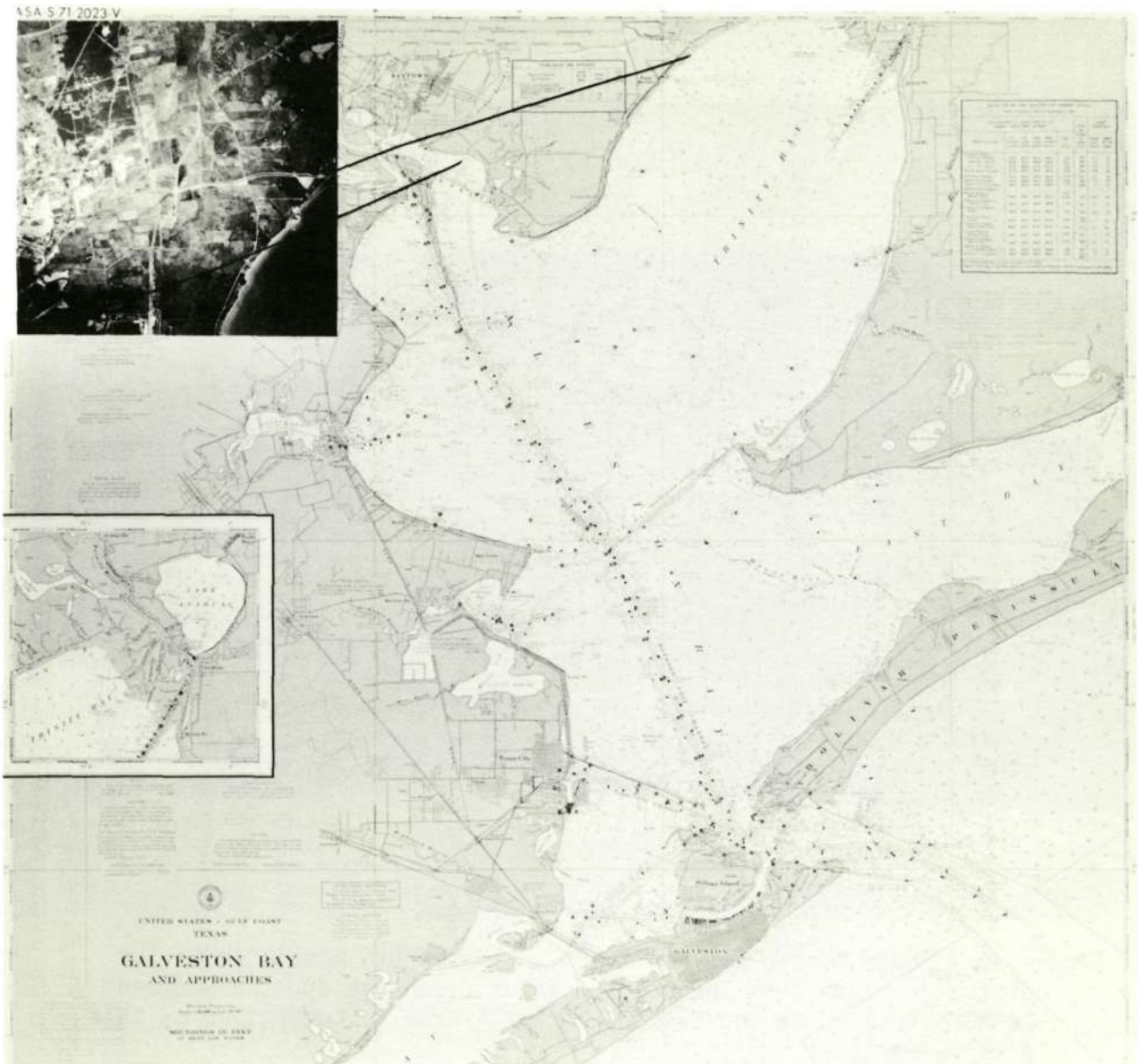

Figure 8. - Trinity Bay Study Area, "Located on Cedar Bayou a major power plant discharges cooling water through a canal (insert) into upper Trinity Bay."

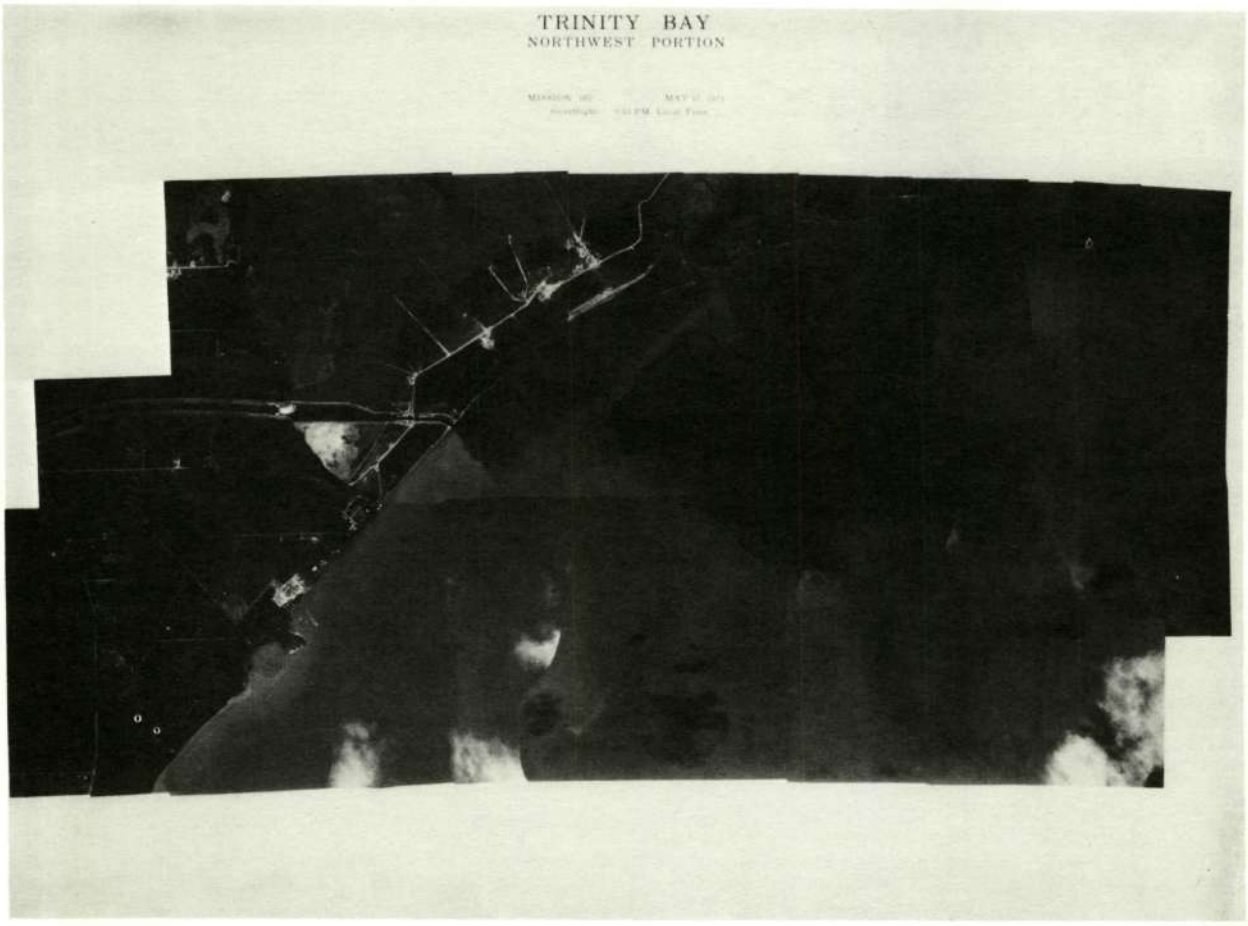

Figure 9. - Photo Mosaic of Trinity Bay, "This photo mosaic shows the discharge plume from the cooling water discharge and the sediment patterns caused by the rather complex hydraulic conditions of this shallow estuary."

Figure 10. - Color Infrared Photograph of Katy, Texas Area, "This photograph of rice and pasture land west of Houston was digitized in a color separation experiment to simulate three channels of spectral data."

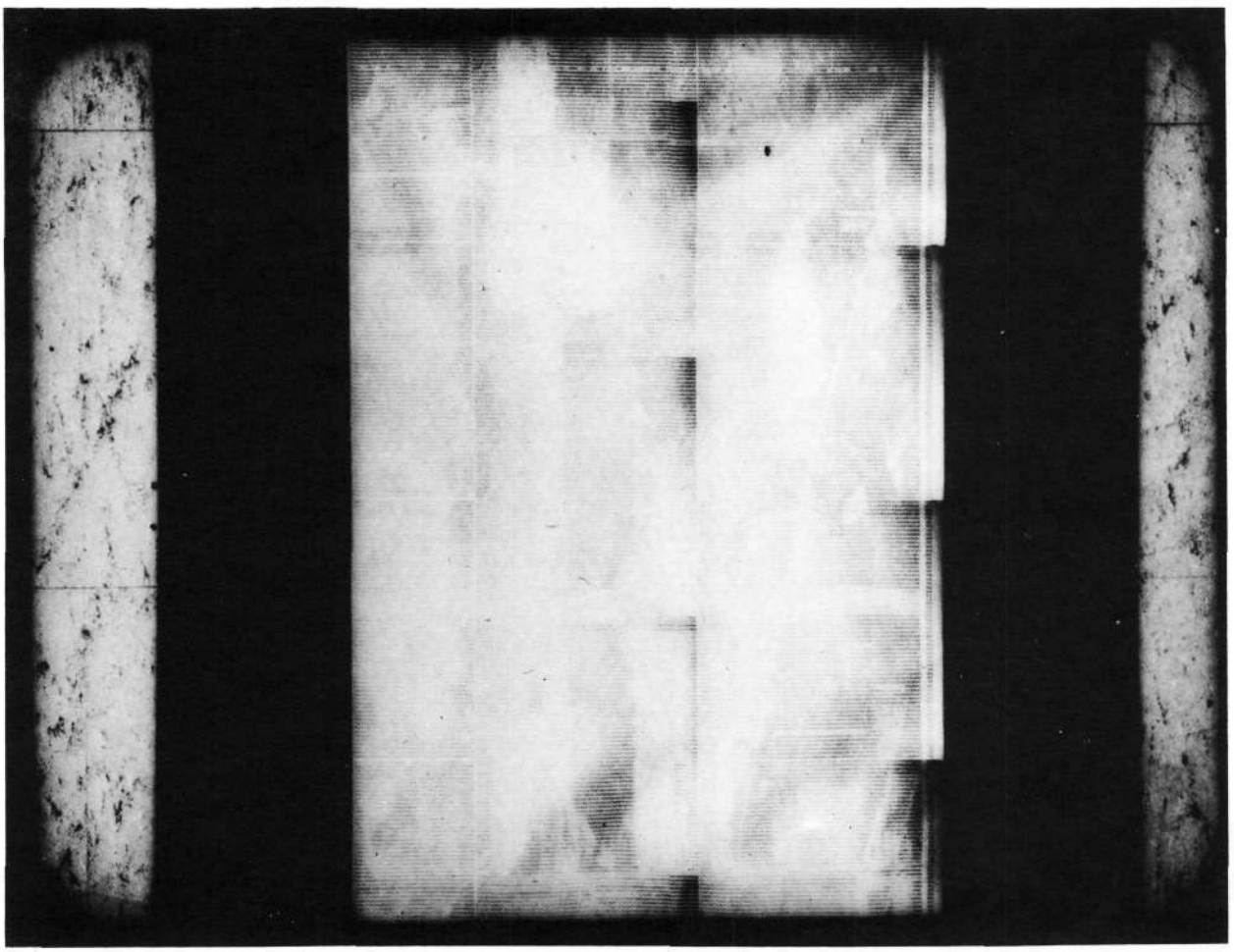

Figure 11. - Grey Scale Printout of Spectral Data, "This computer-generated printout portrays various density levels in the red band by different symbols. It proyides a means for selecting training sets for a digital pattern recognition program."

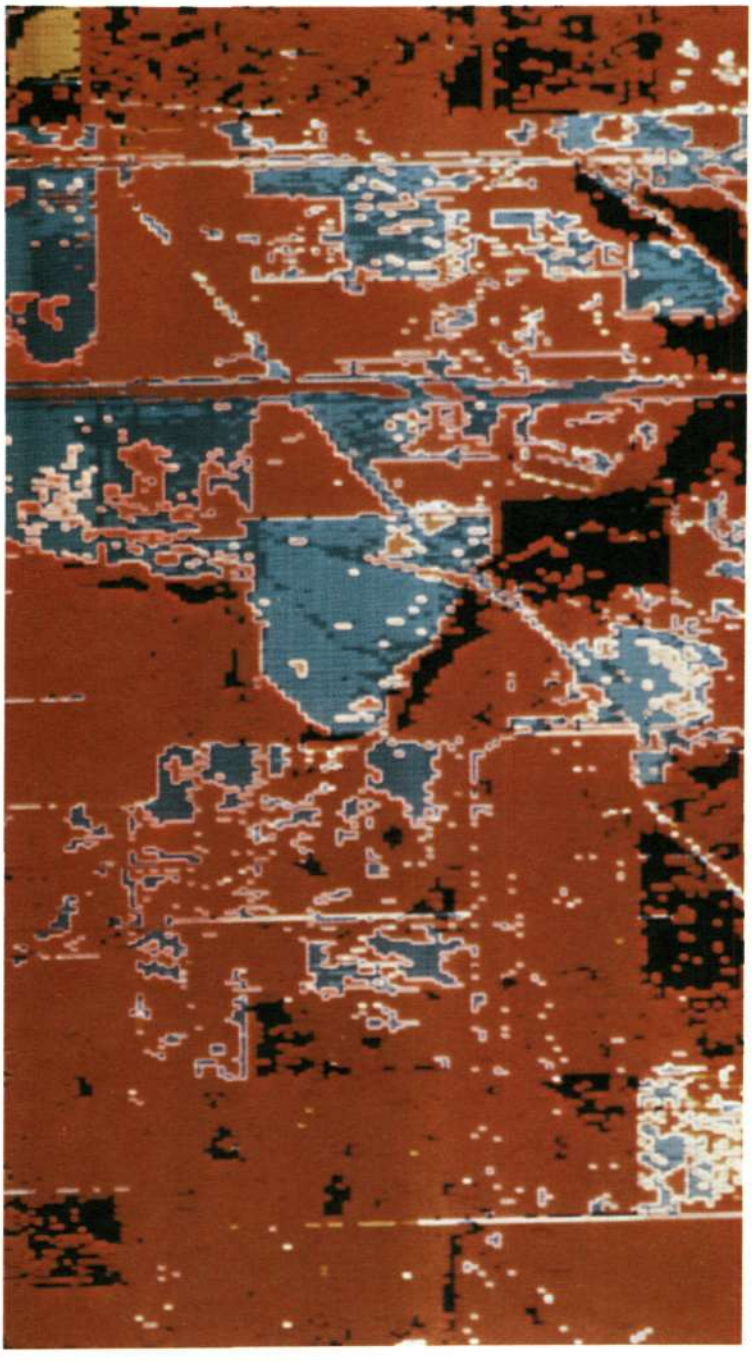

Figure 12. - Recognition Map of Katy, Texas area, "This recognition map was generated from the pattern recognition program and imaged from a digital tape by the film recorder of the Data Analysis Station. The color code is:

black	forest
red	pasture
blue	rice

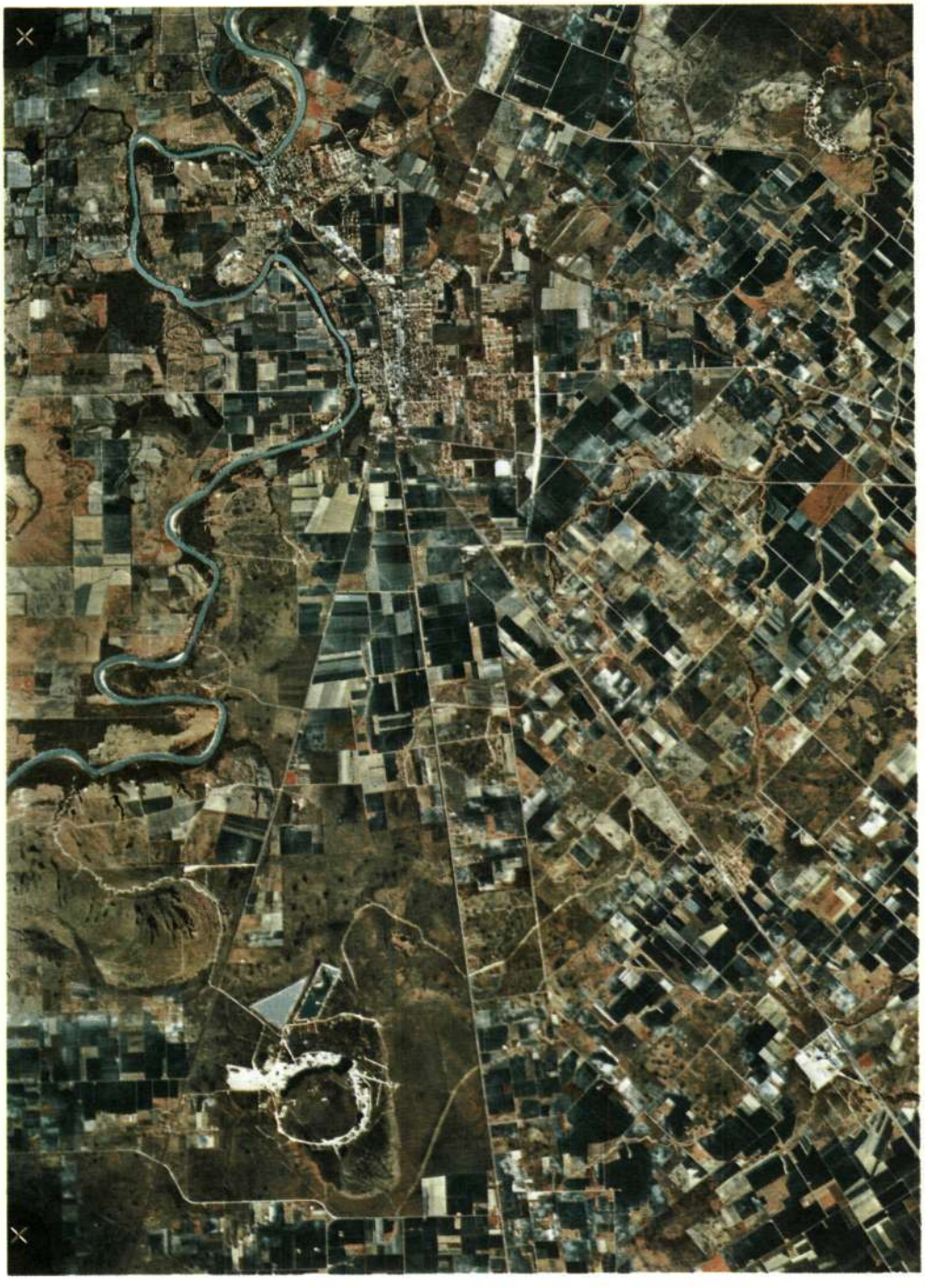

Figure 13. - High Altitude Photo of Rosenberg, Texas area, "This area near Houston provides a site for study of coastal prairie rangeland."

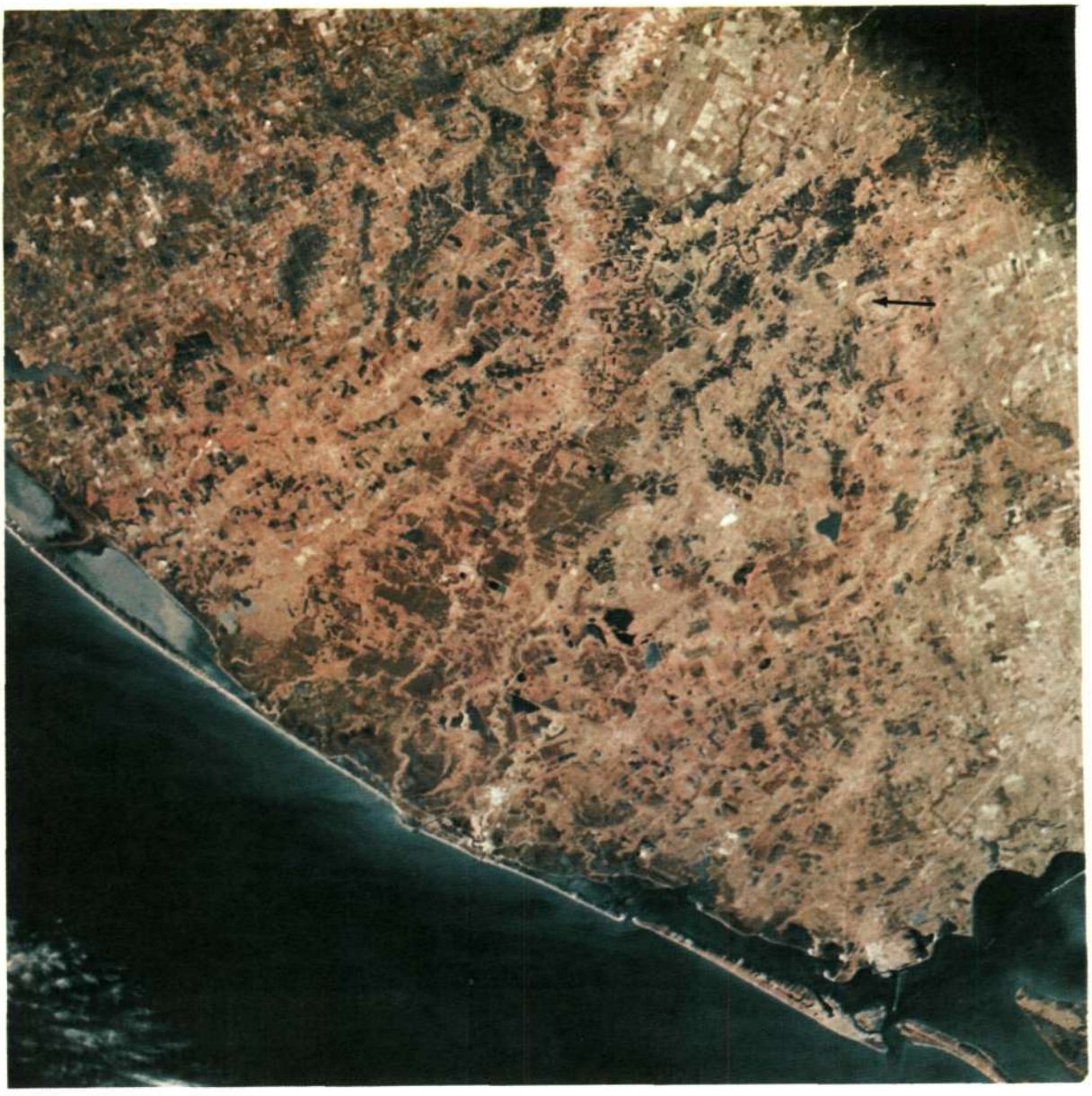

Figure 14. - Space View of Texas Coast, "This frame of color infrared photography from Apollo 9 (S065 multiband experiment) shows various land uses in the Texas Coastal region including (arrow) the range-land study area near Rosenberg."

Figure 15. - Low Altitude View of Rangeland near Rosenberg, Texas, "This view from a helicopter at an altitude of about 200 feet shows the great variety of terrain appearance typical of coastal prairie."

SECTION 22

PUBLIC HEALTH APPLICATIONS OF REMOTE SENSING

by

Charles E. Fuller, D.V.M., M.P.H.
Chief, Public Health Ecology
Preventive Medicine Division
Medical Research & Operations Directorate
NASA Manned Spacecraft Center
Houston, Texas 77058

INTRODUCTION

Since August 1970, a small staff from the Medical Research and Operations Directorate working with the Science & Applications Directorate at the Manned Spacecraft Center has studied the feasibility of using remote sensing in public health applications. Technical assistance to this Public Health Ecology group has been received from the University of Texas School of Public Health at Houston, and from municipal, county, state, and regional government officials. Theoretical evaluations, and practical applications of remote-sensor data have been discussed with representatives from the above groups in addition to those from the U.S. Public Health Service, the Pan American Health Organization, the World Health Organization, and the Food and Agriculture Organization of the United Nations. All discussions have been directed toward potential applications on a pilot study scale.

This Public Health Ecology group has embarked on a three-fold program of research and development. This overall program entails:

First, a program designed to develop and increase awareness in the Public Health Sector of the potential of NASA's remote sensing capabilities for the solutions of public health problems currently engaging these agencies.

Second, a program designed to develop and increase a university and public health sector applied research program into those public health problems which might be most amenable to solution by the application of remote sensing technology.

And third, a program designed to develop and increase an in-house capability to examine, develop and apply remote sensing applications to the solutions of public health problems.

PROGRAM OBJECTIVES

The Public Health Ecology group is encouraged that it will find significant scientific correlations between disease, water, air and urban degradation, and natural disasters as they show relationships to other observed phenomenon such as indicator species, crown signatures of trees, and evidence of other reliable symbiotic relationships.

Of these four areas of endeavor, animal or insect-borne diseases have received the greatest emphasis. These diseases are caused by organisms whose life cycles depend on insect vectors or animal hosts that have a unique and often critical dependency on specific components of the biosphere for their perpetuation and transmission.

Primary reasons for the stubborn persistence of these diseases in our society lies in our lack of understanding and our inability to deal effectively with the interrelationships between man and his physical and biological environment. Remote sensing can provide the investigator with the unique perspective and a different kind of knowledge needed to deal more effectively with these diseases.

The key to this sought after new capability is to determine those highly reliable sensor detectable characteristics which are to a high degree mutually exclusive, all inclusive and replicable when addressing vector-borne disease phenomenon or medical zoology problems.

SUPPORTING RESEARCH AND TECHNOLOGY

Contracts to assist in the accomplishment of this work, as seen in Figure 1, have been awarded to the University of Texas School of Public Health at Houston. This graduate school, one of eighteen in the nation that provides Masters and Ph.D. level training to physicians, veterinarians, dentists, bioenvironmental engineers and other graduate level paramedical people, has also received a contract to assist the Public Health Ecology group in a study of respirable and suspended air-borne particulates.

The basic technique is dependent on contrast imagery. Since suspended particulates scatter light waves of a wavelength equal to that of the suspended particulate diameter the image contrast at that wavelength is reduced. Furthermore, the amount of reduction of that contrast has been successfully correlated to the size, size distribution and total weight of suspended particulates in the air environment. Thus, the method requires a passive detector system which will measure

the amount of scattered light at a particular wavelength or family of wavelengths and a ground truth capability with which to correlate results.

The particulate itself may be harmful to the body or may act as a carrier of substances absorbed upon their surface. The capability to monitor such a hazard would represent a real contribution to community health.

Another study to evaluate the capability of remote sensing in delimiting regions meaningful to urban public health investigators has been initiated at the University of Texas.

This program requires the use of remote sensing to examine the capability for prediction and assessment of socio-economic spatial distribution and those related ecological facets which exert a marked influence on health and health-related activities.

Another contract was just awarded to the University of Texas School of Public Health to investigate the usefulness of remote sensing imagery to identify and quantify specific water pollution parameters that will contribute to the resolution of water degradation problems of public health importance.

Another contract was recently awarded to the Office of Environmental studies, The University of West Florida to conduct an investigation of those botanic species or vegetative communities which have a strong relationship with certain diseases.

PUBLIC HEALTH ECOLOGY PROJECTS

The following specific projects resulting from situations of opportunity have been initiated in the last seven months.

As the epidemic of Venezuelan equine encephalitis crossed the Mexican border and spread through Texas counties in July and August, 1971, as seen in Figure 2, NASA provided low and high altitude aerial photography and health experts trained in remote sensing to a cooperative program with the Public Health Service Center for Disease Control and the University of Texas School of Public Health at Houston.

Currently, detailed research is underway to determine the habitat of Culex quinquefasciatus, as seen in Figure 3, the mosquito vector of St. Louis encephalitis virus in the Houston area. Studies of this mosquito are indicative that in most cases, as seen in Figure 4, the habitat can be associated with effluent from septic tank overflow into collection ditches that are common in the Houston area because of the high water table and the soil conditions. These collecting ditches as

seen in Figure 5, constitute 1600 miles of collecting ditches in Harris County which run into larger ditches as seen in Figure 6, which all run into Galveston Bay.

NASA aircraft provided thermal scanner data, color infrared, color and multiband camera coverage over approximately 12 miles of these ditches containing septic water along Little York Road in north Houston.

As seen in Figure 7, ten test sites were surveyed for physical, chemical, microbiological and entomological characteristics at the time of the flight. This study is still underway.

A project in support of the U.S. Public Health Service Center for Disease Control, Atlanta, Georgia, was initiated in mid-July 1971. An explosive outbreak of anthrax caused the death of more than 500 cattle and numerous other animals in Ascension Parish, Louisiana. This applied research project uses remote sensing to determine the environmental conditions that are conducive to this soil-borne disease outbreak. NASA remote-sensing aircraft have been flown on missions over areas that are highly endemic for the disease.

Final spatial and numerical mortality data concerning the Ascension Parish Anthrax Project in Louisiana has just been received from the Public Health Service Center for Disease Control in Atlanta. This will be transferred as overlay information to color coded soils type map overlays as seen in Figure 8, to the special purpose semi-controlled color infrared mosaic being prepared by the Mapping Sciences Branch. The study has already revealed that essentially no deaths due to anthrax were observed in soil type 7, seen in orange at the northern part of the parish.

This investigation will permit correlative interpretation of NASA remote-sensing data of farms where anthrax exists. Color and color-infrared aerial photography of the epidemic area is now being analyzed in a retrospective epidemiologic study of this test site. The objective is to learn what determinants of anthrax infection can be detected and measured from the air so that aircraft may be used to rapidly evaluate potential for an anthrax outbreak or to determine the natural geographic or physical barriers of an epidemic.

High altitude color infrared aerial photography has been useful to scientists studying the habitat of endemic strains of Venezuelan encephalitis virus as seen in Figure 9, along the southern coast of Florida. It has been particularly difficult from the ground to determine the salt-water/fresh-water interface as seen in Figure 10, that provides the proper environment for vegetation hammocks in which encephalitis vector mosquitoes (Culex atratus) commonly breed.

Late in September a low altitude mission was conducted with the NP3A over a 200 acre test plot as seen in Figure 11, between Lakes Pontchartrain and St. Catherine northeast of New Orleans with color,

color infrared and multiband sensor and film combinations in a joint investigation of the feasibility of using remote sensing to recognize the ecological set necessary to produce salt marsh mosquito populations.

The New Orleans Mosquito Control Districts three years of baseline entomological, vegetative, aquatic, and meteorological data has shown certain heterogeneous vegetative communities to be empirically but strongly related to salt marsh mosquito populations. Heterogeneous vegetative communities are even difficult to assess using color infrared photography as seen in Figure 12.

Major botanical communities in the New Orleans Mosquito Control District Test Site area have been identified and inventoried and are now being compared with multiband photography which has been subjected to edge and color enhancement as a function of emulsion density.

The results of the mission are now being processed by several interpretive means. One of these methods is by simultaneously processing by electronic means three photographic negatives of the same view which records different wavelength portions of visible light. The process enhances the ease of identifying the different vegetative communities and very sharply delineates edge effects and community interfaces by assigning false colors to differentiate subtle density differences. Figure 13 shows the test site frame in the green band, Figure 14 in the red band, and Figure 15, in the near infrared band. As seen in Figure 16, only when the red band and the near infrared band are combined with decreasing density slices are the most subtle differences markedly observed which reveal even the most minor vegetative communities and interface differences.

The importance of this capability is recognized when one observes that approximately 90 percent of the production of Aedes sollicitans mosquito is dependent on the same ecological set that provides support for the Bacopa vegetative community in the New Orleans area.

NASA-S-72-577-X

SUPPORTING RESEARCH AND TECHNOLOGY

PUBLIC HEALTH ECOLOGY

VECTOR BORNE DISEASES	UNIV OF TEXAS SCHOOL OF PUBLIC HEALTH
PUBLIC HEALTH ASPECTS OF WATER DEGRADATION	UNIV OF TEXAS SCHOOL OF PUBLIC HEALTH
PUBLIC HEALTH ASPECTS OF AIR POLLUTION	UNIV OF TEXAS SCHOOL OF PUBLIC HEALTH
BIOENVIRONMENTAL FACTORS OF DISEASE AND HEALTH CONDITIONS	UNIV OF WEST FLORIDA

Figure 1.- Effort to develop a university sector applied research program into those public health problems which might be most amenable to solution by the application of remote sensing technology has resulted in the contracts in the above areas.

Figure 2.- As the epidemic of Venezuelan equine encephalitis crossed the Mexican border and spread through Texas counties in July and August, 1971, NASA provided low and high altitude aerial photography over a test site in the Flour Bluff section of Corpus Christi, Texas. This activity supported a cooperative program with the Public Health Service Center for Disease Control and the University of Texas School of Public Health at Houston.

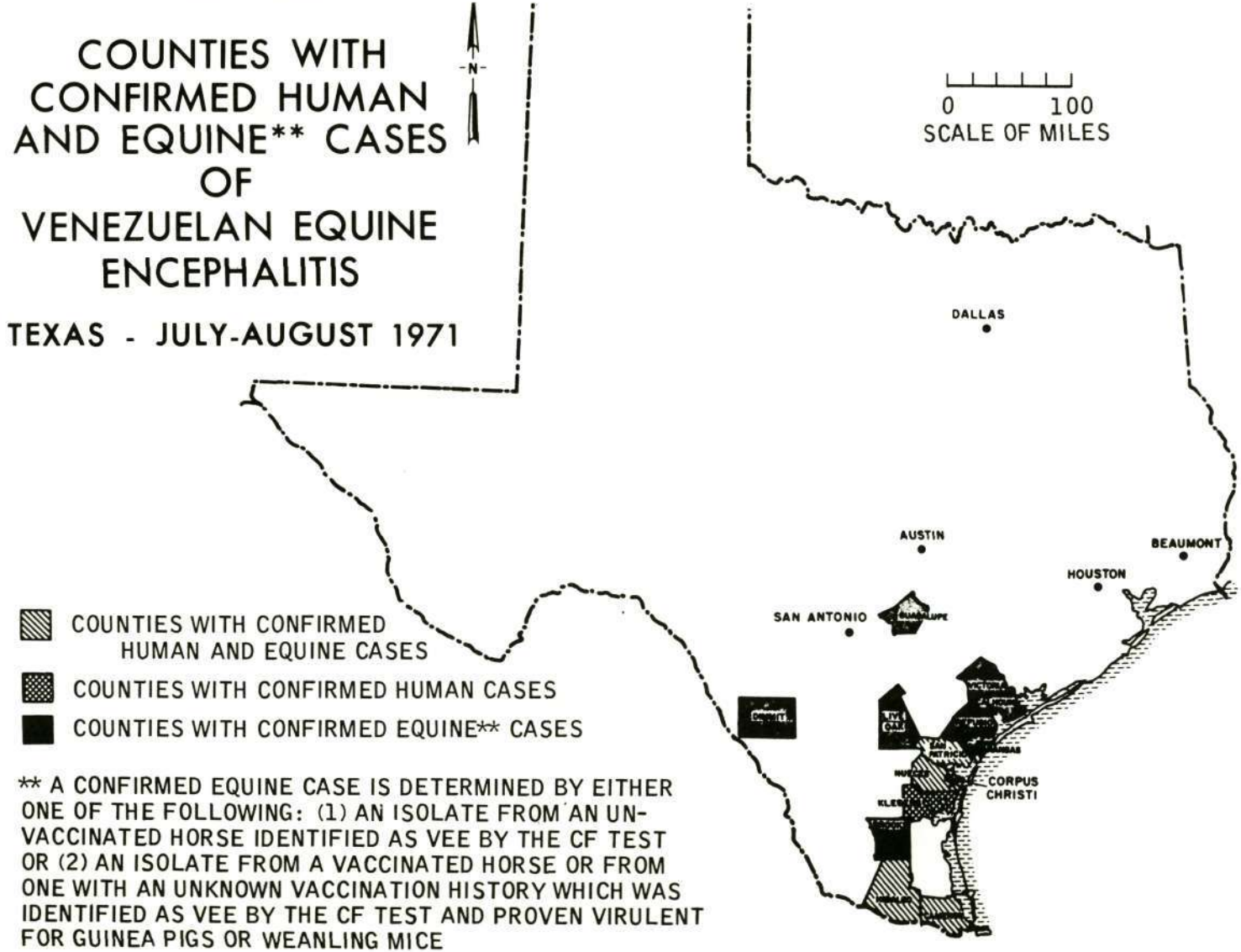

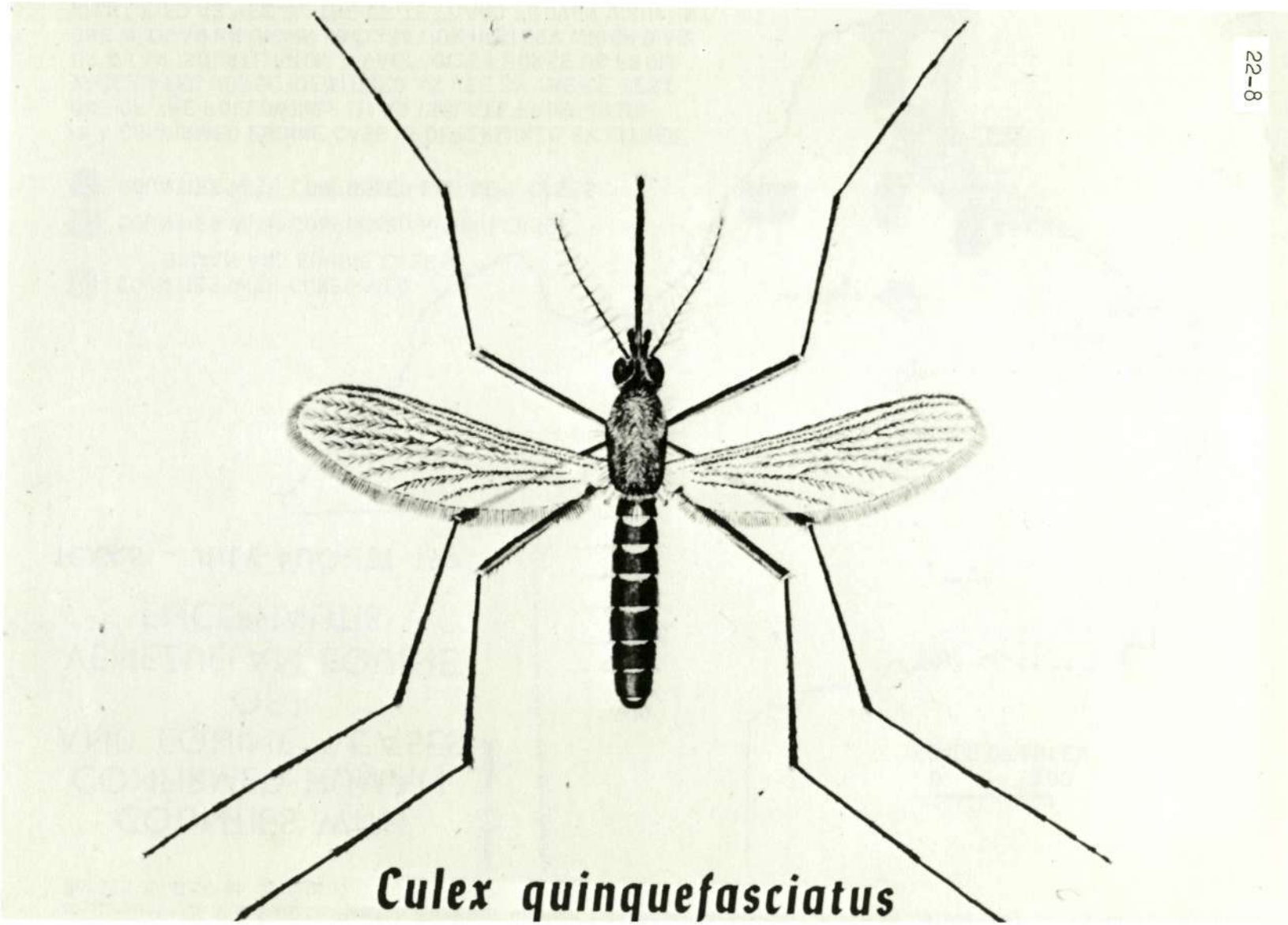

Figure 3.- Culex quinquefasciatus is the mosquito vector of St. Louis encephalitis virus in the Houston area. This mosquito which breeds almost entirely in ditches which contain effluent from septic tanks in the Houston area, caused an epidemic of St. Louis encephalitis in 1964. Control of this disease vector is mandatory.

NASA
S-71-25437

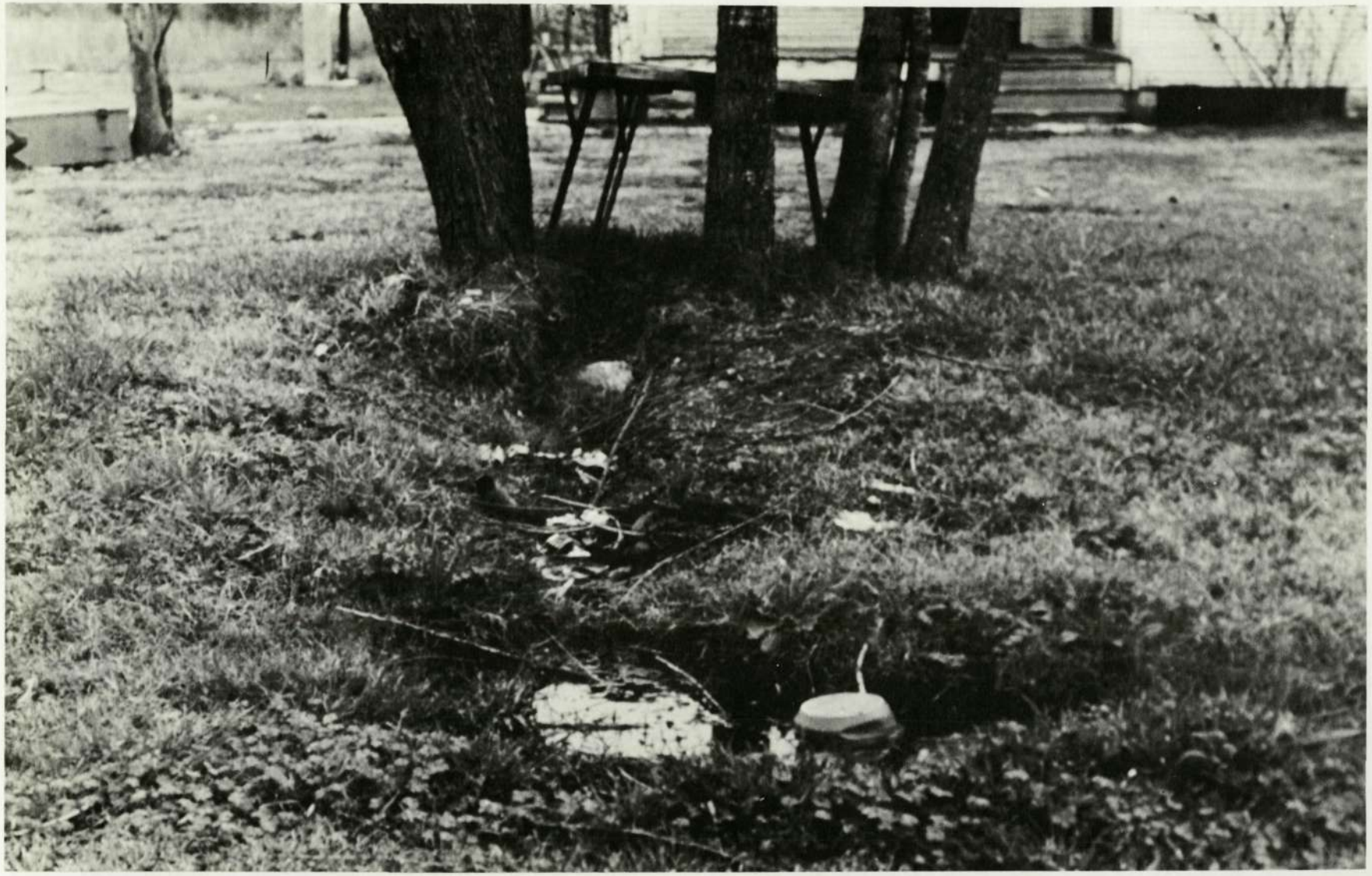

Figure 4.- The effluent from septic tanks in thousands of adjacent homes, unable to percolate thru the hard pan, flows thru pipes to openings near these collecting ditches. In this figure we see septic tank effluent running from a pipe opening in front of the trees in the front yard of this house.

NASA
S-71-38225

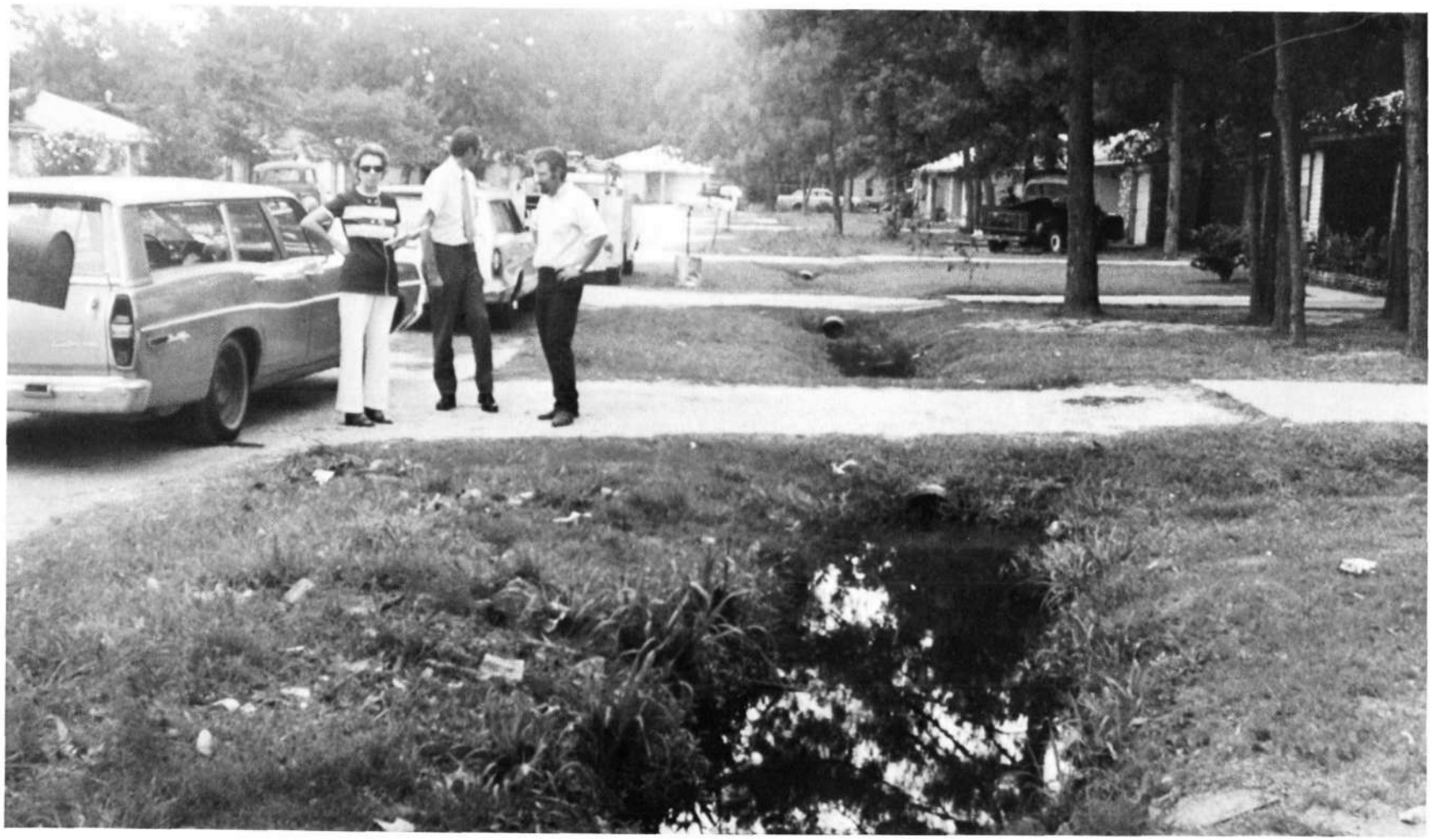

Figure 5.- This collecting ditch is representative of some 1,600 miles of collecting ditches in Harris County. Approximately $900,000 are required each year to find and control Culex quinquefasciatus larvae in Harris County, Houston, Texas.

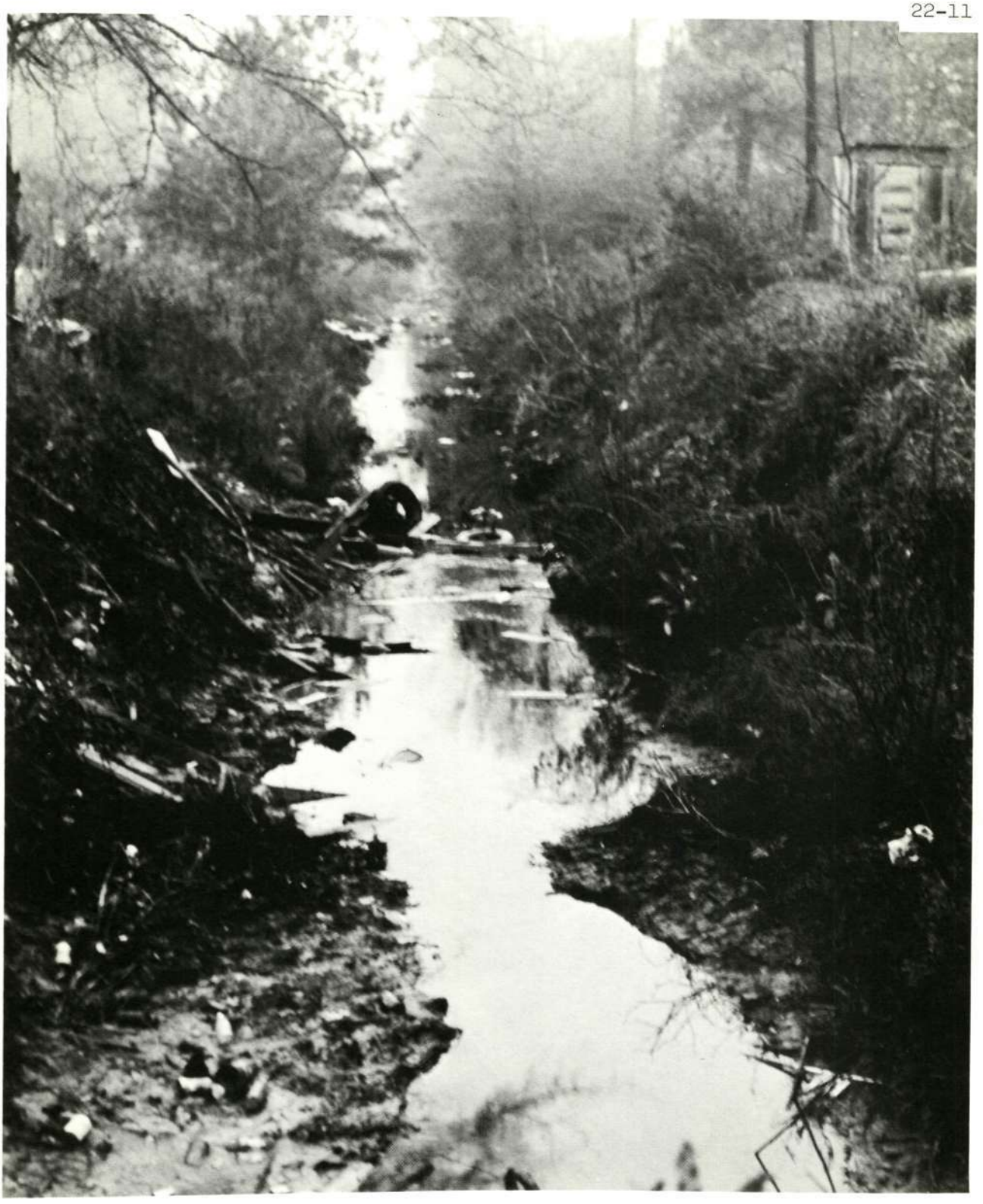

NASA
S-71-25435

Figure 6.- Large ditches such as seen here collect the run off from ditches seen in Figure 5, and channel it to courses which eventually reach Galveston Bay. Culex mosquitoes breed in these larger courses as well as smaller ones provided they contain organic wastes.

NASA
S-71-38217

Figure 7.- A laboratory technician is seen collecting water samples from one of ten test sites near Little York Road in north Houston, Texas. These samples taken at the time of overflight were surveyed for physical, chemical, microbiological and entomological characteristics.

Figure 8.- Color coded soils type map overlays of Ascension Parish, Louisiana, as seen here, as well as mortality, morbidity, soil pH, and soil anthrax organism identification data, will be compared with special purpose semi-controlled infrared mosaics being prepared from data obtained in September 1971, by the NASA NP3A aircraft. This investigation will permit correlative interpretation of NASA remote sensing data with epidemiologic data.

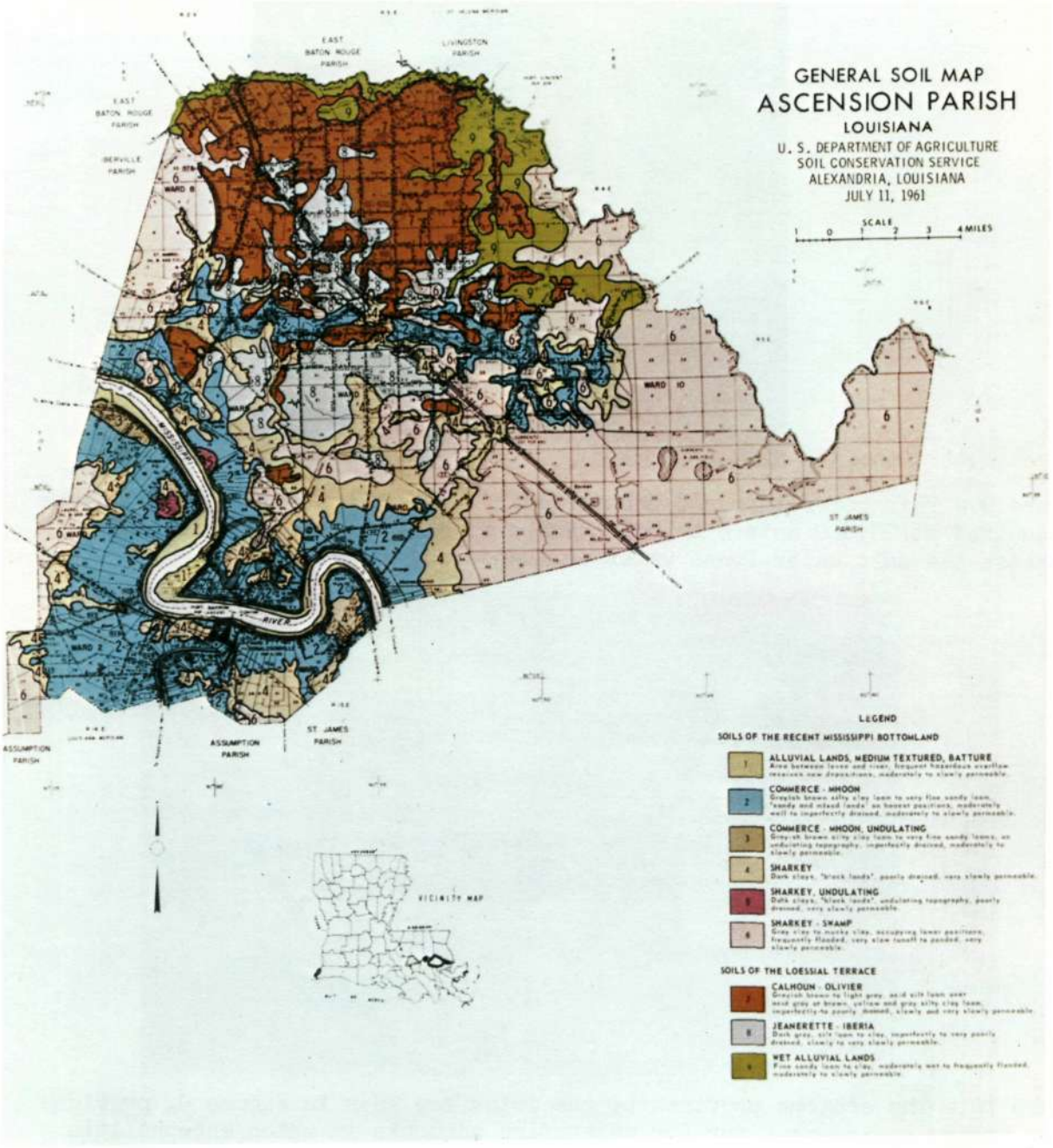

Figure 9.- This color infrared photograph of the south Florida littoral zone acquired at 20,000 meters by NASA remote sensing aircraft readily illustrates the salt water-fresh water influence and interface.

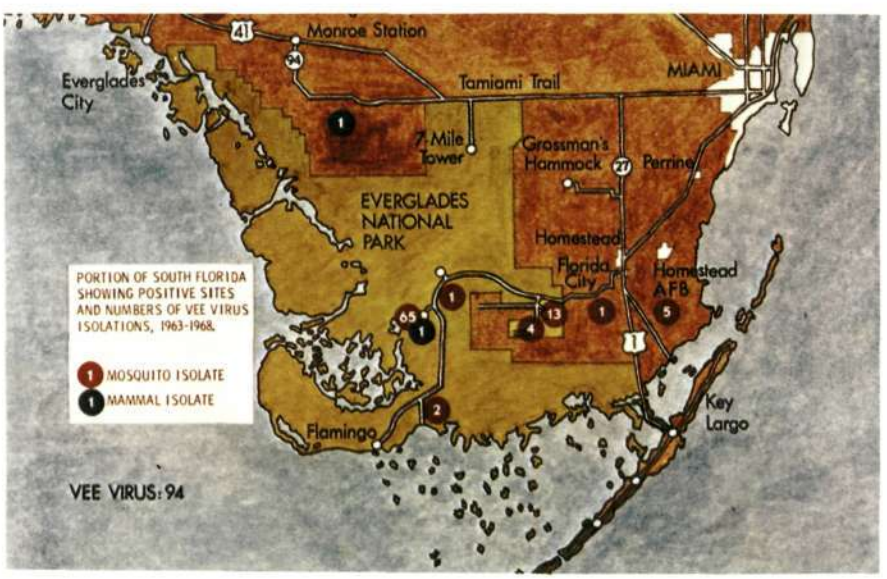

Figure 10.- The ecotone provided by the interface seen in Figure 9, provides the proper environment for for vegetation hammocks in which encephalitis vector mosquitoes (Culex atratus) commonly breed.

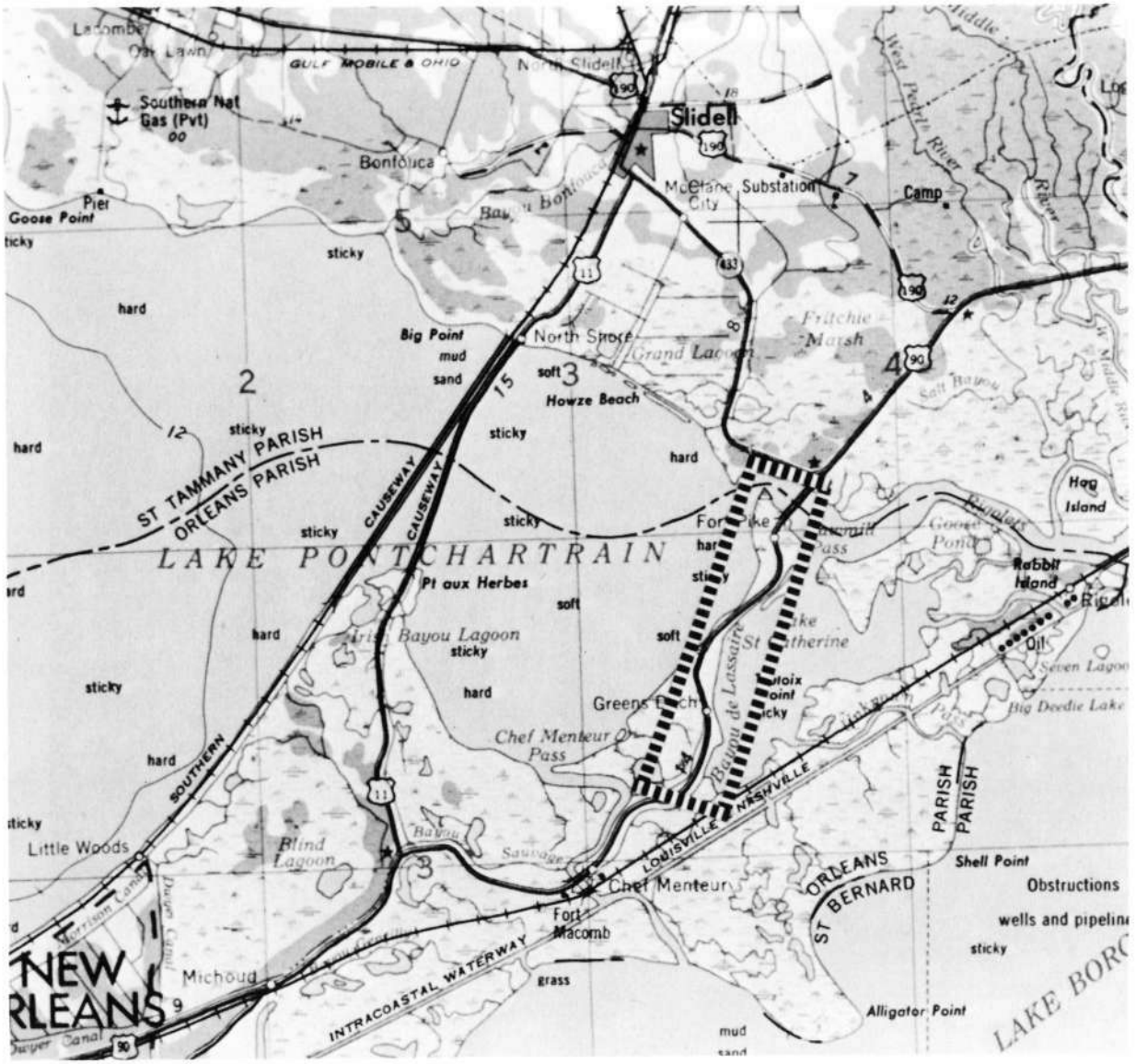

Figure 11.- The area outlined between Lakes Pontchartrain and St. Catherine includes a 200 acre test site of the New Orleans Mosquito Control District. Three years of baseline entomological, vegetative, aquatic and meteorological data has been acquired by that group.

Figure 12.- This color infrared photograph acquired from ektachrome color infrared 2443 film from 770 meters with the NASA NP3A aircraft, illustrates approximately 100 acres of the 200 acre New Orleans Mosquito Control District test site. Several vegetation types can be observed.

Figure 13.- This photograph was acquired from the display of the I^2S Multiband Camera Film Viewer (MCFV) which electronically processed the 2402 black and white film exposed by the KA-62 multiband cameras of the test site. This particular camera recorded the green band. False color assignment and edge enhancement have been accomplished for this band as seen here.

Figure 14.- This photograph, acquired by the same means as that seen in Figure 13, was derived from the KA-62 multiband camera that exposed the 2402 film in the red band.

Figure 15.- This photograph acquired by the same means as that seen in Figures 13 and 14, was derived from the multiband camera that exposed the 2402 film in the near infrared band.

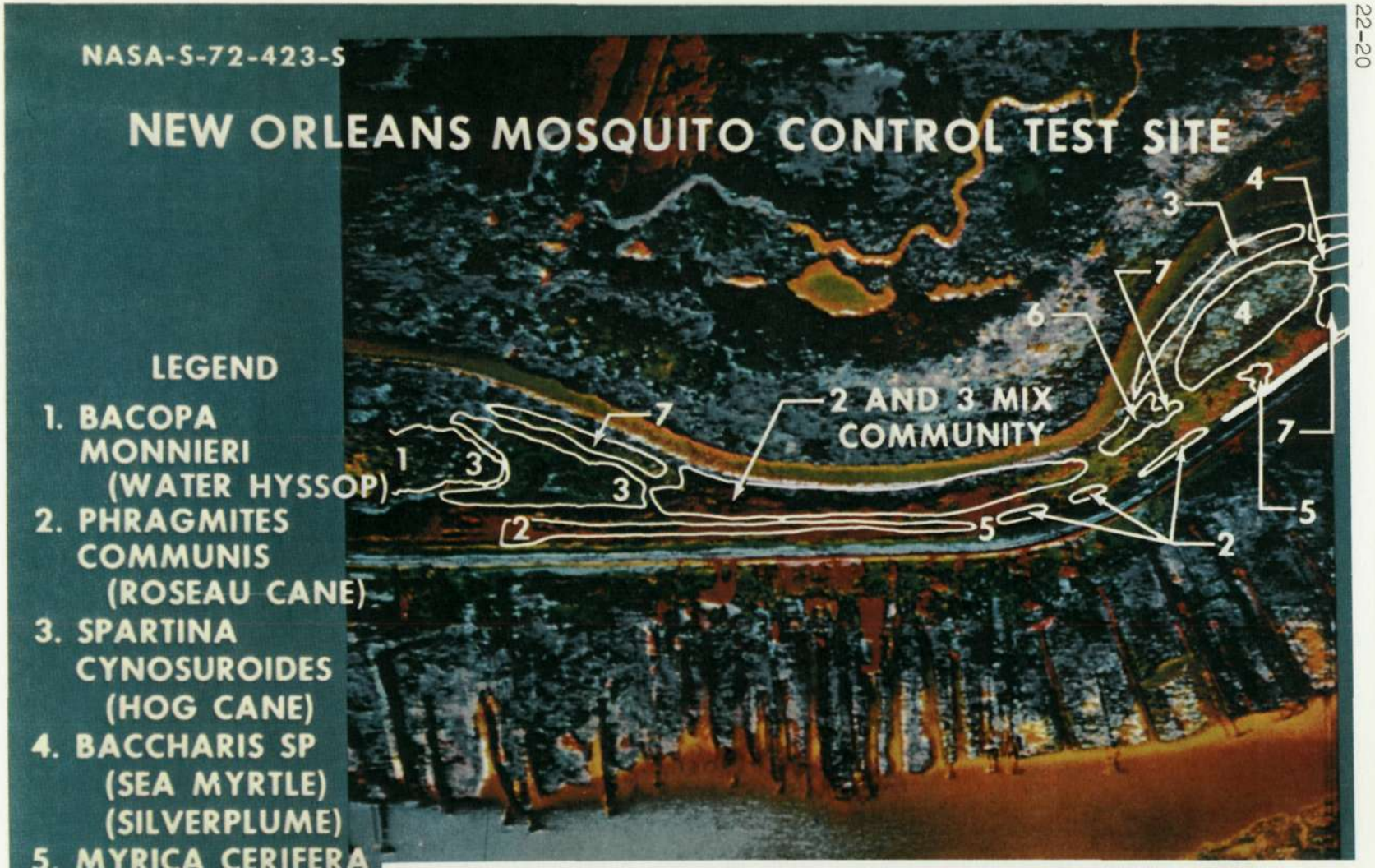

Figure 16.- This photograph acquired by the same means as the preceeding three, was derived by adding the red and near infrared bands. This process enhances the ease of identifying the different vegetative communities and sharply delineates edge effects and community interfaces by assigning false colors to differentiate subtle density differences.

SECTION 23

A BREADBOARD HYBRID MULTISPECTRAL PROCESSING SYSTEM

by Donald Hayden

ABSTRACT

(Not available)

CONSTRUCTING AND MANIPULATING COLOR IMAGERY FROM DIGITAL DATA

by

J. E. Davis, C. A. Helmke, T. R. Kell, M. J. Arldt, E. L. Wilson
Lockheed Electronics Company, Inc.
Houston, Texas

INTRODUCTION

The University Centers of Excellence were the leaders in the development of airborne scanner systems, the related data processing and the application of this data. When the Earth Observations Division at the Manned Spacecraft Center decided to use airborne scanners, much of the technology resulting from the work at these centers was utilized. One of the more significant areas in thich this technology was advanced by MSC was in the development of more sophisticated Data Analysis Station (DAS) Equipment which allows complex manipulation and subsequent idsplay of the sensor output. A major consideration for the new DAS was to have an interactive system which would aid investigators, who were not computer oriented, in examining the data.

EQUIPMENT

The Bendix Corporation developed the 24 band multispectral scanner system (MSS) and a DAS (Fig. 1) which are now at MSC. A second DAS (Fig. 2) was developed by Aerojet General primarily for use with the Passive Microwave Imaging System (PMIS). The manufacturers of these two DAS supplied both the hardware and the software for these systems. The following is a listing of the basic units which make up the DAS's. Some of these units are shared between the two systems.

a. An Ampex FR1900 14-track wide-band tape unit.

b. An ASR-33 teletypewriter.

c. A Systems Engineering Laboratories 810B computer with 16K word memory, 2 digital tape controller units and 3 separate digital magnetic tape units.

d. An operator console containing a color display device.

e. A multi-bay rack assembly containing a 9 inch strip film recorder and system control logic.

f. A 1000-line-per-minute line printer.

g. A 600-card-per-minute card reader.

h. An 800 character numeric display terminal which can be used interactively with the system.

FUNCTIONS OF DAS

Figure 3 shows the MS DAS console and Figure 4 is of the PMIS DAS console with the interactive display terminal on the right. Figure 5 shows how sensor data is processed in the DAS to cut down on the volume of data being handled by the large scale computers. Data from these larger computers comes back to the DAS for display and film recording. The DAS is used to perform the following functions on scanner data:

1. Editing of flight tapes by transferring to 9 track tape only that portion of the data to be studied in detail. Training sample selection is a practical application of editing.

2. Screening flight tapes (or other processed tapes) by creating black and white or color imagery on the T.V.

3. Producing hard copy in the form of film transparencies in color or black and white.

4. Outputting data on the line printer.

Item 2 is the principle part of the discussion in this paper.

After the analog PCM tape from the scanner has been read a tape interface unit converts this to digital data and it is input to the computer. Figure 6 shows how the computer can then convert the sensor based data to color signal data using any of a number of algorithms designed for this purpose. The DAS system then records this processed data on a disc after going through a buffer unit. The disc then feeds the T.V. display through the digital to analog converter.

DATA FORMAT

MS DAS

On the MS DAS the software algorithms must produce color signal data in the format required by the disk. The format is a 5-bit word which allows for 32 distinct values (0-31). The relative intensity of a particular color signal is dictated by the 5-bit color signal word. A word of all zeros produces no signal for that color while a word of all 1's produces a maximum intensity. Values between 0 and 31 produce a proportional brightness. Thus at each addressable element on the T.V., the data stored on the disk controls the color presentation by specifying the intensity of each of the three colors. Since the disk holds one T.V. frame of data each new scan line that is sent to the disk replaces the oldest scan line. The vertical synchronization signal is adjusted automatically so that the new data appears at the top of the screen. This creates a moving scene effect as would be experienced while looking downward through an aircraft window. The rate at which the scene appears to move past the window is determined by the speed at which the computer formats new lines and sends them to the disk.

PMIS DAS

The method used by the PMIS DAS is somewhat different but uses the same principle. A major difference is that while the MS DAS provides for 32 possible intensities for each color the PMIS DAS provides for 16 levels of green, eight of red and four of blue. This seems to be about as many levels as the eye can distinguish as shown in Figure 7.

DATA SOURCES

Many data sources suitable for color imagery on the DAS are now available or in development. The DAS requires that the data be on either a 14 track PCM tape compatible with the Ampex FR1900 or on a 9-track 800 BPI digital tape. Data recorded on other types of tapes must be converted. Analog tapes for example, must be digitized before coming to the DAS. To date, color imagery has been generated from the Bendix 24 channel scanner and from RS14 Infrared Scanner data digitized at MSC. In addition, aerial photos have been digitized on a microdensitometer and subsequently displayed.

COLOR IMAGE CONSTRUCTION

MSDAS

Three specific algorithms are used when processing data with the MS DAS. All of these algorithms are based on a function which is a linear combination of the data channels. This function is called linear transformation (LT) and is of the form:

$$LT = A_0 + A_1C_1 + A_2C_2 + \cdots\cdots A_{24}C_{24}$$

where A's are coefficients and the C's represent sensor values of the designated channels.

One algorithm is called Normal Linear Transformation and is simply three separate linear transformations where the intensity for a CRT gun (I) is proportional to the linear transformation LT

I_R proportional to LT_1

I_G proportional to LT_2

I_B proportional to LT_3

Figure 8 is an example of outputs from this time manipulation. The red display, is of a thermal IR channel (9.3-9.8 μm) from the 24-band scanner. The green display, Figure 9, is of a near IR channel (1.18-1.30 μm) and the blue display, Figure 10, is of the blue channel (.46-.50 μm). Figure 11 shows the combined display. Figure 12 shows one channel of data using a linear transformation to get different intensities of blue. Figure 13 shows this same channel of data after the table of color codes has been applied to the different signal levels.

Another algorithm is called Contrast Enhancement. This algorithm uses only 1 linear transformation. Theresult of the linear transformation is then used as an index to a table of pre-defined color codes.

I_R = RED (LT) i.e. the LTth RED value

I_G = GREEN (LT)

I_B = BLUE (LT)

Figure 12 shows one channel of data using a linear transformation to achieve different intensities of blue. Figure 13 shows this same channel of data after the table of color codes has been applied to the different signal levels.

A third algorithm is called Linear Discriminant. It uses three linear transformations but the intensities are either zero or the maximum depending upon whether the result of the transformation meets a given threshold

$I_R = 0$ if $LT_1 < THRESH_1$ $\quad I_R = 31$ if $LT_1 \geq THRESH_1$

$I_G = 0$ if $LT_2 < THRESH_2$ $\quad I_G = 31$ if $LT_2 \geq THRESH_2$

$I_B = 0$ if $LT_3 < THRESH_3$ $\quad I_B = 31$ if $LT_3 \geq THRESH_3$

Figures 14 (9.3-9.8 m), 15 (1.18-1.30 m), and 16 (.46-.50 m) show data which is above the treshold for these three channels. Figure 17 shows the combined display. White is produced when all 3 channels exceed the treshold. When only the red and green channels exceed this limit yellow is displayed. Where blue and red exceed the limit magenta results and when blue and green exceed the limit the cyan portion of the image (oil tanks) is shown.

PMIS-DAS

The PMIS DAS is used with a program called Color Study which is similar to Contrast Enhancement. The user can very easily define his own color tables with the numeric display terminal. The PMIS scanner had not been flown at the time this paper was written and so none of the data was available for publication. Data from other sensors has been displayed on this DAS in the absence of PMIS data.

Figure 18 shows 2 color charts made up on the interactive console for the Color Study program. The bottom portion shows all 512 possible colors which may be called upon to generate a color chart.

The data for the image in Figure 19 came from digitizing the two analog channels of the RS14 infrared scanner (3.0-5.5 μm and 8-14 μm). The channels are displayed side by side using the same color chart for each. Thus the color differences shown represent actual signal differences between the two channels.

Figure 20 is another example of imagery using the Color Study program. The data was obtained by digitizing infrared color film with a microdensitometer and recording on tape.

The imagery in Figure 21 was produced by a simulation study of temperatures in Trinity Bay. Figure 22 represents the same input data applied to a different color chart.

SUMMARY

The comparison of Figures 21 and 22 adequately demonstrate how much easier it is to distinguish different colors than it is to distinguish shades of grey or in this case shades of green.

All of these examples show what a capable and flexible tool for principle investigators the DAS is and how it can be applied to a large variety of sensors.

Future plans call for processing data from sensors such as the PMIS, the Scanning Imaging Spectroradiometer (SIS), the Skylab S-192 multispectral scanner, and the ERTS systems.

FIGURE LEGENDS

Figure 1

Figure 2

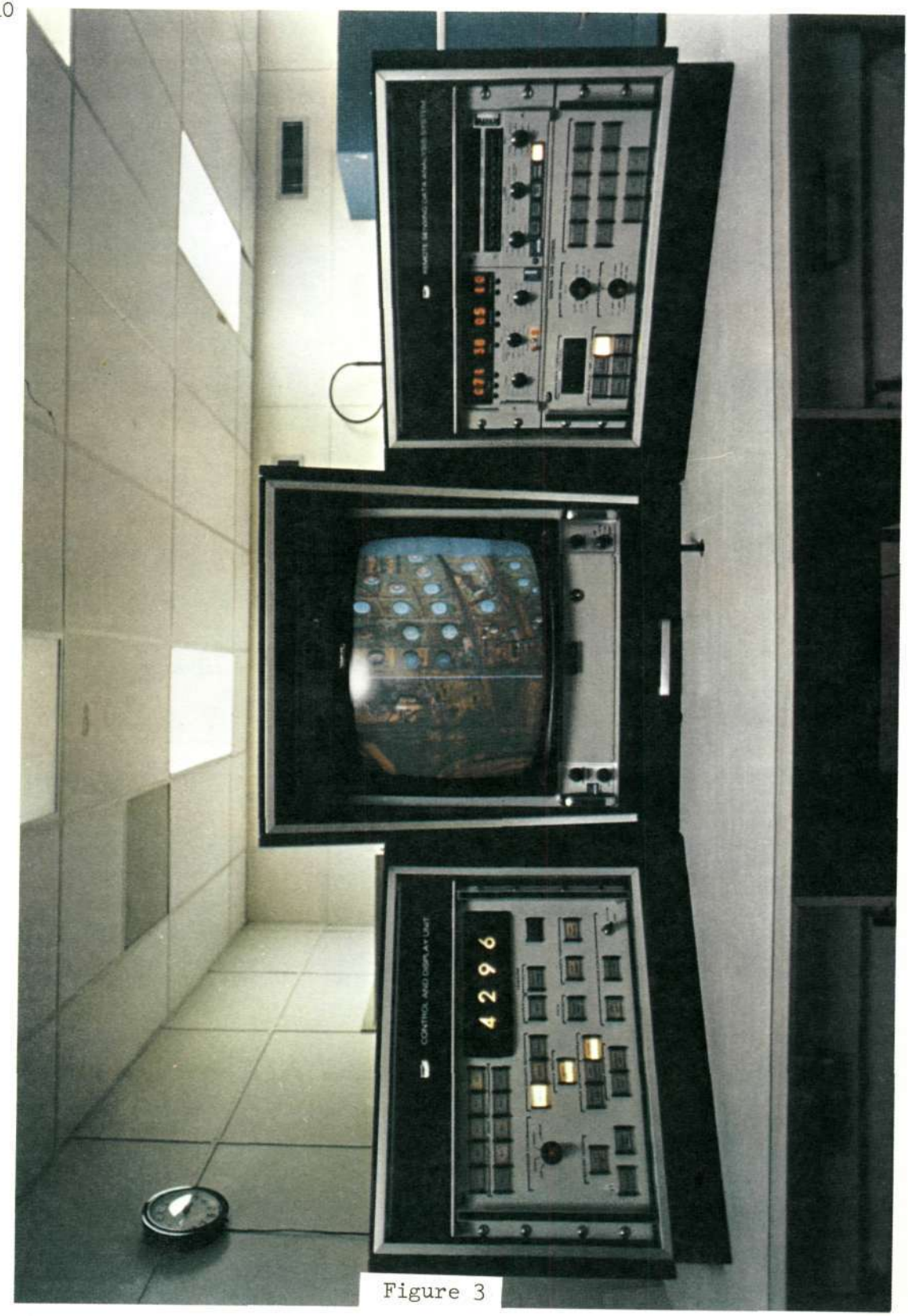

Figure 3

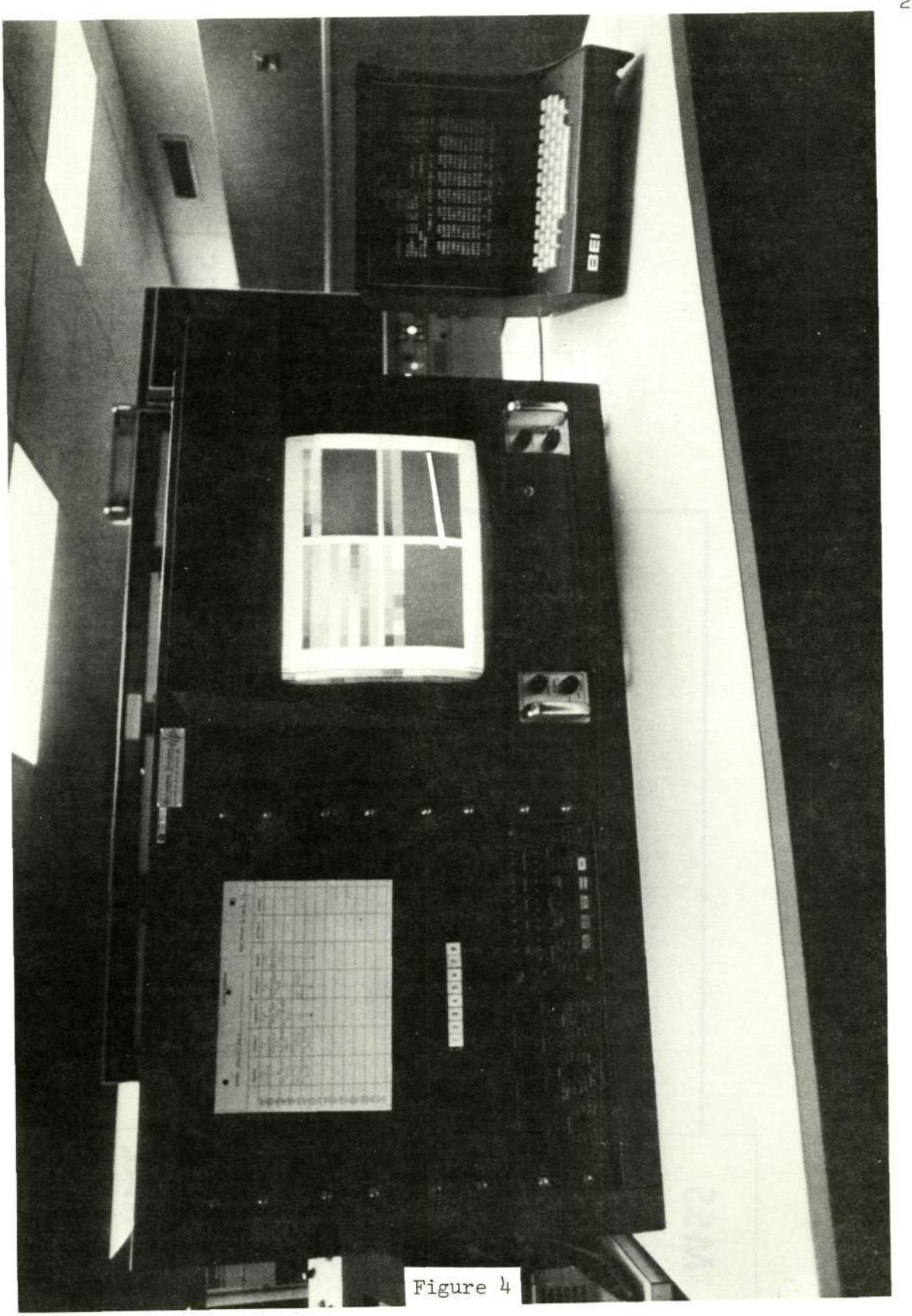

Figure 4

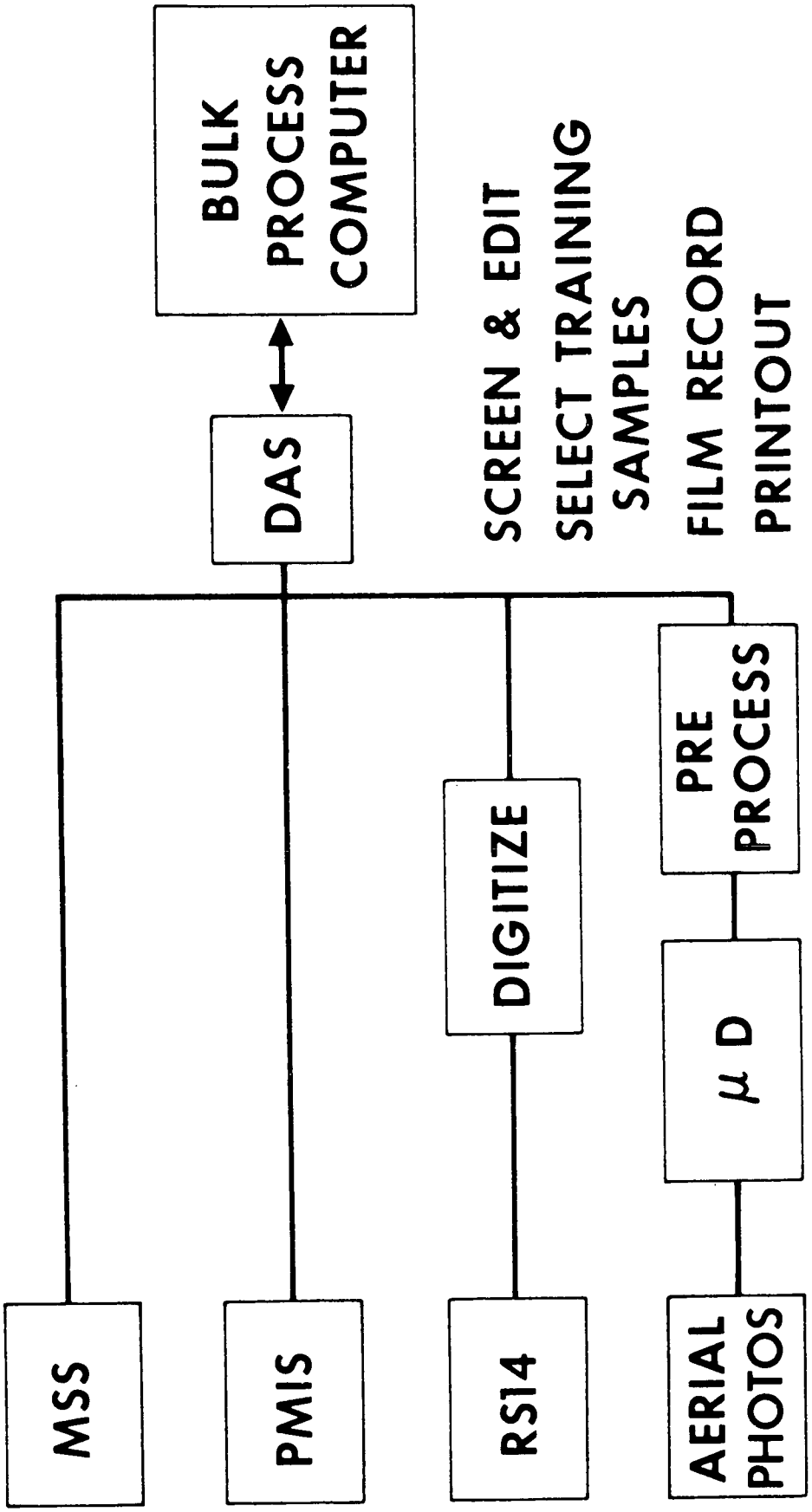
BULK PROCESS COMPUTER
DAS
SCREEN & EDIT
SELECT TRAINING SAMPLES
FILM RECORD PRINTOUT
MSS
PMIS
DIGITIZE
PRE PROCESS
μ D
RS14
AERIAL PHOTOS

Figure 5

DAS DATA FLOW

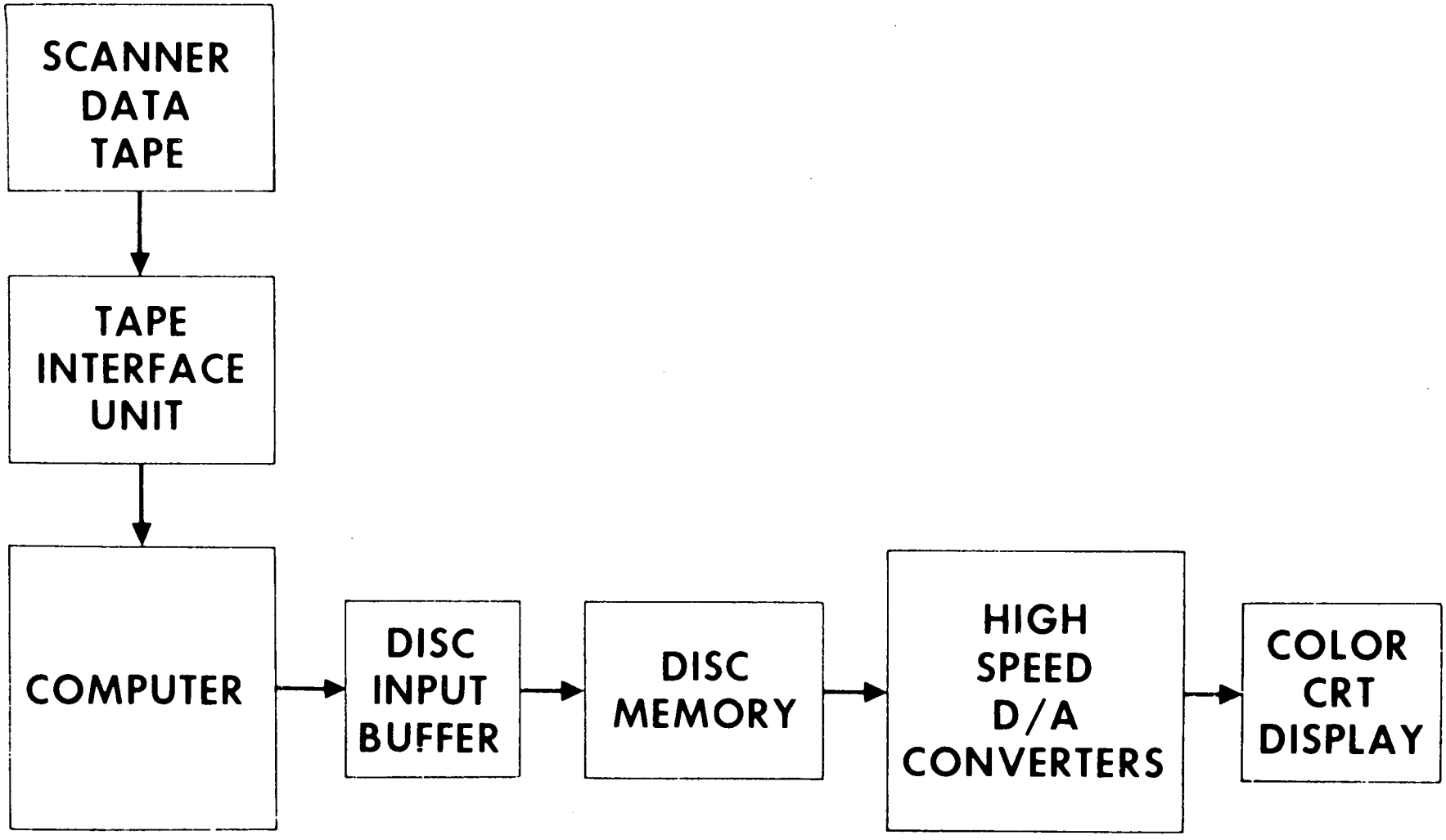

Figure 6

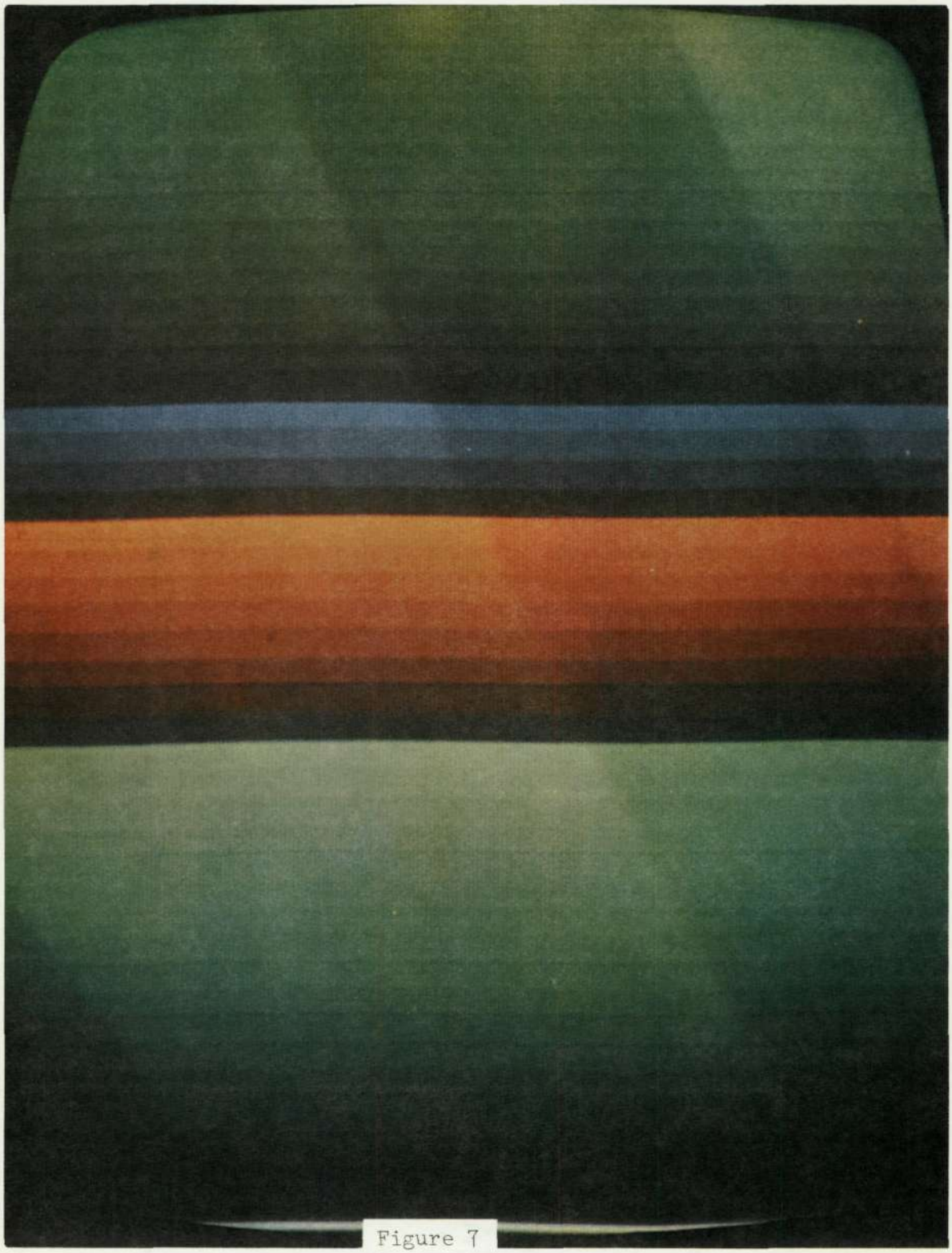

Figure 7

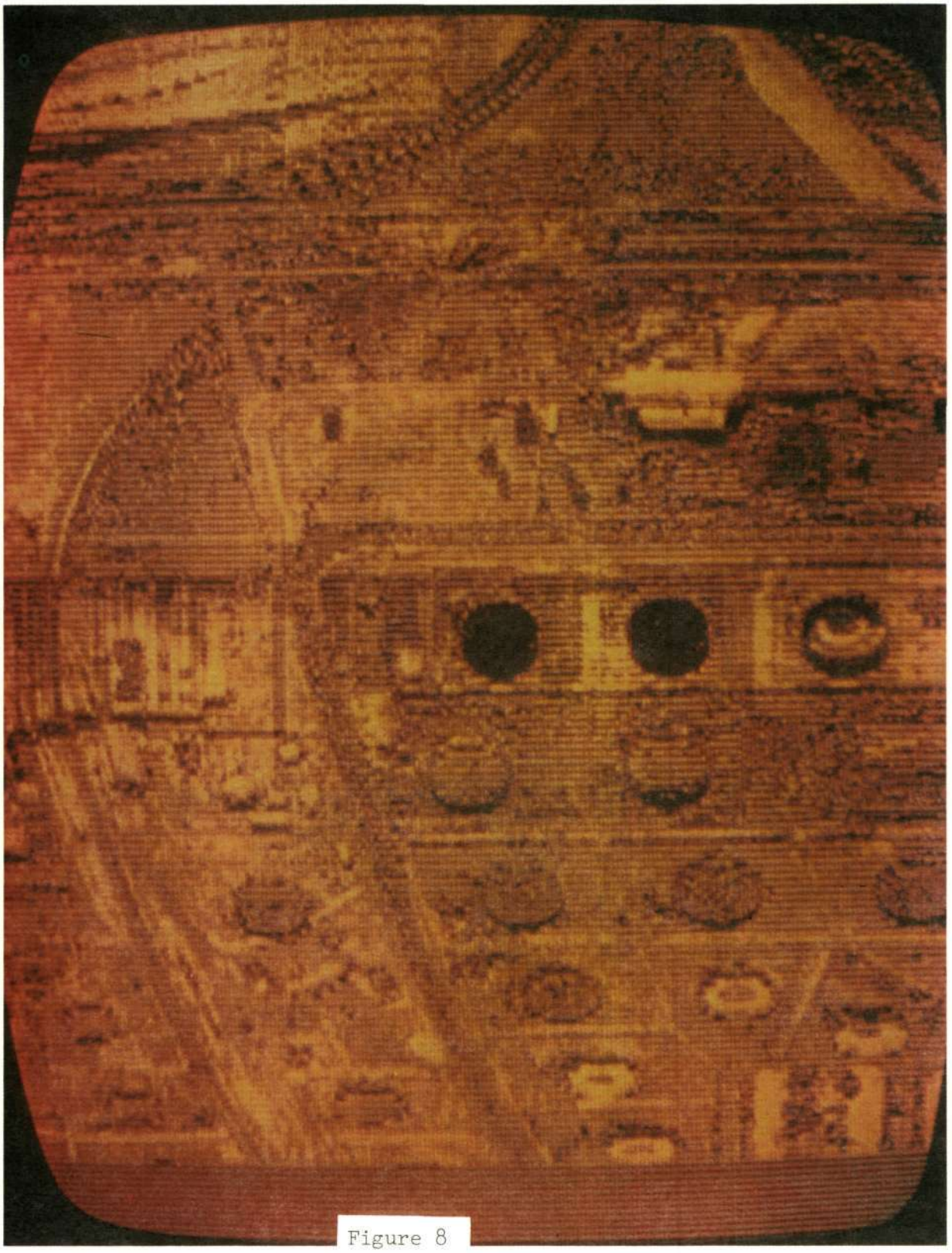

Figure 8

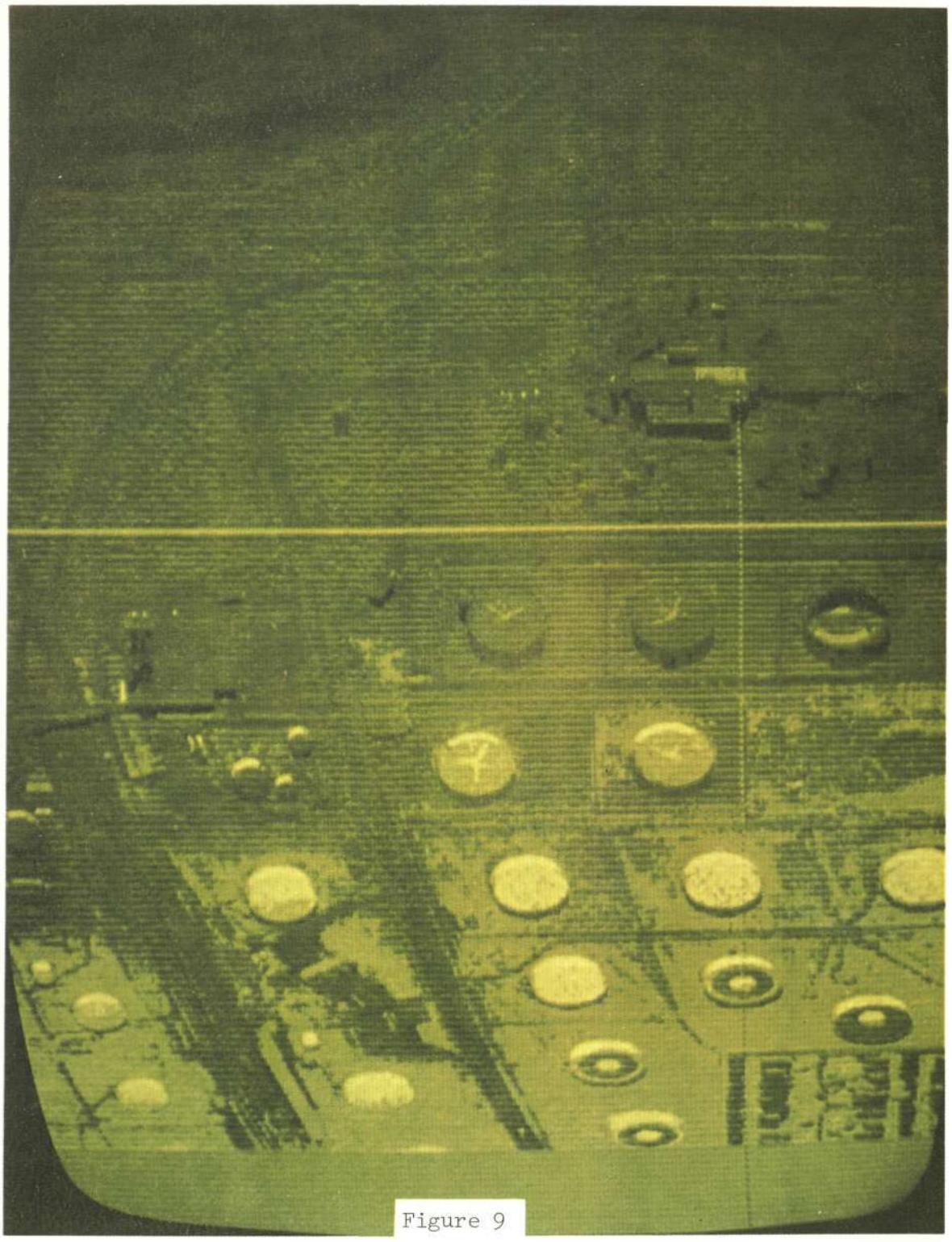

Figure 9

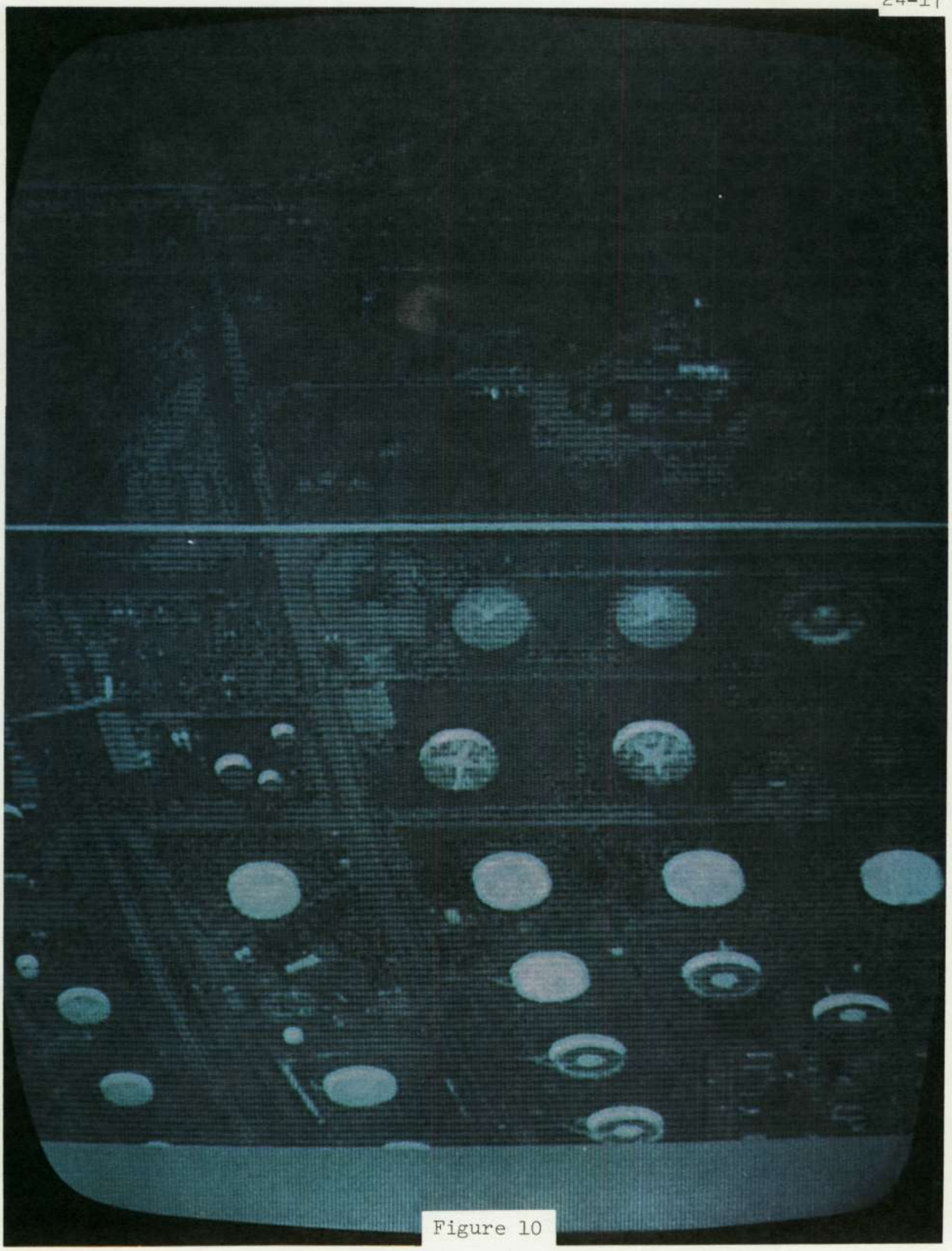

Figure 10

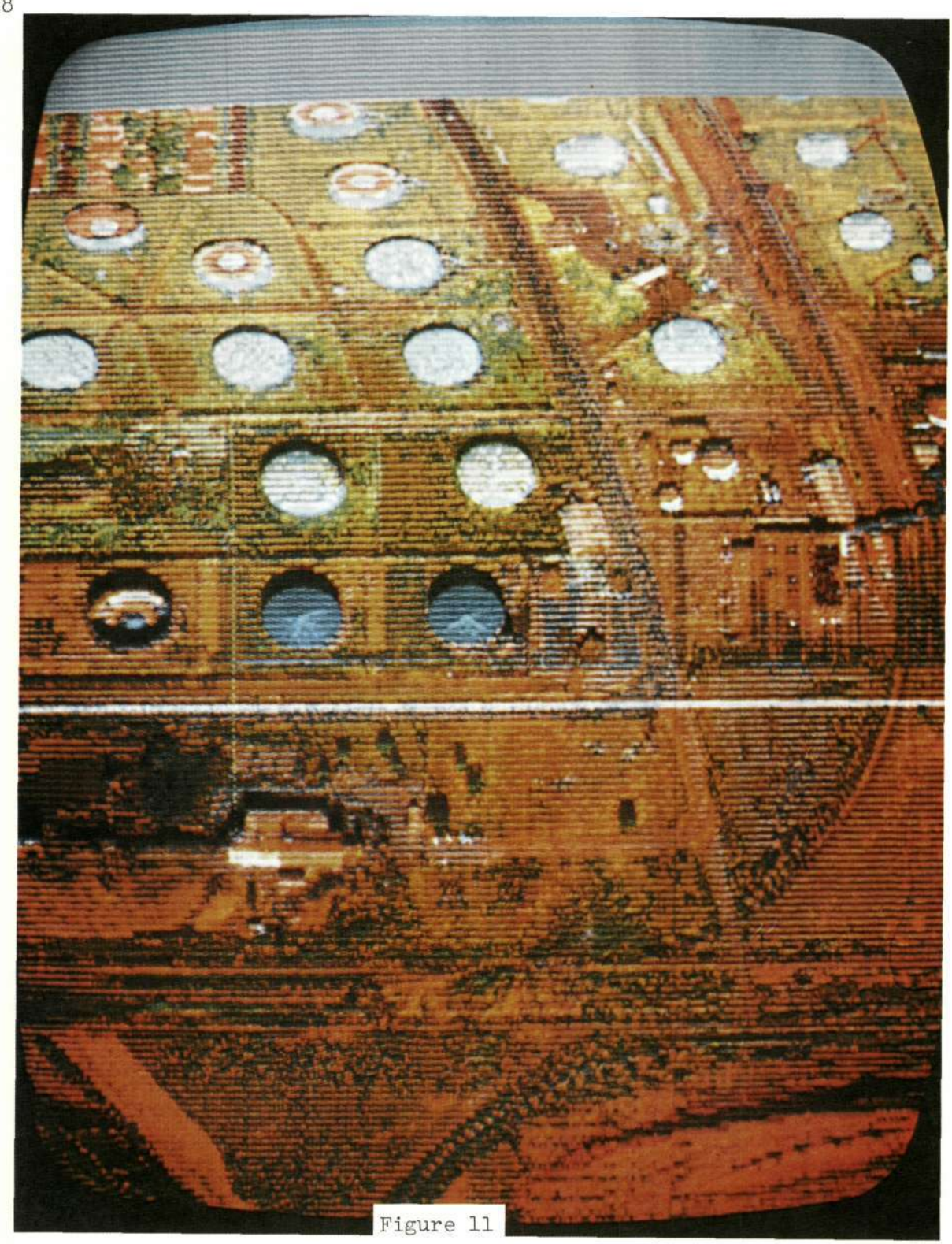

Figure 11

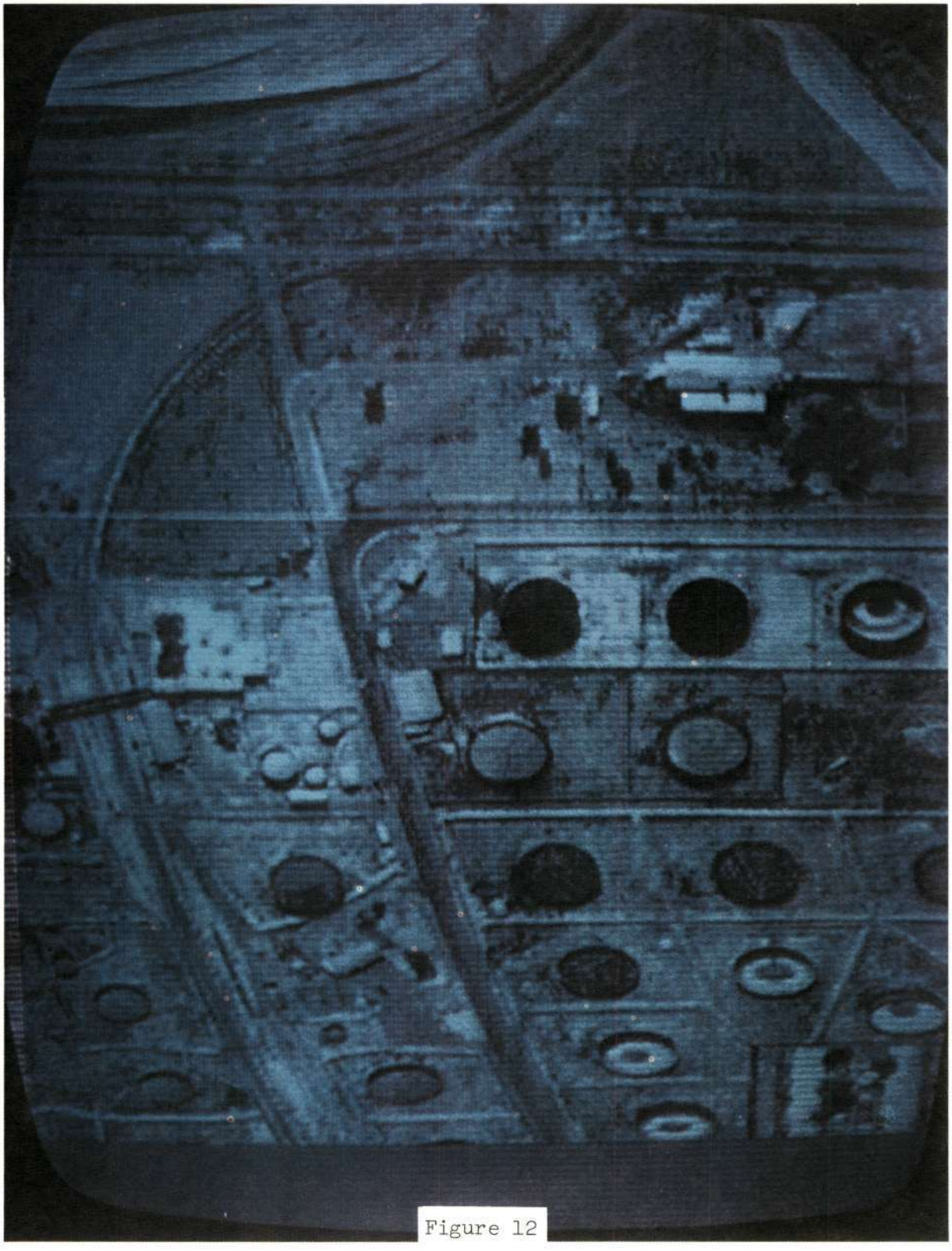

Figure 12

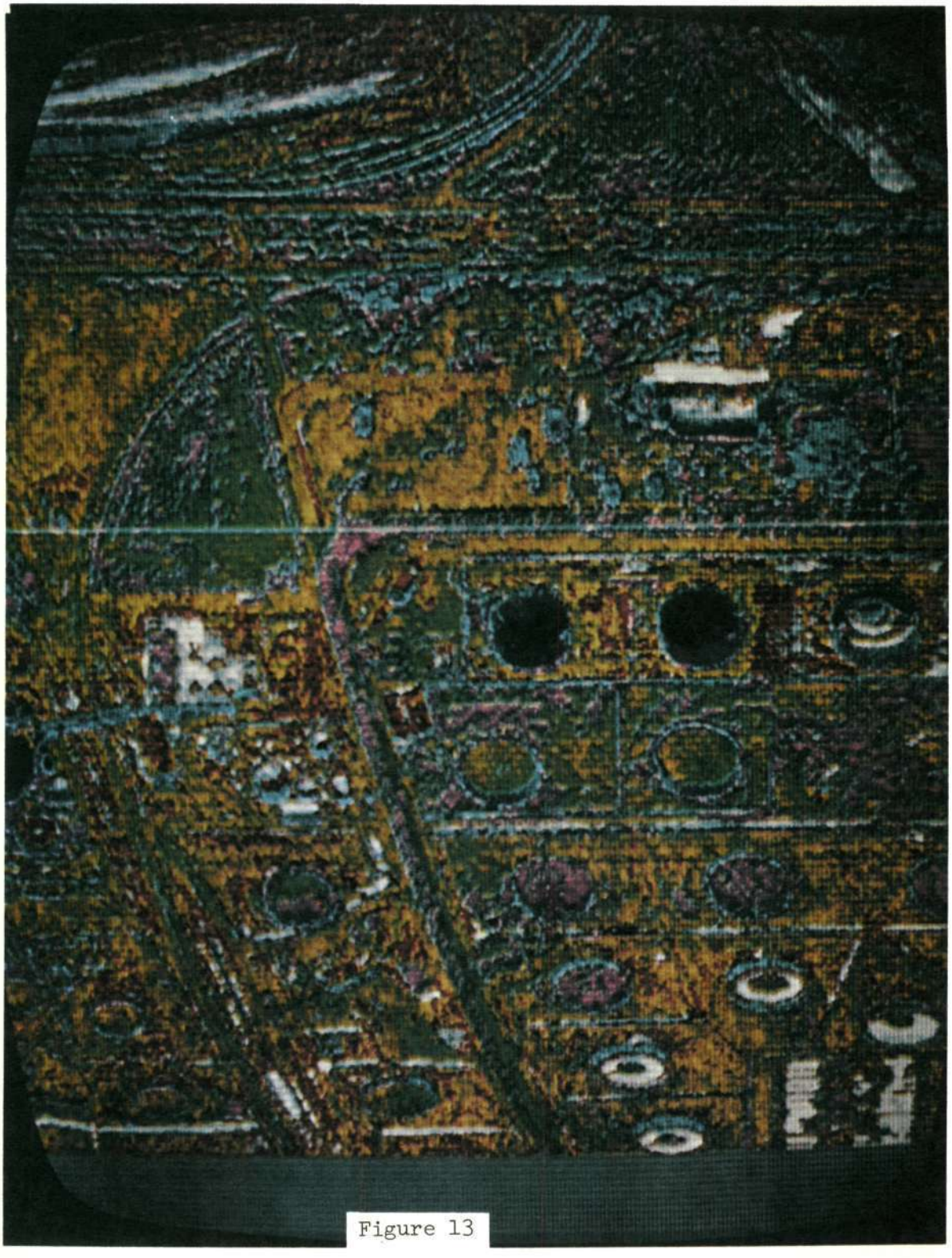

Figure 13

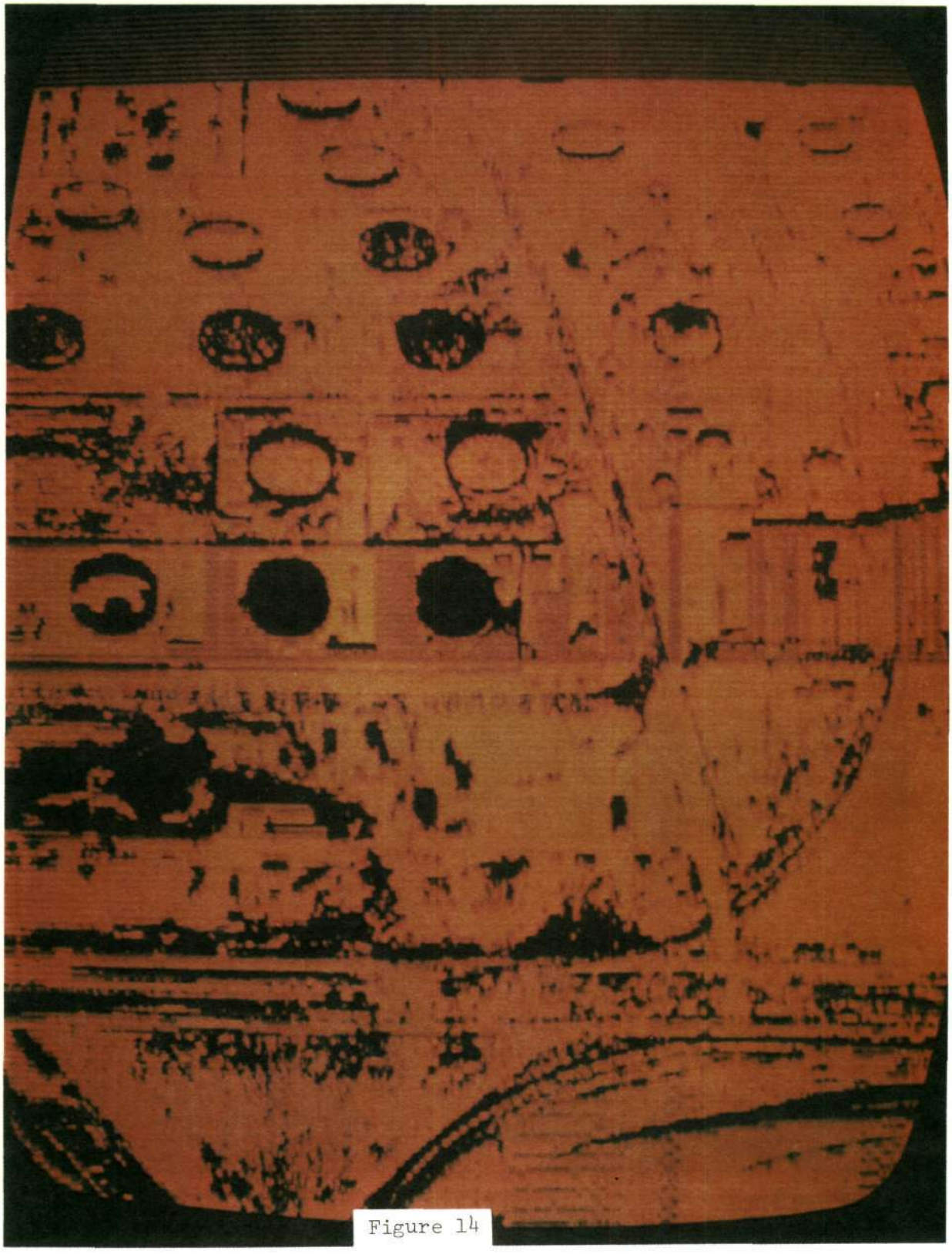

Figure 14

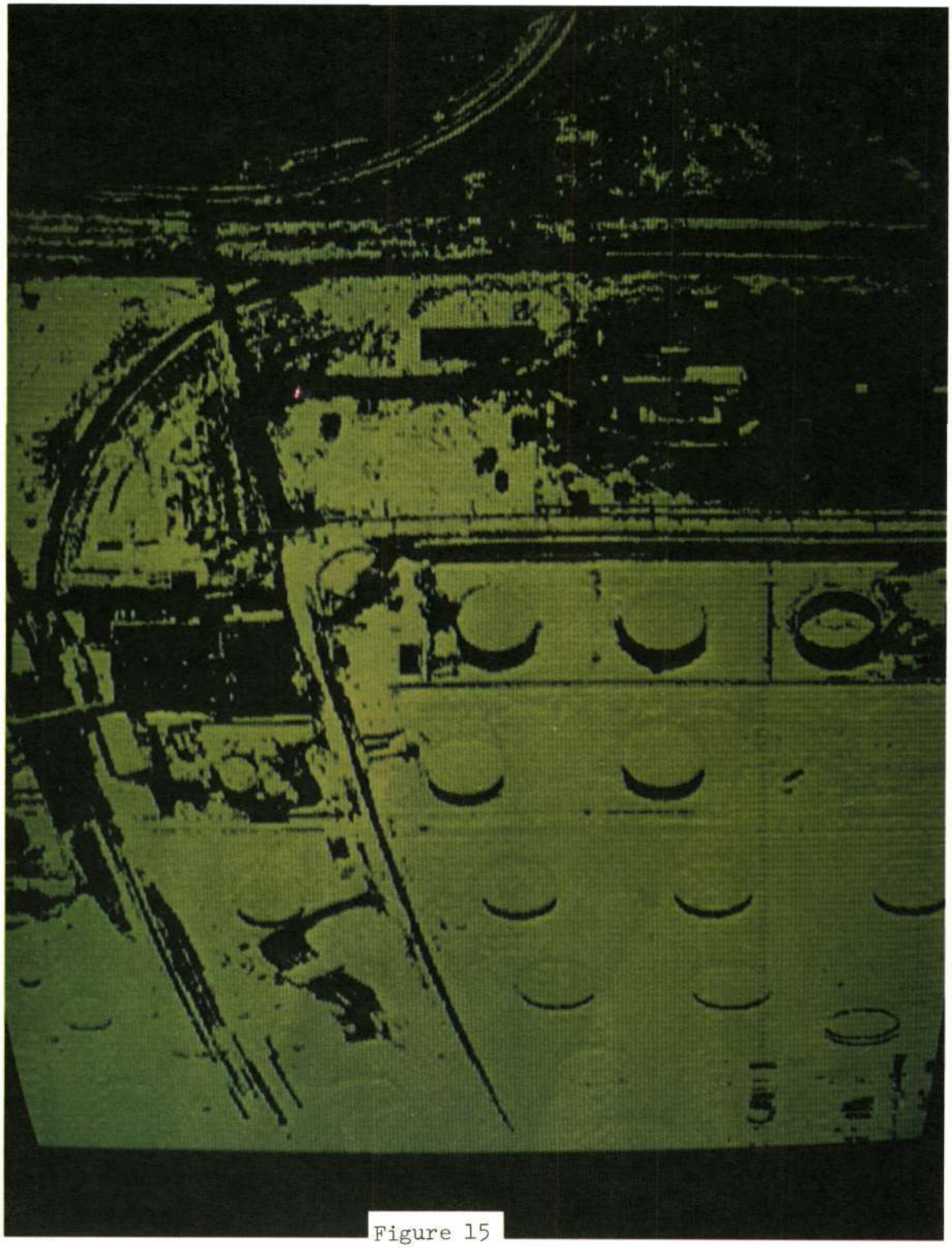

Figure 15

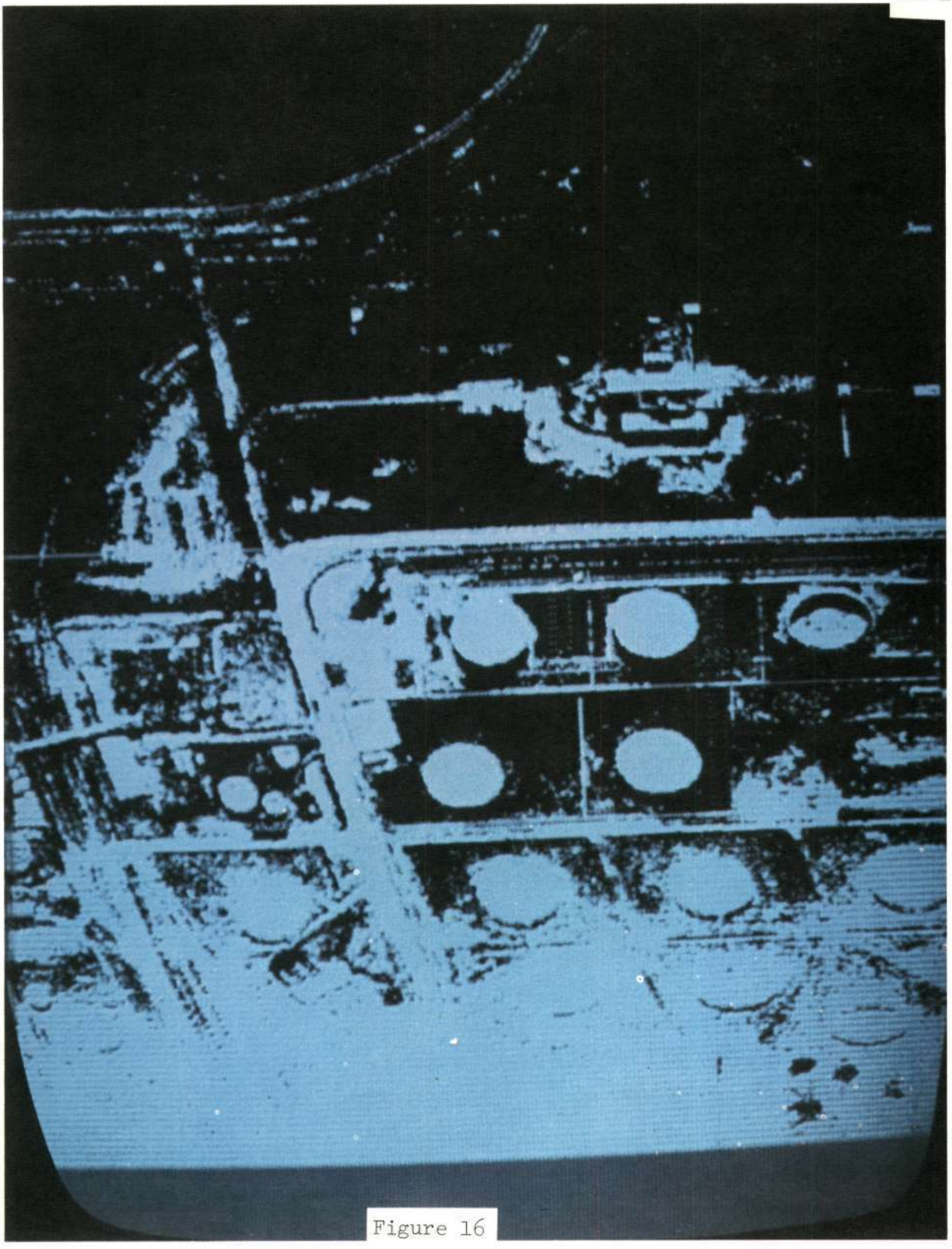

Figure 16

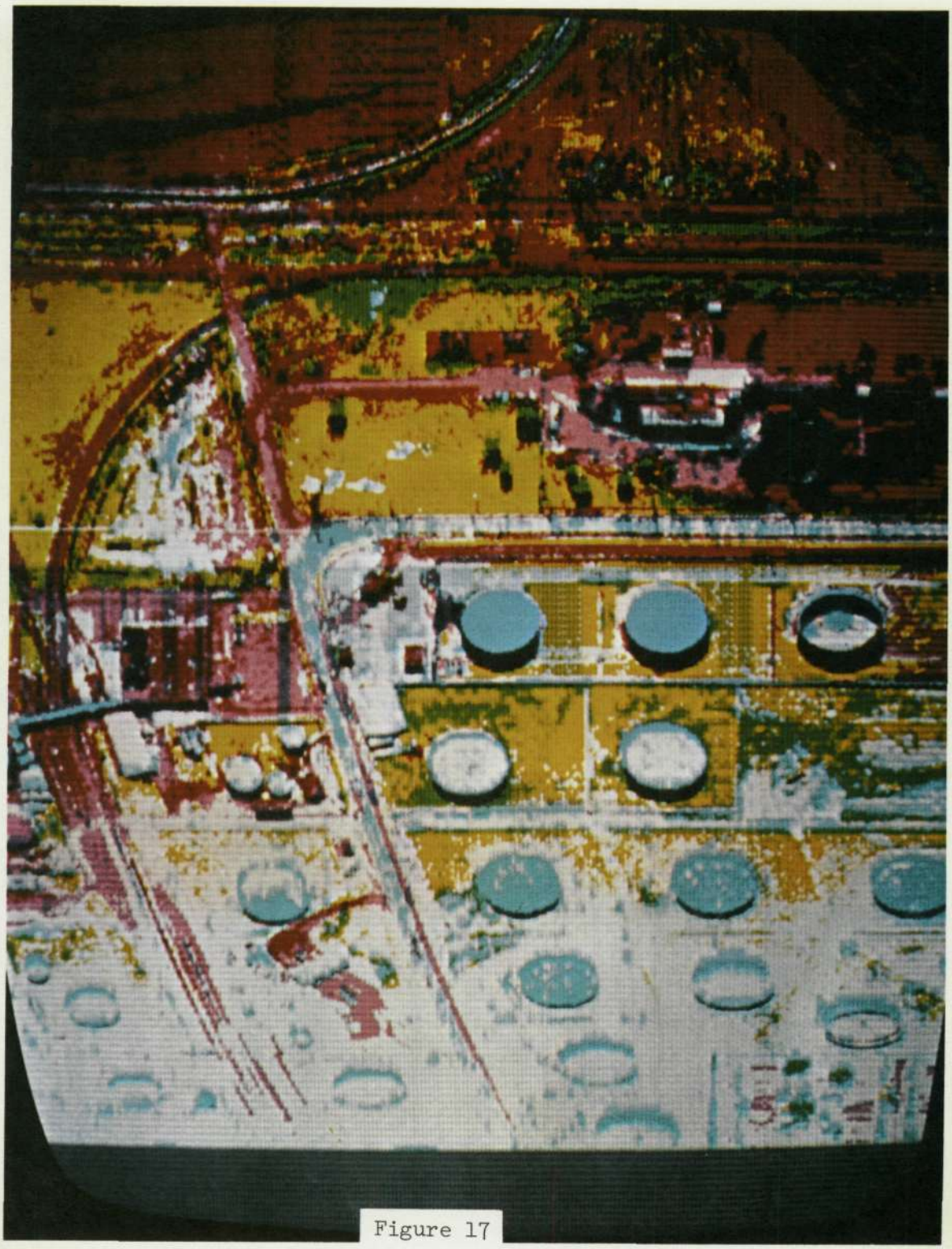

Figure 17

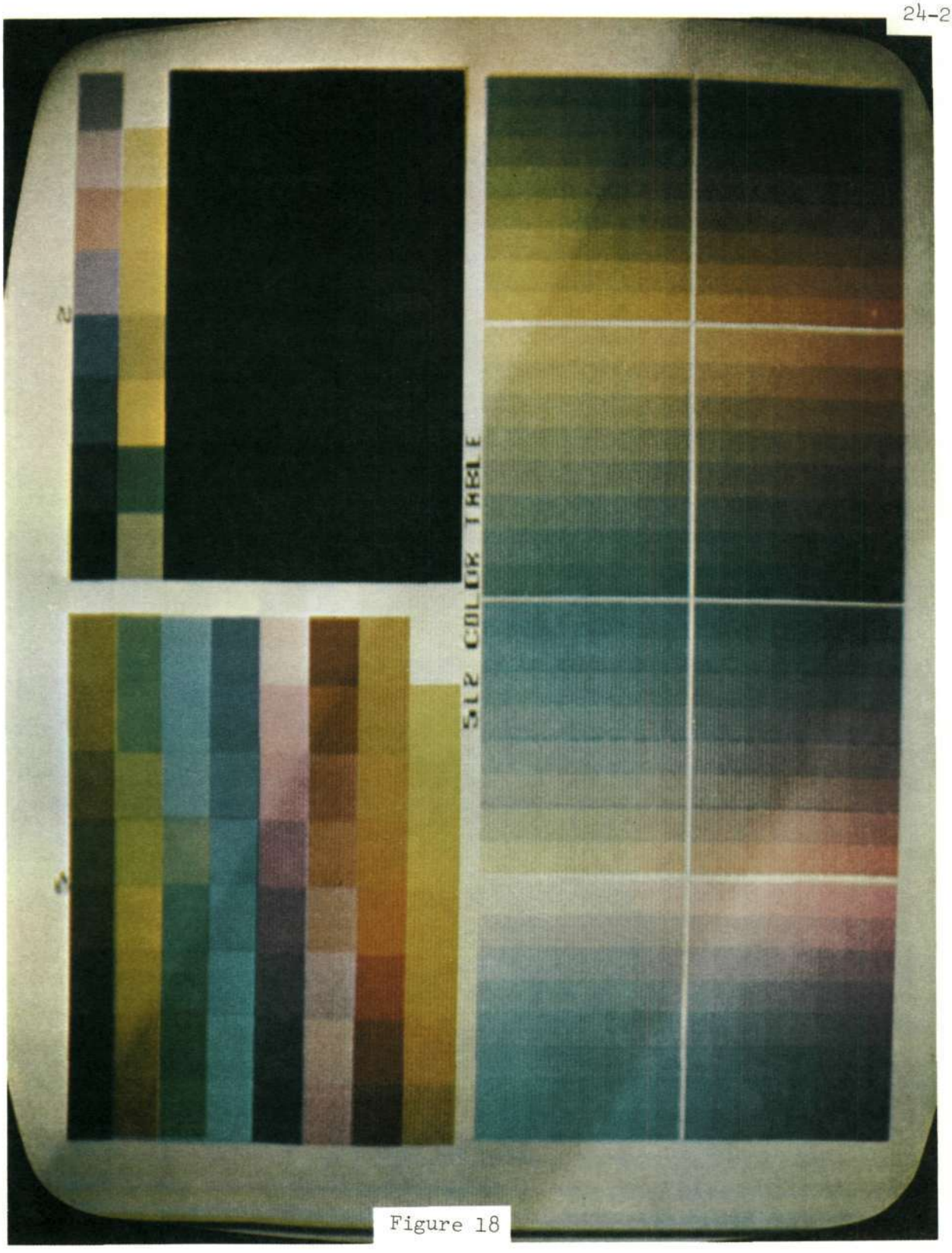

Figure 18

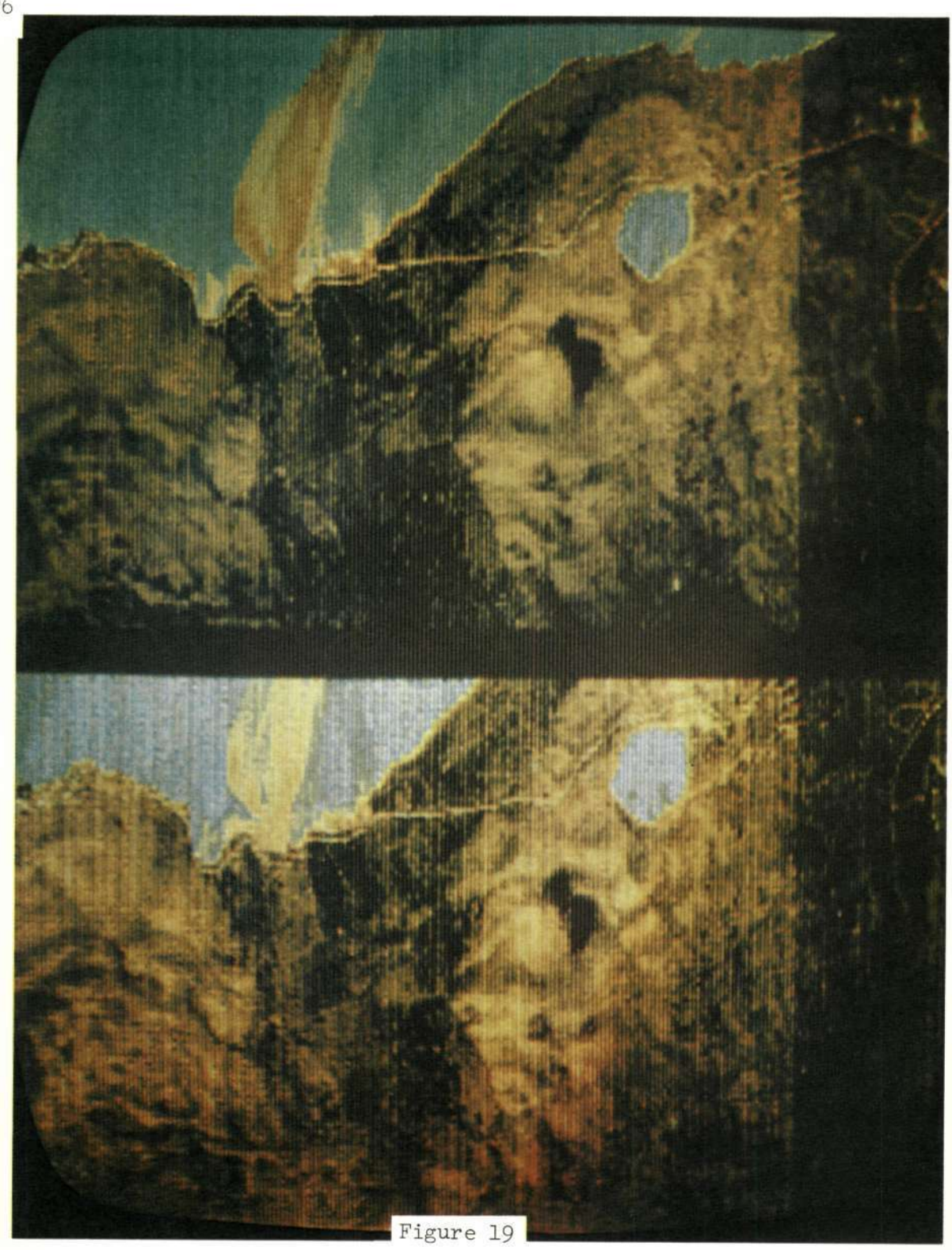

Figure 19

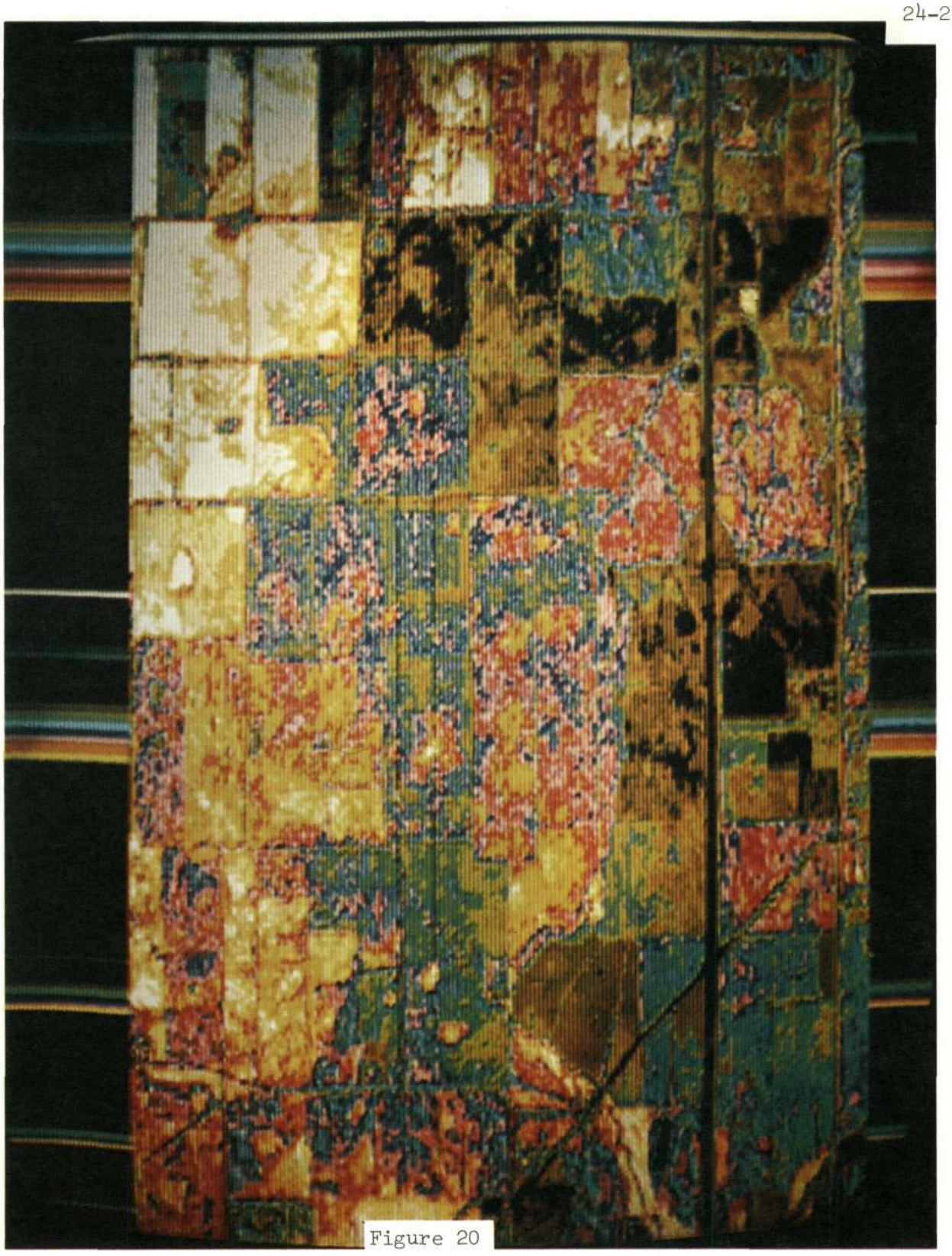

Figure 20

Figure 21

Figure 22

SECTION 25

SALINITY SURVEYS USING AN AIRBORNE MICROWAVE RADIOMETER

J.F. Paris

J.D. Droppleman

Lockheed Electronics Company, Inc.

Houston Aerospace Systems Division

D.E. Evans

NASA Manned Spacecraft Center

ABSTRACT

The Barnes PRT-5 Infrared Radiometer and the L-Band (1.42 GHz) Channel of the Multifrequency Microwave Radiometer (MFMR) are used to survey the distribution of surface water temperature and salinity. These remote sensors were flown repetitively in November 1971 over the outflow of the Mississippi River into the Gulf of Mexico. Data reduction parameters were determined through the use of flight data obtained over a known water area. With these parameters, the measured infrared and microwave radiances were analyzed in terms of the surface temperature and salinity.

INTRODUCTION

Surface water salinity and temperature measurements are useful to studies of coastal processes such as bay circulation and river outflow. Marine organisms are affected by the salinity and temperature of their water habitat. Marine ecologists and biologists thus need the capability for conducting surveys of salinity and temperature. Also, fish forecasting by the National Fisheries Service of the National Oceanic and Atmospheric Administration (NOAA) requires information on the temperature and salinity of breeding grounds of marine organisms.

Past investigations have shown that the microwave emission of water is affected significantly by changes in the salinity of the water surface layer for microwave frequencies less than 3 GHz(Rfs. 1-3). Thus, the possibility existed for making surveys of the water surface salinity from aircraft through the use of an L-band microwave radiometer. A Multifrequency Microwave Radiometer (MFMR) built by Aerojet General Corporation was installed on the NASA 927 (Lockheed P3A aircraft) in 1969. One channel of the MFMR operates in the L-band at 1.42 GHz. The purpose of this paper is to report on the development of an analysis technique whereby the distribution of surface water temperature and salinity along the flight line may be calculated by computer from MFMR and infrared radiometry (PRT-5) data taken along the flight track of the NASA 927 aircraft.

In order to recover the salinity of the water surface from MFMR measurements, one must consider carefully the effects of a number of other parameters, such as, variations in water surface temperature, absorption and emission by the intervening atmosphere, absorption and emission by the MFMR radome antenna, and waveguide, and departures in the calibration constants from the values determined before the aircraft flight. These considerations are discussed in Section II below.

A computer program was developed to analyze the MFMR and PRT-5 data and to produce profiles of water surface salinity and temperature along the aircraft flight track. The development of the computer program is discussed in Section III below.

The computer program was used with flight data acquired during a flight of the NASA 927 over the outflow of the Mississippi River into the Gulf of Mexico in November 1971. The results of the application of the program are given in Section IV below.

Conclusions and recommendations are presented in Section V below.

THEORETICAL DEVELOPMENTS

EMISSION AND REFLECTION OF WATER

In the determination of salinity from measurements of the microwave emission of water, one needs a computationally simple, mathematical model that may be used to predict the microwave emissive and reflective properties of water, given the observable conditions of the water and trial values of salinity. It is known that the microwave emission of water is affected, in general, by changes in water temperature, water salinity, water surface roughness (wind waves and swell), and by the presence of other materials on the surface, such as sea foam and oil. (Refs. 1-7)

Mathematical models exist for predicting the microwave properties of sea foam and oil on water. These models require, however, a knowledge of the thicknesses of foam and oil, of the dielectric constant of the oil, and of the air-to-water ratio of the foam. These parameters are not available through the use of remotely sensed data. On the other hand, visual or photographic data may be used to determine the presence or non-presence of oil or foam on the water surface. Thus, in the mathematical model, it is assumed that there is no foam or oil on the water surface.

Mathematical models exist also for predicting the effect of water surface roughness on the microwave emission of water. These models require a knowledge of the spectrum of water surface slopes which, in turn, may be inferred from a knowledge of the fetch, duration, and speed of the wind over the water. Again, these parameters are not available from remotely sensed data. Studies (Refs. 4 and 6) have shown, however, that the effect of the water surface roughness is small for viewing angles near nadir and for vertical polarization. In the mathematical model developed for use in this paper, it is assumed that the effects of water surface roughness can be ignored.

With the elimination of the above effects, only the effects of temperature and salinity remain. In order to model the microwave properties of water, it is assumed that the water is a homogeneous, semi-infinite dielectric bounded by a plane surface and overlaid by air. Since the water is an absorbing and emitting medium of large depth, the radiation impinging upon the air-water interface from below is the same as that emitted by a black-body at the temperature of the water. That is, the brightness temperature of the radiation just under the air-water interface is equal to the absolute themometric temperature of the water.

At the air-water interface, a fraction, r, of the radiation impinging from below is reflected back into the water mass. The rest of the radiation is transferred through the air-sea interface and emerges as emitted radiation. Thus, the brightness temperature of the emitted radiation, T_e (°K), is

$$T_e = (1 - r)\, T_w \tag{1}$$

where T_w is the water temperature (°K).

The reflectivity, r, for a flat semi-infinite dielectric of dielectric constant, $\varepsilon' - j\varepsilon''$, is given as (Ref. 2)

$$r_v = \left| \frac{(\varepsilon' - j\varepsilon'') \cos\psi - \sqrt{(\varepsilon' - j\varepsilon'') - \sin^2\psi}}{(\varepsilon' - j\varepsilon'') \cos\psi + \sqrt{(\varepsilon' - j\varepsilon'') - \sin^2\psi}} \right|^2 \tag{2}$$

or

$$r_h = \left| \frac{\cos\psi - \sqrt{(\varepsilon' - j\varepsilon'') - \sin^2\psi}}{\cos\psi + \sqrt{(\varepsilon' - j\varepsilon'') - \sin^2\psi}} \right|^2 \tag{3}$$

where ψ is the zenith angle of observation and the subscripts v and h refer to vertical and horizontal polarization, respectively.

The microwave radiation directed downward impinging upon the air-water interface is characterized by a sky brightness temperature, T_{sky} (°K), which is the sum of the transmitted cosmic background brightness and the katabatic emission by the atmosphere.

A portion of the sky radiation is reflected from the air-water interface toward the observer, such that the total radiation leaving the air-water interface and traveling toward the observer has a brightness temperature of

$$T_o = r\, T_{sky} + (1 - r)\, T_w \tag{4}$$

In order to compute the reflectivity for a given angle of observation and polarization, one must be able to specify the dielectric constant, $(\varepsilon'-j\varepsilon'')$ of the water.

Studies (Refs. 8 and 9) have shown that the values of ε' and ε'' for water with dissolved salt (NaCℓ) may be predicted for the microwave spectrum through the use of Debye model. That is,

$$\varepsilon' = \varepsilon_\infty + \frac{\varepsilon_s \quad \varepsilon_\infty}{1 + \omega^2 \tau^2} \tag{5}$$

and

$$\varepsilon' = \frac{\omega \tau(\varepsilon_s - \varepsilon_\infty)}{1 + \omega^2 \tau^2} + \frac{\sigma_i}{\omega \varepsilon_o} \tag{6}$$

where ε_∞ is 4.9, ε_s, τ, and σ_i are functions of water temperature and salinity only, and ω is the circular frequency, [$2 \pi \nu$, where ν is the electromagnetic frequency (Hz)].

The values of ε_s, τ, and σ_i for specific water temperatures and salinities as given in Refs. 8 and 9 are given in Table 1. In order to predict the values of ε' and ε'' for any water temperature and salinity, it is necessary to interpolate between the values given in Table 1. Interpolation formulas exist for this purpose and are indicated in Table 2 (Ref. 10).

With these interpolation formulas and the use of Equations 2-6, one has a mathematical model that may be used to predict the emissive and reflective properties of water at 1.42 GHz for any given water temperature, water salinity, angle of viewing and polarization. This model was used to compute the microwave emission for vertical and horizontal polarization, for viewing angles of 0, 30, and 55 degrees, for water salinities of 0, 5, 10, 15, 20, 25, 30, and 35 0/00, and for water temperatures ranging from 0 to 30°C. The results of the calculations are shown in Figures 1-5.

These figures show that salinity has the maximum effect on microwave emission for angles of viewing near 55 deg, for vertical polarization, for warm water, and for salinities in the range from 10 to 35 0/00.

EMISSION AND ABSORPTION BY THE ATMOSPHERE

A mathematical model that may be used to predict the effect of the atmosphere on the transfer of microwave radiation is needed to allow the proper consideration of this effect. For a given aircraft flight, soundings of atmospheric temperature and humidity are available usually through the use of radiosondes released at National Weather Service stations. At 1.42 GHz, the atmosphere is practically transparent for all conditions including clouds and rain (Ref. 9). In the case of rain, however, the surface water would be disturbed and diluted by the rain water. Also the aircraft radome would be covered by liquid water and would create large and unpredictable losses. For these reasons, rainy weather conditions must be ruled out for the measurement of salinity by the MFMR. The emission and transmission of the atmosphere may be computed from the knowledge of the vertical distribution of temperature and humidity in the atmosphere (Ref. 10).

In addition, the effects of refraction and a spherical geometry may be easily included in the calculation. (Ref. 11). As a result, the relationship between the brightness temperature of the radiation impinging upon the MFMR radome, T_b, and T_o, the brightness temperature of the radiation leaving the air-water interface, is

$$T_b = T_o t + T_{atm} \tag{7}$$

where t is the transmission coefficient for the intervening atmosphere and T_{atm} is the brightness temperature of the radiation emitted by the intervening atmosphere toward the observer.

TRANSMISSION OF SENSOR COMPONENTS

If one neglects the radiation received in the side lobes of the L-band radiometer of the MFMR, then the equivalent radiometric temperature of the radiant power received by the radiometer is given by

$$T_r = \frac{T_b}{L_r L_a L_w} + \frac{(L_r - 1)}{L_r L_a L_w} T_{rd} + \frac{(L_a - 1)}{L_a L_w} T_a + \frac{(L_w - 1)}{L_w} T_w \tag{8}$$

where L_r is the loss factor for the radome,

L_a is the loss factor for the antenna,

L_w is the loss factor for the waveguide,

T_{rd} is the thermometric temperature of the radome,

T_a is the thermometric temperature of the antenna,

and T_w is the thermometric temperature of the waveguide.

CALIBRATION EQUATION

The microwave radiometer is a linear device such that the output, C (counts)*, is given by

$$C = C_{b\ell} - \frac{T_{b\ell} - T_r}{S} \tag{9}$$

where $C_{b\ell}$ is the output of the radiometer when the power emitted by the reference load is being monitored, (counts),

$T_{b\ell}$ is the thermometric temperature and equivalent radiometric temperature of the reference load, (°K),

and S is the response of the instrument or scale factor (°K per count).

In the MFMR, the scale factor may be determined before or after a data run by injecting a known amount of argon noise that has an equivalent noise temperature, T_n (°K), and observing the change in output, ΔC (counts). In this case,

$$S = \frac{T_n}{\Delta C} \tag{10}$$

SUMMARY OF MATHEMATICAL MODELS

Mathematical models were developed above to predict the effects of all measurable parameters and salinity on the output of the MFMR. These models are valid only for the following conditions.

---

*The output of the MFMR is voltage, however, it is recorded as PCM counts.

1. Smooth water surfaces free from foam and oil
2. Non-raining atmospheres
3. Matched radiometer systems
4. Linear radiometer systems

PROGRAM DEVELOPMENT

DATA AVAILABLE FOR ANALYSIS

The data available for analysis consists of the following:

1. One-second averages of the thermometric temperature of the radome, the antenna, and the waveguide of the MFMR and of the equivalent radiometric temperature of the radiation measured by the L-band radiometer as determined from the calibration equations (Eqs. 9 and 10).

2. Averages taken over 0.792 sec. of the equivalent radiometric temperature of the radiation measured by the PRT-5 infrared radiometer.

3. Radiosonde measurements of atmospheric temperature and humidity from the surface to the 10 mb level (approximately 31 km).

4. Flight logs for the aircraft flight.

5. Location (latitude, longitude, and altitude), attitude (heading, drift, roll, pitch), and speed of aircraft sampled once each ten seconds.

6. Surface measurements of salinity and temperature at selected points under the aircraft surface track.

7. Photographic coverage (10% overlap) along flight line.

8. Scale factors, baseline counts, and baseline temperature used to reduce raw MFMR data to produce data in 1 above.

9. Equivalent argon noise temperature, radome loss factor, and waveguide loss factor.

ADEQUACY OF THE AVAILABLE DATA AND MATHEMATICAL MODELS

In the above it has been noted that some minor effects such as surface roughness and sidelobe contributions have been ignored in the development of the mathematical models. In addition, there is some evidence that there are systematic errors in the values of injected argon noise and of the antenna loss factor for the MFMR. All of these factors could create a significant bias in the data if not properly treated. In order to insure consistency in the analysis and to eliminate the effects of systematic errors, a new set of calibration constants (scale factor and antenna loss factor) are obtained through the use of flight data and the mathematical models. Two portions of the flight data are taken — the first over a stretch of water of known temperature and salinity and the second when the radiometrically cold sky is being viewed.

DETERMINATION OF THE NEW CALIBRATION CONSTANTS FOR THE MFMR

If equations (8) and (9) are combined and rearranged, one obtains the expression,

$$T_b = L_r L_a L_w [T_{b\ell} - S\,(C_{b\ell} - C)]$$

$$- (L_r - 1)\, T_{rd} - (L_l - 1)\, L_r T_a - (L_w - 1)\, L_r L_a T_w \qquad (11)$$

The actual output of the radiometer, C, may be obtained from the given values of radiometric temperature through the use of equiations (9) and the old calibration constants.

If T_{bw} is the brightness temperature corresponding to the radiometer reading, C_w, obtained when the known water target is being viewed, and T_{bs} is the brightness temperature of the sky corresponding to the radiometer reading, C_s, then from equation (11),

$$T_{bw} - T_{bs} = L_r L_a L_w S(C_w - C_s) \qquad (12)$$

or

$$S = \frac{T_{bw} - T_{bs}}{L_a L_r L_w (C_w - C_s)} \tag{13}$$

Inserting equation (13) into (11) and solving for L_a, one obtains the expression

$$L_a = \frac{a_1}{a_2} \tag{14}$$

where

$$a_1 = T_b + \frac{(T_{bw} - T_{bs})(C_{b\ell} - C)}{C_w - C_s} + (L_r - 1) T_r - L_r T_a \tag{15}$$

and

$$a_2 = L_r L_w T_b - (L_w - 1) L_r T_w - L_r T_a \tag{16}$$

In equations (14)-(16), one may use either C_w and T_{bw} or C_s and T_{bs} to determine L_a. With the knowledge of L_a, one may obtain the value of the scale factor, S, from equation (13).

The effect of the above determinations is to force the MFMR measurements to agree with the mathematical model at two points, namely, for a selected water point and for a cold sky point. Since all of the radiometric measurements are made for water conditions close to the selected water point, there should be consistency in the values of the derived salinities.

COMPUTATIONAL PROCEDURE FOR OBTAINING SALINITY AND TEMPERATURE FROM MFMR AND PRT-5 DATA

After receipt of all of the flight data and surface and atmospheric measurement data obtained in support of the aircraft flight, the following procedure was followed:

1. A homogeneous area of water with known water temperature and salinity was selected.

2. From an inspection of the surface measurement and PRT-5 tabulations, the difference between the two temperatures was determined for the selected water area. In general, there will be a fixed difference due to the cool skin of the water, the nonunity value of the emissivity of water, and the absorption and emission of the intervening atmosphere.

3. The radiation properties of the atmosphere were calculated through the use of the Microwave Atmospheric and Oceanic Data Analysis Program (MAODAP). The MAODAP uses radiosonde data taken during the flight (Ref. 12).

4. The salinity and temperature analysis program (STANL) was then employed. In the STANL, the following operations are performed:

   a. Controls cards are read.

   b. Data are read from PRT-5 and MFMR data tapes supplied by the Computing and Analysis Division (CAAD) of NASA Manned Spacecraft Center.

   c. Eleven-second running averages are computed for needed MFMR and PRT-5 parameters.

   d. The new calibration constants are determined by use of the flight data and the Eqs. 13-16.

   e. The salinity and temperature are determined from the MFMR and PRT-5 data through the following procedure:

      (1) First, the microwave radiometric temperatures are corrected for the change in scale factor, that is

$$T'_r = T_{b\ell} + S' \frac{(T_r - T_{b\ell})}{S} \tag{17}$$

      (2) Second, the PRT-5 infrared radiometric temperature are used with the correction factor in 2 above to determine the water temperature (°K).

      (3) Last, the value of salinity is determined through iteration such that the predicted radiometric temperatures agrees with the corrected radiometric temperatures determined in (1) above.

PROGRAM APPLICATION

MISSION 190, FLIGHT 3

Mission 190, Flight 3 was flown over the outflow of the Mississippi River into the Gulf of Mexico (Site 128) on November 11, 1971. Nine data runs were made over Line 1 (see Figure 6) at approximately 242 m (860 ft.) above the water surface. The first eight data runs were made with the MFMR antennas pointing 4.8 deg from nadir in vertical polarization. The last run was made with the antennas pointing 45 deg from the zenith in vertical polarization. The first data run began at the ENE end of Line 1 at 0935 CST; the last data run ended at the ENE end of Line 1 at 1803 CST. Two KA-62 cameras, the Barnes PRT-5 Infrared Radiometer, the MFMR Boresite Camera, the MFMR, and the navigation equipment were used on the NASA 927 (Lockheed P3A) aircraft during the flight, and all sensors functioned normally.

Flight support consisted of a radiosonde released at Boothville, La. (approximately 25 n. miles north of the aircraft flight line), and a surface survey along the aircraft flight line. The surface survey was made through the use of a 65 foot crewboat leased at Venice, La. The surface measurements consisted of *in situ* measurements of salinity and temperature with a Beckman In-Situ Salinometer. The measurements were taken at stations approximately every nautical mile along the flight line. In addition, water samples were taken approximately every ten stations. As originally planned, the surface survey was to take place during a time period centered upon the time interval of the aircraft flight. Unfortunately, the crewboat ran into the dock the evening before the day of the aircraft flight and had to undergo repairs before leaving during the morning of the flight. The accident did not come to the attention of the mission manager since the aircraft crew and sensor operators had left for the airport before the surface survey team arrived at the Gulf Docks in Venice to leave on the crewboat. As a result, the surface survey boat arrived at S. Pass and began the survey at 1157 CST just before the aircraft survey was being completed. The surface survey proceeded toward the WSW end of Line 1 and returned to S. Pass at 1641 CST.

In general, the atmosphere was clear and dry, and surface winds were from the ENE at 5 knots. The radiosonde was released at 1715 CST. The results of the radiosonde sounding are shown in Table 3.

DATA PREPARATION

The water area at the Southwest Pass outflow was selected as the calibration point for the water data. The surface measurements of water surface temperature at this point were compared with the PRT-5 radiometric temperatures, and the radiometric temperature was found to be 3.5 °C lower than the bucket temperature of the water surface.

The MAODAP was used to calculate the microwave parameters of interest for the subsequent analysis. The parameters of interest from the MAODAP program are listed in Table 4.

The analysis program (STANL) developed for the study was then used to determine the new calibration constants and to produce a plot of surface water salinity and temperature along the flight track.

RESULTS

The results of the determination of new calibration constants for the MFMR are listed in Table 5. A significant difference was noted between the old and new values of antenna loss factor, scale factor and injected noise. These differences appear to be the result of a bias in the measurement of injected noise as made by the hot/cold load laboratory calibration procedure.

The plot of surface water salinity and temperature along the flight track during run 8 is shown in Figure 7. The symbols in the Figure indicate the values of surface temperature and salinity obtained by the surface survey that was conducted shortly after the aircraft flight. In general, there is good agreement. The times of passage over the river mouths are indicated by the symbol M and the time of passage over surface foam lines as seen in the photography are indicated by the symbol F .

These data confirm the usefulness of L-band measurements of water microwave emission in determining the surface salinity of water.

REFERENCES

REF. NO. 1	Reference
1	Sirounian, V., 1968: The effect of the temperature, angle of observation, salinity, and thin ice on the microwave emission of water. J. Geophys. Res., 73, 4481-4486.
2.	Paris, J.F., 1969: Microwave radiometry and its applications to marine meteorology and oceanography. Ref. No. 69-II, Contract Nonr 2119 (04), College Station, Texas, A&M University, 210 pp.
3	Droppleman, J.D., R.A. Mennella, and D.E. Evans, 1970: An airborne measurement of the salinity variation of the Mississippi River outflow. J. Geophys. Res., 75, 5909-5913.
4	Stogryn, A., 1967: The apparent temperature of the sea at microwave frequencies. IEEE Trans. Ant. Prop., AP-15, 278-286.
5	Williams, G.F., Jr., 1969: Microwave Radiometry of the ocean and the possibility of marine wind velocity determination from satellite observation. J. Geophys. Res., 74, 4591-4594.
6	Hollinger, J.P., 1970: Passive microwave measurements of the sea surface. J. Geophys. Res., 75, 5209-5213.
7	Nordberg, W., J. Conaway, D.B. Ross, and T. Wilheit, 1971: Measurements of microwave emission from a foam-covered, wind-driven sea. J. Atmos. Sci., 28, 429-435.
8	Saxton, J.A., and J.A. Lane, 1952: Electrical properties of sea water: Reflection and altenuation characteristics at v.h.f. Wireless Engineer, 29, 269-275.
9	Saxton, J.A., 1952: Dielectric dispersion in pure polar liquids at very high radiofrequencies. II Relationship of experimental results to theory. Proc. Roy Loc. (London), A213,473-492.

REF. NO. 1	Reference
10	Paris, J.F., 1971: Transfer of thermal microwaves in the atmosphere. Vols. I and II, NASA Grant NGR-44-001-098, Dept. of Meteorology, Texas A&M University, College Station, Texas, 468 pp.
11	Paris, J.F., 1971: A program for computing the brightness temperature of a clear atmosphere from radiosonde data. Tech. Rpt. LEC/HASD 649D.21.068, NASA Manned Spacecraft Center, Houston, Texas, under contract NAS 9-10950, 38 pp.
12	Paris, J.F., 1971: MADDAP — microwave atmospheric and oceanic data analysis program. Earth Observation Division, NASA Manned Spacecraft Center, Houston, Texas, under contract NAS 9-12200, AD 63-0117-3334-15, 150 pp.

TABLE I.-THE DEBYE PARAMETERS OF AQUEOUS SODIUM CHLORIDE FOR SPECIFIC VALUES OF TEMPERATURE AND SALINITY (AFTER SAXTON AND LANE, 1952; SAXTON, 1952)

T_{sea} (C)	Debye Parameter	Salinity (0/00) 0.0	28.3	55.5
-10	ε_s	92.3	——	——
	$\tau_t \times 10^{12}$ s	27.5	——	——
	σ_i $\mho$ m^{-1}	0.0	——	——
0	ε_s	88.2	77.0	69.0
	$\tau_t \times 10^{12}$ s	18.7	17.1	16.4
	σ_i $\mho$ m^{-1}	0.0	2.44	4.77
10	ε_s	84.2	74.0	66.0
	$\tau_t \times 10^{12}$ s	13.6	12.2	11.8
	σ_i $\mho$ m^{-1}	0.0	3.45	6.22
20	ε_s	80.4	71.0	63.0
	$\tau_t \times 10^{12}$ s	10.1	9.2	9.0
	σ_i $\mho$ m^{-1}	0.0	4.44	7.66
30	ε_s	76.7	68.0	68.0
	$\tau_t \times 10^{20}$ s	7.5	7.2	7.1
	σ_i $\mho$ m^{-1}	0.0	5.22	9.22
40	ε_s	73.1	65.0	58.0
	$\tau_t \times 10^{12}$	5.9	5.7	5.6
	σ_i $\mho$ m^{-1}	0.0	6.22	10.8

TABLE II.-REGRESSION COEFFICIENTS FOR THE DEBYE PARAMETERS OF AQUEOUS SODIUM CHLORIDE

Independent variable	Regression coefficients		
	ε_s	$\tau_t \times 10^{12}$ (sec)	σ_i ($\mho$ m^{-1})
constant	0.88195 E 02	0.19390 E 02	———
T_{sea}	-0.40349 E-00	-0.68020 E-00	———
S	-0.43917 E-00	-0.11370 E-00	0.87483 E-01
T_{sea} S	0.43269 E-02	0.58629 E-02	0.45802 E-02
T_{sea}^2	0.65924 E-03	0.95865 E-02	———
S^2	0.16738 E-02	0.11417 E-02	00.25662 E-04
T_{sea}^2 S	-0.92286 E-05	-0.87596 E-04	-0.16914 E-04
T_{sea} S^2	-0.42856 E-04	-0.54577 E-04	-0.37158 E-04
T_{sea}^2 S^2	0.44410 E-07	0.82521 E-06	0.39288 E-06
exp(T_{sea})	———	-0.65303 E-17	———

TABLE III.-RADIOSONDE DATA OBTAINED AT BOOTHVILLE, LA., AT 1715 CST, 11 NOVEMBER 1971, IN SUPPORT OF MISSION 190, FLIGHT 3, SITE 128

Pressure (mb)	Temperature (°C)	Dew-Point Depression (°C)
1023.5	17.2	5.3
1000.	17.3	5.6
953.	13.5	5.1
939.	13.8	27.0
850.	12.2	28.6
776.	9.4	28.0
500.	-13.4	21.9
400.	-26.9	18.3
314.	-39.4	15.8
200.	-61.7	Dry
171.	-65.4	Dry
159.	-63.8	Dry
128.	-68.4	Dry
121.	-66.1	Dry
100.	-70.6	Dry
95.	-73.0	Dry
50.	-62.5	Dry
41.	-55.3	Dry
23.	-53.5	Dry
17.	-46.2	Dry
13.	-47.6	Dry
10.	-40.5	Dry

TABLE IV.-LIST OF PARAMETERS FROM AMODAP NEEDED FOR THE ANALYSIS PROGRAM

Parameter	Value
Temperature of selected water area	22.2 °C
Salinity of selected water area	8.0 0/00
Equivalent radiometric temperature of sky (at 45 deg zenith angle)	7.06 °K
Atmospheric transmission factor for intervening atmosphere	0.99982
Emissive brightness temperature of intervening atmosphere	0.1 °K
Sky brightness temperature at surface for the viewing angle of the MFMR	5.15 °K
Zenith angle of viewing	4.8 deg

TABLE V.-CALIBRATION CONSTANTS FOR THE MFMR

Parameter	Old Value	New Value
Radome loss factor	1.10786	1.10786
Antenna loss factor	1.600	1.509
Waveguide loss factor	1.0423	1.0423
Scale factor	0.5875 °K/cnt	0.49588 °K/cnt
Injected noise	133.0 °K	112.3 °K

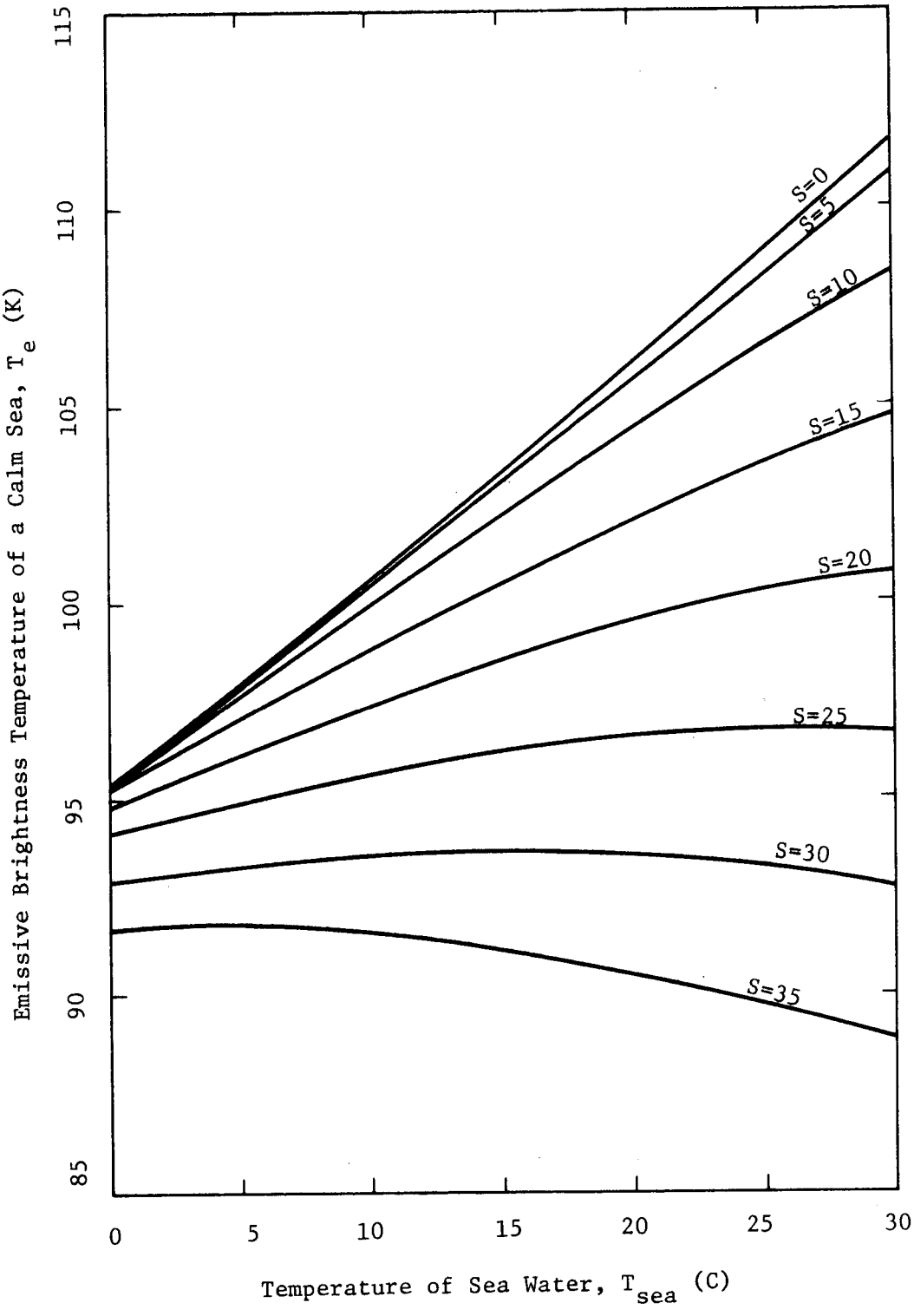

Fig. 1. Microwave emission of a calm sea: ν = 1.42 GHz, θ_a = 0 deg, vertical or horizontal polarization.

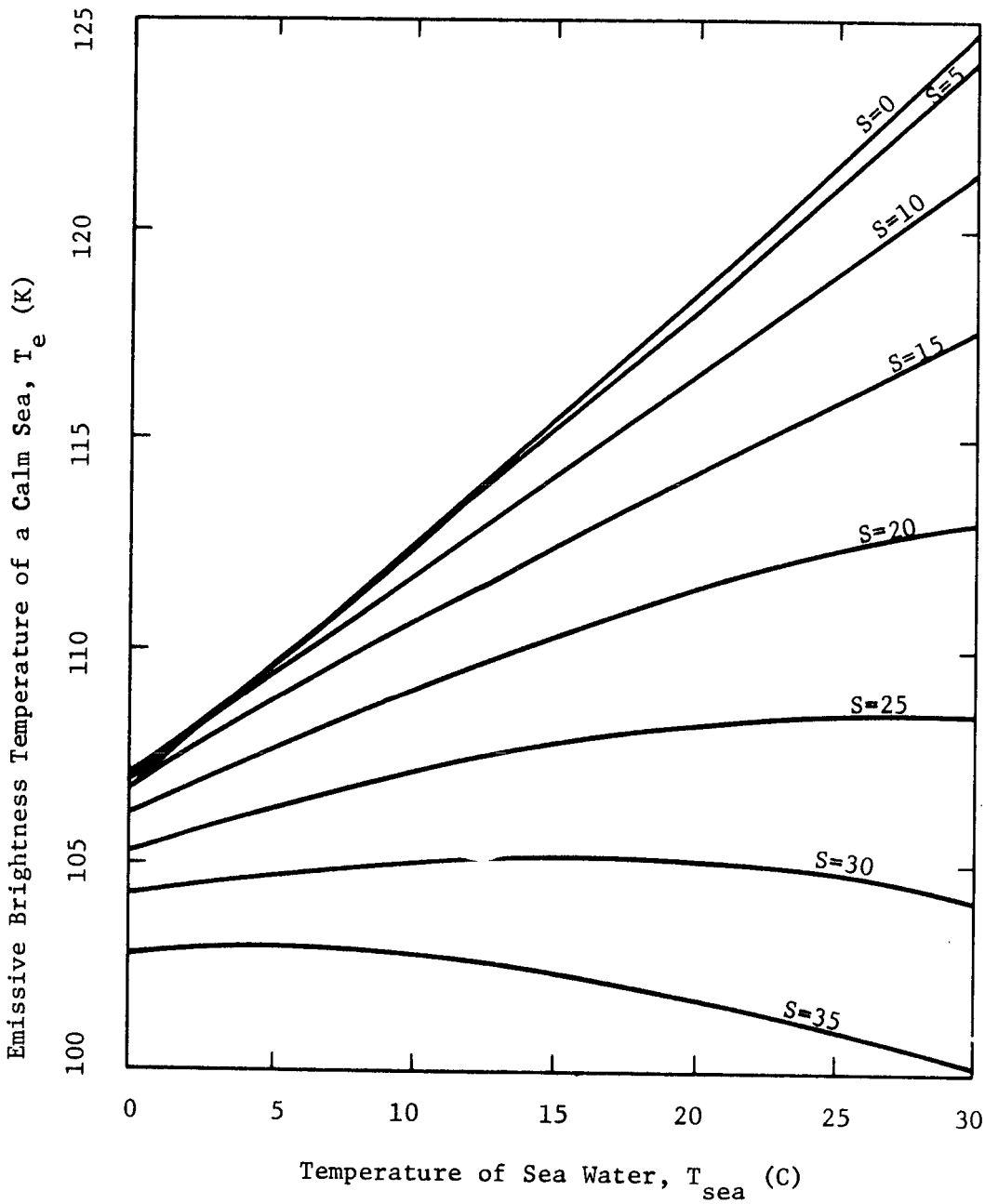

Fig. 2. Microwave emission of a calm sea: ν = 1.42 GHz, θ_a = 30 deg, vertical polarization.

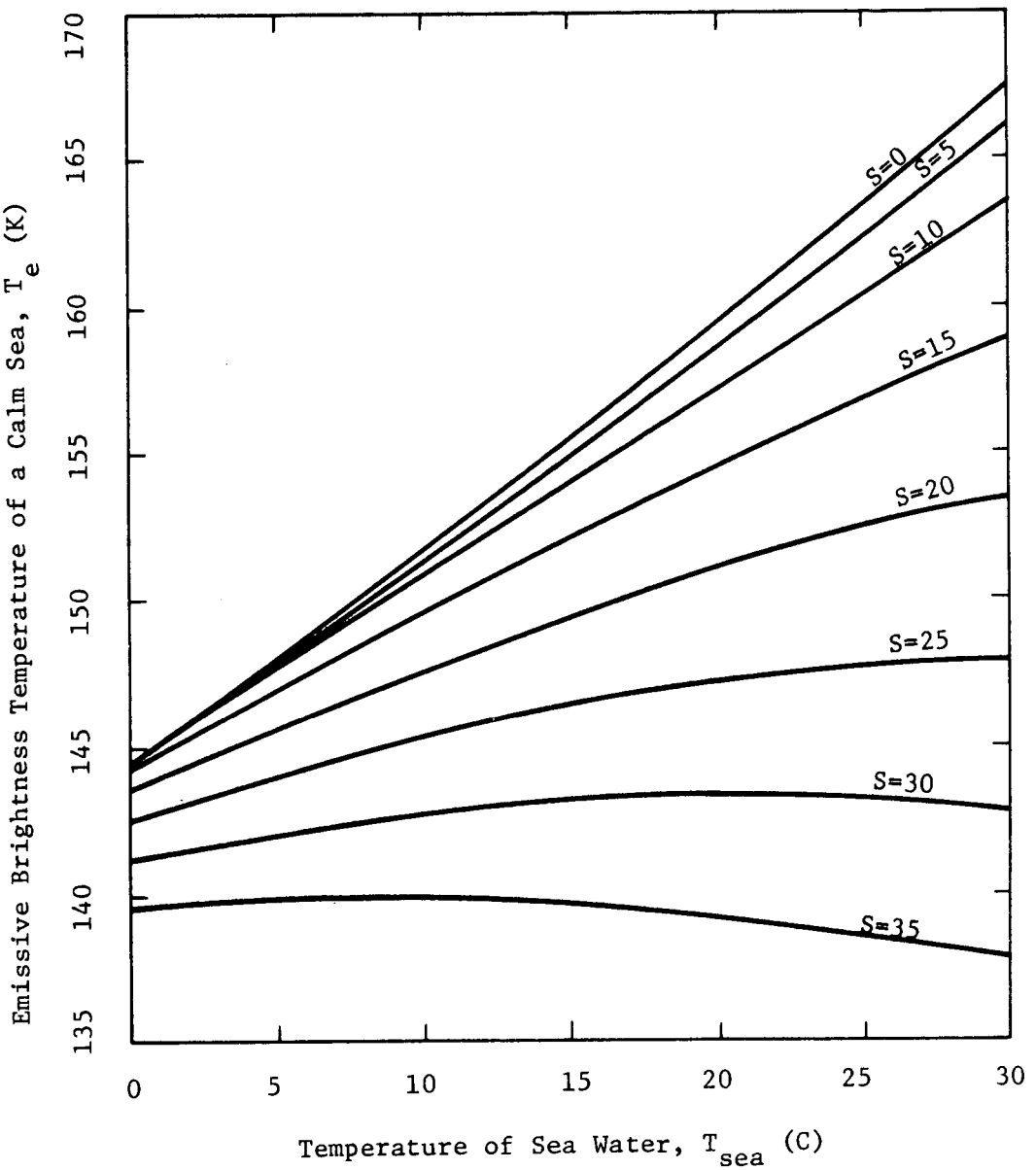

Fig. 3. Microwave emission of a calm sea: ν = 1.42 GHz, θ_a = 55 deg, vertical polarization.

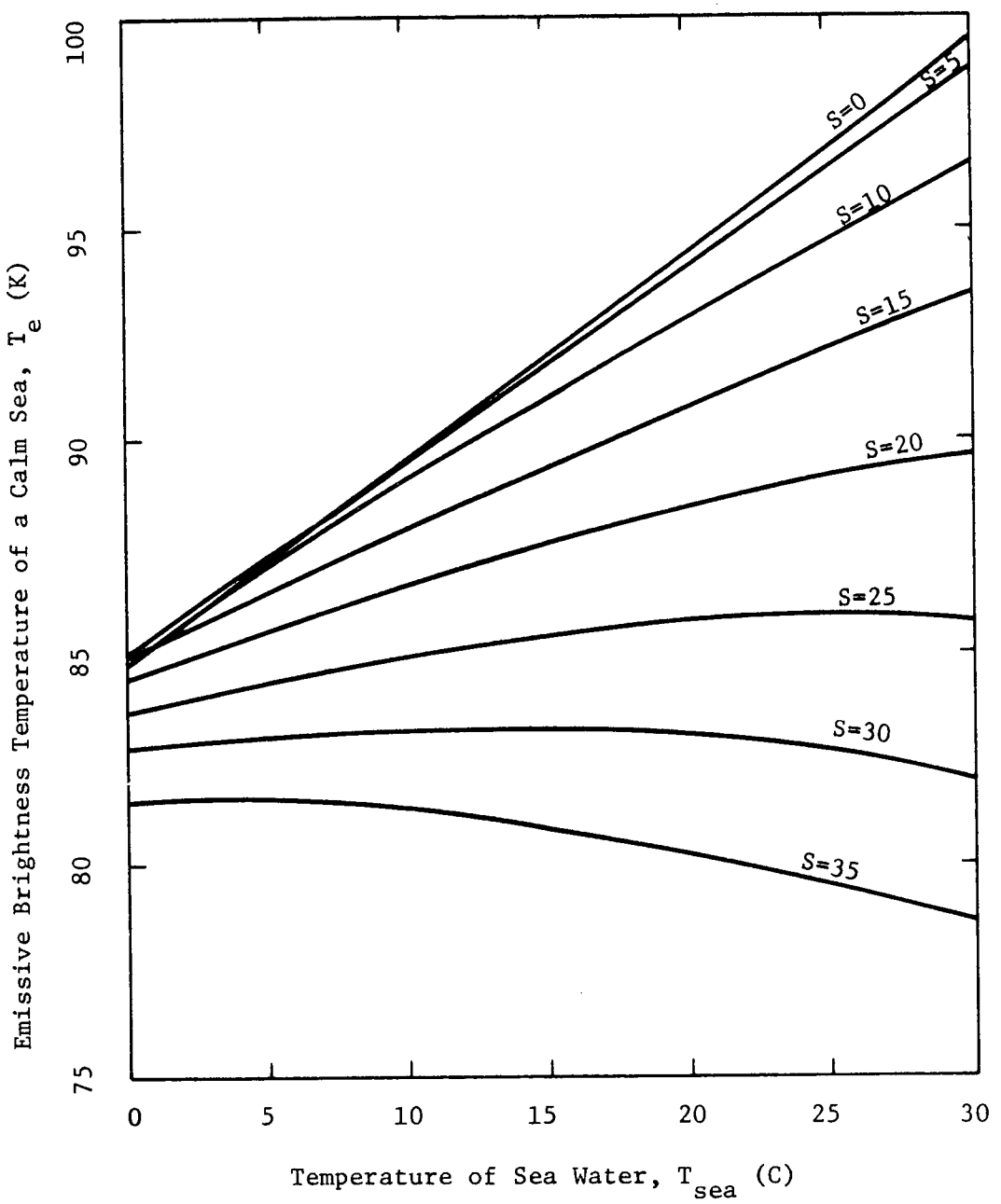

Fig. 4. Microwave emission of a calm sea: ν = 1.42 GHz, θ_a = 30 deg, horizontal polarization.

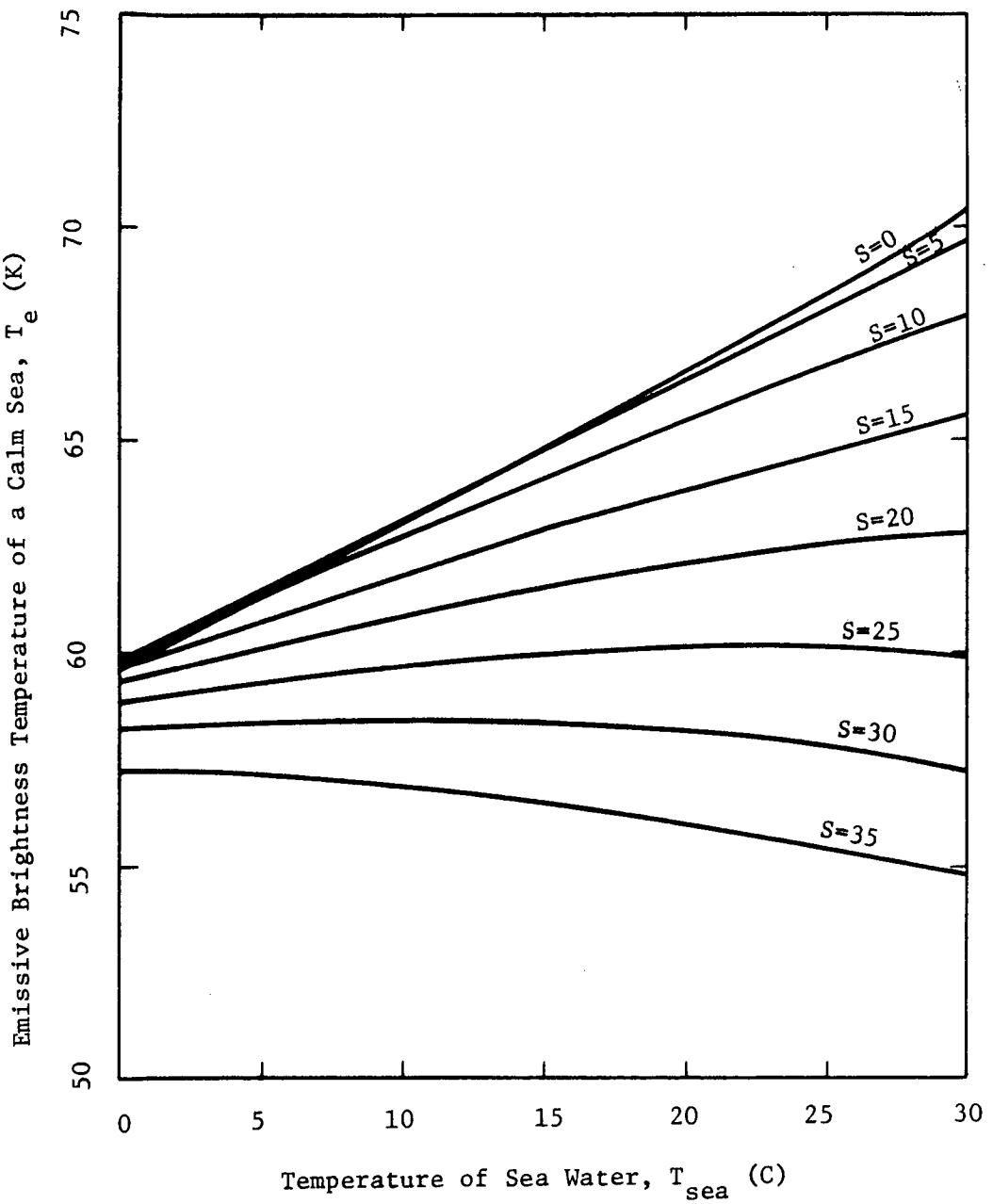

Fig. 5. Microwave emission of a calm sea: ν = 1.42 GHz, θ_a = 55 deg, horizontal polarization.

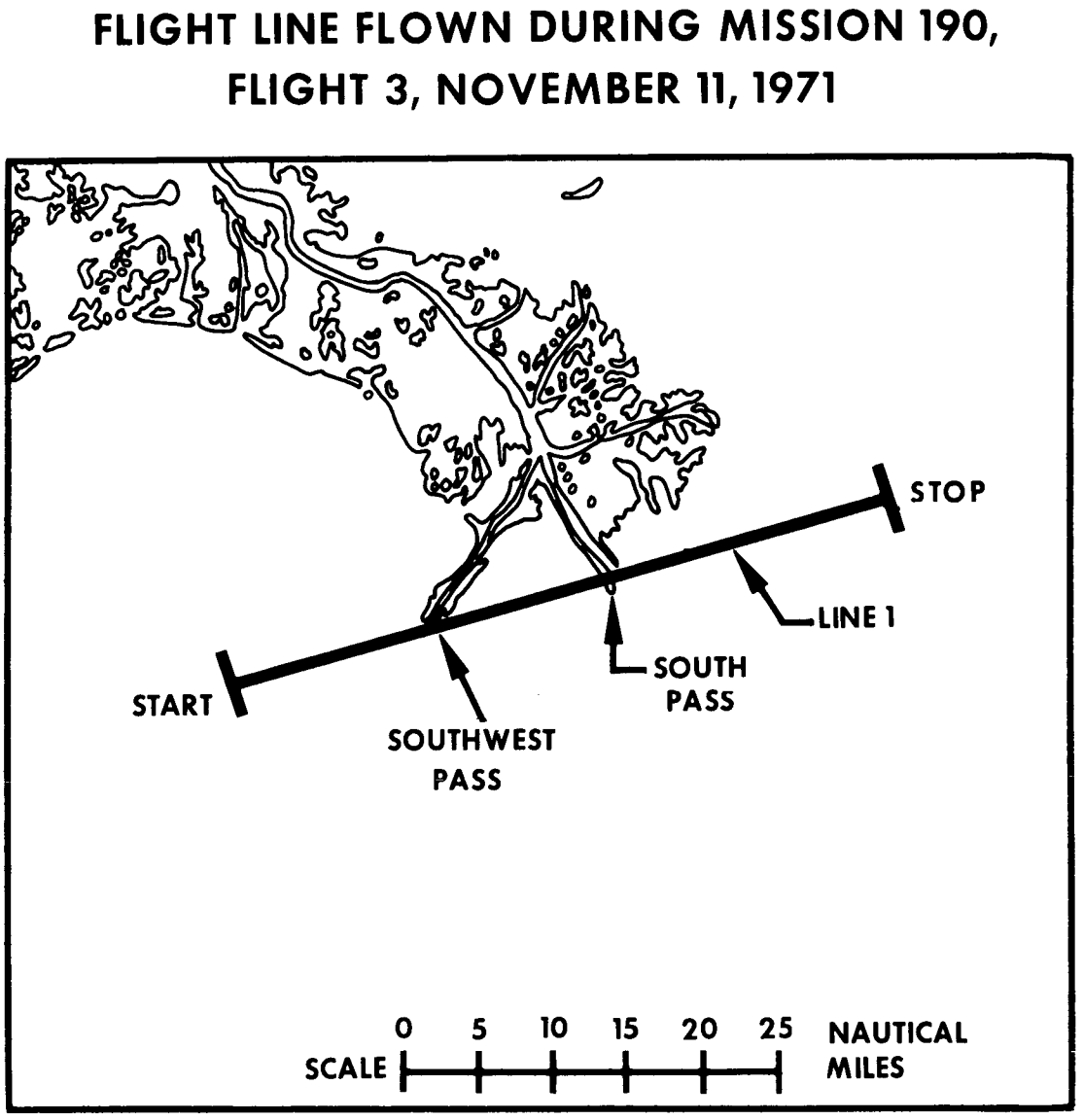

Fig 6. Flight line flown during mission 190, flight 3, site 128, November 11, 1971.

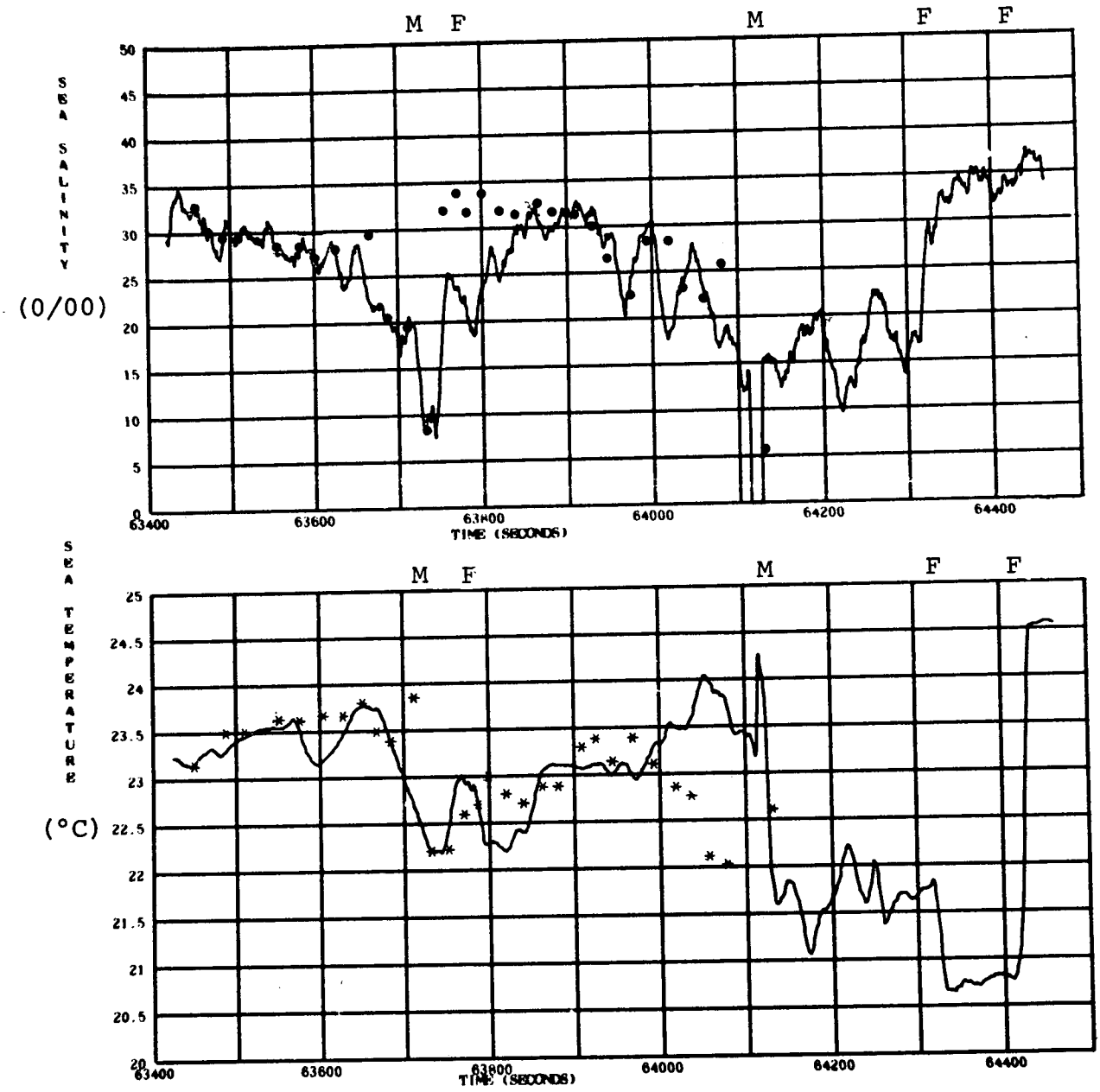

• Surface salinity measurement (0/00)

* Surface Temperature measurement (°C)

Fig 7. Results of mission 190, flight 3, run 8, over site 128, line 1.

SECTION 26

MICROWAVE BRIGHTNESS TEMPERATURE OF A WINDBLOWN SEA

by

Forrest G. Hall
NASA Manned Spacecraft Center
Houston, Texas

INTRODUCTION

The microwave brightness temperature of the windblown ocean surface has been a problem of interest for several years. The problem simply stated is, how is the microwave electromagnetic radiation emitted and reflected from the ocean surface affected by the wind generated roughness of the water surface (waves and white caps)?

The relevance of this problem lies in the fact that the brightness temperature of a sea surface is dependent upon the roughness of the surface, which in turn depends to some extent on the windspeed at the surface. Thus by measuring the microwave brightness temperature remotely and comparing this result to the actual or kinetic temperature of the sea water, the deviation of these two results can be utilized to remotely measure wind speeds over the world's oceans. The importance of such data to accurate weather prediction is discussed at some length by Moore and Pierson (1970) and Aukland et al. (1970).

The problem has been treated in a fundamental way by Peake (1959) and more recently by Stogryn (1967). Stogryn utilizes some of the notions developed by Peake to develop a specific model for the microwave brightness temperature of the sea as a function of wind speed. His model is based on the Kirchoff approximation for scattering from rough, finitely conducting surfaces. In essence, this approximation assumes that the radius of curvature of each surface wave viewed by the microwave sensor, is not exceeded by the characteristic wavelength of the viewing sensor. For a 19.35 GHz radiometer, the characteristic wavelength c/f, is equal to 1.5 cm; thus as the number of the waves which have radii of curvature exceeding 1.5 cm increases, the accuracy of the Kirchoff approximation decreases.

Undoubtedly many surface features on a windblown sea have radii of curvature less than the characteristic wavelengths of currently operating microwave radiometers (0.8-21 cm). Crests of waves, particularly capillaries, sea spray, white caps and foam will all have some surface features which violate the Kirchoff criteria. The extent to which waves violate this criteria and the effects such a violation will have on the Kirchoff model is not known at this time.

The effects of white caps and sea foam, however, are documented in the experimental work of Williams (1971). His work indicates an extremely high emissivity for foam which cannot be consistent with a Kirchoff model. Thus, it is clear that the portion of the sea surface covered by "white water" must be treated by a different model.

That no model exists which treats the compound sea surface (white water plus clear water) invites the line of investigation discussed in this paper.

In essence the model developed here treats the clear water portion of the surface with the Kirchoff approximation and the white water portion with a model for foam emissivity developed by Droppleman (1970). Although the Kirchoff approximation is employed for the clear water, the approach to the calculation of the brightness temperature is different than the one employed by Peake and Stogryn. As will be seen, the ensuing model produces results which differ in certain respects from Stogryn's model: even for the clear water case. A more drastic deviation in the results of the two models occurs when white water begins to appear on the ocean surface. This result is not surprising and has been documented in the field by several investigators: Nordberg et al. (1970), Hollinger (1971), and Ross et al. (1970).

In addition, but not secondary, to those portions of microwave-sea surface model mentioned above, the atmospheric model plays a vital role in the determination of the microwave brightness temperature. In fact, the sea surface and atmosphere interact as a single unit to produce the total microwave effect. The atmosphere is very "hot" at certain microwave frequencies and as a result this atmospheric radiation reflected by the ocean surface produces a major portion of the change in brightness temperature with increasing surface roughness, especially when little or no white water is present. Thus, it is important to incorporate in the total model an accurate atmospheric radiation model which will specify the radiation intensity of the atmosphere as a function of the radiation frequency and condition of the atmosphere. The model shown here was developed by Paris (1971). Paris' model accounts for the absorbtion and reradiation of microwave electromagnetic radiation from the two major atmospheric contributors, oxygen and water vapor. The inputs to his program are radiosonde data, i.e., pressure, temperature, and relative humidity as a function of altitude. Although this feature of his program provides for the inclusion of actual ground truth data into the model, we do not utilize this feature here; instead we read in hypothetical radiosonde data based on a standard atmosphere. Another important feature of the atmospheric model is its treatment of refractive effects in the atmosphere. This feature is especially important for zenith angles near the horizon.

I would like to acknowledge various members of the Lockheed Electronics Company for their contributions to this effort; Dr. Jack Paris and Dr. Jerry Droppleman for providing coded atmospheric and sea water emissivity subroutines; Mr. Walter Hanby for developing the wave slope generator, incorpora-

tion of the atmospheric and sea water subroutines into the main program and the output routines; finally Mr. Mel Shelton for coding and debugging the main program.

METHOD OF ANALYSIS

In this section we will define the composite model for the ocean surface and outline the computer scheme employed to obtain the brightness temperature based on such a model. Detailed derivations are omitted and only the relevant relationships used will be given.

THE COMPOSITE OCEAN SURFACE MODEL

In our analysis we employ a numerical computer scheme to calculate the total amount of microwave power radiated and reflected into an antenna located an altitude h above a continuous, stationary random surface. This analysis is valid only for those surfaces which are reasonably described by the following mathematical model: A composite stationary random surface consisting of I distinct parts, such that each part is either a specular surface or a slightly rough surface at the characteristic radiometer frequency.

We will assume for our analysis that the surface of a wind blown sea can be usefully approximated by the model described above. More specifically, we will employ a Monte Carlo scheme to computor generate a wind speed dependent, three dimensional sea surface consisting of a composite of two parts: (1) a clear water component, representable by a collection of statistically distributed flat, specular surfaces and (2) a white water component consisting of whitecaps, streaks and foam.

The Clear Water Component

We will assume that the clear water portion of the ocean surface, i.e., that portion not obscured by white caps or foam, can be represented by a collection of plane specular facets, whose surface normals are oriented with respect to the local vertical according to the distribution empirically obtained by Cox and Munk (1954). Cox and Munk discovered experimentally that a good approximation to the distribution $P(\alpha,\varphi)$ of the wave slopes with respect to the zenith angle α and the azimuth angle φ (measured from the crosswind axis) is gaussian and of the form

$$P(\alpha,\varphi) = \frac{1}{2\pi\sigma_c\sigma_u} e^{-\frac{1}{2}\tan^2\alpha\left[\frac{\cos^2\varphi}{\sigma_c^2} + \frac{\sin^2\varphi}{\sigma_u^2}\right]} \qquad (1)$$

where σ_c^2 is the mean square slope, crosswind component and σ_u^2 is the mean square slope, upwind component. Cox and Munk found these components to be linearly related to the wind speed W(m/sec.) in the manner shown below. The value $\alpha = \sqrt{\sigma_u^2}$ is plotted in Figure 1.

$$\sigma_c^2 = 0.003 + 1.92 \times 10^{-3} W$$

$$\sigma_u^2 = 3.16 \times 10^{-3} W \qquad (2)$$

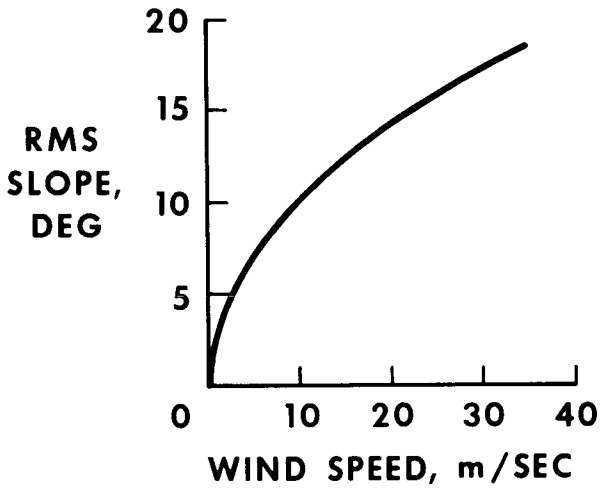

Figure 1.- The rms deviation from the local vertical of the normal to the surface of a wave as a function of wind speed. After Cox and Munk (1954).

In our model then, we develop a MonteCarlo scheme to orient the specular clear water facets, for a given wind speed, according to the distribution of equation (1).

The optical properties of each of these facets are then determined by the Fresnel coefficients and the peculiar geometry which each facet finds itself oriented with respect to the antenna. The dielectric constant for the Fresnel coefficients is calculated using a model developed by Paris (1969).

The White Water Component

Three categories of white water exist on the surface of a heavy sea: whitecaps, spray, and foam. White water makes its appearance when the wind speed increases to the neighborhood of 8 m/sec. Above this speed the percent coverage by white water increases monotonically until the surface is completely obscured around 60 m/sec. (see Neumann and Pierson (1966)). Percent white water coverage as a function of wind speed, has been modeled for wind speeds above 7.5 m/sec. by Cardone (1970). His model agrees roughly with observations by Blanchard (1963). Cardone's results are displayed in Figure 2.

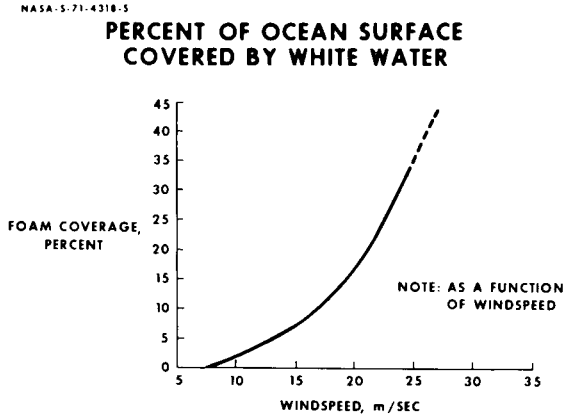

Figure 2.- Percent coverage of the ocean surface as a function of wind speed. After Cardone (1970).

As with wave slopes discussed in the previous section, we employ a Monte Carlo scheme in a computer program to generate white water on the ocean surface. The wind speed is an input to the computer program and the Monte Carlo routine generates an amount of white water specified by Cardone's model.

Once white water has been specified, we use the theoretical model developed by Droppleman to compute the emissivity of the white water patch. For a given electromagnetic frequency, the emissivity in this model is a function of the thickness of the white water patch, the angle at which the patch is oriented with respect to the antenna, and the volumetric ratio of water to air contained in the white water. The emissivity can vary from 0.3 to 1.0 depending on the parameters. The Monte Carlo routine is capable of distributing all of these parameters statistically; however, no data is available for either the thickness distribution or the volumetric ratio distribution. Thus, we choose a thickness and a volumetric ratio to generate an emissivity of about 0.95, depending on the orientation of the foam patch with respect to the antenna. For these values of thickness and volumetric ratio, the emissivity is almost insensitive to geometry so that we allow the surface normals to the foam patches to be gaussianly distributed a'la Cox and Munk. The parameters chosen above are clearly arbitrary. We excuse this on the grounds that to our knowledge no such data presently exists and await the time when such data is available to be used in this model.

APPARENT TEMPERATURE OF THE SEA

At microwave frequencies we are allowed the notion of the apparent temperature of the sea. This number, which characterizes the total amount of microwave power radiated and reflected into a microwave antenna viewing the sea surface, is defined by the relation

$$T_{aj} = \int_G T_{bj}\, G(\beta)\, d\Omega \qquad (3)$$

where T_{aj} is the apparent temperature as seen by the jth polarization mode of the ^{aj} antenna, $G(\beta)$ is the antenna gain function ,and $d\Omega$ is a solid angle element of the gain pattern. We will spend the remainder of this section defining the quantity T_{bj}.

Some rather simple relations emerge as a result of the relation given by eq. (3), and we will use this fortuitous circumstance to build our model. This model differs in approach, if not in principle, from Stogryn's model which is based on Peak's definition of the scattering coefficient. In order to understand eq. (3) more clearly let us consider the physics involved in calculating T_{aj}.

Figure 3 depicts a microwave antenna located at some altitude h* above an ocean surface. The Y axis in the figure is chosen to point in the upwind

* h is assumed to be of a sufficient magnitude to guarantee that the surface is in the far field of the antenna pattern.

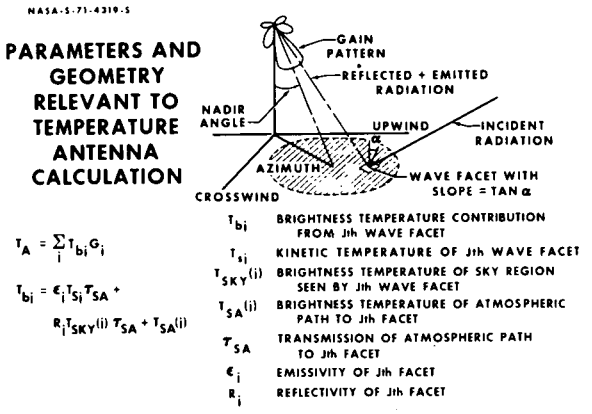

Figure 3.- The Parameters and Geometry relevant to the Antenna Temperature Calculation.

direction and the Z axis along the local normal. The X axis, being right-hand consistent with Y-Z, then points in the crosswind direction.

The angles (θ_o, φ_o) will serve to orient the antenna. We will assume the antenna gain pattern to have a symmetry axis (pointing axis) so that θ_o defines the nadir of the symmetry axis and φ_o defines the azimuth angle with respect to the crosswind X axis. The antenna will then "see" the shaded portion of the ocean surface. We then see from Figure 3 that a wave facet within the shaded area can be located with respect to the symmetry axis by an angle β. β is the angle subtended by the antenna symmetry axis and the dashed line of Figure 3 labeled "reflected + emitted radiation." Each of these wave facets within the shaded area subtends some angle $\Delta\Omega$ in the antenna pattern; thus radiation which is either emitted or reflected from one of these facets will be seen by the antenna. If we partition the gain pattern G into I solid angle increments $\{\Delta\Omega_i\}_{i=1}^{I}$ then I facets will be generated within the shaded area (ignoring antenna side lobes). The integral in equation (3) can thus be transformed into the sum

$$T_{aj} = \sum_{i=1}^{I} T_{bj}^{i} G(\beta_i) \Delta\Omega_i$$

where $\Delta\Omega_i$ is a solid angle increment contained in the gain pattern G and furthermore $\Delta\Omega_i \in \{\Delta\Omega_i\}_{i=1}^{I}$, the partition discussed previously. T_{bj}^{i} is the brightness temperature of the ith facet subtended by $\Delta\Omega_i$.

T_{bj}^{i} is determined by three factors: microwave radiation emitted from the ith facet, microwave radiation emitted from the sky and reflected from the ith facet into the solid angle increment $\Delta\Omega i$ and the radiation attenuated and radiated by the atmosphere contained in $\Delta\Omega_i$. These parts can be represented mathematically by the equation

$$T_{bj}^{i} = \epsilon_j^i T_S^i \alpha_{SA}^i + \rho_j^i T_{SKY}^i \alpha_{SA}^i + T_{SA}^i \qquad (4)$$

where

ϵ_j^i = emissivity of the surface of the ith facet for the jth component of polarization.
T_S^i = kinetic temperature of the surface of ith facet
ρ_j^i = reflectivity of the ith facet for the jth component of polarization
T_{SKY}^i = the sky temperature at the ith facet from that portion of the sky which will be reflected by the ith facet into $\Delta\Omega_i$
α_{SA}^i = fraction of the radiation absorbed by the atmosphere contained in $\Delta\Omega_i$
T_{SA}^i = brightness temperature of the atmosphere contained in $\Delta\Omega_i$

Thus, if we calculate T_{bj}^{i} for each facet, which will be composed either of clear water or white water, and sum the contributions from each facet, then we have calculated the apparent temperature of the sea. As we have seen earlier, the collection of facets must be oriented with slopes corresponding to the distribution found by Cox and Munk. Therefore, a large number of facets must be considered if we are to duplicate their statistics. The volume of calculations arising as a result of this procedure clearly requires the development of a computer program. We have developed such a program at NASA/MSC and will spend the next section describing this program.

THE COMPUTER PROGRAM FOR APPARENT TEMPERATURE OF THE SEA

The logic of the computer program, which calculates the apparent temperature of the sea, follows closely the development outlined so far (see Figure 4 for logic flow chart). First a partition for the gain pattern is selected to conform to the assumed axial symmetry of the pattern and provides a simple iteration scheme for the program. A large part of the program is the iteration logic. This logic selects each $\Delta\Omega_i$ so that a constant area increment ΔA_i is viewed at this surface. This step is needed for statistical purposes. The logic also keeps track of the location of $\Delta\Omega_i$ within the pattern and insures that the entire pattern is exhausted before the program ceases computation. About 20,000 increments are used to divide the pattern. When a particular $\Delta\Omega_i$ has been chosen by the iteration logic, a sequence of steps is initiated which allows calculation of T_{bj}^{i} using equation (4).

The block labeled random foam generator in Figure 4 is a random number generator which decides statistically whether the ith facet is to be white water or clear water. This decision is based on the value for the wind speed and Cardone's model for percent white water coverage (see Figure 2).

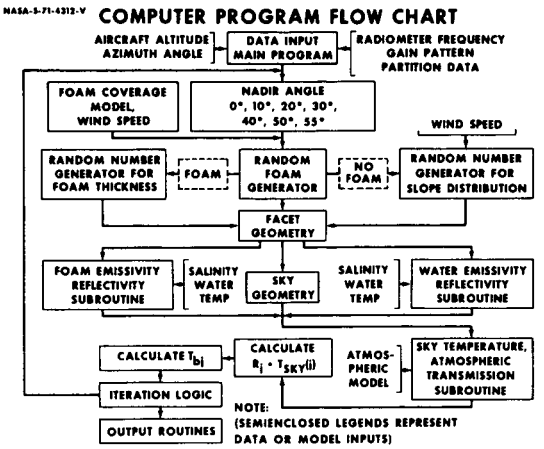

Figure 4.- Computer program flow chart. Random foam generator decides whether left or right side of flow chart is to be executed.

If, for example, the wind speed is 21 m/sec. then for 20 percent of the loops made by the program the sequence (shown in the left side of Figure 4) which calculates T_{bj} for foam is executed.

In the foam sequence, another random number generator, according to yet another distribution function, decides on the thickness of foam to be used. Presently no such data is available and we use a constant thickness as discussed in a previous section in this paper. The geometry of the facet, determined by its location and orientation with respect to the antenna, is then used to calculate the vertically and horizontally polarized emissivities of the facet. These emissivities are calculated using a subroutine developed by Droppleman (1970), also discussed earlier. Once this is accomplished, the program calls a subroutine developed by Paris (1969) which calculates the radiative and absorptive properties of the atmosphere, based on the location of the facet with respect to the antenna and the condition of the atmosphere determined by the radiosonde data input. The program then calculates T_{bj} according to equation (4). This number is stored in the sum register and the program returns to the iteration logic to select another $\Delta\Omega i$.

In case the foam generator decides not to generate a facet covered by white water, then a different sequence is initiated (see right hand side of Figure 4). This sequence contains a random number generator which orients the specular facets according to the distribution of Cox and Munk (1954). Once a facet is oriented with azimuth and zenith angles (φ,α), these angles are used to determine the geometry of the facet with respect to the antenna. This geometry, and the dielectric constant of the sea water (Paris (1969)) are used to determine the horizontal and vertical polarization Fresnel coefficients R_h, R_v. We then assume a randomly polarized incident radiation

(equal intensity in all planes) and use the Fresnel coefficients to calculate the fraction of the incident radiation reflected into the vertical and horizontal polarization planes of the antenna. In terms of the Fresnel coefficients the fraction of incident radiation received by the horizontal mode of the antenna is given by

$$\Pi_v(\theta_p) = \cos^2\theta_p \cdot R_v + \sin^2\theta_p \cdot R_h \qquad (4)$$

The fraction for the vertical polarization mode of the antenna is given by

$$\Pi_h(\theta_p) = \sin^2\theta_p \cdot R_v + \cos^2\theta_p \cdot R_h \qquad (5)$$

where θ_p is the angle subtended by the plane of the surface facet and the antenna horizontal polarization plane.

Once these reflectivities have been calculated then the polarized emissivities are calculated from the coefficients r_v and r_h by

$$\epsilon_j = 1 - \Pi_j \ , \ j = h \text{ or } v \qquad (6)$$

At this point the atmospheric subroutine is called and the sky temperature is calculated along the incident direction defined by the orientation of the specular facet. This subroutine is quite sophisticated. The effects of atmospheric refraction are included, which is quite important at large zenith angles where microwave radiation is strongly refracted. In addition, the program can use radiosonde data taken during the radiometer overflight.

Once the sky temperature T_{sky} (see Figure 3), and the transmission of the atmosphere τ_{sa}, and the brightness temperature T_{SA} of the atmospheric path between the radiometer and the surface facet, have been calculated, equation (4) is evaluated for T_b, the brightness temperature of the facet. A subroutine then retrieves the value for the antenna gain function at this angle β, multiplies this by T_b and adds it to those T_b already calculated. The program is then ready to iterate to another facet.

After the volume of the antenna pattern has been exhausted then the output routines are activated. This output consists of tables and plots of brightness temperature vs. nadir angle for various wind speeds. The program will also print all parameters used in the calculation of T_a: sky temperature vs. zenith angle calculated from radiosonde data: the distribution of surface wave slopes generated by the random number generators: the percent foam coverage generated: a three dimensional wire plot of the antenna pattern.

This general description of the computer program completes the analysis section. We would like now to present some results from this program.

RESULTS

In this section we will present a portion of those results which have so far been obtained from this program. To this date, brightness temperatures versus wind speed data have been generated for each characteristic frequency of all microwave radiometers presently employed on NASA/MSC aircraft. These frequencies are 1.41, 1.42, 4.9, 10.62,10.69, 13.9, 19.35, 22.23, 31.4, 37.0 GHz. As of yet, this model has not been compared to data gathered in a field situation, where for our model we would use an actual gain pattern with radiosonde determined or in situ measured sky temperatures. We will, however, in the first part of this section, compare the results of our model to those results from Stogryn's (1967) model. We will then present curves displaying the increase in brightness temperature with wind speed (wind sensitivity) for winds less than 8 m/sec. (no white water) as a function of radiometer frequency and nadir look angle. Next we will present curves indicating the effects of white water on the brightness temperature. Finally we will examine the wind sensitivity for the 1.4 GHz radiometer at nadir and 55 degrees from nadir for wind speeds above 10 m/sec.

Figure 5 is a sample output from the computer program. These curves are for a 19.35 GHz radiometer viewing a sea surface at 290° K. The curve

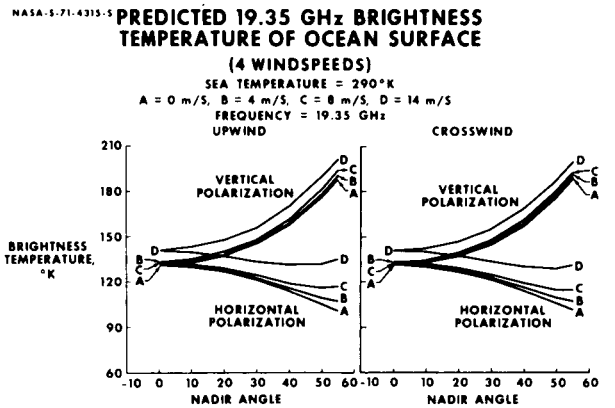

Figure 5.- The predicted brightness temperature of the ocean surface at 19.35 GHz using composite surface model. Aircraft altitude is 1 km.

labeled A is for a calm wind for which the ocean surface is flat. As wind speed increases to 4 meters/sec., curve B is generated. Notice from curve A to curve B that at large nadir look angles the horizontally polarized brightness temperature increases a few degrees Kelvin while the vertically

polarized component increases only slightly. This trend continues until curve D, where a sudden increase from curve C in both the vertically and horizontally polarized brightness temperatures can be observed at all nadir angles. This sudden increase is a result of the onset of significant coverage by white water at 8 m/sec. For the left most curve in this figure, the antenna is pointed directly upwind. In the rightmost curve it is pointed directly crosswind. Some minor differences exist between these two curves. The differences are probably not large enough to capitalize on them experimentally.

Using our model, brightness temperature computations were made at 19.35 GHz and the results compared to those obtained by Stogryn. To effect a better comparison, Stogryn's atmospheric model was substituted for Paris' model. For the horizontally polarized brightness temperature our results are identical to Stogryn's except we predict a slight wind sensitivity (.025 $^{o}K/m\text{-}sec^{-1}$) at nadir. For the vertically polarized case we predict, in contrast to Stogryn's results, a small wind sensitivity at all nadir angles. Thus we do not see the 52° crossover in these curves as predicted by Stogryn. By disabling the foam generator in the computor routine we can see the crossover, but only at windspeeds above 30 m/sec. Such a phenomenon is obscured by the effects of white water.

For the case where no white water exists, we can calculate the increase in brightness temperature with increasing wind speed as a function of nadir look angle. These results are presented in Figure 6. Only the sensitivity for the horizontal polarization mode is plotted. At nadir the wind sensitivity is minimum and increases rapidly beyond 45°. Of the frequencies plotted,

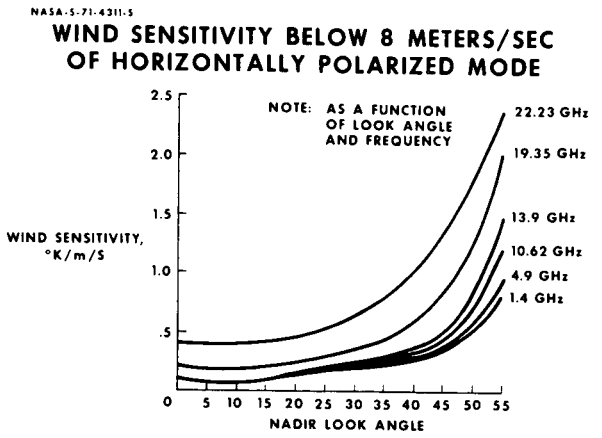

Figure 6.- Increase in brightness temperature with increasing wind speed (wind sensitivity) for wind speeds less than 8 m/sec. (no white water). Aircraft Altitude is 1 km.

the maximum sensitivity is observed for a frequency of 22.23 GHz. This phenomenon will be discussed in the next section. Remember that these sensitivities are for the ocean surface without whitecaps.

In the next figure, figure 7, are displayed the brightness temperature versus lookangle for wind speeds above 10 m/sec. 1.41 GHz was chosen to minimize the effects of clear water roughness. In these plots there is a large increase with wind speed at all nadir angles in both the vertically and horizontally polarized brightness temperature. This is a result of the increasing surface coverage of highly emissive whitecaps and foam.

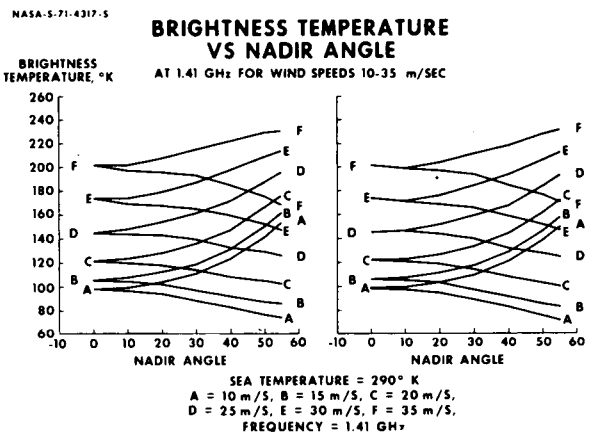

Figure 7.-The predicted brightness temperature increase of the ocean surface at 1.41 GHz using composite surface model. h = 1km.

The data in Figure 7 can be plotted in a different way to reveal a very interesting phenomena. We have done this in Figure 8 where brightness temperature is plotted versus wind speed and percent white water coverage for two nadir look angles. The slope of these curves is thus wind sensitivity or white water coverage sensitivity. For wind speeds less than 20 m/sec., the curve for a nadir angle of 55° has the greatest slope, thus the greatest wind sensitivity; For wind speed above 20 m/sec., however, the nadir pointed radiometer is most wind sensitive.

This result could be of considerable consequence to investigators since data reduction for the nadir pointed radiometer, especially from orbit, is considerably simpler than data reduction at the larger pointing angles. Whether or not this result holds for frequencies other than 1.4 GHz is not known, only because computations at other frequencies for wind speeds above 14m/sec. have not yet been made.

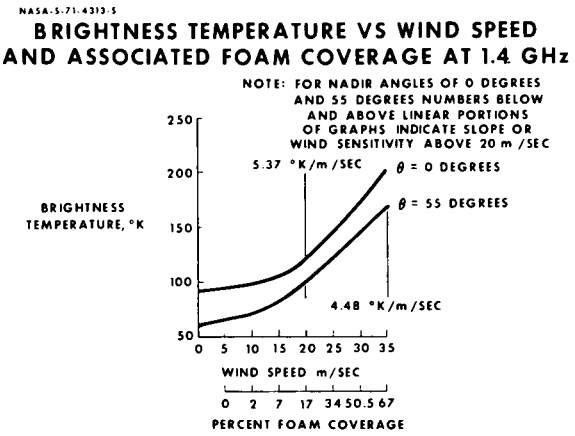

Figure 8.-Brightness temperature versus wind speed and foam coverage at 1.41 GHz for the horizontally polarized mode. h = 1km.

We should reiterate here that our choice to use 1.4 GHz for the initial computations implies no endorsement over other frequencies for wind speed determination.

DISCUSSION

In this section we will address ourselves to a discussion of the deficiencies and merits of the numerical technique and physical models we have employed in calculating the microwave brightness temperature of the ocean surface.

In the discussion of deficiencies we will note some limitation of the particular surface model employed. In addition we will point out certain areas wherefurther experimental or theoretical research could greatly enhance the results from this model.

The merit of our particular approach rests primarily in the ease with which a variety of complicated models can be brought together to model complex situations so often encountered in remote sensing. In addition the mathematical simplicity of this approach facilitates a physical understanding which is often hindered by more involved deductive approaches. We will show in the discussion to follow, how the two factors mentioned directly above, facilitate the investigation of the physics of the increase in microwave brightness temperature with increasing rms wave slope.

LIMITATIONS OF THE COMPOSITE SURFACE MODEL

Although the composite model postulated here for the surface of the ocean seems to be an improvement over previous models, at least three objections can be brought against the validity of the model: 1) The randomly oriented specular facet approximation for the clear water portion of the ocean surface may not characterize surface emission and reflection from those parts of the ocean surface covered by capillary waves whose radii of curvature are less than the wavelength of the emitted and reflected radiation. 2) Multiple surface reflections are ignored. 3) The composite model supposes that the total radiation from the clear water portions and the white water portions of the surface is the sum of the radiation from the individual portions. This model will diverge from reality in case a large percentage of adjacent white water and clear water portions of the surface have dimensions less than the wavelength of the reflected and emitted radiation.

A quantitative theoretical assessment of the magnitudes of items 1) and 3) is a difficult task. While the deviation of the Kirchoff approximation from a more sophisticated model could be assessed theoretically, the percentage of the ocean surface which would violate such a approximation is, to our knowledge, unknown. As for item 3), photographs of the ocean surface (see Pierson (1966)) show for wind speeds less than 20 m/sec. white water and clear water to exist in patches large compared to microwave wavelengths. Above 20 m/sec. white water streaking could affect the validity of assumption 3). More investigation into this matter is needed.

Item 2) should be important only to the radiometric sensing of high sea states at large nadir look angles. If, however, a user application of this nature is uncovered, the model could be altered to include the effects of multiple surface scattering.

LIMITATIONS OF THE SUBMODELS

In addition to the surface model, five other models are used to calculate the apparent temperature of the sea. These are 1) percent white water coverage with wind speed 2) white water optical properties model 3) distribution of the wave slopes, 4) atmospheric radiation model and 5) dielectric constant of sea water. In this section we will discuss extensions for models 1) through 4) which could greatly enhance the accuracy of the total model presented here and would certainly increase the reliability of the remote sensing of wind speeds over the world's oceans.

Percent White Water Coverage Versus Wind Speed

The percent white water coverage as discussed by Cardone (1969) is not a function of the wind speed alone. In addition to the wind speed, foam coverage depends to a large extent upon the state of the wind swept sea surface. Further investigations of the influence on foam coverage by time

varying winds, fetch, depth of water, etc., would increase the reliability of remotely sensing wind speeds.

White Water Optical Properties

The optical properties of sea foam are known to depend on at least three things: 1) Thickness of the foam. 2) Volumetric ratio of air to water in the foam. 3) The incidence angle at which the foam is viewed. Although Droppleman (1970) and Williams (1971) have investigated these effects, more research is justifiable.

Droppleman's investigation into this matter was a theoretical one. The model chosen by him is highly idealized; so it is quite possible that certain optical properties of foam may not be in accordance with Droppleman's predictions.

While the experimental work done by Williams corroborates some of Droppleman's results, a more complete investigation, both in the laboratory and in the field would be a valuable undertaking. Laboratory efforts could establish the effects discussed in the opening paragraph of this section on white water optical properties. Field radiometer measurements could further verify these results.

In addition, the actual configuration of white water on the ocean surface should certainly be established. This configuration could be defined by the statistical distributions of white water thickness, volumetric air to water ratios and surface slopes.

Distribution of the Wave Slopes

Hollinger (1971) has questioned the validity at microwave frequencies of Cox and Munk's optically determined sea slope distribution. He further suggests that this distribution could be seen differently by each microwave frequency and thus explain the dependence of wind sensitivity on frequency. As we will show momentarily, the frequency dependency of wind sensitivity is also a result of the variation of sky temperature with frequency, but as yet Hollinger's suggestion can not be dismissed.

An investigation into this question, using the model developed here, is in progress at NASA/MSC. It is possible that the individual effects of the variation of sky temperature and slope distribution with frequency on wind sensitivity can not be separated without considerable experimental effort.

Atmospheric Radiation Model

The major limitation of the atmospheric model used here is its inability to account for the effects of liquid water in the atmosphere. Such a capability is essential since the radiometric sensing of wind speeds through cloud cover is a most useful application.

Paris (1971) has developed a model to account for such effects, but this model requires as an input, the drop size and spatial distribution of water droplets in the atmosphere. As far as we know, no technique exists which can acquire such data on the scale needed for this application.

Another approach to this problem is multi-frequency sensing which might possibly be used to determine in situ the effects of clouds on the brightness temperature. A theoretical investigation of this possibility, using the model developed here, is in progress here at MSC.

MERITS OF THE NUMERICAL APPROACH

The prime consideration for choosing the numerical model above a more analytical approach to ocean surface modeling, is the ease with which existing submodels may be removed from the computer program circuit (see logic flow chart, Figure 4) and more sophisticated models plugged back in. As an unexpected benefit, we found this approach could be used to further the understanding of the basic physics involved in the wind sensitivity frequency dependence. In this section, the above statements will be discussed in more detail.

In Figure 4 each of the boxes to the right or left of center represent subroutines called within the main program. Thus, when new models for sea foam coverage, etc, become available, the models can be programmed and easily incorporated into the total model.

The main program itself consists of input and output routines, random number generators, geometry logic and iteration logic. Each of these routines are independent of the subroutines and will need no modification to incorporate more sophisticated models.

The iteration logic, shown in the small box in the lower left hand side of Figure 4, is an important portion of the main program. Essentially, this logic keeps track of the location of a solid angle element relative to the entire gain pattern and its position with respect to the atmosphere and surface. The program thus "knows" exactly which point of the surface and atmosphere is being viewed by a particular part of the gain pattern.

The iteration logic thus allows the consideration of a horizontally inhomogenous surface or atmosphere provided the model subroutines are capable of providing data of this nature. Such a feature allows us to consider, for example, surface distributions of white water which are not random. Therefore, if the distribution of surface foam can be specified, (for example,

by a camera boresighted with the radiometer) and this data reduced for input into the main program, then the actual surface can be modeled. In this way, horizontal inhomogeneities in surface temperature and salinity could also be modeled.

The ability to substitute atmospheric models within the program allows a very important point to be proved. Using this method we can show that a variation of sky temperature with zenith angle is necessary to produce the wind sensitivity of the horizontally polarized brightness temperature. Further, the variation of the sky temperature with frequency is sufficient to produce a change in wind sensitivity with frequency.

Figure 9 is a plot of brightness temperature versus nadir look angle calculated for an atmospheric model whose temperature does not vary with zenith angle. We accomplished this simply by disabling the normal atmospheric subroutine and substituting a constant sky temperature of 30° K. 30° K was chosen from Figure 10 as an average temperature of the sky at 19.35 GHz.

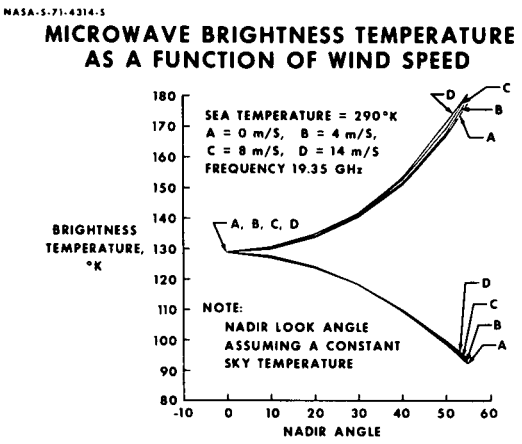

Figure 9.- Brightness temperature versus nadir angle assuming a constant sky temperature of 30° K.

Comparing Figure 9 to Figure 5, we see that the constant sky temperature model completely eliminates the horizontally polarized wind sensitivity. No effect on the vertically polarized component is observed.

We believe the horizontally polarized wind sensitivity is a result of the combined effects of the rms wave slope increase with wind speed and the sky temperature increase with zenith angle. As more and more of the wave

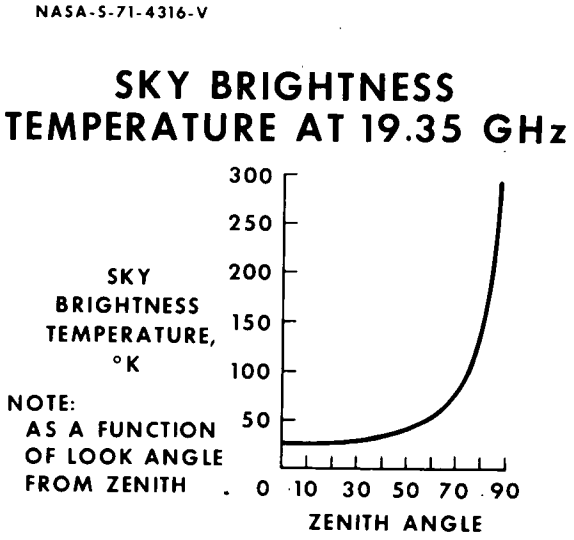

Figure 10.- Sky brightness temperature versus zenith angle for 19.35 GHz.

slopes are oriented toward the horizon by the wind, a hotter portion of the sky is reflected into the radiometer, thus the brightness temperature increases with wind speed. It is believed that the difference in wind sensitivity between the horizontally and vertically polarized brightness temperatures is a result of the difference in the Fresnel reflectivities of a specular facet as shown in Figure 11.

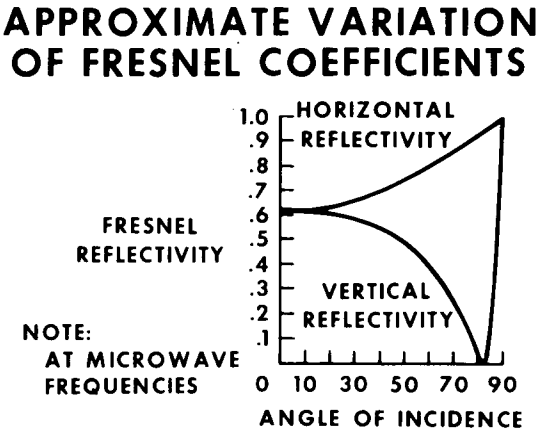

Figure 11.- Approximation variation of Fresnel reflectivities with angle of incidence at 19.35 GHz.

Exactly how the Fresnel coefficients effect this difference is a complex process since for a given facet each polarization mode of the antenna sees the linear combination of the Fresnel coefficients given by equations (4) and (5).

CONCLUSIONS

1. We have developed a mathematical model for the apparent temperature of the sea at all microwave frequencies. The model is a numerical model in which both the clear water wave structure and white water is accounted for as a function of wind speed.

2. This model produces results similar to Stogryn's model at 19.35 GHz for wind speeds less than 8 m/sec. Above 8 m/sec, our model diverges from Stogryn's model which does not include the effects of white water.

3. The model developed here can use radiosonde data to calculate atmospheric effects and can incorporate an empirically determined antenna gain pattern.

4. The computer program is of a modular design. Subroutines called are Cardone's foam coverage vs. wind speed model, Cox and Munk's sea slope distribution model, Droppleman's foam emissivity model, Paris' sea water dielectric constant and atmospheric model. These models can be easily substituted for by other models provided they are coded for the Univac 1108.

5. The computer logic of the main program is capable of treating a horizontally inhomogeneous surface or atmosphere.

6. Computer computation using this model showsthat a variation of microwave sky brightness temperature with zenith angle is <u>necessary</u> to produce the wind sensitivity of the horizontally polarized brightness temperature. The variation of the sky temperature with frequency is <u>sufficient</u> to produce a frequency dependent wind sensitivity.

BIBLIOGRAPHY

1. R.K. Moore and W.J. Pierson, "Worldwide Oceanic Wind and Wave Predictions Using a Satellite Radar Radiometer", AIAA Paper no. 70-310, Presented in Annapolis Maryland, March 1970.

2. J.C. Aukland, P.J. Caruso and W.H. Conway, "Remote Sensing of the Sea Conditions with Microwave Radiometer Systems", AIAA Paper no. 70-318, Presented in Annapolis, Maryland, March 1970.

3. W.H. Peake, "Interaction of Electromagnetic Waves with Some Natural Surfaces", IRE Trans. on Antennas and Propogation, Vol. AP-7, pp. S324-S329, December 1959.

4. A. Stogryn, "The Apparent Temperature of the Sea at Microwave Frequencies", IEEE Trans. on Antennas and Propogation, Vol. AP-15, no. 2, March 1967.

5. G.F. Williams, "Microwave Measurements of Bubbles and Foam", Publisher not located, Univ. Miami, Coral Gables Fla. 33124.

6. J.D. Droppleman, "Apparent Microwave Emissivity of Sea Foam", J. Geophys. Res., Vol. 75, no.3, January 1970.

7. W. Nordberg, J. Conway, Duncan B. Ross, T. Wilheit, "Measurements of Microwave Emission from a Foam Covered, Wind Driven Sea", NASA Preprint X-650-70-384, Oct. 1970 (Submitted for publication to Journal Atmospheric Sciences).

8. James P. Hollinger, "Passive Microwave Measurements of Sea Surface Roughness", IEEE Trans. on Geoscience Electronics, Vol. GE9, no. 3, pp. 165-169, July 1971.

9. Duncan B. Ross, V.J. Cardone and J.W. Conway, "Laser and Microwave Observations of Sea Surface Condition for Fetch-Limited 17-to 25-m/sec. Winds", IEEE Trans. on Geoscience Electronics, Vol. GE 8, no. 4, pp. 326-336, Oct. 1970.

10. J.F. Paris, "Transfer of Thermal Microwaves in the Atmosphere", NASA NGR-44-001-98, Vol. 1, Texas A and M Univ., May 1971.

11. C.Cox and W. Munk, "Measurement of the Roughness of the Sea Surface from Photographs of the Sun's Glitter", J. Opt. Soc. Am., Vol. 44, no. 11, Nov. 1954.

12. J.F. Paris, "Microwave Radiometry and its Application to Marine Meteorology and Oceanography", ONR Contract Nonr 2119 (04), Texas A and M Univ., Jan. 1969.

13. G. Neumann and W.J. Pierson, "Principles of Physical Oceanography", Prentice-Hall, Inc., Englewood Cliffs, N.J., pp.327-329, 1966.

14. D.C. Blanchard "The Electrification of the Atmosphere by Particles From Bubbles in the Sea", Progr. Oceanog., Vol 1, pp. 71-202, 1963.

SECTION 27

DETECTION OF OIL SPILLS USING 13.3-GHz RADAR SCATTEROMETER

by

K. Krishen
Lockheed Electronics Company, Inc.
Earth Observation Department
Houston, Texas

ABSTRACT

This paper describes the results of an analysis of 13.3-GHz Single Polarized Scatterometer data collected during NASA/MSC Mission 135, flown on March 16, 1970. Data were gathered over a crude oil spill on the Gulf of Mexico (Test Site 128) off the Mississippi Delta. With the aid of RC-8 camera photographs, the scattering cross section was correlated with the extent of the oil spill. The scattering cross section at higher incidence angles (25° to 50°) decreased by 5 dB to 10 dB in the presence of the oil spill. This was attributed to oil's damping of small gravity and capillary waves. The composite scattering theory and the scatterometer acquired data were used to obtain an expression of radar scattering over ocean surfaces with oil spills. The study demonstrates that the presence and extent of oil spills can be detected using high frequency radar systems.

INTRODUCTION

In recent years transportation of crude oil using super tankers and stepped up exploration for oil from ocean drilling towers have increased the possibilities of pollution of oceans from oil spills. The desirability of using remote sensors to detect and monitor oil spills is well recognized. Radar's ability to rapidly search wide areas with high resolution offers global scale monitoring of oil spills. Furthermore, radars operated in the frequency range from UHF to X-band are relatively insensitive to bad weather and cloud cover, and can collect data both night and day. Radar's potential for detection and monitoring of oil spills has been demonstrated in experiments conducted by the Naval Research Laboratory[1] (NRL) utilizing the NRL Four-Frequency System at 0.428 GHz, 1.228 GHz, 4.425 GHz, and 8.91 GHz.

At the request of the U.S. Coast Guard, NASA/MSC flew Mission 135 over the Chevron oil spill on March 16, 1970, with the NASA 927 (Lockheed NP3A) aircraft. The NASA 927 remote sensors used on the flight included

RC-8 cameras and a 13.3-GHz Single Polarized Scatterometer. The purpose of the scatterometer was to obtain the radar signature of the oil-covered ocean surface. Ground truth data for Mission 135 were collected by Coast Guard personnel and oceanographers from Louisiana State University.

This paper describes an analysis of the Mission 135, 13.3-GHz vertical-transmit, vertical-receive scatterometer data. The data were collected simultaneously for incident angles between +60° and -60° using doppler coherent wave techniques. A digital processing program yielded a backscattering cross section (σ_0) versus incident angle (θ) curve for the preceding range of incident angles. In the range of incident angles between 25° and 50°, the scattering cross section decreased 5 dB to 10 dB in the presence of the oil spill. The behavior of σ_0 can be explained by a theoretical composite scattering model. The decrease in scattering cross section in the presence of oil is attributed to the damping by oil of small gravity and capillary waves. This decrease in scattering cross section can be used to locate and monitor the oil spill. Repeated coverage of the affected area and presentation of the scatterometer data on either a two-dimensional matrix printout or a black and white or false color image can be used to monitor the movement of oil slicks.

13.3-GHz SCATTEROMETER DATA

A functional and equipment description of the 13.3-GHz Scatterometer used on Mission 135 is contained in Krishen, et al[2]. In operation the scatterometer's radar energy is radiated by an antenna with a wide fore and aft beam and a narrow transverse beam (see Figure 1). The returned energy may be separated as a function of incidence angle using the doppler equation. Radar cross section per unit area is given by the equation:

$$\sigma(\theta) = \frac{P_R}{P_T} \frac{2(4\pi)^3}{\lambda^3} \cdot \frac{Vh^2}{\Delta f_d} \cdot \frac{1}{\int_{-\psi_1}^{\psi_2} \{G_T(\psi) G_R(\psi)\}_\theta \, d\psi} \qquad (1)$$

where,

P_T = transmitted power

P_R = power received in the doppler window defined by Δf_d

G_T, G_R = transmitting antenna and receiving antenna gain, respectively, as a function of θ (incident angle), and ψ (cross track angle)

h = altitude of the aircraft.

Any altitude, pitch, and velocity perturbations in aircraft parameters are properly reflected in the processing plan. A ferrite modulator is used to calibrate the system by providing an absolute power reference for the transmitted signal.

Statistical averages and variance of $\sigma(\theta)$ also are computed in the computer program, using equation (1) and taking logarithms after averaging is performed. The average values of the scattering cross section are represented by $\sigma_0(\theta)$ and $\sigma_0(\theta)_{dB}$ where,

$$\sigma_0(\theta)_{dB} = 10 \log_{10} \left(\sigma_0(\theta)\right) \quad .$$

GROUND TRUTH DATA

The MSC Earth Observations Aircraft Program Mission 135 was conducted over the Chevron drilling platform oil spill on March 16, 1970, from the NASA 927 (NP3A) aircraft. Chevron offshore production platform MP-41C, off the Mississippi Delta, caught fire on February 10, 1970. On March 10 the fire was successfully extinguished, but crude oil continued to spill for approximately 1 month before all wells were capped. Two flights were flown, one during the day and one at night. Figure 2 shows the location of the accident; it is northeast of the Mississippi Delta near the Mississippi River, Gulf outlet channel. The approximate flight lines, as depicted in NASA/MSC Mission 135, Screening and Indexing Report[3] are shown in Figure 3.

Ground truth for Mission 135 was taken from the U.S. Coast Guard's (USCG) on-the-scene situation reports and from data gathered by the Louisiana State University (LSU) staff[4]. The U.S. Coast Guard situation reports, summarized in the appendix of the LSU report, outline chronological developments of the Chevron oil spill. The LSU report contains measurements of tides, winds, waves, salinity, temperature and currents. The USCG routine situation reports list direction and approximate width and length of the oil slick when visibility allowed observations from helicopters or other aircraft. Analysis and interpretation of all ground truth data are given in the LSU report.

The scattering cross sections at the 13.3-GHz frequency are dependent on the local wind velocity[5]; therefore, wind velocity and sea state measurements in the oil spill area are needed for interpretation of the scatterometer data. The measurements of sea state and wind velocity[4] are plotted in Figures 4 and 5. The wind measurements were taken onboard the U.S. Coast Guard Cutter *Dependable* in the vicinity (Figure 2) of Chevron

platform MP-41C. The anemometer height on the *Dependable* is approximately 18.5 meters*. The wave height and wave period measurements were taken from Chevron platform MP-41M (Figure 2). The wind measurements for the same time intervals are given in Figure 5.

The relative direction flown by the NASA 927 aircraft with respect to wind is shown in Figures 6 and 7 for flights 1 and 2, respectively (in these figures F1L10R4 is an abbreviation for Flight 1, Line 10, Run 4).

The extent of oil cover was reported by the U.S. Coast Guard at 1225 hours local time. In summary, USCG reported a major oil slick of approximately 1-1/2 to 2 miles extent approximately 240° true north from the platform, dispersing to medium crude and rainbow slick 3 miles from the rig. The total slick extended 5 miles west, 6 miles north, 3 miles east, and 5 miles south of the rig (Figure 8). Furthermore, USCG reports the slick was well dispersed and areas of medium crude were on the periphery of the total area.

In addition to the ground truth provided in the LSU and USCG reports, photographs were taken by the RC-8 cameras during flight 1. One RC-8 camera was loaded with color film (type SO 397) and the other with color infrared film (type SO 117). Both cameras have a 9 by 9 inch film format and provision for recording time and aircraft attitude and altitude between film frames. The RC-8 field of view is 74°. Photographic coverage was used in this study to correlate scatterometer data with oil covered areas. Identification marks such as MP-41C (Figure 9) and Breton Island (Figure 3) were used to pinpoint the areas over which the aircraft was flying at a particular time. In this paper only typical photographs are presented in reference to scatterometer data interpretation. Analysis of Mission 135 photographic coverage is given in a report by Catoe[6].

CORRELATION OF 13.3-GHz SCATTEROMETER DATA WITH THE OIL SLICK

Radar backscattering cross sections are dependent upon surface roughness, dielectric properties, and angle of incidence. In the recent past, several experimental and theoretical models have given the relationship between radar backscatter and ocean surface parameters (Wright[7] and Krishen[5]). In this paper the radar signature of an ocean surface oil slick is studied. In particular, the signature of an oil slick is compared to a sea surface without oil slick. Differences in the scattering cross sections can be utilized to distinguish an oil slick from its background.

*Telephone conversation with S. P. Murray, LSU.

During Mission 135, several runs of scatterometer data were taken. For this analysis, only those data were processed for which the scatterometer signal-to-noise ratio was highest. The results presented in this paper are based on F1L10R3, F1L10R4, F1L11R1, F2L10R1, F2L10R2, and F2L10R5 data. Photographic coverage was available only for flight 1.

An area with no significant oil slick (Figure 10) was chosen from ground truth data. The average scattering cross section for this area is given in Figure 11. A comparison of Mission 135 (no significant slick) F1L10R4 data with F1L1R1 of Mission 119 data for the same wind conditions is also given in Figure 11. Mission 119 was flown over site 86 near Argus Isle, Bermuda, during January and February 1970. Mission 119 was flown over open ocean during fully developed conditions, while Mission 135 was flown over relatively shallow waters near the coast. In view of this, and the fact that only approximate values of wind velocity are available, one can conclude that an agreement between Mission 119 and 135 data exists within experimental error tolerances.

An area where significant oil was present was chosen (Figure 12), and the corresponding scatterometer data was processed. The data for Mission 135, F1L10R4 with oil slick present, is given in Figure 13, which also shows data from Mission 156 (FCF). Mission 156 (FCF) was flown over the Gulf of Mexico near Galveston, Texas, in relatively calm conditions (5 to 6 knots wind speed) in February 1971. The agreement is striking.

The comparisons shown in Figures 11 and 13 indicate that in the presence of oil, high surface wind velocity ocean radar scattering cross section is similar to that of an ocean with low surface wind speed.

Radar scattering cross sections for ocean surfaces both with and without oil slicks are compared in Figure 14. At higher angles (25° and above) the cross section decreases about 7 dB in the presence of oil. This implies that the power returned from an oil slick is decreased by a ratio of 5 over that returned from an oil-free surface. The data for F1L10R3 was studied and showed a similar relationship.

Flight 1, line 11, run 1 was flown over an area where no significant oil slick was present. The scattering cross section for this data compared to the data shown in Figure 11 showed close agreement.

Flight 2 was conducted at night; consequently, no photographic data is available. But based on the approximate ground track and ground truth, one can select data from flight 2 for an area relatively free of oil slick and for an oil slick covered area. Flight 2 data compared to flight 1 data showed good agreement. Furthermore, the decrease in scattering cross section at higher angles compares very well (Figure 15) with the results obtained for flight 1 (Figure 14). The results of F2L10R1 and F2L10R5

show consistently similar decreases in radar scattering cross section. The feasibility of using radars both day and night for detection and monitoring of oil slicks is thus evident.

If the angle of incidence is kept constant along the flight path, one can generate a graph (Figure 16) of average σ_0 as a function of time/distance. In this graph an average σ_0 for 20-second intervals is plotted. The dip in the graph indicates the presence of oil. Other sets of data over the slick showed similar results.

The behavior of σ_0 can be explained using a theoretical composite scattering model in which the ocean surface is considered a slightly rough surface (high frequency gravity and capillary waves) superimposed on a larger structure (sea waves and swells)[5]. It has often been suggested that near the normal incidence for backscattering cross sections, scattering of the optics type [Kirchhoff method] predominates. In other directions, however, the slight roughness on top of large scale roughness constitutes the major source of scattering. In view of this, Wright[7] and Guinard and Daley[8] ignore the large structure effects to account for scattering at higher backscattering angles. Their procedure parallels Rice[9], Barrick and Peake[10], and Valenzuela[11]. The presence of a large structure introduces a modification which is small for vertical-transmit, vertical-receive cases (Wright[7]). For Rice's method the backscattering cross sections of a slightly rough surface using first order terms are given by

$$(\sigma_{\lambda\delta})_s = 4\pi k_0^4 \cos^4 \theta |\alpha_{\lambda\delta}|^2 W(p,q) \qquad (2)$$

where,

k_0 = wave number of the incident radar energy

θ = the incident angle

$W(p,q)$ = the roughness spectral density of the surface, and p,q are radian wave numbers

$$\alpha_{HH} = \frac{\varepsilon - 1}{\left[\cos\theta + \sqrt{\varepsilon - \sin^2\theta}\right]^2}$$

$$\alpha_{VV} = \frac{(\varepsilon - 1)[(\varepsilon - 1)\sin^2\theta + \varepsilon]}{\left[\varepsilon\cos\theta + \sqrt{\varepsilon - \sin^2\theta}\right]^2}$$

ε = the complex dielectric constant of the surface.

To determine the oil slick's effect on the sea surface, the directional spectrum of the sea's small gravity-capillary structure is expressed as

$$W(r) = kr^{-k_3}$$

where,

$$r = \sqrt{p^2 + q^2} \quad .$$

The values of k and k_3 are dependent on the small structure atop the large structure. After substitution of this spectrum and evaluation at the Bragg scattering condition (Wright[7]), equation (2) yields

$$\sigma_0(\theta) = k_1 |\alpha_{vv}|^2 (\cos\theta)^4 (\operatorname{cosec}\theta)^{k_3} \qquad (3)$$

for the vertical-transmit, vertical-receive polarization combination. In equation (3) k_1 is directly proportional to k. Two sets of data, corresponding to no significant oil slick and significant oil slick, were chosen and the values of k_1 and k_3 sought for best fit. The values of these constants for no significant oil (F1L10R4, from 21:27:26 to 21:27:45 GMT) are

$$k_1 = 0.005118$$

$$k_3 = 5.25 \quad .$$

Using these values for the constants, the calculated values compare very well with the experimental results as shown in Figure 17.

In the presence of oil (F1L10R4, from 21:26:26 to 21:26:45 GMT), the spectrum constants were given by

$$k_1 = 0.0003275$$

$$k_3 = 7.0 \quad .$$

A comparison of the calculated and experimental values is shown in Figure 18. The results of this study demonstrate that the spectrum of small gravity and capillary waves diminishes significantly in the presence of oil. Cox and Munk[12] measured the mean squared slope in both the presence and absence of oil slicks, and found that the mean squared slope in the presence of oil slicks was about one-third that in the absence of slicks. The oil's smoothing of the sea surface is amply verified by the change in the values of k_1 and k_3 determined in this study.

CONCLUSIONS

The presence of oil spill on a water surface can be detected at 13.3 GHz because of a sharp decrease in scattering cross section (for vertical-receive, vertical-transmit polarizations). The decrease in scattering cross section is attributed to damping of small gravity and capillary waves on the water surface. Repeated coverage of an affected area with radars and presentation of the data as false-color photography can be used to detect and monitor the spread of an oil spill. Further experimentation is needed to establish a relationship between thickness of the oil spill and radar backscattering cross sections.

REFERENCES

1. Guinard, N. W., The Remote Sensing of Oil Slicks, *Proc. Seventh International Sym. of Environment*, The University of Michigan, May 1971.

2. Krishen, K., N. Vlahos, O. Brandt, and G. Graybeal, Results of Scatterometer Systems Analysis for NASA/MSC Earth Observation Sensor Evaluation Program, *Proc. Seventh Int'l. Sym. of Environment*, The University of Michigan, May 1971.

3. NASA/MSC, *Screening and Indexing Report, Mission 135, Site 128*, Manned Spacecraft Center, Houston, Texas, May 1970.

4. Murray, S. P., W. G. Smith, and C. J. Sonu, *Oceanographic Observations and Theoretical Analysis of Oil Slicks During the Chevron Spill*, Tech. Rept. No. 87, Louisiana State University, September 1970.

5. Krishen, K., Correlation of Radar Backscattering Cross Sections with Ocean Wave Height and Wind Velocity, *Journal of Geophy. Res.*, 76, No. 27, 6528-6539, 1971.

6. Catoe, C. E., *Results of Chevron Oil Spill in Gulf of Mexico, Final Rept.*, Project 714104/A/004, U.S. Coast Guard, Washington, May 1970.

7. Wright, J. W., A New Model for Sea Clutter, *IEEE Trans. Antennas Propagat., AP-16*, 217-223, 1968.

8. Guinard, N. W., and J. C. Daley, An Experimental Study of a Sea Clutter Model, *Proc. IEEE, 58*, 543-550, 1970.

9. Rice, S. O., *Reflection of Electromagnetic Waves by Slightly Rough Surfaces: The Theory of Electromagnetic Waves* (a symposium), Interscience, New York, 1951.

10. Barrick, D. E., and W. H. Peake, Scatternig from Surface with Different Roughness Scales: Analysis and Interpretation, *Res. Rep. BAT-197A-10-3*, Batelle Memorial Institute, Columbus, Ohio, 1967.

11. Valenzuela, G. R., Depolarization of EM Waves by Slightly Rough Surfaces, *IEEE Trans. Antennas Propagat., AP-15*, 552-557, 1967.

12. Cox, C., and W. Munk, Measurement of the Roughness of the Sea Surface from Photographs of the Sun's Glitter, *J. Opt. Soc. Amer., 44*, 838-850, 1954.

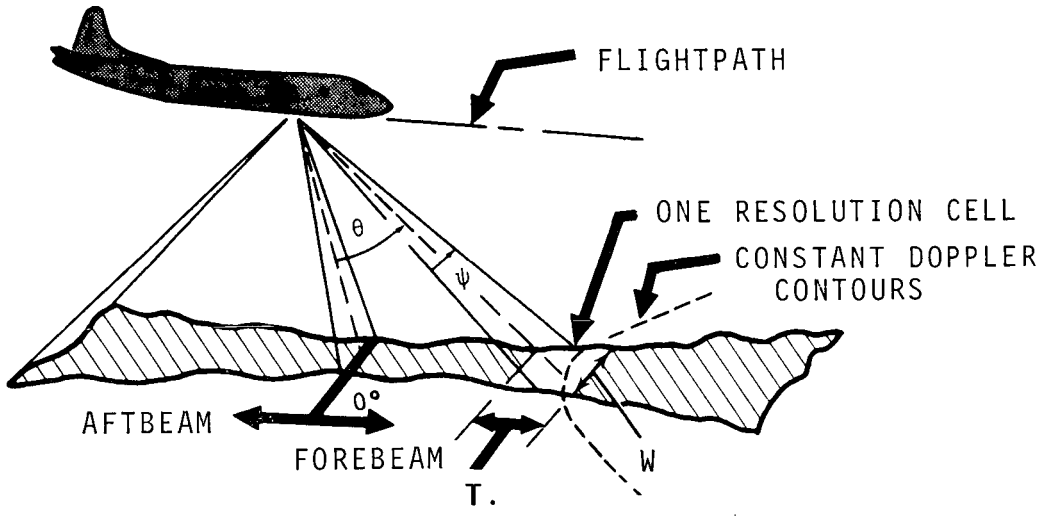

Figure 1. 13.3-GHz Scatterometer resolution cell geometry.

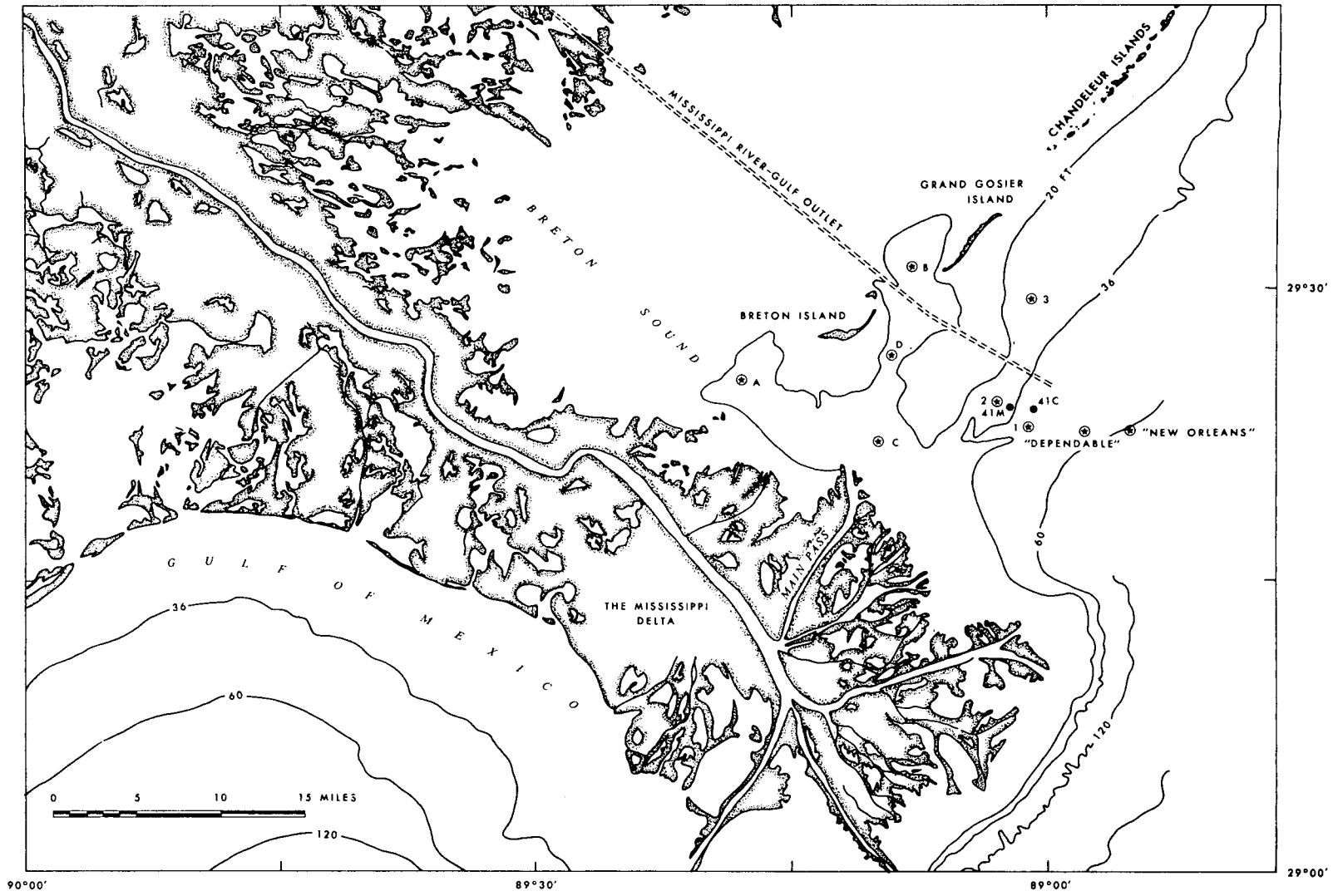

Figure 2. Location map showing stations occupied in study (from Murray et al, 1970).

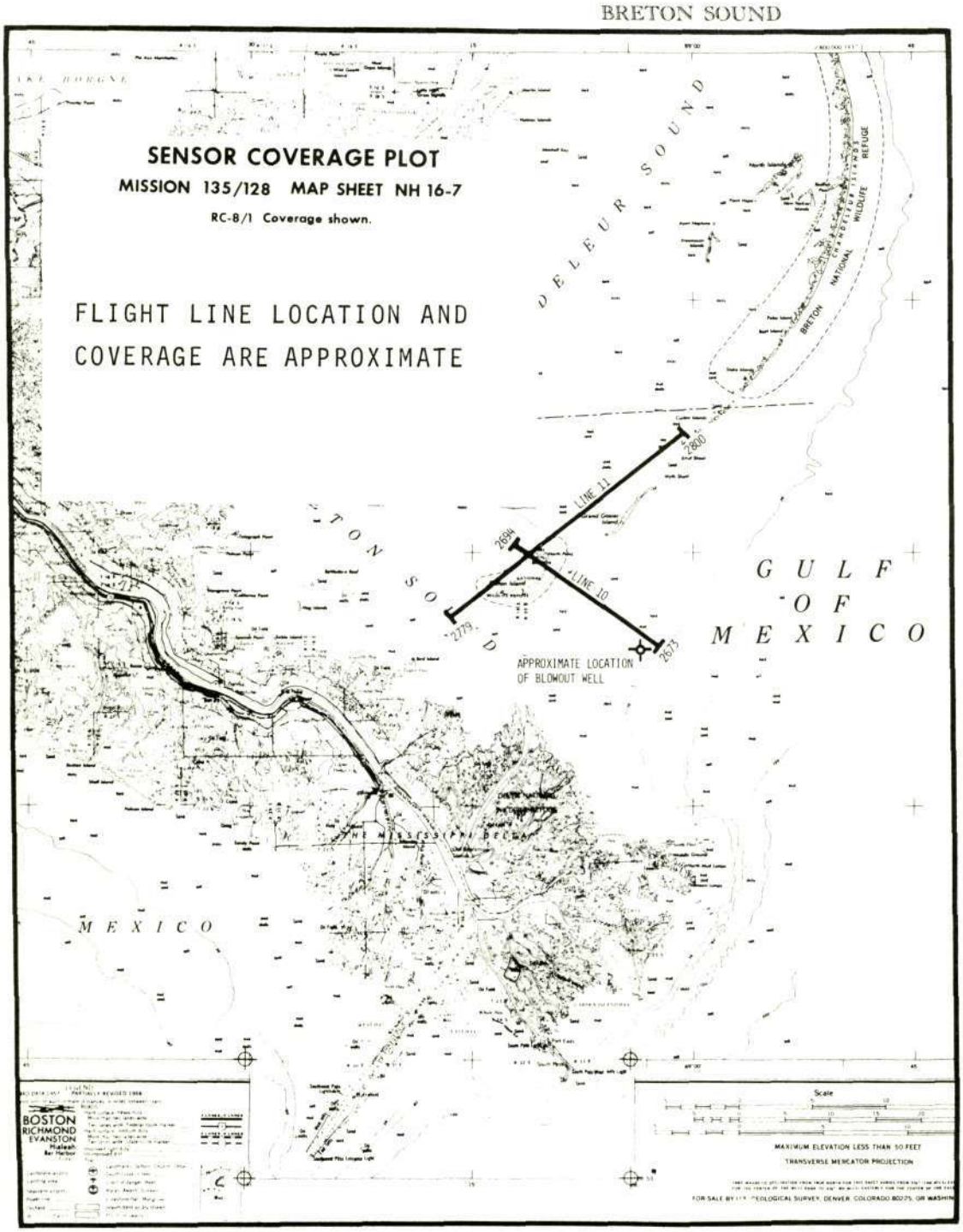

Figure 3. Approximate flight line location, from NASA/MSC Mission 135 Screening and Indexing Report (1970).

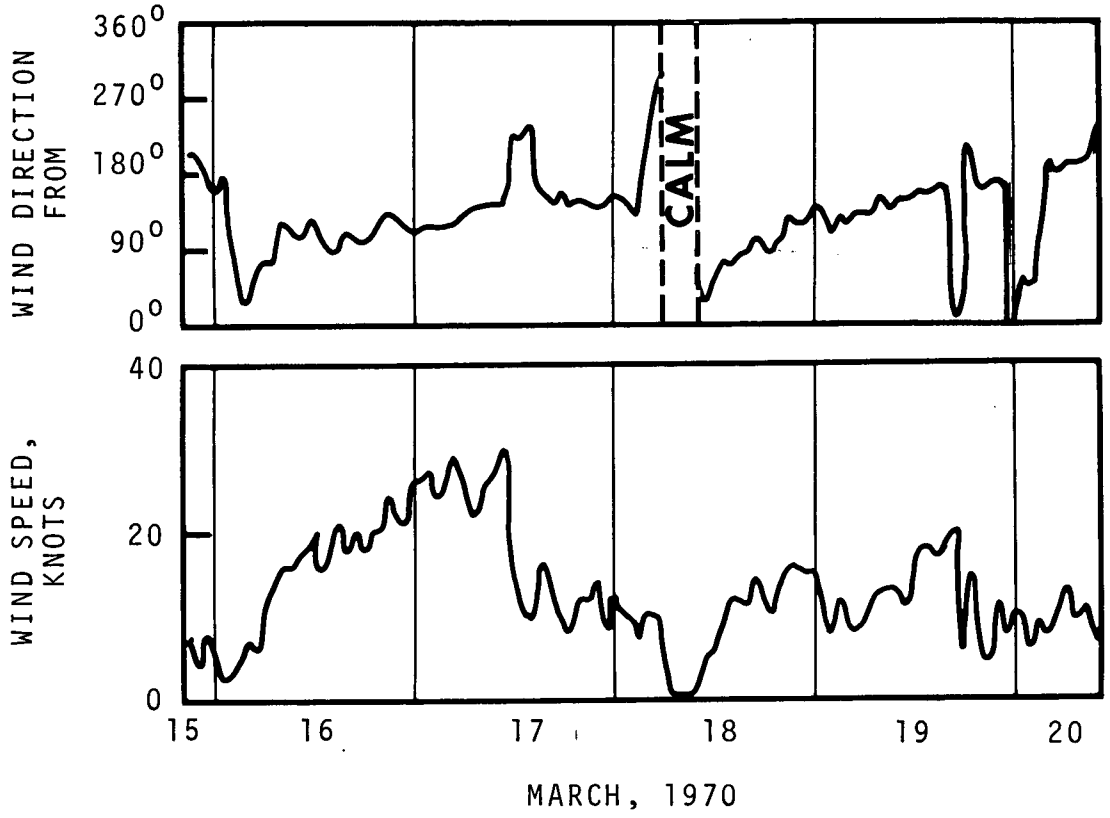

Figure 4. Wind speed and direction at *Dependable* station.

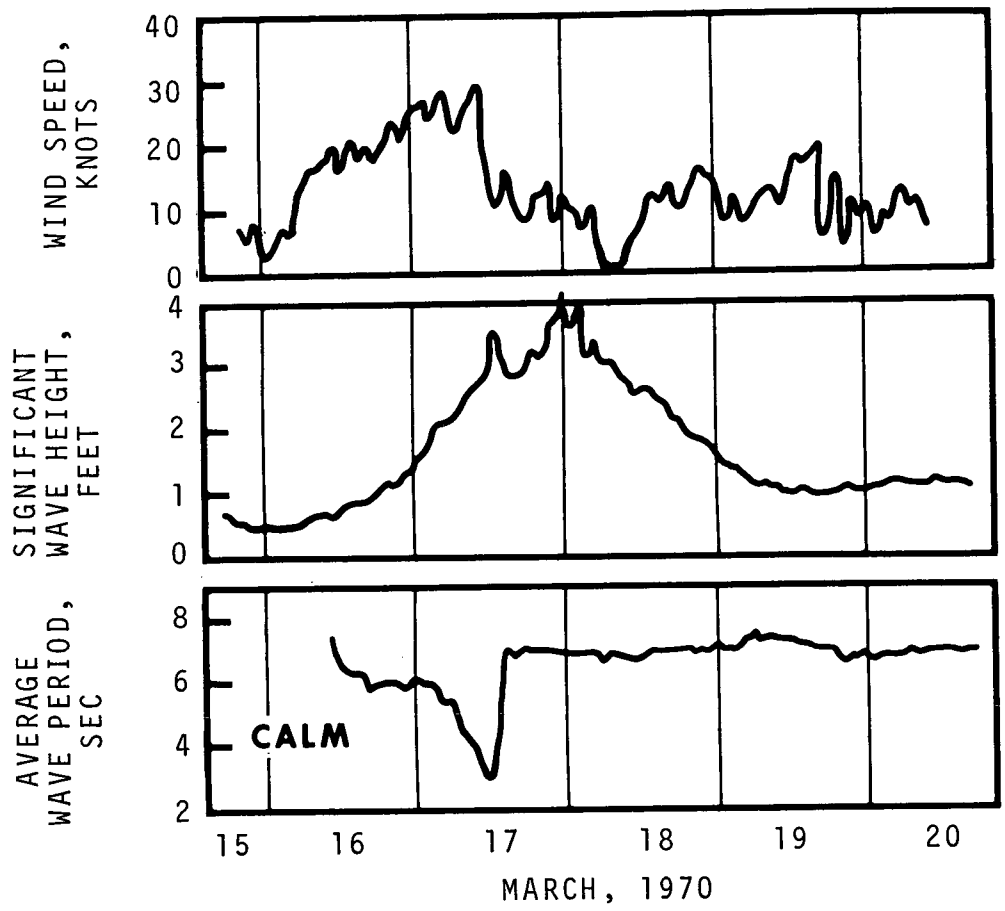

Figure 5. Wave height and wave period from 521 meter installed at Chevron platform MP-41M and wind speed for same intervals.

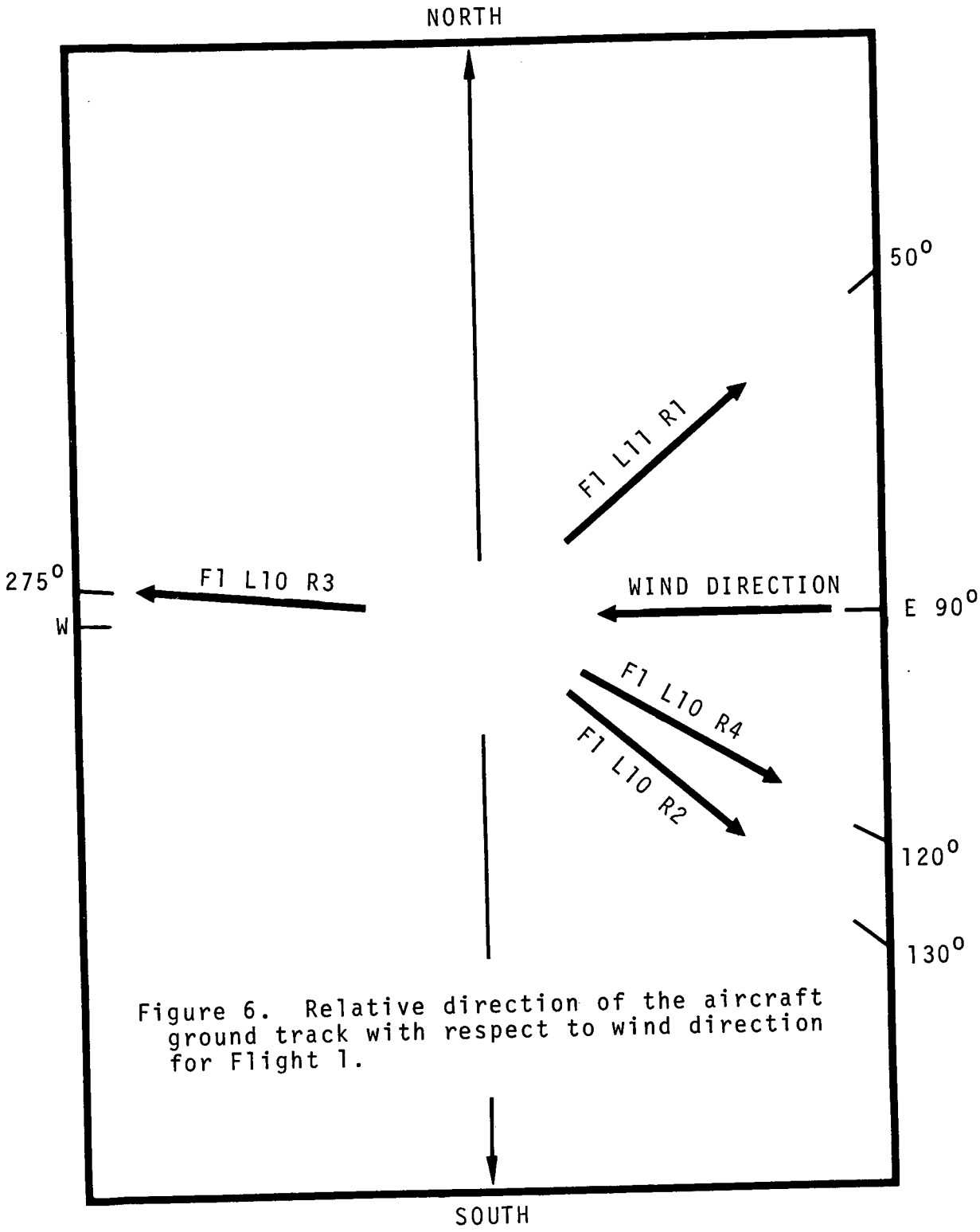

Figure 6. Relative direction of the aircraft ground track with respect to wind direction for Flight 1.

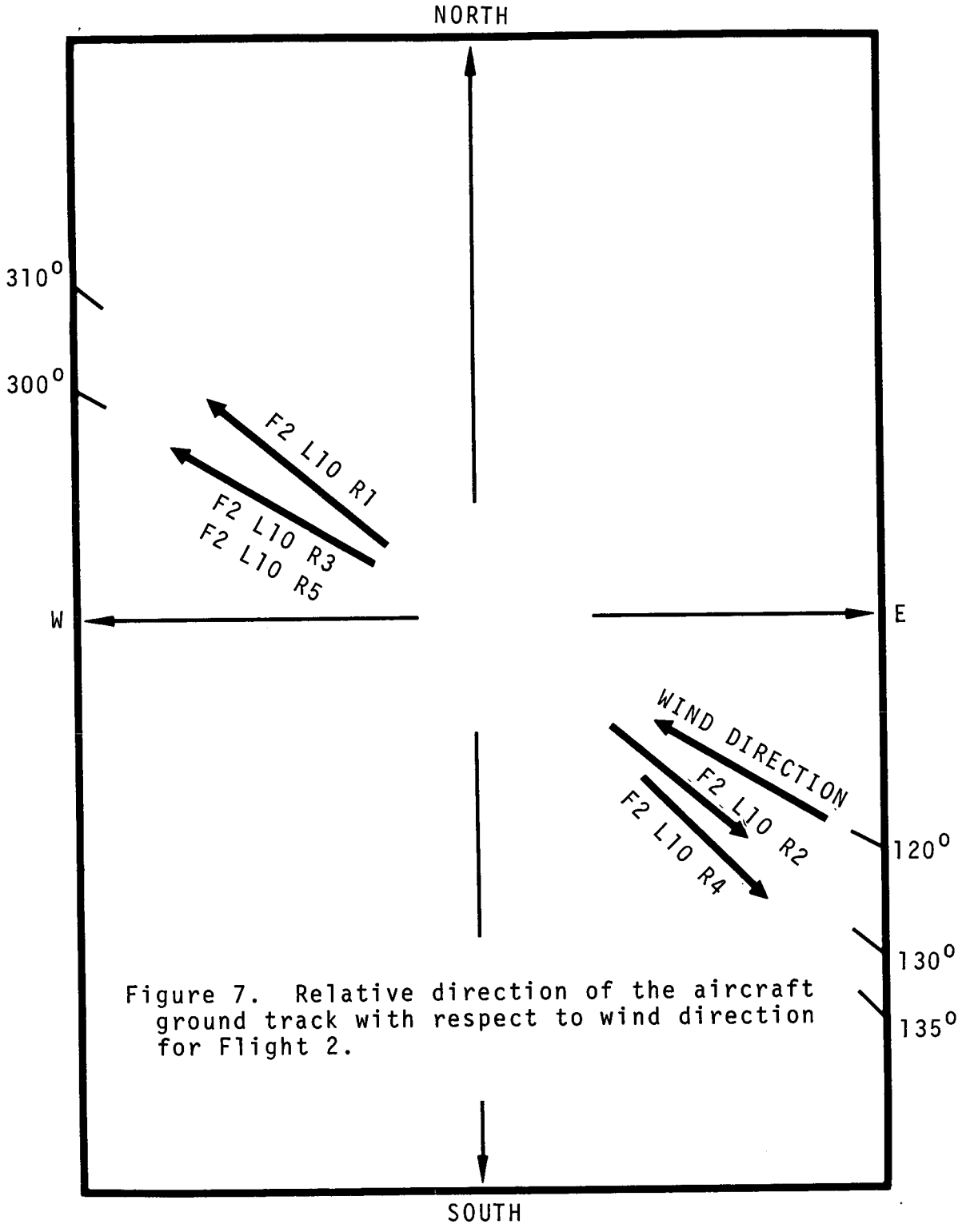

Figure 7. Relative direction of the aircraft ground track with respect to wind direction for Flight 2.

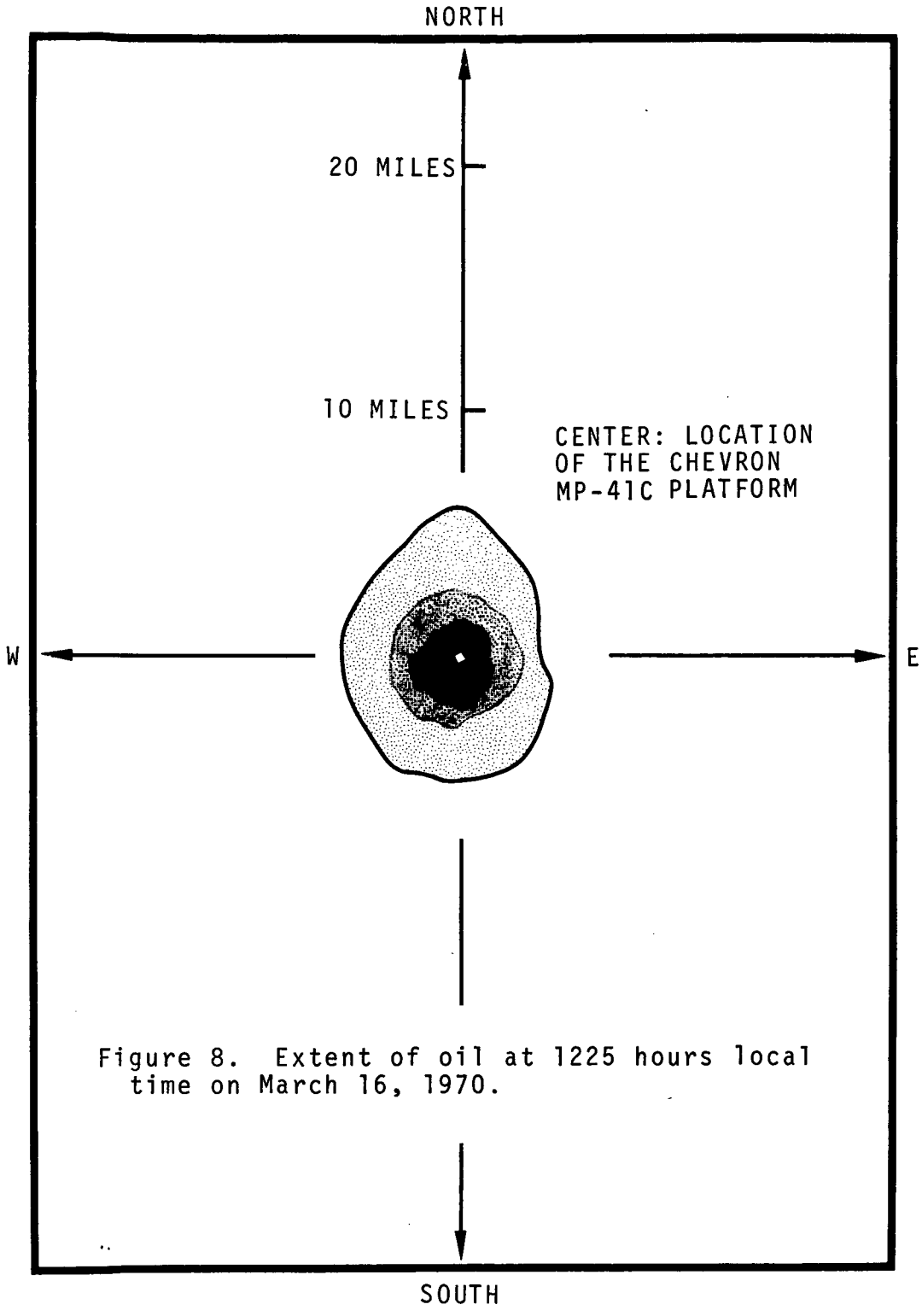

Figure 8. Extent of oil at 1225 hours local time on March 16, 1970.

Figure 9. RC-8 photograph of Chevron MP-41C platform.

Figure 10. RC-8 photograph of an area with no significant oil slick.

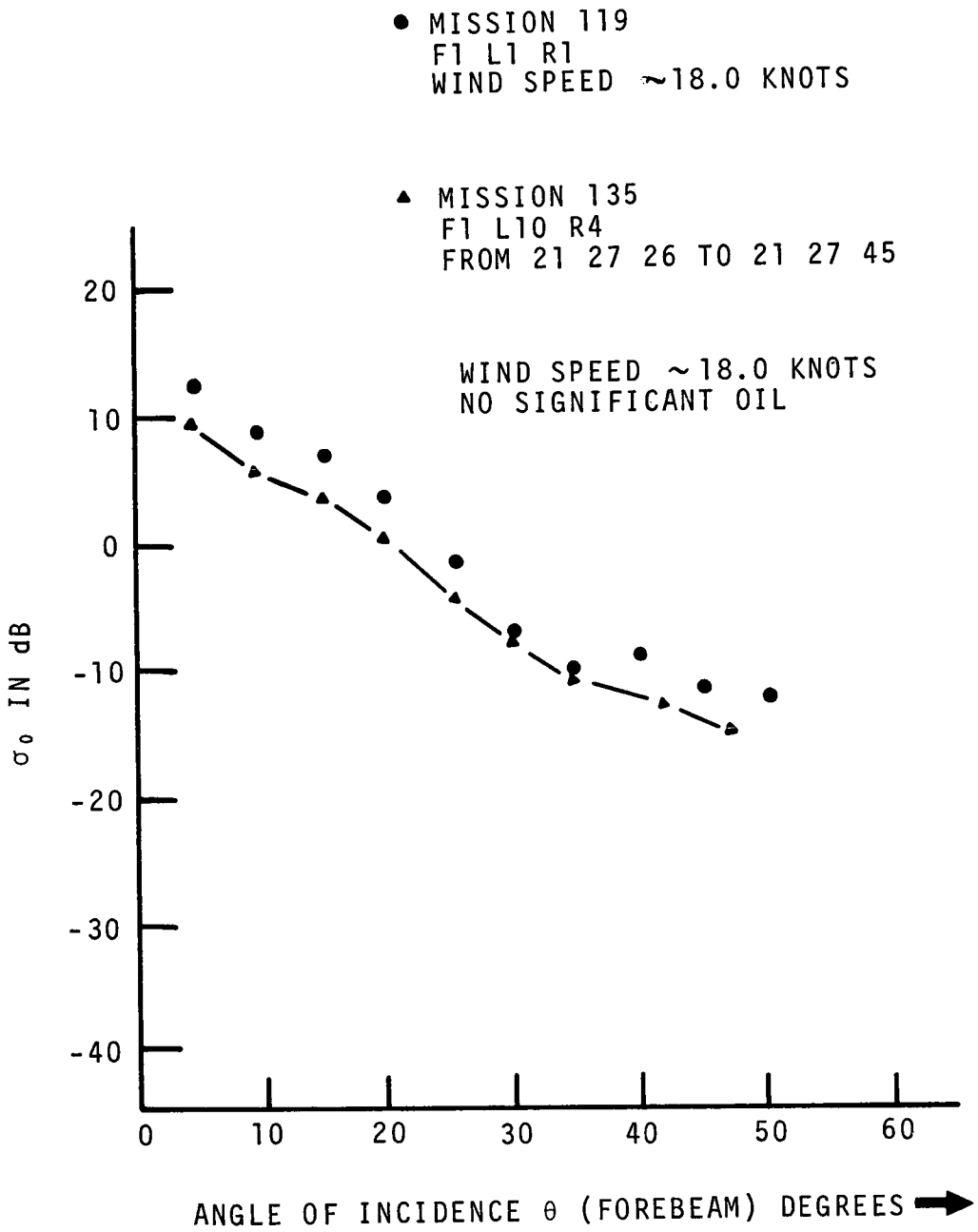

Figure 11. Comparison of Mission 135 data with Mission 119 data.

Figure 12. RC-8 photograph of an area with significant oil slick.

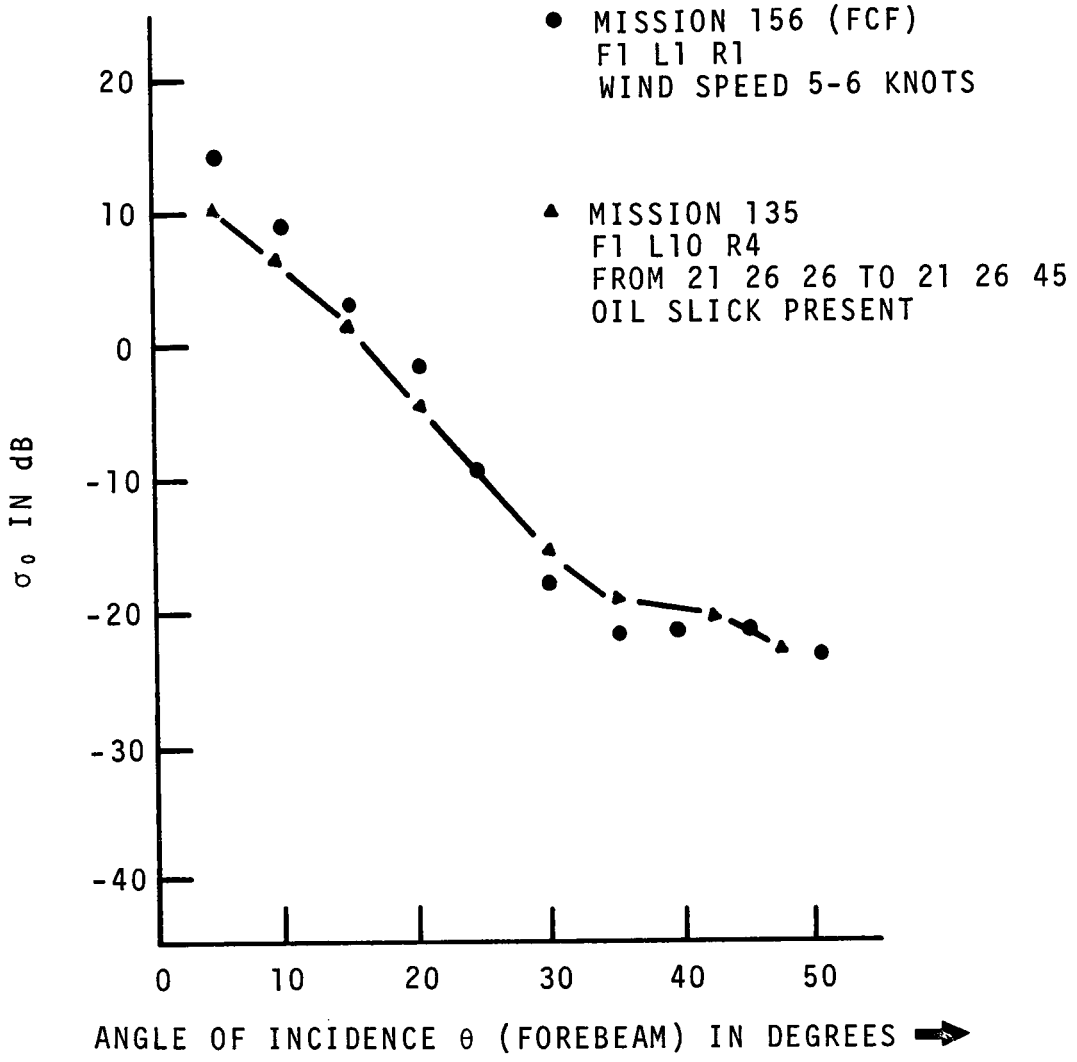

Figure 13. Comparison of Mission 135 data with Mission 156 (FCF) data.

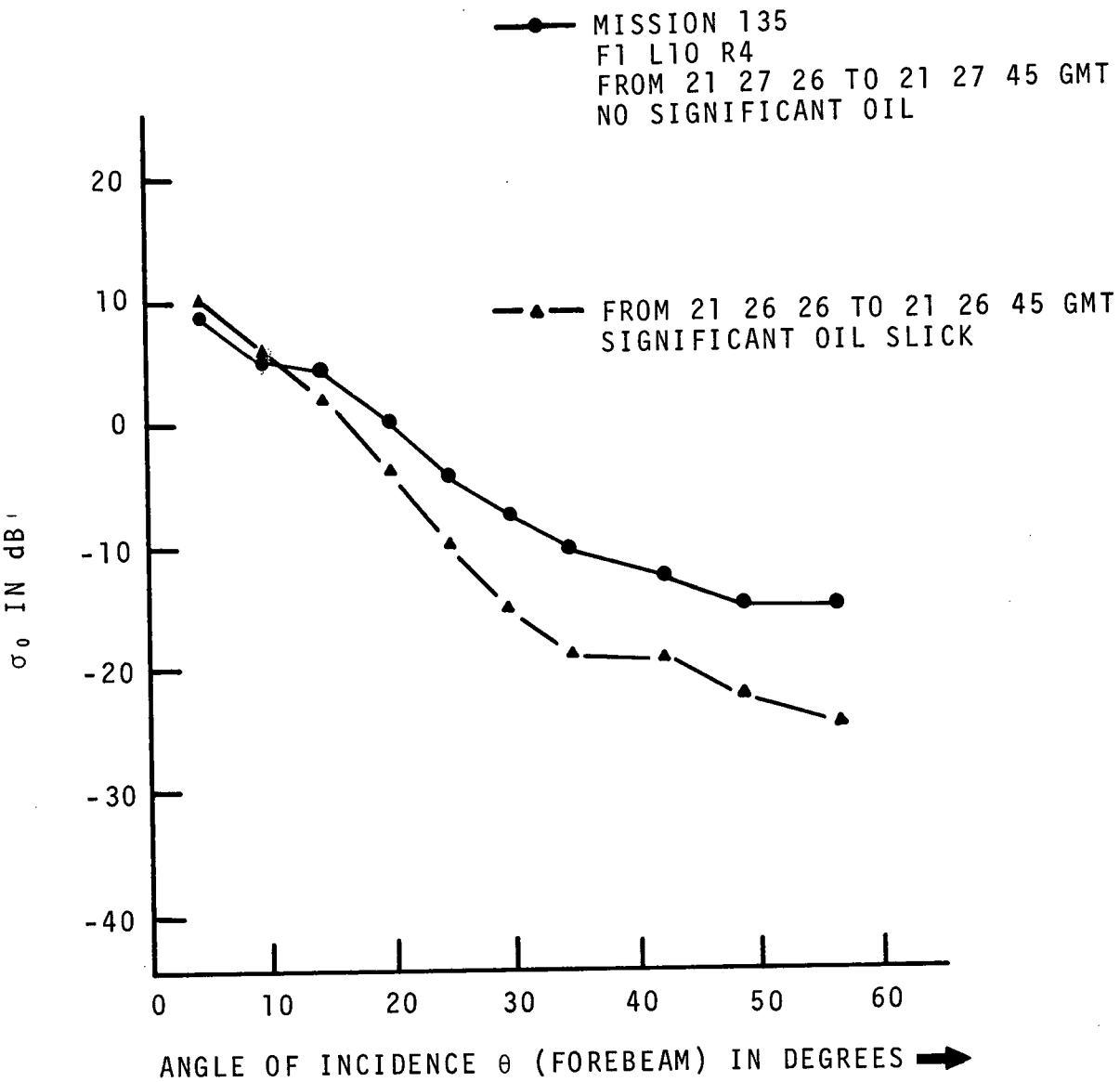

Figure 14. Comparison of scattering cross section of oil slick area and no significant oil slick area for flight 1.

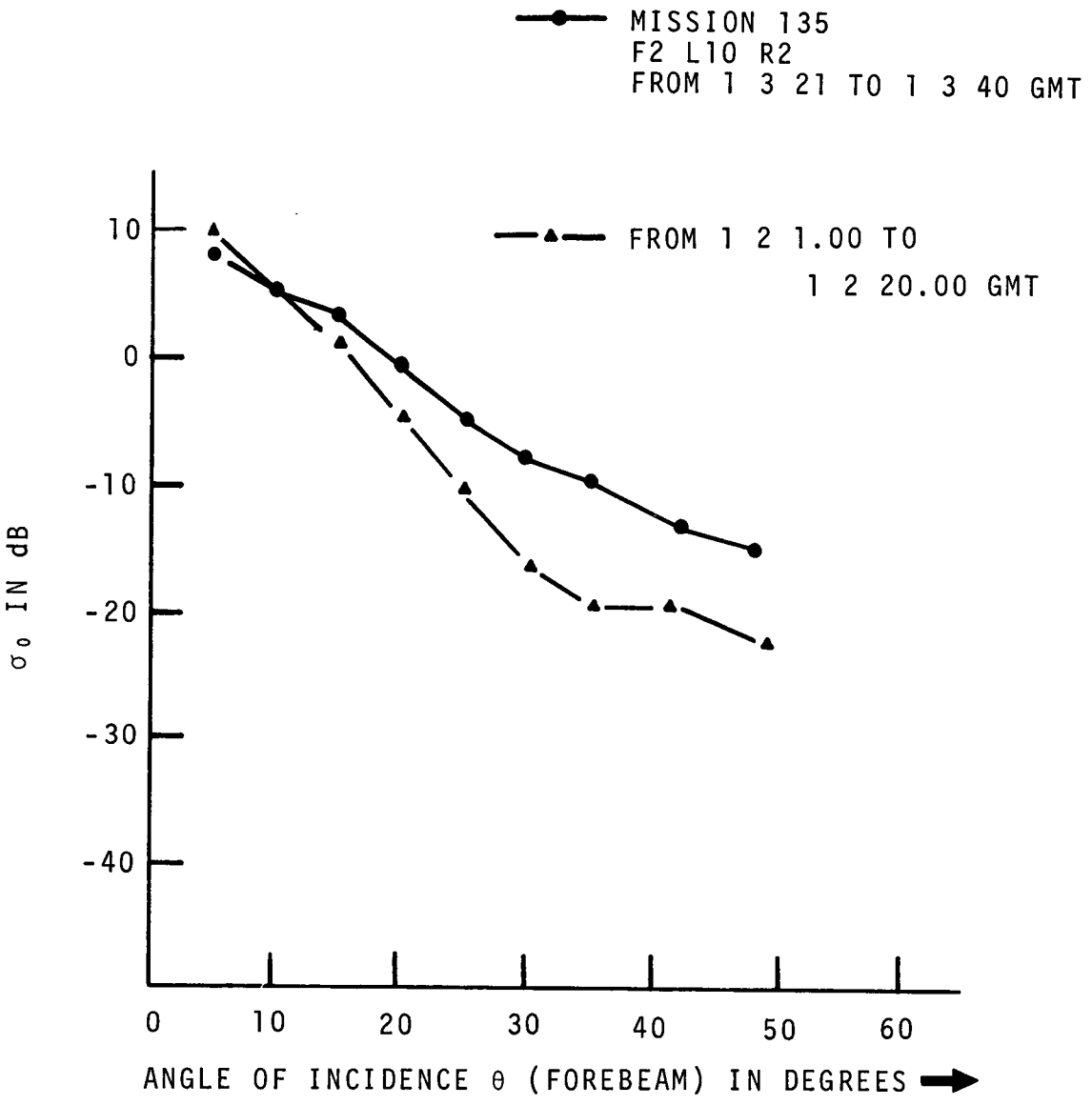

Figure 15. Comparison of $\sigma_0(\theta)_{dB}$ of oil slick and no significant oil slick data for flight 2.

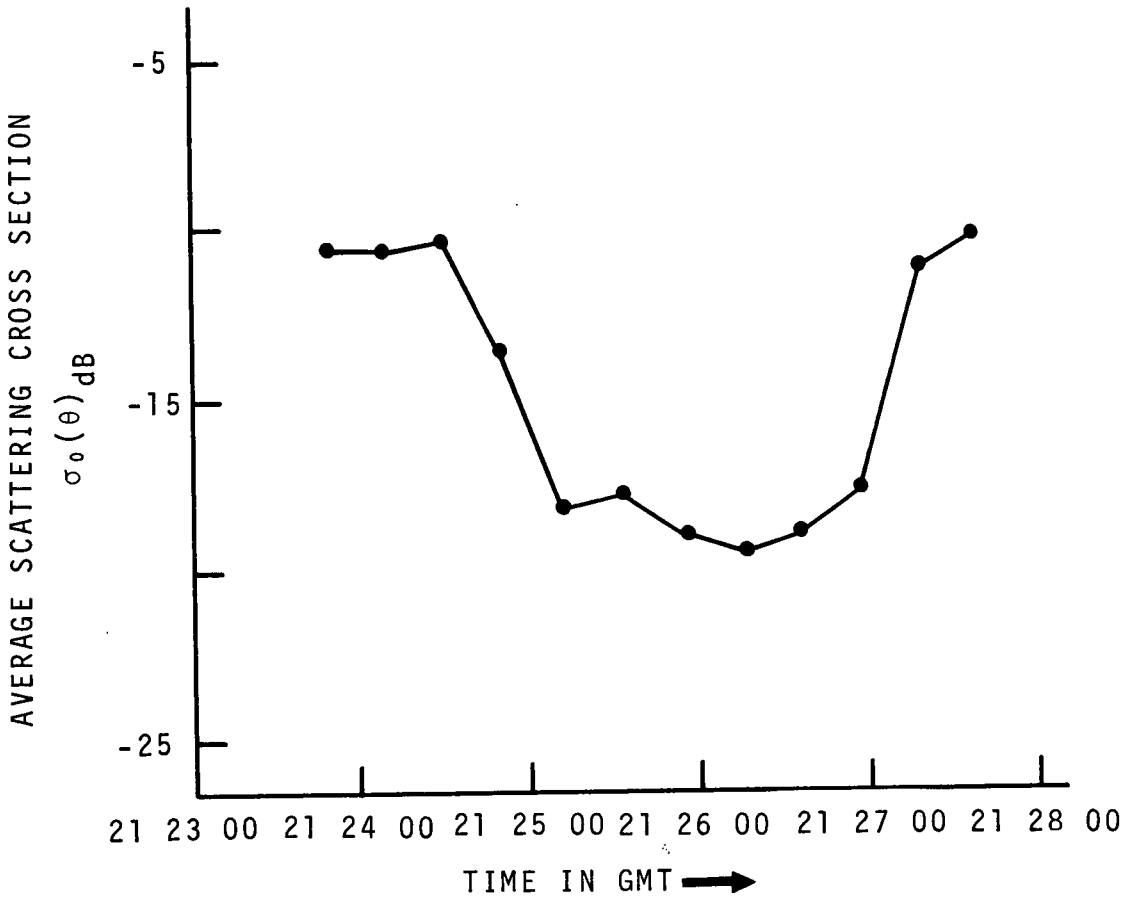

Figure 16. Average value of scattering cross section at $\theta = 35°$ along ground track for F1 L10 R4.

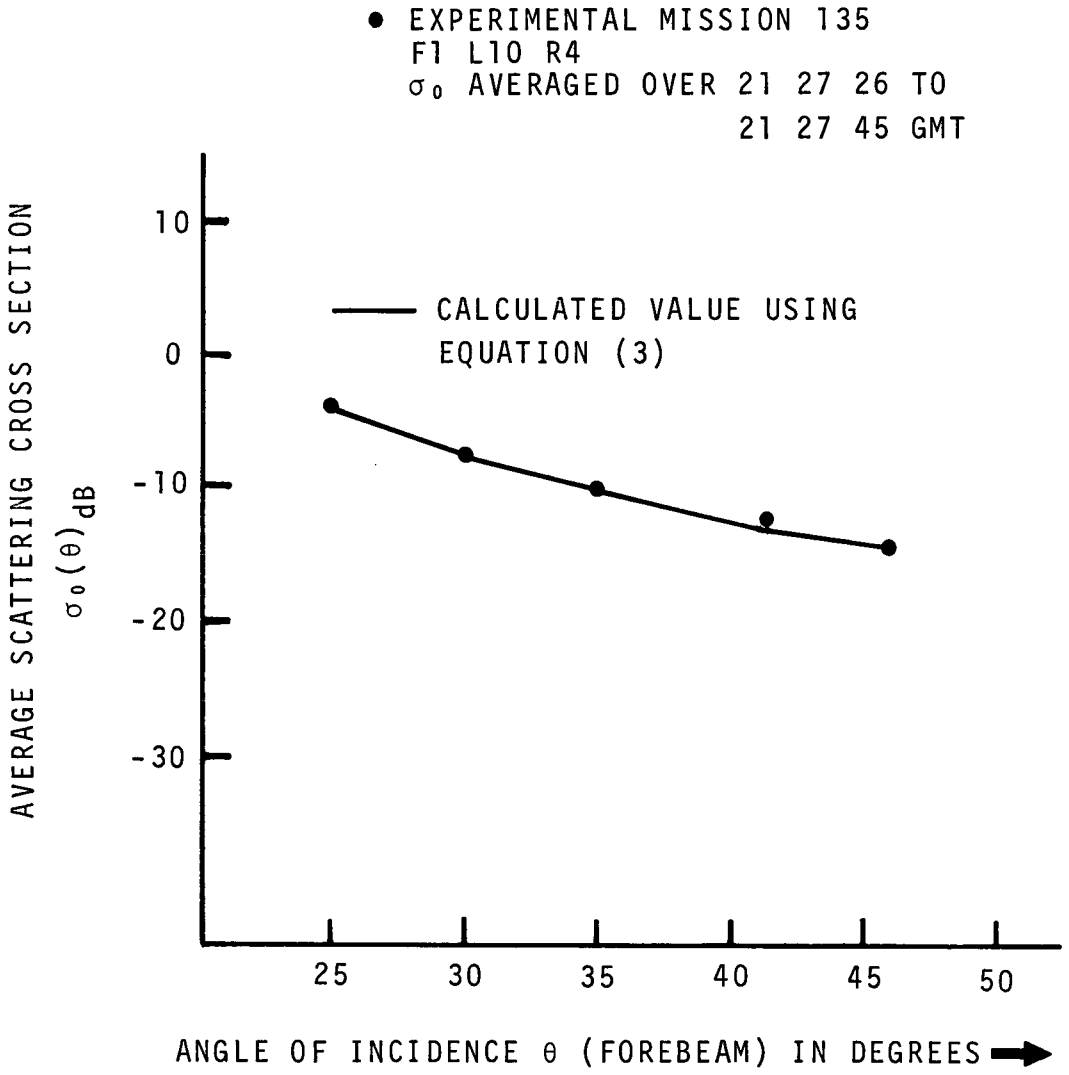

Figure 17. Comparison of calculated and experimental scattering cross section for Mission 135 (no significant oil present).

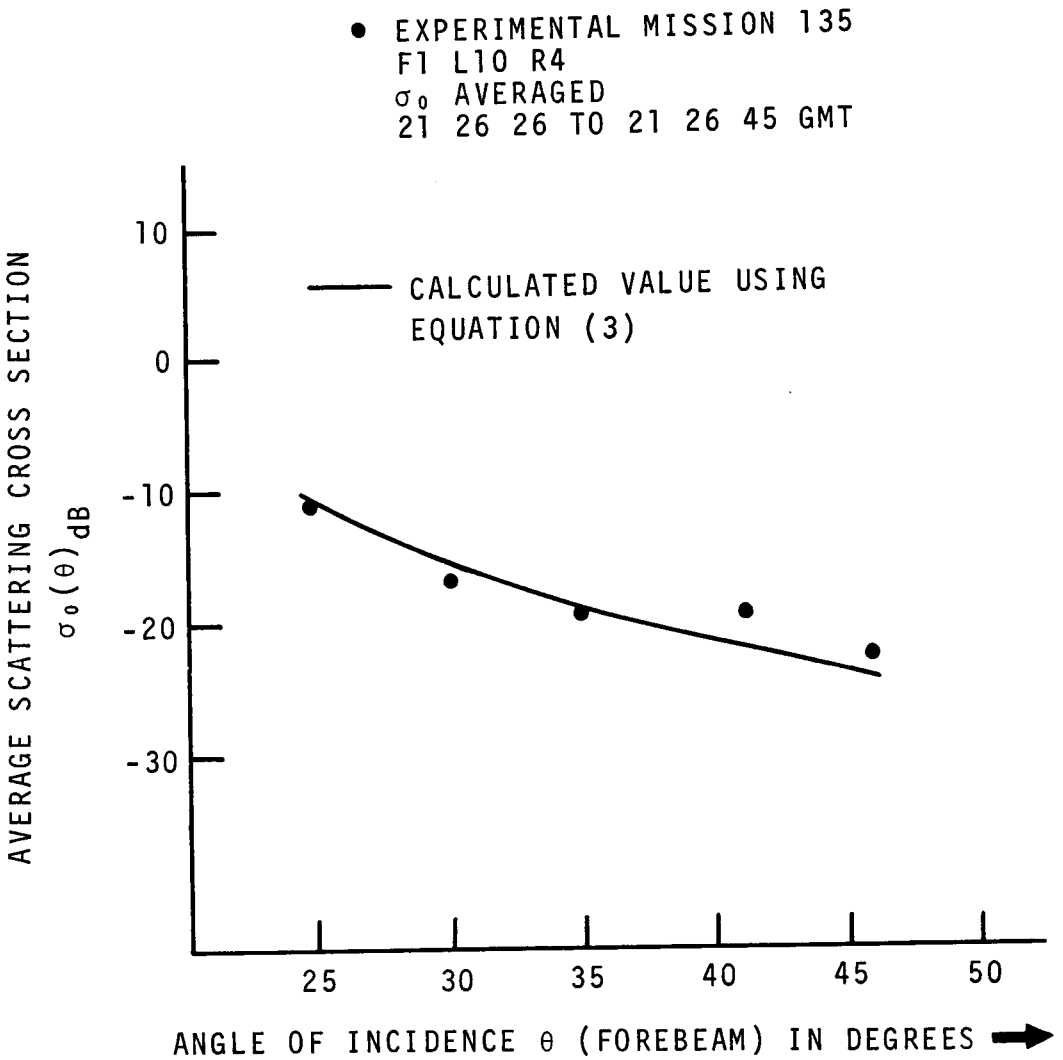

Figure 18. Comparison of calculated and experimental scattering cross section for Mission 135 (significant oil present).

☆ U. S. GOVERNMENT PRINTING OFFICE: 1972—770-624